Abstract Volume
15th Swiss Geoscience Meeting

Davos, 17th – 18th November 2017

Moving Boundaries

SLF

sc | nat

Swiss Academy of Sciences
Akademie der Naturwissenschaften
Accademia di scienze naturali
Académie des sciences naturelles

WSL

Big Picture: The Magic Line

The large picture Shows the Glarus thrust fault and the Martinsloch at the Tschingelhörner (at the boundary between the Cantons of Glarus and Graubünden). This Geological-tectonic structure of scientific and historical significance can be clearly observed as a more or less straight horizontal line through the steep cliffs of the Tschingelhörner. The Martinsloch is a rock hole of cultural, historical and astronomical significance.

At the Tschingelhörner, the line formed by the Glarus thrust fault marks the boundary between dark-colored Permian Verrucano rocks (250 Ma) overthrusted over light-colored Late-Jurassic limestones («Quinten-Kalk» 150 Ma) with slivers of flysch («Sardona flysch» 50 Ma). In other regions along the Glarus thrust fault, the Verrucano rocks are even resting directly over the much younger Sardona flysch.

This superposition of older rocks over much younger rocks is the result of the moving boundaries between the European and African tectonic plates some 20-25 mio years ago. Because of the collision between these two plates, the Verucano rocks were «pushed» northwards along the Glarus thrust fault over a distance of more than 35 kilometers to rest in their actual final position.

The legendary Martinsloch («Martin's hole») is the result of preferential erosion along two zones of geological weakness. Twice a year, for two days in spring and in autumn, the sun shines through the Martinsloch and illuminates the Church tower of Elm in the Valley below. (Photo credit: Pierre Dèzes)

Small Picture:

Ice formation in a mountain stream (Photo credit: Marcia Phillips)

15th Swiss Geoscience Meeting, Davos 2017

Table of contents

http://www.geoscience-meeting.ch

Organisation

Host Institution

WSL-Institute for Snow and Avalanche Research SLF

Patronnage

Platform Geosciences of the Swiss Academy of Sciences SCNAT

Local Organizing Committee

Cornelia Accola
Michael Bründl
Charles Fierz
Marion Hofmänner
Tobias Jonas
Marcia Phillips
Jürg Schweizer (President SGM2017)
Alec van Herwijnen

Coordination

Pierre Dèzes

Sponsors

Swiss Geological Survey, swisstopo
CHGEOL
Edi Meier + Partner
Gebäude Versicherung Graubünden
Geo2X
Geobrugg AG
Geopraevent
Geotest
International Union of Geodesy and Geophysics (IUGG)
International Union of Geological Sciences (IUGS)
Riegl
Roxplore
Swiss Academy of Sciences (SCNAT)
Swiss Drilling
Swiss Gemmological Institute (SSEF)
ThermoFisher Scientific
WSL-Institute for Snow and Avalanche Research SLF

Participating Societies and Organisations

Geothermie-Schweiz (Geothermie.ch)
International Union of Geodesy and Geophysics, Swiss Committee (IUGG)
International Union of Geological Sciences, Swiss Committee (IUGS)
Komission der Schweizerischen Paläontologischen Abhandlungen (KSPA)
Swiss Association of Energy Geoscientists (SASEG)
Swiss Association of Geographers (ASG)
Swiss Commission for Remote Sensing (SCRS)
Swiss Commission on Atmospheric Chemistry and Physics (ACP)
Swiss Committee for Stratigraphy (Platform Geosciences/SCNAT)
Swiss Geodetic Commission (SGC)
Swiss Geological Society (SGG/SGS)
Swiss Geological Survey (swisstopo)
Swiss Geomorphological Society (SGGm/SSGm)
Swiss Geophysical Commission (SGPK)
Swiss Geotechnical Commission (SGTK)
Swiss Hydrogeological Society (SGH)
Swiss Hydrological Commission (CHy)
Swiss Paleontological Society (SPG/SPS, Swiss Geological Society)
Swiss Snow, Ice and Permafrost Society (SIP)
Swiss Society for Hydrology and Limnology (SGHL/SSHL)
Swiss Society for Quaternary Research (CH-QUAT)
Swiss Society of Mineralogy and Petrology (SMPG/SSMP, Swiss Geological Society)
Swiss Tectonics Studies Group (Swiss Geological Society)

Program Committee

Naki Akçar
Daniel Ariztegui
Pascal Blanc
Jean-Pierre Burg
Sébastien Castelltort
Pierre Dèzes
Charles Fierz
Karl Föllmi
Leander Franz
Stéphanie Girardclos
Edwin Gnos
Bernard Grobéty
Marion Hofmänner
Francisco Klauser
Christian Klug
Adrien Mestrot
Klaus Mezger
Alain Morard
Nils Oesterling
Eric Reusser
Elias Samankassou
Torsten Scheyer
Fritz Schlunegger
Michael Schnellmann
Guido Schreurs
Jürg Schweizer
Margit Schwikowski
Vera Slaveykova
Marie Violay
Andreas Voegelin
Stefan Wunderle

1. Structural Geology, Tectonics & Geodynamics

Guido Schreurs, Neil Mancktelow, Paul Tackley, Daniel Egli

Swiss Tectonics Studies Group of the Swiss Geological Society

TALKS:

1.1 **Andrić**, N, Vogt K., Matenco L., Cvetković V., Cloetingh S., Gerya T.
Magmatic pulses during Mediterranean-style continental collisions: A numerical modelling approach

1.2 **Beaussier S.**, Gerya T., Burg J.-P.
3D thermomechanical modeling of the Wilson Cycle: Structural inheritance of alternating subduction polarity

1.3 **Cionoiu S.**, Tajcmanova L., Moulas E., Stünitz H.
Stress distribution in samples from solid confining medium deformation experiments: An experimental and numerical study

1.4 **Hässig M.**, Enukidze O., Galoyan G., Popkhadze N., Moritz R.
Jurassic and Cretaceous geodynamic environments of ore formation along the Tethyan belt: New insights from the structural context along the Somkheto-Karabagh mountain belt, Armenia and Georgia

1.5 **Herwegh M.**, Berger A., Baumberger R., Wehrens P., Kissling E.
The Rise of the Aar Massif by Subvertical Large-Scale Block Extrusion

1.6 **Mosar J.**, Nguyen V.-T., Scheidt N., Gruber M.
The Pontarlier Fault System: Tectonics Revisited

1.7 **Moulas E.**, Schmalholz S., Brandon M.
Analytical two-wedge corner flow model for tectonic nappe evolution in collisional orogens

1.8 **Mozafari Amiri N.**, Tikhomirov D., Sümer Ö., Özkaymak Ç., Uzel B., Yesilyurt S., Ivy-Ochs S., Vockenhuber C., Sözbilir H.H., Akçar N.
Destructive earthquakes history of western Anatolia during the last 15 ka

1.9 **Nibourel L.**, Berger A., Egli D., Luensdorf K., Herwegh M.
Tectonic exhumation of isothermal planes: RSCM thermometry data record intense retrograde deformation in the Aar massif

1.10 **Vaughan-Hammon J.D**. , Luisier C. , Schmalholz S.M., Baumgartner L.P.
Impact of flow law and viscosity ratio on finite strain evolution during buoyancy-driven exhumation with application to the Monte Rosa nappe

1.11 **Zurbriggen R.**
Early Paleozoic orthogneisses in the Alps: products of a peri-Gondwanan peraluminous arc system

1.12 **Zwaan F.**, Schreurs G., Adam J.
Effects of sedimentation on rift basin and transfer zone evolution: insights from 4D analogue models

POSTERS:

P 1.1 **Sanan P.**
StagBL: A Scalable, Portable, High-Performance Discretization and Solver Layer for Geodynamic Simulation

P 1.2 **Tackley P.J**., Lourenco D., Fomin I.
Mantle Compositional Heterogeneity Arising From Magma Ocean Crystallisation Followed by Long-Term Differentiation: Modelling From a Molten Earth to the Present Day

P 1.3 **Gülcher A.**, Beaussier S., Gerya T.
Influence of detachment faults for intra-oceanic subduction initiation: 3D thermomechanical modeling

P 1.4 **Bessat A.**, Pilet S., Duretz T., Schmalholz M.S.
Numerical modelling of lithospheric flexure at subduction zones: what controls the generation of petit-spot volcanoes ?

P 1.5 **Candioti L.G**., Duretz T., Picazo S., Schmalholz S.M.
Orogenic wedge formation starting from hyper-extended passive margins: a self-consistent modelling study with application to the Western Alps

P 1.6 **Petri B.**, Duretz T., Mohn G., Schmalholz S.M.
Thinning of heterogeneous lithosphere: insights from field obsevrations and numerical modelling

P 1.7 **Kiss D.**, Duretz T., Podladchikov Y., Schmalholz S.M.
Scaling laws and numerical simulations for shear zones caused by thermal softening for 1D, 2D and 3D simple and pure shear

P 1.8 **Spitz R.**, Schmalholz S.M., Kaus B.J.P.
3D numerical modelling and finite strain analysis of the transition between viscous overthrusting and folding

P 1.9 **Nabavi S.T**., Alavi S.A., Frehner M.
3D FE-modelling of inclined, brittle-ductile transpression

P 1.10 **Nabavi S.T**., Alavi S.A., Frehner M., Mohammadi S., Ghassemi M.R.
Mechanical evolution of transpression zones affected by fault interactions: insights from 3D elasto-plastic finite element models

P 1.11 **Zwaan F.**, Schreurs G.
Evolution of rifts and rift linkage zones in orthogonal and scissor extension settings: insights from analogue models analysed with 4D X-ray computed tomography

P 1.12 **Waldvogel M.**, Zurbriggen R., Berger A., Herwegh M.
Structural Geology in Applied Material Science: Strain Localisation and Crack Initiation in Waterproofing Membranes during Tensile Tests

P 1.13 **Simon V.**, Kraft T., Tormann T., Diehl T., Herrmann M.
The Swiss-army-knife approach to nearly automatic microearthquake analysis for natural and induced sequences

P 1.14 **Diehl T.**, Kissling E., Lee T., Schmid S.
How deep is shallow? Improving hypocenter locations of upper crustal seismicity in Switzerland

P 1.15 **Lee T.**, Diehl T., Kissling E., Wiemer S.
High-Quality Earthquake Catalogue for a Changing Network Configuration: Application to Southwestern Switzerland

P 1.16 **Hetényi G.**, Molinari I., Clinton I., Kissling E., Alparray Seismic Network Team, Alparray OBS Cruise Crew, Alparray Working Group
The completed AlpArray Seismic Network

P 1.17 **Scarponi M.**, Hetényi G., Plomerová J., Solarino S., Berthet T.
High resolution imaging of the Ivrea Geophysical Body: A receiver function and gravity approach

P 1.18 **Calignano E.**, Zappone A., Madonna C. & The Epos-Ip Wp16 Team
The Swiss participation to a coherent and collaborative network of Solid Earth Multi-scale laboratories: EPOS-TCS MSL

P 1.19 **Rauch A.**, Sartori M., Castelltort S., Volken S., Dall'agnolo S.
A tool to assist bedrock geology interpretation

P 1.20 **Mair D.**, Lechmann A., Herwegh M.M., Schlunegger F.
Insights on the Aar Massif exhumation from new field data from the Jungfrau-Eiger mountain chain

P 1.21 **Berger A.**, Egli D., Herwegh M.
Hydrothermal cockade-like breccias in the Grimsel Breccia Fault: fluidization, flow rates and growth dynamics during seismic events

P 1.22 **Dutler N.**, Nejati M., Amann F., Valley B.
The Measurement of Fracture Toughness Anisotropy in Grimsel Granodiorite using Semi-Circular Samples

P 1.23 **Kakurina M.**, Guglielmi Y., Nussbaum C., Valley B.
A multiparametic evaluation of the Wallace-Bott hypothesis in the presence of a fluid source

P 1.24 **Akker V.**, Kaufmann J., Desbois G., Klaver J., Urai J., Berger A., Herwegh M.
Porosity of slates – from 3D bulk rock measurements to direct imaging

P 1.25 **Pantet A.**, Epard J.-L., Masson H.
Mimicking Alpine thrusts by orogenic passive deformation of synsedimentary normal faults: a record of Jurassic extension of the European margin (Mont Fort nappe, Middle Penninic, Western Alps).

P 1.26 **Schori M.**, Mosar J.
Basement-cover interaction in the Jura Mountains: Where, how and to what degree?

P 1.27 **Radaideh O.M.A.**, Mosar J
Analysis of geomorphic indices in the westernmost area of Switzerland: Implications for neotectonics

P 1.28 **Schmitt N.**, Verbeken B., Gruber M., Miller S., Valley B., Mosar J.
Three-dimensional measurement of limestone fracture network from the La Sarraz Fault Zone using high resolution X-ray µ-computed tomography

P 1.29 **Rime V.**, Mosar J.
Tectonic structure and dynamic of the Neuchâtel Jura Mountains: new insight from detailed mapping and forward modelling techniques

P 1.30 **Schenker L.F**., Ambrosi C., Scapozza C., Czerski D., Maino M., Castelletti C. Gouffon Y.
Distribution of HP rocks in the nappes of the Lepontine Dome

P 1.31 **Buchs N.**, Epard J.-L.
Ophiolites in the North Himalayan nappes and Indus Suture Zone in Eastern Ladakh (NW Himalaya, India)

P 1.32 **Mladenović A.**, Cvetković V., Trivić B., Cvetkov V.
Late Eocene to recent tectonic evolution of the northern Internal Dinarides (western Serbia)

P 1.33 **Alania V.**, Enukidze O., Tevzadze N.
Blind thrusts under Tbilisi, Georgia

P 1.34 **Laziz O.**, Bouaja F., Benabbas C.
Travertine occurrences along major neotectonic normal fault zones in the Hammam Debar- Roknia Guelma region, North-East Algeria

P 1.35 **Bastias J.**, Spikings R., Ulianov A., Schaltegger U., Grunow A., Hervé F., Riley T., Burton-Johnson A.
The tectono-magmatic evolution of the Antarctic Peninsula Batholith, Graham Land: insights from U-Pb zircon ages and geochemical data

P 1.36 **Gilgannon J.**, Herwegh M., Poluet T., Regenauer-Lieb K., Veveakis M.
Revisiting diffusion creep of calcite

P 1.37 **Biermanns P.**, Schmitz B., Ustaszewski K., Sokol K., Reicherter K.
The External Dinarides of Southern Montenegro and Northern Albania: Contraction vs. extension – Instrumentally recorded seismicity vs. field observations

P 1.38 **Youcef Brahim E.H**., Chadi M., Djeffal R.
Diagenesis and Stadial Analysis of Jurassic Dolomite, Case Study : South-setifian Shelf (NE Algerian)

1.1

Magmatic pulses during Mediterranean-style continental collisions: A numerical modelling approach

Nevena Andrić[1,2], Kathatina Vogt[1], Liviu Matenco[1], Vladica Cvetković[2], Sierd Cloetingh[1] & Taras Gerya[3]

[1] Utrecht University, Faculty of Geosciences, Utrecht, The Netherlands
[2] University of Belgrade, Faculty of Mining and Geology, Belgrade, Serbia (nevena.andric@rgf.bg.ac.rs)
[3] Department of Earth Sciences, ETH-Zurich, Sonneggstrasse 5, 8092 Zurich, Switzerland

Magmatism plays an important role in crustal growth during continental collision and occurs through all collisional stages. Collisional orogens are characterized by variable magmatism in terms of volume, composition, spatial extent and temporal distribution of magmas during different stages of continent-continent collision. In some orogens of the Mediterranean domain (e.g. Apennines, Betic - Rif, Carpathians, Dinarides) magmatism migrates towards the foreland following the retreat of the subducting slab. This magmatism migration is commonly accompanied by chemical diversity of igneous rocks across the orogen from more mafic to more felsic rocks. The tectonic processes driving a magmatic variability observed in the collisional orogens along Mediterranean domain are not fully understood and are difficult to quantify by field observations or geochemical techniques. Therefore, we used a series of 2-D magmatic-thermomechanical numerical experiments to study the link between tectonic processes and magmatism in such systems.

Our numerical modelling results demonstrate that the rheological structure and compositional layering of the crust impose a key control on the distribution of magmatic rocks within the collisional orogen. Results indicate that the indentation of the overriding plate`s lower crust into the orogenic wedge can explain the migration pattern of deformational and magmatic fronts in Mediterranean-style continental collision. Furthermore, the modelling shows a gradual change in magma source compositions with time from dominantly mafic to felsic. This is explained as a response to certain lithospheric-scale processes, i.e. like relamination, slab detachment and eduction that followed subduction of oceanic and continental lithosphere along the colliding margins. Finally, modelling results lead to a new model for the lithospheric scale processes driving the magmatic pulses in the Dinarides Mountains, one of the orogens in the Mediterranean domain.

1.2

3D thermomechanical modeling of the Wilson Cycle: Structural inheritance of alternating subduction polarity

Stephane Beaussier[1], Taras Gerya[2], Jean-Pierre Burg[1]

[1] Geological Institute, ETH Zurich, Sonneggstrasse 5, CH-8092 Zurich (stephane.beaussier@erdw.ethz.ch,jean-pierre.burg@erdw.ethz.ch)
[2] Institute of Geophysics, ETH Zurich, Sonneggstrasse 5, CH-8092 Zurich (taras.gerya@erdw.ethz.ch

Alternating subduction polarity along suture zones has been documented in several orogenic systems. Yet, the mechanisms leading to this geometric inversion and the subsequent interplay between the contra-dipping slabs have been little studied. To explore such mechanisms, 3D numerical modelling of the Wilson Cycle was conducted from continental rifting, breakup and oceanic spreading to convergence and self-consistent subduction initiation.
In the resulting models, near-ridge subduction initiating with the formation of contra-dipping slab segments is an intrinsically 3D process controlled by earlier convergence-induced ridge swelling. The width of the slab segments is delimited by transform faults inherited from the rifting and ocean floor spreading stages. The models show that the number of contra-dipping slab segments depends mainly on the size of the oceanic basin, the asymmetry of the ridge and variations in kinematic inversion from divergence to convergence. Convergence velocity has been identified as a second order parameter. The geometry of the linking zone between contra-dipping slab segments varies between two end-members governed by the lateral coupling between the adjacent slab segments: (1) Coupled slabs generate wide, arcuate linking zones holding two-sided subduction (2) Decoupled slabs generate narrow transform fault zones against which one-sided, contra-dipping slabs abuts.

1.3

Stress distribution in samples from solid confining medium deformation experiments: An experimental and numerical study

Sebastian Cionoiu[1], Lucie Tajcmanova[1], Evangelos Moulas[2], Holger Stünitz[3]

[1] Department of Earth Sciences, ETH Zürich, Clausiusstrasse 25, CH-8092 Zürich (sebastian-ci@erdw.ethz.ch)
[2] Institut des sciences de la Terre, Université de Lausanne, Quartier UNIL-Mouline, Bâtiment Géopolis, CH-1015 Lausanne
[3] Department of Geology, University of Tromsø, Naturfagbygget - Dramsveien 201, N-9037 Tromsø

Shear experiments for the Calcite-Aragonite system were performed in a (Griggs-Type) solid medium deformation apparatus at 600°C. The confining pressure (σ_3) was maintained 0.1 – 0.2GPa below the Calcite-Aragonite transition which occurs at 1.47GPa. The first principal stress (σ_1) reached 1.55 – 1.8GPa, depending on the sample strength. Thus the bulk sample pressure, approximated by $P_{2D} = (\sigma_1 + \sigma_3)/2$ or $P_{3D} = (\sigma_1 + 2*\sigma_3)/3$ was closely varying around the transition pressure.

Raman spectroscopic data show a strong, systematic heterogeneity in the distribution of the phase transformation in the shear plane (σ_1-σ_3 plane). Light microscopy reveals heterogeneous, strain and grain-size distribution. The phase transition is complete at the center and thinned parts of the experimental shear zone, while regions close to the corners of the pistons confining the shear and around those show minor transformation. This is interpreted as being a result of stress, strain and pressure variations within the shear zone.

To further investigate different mechanisms contributing to the phase transition, the local distribution of first order parameters as pressure, stress and strain in the experiment must be understood. To achieve this, numerical modelling based on a finite difference code in Matlab is used. The modelling results are then compared to experiments, analyzed in the σ_1-σ_3 and the σ_1-σ_2 plane.

1.4

Jurassic and Cretaceous geodynamic environments of ore formation along the Tethyan belt: New insights from the structural context along the Somkheto-Karabagh mountain belt, Armenia and Georgia

Marc Hässig[1], Onise Enukidze[2], Ghazar Galoyan[3], Nino Popkhadze[4], Robert Moritz[1]

[1] *Department of Earth Sciences, University of Geneva, Rue des Maraîchers 13, 1205 Geneva, Switzerland (marc.haessig@unige.ch)*
[2] *M. Nodia Institute of Geophysics, I. Javakhishvili Tbilisi State University, Georgia*
[3] *Institute of Geological Sciences, National Academy of Sciences of Armenia, 24a Baghramian Avenue, Yerevan 375019, Armenia*
[4] *Al. Jalenidze Institute of Geology, I. Javakhishvili Tbilisi State University, Georgia*

The Somkheto-Karabagh mountain belt marks the southern margin of Eurasia in the Lesser Caucasus. Bordering it to the South, ophiolites mark the limit between Eurasia and the Gondwanian derived South Armenian Block on which they have been thrusted. This volcanic arc was formed along the Southern Eurasian margin during closure of the Tethyan oceanic domain. Arc construction lasted from at least the Mesozoic to the very beginning of Cenozoic times due to North-dipping subduction of Palaeotethys followed by Northern Neotethys until collision between the Eurasian and the South Armenian Blocks. Ore formation along the Lesser Caucasus can be assigned to two different evolution stages: (1) Mesozoic arc construction and evolution along the Eurasian margin, and (2) Cenozoic magmatism and tectonics controlled by structures inherited from Late Cretaceous-Paleogene accretion boundaries along the Eurasian margin. Investigations of the Bolnisi district in Georgia and the Alaverdi district in Armenia along a NS-oriented section across the arc (Figure 1) bring new insight to its structural evolution as well as that of the associated back-arc basin between the Loki and Khrami massifs in relation to the magmatic activity responsible for the deposits found today.

In Armenia, N- to S-oriented debris flows and general E-W-striking syn-depositional normal faults covered by Late Jursassic and younger rocks support N-S extension during Early to Middle Jurassic times. The Alaverdi district features magmatic-hydrothermal systems along with volcanic and sedimentary rock-types which evidence a subaqueous environment during the Middle Jurassic. Intrusive activity is also evidenced during these times. Near the Teghout deposit, also in the Alaverdi district, metamorphic rock foliation argues for post-Middle Jurassic N-S transpressive deformation of early Middle Jurassic tonalite. The Teghout deposit is a Late Jurassic to Early Cretaceous porphyry Cu deposit.

In Georgia, new observations have identified a transgressive contact of Late on Early Cretaceous rock sequences. In addition, angular unconformities between successive stages of the Late Cretaceous have been recognised evidenced by variations of dip direction and/or angle. Locally, small grabens and Gilbert delta systems within the Late Cretaceous argue for an extensional context at that time. The Bolnisi district consist essentially of epithermal systems, and possibly one transitional system previously interpreted as VMS-epithermal. These are the last metallogenic events associated with subduction of the northern branch of the Neotethys before accretion of the South Armenian block with the Eurasian margin during Early Maastrichtian (~73-71 Ma).

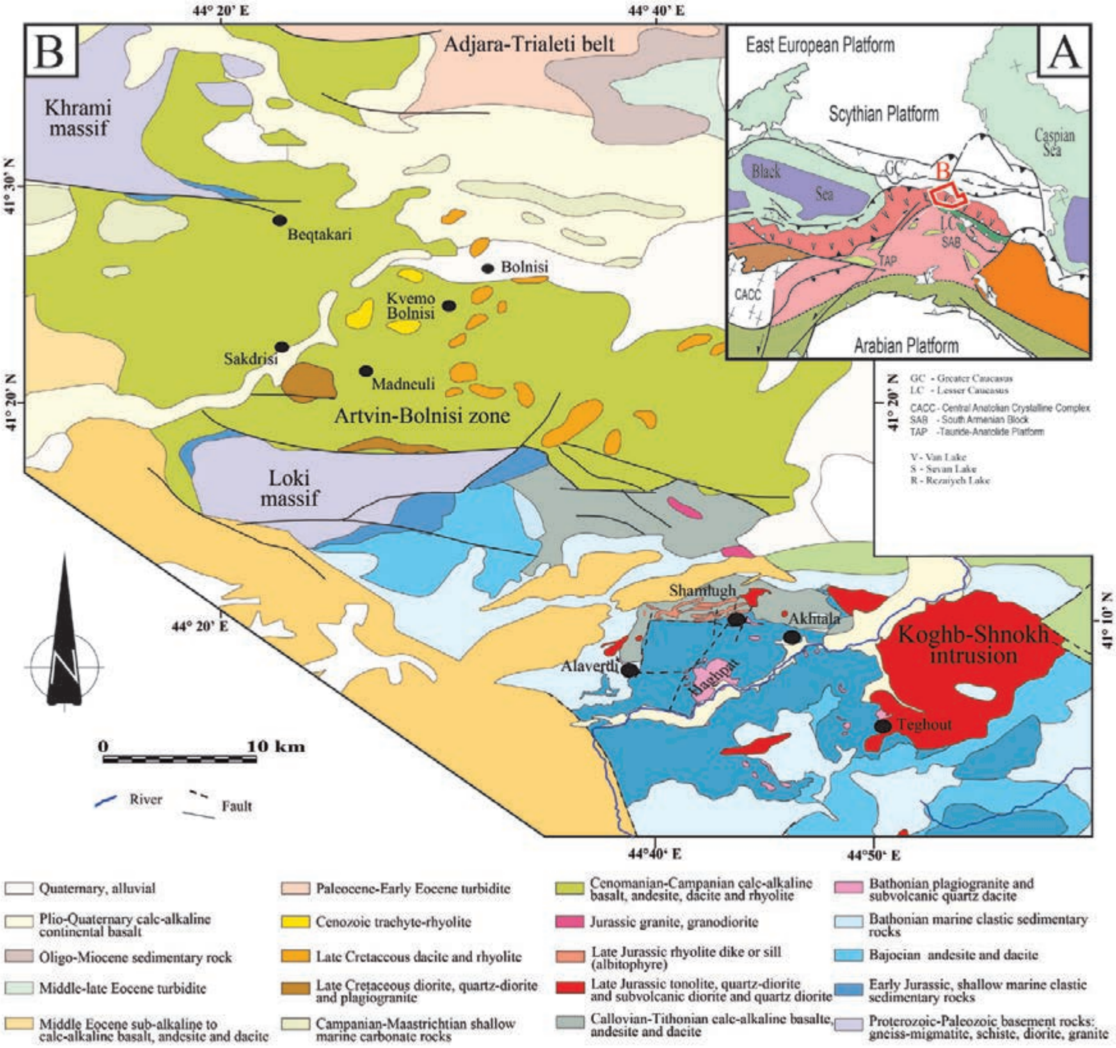

Figure 1. A, tectonic map of the Middle East–Caucasus area, showing the main blocks and suture zones after Avagyan et al. (2005), modified. Position of map B is indicated. B, simplified geologic map of the Bolnisi and Alaverdi mining district, after Moritz et al. (2016), modified.

REFERENCES

Avagyan, A., Sosson, M., Philip, M.H., Karakhanian, A., Rolland, Y., Melkonyan, R., Rebai, S., and Davtyan, V., 2005. Neogene to quaternary stress field evolution in Lesser Caucasus and adjacent regions using fault kinematics analysis and volcanic cluster data. Geodinamica Acta 18, 401–416.

Moritz, R., Melkonyan, R., Selby, D., Popkhadze, N., Gugushvili, V., Tayan, R. & Ramazanov, V. (2016). Metallogeny of the Lesser Caucasus: From Arc Construction to Postcollision Evolution. In Special publications of the Society of Economic Geologists. (No. 19, pp. 157-192). Society of Economic Geologists.

1.5
The Rise of the Aar Massif by Subvertical Large-Scale Block Extrusion

Herwegh Marco[1], Berger Alfons[1], Baumberger Roland[2], Wehrens Philip[2] & Kissling Edi[3]

[1] *Institute of Geological Sciences, University of Bern, Baltzerstrasse 1+3, CH-3012 Bern (marco.herwegh@geo.unibe.ch)*
[2] *Federal Office of Topography, Swiss Geological Survey, Seftigenstrasse 264, 3084 Wabern, Switzerland*
[3] *Institute of Geophysics, ETH Zürich, Sonneggstrasse 5, CH-8092 Zürich, Switzerland*

The Aar Massif belongs to the External Cristalline Massifs of the Alps and three end member models have been proposed for its exhumation: (i) formation of an antiformal nappe stack of upper crustal rocks; (ii) a crustal-scale buckling with massif-internal shortening or (iii) the formation of a pop-up structure because of north- and south-directed thrusts at both ends of the massif (e.g. Burkhard 1999, Choukroune and Gapais, 1983). These models can only in part explain the observed structo-metamorphic evidences which are: (i) A pervasive dissection of the Aar Massif by ta large number of steep massif-parallel reverse/normal faults (Steck 1968; Challandes et al. 2008, Rolland et al. 2009; Handegg phase). (ii) The overprinting of these fault patterns by north directed thrusts in the North (e.g. Labhart 1966; Pfaffenchopf phase) and simultaneous dextral strike-slip reactivation of Handegg faults in the South (Rolland et al. 2009, Oberaar phase). (ii) An increase in metamorphic grade from North to South, which is steep in the North but becomes shallower in the South. Moreover, seismic tomography reveals a positive and negative mass anomaly underneath the Aar Massif and the Gotthard nappe, respectively, suggesting lower crustal rocks and upper crustal rocks at shallower and deeper positions compared to an undeformed continental crust.

The combination of these observations lead us to a new geodynamic model for the exhumation of the Aar Massif. At a late stage of Alpine collision, slab rollback of the European lithospheric mantle, results in delamination in the lower crust. The missing slab pull forces in combination of buoyancy of mid- to upper crustal blocks lead to a steep rise of crustal block (vertical tectonics). This rise is accommodated along the steep reverse faults (Handegg phase, 22-17 Ma), which evolve and propagate from S to N being in charge for todays metamorphic gradient. Ongoing delamination in the lower crust and its buoyancy-driven piling up generates the excess of lower crust underneath the study area as manifest by the lower crustal thickening. In additon to the vertical component a weak compressional plate convergence component still persisted, as manifest by the structures of the Oberaar and Pfaffenchopf phase (<12 Ma). The associated strain partitionning between the northern and southern part of the Aar massif resulted in a further horizontal shortening and tectonic uplift component of several kilometers. It is this long lasting deformation history in combination with surface erosion, which resulted in the today's shape of the North Alpine front.

REFERENCES
Burkhard, M. 1999: Strukturgeologie und Tektonik im Bereich AlpTransit, Vorerkundung und Prognose der Basistunnels am Gotthard und am Lötschberg. 45-57.
Challandes, N., Marquer, D. & Villa, I. 2008: P-T-t modelling, fluid circulation, and 39Ar- 40Ar and Rb-Sr mica ages in the Aar Massif shear zones (Swiss Alps). Swiss Journal of Geosciences 101, 269-288.
Choukroune, P. & Gapais, D. 1983: Strain patterin in the Aar granite (Central Alps): orthogneiss developed by bulk inhomogeneous flattening. Journal of Structural Geology 5, 411-418.
Labhart, T. P. 1966: Mehrphasige alpine Tektonik am Nordrand des Aarmassivs. Eclogae Geologicae Helvetiae 59, 803–830.
Rolland, Y., Cox, S.F., Corsini, M. 2009: Constraining deformation stages in brittle-ductile shear zones from combined field mapping and 40Ar/39Ar dating: The structural evolution of the Grimsel Pass area (Aar Massif, Swiss Alps). Journal of Structural Geology 31,1377-1394.
Steck, A. 1968: Die alpidischen Strukturen in den Zentralen Aaregraniten des westlichen Aarmassivs. Eclogae Geologicae Helvetiae 61, 19-48.
Wehrens P., Baumberger, R., Berger, A., & Herwegh M. 2017: How is strain localized in a meta-granitoid, mid-crustal basement section? Spatial distribution of deformation in the Aar massif (Switzerland). Journal of Structural Geology, 94, 47-67.

1.6

The Pontarlier Fault System: Tectonics Revisited

Jon Mosar[1], Viêt-Thang Nguyen[1], Nicole Scheidt[1], Marius Gruber[1]

[1] *Department of Geosciences, Earth Sciences, University of Fribourg, Chemin du Musée 6, CH-1700 Fribourg (jon.mosar@unifr.ch)*

The Pontarlier Fault system in the western swiss alpine foreland extends from the Jura fold-and-thrust belt into the Molasse Basin. We present here a new structural map of the whole Pontarlier Fault system compiled from french and swiss geological maps, digital elevation models and original field data. The map comprises lithological information, thrust fault traces and steep faults, as well as fold axial traces obtained from structural contours based on bedding dip data. In the Molasse Basin part, we further can rely on interpretation from oil exploration seismic data.
The fault system is made of one major N-S oriented fault string with splays and transpressional lenses and is associated with NW-SE oriented conjugate faults such as the La Sarraz-Mormont; Treycovagnes or La Lance fault systems. The Pontarlier Fault zone shows sinistral offset in the km range and its meridional segment, south of the Dent de Vaulion, is offset to the W by a few km. The conjugate NW-SE oriented faults show a dextral movement, and we can observe a kinematic link between the development of the regional folds such as the Mormont anticline and these dextral strike-slip faults. The corner zones of the “intersection” of the conjugate fault systems are characterized by top to the NW directed thrusts and associated folds. These faults become less prominent towards the North. Here, curved fold axis and thrust planes can be associated with diffuse shear zones of similar orientation and kinematics as the discrete fault systems.

To the North the Pontarlier Fault zone terminates at the meridional edge of the Plateau d’Ornans near St. Gorgon, where the Faisceau Salinois and the Haute Chaîne Jura join. The fault zone grades into thrust faults and into a more diffuse system of NNE-SSW oriented, large vertical faults. Based on their orientation they can be seen as related to the Rhine Graben structure.

The Pontarlier fault system thus connects/separates different structural domains with distinct fault and fold patterns. The fault system is probably an inherited paleotectonic structure that has subsequently been reactivated (thus faults and folds E and W of the fault zone need not correlate). Based on recent data it appears that the Pontarlier Fault zone and the conjugate fault systems are “youngest” along their southern segment. Different scenarii and prior reference studies will be discussed.

Detailed analysis of the paleostress and the fault architecture along the La Sarraz-Mormont fault system reveals the complexity of these fault systems. The development of a multi-hierarchical Riedel system leads to important regional and local changes in the stress field orientation with differences of more than 90°, as opposed to a temporal superposition of successive tectonic events (“phases”) with distinct regional stress orientations*. Thus locally the paleostress orientation from fault and striation data and the stress orientation obtained from borehole modelling show compression parallel to the La Sarraz Fault system.

*The polyphase interpretation based on orientation of local stress tensors only, is strongly dependent on the measured stress indicators and their position in a possible fault hierarchy.

1.7

Analytical two-wedge corner flow model for tectonic nappe evolution in collisional orogens

Evangelos Moulas[1], Stefan Schmalholz[1] & Mark Brandon[2]

[1] *Institute of Earth Science, University of Lausanne, CH-1015 Lausanne (evangelos.moulas@unil.ch)*
[2] *Department of Geology and Geophysics, Yale University, New Haven*

Many collisional orogens are made of tectonic nappes and are characterized by doubly-vergent wedge kinematics, but the mechanical conditions for nappe evolution remain contentious. The Western Alps are a prominent example of such orogens and their kinematic evolution is described by two main phases: 1) nappe formation by top-to-foreland shearing with extrusion and 2) subsequent backfolding of the ordered nappe stack. However, the mechanical conditions for nappe formation and for the subsequent switch to backfolding are still unclear. Here we apply a new analytical corner-flow model exhibiting two wedges of different viscosity, and show that nappe formation by forced return flow in the lower wedge, with acute angle, requires an upper wedge with a viscosity that is at least three orders of magnitude larger. In contrast, the switch to backfolding only takes place when the viscosity ratio between the two wedges decreases to approximately one. The exhumation path and corresponding velocities for nappe formation and backfolding, which are based on geological data for the prominent Monte Rosa nappe in the Western Alps, are reproduced by our model suggesting that nappe formation took place by forced flow and not by buoyancy-driven flow. We show that during nappe formation collisional orogens are mechanically characterised by two tectonic wedges with significantly different strength whereas during subsequent backfolding the orogens are characterised by essentially one wedge. Our two-wedge model elaborates the doubly-vergent wedge model and allows investigating a much wider variety of nappe geometries.

1.8

Destructive earthquakes history of western Anatolia during the last 15 ka

Nasim Mozafari Amiri[1], Dmitry Tikhomirov[1], Ökmen Sümer[2], Çağlar Özkaymak[3], Bora Uzel[2], Serdar Yesilyurt[1], Susan Ivy-Ochs[4], Christof Vockenhuber[4], Hasan Sözbilir[2] & Naki Akçar[1]

[1] Institute of Geological Sciences, University of Bern, Baltzerstrasse 3, 3012 Bern, Switzerland (nasim.mozafari@geo.unibe.ch)
[2] Department of Geological Engineering, Dokuz Eylül University, 35160 İzmir, Turkey
[3] Department of Geological Engineering, Afyon Kocatepe University,03200 Afyonkarahisar, Turkey
[4] Swiss Federal Institute of Technology, Institute for Particle Physics, Otto-Stern-Weg 5, 8093 Zürich, Switzerland

Investigation of seismic behavior of faults in regional scale is an essential key in order to improve our estimation on the timing and magnitude of future destructive earthquakes. Well-preserved fault scarps, basically include the most direct evidence of paleoearthquakes. Using fault scarp dating with cosmogenic ^{36}Cl, the age and vertical component of slip of past ruptures are recoverable prior to and within the seismic archives. An appropriate place to apply ^{36}Cl dating is western Anatolia, one of the most seismically active regions in the world, characterized by well-preserved normal faults.
In this study, we collected 584 samples from seven well-preserved fault surfaces within the Büyük Menderes Graben, Gediz Graben and Gökova Graben (Fig. 1) in order to date the past ruptures, determine the vertical component of slips, evaluate magnitude of potential earthquakes and estimate slip rates of the faults. We reconstructed at least 12 major seismic events beyond the existing earthquake records. According to our results the oldest earthquake approximated to be occurred at ca. 15 ka. The seismic events mainly occurred as clustered earthquakes of 6.2 to 7.1 in magnitude with vertical component of slips of ca. 0.6 to 3.5 m. The time correlation of the modeled seismic events in regional scale indicates that western Anatolia experienced at least four periods of high seismic activity at ca. 2.0, 3.5, 6.0 and 8.0 ka. This earthquake return period of approximately 2000 years is compatible with the time interval of earthquakes of several normal faults within the extensional region of Aegean Sea. The increment of average vertical slip rates, from 0.1 to 1.9 mm/yr through time shows that our century with records of many destructive earthquakes is the most seismically active period during Holocene time in western Anatolia.

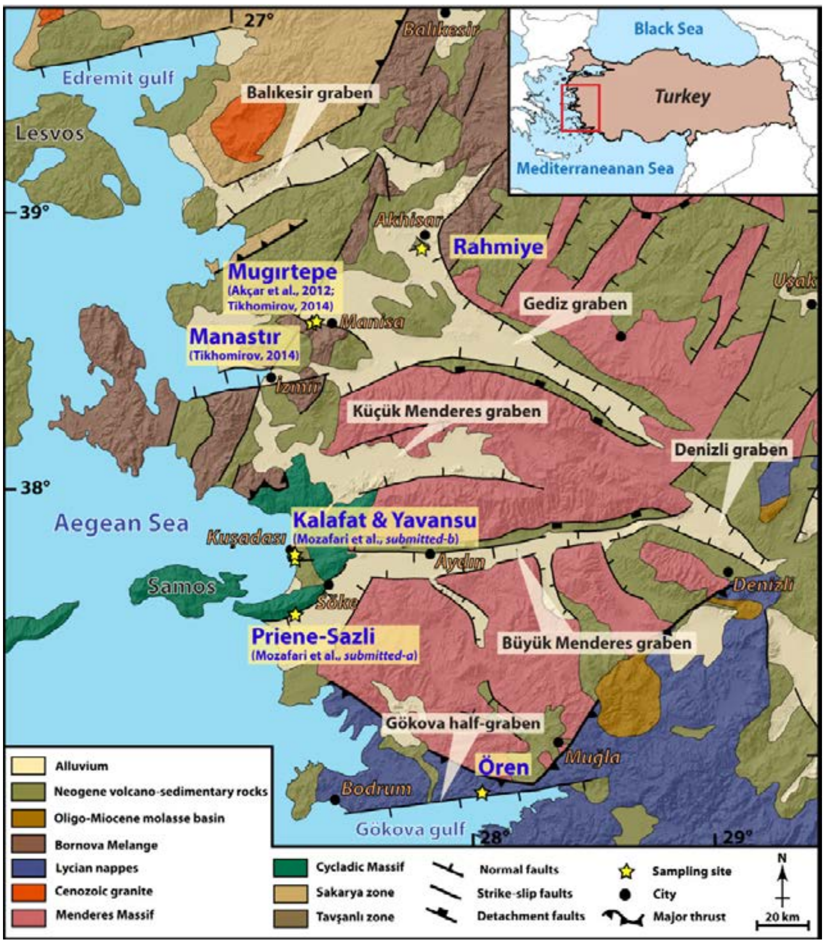

Figure 1. Simplified geological map of western Anatolia (modified after Akçar et al., 2012; Sümer et al., 2013). The yellow stars show locations of the sampling sites in Priene-Sazlı, Yavansu and Kalafat faults within Büyük Menderes Graben, Ören Fault in Gökova Graben, Mugırtepe Fault (Akçar et al., 2012), Manastır Fault (Tikhomirov, 2014) and Rahmiye Fault within Gediz Graben.

REFERENCES

Akçar, N., Tikhomirov, D., Özkaymak, Ç., Ivy-Ochs, S., Alfimov, V., Sözbilir, H., Uzel, B. & Schlüchter, Ch.: 2012. ^{36}Cl Exposure Dating of Paleoearthquakes in the Eastern Mediterranean: First Results from Western Anatolian Extensional Province, Turkey. GSA Bulletin 124, no. 11/12, 1724-1735.

Mozafari, N., Sümer, Ö., Tikhomirov, D., Ivy-Ochs, S., Alfimov, V., Vockenhuber, Ch., İnci, U., Sözbilir, H. & Akçar, N., *submitted (a):* Holocene seismic activity of the Priene-Sazlı Fault revealed by cosmogenic ^{36}Cl, western Anatolia, Turkey.

Mozafari, N., Tikhomirov, D., Sümer, Ö., Özkaymak, Ç., Uzel, B., Yesilyurt, S., Ivy-Ochs, S., Vockenhuber, Ch., Sözbilir, H. & Akçar, N., *submitted (b):* Seismic activity of the Büyük Menderes Graben (western Turkey) during the last 20 ka: Insights from cosmogenic ^{36}Cl analysis.

Sümer, Ö., Inci, U. & Sözbilir, H., 2013: Tectonic evolution of the Söke Basin: Extension-dominated transtensional basin formation in western part of the Büyük Menderes Graben, Western Anatolia, Turkey. Journal of Geodynamics 65, 148-175.

Tikhomirov, D., 2014: PhD thesis, University of Bern, An advanced model for fault scarp dating and paleoearthquake reconstruction, with a case study of the Gediz Graben formation (Turkey).

1.9

Tectonic exhumation of isothermal planes: RSCM thermometry data record intense retrograde deformation in the Aar massif

Lukas Nibourel[1], Alfons Berger[1], Daniel Egli[1], Keno Luensdorf[2] & Marco Herwegh[1]

[1] *University of Bern, Institute of Geological Sciences, Baltzerstrasse 1+3, 3012 Bern, Switzerland (lukas.nibourel@geo.unibe.ch)*
[2] *Dept. of Sedimentology & Environmental Geology Geoscience Center, Georg-August-Universität Göttingen, Goldschmiedstrasse 3, D-37077 Göttingen, Germany*

The thermo-kinematic evolution of the eastern Aar massif (Switzerland) is investigated through peak metamorphic temperatures, quantified on 60 metasedimentary samples, using thermometry based on Raman spectroscopy on carbonaceous material (RSCM). Estimated temperatures, reached during Oligocene/Miocene metamorphism, range from <250°C in the north to 375-500°C south of the Aar massif and are presented along four massif-perpendicular transects. The average horizontal thermal field gradient gradually rises from 6°C/km along the easternmost transect to 15°C/km in the westernmost transect. Very steep horizontal gradients of more than 30°C/km are locally observed at the massif front, local minima in the vicinity of the southern Aar massif boundary.

Inferred isothermal planes strike approximately parallel to the Aar massif and were, assuming sub-horizontal isotherms at peak temperature, exhumed and rotated to a near-vertical present-day position, especially at the massif front. Generally increasing peak temperatures from east to centre are consistent with the easterly axial dip of the eastern Aar massif. The pronounced temperature step situated at the massif front coincides with field observations of steep to vertical shear zones and with intense deformation and steepening reported at the basement cover contact. This indicates that substantial amounts of basement shortening and related thickening have occurred near or after the thermal peak, making the peak temperature envelope a potential tracer for retrograde deformation and/or exhumation. Our data are in good agreement with kinematic observations all along the Aar massif basement indicating Neogene exhumation, with deformation being mainly concentrated along the massif front.

1.10

Impact of flow law and viscosity ratio on finite strain evolution during buoyancy-driven exhumation with application to the Monte Rosa nappe

Joshua Vaughan-Hammon[1], Cindy Luisier[1], Lukas Baumgartner[1], Stefan Schmalholz[1]

[1]Institute of Earth Sciences, University of Lausanne (Joshua.vaughan-hammon@unil.ch)

Several mechanisms have been proposed to explain the exhumation of (ultra)high-pressure, (U)HP, tectonic units, such as (i) synconvergent return flow within a subduction channel, (ii) lithospheric extension associated with slab rollback, and (iii) buoyancy-driven flow such as crustal delamination or trans-mantle diapirs. We study here with simple 2D numerical simulations the finite strain evolution in and around tectonic units which exhume due to buoyancy-driven flow. We quantify the impact of the flow law and the viscosity ratio between exhuming unit and surrounding material on the finite strain evolution. One aim of the models is to eventually use the observed finite strain pattern in and around exhumed (U)HP units to assess the viscosities and flow laws of the exhumed units.

Buoyancy-driven flow has been suggested as exhumation mechanism for the Monte Rosa nappe which is a major HP tectonic unit in the Western Alps. However, the tectono-metamorphic evolution during exhumation still remains ambiguous. One reason for this ambiguity is that the published estimates of peak metamorphic pressure and temperature vary significantly, namely between 1.2 - 2.7 GPa and 490 - 650 oC, respectively. Furthermore, field observations of the Monte Rosa basement complex show remarkable differences in deformation intensity between (i) relatively undeformed granite with essentially undisturbed igneous textures, (ii) variably deformed HP ‘whiteschist’ lenses, and (iii) highly deformed metapelites. These differences in deformation intensity are likely related to differences in mechanical strength and, hence, provide a unique setting to estimate strength differences within the Monte Rosa nappe.

We apply 2D numerical simulations to the Monte Rosa nappe assuming exhumation by buoyancy-driven flow. Assuming further that the Monte Rosa peak and retrogressive pressures relate to lithostatic pressure, it is possible to estimate an exhumation velocity using age estimates for the respective pressures. This estimate provides an exhumation velocity of approximately 1 to 2 cm/yr. Using this velocity to solve Stokes’ law for a rising sphere enables a first-order viscosity estimate for the lithology surrounding the Monte Rosa nappe during its buoyant rise, which is in the order of 1020 Pas. Implementing this viscosity within the 2D numerical finite difference model for the buoyant rise of an ellipse, mimicking the granitic Monte Rosa unit, can provide viscosity estimates for the Monte Rosa unit by requiring that the unit does not deform significantly during its rise. Both linear and non-linear creep flow laws are applied together with reasonable model conditions at high numerical resolutions of 1000 x 2000 (for linear viscosity) and 600 x 1200 (for power-law viscosity) numerical grid points. Viscosity estimates resulting from the 2D modelling are compared with estimates from laboratory-derived flow laws for granite, quartz and feldspar.

This study aims to evaluate effective viscosity variations within the Monte Rosa nappe by combining structural field observations with 2D numerical modelling and experimentally derived flow laws. A future aim of this research is to evaluate whether different observed metamorphic conditions within the Monte Rosa nappe could be linked to different deformation intensities and, hence, stress and strength variations within the nappe.

1.11

Early Paleozoic orthogneisses in the Alps: products of a peri-Gondwanan peraluminous arc system

Roger Zurbriggen

Feldmatt 10, CH-6206 Neuenkirch (roger-zurbriggen@bluewin.ch)

Early Paleozoic (mainly Ordovician) orthogneisses and associated migmatites are widespread in pre-Mesozoic basement units of the Alps. They belong to a peri-Gondwanan arc system of a global scale with an approximate length of 20'000 km (Fig. 1). The European part of it was recently referred as Cenerian belt (Zurbriggen 2017).

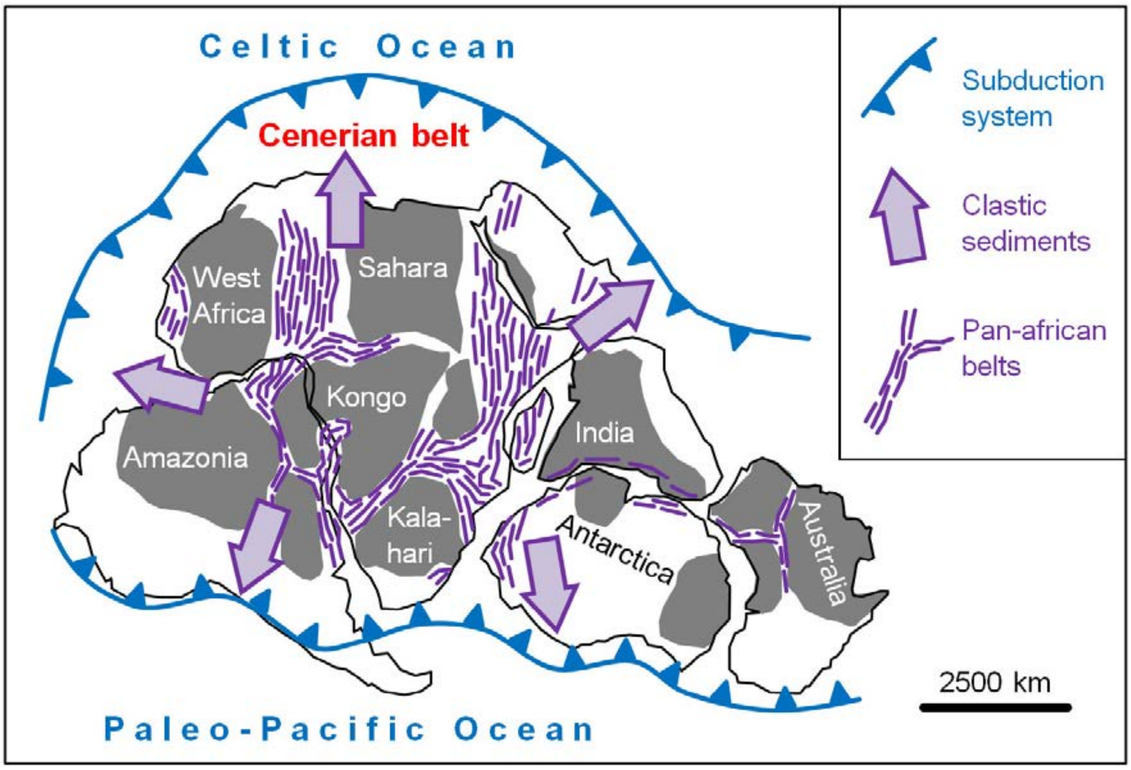

Figure 1. Early Paleozoic plate tectonics were characterized by a cricum-Gondwanan system of subduction zones, which were fed by extraordinary large amounts of Pan-african detritus. This led to the formation of fast growing subduction-accretion complexes, which cratonized during peraluminous arc magmatism. (Drawn after Gray et al., 2008).

The main characteristic of this magmatism was its peraluminosity. A majortity of the orthogneisses are peraluminous low-temperature S- and I-type metagranitoids. Whereas S-types metagranitoids and the associated migmatites clearly point to the anatexis of metasediments (green field in Fig. 2), low-temperature I-type metagranitoids can be explained by the mixing of thermally and rheologically compatible granitic magmas from both sources, sediments and mantle. Only a few of the orthogneisses are metaluminous high-temperature I-type metagranitoids generated by fractionation from mantle derived melts.

The paper discusses the different magmatic processes (sources of heat and materials) of the orthogneisses (i) on the base of their chemical trends in the Debon-Le Fort diagram, and (ii) in the context of the tectonic setting of cratonizing subduction-accretion complexes at the periphery of Gondwana.

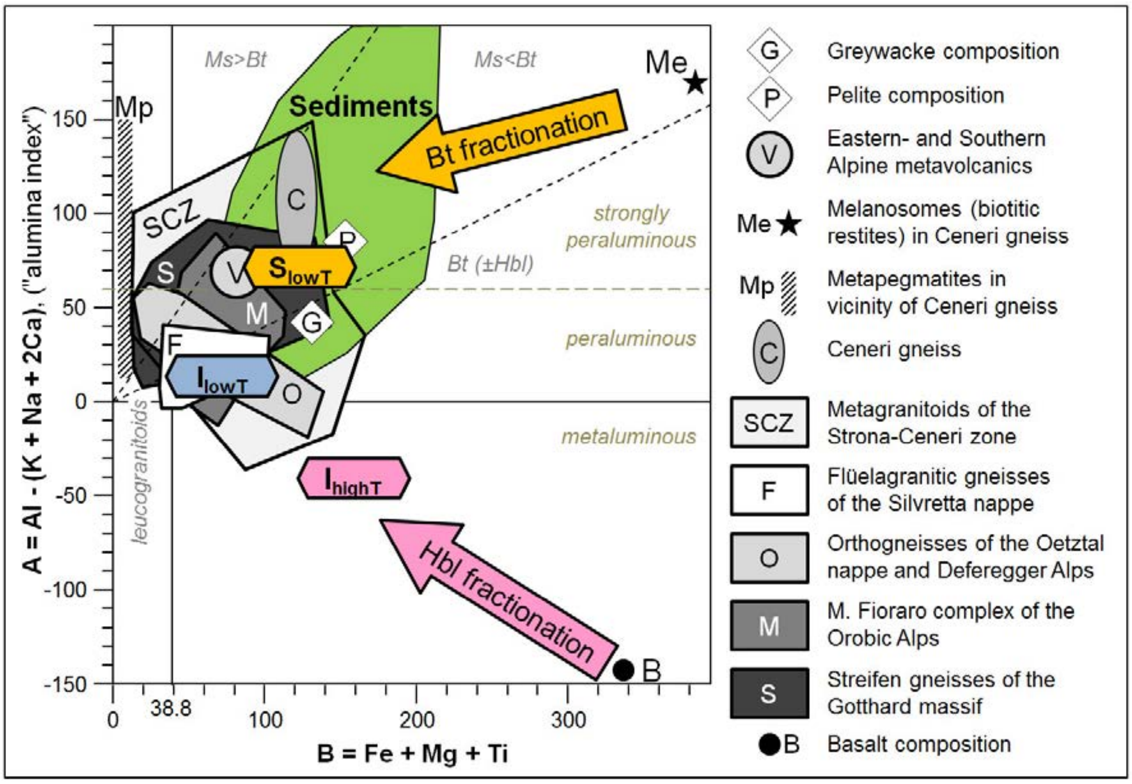

Figure 2. Granite discrimination diagram after Debon and Le Fort (1988). Data from early Paleozoic orthogneisses and metavolcanics are taken from Zurbriggen (2015) and references therein. $\mathbf{S}_{lowT}$, $\mathbf{I}_{lowT}$ and $\mathbf{I}_{highT}$ refer to low-temperature (strongly) peraluminous S- and I-type granitoids, and metaluminous high-temperature I-type granitoids, respectively (Chappell et al. 2004).

REFERENCES

Chappell, B., White, A., Williams, S. & Wyborn, D. 2004: Low- and high-temperature granites. Transactions of the Royal Society of Edinburgh, Earth Sciences, 95, 125-140.

Debon, F. & Le Fort, P. 1988: A cationic classification of common plutonic rocks and their magmatic associations: principles, method, applications. Bulletin de minéralogie, 111, 493-510.

Gray, D., Foster, D., Meert, J., Goscombe, B., Armstrong, R., Trouw, R., & Passchier, C. 2008: A Damara orogen perspective on the assembly of southwestern Gondwana. Geological Society, London, Special Publications 2008, 294, 257-278.

Zurbriggen, R. 2015: Ordovician orogeny in the Alps: a reappraisal. International Journal of Earth Sciences, 104, 335–350.

Zurbriggen, R. 2017: The Cenerian orogeny (early Paleozoic) from the perspective of the Alpine region. International Journal of Earth Sciences, 106, 517–529.

1.12

Effects of sedimentation on rift basin and transfer zone evolution: insights from 4D analogue models

Frank Zwaan[1], Guido Schreurs[1], Jürgen Adam[2]

[1] *Institute of Geological Sciences, University of Bern, Baltzerstrasse 1+3, CH-3012 Bern, Switzerland (frank.zwaan@geo.unibe.ch)*
[2] *Department of Earth Sciences, Royal Holloway, University of London, Egham, Surrey, TW20 0EX, United Kingdom*

During the early evolution of rift systems, individual rift segments often develop along pre-existing, non-continuous and laterally offset crustal weaknesses. As extension progresses, these initial rift segments must establish linkage in order to develop a continuous rift system that might eventually lead to continent break-up. Previous analogue and numerical modelling efforts have demonstrated that rift interaction structures are influenced by structural inheritances, detachment layers, magma bodies, rate and direction of extension, as well as distance between rift segments on rift interaction structures (e.g. Allken et al., 2012; Zwaan & Schreurs, 2017). However, the effects of syn-tectonic sedimentation have been largely ignored to date.

In this study we therefore assess how sedimentation influences rift segment and rift transfer zone evolution in orthogonal and oblique extension settings, by means of brittle-ductile analogue models, analysed with 4D X-ray computed tomography (XRCT or CT) methods and 3D digital volume correlation (DVC) techniques (Adam et al., 2013).

Our models show that syn-rift sedimentation does not significantly influence the large-scale evolution of rift and transfer zone structures. Yet syn-rift sedimentation can strongly affect rift-internal structures: sedimentary loading reinforces the rift wedge, decreasing rift wedge faulting and increases subsidence within the rift basin (Fig. 1a, b). These effects are strongest in areas where most accommodation space is available, that is, along the main rift segments. In contrast, rift segments that undergo high degrees of oblique extension develop less accommodation space and are significantly less influenced by sedimentary loading. Rift interaction structures are least affected by sediment influx, as they experience relatively low amounts of subsidence so that little accommodation space is available.

Our conclusions are valid for the early stages of rift development, when a high sediment influx could delay continental break-up, as other processes are likely to become dominant during later stages of continental extension. Finally DVC analysis of CT data proves to be a powerful tool to extract and fully quantify 3D internal model deformation in great detail and could be useful for comparing and calibrating analogue and numerical models (Fig. 1c).

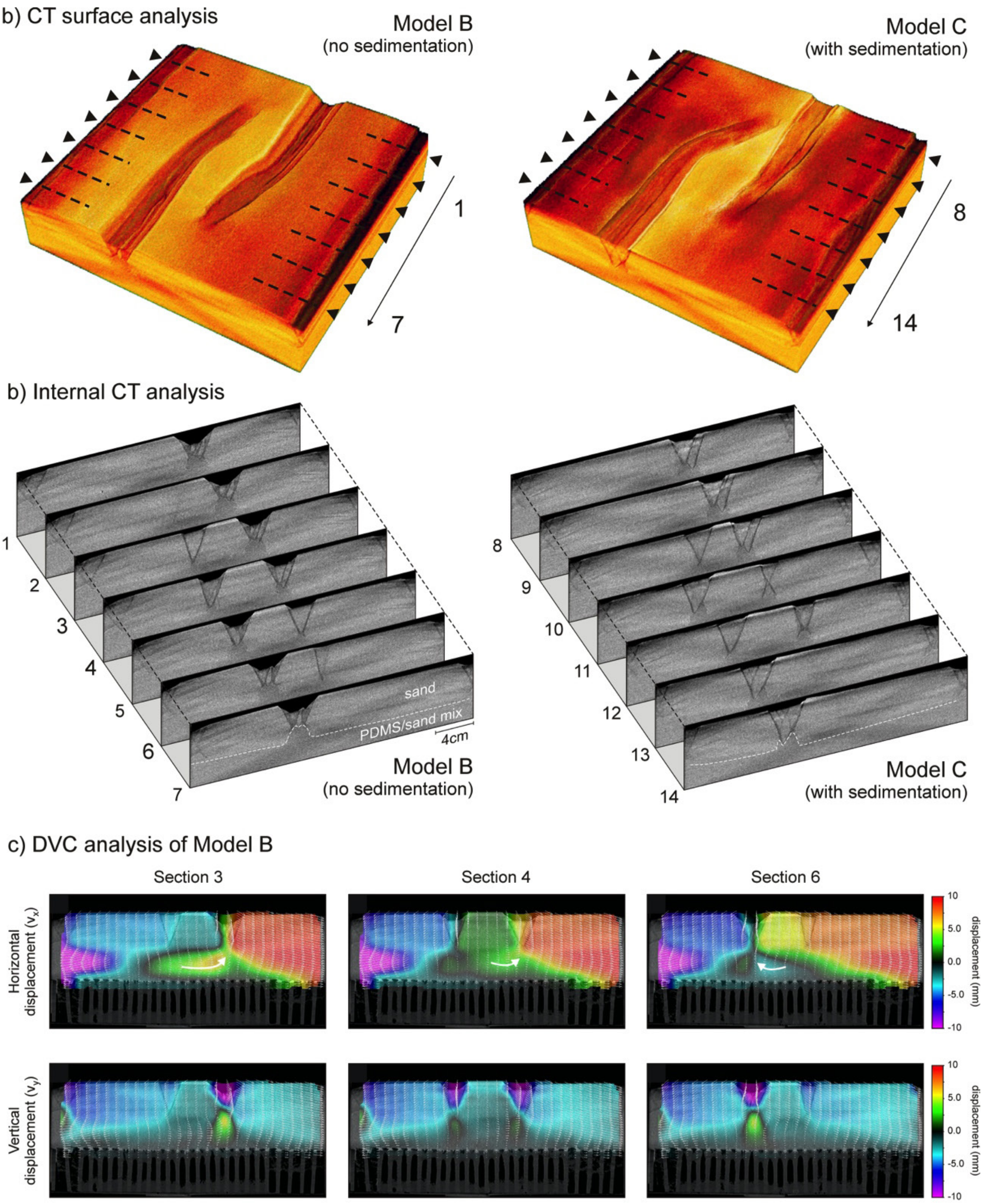

Figure 1. *Use of CT-scanning (a, b) and DVC techniques (c) for model analysis.*

REFERENCES

Adam, J., Klinkmüller, M., Schreurs, G. & Wieneke, B. 2013: Quantitative 3D strain analysis in analogue experiments simulating tectonic deformation: Integration of X-ray computed tomography and digital volume correlation techniques. Journal of Structural Geology, 55, 127-149.

Allken, V., Huismans, R. &Thieulot, C. 2012: Factors controlling the mode of rift interactionin brittle-ductile coupled systems: A 3D numerical study. Geochemistry, Geophysics, Geosystems,13, Q05010.

Zwaan, F. & Schreurs, G. 2017. How oblique extension and structural inheritance influence rift segment interaction: Insights from 4D analog models. Interperation, 5, SD119–SD138.

P 1.1

StagBL: A Scalable, Portable, High-Performance Discretization and Solver Layer for Geodynamic Simulation

Patrick Sanan[1]

[1]*Institut für Geophysik, ETH Zürich, NO H 23, Sonneggstrasse 5, 8092 Zürich (patrick.sanan@erdw.ethz.ch)*

StagBL is an open-source parallel solver and discretization library for geodynamic simulation,encapsulating and optimizing operations essential to staggered-grid finite volume Stokes flow solvers.It provides a parallel staggered-grid abstraction with a high-level interface in C and Fortran.
On top of this abstraction, tools are available to define boundary conditions and interact with particle systems.

Tools and examples to efficiently solve Stokes systems defined on the grid are provided in small (direct solver), medium (simple preconditioners), and large (block factorization and multigrid) model regimes.

By working directly with leading application codes (StagYY, I3ELVIS, and LaMEM) and providing an API and examples to integrate with others, StagBL aims to become a community tool supplying scalable, portable, reproducible performance toward novel science in regional- and planet-scale geodynamics and planetary science.

By implementing kernels used by many research groups beneath a uniform abstraction layer, the library will enable optimization for modern hardware, thus reducing community barriers to large- or extreme-scale parallel simulation on modern architectures. In particular, the library will include CPU-, Manycore-, and GPU-optimized variants of matrix-free operators and multigrid components.

The common layer provides a framework upon which to introduce innovative new tools. StagBL will leverage p4est to provide distributed adaptive meshes, and incorporate a multigrid convergence analysis tool.
These options, in addition to a wealth of solver options provided by an interface to PETSc, will make the most modern solution techniques available from a common interface. StagBL in turn provides a PETSc interface, DMStag, to its central staggered grid abstraction.

We present the development version of StagBL, including preliminary integration with application codes and demonstrations with its own demonstration application, StagBLDemo. Central to StagBL is the notion of an uninterrupted pipeline from toy/teaching codes to high-performance, extreme-scale solves. StagBLDemo replicates the functionality of an advanced MATLAB-style regional geodynamics code, thus providing users with a concrete procedure to exceed the performance and scalability limitations of smaller-scale tools.

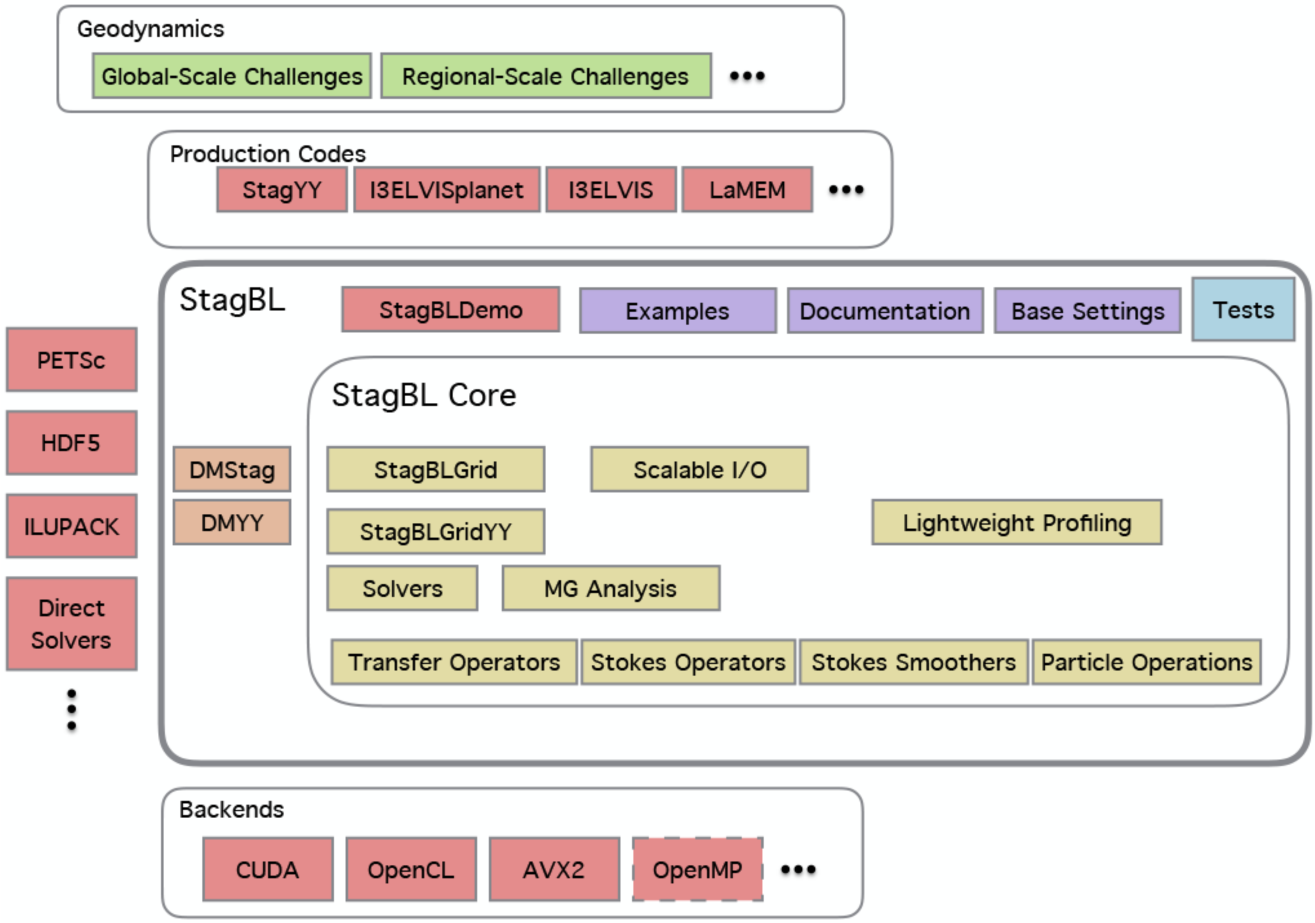

Figure 1. StagBL Components

P 1.2

Mantle Compositional Heterogeneity Arising From Magma Ocean Crystallisation Followed by Long-Term Differentiation: Modelling From a Molten Earth to the Present Day

Paul J. Tackley[1], Diogo Lourenco[1] & Ilya Fomin[1]

[1] *Institut für Geophysik, Departement Erdwissenschaften, ETH Zürich, CH-8092 (ptackley@ethz.ch)*

There is geochemical evidence both for primordial material and recycled material in the mantle. Large deep mantle structures that are inferred to be chemically distinct, as well as small-scale heterogeneity distributed everywhere, may thus be made of a mixture of differentiated materials that formed at different times, from an early magma ocean phase to ongoing melting at the present day. Early solidification of a magma ocean may have left the mantle compositionally stratified, while throughout Earth‘s history melting in the shallow mantle has produced crust, most of which was recycled into the interior and some of which may have segregated above the core-mantle boundary, joining possible enriched products from early differentiation, internal differentiation and basal magma ocean solidification to produce a Basal Melange (BAM)[1].

We will present simulations of mantle evolution from a 100% molten state (magma ocean) to the present day. This allows both early and long-term differentiation processes to be included in a self-consistent manner, using the simulation code StagYY. Dynamics occuring in regions that are mostly solid are fully resolved, while turbulent convection in regions that are mostly molten is parameterised by the use of an effective diffusivity. We investigate and characterize the evolution of a magma ocean as a function of various uncertainties including the shape of the solidus/liquidus (controlling whether crystallization starts in the middle or at the base), melt-solid density difference, fractional vs. batch crystallization, iron partitioning, and early cooling rate. Solid-state convection probably onset before the magma ocean is completely crystallized, making a strongly stratified mantle unlikely, but some early deep layering may have resulted. The core rapidly cools to the rheological transition of the mantle, making a straightforward basal magma ocean difficult to maintain; compositional differences due to iron partitioning are needed. Selected cases are run for subsequent billions of years beyond the magma ocean stage to predict modern-day mantle structure, with a focus both on the deep mantle and volumetric distribution of chemically distinct components.

REFERENCE

Tackley, P. J. 2012: Dynamics and evolution of the deep mantle resulting from thermal, chemical, phase and melting effects, Earth Science Reviews, 110, 1-25.

P 1.3

Influence of detachment faults on intra-oceanic subduction initiation: 3D thermomechanical modeling

Anna Gülcher[1], Stéphane Beaussier[2] & Taras Gerya[1]

[1] Institute of Geophysics, Department of Earth Sciences, ETH Zürich, Sonneggstrasse 5, CH-8092 Zürich (guanna@student.ethz.ch)
[2] Geological Institute, Department of Earth Sciences, ETH Zürich, Sonneggstrasse 5, CH-8092 Zürich

Extensional detachment faults have been widely documented in slow-spreading ridges on Earth and due to their weakness can effectively localize deformation. It has been proposed that these weak detachments provide ideal conditions for the nucleation of a subduction zone parallel to the ridge axis when ridge-perpendicular compressional forces are applied, i.e. like in the western Neotethys in Jurassic times (Maffione et al., 2015, figure 1). However, only 2D numerical models were carried out to support this theory, whereas the geometry of detachment faults is intrinsically 3D. To explore the concept of intra-oceanic subduction initiation along detachment faults, we conducted 3D numerical modelling experiments with the I3ELVIS code (Gerya and Yuen, 2007) in order to investigate both the formation of detachment faults in slow oceanic spreading systems and their response upon inversion from oceanic spreading to convergence.

According to the numerical experiments, the formation of detachment faults strongly depends on the magnitude of the healing rate of faulted rocks in oceanic lithosphere. The detachment faults formed in our numerical models deviate from the simple conceptual model of oceanic detachment faulting where fault footwalls are rotated, leading to the formation of oceanic core complexes (Escartín et al., 2015). The controlling parameters for oceanic core complexes are not necessarily similar to those for detachment faults, and the formation of detachment faults is therefore less strongly coupled with the formation of oceanic core complexes than formerly proposed.

Upon compression, an asymmetric spreading pattern is prone to asymmetric inversion, where underthrusting of one oceanic plate under the other occurs. The detachment faults localize extensive deformation, but the conceptual model for the direct inversion of a single detachment fault into an incipient subduction zone has not been supported numerically. Our results show instead a widespread interaction of multiple detachment faults when convergence is being applied. The nascent subduction zone cuts through the base of several detachment faults, thereby forming an initial accretionary wedge in the incipient fore-arc.

Our results therefore call for further research on three-dimensional modelling of the interplay between detachment faults and oceanic core complexes and on the initiation of a self-sustaining subduction zone adjacent to a pre-existing oceanic ridge.

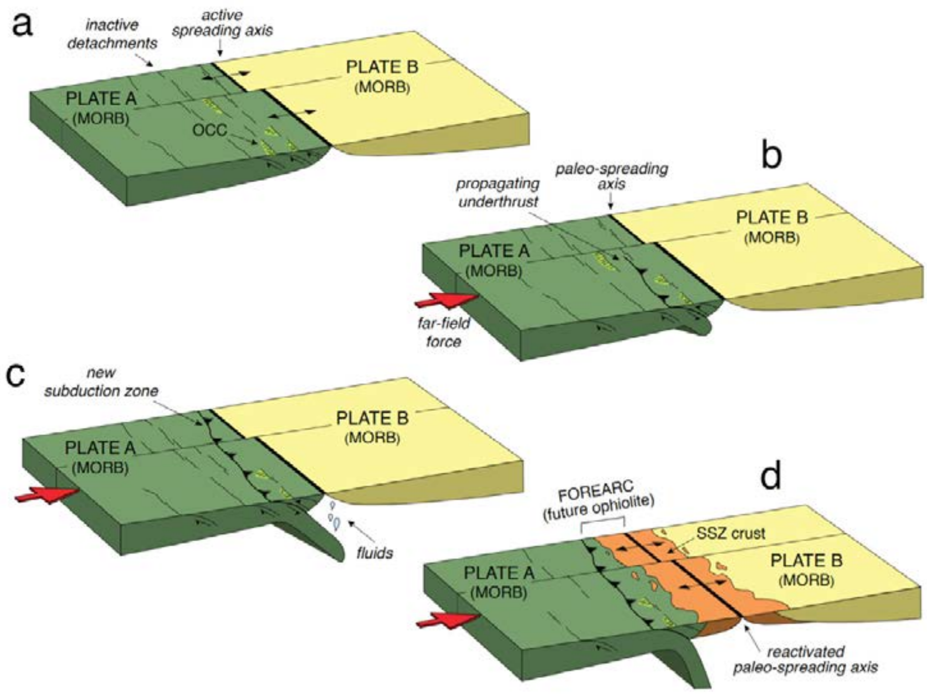

Figure 1. The proposed evolutionary tectonic model of intra-oceanic subduction initiation at detachment faults, thought to have occurred in

the western Neotethys in the Middle Jurrasic (a) (Ultra-)slow spreading ridge with detachment faults yielding local oceanic core complexes (OCC's) (b) Upon ridge-orthogonal compression, detachment faults localize deformation (c) Lateral propagation of underthrust resulting in a extensive subduction zone (d) Reactivated paleo-spreading axis where magmatic activity generates SSZ-crust (from (Maffione et al., 2015))

REFERENCES

Maffone et al. (2015) Dynamics of intraoceanic subduction initiation: 1. Oceanic detachment fault inversion and the formation of supra-subduction zone ophiolites. Geochemistry Geophysics Geosystems, 18, 1541-1576.

Gerya, T. V., and Yuen, D. A. (2007). Robust characteristics methods for modelling multiphase visco-elasto-plastic thermo-mechanical problems. Physics of the Earth and Planetary Interiors, 163, 83-105.

Escartín, J. and Canales, J. P. (2011). Detachments in oceanic lithosphere: Deformation, magmatism, fluid flow, and ecosystems. Eos Trans. AGU, 92, 31.

P 1.4

Numerical modelling of lithospheric flexure at subduction zones: what controls the generation of petit-spot volcanoes ?

Annelore Bessat[1], Sébastien Pilet[1], Thibault Duretz[1], Stefan Markus Schmalholz[1]

[1] *Institute of Earth Sciences, University of Lausanne, Géopolis, CH-1015 Lausanne (annelore.bessat@unil.ch)*

Petit-spot volcanoes were found fifteen years ago by Japanese researchers at the top of the subducting plate in front of Japan (Hirano *et al.,* 2006). This discovery is of great significance as it highlights the importance of tectonic processes for the initiation of intraplate volcanism. The location of these small lava flows is unusual and seems to be related to the plate flexure, which may facilitate the extraction of low degree melts from the base of the lithosphere. The presence of melts (0.1 to 2%) at the base of the lithosphere has been hypothesized previously to explain changes in electric and seismic properties at 70-90 km depth, i.e. within the low velocity zone (LVZ) (Sifré *et al.,* 2014).

A critical question is related to the process associated with the extraction of this low degree melts from the LVZ to produce the petit-spot volcanoes observed at the surface. First models suggested that the extension associated to plate bending allows large cracks to propagate across the lithosphere and could promote the extraction of low degree melts from the base of the lithosphere (Hirano *et al.,* 2006 & Yamamoto *et al.,* 2014). However, the study of petit-spot mantle xenoliths from Japan (Pilet *et al.,* 2016) has demonstrated that low degree melts are not directly extracted to the surface but percolate, interact and metasomatize the oceanic lithosphere.

In order to understand the melt extraction process in the region of plate bending, we performed 2D thermo-mechanical numerical simulations of subduction based on the general plate geometry observed in Japan. The numerical model considers viscoelastoplastic deformation, a combination of laboratory-derived flow laws (e.g. diffusion creep, dislocation creep and Peierls creep) and heat transfer. The models are applied to quantify the distribution of stress, strain rate, and viscosity in and around the flexed lithosphere since these quantities likely control the percolation of melt initially stocked at the base of the lithosphere. Furthermore, we quantify the evolution of lateral variations of the gravitational potential energy (GPE) during subduction to quantify the forces driving subduction.

Initial results show that plate flexure changes the distribution of the deformation mechanism in the flexure zone, between 40 km to 80 km depth. A change of the dominant deformation mechanism from diffusion creep to dislocation creep and from there to Peierls creep was observed about 200 to 300 km away from the trench in the subducting lithospheric slab. These changes are linked to the augmentation of the stresses in the flexure zone. At the base of the lithosphere diffusion creep is observed as a thin layer (20 km), which becomes even smaller (10 km) as subduction progresses in favor of dislocation creep. Further work will be necessary to prove whether or not the associated stress distribution is compatible with the development of porosity waves, a critical process to extract melts in low porosity media.

REFERENCES

Hirano, N., Takahashi, E., Yamamoto, J. et al. 2006: Volcanism in Response to Plate Flexure. Science, 313, 1426-1428

Pilet, S., Abe, N., Rochat, L. et al. 2016: Pre-subduction metasomatic enrichment of the oceanic lithosphere induced by plate flexure. Nature Geoscience, 9, 898-904

Sifré, D., Gardés, E., Massuyeau, M. et al. 2014: Electrical conductivity during incipient melting in the oceanic low-velocity zone. Nature, 509, 81-87

Yamamoto, J., Korenaga, J., Hirano, N., and Kagi, H. 2014: Melt-rich lithosphere-asthenosphere boundary inferred from petit-spot volcanoes. Geology, 42, 967-970

P 1.5

Orogenic wedge formation starting from hyper-extended passive margins: a self-consistent modelling study with application to the Western Alps

Lorenzo G. Candioti[1], Thibault Duretz[1], Suzanne Picazo[1], Stefan M. Schmalholz[1]

[1] *Institut des sciences de la Terre, Bâtiment Géopolis, Université de Lausanne, CH-1015 Lausanne (lorenzo.candioti@unil.ch)*

The concept of orogenic wedges has been applied to explain the geodynamic evolution of many orogens worldwide. Recent numerical modelling studies have investigated orogenic wedge formation in a shortening lithosphere which was initially homogeneous, that is, having initially a constant crustal thickness. However, many orogens, such as the Western Alps, are characterised by the collision of hyper-extended passive margins which exhibited a significant variation of crustal thickness from the onset of orogenic wedge formation. Also, the pre-Alpine Liguria-Piemonte basin likely lacked newly formed oceanic crust and consisted mainly of inherited and impregnated subcontinental mantle exhumed to the seafloor until embryonic ocean formation.

To study the impact of hyper-extended passive margins and exhumed subcontinental mantle on subsequent orogenic wedge formation we perform 2D thermo-mechanical numerical simulations. We model first the formation of hyper-extended passive margins with exhumed subcontinental mantle during lithospheric extension and then subsequently shorten the evolved basin to model orogenic wedge formation. Hence, the starting configuration for orogenic wedge formation has been modelled in a self-consistent way by a prior lithospheric extension phase. We quantify the impact of the thermal state and the associated strength distribution of the exhumed subcontinental mantle by starting the compression of the extended lithosphere after different durations of cooling. During cooling, the lithosphere is neither extended nor compressed. Lateral variations of gravitational potential energy in the lithosphere are calculated to quantify the associated horizontal forces during extension and the subsequent cooling period. The role of cooling of the exhumed subcontinental mantle for subduction initiation is discussed. Furthermore, potential applications of the model results to the Western Alpine orogeny are discussed.

P 1.6

Thinning of heterogeneous lithopsphere: insights from field obsevrations and numerical modelling

Benoit Petri[1], Thibault Duretz[2], Geoffroy Mohn[3] & Stefan M. Schmalholz[1]

[1] Institut des sciences de la Terre, Université de Lausanne, 1015 Lausanne, Switzerland (bpetri@unil.ch)
[2] Géosciences Rennes, Université de Rennes 1, UMR 6118, Rennes Cedex 35032, France
[3] Département Géosciences et Environnement, Université de Cergy-Pontoise, 5, mail Gay Lussac, Neuville-sur-Oise, 95031 Cergy-Pontoise Cedex

The nature and mechanisms of formation of extremely thinned continental crust (< 10 km) and lithosphere during rifting remain debated. Observations from present-day and fossil continental passive margins document the heterogeneous nature of the lithosphere characterized, among others, by lithological variations and structural inheritance. This contribution aims at investigating the mechanisms of extreme lithospheric thinning by exploring in particular the role of initial heterogeneities by coupling field observations from fossil passive margins and numerical models of lithospheric extension.

Two field examples from the Alpine Tethys margins outcropping in the Eastern Alps (E Switzerland and N Italy) and in the Southern Alps (N Italy) were selected for their exceptional level of preservation of rift-related structures. This situation enables us to characterize (1) the pre-rift architecture of the continental lithosphere, (2) the localization of rift-related deformation in distinct portion of the lithosphere and (3) the interaction between initial heterogeneities of the lithosphere and rift-related structures. In a second stage, these observations are integrated in high-resolution, two-dimensional thermo-mechanical models taking into account various patterns of initial mechanical heterogeneities.

Our results show the importance of initial pre-rift architecture of the continental lithosphere during rifting. Key roles are given to high-angle and low-angle normal faults, anastomosing shear-zones and decoupling horizons. We propose that during the first stages of thinning, deformation is strongly controlled by the complex pre-rift architecture of the lithosphere, localized along major structures responsible for the lateral extrusion of mid to lower crustal levels. This extrusion juxtaposes mechanically stronger levels in the hyper-thinned continental crust, being exhumed by subsequent low-angle normal faults.

Altogether, these results highlight the critical role of the extraction of mechanically strong layers of the lithosphere during the extreme thinning of the continental lithosphere and allows to propose a new model for the formation of continental passive margins.

P 1.7

Scaling laws and numerical simulations for shear zones caused by thermal softening for 1D, 2D and 3D simple and pure shear

Dániel Kiss[1], Thibault Duretz[1 2], Yuri Podladchikov[1] and Stefan M. Schmalholz[1]

[1] *Institute of Earth Sciences, University of Lausanne, Lausanne, Switzerland (daniel.kiss@unil.ch)*
[2] *CNRS, Geosciences Rennes, Rennes, France*

Localization of strain plays a major role during geodynamic processes, such as mountain building, and in particular during the formation of shear zones on all geological scales. Strain localization in a homogenous material requires a softening mechanism and we consider here thermal softening. Thermal softening is a result of the conversion of mechanical work into heat (i.e. shear heating) and of the temperature dependence of rock viscosities. Previous studies have shown that thermal softening can cause strain localization and the formation of large-offset shear zones in ductile materials whose deformation behavior is described with creep flow laws (e.g. dislocation creep).

Systematic analysis of data resulting from one-dimensional (1D) numerical simulations of simple shear provides scaling laws involving dimensionless parameters which can be used to predict the width of the shear zone and its temperature evolution. The applied 1D simple shear model is made of a homogenous medium and the bulk shear deformation is controlled by a constant, far-field shear velocity. The initial configuration exhibits a small thermal perturbation to nucleate the localization. To show the general applicability of the scaling laws which have been derived from 1D simple shear models we compare predictions of these scaling laws with results of 2D and 3D models of shear zone development under far-field pure shear. The results of the 1D model are practically identical with the results of the more sophisticated 2D and 3D pure shear models. The presented scaling laws are, hence, applicable to a wide range of shear zones caused by thermal softening. Finally, we discuss applications of the scaling laws to a variety of natural shear zones and for laboratory-derived dislocation creep flow laws for quartzite (representing upper crust), plagioclase (representing lower crust) and olivine (representing mantle lithosphere).

P 1.8

3D numerical modelling and finite strain analysis of the transition between viscous overthrusting and folding

Richard Spitz[1], Stefan M. Schmalholz[1] & Boris J.P. Kaus[2]

[1] *Institute of Earth Sciences, University of Lausanne, Bâtiment Géopolis, CH-1015 Lausanne (richard.spitz@unil.ch)*
[2] *Institute of Geosciences, Johannes Gutenberg University Mainz, J.-J.-Becher-Weg 21, D-55128 Mainz*

The Helvetic nappe system in Switzerland is generally described as fold and thrust belt. While the overall geology has been studied in detail, the tectonic development and mechanical interconnection between overthrusting and folding is still not fully understood. One important clue comes from the mechanical stratigraphy and the corresponding lateral transition from overthrusting to folding, which is characteristic for the Helvetic nappe system.

To investigate the control of the lateral variation in the thickness of a weak detachment horizon on the transition between overthrusting and folding during bulk shortening, we employ a three-dimensional numerical model with linear and non-linear viscous rheology. The lateral thickness variation of the detachment horizon mimicks the lateral variation of the pre-Alpine half-graben depth.

Our model configuration is based on published work based on 2D numerical simulations and consists of a stiff viscous layer, with a pre-existing weak zone, resting within a weaker viscous matrix. The thickness of the stiff layer H_L is constant at 1 km, the detachment horizon thickness H_D ranges from 0.2 to 1 km and the total width and length of the model is 50 km. The reference viscosity ratio μ_L/μ_M (for the same strain rate) between the layer and matrix is 100 and both units employ a power-law stress exponent of n = 3. We consider several initial geometries whereby we vary the detachment horizon thickness linearly or stepwise by introducing a flat-ramp geometry. Additionally, we also investigate the effect of shear zone obliqueness on the overthrusting behavior.

To quantify the deformation we compute the finite strain tensor, which we utilize to calculate the strain magnitude and the strain symmetry. The strain magnitude is expressed by the so-called Nadai strain ε_S and the strain symmetry is described by the Lode's ratio ν. Values for the Lode's ratio indicate the mode of deformation: $\nu = -1$ to 0 corresponds to a general constriction, $\nu = 0$ to pure plane strain and $0 < \nu \leq 1$ to flattening. We connect both parameters by the usage of Hsu-diagrams to illustrate the three-dimensional strain magnitude. For instance, Lode's ratios from the rear and frontal limb of the nappe remain close to 0, whereas values along the fold axis display modes of constriction and flattening for the same bulk strain magnitude. Our results demonstrate that finite strain can deviate significantly from plane strain along the fold axis and in the transition zone between folding and overthrusting, depending on the initial geometry.

P 1.9

3D FE-modelling of inclined, brittle-ductile transpression

Seyed Tohid Nabavi[1], Seyed Ahmad Alavi[1] & Marcel Frehner[2]

[1] *Faculty of Earth Sciences, Department of Geology, Shahid Beheshti University, Tehran, Iran (tohidnabavi@gmail.com)*
[2] *Geological Institute, ETH Zürich, Sonneggstrasse 5, 8092 Zürich, Switzerland*

Transpression kinematic is a direct consequence of oblique convergence where velocity vectors are oblique to boundaries between deforming crustal blocks. Transpression zones form from the simultaneous operation of two components (Frehner 2016; Nabavi et al. 2017a): (i) simple shearing parallel with the shear zone boundaries; and (ii) coaxial flow producing shortening orthogonal to the shear zone and stretching parallel to it. Many natural transpression zones develop as the non-vertical zones, which may be termed “inclined transpression” (Nabavi et al. 2016, 2017b). The simple inclined transpression of Jones et al. (2004) involves simultaneous pure shearing (coaxial deformation) and strike-slip and dip-slip simple shearing resulting in triclinic flow.

The mechanical evolution of inclined transpression zones is investigated by a static 3D elasto-plastic mechanical model solved with the finite-element (FE) method using the commercial FE-package ABAQUS™. The model comprises three blocks – an upper ‘active’ block (made up of three layers with different rheologies), which slides frictionally on top of a rigid lower block with 5 km thickness. The lateral dimensions of the ‘active’ block are 75.5×50×9.5 km and two parallel primary dipping faults (=70°) have a length of 50 km length. A regional oblique shortening of 16% (3 km shortening) is imposed at a convergence angle of 25° (α=25°).

The imposed oblique convergence results in inclined transpression accommodated throughout the entire model (Fig. 1). Oblique convergence is accommodated along mixed dextral-thrust faults, where the higher values of incremental shear strain are recorded. The incremental boundary-normal shortening accommodated within the transpression zone is compensated by differential uplift, such that the total thickness increases from 9.5 km in the undeformed stage to ~15 km after the maximum shortening (16%) (Fig. 1a). The incremental shear strain pattern shows that maximum strain is concentrated within the transpression zone and with the largest strain values along the oblique reverse faults (Fig. 1b,d). In addition, results show high shear strain values located along the left boundary (fault 2) of the inclined transpression zone, suggesting that this fault is more active than the right boundary (fault 1). In addition, there are different shear strain in competent (high amount) and incompetent (low amounts) layers. The overall oblique displacement results in shortening and associated up-dip extrusion, mainly produced at the frontal part of the oblique-reverse faults. Displacement vectors within the inclined transpression zone are rotated counter-clockwise with respect to vectors in the fixed backstop. Rotation of the displacement vectors with time suggests that the transpression zone evolves under an overall non-plane strain deformation. Structures observed in this model are mainly mixed dextral-reverse faults sub-parallel with the backstop and obliquely oriented, related folds, accountable for contraction-dominated transpression. Results demonstrate that deformation can be accommodated by folding in all blocks. Deformation accommodated as folding in the mobile backstop produces an asymmetric anticline so that permanent strains develop principally in the forelimb. As the simulated oblique convergence increases, inclined transpression begins to accommodate a progressively greater fault slip and the overall anticline growth in the mobile backstop is characterized by an increase in fold amplitude rather that its width. The model results demonstrate that the transpression zone evolves in a 3D strain field and along non-coaxial strain paths. The results show the mean and maximum principal stress increases inside the transpression zone (Fig. 1c).

Also, the fault slip distributions in the elasto-plastic model is asymmetric. Generally, the transpression zone undergoes lateral and up-dip extrusion. Modelling results show that strain partitioning occurs between a narrow simple-shear-dominated domain and a broad contraction-dominated domain (Fig. 1). This type of strain partitioning is defined as discrete partitioning.

REFERENCES

Frehner, M. 2016: 3D fold growth in transpression, Tectonophysics 693, 183-196.
Jones, R. R., Holdsworth, R. E., Clegg, P., McCaffrey, K., & Tavarnelli, E. 2004: Inclined transpression. Journal of Structural Geology 26, 1531-1548.
Nabavi, S. T., Alavi, S. A., Mohammadi, S., Ghassemi, M. R., & Frehner, M. 2017a: Analysis of transpression within contractional fault steps using finite-element method, Journal of Structural Geology 96, 1-20.
Nabavi, S. T., Díaz-Azpiroz, M., & Talbot, C. J. 2017b: Inclined transpression in the Neka Valley, eastern Alborz, Iran, International Journal of Earth Sciences 106, 1815-1840.
Nabavi, S. T., Rahimi-Chakdel, A., Khademi, M. 2016. Structural pattern and emplacement mechanism of the Neka Valley nappe complex, eastern Alborz, Iran, International Journal of Earth Sciences, doi:10.1007/s00531-016-1433-x.

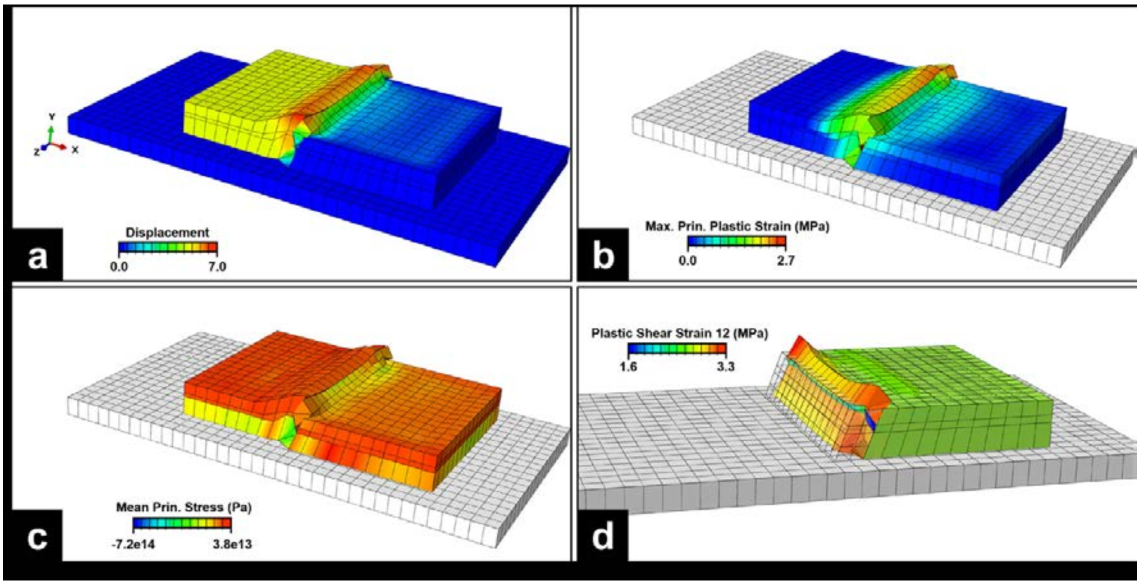

Figure 1. Model results of a) displacement, b) maximum plastic strain, c) mean principal stress, and d) shear strain distributions.

P 1.10

Mechanical evolution of transpression zones affected by fault interactions: insights from 3D elasto-plastic finite element models

Seyed Tohid Nabavi[1], Seyed Ahmad Alavi[1], Marcel Frehner[2], Soheil Mohammadi[3] & Mohammad Reza Ghassemi[4]

[1] Faculty of Earth Sciences, Department of Geology, Shahid Beheshti University, Tehran, Iran (tohidnabavi@gmail.com)
[2] Geological Institute, ETH Zürich, Sonneggstrasse 5, 8092 Zürich, Switzerland
[3] High Performance Computing Laboratory, School of Civil Engineering, University of Tehran, Tehran, Iran
[4] Research Institute for Earth Sciences, Geological Survey of Iran, Tehran, Iran

Transpression zones, as a common tectonic setting in strike-slip fault systems, orogenic belts, and plate boundaries, result from oblique convergence between deforming crustal plates (Frehner 2016; Nabavi et al. 2017b). Transpression is characterized by simultaneous simple shearing parallel to the shear zone boundaries and coaxial flow producing shortening orthogonal to the shear zone boundaries. Transpression can have either a monoclinic or a triclinic kinematic symmetry, depending on the orientation of the pure shear axes with respect to the simple shear axes (Fernández & Díaz-Azpiroz 2009).

The mechanical evolution of transpression zones affected by fault interactions is investigated by a static 3D elasto-plastic mechanical model solved with the finite-element (FE) method using the commercial FE-package ABAQUS™. Ductile transpression between non-rigid walls implies an upward and lateral extrusion. The model demonstrates that the transpression zone evolves in a 3D strain field and along non-coaxial strain paths. Distributed plastic strain, slip transfer, and maximum plastic strain occurs within the transpression zone. Outside the transpression zone, fault slip is significantly reduced because shear offset is accommodated by distributed plastic shear. The results show that the mean and maximum principal stress increase inside the step between the fault segments compared to the region outside the step (Fig. 1a) (e.g., Nabavi et al. 2017a). With progressive deformation, the σ_3 axis rotates within the transpression zone forming an oblique angle to the regional transport direction (~9°-10°).

Rotation of the displacement vectors with the evolution of the oblique convergence suggests that the transpression zone evolves under an overall non-plane strain deformation. Slip decreases along fault segments and with increasing depth so that we can see a distinct slip decrease at depths from 0-5 km to 5-15 km (Fig. 1b). This can be attributed to the accommodation of bulk shortening over adjacent fault segments. Also, fault slip distributions in the elasto-plastic model shows quite some asymmetry (Fig. 1b). The model shows an almost symmetrical domal uplift, which is due to off-fault deformation, generating a doubly plunging fold (Fig. 2a) and a positive flower structure (Fig. 2c). Outside the overlap zone, expanding asymmetric subsidence basins showing negative flower structures develop on both sides of the transpression zone, and are called 'transpressional basins' (Fig. 2a).

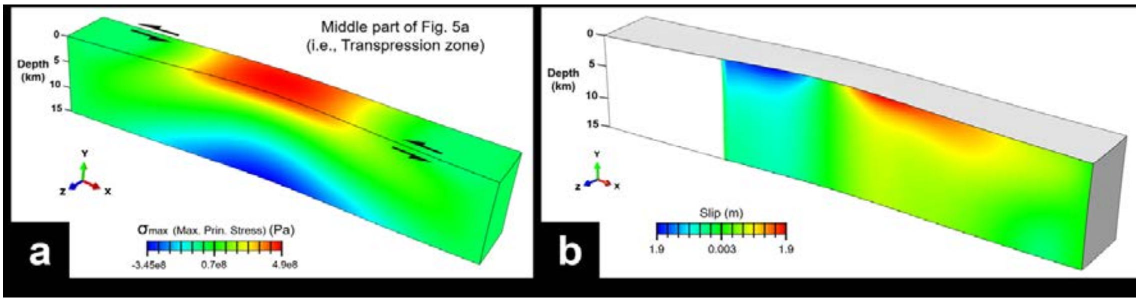

Figure 1. a) Maximum principal stress within contractional fault step. Here, the model dimension is 70×10×15 km. The compressive (positive values) and tensile zones are specified. b) Slip distribution along one fault segment in vertical section.

Generally, the transpression zone undergoes lateral and vertical extrusion (Fig. 2b). Deflection at fault segments causes the fault dip to change to less than 90° (~86-89°) near the surface (~1.5 km). This results in a pure-shear-dominated, triclinic, and discontinuous heterogeneous flow of transpression zone (Fig. 2d).

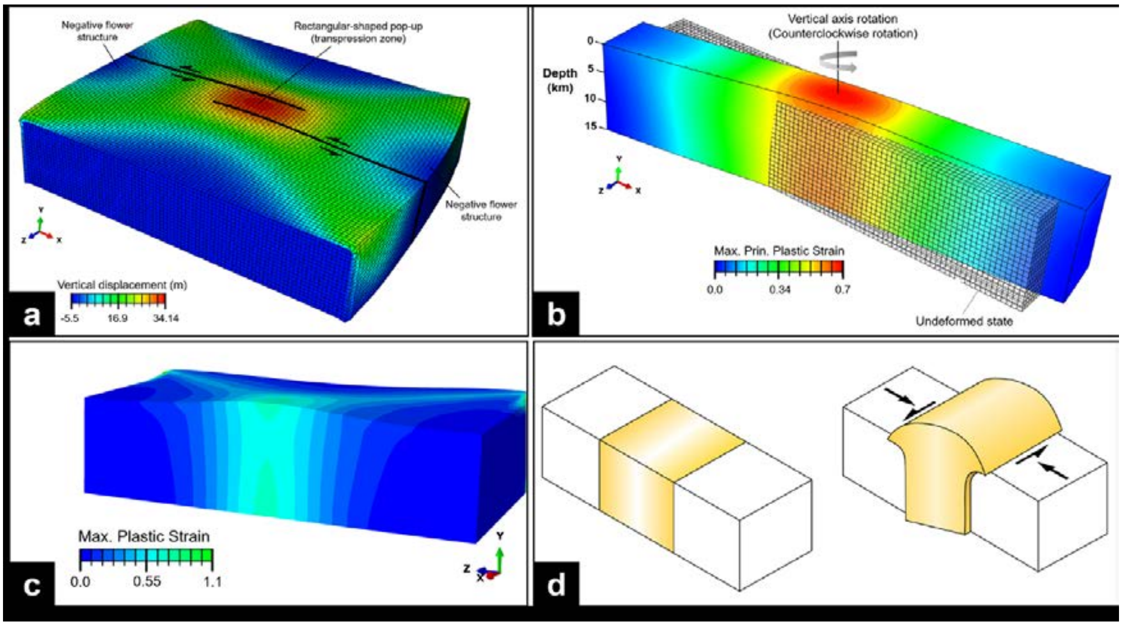

Figure 2. a) Model result showing vertical displacement (U_y) of the transpression zone. b) Vertical and lateral extrusion, and also rotation of fold axis with respect to undeformed state (grey meshed block) within the resulting transpression model. c) Maximum principal strain distribution. d) Discontinuous heterogeneous flow of the transpression zone.

REFERENCES

Fernández, C., & Díaz-Azpiroz, M. 2009: Triclinic transpression zones with inclined extrusion, Journal of Structural Geology 31, 1255-1269.

Frehner, M. 2016: 3D fold growth in transpression, Tectonophysics 693, 183-196.

Nabavi, S. T., Alavi, S. A., Mohammadi, S., Ghassemi, M. R., & Frehner, M. 2017a: Analysis of transpression within contractional fault steps using finite-element method, Journal of Structural Geology 96, 1-20.

Nabavi, S. T., Díaz-Azpiroz, M., & Talbot, C. J. 2017b: Inclined transpression in the Neka Valley, eastern Alborz, Iran, International Journal of Earth Sciences 106, 1815-1840.

P 1.11

Evolution of rifts and rift linkage zones in orthogonal and scissor extension settings: insights from analogue models analysed with 4D X-ray computed tomography

Frank Zwaan*, Guido Schreurs1*

[1] *Institute of Geological Sciences, University of Bern, Baltzerstrasse 1+3, CH-3012 Bern, Switzerland (frank.zwaan@geo.unibe.ch)*

When simulating rift systems, analogue and numerical modellers often apply a continuous magnitude along the strike of an extensional structure, rift or rift system. Yet in nature, significant extension intensity variations are observed along strike of a rift system, as the natural consequence of tectonic plates moving apart about a pole of rotation, resulting in scissor extension and rift propagation.

We performed various analogue tectonic experiments with a 2 set-ups based on previous work by Zwaan et al. (2016) to assess the differences in 1) rift development and 2) between rifts and transfer zones (zones of interaction between individual rift segments) forming in traditional orthogonal extension settings versus scissor extension settings. Various models are analyzed with X-Ray computed tomography (XRCT or CT) techniques, allowing a detailed 4D assesment of the internal model deformation.

Our modelling efforts give the following results: 1) Rift development in scissor tectonics settings develops a strong structural gradient in both space and time along the strike of the system. 2) Although scissor extension and orthogonal extension produce quite different large-scale structures, local features in a scissor extension systems can be regarded as forming in an orthogonal extension setting. 3) Various degrees of underlap produce three basic modes of rift linkage structures. Low underlap (high angle φ) experiments develop rift pass structures. With increasing underlap (φ = ca. 40˚), transfer zone basins develop. High degrees of underlap (φ ≤ 30˚), tend to result in sub-basins.

Several of these structures are found in previous model studies and in nature. Yet a direct comparison is challenging, as various parameters might modify their structural development significantly.

REFERENCES

Zwaan, F., Schreurs, G., Naliboff, J. & Buiter, S.J.H., 2016: Insights into the effects of oblique extension on continental rift interaction from 3D analogue and numerical models, Tectonophysics, 693, 239-260.

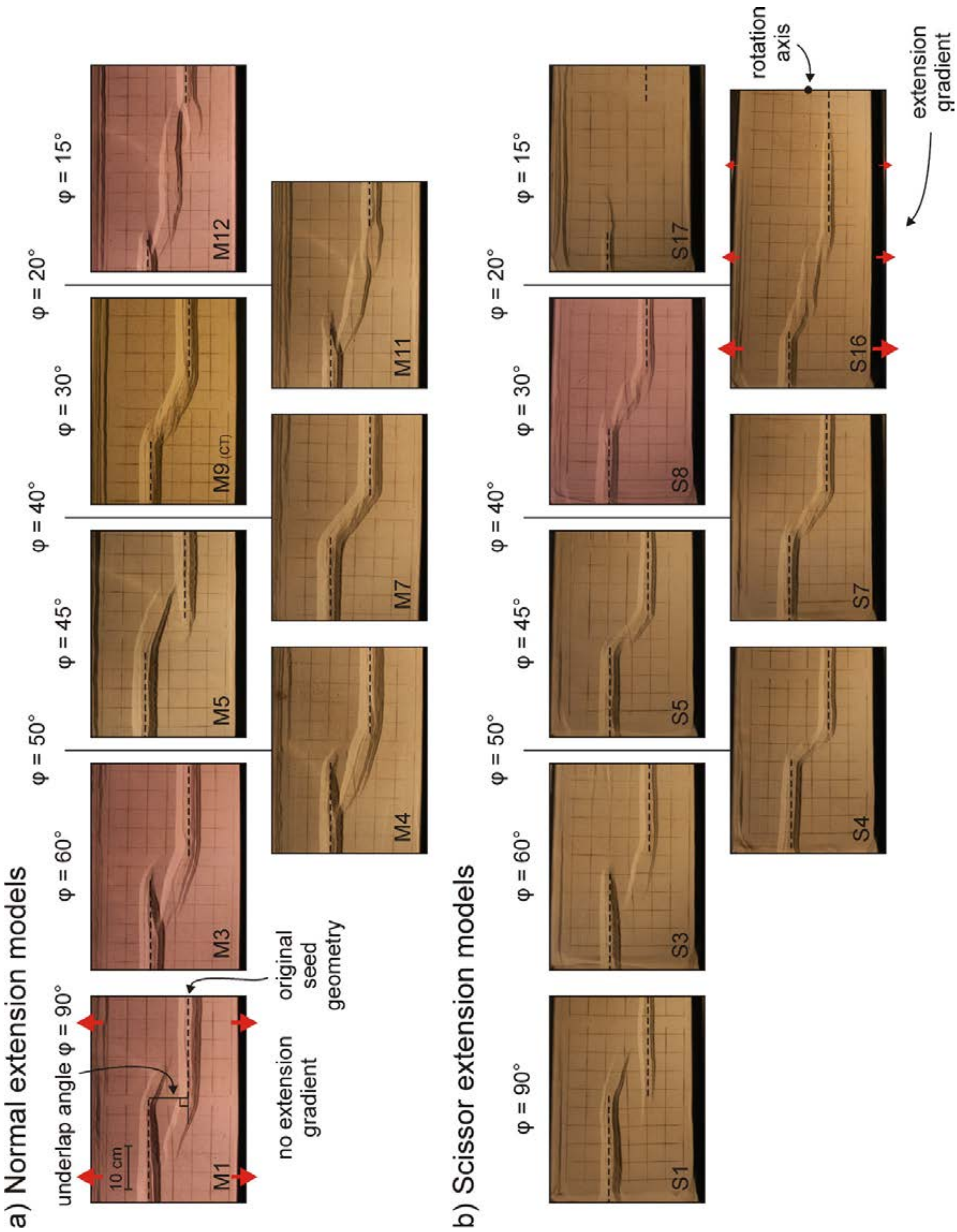

Figure 1. Surface structure overview of model results from both the orthogonal extension models and the scissor extension models as a function of rift underlap (angle φ).

P 1.12

Structural Geology in Applied Materials Science: Strain Localisation and Crack Initiation in Waterproofing Membranes during Tensile Tests

Marius Waldvogel[1], Roger Zurbriggen[2], Alfons Berger[1], Marco Herwegh[1]

[1] Institute of Geological Sciences, University of Bern, Baltzerstrasse 1+3, CH-3012 Bern (marius.waldvogel@geo.unibe.ch)
[2] RD&I Department, Akzo Nobel Chemicals AG, Industriestrasse 17a, CH-6203 Sempach Station

Strain localisation and the initiation of brittle deformation in the Earth's crust is an important topic to understand plate tectonics. In the current study, which is an applied materials science project, we investigate the initiation of crack formation within a polymer-cement-composite material, i.e. a waterproofing membrane. Such membranes are applied onto concrete substrates in order to maintain their durability preventing the propagation of cracks, forming during expansion/shrinkage of the concrete substrate. Generally, such one-component flexible cementitious waterproofing membranes are composed of a mortar (mix of quartz sand (d=0.1-0.3 mm) and ordinary Portland cement (OPC, CEM I 52.5 N)), modified with a spray-dried redispersible polymer powder (Schulze & Killermann, 2001). The elasto-plastic polymers are added to the mechanically rigid cement matrix forming the composite material. It is therefore the elastic to ductile deformation behaviour of the polymers, which enhances the tensile strength of the composite (Ohama, 1995; Schulze & Killermann, 2001) and helps to reduce the formation of microcracks (Ohama, 1995), i.e. which enhances the so-called crack-bridging ability (CBA). The CBA is measured using normed uniaxial tensile testing during which the waterproofing membrane must bridge a specified displacement without cracking (FprEn, 2011). Therefore, the waterproofing membrane is applied on a fibre cement board substrate, in which a pre-defined crack is incorporated. The samples were subjected to tensile loading until cracking occurred, while the evolution in strength and surface structures were continuously monitored. Additionally, samples were deformed to pre-defined displacements, then fixated and images of the surface of the waterproofing membrane were acquired. Image analysis is exerted to investigate strain localisation and crack initiation. Strain localisation is recognized as white lines forming, growing and connecting in a distinct zone on the sample surface (called “strain whitening” hereafter) above the pre-defined crack in the substrate material. After a strain hardening period, strain whitening starts at or shortly after the peak load, indicating that strain localisation processes and associated strain softening are taking place. Furthermore, strain whitening is the visualisation of the formation of crazes in the polymers (Trimiño et al., 2015). The width of the strain whitening domain increases non-linearly with displacement with a decreasing growth rate. The growth behaviour of the strain whitening zone can provide additional information of initiation of strain localisation and crack initiation in the waterproofing membrane. Elongated holes and cracks form and evolve only inside this zone. With image analysis, initiation and evolution of pores, elongated holes and cracks can be quantitatively investigated using the angular orientation of their major axes, their surface areas, and geometrical shape descriptors (circularity and roundness (Heilbronner & Barrett, 2014)). Initially, pores generally show high roundness and circularity indicating a circular geometry. Due to their shape, the angular orientation of pores is random irrespectively of displacement during the first few strain increments. With increasing displacement, elongated holes evolve showing an increasing elliptical shape and a change from a random angular orientation towards a preferred orientation of the major axis of the elongated hole parallel or perpendicular to the tensile load direction. Several individual elongated holes grow and eventually coalesce to macrocracks, which can be seen by the smooth transition from elongated pores to macrocracks in terms of circularity and roundness. Macrocracks show a tendency to orient perpendicularly to the extension direction. In order to improve the CBA of waterproofing membranes the elastoplastic behaviour of the composite mortar has to be increased. This reduces the stress concentrations around mechanical heterogeneities (pores, rigid cement particles) allowing for a more homogeneous uptake of strain over a wider membrane volume. Along this behaviour, also the crack formation is reduced enhancing the performance of the waterproofing capacity. Although being industry products, the mechanical behaviour of these materials is not unlikely that of some polymineralic rocks in the Earth's crust. In this sense, polymer-modified mortars might be suitable analogue materials to model the behaviour of a porous soft material with minor sand composition, e.g. a low-consolidated sandy to silty claystone.

REFERENCES

European Committee for Standardization. 2011: FprEN 14891 Liquid-applied water impermeable products for use beneath ceramic tiling bonded with adhesives – Requirements, test methods, evaluation of conformity, classification and designation.

Heilbronner, R. & Barrett, S. 2014: Image Analysis in Earth Sciences Microstructures and Textures of Earth Materials. Springer-Verlag Berlin Heidelberg, pp 520.

Ohama, Y. 1995: Handbook of Polymer-modified Concrete and Mortars Properties and Process Technology. Noyes Publications, pp. 236.

Schulze, J. & Killermann, O. 2001: Long-term performance of redispersible powders in mortars. Cement and Concrete Research 31, 357-362.

Trimiño, L.F., Cronin D.S. & Caruso Dailey, M.M. 2015: Characterization of Structural Epoxy Adhesives. In: Dynamic Behavior of Materials, Volume 1: Proceedings of the 2014 Annual Conference on Experimental and Applied Mechanics (Ed. By Song, B., Casem, D. & Kimberley, J.). The Society for Experimental Mechanics, Inc., 185-191.

P 1.13

A Swiss-army-knife approach to nearly automatic microearthquake analysis for natural and induced sequences.

Verena Simon[1], Toni Kraft[1], Thessa Tormann[1], Tobias Diehl[1], Marcus Herrmann[1]

[1]Swiss Seismological Service, ETH Zurich, Sonneggstr. 5, 8092 Zurich, Switzerland (verena.simon@sed.ethz.ch)

Many Swiss earthquake sequences have been studied using relative location techniques, which often allowed to constrain the active fault planes and shed light on the tectonic processes that drove the seismicity. Yet, in the majority of cases, the number of located earthquakes was too small to infer the details of the space-time evolution of the sequences, or their statistical properties. Therefore, it has mostly been impossible to resolve seismicity patterns of individual sequences in a sufficiently high precision needed to improve the understanding of the mechanisms behind them.

Here we present a nearly automatic workflow that combines well-established seismological analysis techniques and allows to significantly improve the completeness of detected and located earthquakes of a sequence.

We start from the manually timed routine catalog of the Swiss Seismological Service (SED), which contains the larger events of a sequence. From these well-analyzed earthquakes, we dynamically assemble a template set and perform a matched filter analysis on the station with: the best SNR for the sequence; and a recording history of at least 10-15 years, our typical analysis period. This usually allows us to detect events several orders of magnitude below the SED catalog detection threshold. The waveform similarity of the events is then further exploited to derive accurate and consistent magnitudes. The enhanced catalog is then analyzed statistically to derive high-resolution time-lines of the a- and b-value and consequently the occurrence probability of larger events.

Many of the detected events are strong enough to be located using double-differences. No further manual interaction is needed; we simply time-shift the arrival-time pattern of the detecting template to the associated detection. Waveform similarity assures a good approximation of the expected arrival-times, which we use to calculate event-pair arrival-time differences by cross-correlation. After a SNR and cycle-skipping quality check these are directly fed into hypoDD. Using this procedure we usually improve the number of well-relocated events by a factor 2-5.

We demonstrate the successful application of the workflow at the example of natural sequences in Switzerland and present first results of the advanced analysis the was possible with the enhanced catalogs.

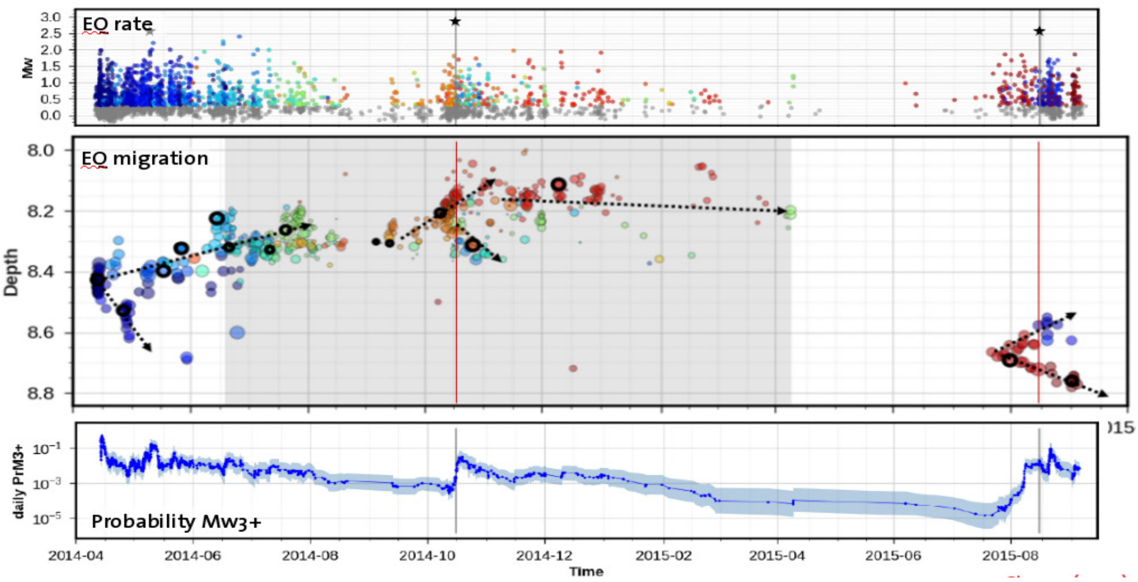

Figure 1. Temporal evolution of the Diemtigen/BE sequence 2014/15: Top: earthquake rate, middle: migration of earthquakes with depth (absolute depth uncertainty of seismic cloud app. 1km), bottom: probability for a Mw ≥ 3 event. Colors indicate the associated template. ML3.2 event in Oct. 2014 and ML2.7 event in Aug. 2015 are indicated by vertical lines.

REFERENCES

Simon, V., (2017) High precision analysis of natural earthquake sequences in Switzerland. Master Thesis, IDEA League, Joint Master Program in Applied Geophysics, ETH Zurich, 11. Aug. 2017, pp. 92.

P 1.14

How deep is shallow? Improving hypocenter locations of upper crustal seismicity in Switzerland

Tobias Diehl[1], Edi Kissling[2], Timothy Lee[1] & Stefan Schmid[2]

[1] *Swiss Seismological Service, ETH Zurich, CH-8092, Switzerland (tobias.diehl@sed.ethz.ch)*
[2] *Institute of Geophysics, ETH Zurich, 8092, Switzerland*

The M_L 4.6 Urnerboden and M_L 4.3 Château d›Oex earthquakes of 2017 illustrate that the tectonic interpretation of upper crustal fault systems crucially depends on the accuracy of absolute focal depth estimates. Routine earthquake location procedures locate both earthquakes in the region of the sediment-basement contact, which raises the question whether or not the associated fault systems connect from the sedimentary cover into the basement. In the Urnerboden case, geometries and kinematics of relocated seismicity at 4-5 km depth correlate remarkably well with subvertical faults measured at the surface. This correlation suggests the existence of a left-lateral fault system in the Linthal region, which cuts through the Helvetic nappes and underlying flysch, possibly also affecting the autochthonous basement.

In the case of the M_L 4.3 Château d›Oex earthquake, relative relocations and focal mechanisms image a normal fault in the Préalpes domain, which dips towards the northeast. The top of the basement in this area is likely located in a depth of about 5-6 km. Focal depths constrained by temporary aftershock stations, on the other hand, range between 3-4 km, supporting a source in the sedimentary cover. The accuracy of the derived focal depths, however, is strongly linked to uncertainties on the seismic velocity structure within the uppermost crust. Particularly systematic errors in the S-wave velocities may significantly bias absolute locations and therefore the tectonic interpretation. Normal faulting near Château d›Oex suggests the existence of an extensional corridor extending to from SW to NE from the eastern end of Lake Geneva towards Thunersee, which contrasts with well known dextrally transtensional WSW-ENE striking corridor that follows the Rhone valley floor.

In this study, we aim to reduce uncertainties in location by improving P and S-wave velocity models on local and regional scales. In particular, we take advantage of significant improvements in the Swiss National Seismic Network in terms of station density and data quality. High-quality travel-time data collected by the Swiss Seismological Service (SED) over the last 17 years are used to solve the coupled hypocentre-velocity structure problem in 1D. Within the 1D inversion, the quality of travel-time data will be assessed and possibly erroneous picks in the SED bulletin data identified. Initially, we apply the 1D inversion to north and northeast Switzerland to improve absolute locations in the northeastern Alps and its foreland. Seismicity in the northern foreland is of particular interest, since this region is targeted for radioactive waste repositories. In addition, we will assess the potential spatial resolution of a 3D local earthquake tomography using the improved travel-time data and explore possible methods to constrain host formations of seismicity by comparison of hypocentre solutions with the resolved 3D velocity structure.

P 1.15

High-Quality Earthquake Catalogue for a Changing Network Configuration: Application to Southwestern Switzerland

Timothy Lee[1], Tobias Diehl[1], Edi Kissling[2], Stefan Wiemer[1]

[1] Swiss Seismological Service, ETH Zurich, 8092, Switzerland
[2] Institute of Geophysics, ETH Zurich, 8092, Switzerland

Earthquake catalogues derived from several decades of observations are often biased by changing network configurations and processing procedures. Changing station network geometries over time within the same region cause varying hypocentre location quality and completeness of earthquake catalogues. Moreover, changing procedures and algorithms used for earthquake location can introduce systematic errors when combined into one single catalogue. Such catalogues are largely inconsistent in terms of location accuracy. To study the long-term spatio-temporal behaviour of seismogenic fault zones at high-resolution, accurate and consistent earthquake catalogues are required. Usually, routine hypocentre locations reported in earthquake catalogues are determined with an a priori 1D or 3D velocity model. However, travel times depends on hypocentral parameters as well as seismic velocities (the coupled hypocenter-velocity problem). To solve the coupled problem, it is necessary to invert for hypocentral and velocity model parameters simultaneously. The so-called minimum 1-D model calculation, which involves simultaneous inversion of arrival time data from local earthquakes to derive hypocentre locations, seismic velocities, and station delays, is a well-established approach to solve the coupled-problem for a region and therefore provides robust and accurate absolute locations.

Relative earthquake relocation techniques, on the other hand, minimize the impact of the remaining (un-modelled) 3D velocity structure by directly inverting travel-time differences between pairs of events. In addition, differential-times derived from waveform cross-correlation reduce the impact of inconsistencies compared to catalogue picks. Inverting differential-times for their hypocentre separation thus provides high-precision relative locations of hypocentres, imaging the fine scale structure of seismogenic faults. High-resolution seismotectonic studies, comparing e.g. geologically or geophysically mapped faults with seismicity, require accurate absolute as well as precise relative hypocentre locations.

In this study, we establish a high-quality earthquake catalogue by relocating absolute hypocentre locations of the last 33 years with the minimum 1-D model approach for the Valais region. To account for the changing network geometry over this time interval, we first constrain the 1D velocity structure by using high-quality data from the last 15 years obtained by the digital broadband network of the Swiss Seismological Service. The network was continuously improved and densified in this period. For events, which occurred prior to the digital era, we fix the 1D velocity structure and invert only for station delays and hypocentres. The derived consistent catalogue of absolute locations and 1D velocity structure is then used as initial value for a regional relative relocation.

The new catalogue will provide new insights into the seismotectonics of the Valais and allows the detailed comparison of seismicity and geologically mapped faults. In particular, we are interested in the prominent seismogenic structure located in the Rawil depression north of the Rhone Valley and its relationship to the Rhone-Simplon line, which is considered to be the tectonic (dextral) boundary between Helvetic nappes to the north and Penninic nappes to the south in this area.

P 1.16

The completed AlpArray Seismic Network

György Hetényi[1,2,3], Irene Molinari[2], John Clinton[3], Edi Kissling[2], AlpArray Seismic Network Team, AlpArray OBS Cruise Crew & AlpArray Working Group

[1] University of Lausanne, Institute of Earth Sciences, UNIL-Mouline Géopolis, 1015 Lausanne (gyorgy.hetenyi@unil.ch)
[2] ETH Zürich, Department of Earth Sciences, Institute of Geophysics, Soneggstrasse 5, 8092 Zürich
[3] Swiss Seismological Service at ETH Zürich, Soneggstrasse 5, 8092 Zürich

The AlpArray program is a European initiative to advance our understanding of orogenesis and its relationship to mantle dynamics, plate reorganizations, surface processes and seismic hazard in the Alps-Apennines-Carpathians-Dinarides orogenic system. To obtain new, high-resolution geophysical images of structures and map physical properties of the lithosphere and of the upper mantle in 3D, the AlpArray Seismic Network has been deployed in a multi-national effort. With over 600 broadband stations operated for 2 years, this is one of the largest simultaneously operated seismological arrays in the academic domain. This gap-filling network became possible with the coordinated funding and deployment of temporary stations, including ocean-bottom seismometers, which overarch the permanent networks to fill coverage gaps. Here we present the goals, construction and properties of the completed AlpArray Seismic Network (Figure 1), which we expect will provide unprecedented resolution and quality data to image the geologically complex greater Alpine area at depth.

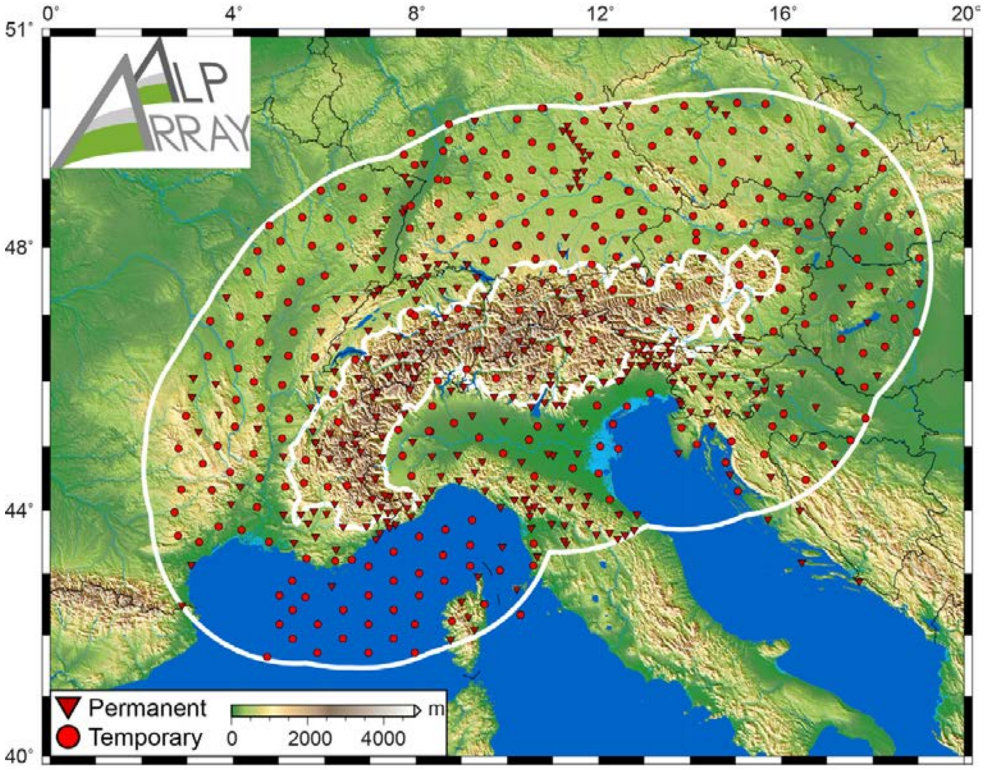

Figure 1. The completed AlpArray Seismic Network

P 1.17

High resolution imaging of the Ivrea Geophysical Body: A receiver function and gravity approach

Matteo Scarponi[1], György Hetényi[1], Jaroslava Plomerová[2], Stefano Solarino[3], Théo Berthet[4]

[1] Institute of Earth Sciences, University of Lausanne, Quartier UNIL-Mouline, Bâtiment Géopolis, CH-1015 Lausanne, Switzerland
[2] Institute of Geophysics, Czech Academy of Sciences, Prague, Czech Republic
[3] Istituto Nazionale di Geofisica e Vulcanologia INGV, c/o DICCA University of Genova, Via all'Opera Pia 15A, 16145 Genova, Italy
[4] Institut des Sciences de la Terre, Grenoble Alpes University, Grenoble, France

The IvreaArray project aims at refining the structure of the Ivrea geophysical body: a fast velocity anomaly beneath the Ivrea-Verbano Zone. Based on the most recent local earthquake tomography result (Diehl et al., 2009), the Ivrea body starting model is defined over a 25 x 25 x 15 km grid. The Moho discontinuity is expected to present both planar and dipping segments (Figure 1). To achieve higher resolution images, we installed ten broadband seismic stations along a profile crossing the Insubric Line and the Ivrea-Verbano Zone at the level of the Sesia Valley (Figure 2). The seismic array geometry has been carefully designed in a linear West-East orientation with 5-km spacing to catch strong-energy phases converted at dipping interfaces. Data from one year of teleseismic earthquakes will be used to image the target Moho discontinuity by means of P-to-S receiver function (RF) analysis. Both inversion and migration techniques are taken into consideration. Secondary reflections and multiple phases will play a key role in estimating the Vp/Vs ratio. The frequency-dependence of RFs is expected to characterize the velocity gradient across the main discontinuity (e.g. James et al., 2003).

A series of gravity survey campaigns is also carried out in the same area to provide additional constraints on the structure and physical properties of the Ivrea geophysical body. The surveys will provide new relative gravity data which, together with already existing measurements, will be used to constrain a 3D density model of the Ivrea geophysical body.

Seismology and gravity will be jointly used to characterize the density contrast across interfaces and density distribution within the media, and hence to map how shallow the mantle rocks are in the Ivrea-Verbano Zone.

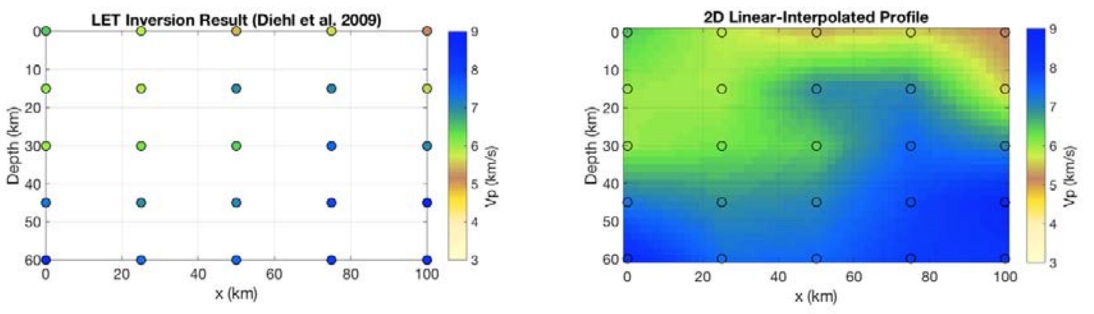

Figure 1: Local Earthquake Tomography model result (left) and its associated linear interpolation (right) from Diehl et al. (2009).

Figure 2: IvreaArray seismic station locations.

REFERENCES

Diehl T, Husen S, Kissling E, Deichmann N (2009) High-resolution 3-D P-wave model of the Alpine crust. Geophys J Int 179(2): 1133-1147. doi:10.1111/j.1365-246X.2009.04331.x

James DE, Niu F, Rokosky J (2003) Crustal structure of the Kaapvaal craton and its significance for early crustal evolution. Lithos 71(2): 413-429.

P 1.18

The Swiss participation to a coherent and collaborative network of Solid Earth Multi-scale laboratories: EPOS- TCS MSL

Elisa Calignano[1], Alba Zappone[2,3], Claudio Madonna[2], and the EPOS-IP WP[16] Team

[1] Utrecht University, Department of Earth Sciences, Heidelberglaan 2, NL-3584 Utrecht, The Netherlands
[2] Department of Earth Sciences, ETH Zurich, Sonneggstrasse 5, CH-8092 Zurich, Switzerland (alba.zappone@sed.ethz.ch)
[3] Department of Process Engineering, ETH Zurich, Sonneggstrasse 3, CH-8092 Zurich, Switzerland

Earth Science research is largely based on data from laboratories, which provide a controlled enviroment, essential for the understanding of processes in Earth's evolution, for the sustainable exploitation of geo-resources, and for the assessment of geo-hazards. The methods adopted in laboratories are largely heterogeneous and multi-scale, reflecting the complexity of the Earth system.

The Rock Deformation Laboratory (RDL) at ETH Zurich conducts research into the mechanical behavior and transport properties of Earth materials at different enviromental conditions. It focuses on a range of problems, including rock deformation, rock physics, volcano-tectonics, coupled thermo-hydro mechanical process in the crust and upper mantle. The RDL is actively partecipating in the European Plate Observing System (EPOS), and particularly in the Thematic Core Service Multi-scale Laboratories (TCS MSL), where a network of European solid Earth science Multi-scale laboratories is currently being developed.

The collaboration of institutions from the Netherlands, Italy, Spain, France, Germany, United Kingdom, Portugal and Switzerland aims to provide , within EPOS – TCS MSL 1) a virtual access to data from laboratories (data service), and 2) a physical access to laboratories (Trans-National Access program).

The first aspect implies an effort in harmonization of the data, which at present are produced and stored in the databases of each laboratory, following lab-individual schemes and formats. The EPOS TCS MSL community is developing a scheme to level out metadata, allowing to collect available data on the properties and processes controlling the rock system behavior at all relevant scales. The aim is to generate a common platform, accessible and interoperable through services for supporting research activities into geo-resources and geo-hazards and Earth System Evolution. The ultimate goal of the EPOS-TCS MSL community is to maximize the accessibility of data and optimize their preservation.

The second aspect, the physical access to laboratories, gives the opportunity for scientific visitors to perform experimental activities in lababoratories outside their own institution. It aims at facilitating access to research infrastructures and maximizing their use, and at the same time it enhances the transparency of access rules and provides a streamlined mechanism of access.

P 1.19
A tool to assist bedrock geology interpretation

Anna Rauch[1], Mario Sartori[1], Sébastien Castelltort[1], Stefan Volken[2], Stéphan Dall'Agnolo[2]

[1] *Département des sciences de la Terre, Université de Genève, Rue des Maraîchers 13, CH-1205 Genève (anna.rauch@unige.ch)*
[2] *Office fédéral de topographie swisstopo, Service géologique, Seftigenstrasse 264, CH- 3084 Wabern*

To support decisions across industrial, civil and academic fields, three-dimensional models of the geological structure are increasingly in demand. Very often, and particularly in mountainous terranes, only (or mainly) surface information in form of geological maps are at hand to tackle such challenge. However, the bedrock geology and structurally relevant information is covered on large areas by Quaternary deposits and glaciers. Therefore, an indispensable first step in a structural investigation is the interpretation of a Bedrock Geology Map (BGM). A BGM is an 'undressed' geological map, unconsolidated deposits being omitted, showing only the bedrock information at the top-bedrock topography. As a map itself, a BGM represents a direct constrain regarding subsurface models (e.g. hydrogeology, reservoir geology, natural hazard assessment etc.). Moreover, it allows ensuring coherency between cross sections, which represent the skeleton of the entire 3D structure.

Yet, the interpretation of the bedrock geology is a complicated process, in which one has to combine various types of information such as outcrop observations, geological concepts, geometrical rules and local geological knowledge. Naturally, a BGM interpretation integrates a significant amount of subjectivity and uncertainty, which leave map users unable to assess the reliability related to the information.

To face such difficulties, we are developing a tool that analyses bedrock and structural content in maps. By means of a high-resolution DEM, an algorithm extracts geometric information from outcropping geological boundaries in 3D, i.e. the stretches of interfaces between different bedrock bodies where they intersect with the topography, hereafter named Topography-Interface-Line (TIL). The analysis will determine whether the geometry of the TIL is most consistent with a planar, a curved or an irregular interface. In case of a plane-consistent TIL, one directly obtains a well-confined range of plane orientations that fit the TIL. For a curve-consistent TIL, the degree of curvature is extracted. An irregular, non-consistent TIL occasionally represents a highly irregular bedrock interface, but more often highlights a poorly located bedrock boundary. In all three cases, the proposed tool strongly facilitates the extraction of elusive structural information and/or locates and identifies potential inconsistencies on the geological map. It therefore can be of great assistance during the process of bedrock geology interpretation. Moreover, the range of structural possibilities proposed by the tool can be recorded and accessed by the map users. This record reflects the uncertainty, in which decisions had to be made regarding bedrock geology interpretation.

We present and discuss the different steps involved in the proposed automated TIL analysis with a case study example of the region of Boltigen in the Swiss Prealps by means of the official 1:25'000 geological map of Boltigen (Braillard 2015).

REFERENCES

Braillard, L. 2015: Boltigen (LK 1226). Bundesamt für Landesopographie swisstopo. ISBN: 978-3-302-40075-4

P 1.20

Insights on the Aar Massif exhumation from new field data from the Jungfrau-Eiger mountain chain

David Mair[1], Alessandro Lechmann[1], Marco Herwegh[1] & Fritz Schlunegger[1]

[1]Institute for Geological Sciences, University of Bern, Baltzerstrasse 1+3, CH-3012 Bern (david.mair@geo.unibe.ch)

The SW-NE striking mountain chain of Jungfrau, Mönch and Eiger is made up of up-domed and over-thrusted Pre-Variscian basement units of the Aar massif and its Mesozoic sedimentary cover. The complex structure involves the migmatites of the Innertkirchen-Lauterbrunnen Gneiss zone (ILGZ, Berger et al. 2017) and the migmatites of the the Erstfeld Zone (EZ, Berger et al. 2017) which form the summits of the Mönch and Jungfrau peaks. The Mesozoic sediments of the authochtonous cover are wedged in-between the two basment units, a situation already recognized as peculiar by Geologists in the 1st half of the 19th century.

While the Mesozoic sediments are only present as a few meters-thin, strongly deformed band within the southern flanks of the Mönch and Jungfrau, they form the bulk of the northern flanks of the mountain chain. Despite having been named “Jungfraukeil” and described as mechanical contact in the 19th century subsequent interpretations attribute the structural complexity merely to a syncline. More precisely, they explain the north flanks’ geology as result of a series of overturned tight to isoclinal folds (i.e. Collet and Paréjas 1931). Consequently the crystalline in the summit regions is seen as core of a large scale anticline structure. On a regional scale the sediment wedge of the “Jungfrau syncline” separates the most frontal unit of the Aar massif (the Gastern intrusion along with its protolith the ILGZ) from the more intern units (Lötschberggneis and Erstfelgneis), which are thrusted on top of the former one. The sediments form the overturned limb of a large recumbent fold (Herwegh & Pfiffner 2005). According to these previously mentioned interpretations, the basal Doldenhorn thrust would die out within the study area. Hence the prefered assignment of the structural style mainly considers the occurrence of tight to isoclinal folds, formed under ductile conditions for the basement rocks (i.e. Krayenbuhl and Steck 2009). Ductile folding of basement rocks under lower to midgreenschist facies metamorphic conditions, however, is very unlikely to occur requiring alternative explanations.

Here, we present evidence from the field and the Jungfrau raillway tunnel to propose that the tectonic architecture of the Jungfrau region including the Eiger is rather complex. Based on cross-cutting and kinematic arguments, we discriminate at least three different deformation stages. Early wedging off and imbrication of sediment slivers related to late-emplacement stage of the Helvetic nappes (Kiental phase of Burkhard 1988). Development of steep south-dipping shear zones, mainly accommodating reverse faulting, which is attributed to the Handegg phase (Wehrens et al. 2016, 2017; Herwegh et al. 2017). An even younger deformation stage is characterized by tectonically sheared-off slivers of basement rocks that are frequently wedged-in between mostly ductile deformed Mesozoic sediments. In addition, we observe that slivers made up of dolomites, iron-bearing sandstones and carbonates form similar boundins and sigma clasts from millimetres to tens of meters thickness, which we relate to their rheological behaviour. Repeated stratigraphic sequences, sheared off along a set of discrete (ultra-)mylonitic shear zones, document the fault zone nature of the Jungfrau syncline. The thrust faults follow stratigraphic and tectonic weaknesses, especially accomodating displacement along the basement cover contact.

At a large-scale, the combination of folded sediments and basement slivers resembles an isoclinally folded system as suggested by the old studies. In detail, however, brittle deformation and thrusting of basement slivers being accommodated by the preferentially ductile folding of the sediments into which the slivers are wedged in show a clear brittle to semibrittle deformation style in the basement. We correlate this young NW thrusting to the Pfaffenchopf phase (Wehrens 2015, Herwegh et al. 2017). This interpreation is in line with the recent geodynamic model of the exhumation of the Aar massif (Herwegh et al. 2017), rendering the summits of the Eiger and Mönch as “Klippen” and allowing to connect the Jungfrau fault zone to Wenden zone in the east.

REFERENCES

Berger, A., Mercolli, I., Herwegh, M., Gnos, E. 2017: Geological Map of the Aar Massif, Tavetsch and Gotthard Nappes. Geological Special Map 129.

Burkhard, P. M. 1988: L’Helvétique de La Bordure Occidentale Du Massif de l’Aar (Évolution Tectonique et Métamorphique). Eclogae Geologicae Helvetiae, 81, 63–114.

Collet, L., & Paréjas, E. 1931: Géologie de La Chaîne de La Jungfrau.” Beiträge zur Geologischen Karte der Schweiz.

Herwegh, M., & Pfiffner, O.A. 2005: Tectono-Metamorphic Evolution of a Nappe Stack: A Case Study of the Swiss Alps.” Tectonophysics, 404, 55–76.

Herwegh, M., Berger, A., Baumberger, R., Wehrens, P., & Kissling, E. 2017: Large-Scale Crustal-Block-Extrusion During Late Alpine Collision. Scientific Reports, 7, 413.

Krayenbuhl, T., & Steck. A. 2009: Structure and Kinematics of the Jungfrau Syncline, Faflertal (Valais, Alps), and Its Regional Significance. Swiss Journal of Geosciences, 102, 441–56.

Wehrens, P. 2015: Structural evolution in the Aar Massif (Haslital transect): Implications for mid-crustal deformation. PhD thesis, University Bern.Ziegler,

Wehrens, P., Berger, A., Peters, M., Spillmann, T. & Herwegh, M. 2016: Deformation at the Frictional-Viscous Transition: Evidence for Cycles of Fluid-Assisted Embrittlement and Ductile Deformation in the Granitoid Crust. Tectonophysics 693, 66–84.

Wehrens, P., R. Baumberger, A. Berger, & Marco Herwegh. 2017. How Is Strain Localized in a Meta-Granitoid, Mid-Crustal Basement Section: Spatial Distribution of Deformation in the Central Aar Massif (Switzerland).” Journal of Structural Geology, 94, 47–67.

P 1.21

Hydrothermal cockade-like breccias in the Grimsel Breccia Fault: fluidization, flow rates and growth dynamics during seismic events

Alfons Berger[1], Daniel Egli[1], Marco Herwegh[1]

[1]Institut für Geologie, University of Bern, Baltzerstr. 1 +3, CH-3012 Bern (alfons.berger@geo.unibe.ch)

The different mechanical behavior between aseismic and seismic deformation is related to the mechanical strength of the fault rocks, which is closely linked to local hydrothermal growth of minerals in fault zones. In this context, we investigate the size and processes of cockade-like breccias in the Grimsel breccia fault (Central Alps, Switzerland). The cockades consist of rock clasts (‹particles›) of different size, surrounded by 30–40 µm thick concentric layers of hydrothermal minerals, chiefly quartz. These textures record multiple episodes of particle fluidization, which is a paleo-earthquake recorder.

Particle-size distributions indicate that fluid velocities during fluidization were at least in the range of ~0.1 ms^{-1}, but such flow rates are local and transient. They require rupture processes and concomitant pressure drops typical of earthquakes. In the literature similar cockade textures are interpreted as products of swarm seismicity rather than aftershock seismicity.

The record of episodic mantle growth around the cockade cores (clasts) is used to calculate fluid/particle mass ratios and the local hydrodynamics of quartz growth. Based on the solubility of SiO_2 in the fluids, these data indicate water/new-particle mass ratios of ~20–40 to precipitate each cockade. Due to the high local flow rates, fast quartz growth rates have to be inferred. The episodic nature of quartz precipitation is demonstrated by fluctuations in its trace element concentrations (e.g., Al). Such changes in Al-content may be related to kinetic effects during dissolution in the source region, to variations in precipitation rates or, more likely, dynamic versus stagnant fluid hydrodynamics in seismic versus interseismic stages.

The overprinting relationships between comminuted (non-cockade) breccias and cockade-like breccia show that seismic rupture processes and frictional granular creep alternate within the same structure. The creep versus rupture mechanisms depend, beside other factors, on the healing (cementation) processes inside such breccias, which are controlled by the above-mentioned hydrothermal processes

P 1.22

The Measurement of Fracture Toughness Anisotropy in Grimsel Granodiorite using Semi-Circular Samples

Nathan Dutler[1], Morteza Nejati[2], Florian Amann[3], Benoît Valley[1]

[1] *Centre for Hydrogeology and Geothermics, University of Neuchâtel, Rue Emile-Argand 11, CH-2000 Neuchâtel*
[2] *SCCER-SOE, ETH Zurich, Sonneggstrasse 5, CH-8092 Zurich*
[3] *Geological Institute, ETH Zurich, Sonneggstrasse 5, CH-8092 Zurich*

This experimental work aims at assessing the variation of mode I fracture toughness (K_{Ic}) with the variation of the angle between the fracture growth direction and the isotropy (foliation) plane. for a series of Grimsel Granodioritic specimens collected from cores of the in-situ stimulation and circulation project (Amann et al., 2017). Three-point-bending tests on semi-circular specimens were performed. The deformation field of the specimens was monitored using Digital Image Correlation (DIC). The foliation consist essentially of aligned phylosilicates minerals and influences the mechanical properties such as elasticity parameters, strength and fracture toughness. This is due to the fact that microcracks align preferentially within the foliation plane. Ultrasonic measurement indicates that the first p-wave arrival time varies in the range of 3.8 to 5.9 km/s. The strong velocitiy anisotropy with highest velocities (i.e. 5.9 km/s) are observed parallel and lowest velocities are observed normal to the foliation plane. Specimens were prepared with the foliation striking with a low anlge of 11 degree with the core axis and with the loading axis making angles of φ = 0° (loading paralell to foliation), 45°, 60° and 90° (loading perpendicular to foliation) with respect to the foliation plane. Depending on the angle, the strain field and the fracture trace show distinct characteristics. The critical fracture toughness values range from 0.63 to 1.89 MPa(m)$^{1/2}$. For a loading angle φ = 0°, the mean value is 0.73 MPa(m)$^{1/2}$, increasing to 0.99 MPa(m)$^{1/2}$ for φ = 45°, 1.30 MPa(m)$^{1/2}$ for φ = 60° and 1.66 MPa(m)$^{1/2}$ for φ = 90°. Figure 1 shows how the normalized fracture toughness values (i.e. normalized by the mean of the value corresponding to φ = 90° configuration) varies depending on the loading direction. The experimental findings are:

- As expected, critical fracture toughness is the lowest when the loading direction facilitate fracture propagation along foliation planes (φ=0°). Fracture toughness increase by a factor of -two to three when fracture popagation is forced to crosscut the foliation planes.
- The amount of intragranular fractures increase with fracture toughness value.
- Fracture propagation angle, fracture offsets along the fracture trace and strain fields are substantially affected by the orientation of the foliation plane with respect to the direction of fracture growth.

The experimental findings may explain an observation made during an in-situ hydraulic fracturing test in Grimsel Granodiorite at the Grimsel Test Site. Impression packer tests conducted after the hydraulic fracturing test indicate that the initial fracture trace coincides with the foliation plane, which is expected to show the lowest fracture toughness value. Further fracture propagation lead to a change in fracture orientation showed by seismic plane (Gischig et al, 2017). Theoretical considerations suggest that the change of orientation takes place in a clear fracture toughness-dominated region, which raises the question how the fracture toughness anisotropy and stress anisotropy compete to determine the direction of fracture propagation.

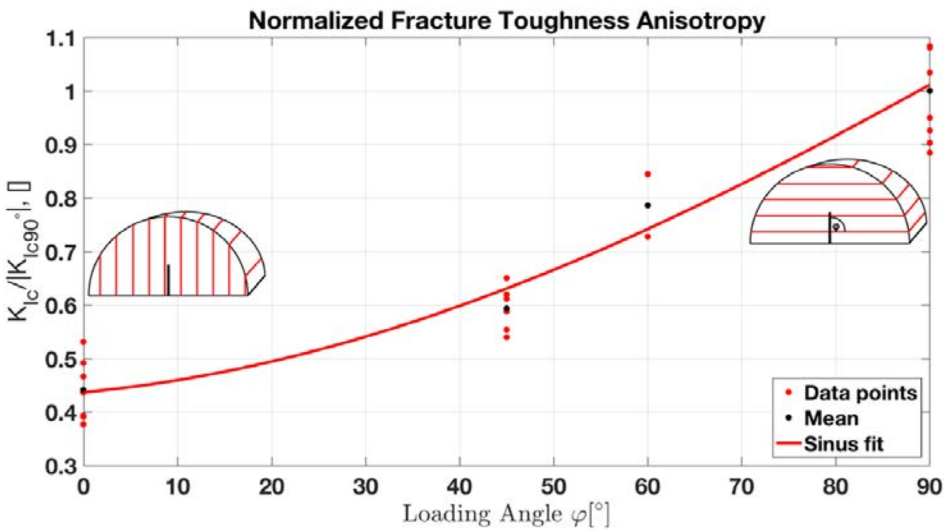

Figure 1: Normalized critical fracture toughness values (red dots) (i.e. normalized by the mean of K_{Ic90°) depending on the loading direction relative to the foliation orientation φ. The black points indicate the mean of each experimental configuration and the red solid one is a sinusoidal fit of the form Asin(φ+ϕ). The best fit parameters are an amplitude A=0.56 and a phase shift ϕ=0.7°.

REFERENCES

Amann, F., et al. (2017), The seismo-hydro-mechanical behaviour during deep geothermal reservoir stimulation: open questions tackled in a decameter-scale in-situ stimulation experiment. Solid Earth Discuss., https://doi.org/10.5194/se-2017-79

Dutler, N., Amann, F., Nejati, M., Valley, B. and Molinari, G. (in preparation), Experimental Investigation of Fracture Toughness and Critical Energy Release Rate on Grimsel Granodiorite

Gischig, V.S., Doetsch, J., Maurer, H., Krietsch, Amann F., H., Evans, K.F., Nejati, M., Jalali, M., Valley, B., Obermann, A., Wiemer, S. and Giardini, D. (2017), On the link between stress field and small-scale hydraulic fracture growth in anisotropic rock derived from microseismicity. Solid Earth Discuss., https://doi.org/10.5194/se-2017-78

P 1.23

A multiparametic evaluation of the Wallace-Bott hypothesis in the presence of a fluid source

Maria Kakurina[1], Yves Guglielmi[2], Christophe Nussbaum[3], Benoît Valley[1]

[1] *Center for Hydrogeology and Geothermics, University of Neuchâtel, Rue Emile-Argand 11, CH-2000 Neuchâtel (maria.kakurina@unine.ch)*
[2] *Lawrence Berkeley National Laboratory, University of California, 1 Cyclotron Rd, CA 94720 Berkeley*
[3] *Swisstopo, Seftigenstrasse 264, CH-3084 Wabern*

Wallace-Bott hypothesis postulates that the slip on each fault plane is colinear with the orientation of the resolved shear stress. Generally, stress inversion methods from fault/striae or focal mechanism datasets are based on this hypothesis. However, if this hypothesis is valid with a single planar fault plane situation in a homogeneous stress state, its validity is questionable when multiple faults or fault segments interact or when other processes like pore pressure diffusion due to fluid injections generates a non-uniform stress field. Earlier numerical methods confirmed that the slip orientation is not necessary parallel to the maximum resolved shear stress when computed from the far field stress tensor, but consistent with the local stress perturbations (Maerten, 2000, Xu et al., 2013, Lisle, 2013). In this work we focus on validation of the Wallace-Bott hypothesis in the presence of a fluid point source that may induce slip reorientations. We used the 3D distinct element method to build a numerical model consisting of deformable block with an embedded fracture. We applied fluid injection sequentially in the middle of the fracture to trigger the shear displacement and then compared the numerical slip vector with an analytical Wallace-Bott solution. Here, a multi-parametric study covering (i) fault geometry such as planar and non-planar faults (Figure 1), (ii) fault orientation, (iii) friction angle, (iv) dilation angles, (v) joint stiffness, was performed to understand the effect of each parameter on the misfit angle between the simulated slip vectors and the resolved shear stresses in the presence of the fluid source. It is shown that significant misfit can be found under specific configurations invalidating the Wallace-Bott assumptions (Figure 2). This misfit is a consequence of non-synchronous development of the slip that leads to the different displacement magnitudes within the fracture and, therefore, causes the stress perturbation.

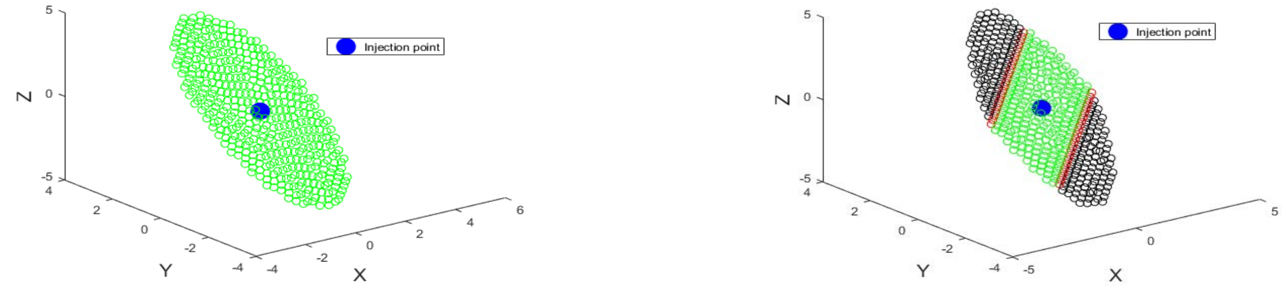

Figure 1. Geomentry of planar (left) and non-planar fractures (right)

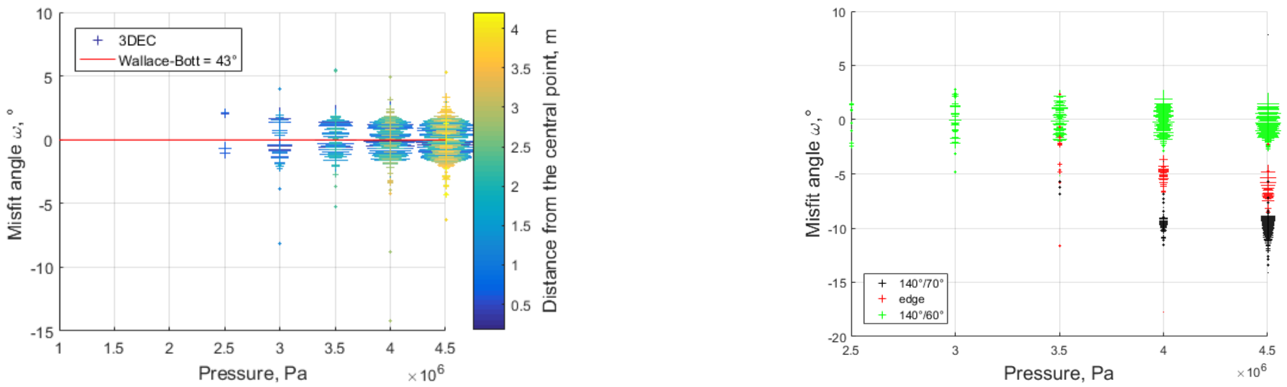

Figure 2. Left - The misfit angle between the slip vector computed using 3DEC and the analitical solution for the planar fracture (left) and non-planar fracture (right). The size of the crosses indicates relative displacement magnitudes. The colorbar on the left chart indicates the distance from the fluid injection source. Different orientation in the legend on the right chart correspond to the orientation of the fracture ramps.

REFERENCES

Lisle, R. J. (2013). A critical look at the Wallace-Bott hypothesis in fault-slip analysis. Bulletin de la Société Géologique de France, 184(4-5), 299-306.

Maerten, F. (2010). Adaptive cross-approximation applied to the solution of system of equations and post-processing for 3D elastostatic problems using the boundary element method. Engineering Analysis with Boundary Elements, 34(5), 483-491.

Xu, S., Nieto-Samaniego, A. F., & Alaniz-Álvarez, S. A. (2013). Origin of superimposed and curved slickenlines in San Miguelito range, Central México. Geologica Acta: an international earth science journal, 11(1).

P 1.24

Porosity of slates – from 3D bulk rock measurements to direct imaging

Vénice Akker[1], Josef Kaufmann[2], Guillaume Desbois[3], Jop Klaver[4], Janos Urai[3], Alfons Berger[1] & Marco Herwegh[1]

[1] *Institute of Geological Sciences, University of Bern, Baltzerstrasse 1+3, CH-3012 Bern (ismay.akker@geo.unibe.ch)*
[2] *Empa, Swiss Federal Laboratories for Materials Testing and Research, Überlandstrasse 129, CH-8600 Dübendorf*
[3] *Structural Geology, Tectonics and Geomechanics, Energy and Mineral Resources Group, RWTH Aachen University, Germany, Lochnerstrasse 4-20, 52056 Aachen, Germany*
[4] *Structural Geology, Tectonics and Geomechanics, Energy and Mineral Resources Group, RWTH Aachen University, Germany, Lochnerstrasse 4-20, 52056 Aachen, Germany & Map Microstructures and Pores GmbH, Lochnerstrasse 4-20, Aachen, Germany*

Sheet-silicate-rich rocks gain interest as they present a mechanically weak phase often associated with accretionary wedges. Under low grade metamorphic conditions, such rock types are able to take up large amounts of strain, hence representing the dominant mechanical weak phase in the upper crust. Their rheological behaviour is strongly dominated by the highly anisotropic deformation behaviour of the sheet silicates. In addition, their water content represents a second component weakening the overall strength of such aggregates either by reducing the strength of the individual grains: (i) crystal and interlayer water or (ii) of the entire aggregate by increased pressure of interstitial pore fluids. Studying the pore network of slates is therefore crucial, as these present the main fluid conduits. In the current study, we aim to gain a profound understanding of the porosity network in slates and access problems such as sample heterogeneity, pore connectivity and the originality of the studied pores. Presented is an overview of different analytical techniques to estimate porosity in slates, including representative element volumes and areas (REV and REA) at different scales.

Porosity analyses are performed on slates from the Flysch units in the Glarus Alps in Switzerland. We include bulk rock porosity measurements such as helium pycnometry and mercury intrusion porosimetry (MIP) as well as direct imaging of porosity using BSE-SEM and high-resolution BIB-SEM images. A combination and comparison of these methods is used to unravel and discuss strengths and weaknesses of the different methods for pore characterisation at different REV and REA: (a) cm^3, (b) mm^3, (c) mm^2, (d) μm^2.

(a-b) Bulk rock porosity measurements have the advantage of providing the connected porosity on a 3D bulk volume. These bulk methods give a higher porosity value than the direct image analysis (c-d), which is due to the strong influence of fractures and potential sample heterogeneity in large cm^3-sized REV. With this respect, the discrimination of type and amount of fracture porosity is crucial, since it might be either in-situ or not in-situ induced by unloading requiring spatial information.
(c) Therefore a combination of bulk rock methods with digital image analysis provides information on a sample's 2D heterogeneity and the different fracture and porosity types. Moreover, image analysis on BSE-SEM images of polished thin sections is based on areas of about 0.5 mm^2 and excludes fractures at the mm-scale but gives insights into microcracks and matrix porosity.
(d) At the smallest scale BIB-SEM analysis allows detecting pores until tens of nm size. Besides, this technique gives information about pore morphologies, the spatial resolution of pores and pore related mineral phases.

Combining the different results has the great opportunity to evaluate and estimate the porosity values over a large range in scales. We use direct imaging of porosity by BSE-SEM and BIB-SEM as feedback on the bulk rock measurements. This enables to discriminate not in-situ pores (i.e. unloading, weathering, and drying) included in bulk rock measurements from the in-situ ones along the deformation path using direct BIB-SEM imaging.

P 1.25

Mimicking Alpine thrusts by orogenic passive deformation of synsedimentary normal faults: a record of Jurassic extension of the European margin (Mont Fort nappe, Middle Penninic, Western Alps).

Adrien Pantet[1], Jean-Luc Epard[1] & Henri Masson[1]

[1]Institut des sciences de la Terre, Université de Lausanne, Bâtiment Géopolis, CH-1015 Lausanne (adrien.pantet@unil.ch)

The Mont Fort nappe is the upper tectonic subdivision of the former Grand St-Bernard (GSB) nappe (Escher 1988, Escher et al. 1997). Subsequent research has confirmed its tectonic and stratigraphic independence from the rest of the GSB nappe (e.g. Gouffon 1993). It consists of a Paleozoic basement overlain by a thin Mesozoic sedimentary cover, comprised of very thin, discontinuous Triassic quartzite and dolomite, a thin limestone layer, and for the greater part of breccias of variable thickness mostly made of dolomitic elements ("reconstituted Triassic"). These breccias are overlain by a more massive limestone topped by a thinner upper breccia rich in elements of quartzite. Called by Escher (1988) the Evolène series, this sequence presents remarkable similarities with the stratigraphic column of the Breccia nappe in the Prealps which typically belongs to the Prepiemontese paleogeographic domain (Lemoine 1961, Escher 1988). This similarity strongly suggests an earliest Jurassic age for the lower limestone, a late Early to Middle Jurassic age for the main mass of breccias (Lower Breccia), and a Late Jurassic to earliest Cretacous age for the upper limestone and the Upper Breccia. We will not discuss here the status of the Cretaceous calcschists (Série Rousse, Marthaler 1984) that overlie the Evolène series and are the subject of research in progress.

These ages are generally accepted. However, several authors proposed a different tectonic model where the Evolène series would be allochthonous over the Mont Fort basement (e.g. Sartori & Marthaler 1994, Marthaler et al. 2008). Their contact would be an Alpine thrust. The main argument would be that this contact surface often cuts with an angular discordance the stratigraphy of the Evolène series. Consequently, this series would not be the original sedimentary cover of the Mont Fort basement but would belong to a distinct tectonic unit that these authors identified with the Cima Bianca nappe (classically defined as a slice of Late Paleozoic to Mesozoic sediments separating the ophiolitic Zermatt-Saas and Tsaté nappes; Vannay & Allemann 1990, Steck et al. 2015). This proposition has been widely accepted (e.g. Tectonic map of Switzerland 2005).

Our observations don't support this proposition. They rather confirm the tectonic reconstruction of Escher (1988) and suggest that the Evolène series is indeed the autochthonous cover of the Mont Fort basement. The main points are:
-- At many places the contact is concordant and shows a good preservation of the basal levels of the Mesozoic sequence, without any hint of tectonic disturbance or anomalous rock deformation.
-- The discordance observed at other places, which can put the Jurassic breccia in contact with all older formations, can be conveniently explained by synsedimentary normal paleofaults. By means of strain theory (e.g. Ramsay 1967) it is easy to demonstrate that passive deformation of such faults during Alpine compression can mimic thrusts.
-- The sedimentary characteristics of the Evolène series, typicall of the Prepiemontese domain, are very different from those of the Cima Bianca unit, much poorer in breccias and whose relatively thick Triassic formations of quartzite and carbonates show a Briançonnais affinity.

Conclusion : The Evolène series is the sedimentary cover of the Mont Fort nappe. During Jurassic times it has been strongly affected by synsedimentary normal faulting, generating stratigraphic gaps, synsedimentary anomalous contacts and internal discordances. These structures provide a spectacular record of the extension of the European margin during the opening of the Alpine Tethys. Then Alpine compression passively deformed these faults in such a way that they mimic Alpine thrusts.

REFERENCES

Escher, A. 1988: Structure de la nappe du Grand Saint-Bernard entre le val de Bagnes et les Mischabel. Service hydrologique et géologique national, Berne.

Escher, A., Hunziker, J., Marthaler, M., Masson, H., Sartori, M., & Steck, A. 1997: Geologic framework and structural evolution of the western Swiss-Italian Alps. In O. A. Pfiffner et al. (Eds.): Deep structure of the Swiss Alps: results of NRP 20, 205–221. Birkhaüser, Basel.

Gouffon, Y. 1993: Géologie de la «nappe» du Grand St-Bernard entre la Doire Baltée et la frontière suisse (Vallée d'Aoste, Italie). Mém. Geol. (Lausanne) 12.

Marthaler, M., Sartori, M., Escher, A. & Meisser, N. 2008. Feuille 1307 Vissoie. Atlas géologique Suisse 1:25'000, Carte et Notice explicative 122.

Sartori, M. & Marthaler, M. 1994: Exemples de relations socle-couverture dans les nappes penniques du Val d'Hérens. C.-r. Excursion Soc.Géol. Suisse et Soc. Suisse Minér. Pétr., Schweiz. Miner. Petr. Mitt. 74, 503-509.

P 1.26

Basement-cover interaction in the Jura Mountains: Where, how and to what degree?

Marc Schori[1], Jon Mosar[1]

[1] *Department of Geosciences, Earth Sciences, University of Fribourg, Chemin du Musée 6, CH-1700 Fribourg (marc.schori@unifr.ch, jon.mosar@unifr.ch)*

The compelling shape of the Jura Mountains fold-and-thrust belt and its role in the Northern Alpine Foreland has been investigated for more than a century. Until the present day we know two important parameters that have controlled the large-scale geometry of the fold-and-thrust belt: First, *the presence of weak Triassic evaporites* allowed a décollement above which the Jura Mountains evolved during Miocene, while the Molasse basin was pushed north-westwards as an intact unit (Buxtorf 1907). Secondly, the limits of the décollement arose from *discontinuities in the Triassic evaporites* which controlled the spatial extent of the Jura Mountains.

Abundant studies have shown that continental Europe underwent several deformation phases with changing regional stress, both before and after Triassic times. The Permo-Carboniferous grabens known from NE Switzerland are evidence of a pre-Mesozoic deformation phase. Geomorphologically more striking is the younger Eocene-Oligocene European Cenozoic Rift System (ECRIS) with the Bresse Graben (BG) and Upper Rhine Graben (URG) bordering the Jura Mountains. These two grabens and the associated transfer zone determined the farthest extent of the Jura Mountains fold-and-thrust belt. The Triassic evaporites are substantially offset at the graben borders which prevented a further north-westwards progression of the décollement during Miocene. Boreholes in the outmost external Jura reveal a thrusting of the Mesozoic cover of the Jura Mountains onto Tertiary sediments of the adjacent graben (Michel et al. 1953).

The example of the ECRIS gives rise to questions that are still difficult to answer. How far underneath the Jura Mountains does the ECRIS stretch its influence? Where, how and to what degree did older pre-Eocene deformations determine the shape of the Jura Mountains?

Numerous pioneering ideas and works on the topic of basement-cover interaction in the Jura Mountains are restricted to subareas in the Jura, where boreholes or seismic lines are available. However, it became apparent that a single deformation solution for the whole of the fold-and-thrust belt is unlikely and indeed, intriguing geomorphological differences between Eastern, Central and Western Jura Mountains encourage more investigation. Therefore, in a more holistic approach, we compile and combine geophysical and structural information all across the Jura Mountains and still more importantly, across the surrounding area which is unaffected by Miocene thin-skinned tectonics in order to discuss possible basement-cover interactions on regional scale, underpinned by distinct exemplary structures.

REFERENCES

Buxtorf, A. 1907: Zur Tektonik des Kettenjura. Bericht der Versammlung des Oberrheinischen Geologischen Vereins , 40, 79-111.

Michel, P., Appert, G., Lavigne, J., Lefavrais, A., Bonte, A., Lienhardt, G. & Ricour, J. 1953: Le contact Jura-Bresse dans la région de Lons-le-Saunier. Bulletin de la Société Géologique de France , 6, 593-611.

P 1.27

Analysis of geomorphic indices in the westernmost area of Switzerland: Implications for neotectonics

Omar M.A. Radaideh[1] & Jon Mosar[1]

[1] *Department of Geosciences and Earth Sciences, University of Fribourg, Chemin du Musée 6, 1700 Fribourg, Switzerland (o.sabbah@ymail.com)*

Geomorphic responses to tectonic forcing have been evaluated by analysis of five morphometric parameters, including elevation-gradient index, bankfull channel dimensions, Transverse Topographic Symmetry index (TTS), drainage basin asymmetry index (AI), and hypsometry curves, together with geological field work and available geophysical data (gravity and magnetic). We analysed sixty-five catchments, topographic swath and longitudinal profiles of three main rivers that are located at transition of the Jura fold-and-thrust belt and the Molasse basin in the vicinity of Pontarlier Fault system in western Switzerland. Field work was conducted to identify drainage anomalies and verified whether they are or not caused by lithological or/and structural controls. Geophysical data was used to delineate the subsurface structures that can be correlated with surface-identified anomalies. Bankfull channel dimensions were obtained from a high-precision DEM using the River Bathymetry Toolkit (RBT). A hypsometric curve describes the relative distribution of an area at different elevations within a drainage catchment (Strahler 1952).

Indeed the change in dimension of drainage area may play a more important influence on hypsometry than the uplift and erosion rates themselves. To avoid any obvious pitfalls related to changes in drainage area, we propose calculating HI values not only for the catchments but also for three different regularly spaced grids (1km, 2km, and 3km) using two different resolution DEMs (2m and 30m). This allowed us to quantify the degree of similarity between the results obtained from different scale sizes and DEM resolutions. A significant degree of similarity was found between the hypsometric integral maps obtained from different resolution DEMs and different grid sizes, indicating that there is no clear dependency in the study area between the hypsometry values and both grid size and DEM resolutions. The hypsographic curves of the selected catchments, however, reveal twenty-one different patterns of landscape, representing all types of landform development described by Strahler (1952).

Lateral stream migration or asymmetric basins, which are generally caused by tectonic tilting effects, can be identified by TTS and AI analysis (Cox 1994; Keller & Pinter 2002). Different directions of lateral channel migrations were detected in the area (Figure 1). Analysis of swath and longitudinal profiles of three rivers shows sudden and dramatic changes in the elevation-slope gradient and the bankfull channel dimensions along the whole length of their courses. These geomorphic anomalies which are associated with pronounced changes in gravity and magnetic properties are linked to the role of neo-tectonic activity within the area.

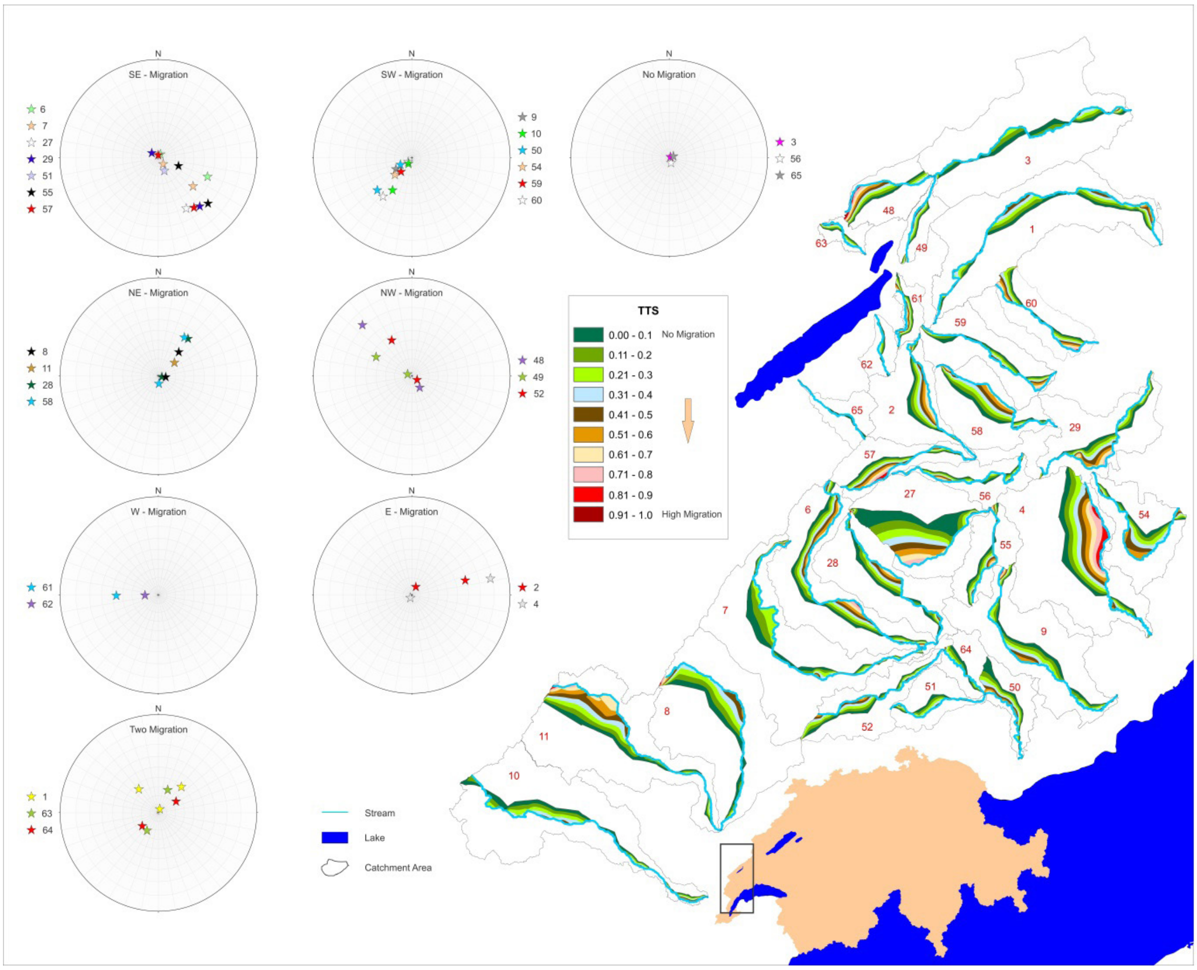

Figure 1. Transverse Topographic Symmetric index (TTS) of selected catchments in the westernmost area of Switzerland. Polar plots showing estimated TTS averages for each watershed. T-index values range from 0 on the centre of polar plot (stream flowing near the catchment midline) to 1 on the outer margin of the polar plot (stream flowing near vicinity of catchment margins).

REFERENCES

COX, R. T. (1994): Analysis of drainage basin symmetry as a rapid technique to identify areas of possible Quaternary tilt-block tectonics: an example from the Mississippi Embayment. Geological Society ofAmerica Bulletin, 106(5), 571—581.

Keller, E.A. & Pinter, N. (2002): Active Tectonics, Earthquakes, Uplift and Landscape. 2nd Edition, Prentice Hall, Upper Saddle River, 362.

Strahler, A. N. (1952): Hypsometric Area-Altitude Analysis of Erosional Topography. Geological Society of America Bulletin, 63(11), 1117-1142.

P 1.28

Three-dimensional measurement of limestone fracture network from the La Sarraz Fault Zone using high resolution X-ray µ-computed tomography

Nicole Schmitt[1], Benjamin Verbeken[1], Marius Gruber[1], Stephan Miller[2], Benoît Valley[2] & Jon Mosar[1]

[1] *Départment de Géosciences - Sciences de la Terre, Université de Fribourg, Chemin du Musée 6, CH-1700 Fribourg, (jon.mosar@unifr.ch)*
[2] *Center for Hydrogeology and Geothermics, University of Neuchâtel, Rue Emile-Argand 11, CH -2000 Neuchâtel*

The Eclépens quarry is located between two branches of the La Sarraz Fault system, in the Upper Cretaceous limestone of the Jura Fold-and-Thrust Belt (JFTB), and is geographically situated in the Molasse Basin. The dextral strike-slip La Sarraz Fault system is a conjugate fault system to the larger N-S trending sinistral Pontarlier fault system. The fault systems reach from the folded and detached (JFTB) into the detached and weakly deformed Molasse Basin and do not extend into the underlaying basement. The hectometre-scale subvertical faults outcropping in the Eclépens quarry strike NW-SE. Minor faults in the quarry are oriented NW-SE, N-S and NE-SW, indicating the development of a complex Riedel system. The Mormont Anticline exposed at the southeastern termination of La Sarraz fault northern branch (Mormont Fault) shows a NE-SW orientation. This anticline is absent to the southwest of the of the fault zone. The location and geometry of the faults were reconstructed using seismic profiles and the Eclépens-1 borehole and surface data. Our study is part of a larger joint venture between Swisstopo, the Department of Geosciences of University of Fribourg and Center for Hydrogeology and Geothermics of the University of Neuchâtel. We present results from a set of twenty-four oriented samples collected from the Eclépens quarry in the near vicinity of two main dextral strike-slip faults with an orientation NW-SE and E-W. Cylinders, varying from 2 to 8 cm diameter and 4 to 9 cm length, were drilled from hand samples and subsequently scanned by Bruker CT-scan 2211 beam hardening µCT-scan (Parameters: microfocus, high energy, voltage (160-170 kV) cupper filter, current (120 µA) and pixel size varying from 15 – 56 µm). The size of the sample determines the scan resolution; the smaller the sample the higher the resolution. This method provides 3D volume reconstruction, visualisation and quantification of the internal features, such as fractures and mineral content. Once the internal features are selected, a 3D skeleton model is generated (figure 1). The construction of a 3D skeleton model permits the quantification of parameters from the internal features, i.e porosity, connectivity and area/volume. One sample from each segment of the damage zone was analysed in order to observe the changes of the internal features of each sample. The obtained results are described as a function of its location in the damage zone of the specimen: [i] Fractured host rock (Sample (S):15, Porosity (P): 0%, Pyrite (Py): 0%); [ii] discrete fault zone between fractured host rock and non-foliated cataclasite (S:16, P:3.4%, Py:0.06%); [iii] Non-foliated cataclasite (S:30, P:2.99%, Py 0.7%); [iv] Foliated cataclasite (S:32, P:3.4%, Py:0.1%) & (S:36, P:1.3%, Py: 0.3%); [v] Fault breccia (S:39, P:5.43%, Py: 0.1%). The fractures of the analysed samples are connected and the density (/mm^3) of the open space is measured: sample 16 (0.89/mm^3), sample 30 (3.77/mm^3), sample 32 (0.82/mm^3), sample 36 (0.2/mm^3), sample 39 (3.91/mm^3). On the 3D skeleton large fractures are identified cross-cutting the samples from the top to the bottom, we define the area of these fractures on sample 30 (12’966 mm^2), 32 (11’764 mm^2) and 39 (22’536 mm^2). On sample 16 and 36 the fractures are non-connected open spaces, further open space is dispersed in the matrix. From our investigation we see that the porosity in Mormont Fault varies from 2.99% to 5.43%, the open spaces are connected in only a few samples such as sample 30, 32 and 39. It is important to quantify the connection of the pores in a sample to understand the pathway of fluid circulation. With the utilisation of the present method, it is possible to visualise, model and quantify the open spaces, area and connectivity from each sample.

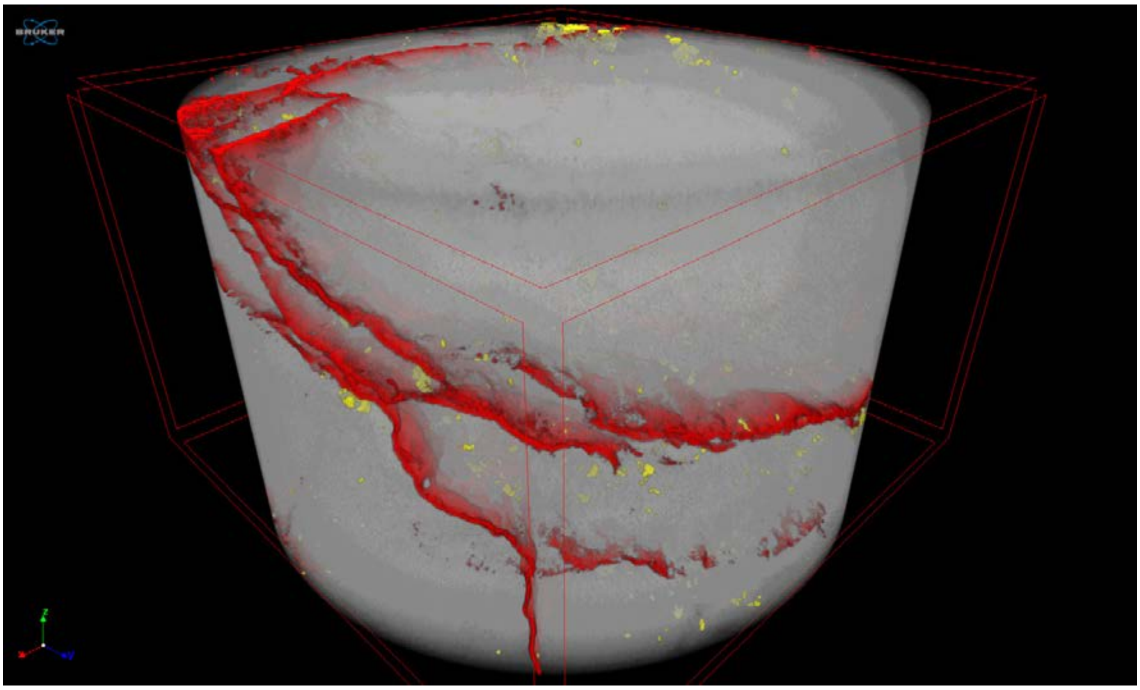

Figure 1 : Reconstructed 3D skeleton model from sample 30 (D: 4x3.6 cm), is from the non-foliated cataclasite of Mormont Fault, pixel resolution of 22 μm. The idiomorphic shape of pyrites (yellow) are in the border of the fractures and dispersed on the matrix of the sample resulted from iron-sulphur rich fluid circulation. It was calculated porosity of 2.99% and pyrite content of 0.7%.

P 1.29

Tectonic structure and dynamic of the Neuchâtel Jura Mountains: new insight from detailed mapping and forward modelling techniques

Valentin Rime[1], Jon Mosar[1]

[1]*Department of Geoscience, Unit of Earth Sciences, University of Fribourg, Chemin du Musée 6, CH-1700 Fribourg (valentin.rime@unifr.ch)*

The Jura fold-and-thrust belt is probably one of the most studied worldwide. Nevertheless, several interesting scientific questions remain unanswered, in particular about the deep tectonic structure for which few data exist. Almost no wells were drilled in the Internal Jura and the scarce seismic lines shot in the area of investigation are not of a sufficient quality to precisely constrain the deep tectonic structure. On the other hand, good outcropping conditions allow a precise understanding of the shallow structure.

This study focusses on the Neuchâtel Jura Mountains and its neighbouring French part on a Travers - Brévine - Morteau section, where the Mesozoic cover is situated at relatively high topographic elevation. Detailed field mapping was conducted in order to constrain a near surface cross-section. Forward modelling was subsequently done in the Move™ software by Midland Valley. The goal of this modelling was to understand the observed surface structure in a kinematically and geometrically consistent forward model.

The proposed solution features a large-scale low-angle thrust fault with a staircase trajectory on which several hinterland-verging thrust are rooting. Our model implies a secondary detachment in the *Opalinus Ton* and a partial doubling of the Mesozoic cover which explains the high topographic position of outcropping sediments. This type of structure is similar to the one proposed by Schori et al. (2015) and is an alternative to the traditional overthickening of Triassic evaporites associated with a unique décollement “zone” and which induces balancing inconsistencies. Along our profile the Jura Mountains accommodate a shortening of 8.5 km, corresponding to a relative shortening of 33%. According to Smit et al. (2003), this amount of shortening implies that locally, the orogenic wedge already attained a state of equilibrium with stable sliding along the basal détachment level.

The kinematic implications of the forward model indicate an oscillating, sequence of thrusting, rather than a forward directed in sequence thrust succession. Interestingly the first formed anticline (according to our model) also marks the northernmost limit of tertiary marine sediments (Piquerez et al., 2011). It is therefore tempting to imagine that this nucleating anticline formed a physical barrier which marked the northern coast of the sea associated with the Molasse Basin. Terrestrial sediments, including coarse breccia, north of this limit have been dated at 17 Ma, while marine conditions were still prevailing south of it at the same time (Kälin et al., 2001). Supported by our kinematic modelling and the sedimentary record, the question therefore arises to know whether this could be used to constrain the dating of the first deformation of the Jura Mountains which would then be older than previously accepted.

REFERENCES

Kälin, D., Weidmann, M., Engesser, B., and Berger, J. P. (2001). Paléontologie et âge de la Molasse d’eau douce supérieure (OSM) du Jura neuchâtelois. Mémoires suisses de Paléontologie, 121, 65-99.

Piquerez, A., Berger, J.-p., Mennecart, B., and Mosar, J. (2011). Molasse Basins in the Jura mountains - an ArcGIS database. Poster of the 19th SwissSed Meeting.

Schori, M., Mosar, J., and Schreurs, G. (2015). Multiple detachments during thin-skinned deformation of the Swiss Central Jura : a kinematic model across the Chasseral. Swiss Journal of Geosciences, 108 (2-3), 327-343.

Smit, J. H. W., Brun, J. P., and Sokoutis, D. (2003). Deformation of brittle-ductile thrust wedges in experiments and nature. J. Geophys. Res., 108(B10).

P 1.30

Distribution of HP rocks in the nappes of the Lepontine Dome

Filippo Luca Schenker[1], Christian Ambrosi[1], Cristian Scapozza[1], Dorota Czerski[1], Matteo Maino[2], Claudio Castelletti[1,4] & Yves Gouffon[3]

[1] *Institute of Earth Sciences, University of Applied Sciences and Arts of Southern Switzerland (SUPSI), Via Trevano, CH-6952 Canobbio (filippo.schenker@supsi.ch)*
[2] *Dipartimento di Scienze della Terra e dell'Ambiente, University of Pavia, via Ferrata 1, 27100 Pavia, Italy*
[3] *Swiss Geological Survey, Federal Office of Topography swisstopo, Seftigenstrasse 264, CH-3084 Wabern*
[4] *now at CSD Ingegneri SA, Via P.Lucchini 12, 6901 Lugano, Svizzera*

Published petrological data on pressure and temperature are critically reviewed, and positioned on the new geological map and cross sections (1:10'000) of the Osogna sheet that includes most nappes of the Lepontine Dome (Central Alps). The goal is to place the P-T metamorphic conditions on the geological, structural and tectonic framework that was recently mapped.
The questions we seek to answer are: How is the pressure distributed within the tectonic units and within the Lepontine Dome? Do we observe sharp or gradual pressure gradients within the tectonic units? Can the HP conditions be averaged/ extended over the tectonic units? If not, do they correspond to conditions of observable subunits, or do they reflect anomalies in the pressure field? Answering these questions may lead to controversial results and is fundamental to better understand the thermobarometric evolution patterns of the Lepontine Dome and the formation of tectonic nappes in general.

P 1.31

Ophiolites in the North Himalayan nappes and Indus Suture Zone in Eastern Ladakh (NW Himalaya, India)

Nicolas Buchs[1] and Jean-Luc Epard[1]

[1]*Institut des sciences de la Terre, Université de Lausane, CH-1015 Lausanne*

Ophiolites are fragments of ancient oceanic lithosphere, preserved in orogenic belts in a context of plate convergence. They are generated at mid-ocean ridges, in a supra-subduction zone or volcanic arc. Commonly, several magmatic events are recorded, as shown, for instance, in the Oman Ophiolite (Goodenough et al. 2014).
The Ophiolitic rocks of Eastern Ladakh are subdivided in two main groups, based on the geodynamic setting during their formation: the supra-subduction zone ophiolite and the ophiolitic "mélanges", corresonding both to the Indus Suture Zone. Recent detailed studies North-East of the Tso Moriri area revealed a large diversity of ophiolitic rocks and associated sediments. We identified three distinct tectonic units containing ophiolites: The Nidar Ophiolite, the Drakkarpo nappe and the Karzok-Ribil nappe.
The Nidar supra-subduction zone Ophiolite represents a complete ophiolitic sequence, from mantle to sediments, which underwent a low greenschist facies metamorphism. This ophiolitic sequence was thrusted towards the South. They record a first magmatic event in a mid-ocean ridge setting, and a second one in a supra-subduction zone at around 130 Ma.
The Drakkarpo nappe is a "mélange" unit composed of thick polygenic conglomerates and volcano-sedimentary rocks, mainly composed of tuffs and augite-basalts (OIB), serpentinites, pillow lavas and gabbros. This unit is interpreted as being a part of an accretionary wedge containing slices of oceanic islands arc. This nappe marks the Indus Suture Zone.
The Karzok-Ribil nappe is a newly defined tectonic unit involved in the North Himalayan nappe stack. It can be followed at the top of the Tetraogal nappe and around the Tso Morari dome. The Karzok-Ribil nappe is composed of segments of ophiolitic sequence (serpentinites, gabbros, pillow lavas), radiolarites, polygenic conglomerates, agglomeratic slates from the indian margin, augite-basalts (OIB) and limestones. It is interpreted as being originally a seamount, located close to the Indian passive margin in a ocean-continent transition zone.
The new lithostratigraphy and structural analyses of the Eastern Ladakh ophiolites and their associated sediments allow us to better constrain the formation and emplacement mechanisms of these tectonic units. It defines or precises the paleogeography and geometry of the north Indian passive margin, prior to the Himalayan collision.

REFERENCES

Goodenough, Kathryn M., Robert J. Thomas, Michael T. Styles, David I. Schofield, and Christopher J. MacLeod. 2014. "Records of Ocean Growth and Destruction in the Oman–UAE Ophiolite." *Elements* 10 (2): 109–114.

P 1.32

Late Eocene to recent tectonic evolution of the northern Internal Dinarides (western Serbia)

Ana Mladenović[1], Vladica Cvetković[1], Branislav Trivić[1], Vesna Cvetkov[1]

[1]University of Belgrade – Faculty of Mining and Geology, Đušina 7, Belgrade, Serbia

The Internal Dinarides are part of a complex suture zone situated in the central area of the Balkan Peninsula, which present-day tectonic pattern is the result of the latest Jurassic – Cretaceous subduction of the Neotethys ocean, followed by Cenozoic post-collisional and neotectonic phases. Although some of these tectonic phases are relatively well studied, facts about others are still under debate. In this study, we integrate data on fault kinematics, anisotropy of magnetic susceptibility and focal mechanisms of earthquakes in order to determine and discuss tectonic phases that were active in the area of the northern Internal Dinarides in western Serbia since the Late Eocene.

Data for paleostress analysis were collected in different geological and tectonic units, using all outcrops where fault-slip indicators could be observed. In total, fourteen stations were located in Permian and Triassic limestones, Jurassic serpentinized peridotites and rocks of the ophiolitic mélange (mostly limestones), Oligocene dacites and Miocene granites, limestones and marls. Slip along the studied fault planes was determined using linear slip sense indicators: striations, fibers of calcite, magnesite and serpentine minerals, systematic elongation of feldspars, among other indicators. Database of earthquakes in this research was formed using the catalogues of the International Seismological Center and the Serbian Seismological Survey. In total, 38 focal mechanisms for earthquakes with magnitudes higher than 3 were calculated based on the polarities of first P-wave arrivals. In order to calculate tectonic stress tensor, formal stress inversion of the focal mechanisms was performed. Anisotropy of magnetic susceptibility (AMS) was carried out on the Bukulja Mts. S-granite, in order to directly correlate these data with paleostress data. Standard cores for AMS analysis were drilled and oriented in situ at nine locations. Based on these data, the principal AMS ellipsoid axes were calculated on specimen and locality levels.

The obtained results indicate that in the area of the northern Internal Dinarides at least three brittle post-collisional phases occurred since Middle/Late Eocene times. These brittle tectonic phases caused shortening and thrusting within the Dinaric orogen, and were most probably associated with magmatism and formation of smaller sedimentary basins within the Internal Dinarides.

The first deformational phase is characterized by generally NNW – SSE oriented compressional axis that acted in a transpressional tectonic regime. It was most probably active from the end of the Middle Eocene up to the Late Oligocene. This tectonic phase may have represented the prolongation of thrusting within the Dinaric orogen, and was likely a controlling factor for the genesis of Oligocene intermediate/acid volcanism in the northern Internal Dinarides.

The second deformational phase most likely started by the beginning of the Early Miocene and was characterized by NE – SW extension. It was related to the Pannonian extension, and in this area of the northern Internal Dinarides it caused formation of smaller sedimentary basins of the so-called Dinaric Lake System. However, based on previous petrological research as well as on new AMS results from the Bukulja Mts. S-granite, we suspect that this tectonic phase could be separated into two sub-phases – the older one that likely controlled Miocene quartzlatitic volcanisam within the wider research area, and the younger one that was related to the formation and exhumation of the S-type granites situated along the contact of the Dinarides and the Pannonian basin.

The beginning of the youngest deformational phase likely coincides with the onset of the basin inversion in the Pannonian area and Dinaric Lake System, which started in the Late Miocene. According to the study of focal mechanisms, the same stress field remained active in the recent time. The results of formal inversion of earthquake focal mechanisms show that the recently active stress tensor is characterized by a NE – SW maximal compressional axis that operates in a strike-slip regime. The recent stress field in the research area is characteristic for the areas situated relatively far from the source of the main tectonic stress, where local influences are expected to play an important role. These local influences here are superposed to the main tectonic controlling factors in the research area, which is defined as the northward motion and simultaneous counterclockwise rotation of the Adriatic microplate.

P 1.33

Blind thrusts under Tbilisi, Georgia

Victor Alania[1], Onise Enukidze[1], Niko Tevzadze[2]

[1] *Tbilisi State University, M. Nodia Institute of Geophysics, Alexidze str.1. 0161, Tbilisi, Georgia (victor.alania@tsu.ge)*
[2] *Georgian Oil and Gas Ltd., Freedom Square 4a, Tbilisi, Georgia*

Our study area, Tbilisi and surrounding area is located frontal part of eastern Achara-Trialeti fold-and-thrust belt. The Achara-Trialeti fold-and-thrust belt, which is one of the good examples of the collision-driven far-field deformations, locates within the northernmost part of the Lesser Caucasus and is associated with Arabia-Eurasia convergency. Building of thick-skinned structures of eastern Achara-Trialeti was formed by basement wedges propagated along detachment horizons within the cover generating thin-skinned structures (Alania et al., 2017a, 2017b).

Our interpretation has integrated seismic reflection profiles, several oil-wells, and the surface geology data to reveal structural characteristics of the eastern Achara-Trialeti fold-and-thrust belt. Fault-related folding theories were used to seismic interpretation (Shaw et al., 2006; Suppe, 1983). Seismic reflection data reveal the presence of south-vergent and north-vergent fault-propagation folds, duplex and structural wedge. The rocks are involved in the deformation range from Mesozoic to Cenozoic strata.

Interpreted industrial seismic refection profiles, serial balanced cross-sections, and recent earthquakes reveal the presence of an active blind thrust fault beneath Tbilisi. 2-D and 3-D structural models show that 2002 M_w 4.5 Tbilisi earthquake related to a north-vergent blind thrust. Empirical relations between blind fault rupture area and magnitude suggest that these fault segments could generate earthquakes of $M_w \sim 6.5$.

On base of published information about historical and recent earthquake data (Tsereteli et al., 2016), and syntectonic units from frontal part of eastern Achara-Trialeti fold-and-thrust belt (Alania et al., 2016) we conclude that compressive deformation started in Middle Miocene and continues today.

REFERENCES

Alania, V., Chabukiani, A., Enukidze, O., Razmadze, A., Sosson, M., Tsereteli, N., & Varazanashvili, O. 2017a: Structural model of the eastern Achara-Trialeti fold and thrust belt using seismic reflection profiles. Geophysical Research Abstracts, Vol. 19, EGU2017-5064.

V. Alania, Sosson, M., Enukidze, O., Asatiani, N., Beridze, T., Candaux, Z., Chabukiani, A., Giorgadze, A., Gventsadze, A., Kvavadze, N., Kvintradze, G., & Tsereteli, N. 2017b: Structural architecture of the eastern Achara-Trialeti fold and thrust belt, Georgia: Implications for kinematic evolution. Geophysical Journal, 4, 81-82.

Alania, V., Chabukiani, A., Chagelishvili, R., Enukidze, O., Gogrichiani, K., Razmadze, A., & Tsereteli, N: 2016. Growth structures, piggyback basins and growth strata of Georgian part of Kura foreland fold and thrust belt: implication for Late Alpine kinematic evolution. In: Tectonic Evolution of the Eastern Black Sea and Caucasus (eds. Sosson M., Stephenson R., Adamia Sh.). Geological Society, London, Special Publications no. 428. First published on October 27, 2015, doi:10.1144/SP428.5.

Tsereteli, N., Tibaldi. A., Alania, V., Gventsadse, A., Enukidze, O., Varazanashvili, O.,& Müller, B.I.R. 2016: Active tectonics of central-western Caucasus, Georgia. Tectonophysics, 691, 328–344.

Shaw, J., Connors, C. & Suppe, J. 2006: Seismic interpretation of contractional fault-related folds. AAPG Studies in Geology 53, 156.

Suppe, J. 1983: Geometry and kinematics of fault-bend folding. American journal of Science 283, 684 - 721.

P 1.34

Travertine occurrences along major neotectonic normal fault zones in the Hammam Debar- Roknia Guelma region, North-East Algeria

Ouided laziz[1], Fouad Bouaja[1], Chaouki Benabbas[1]

[1]*Geology and Envirmnment Constantine University Ain Elbey Constantine Algeria*

The tectonic history of Pliocene-Quaternary structures has been documented in Guelma region from Quaternary travertines and faults relationships. Quaternary travertines deposited from hot springs can reveal much about the neotectonic attributes and histories of structures. The largely developed travertines in the Roknia- Hammam Debar are subdivided into several sequences including the most recent Are observed at the level of the Hammam Debar recent sources. For facies are observed; the mammal and reed facies in proximal bed, massive and laminated facies in distal bed. In Roknia- Hammam Debar structural studies, field mapping and tectono-stratigraphical considerations on Pliocene and Quaternary units indicate two fault populations: N10 ° E are associated with Block detachments, collapses and the development of several fibrous calcite generations. These observations prompted us to Classify as probably seismic tectonic structures. N140 ° E structures already mapped as Seismic structures (Maouche et al 2013) are also affected Roknia travertine .

P 1.35

The tectono-magmatic evolution of the Antarctic Peninsula Batholith, Graham Land: insights from U-Pb zircon ages and geochemical data

Joaquin Bastias[1], Richard Spikings[1], Alexey Ulianov[2], Urs Schaltegger[1], Anne Grunow[3], Francisco Hervé[4], Teal Riley[5], Alex Burton-Johnson[5]

[1] Earth Science Department, University of Geneva, Rue de Maraîchers 13, 1205 Geneva, Switzerland (joaquin.bastias@unige.ch)
[2] Institute of Earth Sciences, University of Lausanne, Géopolis, 1015 Lausanne, Switerland
[3] Byrd Polar and Climate Research Center, Ohio State University, 108 Scot Hall, 1090 Carmack Road, Columbus, OH 43210, USA
[4] Departamento de Geología, Universidad de Chile, Plaza Ercilla 803, Santiago, Chile
[5] British Antarctic Survey Cambridge, CB3 OET, UK.

Concordant zircon U-Pb dates of rocks of the Antarctic Peninsula Batholith span between ~240 to 9 Ma and are emplaced along a strike of 1300 km with an overall width of 200 km. The spatial and temporal extent of the plutons provides an opportunity to use magmatic rocks to constrain the tectonic history of the Peninsula. We aim to increase the understanding of the mechanisms that were involved in the formation of the plutonic rocks in the northern Antarctic Peninsula. These tectonic constraints will improve paleogeographic reconstructions of West Antarctica and South America within the Gondwana supercontinent. These models would benefit of a more precise understanding of the tectonic evolution of the Antarctic Peninsula, also it will give insights in how continents growth and margins evolve.

We present i) 40 concordant U-Pb zircon and 4 hornblende $^{40}Ar/^{39}Ar$ plateau ages, ii) whole rock major oxide and trace element analyses, and iii) Nd-Sr-Pb bulk-rock isotopic compositions.

The Antarctic Peninsula Batholith in the north intrudes Paleozoic-Mesozoic low-grade meta-sedimentary rocks of the Trinity Peninsula Group and the Late Jurassic-Paleogene volcanic and sedimentary rocks of the forearc deposits at the west of the magmatic arc. Further south, it intrudes schists and ortho- and paragneisses with Carboniferous to Triassic metamorphic ages. Magmatic activity spans from the Middle Triassic to the Miocene with gaps in the Early Jurassic and Late Jurassic-Early Cretaceous. Isotopic compositions show that most of the Antarctic Peninsula granitoids were formed as a result of subduction of the Phoenix Plate oceanic lithosphere under the Antarctic Plate continental lithosphere. They fall on trends between a component derived from subduction-modified mantle or juvenile basaltic underplate (εNd>6, $^{207}Pb/^{204}Pb$=15.61, $^{87}Sr/^{86}Sr$<0.704) and an interpreted Proterozoic lower crust (εNd=-7, $^{207}Pb/^{204}Pb$=15.67, $^{87}Sr/^{86}Sr$=0.709; Millar et al., 2001).

Plutonic lithologies of the northern Antarctic Peninsula range in chemical composition from granite to gabbro. Concordant U-Pb zircon ages from the northern Peninsula span between ~160 Ma (Stonington Island) to ~9 Ma (Cornwallis Island), with a peak in the Early Cretaceous (Albian and Aptian).

Major oxides and trace elements of the rocks analyzed in the northern Antarctic Peninsula reveal calc-alkaline, metaluminous, supra-subduction zone rocks (Pearce et al., 1984), with no significant variation in time, although, some intrusions that crystallised between ~118-112 Ma yield peraluminous signatures. Further, trace element data have been used to study the multi-trace-element plots of Pearce et al. (1984). They shows a lack of HREE fractionation, characteristic of a garnet-dominant source, and display an overall enrichment in LILE relative to HSFE, which is a pattern typically associated to subduction. The geochemical data suggest that the plutonic rocks of the Batholith from Graham Land formed in an arc setting.

Geographic variations in dates show that magmatism remained in an approximately stationary position along the west flank of the Antarctic Peninsula from the ~160 Ma to the 19 Ma. Miocene magmatism displaced ~50 km westwards, and is currently exposed on Watkin Island (~22 Ma), Snodgrass Island (~19 Ma), Litchfield Island (~19 Ma) and Cornwallis Island (~26 Ma).

The stationary position of the magmatic arc and the consistent arc setting during the period from ~160 Ma to 41 Ma does not support previous interpretations that the Antarctic Peninsula Batolith formed on an allochthonous crustal block that collided with a former Gondwanan margin during the Early Cretaceous (e.g. Vaughan et al 2002). Further, the collision and following accretion would have altered the plate kinematics, and therefore, it could be expected that the plutonic rocks show a change in the location of the eruption of arc magmas relative to the upper plate. Additional isotopic tracing Nd-Sr-Pb (whole rock), Hf (zircon) and O (quartz) is being conducted to improve our uderstanding of the tectonic environment within which the magma formed and was emplaced.

REFERENCES

Leat, P., Scarrow, J., Millar, I. 1995. On the Antarctic Peninsula batholith. Geological Magazine. 132 (4), 399-412.

Millar, I.L., Willan, R.C.R., Wareham, C.D. & Boyce, A.J. 2001. The role of crustal and mantle sources in the genesis of granitoids of the Antarctic Peninsula and adjacent crustal blocks. JGS, 158, 855–867.

Pearce, J., Lippard, S., Roberts, S. 1984. Characteristics and tectonic significance of supra-subduction zone ophiolites. Journal of Petrology 25(4), 986-983.

Pearce, J. 1996. Sources and settings of granitic rocks. Episodes 19, 120-125.

Vaughan, A.; Storey, B. 2000. The eastern Palmer Land shear zone: A new terrane accretion model of the Mesozoic development of the Antarctic Peninsula. JGS 157, 1243-1256.

Vaughan, A.P.M., Kelley, S.P. & Storey, B.C. 2002. Mid-Cretaceous ductile deformation on the Eastern Palmer Land Shear Zone, Antarctica, and impli- cations for timing of Mesozoic terrane collision. Geological Magazine, 139, 465–471.

P 1.36

Revisiting diffusion creep of calcite

James Gilgannon[1], Marco Herwegh[1], Thomas Poluet[2], Klaus Regenauer-Lieb[2] and Manolis Veveakis[2]

[1] *Institute of Geological Sciences, University of Bern, Baltzerstrasse 1+3, CH-3012 Bern, Switzerland (james.gilgannon@geo.unibe.ch)*
[2] *School of Petroleum Engineering, The University of New South Wales, Kensington NSW 2033, Australia*

The experimental descriptions of how rocks behave at higher temperatures and confining pressures are our only tangible window into actual crustal or mantle rheologies. One fundamental concept that has come from deformation experiments is the idea of steady state end member flow laws. The core assumption of these flow laws is that, at the scale of the continuum, they describe one rate limiting process in a rock. For example in the case of a grain size sensitive rheology the rate limiting process could be self diffusion of the slowest diffusing species, or for grain size in-sensitive behaviours it maybe the overcoming of a lattice's intrinsic energy barriers by a line defect. However, it is not clear that with in the window of an experiment's conditions only one of these processes will dominate the rheological characteristics of a rock. Furthermore, in the material sciences it is know that the superposition of deformation mechanisms can make a flow law less generally useful (Kocks, 1987).

We revisited the diffusion creep experiments of Herwegh et al. (2003) and found that both the activation energy and pre-exponential factor evolve as a function of stress. These dependancies are attributed to the coeval activity of dislocation glide with grain boundary diffusion. It is shown that even in domains classically interpreted to be grain size sensitive and creeping by diffusion creep ($n \approx 1$), dislocation glide may make significant contributions to the accommodation of strain. Most importantly we find that for the data to be correctly fitted, the resultant flow law must contain knowledge of these stress dependancies because they exist even when $n \approx 1$. These results may raise questions over the assumptions of constant material parameters that are ubiquitous across the literature.

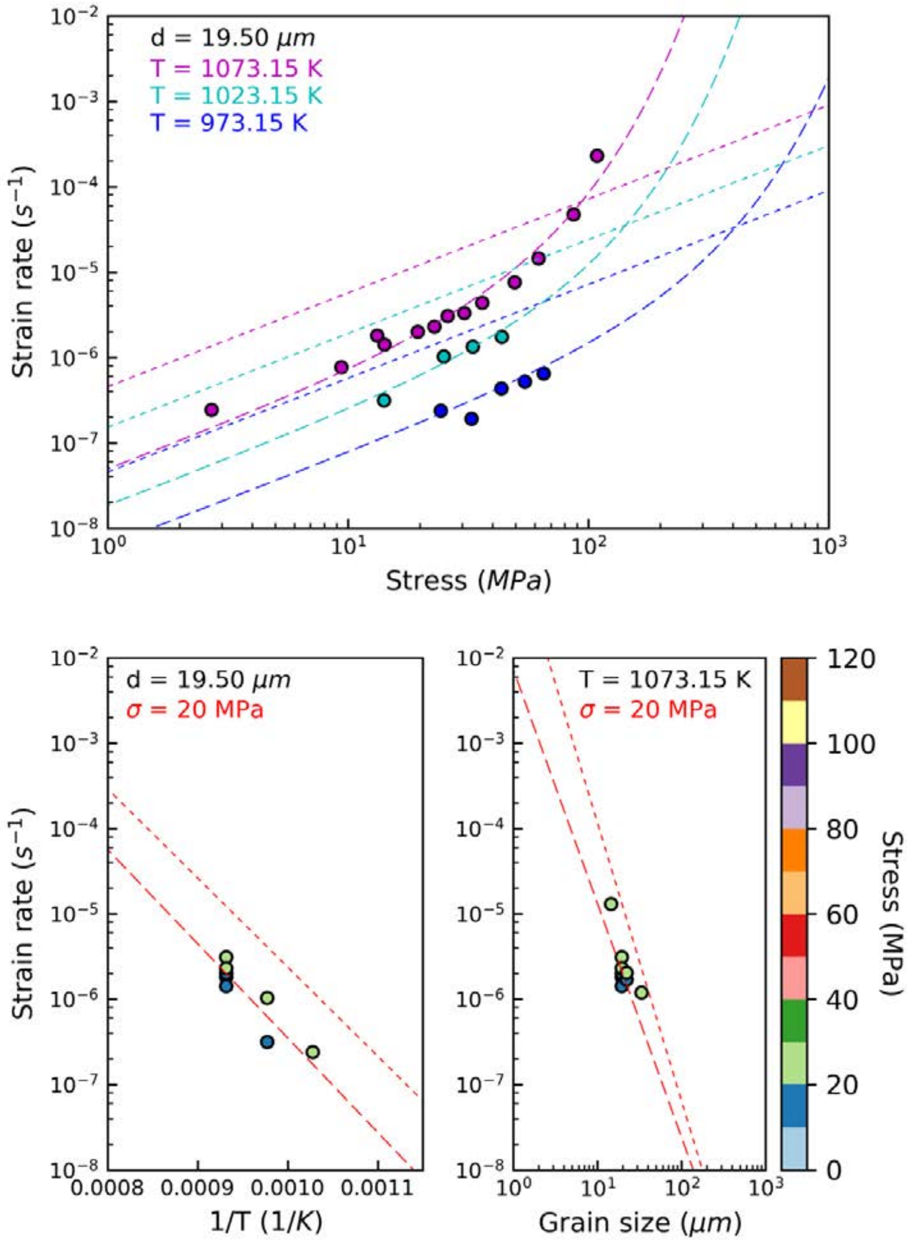

Figure 1. Comparing new flow law fit to data and to the flow law of Herwegh et al. (2003). The small dashed line represents the fit of Herwegh et al. (2003), while the larger dashed lines represents the new fit.

REFERENCES

Herwegh, M., Xiao, X., & Evans, B. 2003: The effect of dissolved magnesium on diffusion creep in calcite, EPSL, 212(3), 457-470.

Kocks, U.F. 1987: Constitutive Behavior Based on Crystal Plasticity, Springer Netherlands, ed. by A.K. Miller, 1-88.

P 1.37

The External Dinarides of Southern Montenegro and Northern Albania: Contraction vs. extension - Instrumentally recorded seismicity vs. field observations

Peter Biermanns[1], Benjamin Schmitz[2], Kamil Ustaszewski[2], Kristijan Sokol[3] & Klaus Reicherter[1]

[1] Neotectonics and Natural Hazards Group, RWTH Aachen University, Lochnerstr. 4-20, 52056 Aachen, Germany (p.biermanns@nug.rwth-aachen.de)
[2] Institute for Geosciences, Friedrich-Schiller-Universität Jena, Burgweg 11, 07749 Jena, Germany
[3] Faculty of Mining and Geology, University of Belgrade, Đušina 7, 11000 Beograd, Serbia

Albania and Montenegro, hosting the transition from Dinarides in the N to Hellenides in the S, comprise some of the seismically most active regions in Europe. Seismicity results from an interplay between NE-ward continental subduction of the Adriatic microplate below Eurasia and oceanic subduction along the Aegean Arc. Earthquake epicentres are aligned in rather well-defined orogen-parallel and orogen-perpendicular belts with characteristic focal mechanisms (e.g. Aliaj, 2006): While the hinterland is mostly dominated by slab rollback-induced extensional tectonics (Burchfiel, 2008), contractional tectonics prevail in the frontal ‘External Dinarides-Hellenides’, proving an ongoing convergence between Adria and Eurasia (Fig.1).

Although instrumentally recorded seismicity shows a rather clear E-W delineation between extensional and contractional domains, field observations in our per se contractionally dominated study area between Bar (Montenegro) and Bulqizë (Albania) suggest a more complex pattern involving co-existing contraction, extension, uplift and subsidence (Fig.1). While dry valleys are formed as a response to ongoing growth of NW-SE-striking anticlines involving deformation of sediments as young as Serravallian, we report widespread regional-scale active normal faulting in the immediate vicinity: Most prominent example is a NW-SE to E-W-trending normal fault scarp that can, despite minor hiatuses, be traced for c. 16 km along the Southern Montenegrin Rumija chain. Its sheer dimensions as well as the regularity of fault striae on the undulating fault planes strongly imply a tectonic origin of the structure. The preliminarily supposed movement rates in the range of ≤ 0.5 mm/yr (based on an LGM-conditioned estimate of the average fault offset), the occurrence of rather narrow varicoloured horizons of consistent height along the scarp base as well as the obviously lacking record of normal faulting in instrumental seismicity suggest the fault(s) to undergo an embryonic stage, possibly indicating the onset of a westward migration of ‘Aegean-style extension’ (sensu Burchfiel, 2008) towards the W. However, exact movement rates and the connection to evidently seismogenic faults, e.g. the causative fault of the 1979 earthquake, and other contractional features are hitherto unknown. We aim to overcome this shortcoming with our ongoing research, generally targeting an improved understanding of how contraction, extension, uplift and subsidence co-exist. This includes (i) further detailed mapping and delineation of domains affected by ‘contradictory’ tectonic styles, (ii) quantification of uplift and subsidence rates by ^{10}Be dating of river gravels from dry valleys on anticlines and ^{14}C dating of organic material from shallow drill cores, as well as (iii) ^{36}Cl dating of exposed surfaces on the normal fault scarp in order to achieve more reliable movement rates.

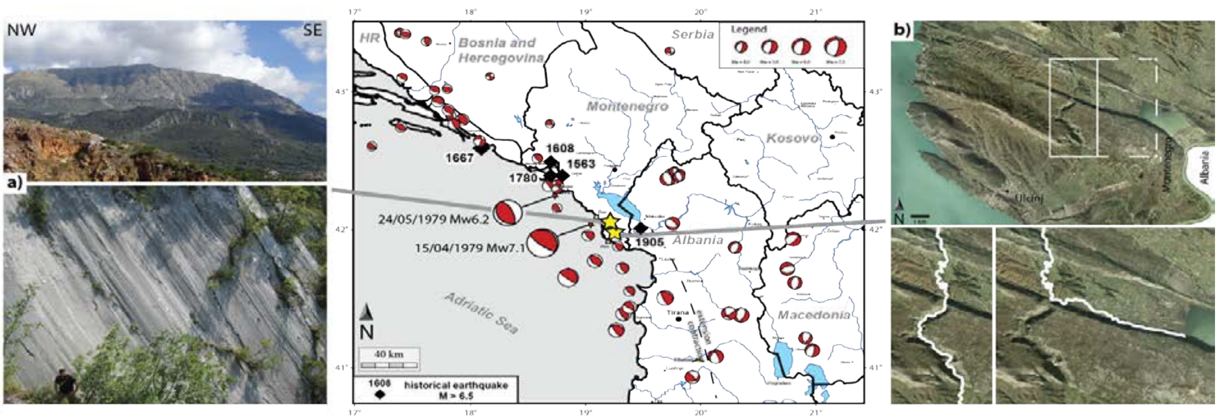

Figure 1. Map of Montenegro, Northern Albania and surroundings showing earthquake focal mechanisms that indicate prevailing extensional tectonics in the hinterland and thrust faulting along the coast. Contradicting this apparently uniform pattern, we report significant regional-scale active extension (e.g. normal fault scarps, ‘a’) in the coastal domain, co existing with young contractional structures (dry valleys on anticlinal ridges formed by uplift-induced redirection of rivers, ‘b’).

REFERENCES

Aliaj, S.,2006: The Albanian Orogen: Convergence Zone between Eurasia and the Adria microplate. In: Pinter, N., Grenerczy, G., Weber, J., Stein, S. and Medak, D. (eds.). The Adria Microplate: GPS Geodesy, Tectonics and Hazards. Springer, 133-149

Burchfiel, B.C., Nakov, R., Dumurdzanov, N., Papanikolaou, D. Tzankov, T., Serafimovski, T., King, R.W., Kotzev, V., Todosov, A., Nurce, B., 2008: Evolution and dynamics of the Cenozoic tectonics of the South Balkan extensional system. Geosphere 4, 919-938.

P 1.38

Diagenesis and Stadial Analysis of Jurassic Dolomite, Case Study : South-setifian Shelf (NE Algerian)

El Hadj Youcef Brahim[1] , Mohamed Chadi[2] & Rami Djeffal[3]

*Department of Geology, Université of Batna 2, Fisdis (wahidyb@yahoo.fr)
** Management of urban technics department Constantine 3 University, (chadi43@yahoo.fr).
[3] Geologic sciences department Constantine 1 University, (djeffal.rami@umc.edu.dz).

The carbonate series of South-Setifian shelf provides a good example of the carbonate shelf sedimentation study in the external zones of the Eastern Algerian Alpine Belt. It's about deposits which by their vertical concatenation, lithology and their diagenetic evolution are similar to those of the actual Bahamian shelf.
Detailed diagenetic analysis has allowed the distinction of many petrographic types (Fig. 1), also, it has allowed the retracement of paleogeography and dolomitisation model of the series.

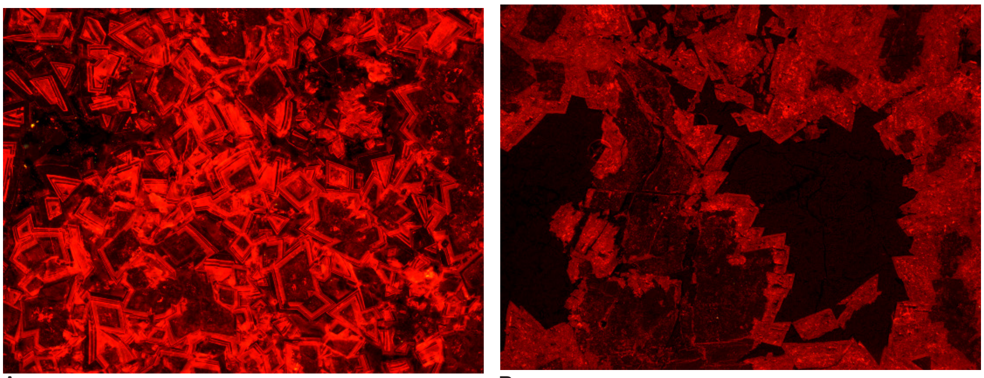

A B

Figure 1. A and B: Dolomite under a cold cathode microscope

2. Mineralogy, Petrology, Geochemistry

Sébastien Pilet, Bernard Grobéty, Eric Reusser

Swiss Society of Mineralogy and Petrology (SSMP)

TALKS:

2.1 **Belgrano T.M**., Diamond L.W.
Supra-subduction zone spreading in the Oman ophiolite

2.2 **Gugushvili V.**, Beridze T., Chkhotua T., Khutsishvili S., Migineishvili R.
Interrelation of Regional Metamorphism, Volcanism, Hydrotermal Activity and Metallogeny During the Tethys Ocean Subduction and at Post-collision Stage of Eurasian Continental Margin Development

2.3 **Hartung E.**, Caricchi L., Floess D., Wallis S., Harayama S.
The volcanic-plutonic connection unveiled

2.4 **Hörler J.**, Burkhard R.
The Karavansalija Mineralized Center in southwestern Serbia: Time relationship of intrusive events, gold skarn mineralization and overlying volcanics and characterization of the ore mineral assemblage.

2.5 **Kaufmann A.**, Pettke T., Baumgartner L.
Fluid-involved processes at the magmatic-hydrothermal transition in Torres del Paine, Chile, studied through inclusions in miarolitic quartz

2.6 **Kempf E.**, Hermann J.
Water incorporation into metamorphic olivine at high pressures in the Zermatt-Saas serpentinites

2.7 **Maltese A.**, Mezger K.
A Model for the Pb-isotope Evolution of the Bulk Silicate Earth

2.8 **Myint M.P**., Franz L., de Capitani C., Balmer W., Krzemincki M..
Petrology and PT-conditions of quartz- and nepheline-bearing gneisses from Mogok Stone Tract, Myanmar

2.9 **O'Sullivan E**., Kamber B., Nägler T.
Molybdenum isotopic composition of the 1.85 Ga Sudbury impact basin fill, Ontario: insights into volatile element loss and post-impact biological activity

2.10 **Paul A.**, Spikings R., Chew D., Daly J.S.
Apatite in-situ U-Pb thermochronology: the effect of parent uranium isotope zonation

2.11 **Popov D.**, Spikings R.
Effect of apatite crystal geometry, parent isotope zonation and petrological environment on its closure temperature (U-Th-Pb system)

2.12 **Prelević D.**
The origin of Alpine-Himalayan K-rich orogenic lavas: an integrated experimental and geochemical approach

2.13 **Schmidt K.**, Vrijmoed J., Tajcmanova L., Moulas E.
Mechanically controlled chemical zoning in UHP garnets from the Western Gneiss Region, Norway

2.14 **Tollan P.**, Dale C., Hermann J., Davidson J., Arculus R.
Melting and modification of the mantle wedge beneath the West Bismarck island arc, evidenced by the chemical and isotopic composition of peridotite xenoliths

2.15 **Vho A.**, Rubatto D., Lanari P., Giuntoli F., Regis D.
Garnet chemical and oxygen isotope zoning and accessory mineral investigation to constrain the evolution of subducted continental crust (Sesia Zone, Italy)

2.16 **Weber S.**, Diamond L.W., Alt-Epping P.
Epidosite alteration of the oceanic crust: cumulative water–rock ratios derived from reactive-transport modelling

2.17 **Wolf M.**, Romer R.L., Franz L.
Metal enrichment in granitic melts: the role of protolith chemistry and partial melting conditions

POSTERS:

P 2.1 **Brunner M.**, Müller L.
High-precision zircon dating of miocene magmatism in the Apuseni Mountains (Romania) with TIMS

P 2.2 **Naumenko**-Dèzes M., Rolland Y., Gallet S., Villa I.
Heterogeneities in natural $^{40}Ar/^{39}Ar$ flux monitors and pristine magmatic micas

P 2.3 **Bulle F.**, Rubatto D., Ruggieri G.
Oxygen isotopes in white mica from the Larderello geothermal field – a potential tool to trace fluid flow in complex magmatic – hydrothermal systems

P 2.4 **Glauser A.**, Eggenberger U., Weibel G., Mäder U.K.
Quality criteria for municipal solid waste incineration bottom ash with regard to recycling and deposition without aftercare

P 2.5 **Richter L.**, Diamond L.W.
Hydrothermal Epidosite Formation in the Oceanic Crust

P 2.6 **Rouwendaal S.E**., Eglinton T.I., Al-Kuwari A., H., Haghipour N., Bontognali T.R.R.
The fossilization potential of gypsum and its relevance to the search for life on Mars

P 2.7 **Curry A.**, Caricchi L., Sheldrake T., Simpson G. Lipman P.
Determining the physical and chemical processes behind four caldera-forming eruptions in rapid succession in the San Juan caldera cluster, Colorado, USA

P 2.8 **Edwards M.**, Pioli L., Andronico D., Cristaldi A., Scollo S.
Mafic magma fragmentation and eruption dynamics of the May 2016 Etna eruption

P 2.9 **Devoir A.**, Müntener O.
Monitoring local-scale igneous underplating crystallization and interactions with country-rocks by garnet Y+REE chemistry

P 2.10 **El Korh A.**, Deloule E., Boiron M.C., Luais B.
Lithium partitioning and isotope fractionation in the Limousin ophiolite (Massif Central, France)

P 2.11 **El Korh A.**, Luais B., Boiron M.C., Deloule E., Cividini D.
Iron isotope fractionation in the Limousin ophiolite (Massif Central, France)

P 2.12 **Gabarashvili K.**, Lobzhanidze K., Beridze T., Vashakidze G., Kavsadze M., Togonidze M.
Morphological Features of Chkheri (the Great Caucasus) and Khertvisi (Southern Georgia) Lava Flows

P 2.13 **Grosjean M.**, Moritz R., Melkonyan R., Hovakimyan S., Ulianov A.
Cenozoic subduction to post-collision magmatic evolution of the Lesser Caucasus: new constraints from the Tejsar and Amulsar areas, Armenia

P 2.14 **Sheldrake T.**, Caricchi L., Gander M., Wallace G., Simpson G.
Cross correlation of magmatic crystals: intepreting correlations and identifying families

P 2.15 **Weber G.**, Caricchi L., Sheldrake T., Arce J.L.
Magma dynamics and long-term evolution of Nevado de Toluca volcano, Mexico

P 2.16 **Jensen M.**, Caricchi L., Blundy J., Melekhova L., Cooper G.
The Temporal Evolution of an Arc Volcano through Thermobarometry and Petrography of Intrusive and Volcanic Products

P 2.17 **Marxer F.**, Ulmer P.
Differentiation of intermediate calc-alkaline magmas at 2 kbar

P 2.18 **Hantsche A.L**., Kouzmanov K., Dini A., Vassileva R., Guillong M., Quadt V.A.
U-Pb age constraints on skarn formation in the Madan Pb-Zn district, Bulgaria: zircon evidence from Tertiary magmatism

P 2.19 **Hetényi G.**, Pistone M., Nabelek P., Baumgartner L.
Lhasa Block partial melt zones: matching geophysical characteristics and petrological origin

P 2.20 **Ravindran A.**, Mezger K., Balakrishnan S., Raith M.M.
Archaean Barite: Strontium Isotopes as a tracer of early crust-mantle evolution

P 2.21 **Roggero D.**, Müntener O., Pilet S.
Neogene retro-arc basaltic magmatism in southern Patagonia: magmatic arc connection and alternatives to subslab models

P 2.22 **Demers**-Roberge A., Tollan P., Müntener O.
Water content of Nominally Anhydrous Mineral in mantle xenoliths from Southern Patagonia: Spatial variability and implications

P 2.23 **Reynes J.**, Hermann J., Jollands M.
Water incorporation and site-specific hydrogen diffusion in garnets

P 2.24 **Manzotti P.**, Rubatto D., Korh E.A., Ballèvre M., Cenki-Tok B., Zucali M., Engi M.
Permian magmatism and metamorphism in the Dent Blanche nappe: constraints from field observations and geochronology

P 2.25 **Ricchi E.**, Gnos E., Bergemann C., Whitehouse M.
Th-U-Pb cleft monazite crystallization ages linked to exhumation history and shear zone activity in the Tauern Window

P 2.26 **Klimentyeva D.**, Heinrich C., Quadt V.A.
Veining and mineralizaton history of Bor (Serbia)

P 2.27 **Zucha W.**, Eggenberger U., Weibel G.
Recovery Potential of Heavy Metals from Swiss Fly Ash

P 2.28 **Schlatter D.M**., Schlöglova K., Fettweis R., Bark G., Hughes J.W.
Lithogeochemical classification of hydrothermally altered Paleoproterozoic plutonic rocks associated with gold mineralisation: examples from South Greenland and Northern Sweden

P 2.29 **Stefanova E.**, Marchev P., Georgiev S., Peytcheva I., Raicheva R.
Trace element geochemistry of pyrites from porphyry systems in Elatsite ore field, Bulgaria: a reliable tool for exploration of porphyry (Cu-Au-Mo) and epithermal base metal-Au deposits

P 2.30 **Kavsadze M.**, Dudauri O., Togonidze M., Vasahkidze G., Gabarashvili K., Beridze T.
Shirimi – Georgian Travertine

P 2.31 **Lukovic A.**, Zavasnik J., Vulic P., Banjesevic M., Saric K., Cvetkovic V., Pacevski A.
Hemoilmenite from andesite of the Late Cretaceous Timok Magmatic Complex, Serbia

P 2.32 **Sadradze N.**, Beridze T.T., Sadradze G.
Upper Cretaceous Kachagiani (Sakdrisi) Ore deposit host rocks analysis, Bolnisi ore field, Georgia

P 2.33 **Georgiev S.**, Peytcheva I., von Quadt A., Grozdev V., Marchev P., Serafimovski T.
Cenozoic magmatic/metalogenic activity of distinct areas of SW Bulgaria, FYR of Macedonia and Northern Greece

P 2.34 **Peretti A.** , Mullis J. , Franz L. , Günther D.
Spinel formation by sulphur-rich saline brines from Mansin (Mogok area, Myanmar)

2.1
Supra-subduction zone spreading in the Oman ophiolite

Thomas M. Belgrano[1] and Larryn W. Diamond[1]

[1]*Water–Rock Interaction Group, Institute of Geological Sciences, University of Bern, Balterzstrasse 3, 3012 Bern, Switzerland (thomas.belgrano@geo.unibe.ch*

Over 40 years of research on the Semail ophiolite (Oman–U.A.E.) has influenced our understanding of crust produced at fast-spreading ocean ridges. While the vast sheeted dike complex and comagmatic pillow lavas prove that the early Semail crust formed at an axial spreading center, the precise tectonic setting of this center – whether true mid-ocean, back-arc or fore-arc – is debated, resulting in increasingly divergent schools of thought. The geochemical signature of the main axial-spreading volcanic unit (Geotimes/V1) is ambiguous and obscured by hydrothermal alteration. We bypass this issue by recognizing the localized occurrence of Lasail unit lavas that have an unambiguously slab-derived geochemical character and that are intercalated within the early Geotimes stratigraphy at three separate locations throughout the northern ophiolite. Thus, the early incipient-arc volcanism recorded by these deep Lasail layers confirms a supra-subduction zone setting for the entire axial spreading phase of the world's largest ophiolite, ruling out subduction initiation by inversion of the spreading axis responsible for Geotimes/V1 magmatism.

2.2

Interrelation of Regional Metamorphism, Volcanism, Hydrotermal Activity and Metallogeny During the Tethys Ocean Subduction and at Post-collision Stage of Eurasian Continental Margin Development

Vladimir Gugushvili[1], Tamar Beridze[1], Tamar Chkhotua[1], Sopio Khutsishvili[1], Ramaz Migineishvili[1]

[1]Alexander Janelidze Institute of Geology, Tbilisi State University, Tbilisi, Georgia (vgug34@yahoo.com)

The evolution of Tethys ocean as at subduction stage, so at postcollision development revealed in regional metamophism, volcanic activity, hydrothemal alteration and metallogeny in the western segment of metallogenic belt of Eurasian actve margin within the borders of Iran, Caucasus, Turkey and Carpathian-Balcans regions.

At the first stage of subduction, the regional metamorphism and formation of the granite-metamorphic complexes occured. At the next stage, calc-alkaline volcanism of island arc setting took place with background chlorite-albite and zeolite propylitization and gold-copper base metal mineralization. The downgoing slab temporally and spatialy was steepening (roll back, break off, detachment and delamination) stipulating incursion of mantle diapir in the lithosphere which revealed in interarc-balkarc rifting, shoshonite-trachyandesite and tholeiite-alkali basaltic volcanism, coinciding with chlorite-albite and epitode-zoisite propylitization and copper-zinc-pyrite mineralization. The following intensification of slab steepening and incursion of diapir at upper levels, provoked spreading and revealed in minor ocean setting, occured in the ophyolites formation, ultramaphic dunite-peridotite magmatism, coincided with high temperature epidote-actinolite prophylitization, serpentinization and copper-pyrite mineralization.

The steepening of subducting slab and related volcanic activity and metallogeny is developed in three directions: along downgoing slab, lateraly to its deepening and in the way-up succession. The transformation is controlled by the intensity of slab deformation temporally and spatialy during subduction. The above mentioned transformation is confirmed by investigation within the borders of metallogenic belt (Gugushvili, 2015, 2017).

The type of mineralisation is depended on the scale of participation sialic, basaltic crusts and mantle in process of ore formation. (Gugushvili et al., 2010; Gugushvili 2017). In the island arc setting in the process of mineralization participated sialic, basaltic crusts and mantle revealed in gold-lead-zinc and copper ores formation. In interarc-backar setting mantle related volcanic activity occurs and only copper-pyrite deposition took place without gold, lead and zinc. Therefore the source of gold and lead is sialic crust, source of zinc would be basaltic crust, whereas source of copper is the mantle.

During subduction, in the island arc and interarc-backarc setting developed volcanic series common for synvolcanic block faulting. It is in distinctly examplified within the Bolnisi ore district. (Lesser Caucasus). Here orebearing Upper Cretaceous volcanics are disposed on the Paleozoic granite-metamorphic hard (solid) substatum. Cretaceous volcanic activity took place in shallowmarine conditions. The block faulting was controlled by magmatic and volcanic activity. The invasion of granodiorite intrusive stocks revealed in tumiscence of the sea bottom and island elevation. The ignimbrite explosion on the island was terminated by the cauldron subsidence. The mineralization in uplifted blocks is controlled by intrusive stocks. The blocks at the cauldron subsidence stage were already orebearing. In the Bolnisi ore district both – syn and postvolcanic block faulting is determined. Here Cretaceous volcanic series is devided by regional fault in two postvolcanic,, giant“ blocks. The ,,giant“ blocks formation would be related to detachment of subduction slab in the Late Campanian. (Gugushvili, et al., 2017).

Tethyan subduction was terminated by ocean collision and suturing in the Oligocene-Miocene. The postcollision setting was established and developed by stress of Gondvana at the Eurasian margin, revealed in orogenesis, fold-thrust structures, invasion of granitoid intrusions and gold-porphyry and low sulfidation epithermal gold mineralization. The porphyry and low sulfidation ores are characterized by high grades of gold, but relatively-low abundunces of base metals. Defined here trace metals associations are indicators of postcollision activity overlapped on the precollision setting. (Gugushvili 2015)

The next stage of postcollision activity in the studied region revealed in the Pliocene-Quartenary volcanics represcented of shoshonite-alkali basalt series. It is characterized by geochemical indicators of the similar rocks of precollision setting interarc-backarc riftogenic rocks (Dilek et al., 2010) however postcollision volcanic series are not characterized by rifting and mineralization.

REFERENCES

Dilek J., Imamverdiev N., Altunkayna K., 2010; Geochemistry and tectonics of Cenozoic volcanism in the Lesser Caucasus (Azerbaijan and the Peri-Arabian region: collision induced mantle dynamic and its magmatic fingerprints, 536-578

Gugushvili V., Popkhadze N., Beridze T., Khutsishvili S., 2010: Sources of base, precious and rare metals during Tethyan evolution of the Caucasus and Pontides. Proceedfings of the XIX CBGA Congress, Thessaloniki, Greece, Special Volume 100, 333-341
Gugushvili V., 2015: Pre-collision and post-collision metallogeny of gold-copper-base metal ores at the Phanerozoic evolution of Tethys Ocean. Eds Sh. Adamia, R. Goldfarb and R. Moritz, A. Janelidze Institute of Geology, Tbilisi, 131.
Gugushvili v. Pre-collision and post-collision geodynamic evolution of the Tethys Ocean and its relation with regional metamorphism, volcanism, hydrotermal activity and metallogeny along the Eurasian continental margin, Eds. R. Goldfarb, R. Moritz, G. Zakariadze, Iv. Javakhishvili Tbilisi State University, A. Janelidze Institute of Geology, New Series, V 129, 179.

2.3

The volcanic-plutonic connection unveiled

Eva Hartung*, Luca Caricchi*, David Floess*, Simon Wallis**, [3] & Satoru Harayama[4]

* Department of Earth Sciences, University of Geneva, Rue Maraîchers 13, CH-1205 Geneva (eva.hartung@unige.ch)
** Department of Earth and Planetary Science, The University of Tokyo, Tokyo 113-0033, Japan
[3] Department of Earth and Planetary Sciences, Nagoya University, Nagoya 464-8601, Japan
[4] Department of Geology, Shinshu University, Matsumoto 390-8621, Japan

Are upper crustal plutons solidified magma bodies or residues from extracted and erupted liquids? This remains one of the key questions to address to understand the construction and eruption of upper crustal magmatic systems.
We have investigated the Takidani Pluton and contemporaneous volcanic deposits (Nyukawa PFD, Chayano Tuff and Ebisutoge PD) distributed around this crustal intrusion to understand whether they were sourced from this pluton. The Takidani Pluton is a good candidate because it contains petrographic and geochemical evidences for residual melt extraction, and pressure quenching associated with eruptive activity (Hartung et al., 2017).

We analysed major and trace element concentrations of 18 plagioclase phenocrysts (core to rim) from the Takidani Pluton and Nyukawa-Chayano-Ebisutoge eruptions. Major elements were first analysed using an electron microprobe and trace elements were subsequently determined by laser ablation inductively coupled mass spectrometry in the same spot. Plagioclase chemistry shows that the Chayano and Ebisutoge rhyolitic deposits are not petrogenetically related to either the Takidani Pluton or the Nyukawa PFD. However, plagioclase of the Nyukawa PDF and the Takidani Pluton show indistinguishable REE patterns suggesting a common source domain for plagioclase from the two units. Ebisutoge plagioclase grains commonly contain xenocrystic cores that have major and trace element compositions comparable to the plagioclase grains observed in the Takidani Pluton and Nyukawa PFD.
Our data show that the Nyukawa and Takidani plagioclase are geochemically indistinguishable, suggesting that the Takidani pluton was the magma reservoir that fed this large eruptive unit (400 km^3, Oikawa, 2003). The Ebisutoge magma was not extracted directly from the pluton, but interacted with Takidani-Nyukawa when it was still molten. We have no evidence to suggest that the Takidani Pluton was the source of either the Chayano Tuff or the Ebisutoge PD.

REFERENCES

Hartung, E., Caricchi, L., Floess, D., Wallis, S., Harayama, S., 2017, Evidence for Residual Melt Extraction in the Takidani Pluton, Central Japan, Journal of Petrology, 58, 763-788
Oikawa, T., 2003, The spatial and temporal relationship between uplifiting and magmatism in the Hida Mountain Range, central Japan, Quarternary Research, 42, 141-156

2.4

The Karavansalija Mineralized Center in southwestern Serbia: Time relationship of intrusive events, gold skarn mineralization and overlying volcanics and characterization of the ore mineral assemblage.

Hörler J., Burkhard R.

Karavansalija mineralised Centre (KMC) is an active Cu-Au skarn exploration project near Novi Pazar in south-western Serbia, currently developed by Eldorado Gold. It is situated within the Rogozna Mt. magmatic suite and belongs to the Oligocene Serbo- Macedonian Magmatic and Metallogenic Belt (SMMMB). Samples from KMC show typical arc signatures of subduction derived magmas, through enrichment of large ion lithophile elements (LILE) and depletion of high field strength elements (HFSE). The magmas follow a high-K (calc-alkaline) fractionation trend and evolve towards shoshonites.

Zircon LA-ICP-MS and ID-TIMS dating, together with zircon trace element and Hf isotope measurements, were carried out to establish the geochronologic and geochemical evolution of KMC. The results suggests that magmatism started at around 29.3 Ma with andesitic to trachyandesitic extrusives and shallow subvolcanic intrusives, and was followed by a more evolved phonolitic shallow intrusion into Cretaceous limestone, generating a skarn field at ca. 29.0 Ma. During a quiescence period of about 1.2 Ma, a new plutonic body evolved, which possibly also partly cannibalized the older plutonic body, as inferred by zircon xenocrysts. Geochemical signals from REE ratios shift from apatite, titanite ± amphibole dominated fractionation of the older magmatic session, to crystallization of allanite, efficiently depleting the LREE and Th/U in the newly formed upper crustal pluton. After a lamproite-like melt was injected, the increased heat and fluid pressure lead to the expulsion of a crowded porphyritic stock at ca. 27.76 Ma, strongly interacting with the skarn and establishing a new hydrothermal system. Ore precipitation took place in the retrograde skarn stage.

Ore mineralization is present as (1) assemblage of base metal sulfides (pyrite, arsenopyrite, pyrrhotite, chalcopyrite, galena, sphalerite) with associated Bi-phases (bismuthinite, cosalite, native Bi) and native Au in quartz-calcite vein/ stockwork zones in exoskarn, (2) in retrograde endoskarn, composed of clinopyroxene-epidote-chlorite along with quartz and calcite, as base metal sulfides (pyrite, chalcopyrite, pyrrhotite, sphalerite, galena, arsenopyrite), (3) massive sulfide (arsenopyrite, pyrrhotite, sphalerite, galena, chalcopyrite) replacement in endoskarn, and (4) late sphalerite-dominated base metal mineralization hosted in calcite veins that cut through retrogressed garnet skarn. Native Au is primarily related to calcite-hosted arsenopyrite, where it occurs as grains on the arsenopyrite surface, and as inclusions in the latter. LA-ICP-MS revealed significant Au content in native Bi, which also forms small (<5 µm) inclusions in arsenopyrite, leading to invisible Au mineralization in the latter. Native Bi occurs in greater abundance near and partly in direct contact with the arsenopyrite grain surfaces. The incorporation of Au in native Bi indicates the liquid Bi collector model as important precipitation mechanism for the Au mineralization. Fluid inclusion data of quartz and calcite from Bi-Au mineralized samples support this idea. This style of Bi-Au mineralization is present as discrete vein zones in exoskarn, and as endoskarn veins in the crowded porphyry.

Soon after the ore deposition, a second, unmineralized pulse of porphyry dykes cut the previous crowded porphyries and skarns at 27.62 Ma, thus bracketing the maximum timespan of ore mineralization to about 140 ka.
This study has shown that with high precision ID-TIMS age dating, several pulses of porphyry dykes could be distinguished, and together with field relations, the timing of ore mineralization could be parenthesized. Furthermore, the style and temperature conditions of Au mineralization was established.

2.5

Fluid-involved processes at the magmatic-hydrothermal transition in Torres del Paine, Chile, studied through inclusions in miarolitic quartz

Anne Kaufmann[1], Thomas Pettke[1], Lukas Baumgartner[2]

[1]*Institute of Geological Sciences, University of Bern, Baltzerstrasse 1+3, CH-3012 Bern (anne.kaufmann@geo.unibe.ch)*
[2]*Institute of Earth Sciences, University of Lausanne, CH-1015 Lausanne*

The study of coexisting inclusions of multiple fluid phases (aqueous liquid, vapour, salt, and silicate melt) allows for direct quantification of the partitioning behaviour of elements between residual water-saturated melt and exsolving aqueous fluid(s) at the magmatic-hydrothermal transition. This stage is decisive for the mass transfer of elements between geological reservoirs and is central to ore deposit forming processes.

The Torres del Paine bimodal igneous complex intruded as laccoliths at a depth of 2-3 km (~0.75 kbar) between 12.43 and 12.59 Ma (Leuthold et al., 2013). It is characterised by numerous fluid exsolution features exposed in the field, including miarolitic cavities, frothy zones, and pegmatoid features, which record magmatic-hydrothermal processes from 750 °C down to <300 °C. The complex is thus a perfect natural laboratory to investigate processes in very shallow subvolcanic magma reservoirs that may ultimately trigger porphyry-type ore deposit formation (e.g. Audétat et al., 2008).

SEM-VPSE images visualise distinct growth phases of miarolitic quartz (see fig. 1b), (I) magmatic quartz associated with feldspar in graphic texture domains, (II) high temperature magmatic-hydrothermal quartz characterised by irregular, patchy patterns, (III) rhythmically zoned hydrothermal growth, and a dark, terminal overgrowth (IV). Seven inclusion types can be distinguished based on phase relations observed at room temperature. These include dominantly aqueous fluid inclusions ranging from vapour-rich inclusions (Type I) over 2-phase vapour-liquid (Type II) to simple and complex brines (Type IV+V), as well as CO_2-bearing 3-phase fluid inclusions (Type III), and crystallised silicate melt inclusions (Type VI). Figure 2 displays the spatial association of these inclusion types with growth domains of the miarolitic quartz crystals.

Preliminary fluid-melt partition coefficients for 42 elements from Li to U have been determined from LA-ICP-MS analyses of co-existing aqueous fluid and silicate melt inclusions following the analytical protocol described in Pettke et al. (2012). Highest K_D values are determined for elements such as Zn, Ag, Pb, and Cu that are typical of magmatic-hydrothermal ore deposits, while lowest values are observed for e.g. Zr, Th, Nb, Ta, and Al and testify to their limited mobility in low-P aqueous fluids. Our data agree to a first order with data published for miarolitic cavities from generally deeper intrusions. Whether the slight differences between published data and our new data are a function of variable pressure during partitioning or are a consequence of different rock chemistries is a matter to be further explored.

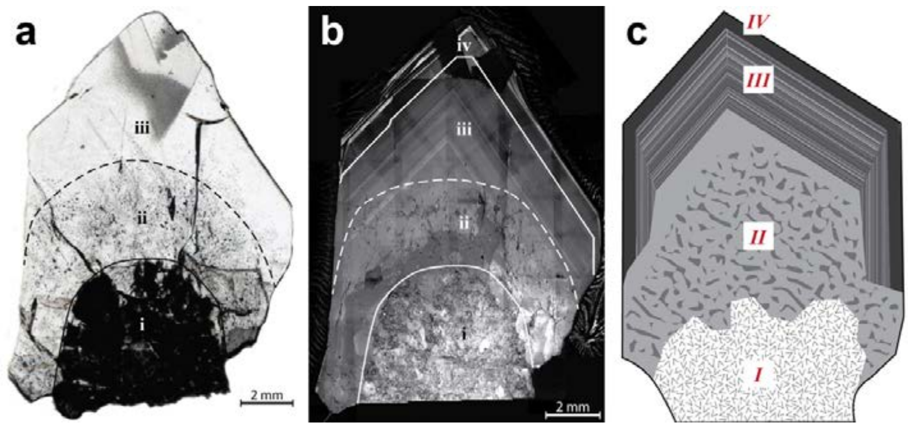

Figure 1. Microphotograph (a), VPSE image (b), and sketch of typical growth domains in miarolitic quartz from Torres del Paine.

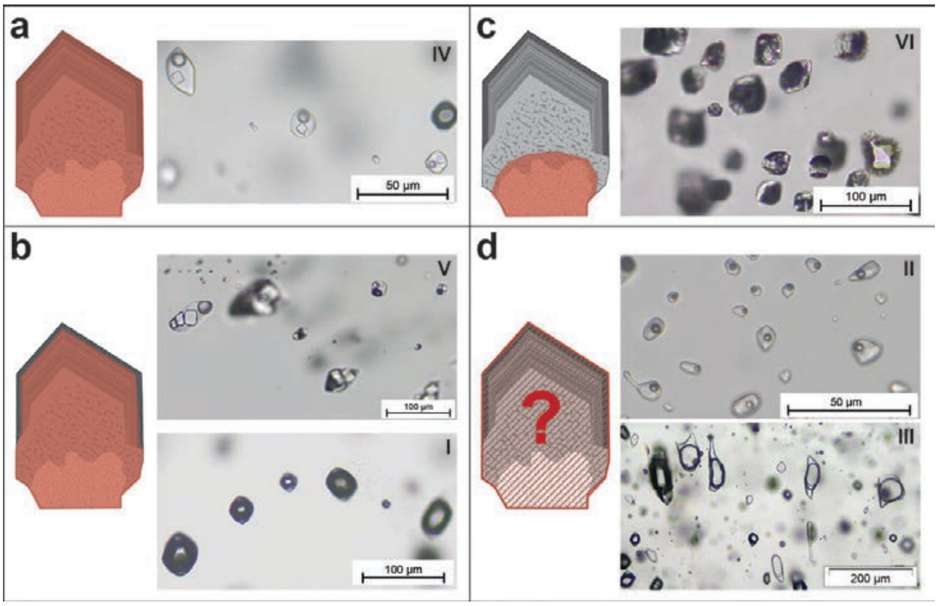

Figure 2. Occurence of assemblages of identified inclusion types as indicated by red shaded areas overlaying the miarolitic quartz sketch; a – type IV brines, b – type V brines and type I vapour-rich inclusions, c – type VI silicate melt inclusions, d – rarely occuring CO_2-bearing (III) and 2-phase liquid-vapour (II) inclusions indicate no definite association with growth domains.

REFERENCES

Audétat, A., Pettke, T., Heinrich, C. A. & Bodnar, R. J. 2008: The composition of magmatic-hydrothermal fluids in barren and mineralized intrusions. Economic Geology 103, 877-908.

Leuthold, J., Müntener, O., Baumgartner, L. P., Putlitz, B. & Chiaradia, M. 2013: A detailed geochemical study of a shallow arc-related laccolith; the Torres del Paine Mafic Complex (Patagonia). Journal of Petrology 54, 273-303.

Pettke, T., Oberli, F., Audétat, A., Guillong, M., Simon, A. C., Hanley, J. J. & Klemm, L. M. 2012: Recent developments in element concentration and isotope ratio analysis of individual fluid inclusions by laser ablation single and multiple collector ICP-MS. Ore Geology Reviews 44, 10-38.

2.6

Water incorporation into metamorphic olivine at high pressures in the Zermatt-Saas serpentinites

Elias Kempf[1], Jörg Hermann[1]

[1] *Institut für Geologie, University of Bern, Baltzerstrasse 3, CH-3012 Bern (elias.kempf@geo.unibe.ch, joerg.hermann@geo.unibe.ch)*

Metamorphic olivine occur in massive antigorite serpentinites, in shear zones and in veins in the eclogite-facies Zermatt-Saas serpentinites. The metamorphic olivine formed at 2.5 GPa and 550°C through the reaction antigorite + brucite = olivine + fluid. Fourier Transform Infra Red (FTIR) measurements of the metamorphic olivines display absorbance bands at 3613, 3600, 3580, 3566, 3551, 3535 and 3480 cm^{-1} (Figure 1), which are characteristic for Si-vacancy in olivine (Walker et al., 2007). The total integrated absorbance of these bands in clear olivines correspond to water contents between 100 - 140 ppm H_2O, calculated with the absorption coefficient of Bell et al. (2003). Olivine from the massive antigorite serpentinite, shearzones and veins all display the same high water contents. The involvement of brucite in the olivine-forming reaction ensures a low Si-activity, which is manifested by the predominance of water incorporation in Si-vacancies in olivine. As these olivines grow during a dehydration reaction, water activity is close to unity. Mapping the water distribution with a FPA detector shows no signs of gain or loss of H_2O after olivine formation, however, growth zoning is observed parallel to the crystallographic a-xis. This supports experimental findings that diffusion of H in Si-vacancies is slow (Padron-Navarta *et al.,* 2014). Even for metamorphic timescales at 550°C, no diffusion modification is expected. Dusty, inclusion-rich olivines show both the characteristic Si-vacanies and additional bands characteristic of Ti-Clinohumite lamella with main bands at 3416 and 3400 cm^{-1}. This shows a second important water incoroporation mechanism that is related to the trace element Ti. The 100-140 ppm H_2O found in the metamorphic olivine are similar to the highest values found in mantle xenoliths (Peslier 2010). It has to be evaluated in future studies, if this process represents an imporant mechanism to transport water into the deeper mantle in subduction zones. Already a few ppm H_2O in Si-vacncies can significantly weaken the crystal structure of olivine (Walker *et al.,* 2007). Thus in subduction zones olivines formed at low Temperatures through the reaction antigorite + brucite = olivine + fluid have the potential to provide a weak interface between the mantle wedge and the subducted oceanic crust.

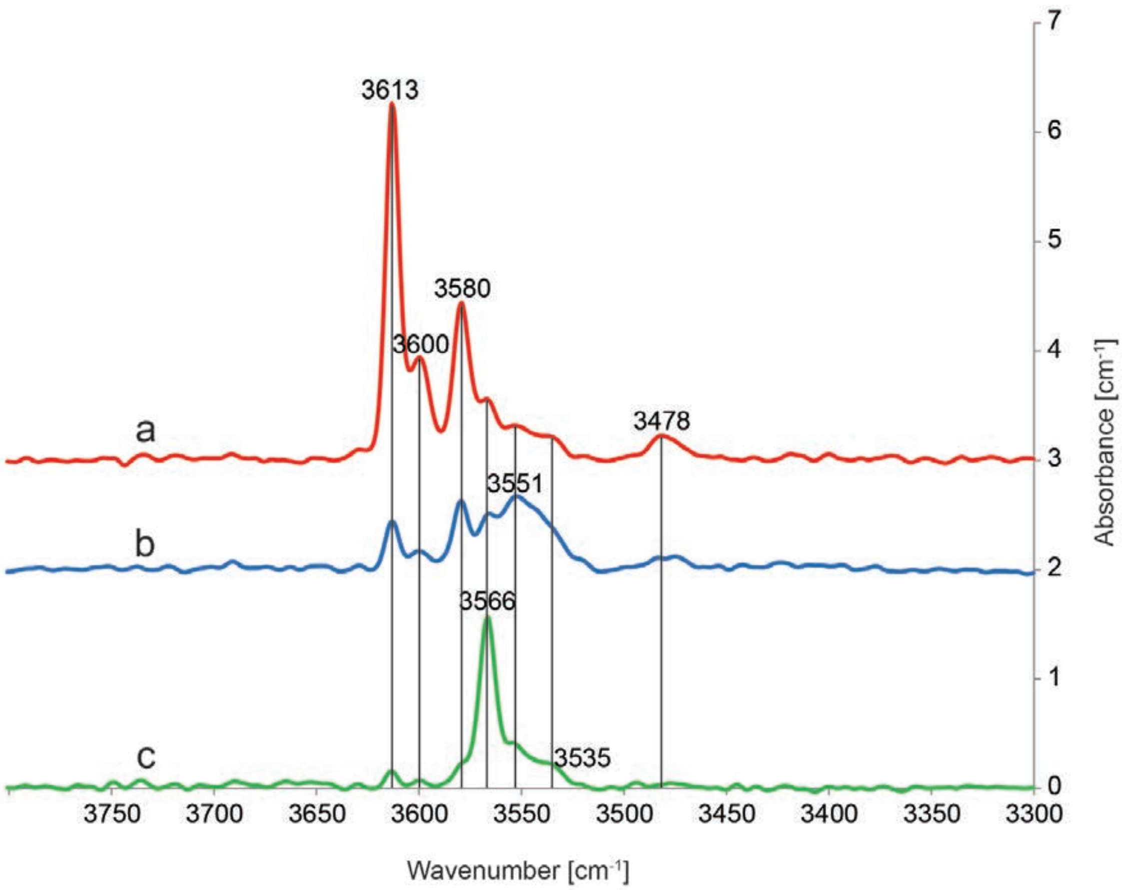

Figure 1. Absorption bands, for each crystallographic orientation are characteristic for Si-vacancies (Walker et al., 2007; Padron-Navarta et al., 2014). Polarised measurements were conducted with a FTIR spectrometer using a MCT detector.

REFERENCES

Bell, D.R., Rossman, G.R., 2003: Hydroxide in olivine: A quantitative determination of the absolute amount and calibration of the IR spectrum, Journal of Geophysical Research, 108, 1-8.

Padron-Navarta, JA., Hermann, J., O'Neill H.St.C., 2014: Site-specific hydogen diffusion rates in forsterite, Earth and Planetary Science Letters, 392, 100-112.

Peslier, A.H., 2010: A review of water contents of nominally anhydrous natural minerals in the mantles of Earth, Mars and the Moon, Journal of Volcanology and Geothermal Research, 197, 239-258.

Walker A.M., 2007: Three water sites in upper mantle olivine and the role of titanium in the water weakening mechanism, Journal of Geophysical Research 112, 1-12.

2.7
A Model for the Pb-isotope Evolution of the Bulk Silicate Earth

Alessandro Maltese[1] & Klaus Mezger[1]

[1]Institut für Geologie, Universität Bern, Baltzerstrasse 1+3, CH-3012 Bern (alessandro.maltese@geo.unibe.ch)

The reconstruction of the Earth's differentiation history is in part tied to isotopic mass balancing among the terrestrial reservoirs (e.g. Kumari et al., 2016). Models that utilize the U-Pb isotope systematics have played a crucial role in advancing our understanding of planetary scale differentiation (e.g. Kamber 2011). While the initial and modern Pb isotopic compositions of the bulk silicate Earth (BSE) are relatively well-constrained (e.g. Murphy et al., 2003), its evolution cannot easily be modelled. This is because in $^{207}Pb/^{204}Pb$ vs $^{206}Pb/^{204}Pb$ space, the BSE plots in an area inaccessible by a single-stage terrestrial evolution model. Previous attempts to solve this paradox rely on assumptions that are in disagreement with more recent observations (e.g. Stacey & Kramers 1975; Allègre et al., 1982). Solving this issue can help to further constrain other existing models and to refine our view of Earth's (early) differentiation history.

Here we present a two-stage mixing model that ties together the giant-impact hypothesis and the possible compositions of proto-Earth and the impactor to resolve the evolution of the BSE through time and the timing of the giant-impact.

The model is fully consistent with Pb isotopic estimates of the BSE and provides a mechanism that can explain the (first) Pb paradox. In addition, it puts an independent constraint on the timing of the formation of the Moon at ca. 70 Myr after the beginning of the solar system.

REFERENCES
Allègre, C. J., Dupré, B. & Brévart, O. 1982: Chemical aspects of the formation of the core. Philos. Trans. R. Soc. Lond. 306, 49-59.

Kamber, B. S. 2011: Geochemistry and Secular Geochemical Evolution of the Earth's Mantle and Lower Crust. In: Frontiers in Geochemistry (Ed. by Harmon, R. S. & Parker, A.). Published 2011 by Blackwell Publishing Ltd.

Kumari, S., Paul, D. & Stracke, A. 2016: Open system models of isotopic evolution in Earth's silicate reservoirs: Implications for crustal growth and mantle heterogeneity. Geochim. Cosmochim. Acta. 195, 142-157.

Murphy, D. T., Kamber, B. S. & Collerson, K. D. 2003: A Refined Solution to the First Terrestrial Pb-isotope Paradox. J. Petrol. 44, 39-53.

Stacey, J. S., Kramers, J. D. 1975: Approximation of terrestrial lead isotope evolution by a two-stage model. Earth Planet. Sci. Lett. 26, 207-221.

2.8

Petrology and PT-conditions of quartz- and nepheline-bearing gneisses from Mogok Stone Tract, Myanmar

Myint Myat Phyo[1], Franz Leander[1], de Capatini Christian[1], Balmer Walter[2], Krzemnicki Michael[3]

[1] *Institute of Mineralogy and Petrography, Department of Geosciences, University of Basel, Bernoullistrasse 30, CH-4056 Basel (myintmyat.phyo@unibas.ch)*
[2] *Department of Geology, Faculty of Science, Chulalongkorn University, Bangkok, Thailand.*
[3] *SSEF (Schweizerische Stiftung für Edelsteinforschung), Aeschengraben 26, CH-4051 Basel / Switzerland (gemlab@ssef.ch)*

The Mogok Stone Tract is mainly composed of high-grade metamorphic rocks such as marbles, calc-silicate rocks, gneisses, peridotites and igneous rocks such as granites, syenites and gabbros, etc. Furthermore, the Mogok Stone Tract is eminent for its finest quality gemstones like rubies, sapphires, spinels and others semi-precious gemstones.

This study focuses on the metamorphic petrology and the P-T conditions of their host rocks. Three quartz gneisses were selected for petrologic investigations. Sample ALT_03 is a biotite-garnet-orthopyroxene gneiss showing a granoblastic, slightly foliated fabric. Conventional thermobarometry using the Grt-Opx-Pl-Qtz-thermobarometry of Lal (1993) yields 758 (±30)°C at 7.3 (±0.5) kbar. The Domino program of de Capitani & Petrakakis (2010) indicates water activities of 0.13-0.55 for an intersection of the garnet isopleths in the stability field of the observed paragenesis.

The closest match between conventional thermobarometry and isopleths method of the DOMINO are found at aH_2O=0.4 (Fig.1a). Sample BPD_02 is a sillimanite-garnet-biotite gneiss with a distinctly foliated fabric. Grt-Bt-thermometry of Holdaway (2000) and GASP-barometry of Koziol & Newton (1988) yield 792 (±30)°C and 7.6 (±0.5) kbar while the garnet isopleths method of the Domino program indicates 789°C at 8.4 kbar (aH_2O=0.34). Sample K1, a foliated garnet-biotite gneiss reveals similar PT-conditions of 752 (±30)°C at 7.5 (±1.2) kbar using the Grt-Bt-thermometry of Holdaway (2000) and the Grt-Bt-Pl-Qtz-barometry of Wu et al. (2004). The garnet isopleth method of the Domino yields 766°C and 6.6 kbar (aH_2O=0.4). Intercalated with ruby- and spinel-bearing marbles were different layers of melanocratic nepheline gneisses. Sample M25 is a granoblastic garnet-K-feldspar-clinopyroxene-nepheline gneiss with accessory calcite, titanite and magnetite.

Stoichiometric calculations of microprobe analyses reveal elevated contents of Fe^{3+} in garnet and clinopyroxene. Conventional thermobarometry is problematic due to the peculiar mineral compositions. Nepheline-alkali feldspar thermometry of Powell & Powell (1978) indicates temperatures of 709 (±70)°C and the Domino program shows a stability field, which is in accordance with the PT-conditions of the quartz gneisses (Fig. 1b). For sample YKK_1a, a nepheline gneiss with an identical paragenesis from a different location, nepheline-alkali feldspar thermometry of Powell & Powell (1978) reveals 790 (±70)°C. Interlayered with sample YKK_1a is sample YKK_2d, a clinopyroxene-Ti-hornblende-plagioclase gneiss with a medium-grained granoblastic texture. Ti-in-hornblende thermometry of Colombi (1988) indicates temperatures of 729-765 (±50)°C. Pressures of 11.0 (±1.5) kbar calculated using the amphibole-plagioclase barometry of Bhadra & Battacharia (2007) have to be regarded as a maximum estimate due to the absence of quartz.

The thermobarometric results of the quartz gneisses are well in accordance with recent investigations on metamorphic rocks from the Mogok area (Thu et al. 2016) highlighting their granulite facies overprint. The newly discovered nepheline gneisses also underwent this high-grade metamorphism. Their occurrence as mafic layers within marbles and their chemical composition point to strongly SiO_2-undersaturated, magmatic dykes (tephritic foidites) as host rocks. Further investigations will focus on the geochronology of these rocks and on the petrology of the ruby- and spinel-bearing marbles.

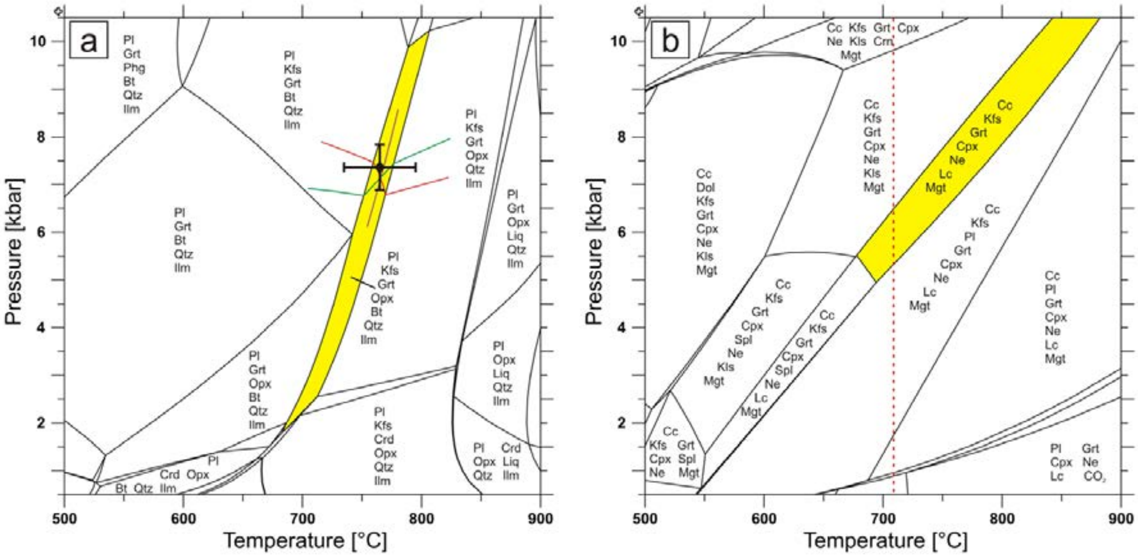

Figure 1. (a) Equilibrium phase diagram of sample ALT_03 calculated with the Domino program at aH_2O=0.4 showing the stability field of the observed paragenesis, the intersection of the garnet isopleths and the estimate of the conventional thermometry (diamond with error bars). (b) Equilibrium phase diagram of sample M25 calculated with the Domino program showing the result of the nepheline-alkali feldspar thermometry (broken red line). The presence of leucite (Lc) in the stability field of the observed paragenesis (yellow) is due to the SiO_2-undersaturated composition and K-content of the nepheline in the sample.

REFERENCES

Bhadra, S. & Bhattacharya, A. 2007: The barometer tremolite + tschermakite + 2 albite = 2 pargasite + 8 quartz: constraints from experimental data at unit silicic activity, with application to garnet-free natural assemblages. American Mineralogist, 92, 491-502.

Colombi, A. 1988: Métamorphisme et géochimie des roches mafiques des Alpes ouest centrales (géoprofil Viége–Domodossola–Locarno): PhD Thesis, University Lausanne, Switzerland, 216 pp.

De Capitani, C. & Petrakakis, K. 2010: The computation of equilibrium assemblage diagrams with Theriak/Domino software. American Mineralogist, 95, 1006-1016.

Holdaway, M.J. 2000: Application of new experimental and garnet Margules data to the garnet–biotite geothermometer. American Mineralogist, 85, 881-892.

Koziol, A.M. & Newton, R.C. 1988: Redetermination of the anorthite breakdown reaction and improvement of the plagioclase-garnet-Al_2SiO_5-quartz geobarometer. American Mineralogist, 73, 216-223.

Lal, R.K. 1993: Internally consistent recalibrations of mineral equilibria for geothermobarometry involving garnet-orthopyroxene-plagioclase-quartz assemblages and their application to the South Indian granulites: Journal of Metamorphic Geology, 11, 855-866.

Powell, M. & Powell, R. 1978: A nepheline-alkali feldspar geothermometer. Contributions to Mineralogy and Petrology, 62, 193-204.

Thu, Y.K., Win, M.M., Enami, M. & Tsuboi, M. 2016: Ti-rich biotite in spinel and quartz-bearing paragneiss and related rocks from the Mogok metamorphic belt, central Myanmar. Journal of Mineralogical and Petrological Sciences, 111, 270-282.

Wu, C.M., Zhang, J. & Ren, L.D. 2004: Empirical garnet-biotite-plagioclase-quartz (GBPQ) geobarometry in medium- to high-grade metapelites. Journal of Petrology, 45, 1907-1921.

2.9

Molybdenum isotopic composition of the 1.85 Ga Sudbury impact basin fill, Ontario: insights into volatile element loss and post-impact biological activity

Edel O'Sullivan[1], Balz Kamber[2] and Thomas Nägler[1]

[1] Institute for Geological Sciences, University of Bern, Baltzerstrasse 1+3, 3012 Bern (edel.osullivan@geo.unibe.ch)
[2] Department of Geology, Trinity College Dublin, College Green, Dublin 2

The early Earth was inundated by giant meteorites during the late heavy bombardment (LHB) between 4.0 and 3.8 Ga. Despite the hostility, the earliest life forms allegedly appeared directly after this period. Analogies to these early impacts are critical to our understanding of the effects of repeated large impacts on the surface of the early Earth. Here we report on the Mo isotopic composition of the 1.85 Ga Sudbury impact crater fill as a multiple-purpose proxy to explore the physical and chemical evolution of a large marine crater, from its effect on crustal geology to the environment that developed within. We build on a recent reconstruction of the impact-related processes and post-impact evolution of the Sudbury basin by the current authors (O'Sullivan et al., 2016) focusing on two features: 1) the anomalous loss of volatile elements such as Pb and Sb from crustal rocks by volatilisation due to the extreme conditions upon impact, and 2) the growth and prosperity of life within the resulting marine environment inside the crater, isolated from the surrounding ocean by the crater rim.

1) Volatile element loss
It has been shown that the Earth's crust is relatively depleted in volatile elements such as Pb, as compared to expected abundances from planetary accretion models. The extreme conditions imposed on the crustal rocks upon impact have previously been proposed to result in volatilisation and loss of these elements. Our data support this view in that the immediately impacted material is extremely depleted in the volatile elements Pb, Zn and Sb in comparison to the average upper continental crust. As expected from the literature, the volatilisation of these elements was recently shown to be mass dependent in a study of Zn isotopes of the same samples (Kamber et al., 2017), with preferential loss of the lighter isotopes, consequently enriching the remaining crustal material in heavy Zn isotopes. This prompted the question as to whether the conditions were extreme enough to affect even the more refractory elements such as Mo and V; large impact events like Sudbury produce enormous amounts of energy, generating temperatures much higher than the vaporisation temperatures of many refractory elements. This gave rise to our first hypothesis: that the Mo isotopes will also show fractionation towards heavy isotopes compared to the upper continental crustal average. We examined this by measuring the Mo isotopic composition of the immediate crater fill, representing the directly targeted crustal rocks.

2) Biological activity
The Sudbury impact crater is unique for many reasons; one of its most notable features is the unusual abundance and preservation of reduced C in the (essentially volcanic) impact-related deposits within the crater. Carbon isotope analysis revealed extremely light $\delta^{13}C$ values, consistent with biogenically produced C. Previous studies speculated that the organic C was washed in from outside the crater. Conversely, our previous work confirmed that this organic C was produced within the crater; the increasing abundance of C would be expected to be accompanied by an increase in particle-reactive Mo, as it is efficiently scavenged by organic particles in the water column and buried. However, a negative correlation is observed, indicating that the Mo inventory was supply-limited, being depleted from the water column by sinking organic particles in an isolated, restricted basin. This lead us to our second hypothesis: as the scavenging of Mo by organic matter is mass dependent, with preferential uptake of the lighter isotopes, the Mo isotopic composition of the C-rich deposits of the basin would initially be light, becoming progressively heavier upwards through the basin fill as the reservoir was depleted over time. We investigated this by analysing the Mo isotopic composition of the entire basin fill sequence, and comparing to the post-impact, open-water black shales of the overlying formation.

REFERENCES

Kamber, B.S., Guyett, P.C., Schoenberg, R., Kenny, G.G., Petrus, J.A. and Ames, D.E. 2017: Volatility-related element loss during large impact events: new Pb and Zn insight from the Sudbury basin. Goldschmidt abstracts, 2017.
O'Sullivan, E.M., Goodhue, R., Ames, D.E. & Kamber, B.S. 2016: Chemostratigraphy of the Sudbury impact basin fill: Volatile metal loss and post-impact evolution of a submarine impact basin. Geochimica et Cosmochimica Acta, 183, 198-233.

2.10

Apatite in-situ U-Pb thermochronology: the effect of parent uranium isotope zonation

A. Paul[1], R. Spikings[1], D. Chew[2], J. S. Daly[3]

[1] *University of Geneva, Geneva, Switzerland (Andre.Paul@unige.ch)*
[2] Trinity College Dublin, Dublin, Ireland
[3] *University College Dublin, Dublin, Ireland*

Uranium-Pb high temperature (>350°C) thermochronometers exploit thermally activated volume diffusive loss of daughter isotopes in accessory minerals such as apatite, titanite and rutile. Previous studies (Cochrane et al., 2014) have shown that U-Pb data can be used to generate accurate, continuous t(time)-T (temperature) solutions spanning hundreds of millions of years. Single grain ID-TIMS analysis yields the highest precision, but detailed analyses of $^{238}U/^{206}Pb$ date vs diffusion length scale reveal scatter beyond predictions from volume diffusion through a single set of intrinsic diffusion parameters. The causes of this scatter can be numerous, and include i) metamorphic overgrowth, ii) fluid catalysed Pb-removal, iii) parent isotope zonation, iv) metamictization, and v) changes in diffusion length. We compare single grain ID-TIMS with LA-MC-ICP-MS *in-situ* U-Pb dates, combined with apatite trace element data (Triassic leucosomes from the Northern Andes of South America), to examine the influence of parent isotope zonation on the distribution of radiogenic Pb, and its impact on the recovery of accurate thermal history paths. Time-T solutions are derived from the *in-situ* dates and U concentrations using controlled random search Monte Carlo simulations and the intrinsic Pb-in-apatite diffusion parameters of Cherniak et al. (1991; Figure 1). The solutions were constrained by crystallisation ages (zircon U-Pb), plateau $^{40}Ar/^{39}Ar$ muscovite dates and low temperature (<350°C) thermochronological constraints (e.g. Spikings et al., 2010). A comparison of the best-fit t-T solutions with the well-constrained tectonic history of the region (Andes of Ecuador and Colombia; Spikings et al., 2015) suggests the solutions are accurate, validating the hypothesis that Pb has been lost by thermally activated diffusion. Accounting for uranium parent isotope zonation is paramount to obtaining accurate t-T solutions. Uranium zonation is ubiquitous in magmatic and metamorphic apatite, and thus in-situ methods are required by U-Pb thermochronology. We also provide a preliminary exploration of the effect of boundary conditions (e.g. apatites as inclusions, or hosted by groundmass) on Pb loss.

REFERENCES

Cochrane R., Spikings R. A., Chew D., Wotzlaw J.-F., Chiaradia M., Tyrrell S., Schaltegger U. & Van der Lelij R. 2014: High temperature (>350°C) thermochronology and mechanisms of Pb loss in apatite. Geochim. Cosmochim. Acta 127, 39–56.

Cherniak D. J., Lanford W. A. & Ryerson F. J. 1991: Lead diffusion in apatite and zircon using ion implantation and Rutherford Backscattering techniques. Geochim. Cosmochim. Acta 55, 1663–1673.

Spikings R. A., Crowhurst P. V., Winkler W. & Villagomez D. 2010: Syn- and post-accretionary cooling history of the Ecuadorian Andes constrained by their in-situ and detrital thermochronometric record. J. South Am. Earth Sci. 30, 121–133.

Spikings R., Cochrane R., Villagomez D., Van der Lelij R., Vallejo C., Winkler W. & Beate B. 2015: The geological history of northwestern South America: From Pangaea to the early collision of the Caribbean Large Igneous Province (290-75 Ma). Gondwana Res. 27, 95–139.

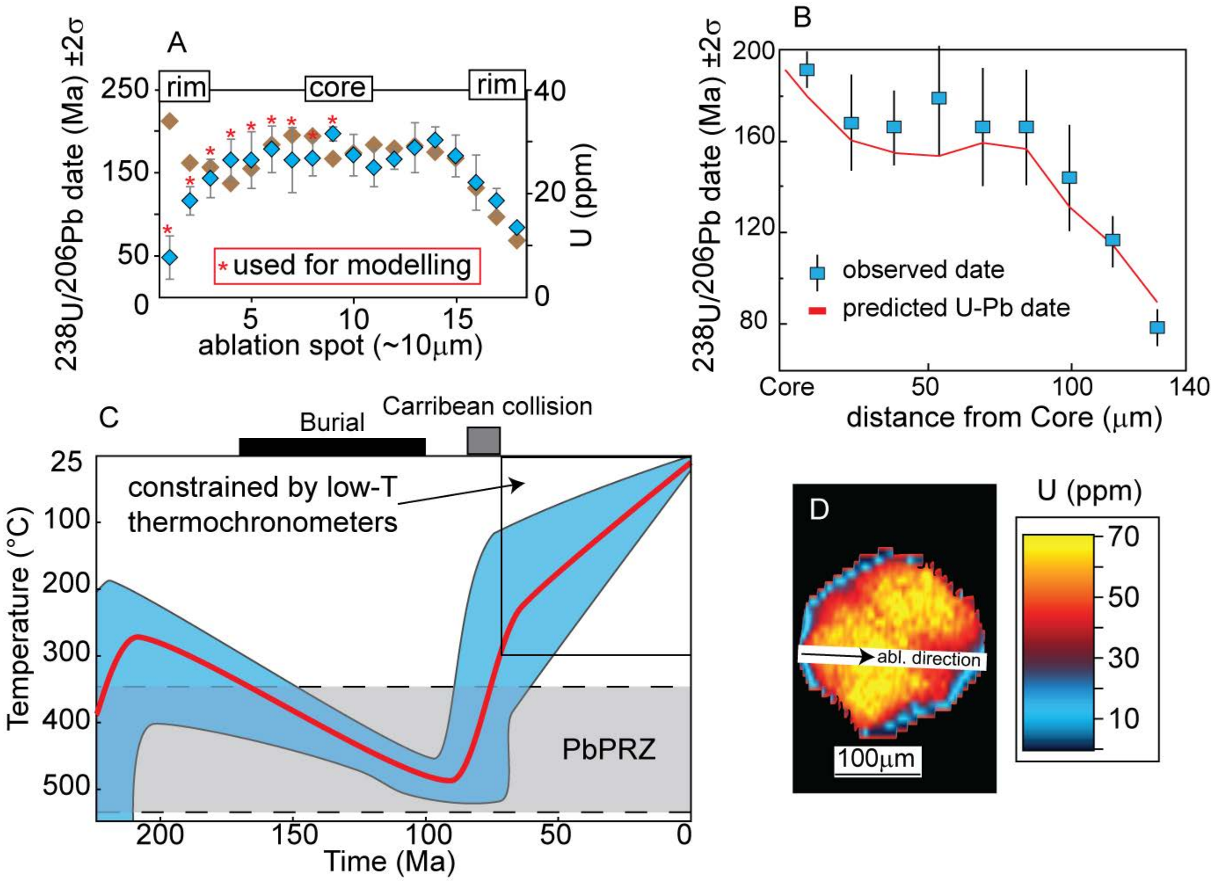

Figure 1. A) Rim-core-rim U-Pb date profile and U concentrations measured perpendicular to the crystallographic c-axis (the rock is a Triassic monzogranitic leucosome). The profile was measured as a raster and segemented into 10mm increments to facilitate input into the inversion model. The observed and predicted dates are presented in B). C) Thermal history solutions obtained by inversion reveal reheating into the apatite Pb Partial Retention Zone (PbPRZ; red line is the best-fit solution), which is defined as the closure temeprature at the core of the grain and at 95% distance from the core towards the rim (Dodson, 1986). D) U-distribution map (5 micron spatial resolution) reveals core enrichment, which is interpreted as a primary magmatic feature.

2.11

Effect of apatite crystal geometry, parent isotope zonation and petrological environment on its closure temperature (U-Th-Pb system)

Daniil Popov[1], Richard Spikings[1]

[1]Department of Earth Sciences, University of Geneva, Rue des Maraîchers, 13, CH-1205 Geneva (Daniil.Popov@unige.ch)

High temperature thermochronology (>150°C) is used to study a range of processes from planetary accretion and meteorite impacts to exhumation of deep crust. Thermochonology assumes that radiogenic daughter isotopes are dispersed by volume diffusion. Additional important assumptions made by previous studies (e.g. Cochrane et al. 2014, Dodson 1973) are (1) daughter isotopes are completely lost once they reach the crystal boundary, (2) crystals can be approximated by a simple geometry (e.g. sphere, infinite slab or infinite cylinder), and (3) parent isotopes are homogeneously distributed within crystals. However, within rocks minerals are surrounded by other minerals, which possibly inhibits radiogenic isotope loss at their boundaries. Furthermore, crystals frequently have complex geometries and uranium zonation in apatite is ubiquitous. This study aims to test the assumptions listed here for the U-Th-Pb-in-apatite thermochronometer.

The problem was explored numerically by finite difference modelling of the radiogenic ingrowth and volume diffusion of $^{208, 207, 206, 204}Pb$ in apatite crystals of different geometry and $^{238,235}U$ and ^{232}Th zonation. At the grain boundary, modelled grains were either open to complete daughter isotope loss or were juxtaposed against another phase. In the latter case apatite and the surrounding mineral were assumed to be in equilibrium at the boundary according to the partition coefficient between the phases ($Kd=C_{host}/C_{inclusion}$), which was assumed to be constant through time. Pb-in-apatite diffusion parameters were taken from (Cherniak 2010a), while diffusion through host alkali feldspar utilises parameters of (Cherniak 2010b). Calculations were done using MATLAB.

Our preliminary results indicate that the apatite crystal environment, geometry and compositional zonation can significantly influence the bulk grain date and in-situ dates of crystals that have experienced protracted thermal histories within a temperature zone where Pb is partially lost by volume diffusion. Depending on the approach, knowledge of all these factors may be necessary for the accurate reconstruction of thermal histories. (1) Crystal environment may significantly affect the closure temperature (Fig. 1a). (2) If daughter isotopes are completely lost at the boundary, crystal zonation has a considerable effect on the bulk grain date (Fig. 1b). . In contrast, if isotopes are dispersed into a surrounding phase with diffusion properties similar to alkali feldspar, the zonation effect diminishes. (3) For grains with equivalent smallest dimensions, the predicted bulk grain date and within-grain date profiles depend on both crystal zonation and geometry.

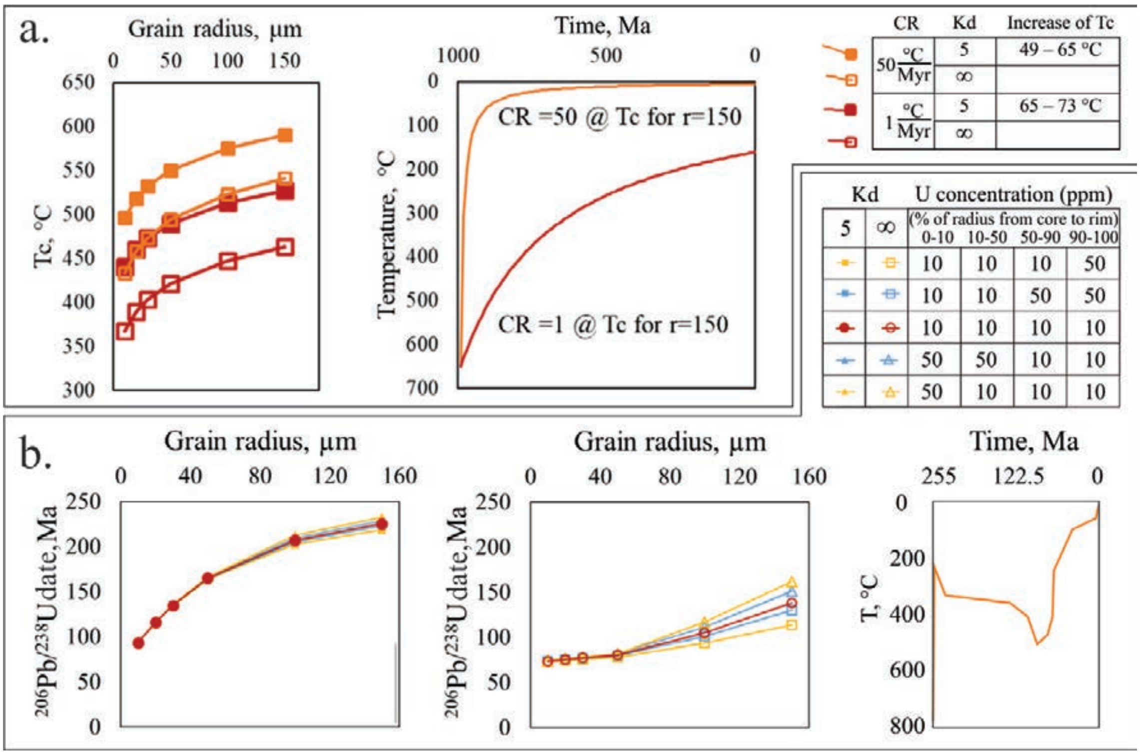

Figure 1. Results of calculations for spherical crystals either open to complete radiogenic isotope loss at the interface (Kd=∞) or having another adjacent phase at the boundary (Kd=5). *a*: Pb-in-apatite closure temperatures for compositionally homogeneous spherical crystals; thermal histories and values for Kd=∞ are are equivalent to using Dodson's equation (Dodson, 1973). *b*: bulk grain $^{206}Pb/^{238}U$ dates for compositionally zoned crystals that have experienced the same thermal history.

REFERENCES

Cherniak, D.J. 2010a: Diffusion in Accessory Minerals: Zircon, Titanite, Apatite, Monazite and Xenotime, Reviews in Mineralogy and Geochemistry, 72, 827-869.

Cherniak, D.J. 2010b: Cation Diffusion in Feldspars, Reviews in Mineralogy and Geochemistry, 72, 691-733.

Cochrane, R., Spikings, R. A., Chew, D., Wotzlaw, J. F., Chiaradia, M., Tyrrell, S., Schaltegger, U., & Van der Lelij, R. 2014: High temperature (> 350 C) thermochronology and mechanisms of Pb loss in apatite, Geochimica et Cosmochimica Acta, 127, 39-56.

Dodson, M. H. 1973: Closure temperature in cooling geochronological and petrological systems, Contributions to Mineralogy and Petrology, 40(3), 259-274.

2.12

The origin of Alpine-Himalayan K-rich orogenic lavas: an integrated experimental and geochemical approach

Prelević Dejan

Faculty of Mining and Geology, University of Belgrade, Djušina 7, (dejan.prelevic@rgf.bg.ac.rs)

The Alpine-Himalayan orogeny is one of the three major orogenic phases defining the geology of Europe and Asia. It generated accretionary orogen that occurs at a diffuse and long lived convergent zone between Eurasia and Gondwana, which has been active since Permian-Mesozoic times resulting in the consumption of major Tethyan ocean(s). The convergence varies in style involving accretion of small continental slivers and numerous oceanic island arcs in the west, to the world's most comprehensive continental collision in the east. It eventually gave rise to a complex collage enclosing continental crustal blocks intercalated with ophiolitic terrains of various sizes and ages forming superimposed mountainous belts.

Magmatism that occurs within these belts postdates final accretionary events forming the Alpine–Himalayan chain. It is diachronous with the most voluminous and widely distributed episode(s) beginning from the late Cretaceous. The magmatism is derived from both the mantle and the crust, and is geochemically extremely heterogeneous, but dominantly potassium enriched. Its origin and relationship to the large-scale elevations in several massifs (Tibet, Menderes etc.) of the orogen is controversial, particularly the significance of the widespread geochemical signal typical for recycled continental crust. Two competing scenarios invoke direct melting of continental crust during deep intercontinental subduction versus removal of heavily metasomatised mantle lithosphere by delamination into the convecting mantle. However, no direct evidence has been found to distinguish between these two models so far.

In my contribution I will draw conclusions about the geodynamic interpretation of orogenic lithospheric mantle within the Alpine–Himalayan combining the field and geochemical studies of K-rich post-collisional mantle-derived lavas from Spain, Italy, Balkans, Turkey, Iran and Tibet with newly developed high-pressure experimental approach. The composition of K-rich postcollisional lavas suggests that the orogenic mantle underwent much more intense and complex material recycling than anticipated only by fluid- or melt- dominated transport. This is based on several fundamental constraints: i) The lavas are strongly incompatible-element enriched with elevated $^{87}Sr/^{86}Sr$, $^{207}Pb/^{204}Pb$, $^{187}Os/^{188}Os$ and low $^{143}Nd/^{144}Nd$ and $^{176}Hf/^{177}Hf$ ratios. All these tracers represent a hallmark for continental crust; ii) The presence of an ultra-depleted component in the source of the K-rich lavas is identified by usual presence of refractory Cr-spinel, high Fo olivine and relatively low whole-rock FeO abundances; iii) Finally, extremely high Th/La is coupled with high Sm/La of potassic mantle-derived lavas points to a genetic relationship with the melange.

The above observations suggest that neither fluids nor melts alone can precondition orogenic mantle using known mechanisms that are active during material recycling within subduction zones, thus a new model is required. I will present a hypothesis that the orogenic mantle along the Alpine-Himalayan system is preconditioned during the previous episode(s) of "dirty" subduction. This process involves the formation of a new mantle lithosphere formed by accretion of suprasubduction fore-arc oceanic lithosphere plus trench sediments beneath older lithosphere during convergence within the Alpine-Himalayan system. The model demands conversion of the principally oceanic lithosphere (including melange) into the phlogopite-bearing continental lithospheric mantle and production of K-rich post-collisional lavas, which is a multi-component and multi-episodic process.

2.13

Mechanically controlled chemical zoning in UHP garnets from the Western Gneiss Region, Norway

Katharina Schmidt[1], Johannes Vrijmoed[2], Lucie Tajcmanova[1], Evangelos Moulas[3]

[1] Insitut für Geochemie und Petrologie, ETH Zürich, CH-8092 Zürich (katharina.schmidt@erdw.ethz.ch)
[2] Mineralogie & Petrologie, Freie Universität Berlin, D-12249 Berlin
[3] Institute of Earth Sciences, Universite de Lausanne, CH-1015 Lausanne

Garnets from the Western Gneiss Region (WGR) experienced Caledonian ultra-high pressure (UHP) metamorphism with peak metamorphic conditions around 800°C at > 3.2 GPa, and a post-UHP amphibolite-facies overprint during exhumation. Garnets from this region preserve prograde chemical zoning, despite being exposed to high temperature during slow subduction and exhumation of the WGR. Current knowledge on chemical diffusion rates in garnet may not be enough to explain the preservation of zonation in these garnets because at the million-year time scale it predicts complete chemical re-equilibration at such high temperature. Interestingly, when chemical diffusion is relatively fast, the development and preservation of compositional zoning in minerals can be strongly influenced by mechanically maintained pressure variations (Tajcmanova 2015).

Here, we compare the application of conventional diffusion methods with the newly developed unconventional quantification methods (Vrijmoed & Podladchikov, 2015) on natural garnets from the WGR. The new approach predicts compositional zoning as a result of spatially varying pressure at chemical equilibrium. The results are used to test whether the observed chemical zoning can be fit by equilibrium at heterogeneous pressure. First results show a good fit with natural observed chemical zoning in garnet multi-component systems. This enables an explanation for chemical zoning by local pressure variations instead of sluggish kinetics.

REFERENCES

Tajcmanova L., Vrijmoed J., Moulas E., (2015) Grain-scale pressure variations in metamorphic rocks: implications for the interpretation of petrographic observations. Lithos 216–217:338–351.

Vrijmoed, J. & Podladchikov, Y.Y., (2015) Thermodynamic equilibrium at heterogeneous pressure. Contributions to Mineralogy and Petrology, 16, p.14910.

2.14

Melting and modification of the mantle wedge beneath the West Bismarck island arc, evidenced by the chemical and isotopic composition of peridotite xenoliths

Peter Tollan[1,2], Chris Dale[1], Jörg Hermann[2], Jon Davidson[1], Richard Arculus[3]

[1] *Department of Earth Sciences, Durham University, Durham, United Kingdom*
[2] *Institut für Geologie, Universität Bern, Bern, Switzerland*
[3] *Research School of Earth Sciences, The Australian National University, Canberra, Australia*

Pristine peridotite xenoliths erupted from seamounts surrounding Ritter Island, West Bismarck island arc provide a rare opportunity to study the chemical and physical manifestation of processes which modify the upper mantle wedge beneath active oceanic arcs. The sample suite consists of a lithologically and texturally diverse array of ultramafic rocks; dominantly harzburgites but also subordinate dunites and pyroxenites. A broad range of textures can be observed within the harzburgite samples. Coarse protogranular textures are most common, but the frequent occurrence of disequilibrium (reaction) textures, such as secondary mineral patches and veins indicates a complex and spatially heterogeneous record of petrogenetic processes. The secondary textures consist dominantly of veins of pure orthopyroxene, forming at the expense of olivine, however occasionally veins or patches of inter-grown, fine-grained clinopyroxene, orthopyroxene(s) and/or glass can be observed. More rarely, veins of coarse clinopyroxene are found, which display better grain-boundary equilibration than the other vein types.

Chemical and isotopic differences between the texturally distinct samples are clear. Samples with protogranular textures have highly refractory bulk-rock trace element compositions indicative of extensive degrees of partial melting, in agreement with the high olivine Mg# (0.905-0.922) and spinel Cr# (0.495-0.614). The heavy rare earth element systematics of coarse-grained orthopyroxene were modelled to quantify this melting history, and indicate that wet melting must have occurred in order to generate such depleted compositions, close to or beyond the point of clinopyroxene exhaustion (and clearly distinct from the melting trend displayed by orthopyroxene from global abyssal peridotites). It is therefore concluded that melting to form the Ritter peridotite residues took place in a subduction zone setting. This is confirmed through their bulk-rock Sr isotope composition, which, despite the very low Sr concentrations is substantially enriched isotopically over typical MORB and overlapping in composition with sediments being subducted in the broad tectonic region ($^{87}Sr/^{86}Sr$ up to ~0.7049).

Samples with reaction textures show considerable enrichment in most whole-rock trace elements, with the exceptions of the high field strength elements and Ti, which show no or minimal enrichments compared to protogranular samples. Bulk laser ablation of glass-bearing reaction patches provides a more direct view of the trace element composition of the melt responsible for generating the observed textures. Both these analyses and the compositional difference between enriched and depleted whole-rock peridotites bear striking resemblances to the trace element composition of locally erupted basalts, indicating that similar melts were involved in the reaction textures observed. This is further supported by bulk-rock $^{87}Sr/^{86}Sr$ of samples which overlap with the isotopic composition of West Bismarck lavas (down to 0.7034). Thermometry results on secondary reaction patches reveal very high temperatures of formation, close to the wet basalt liquidus at upper mantle pressures (1220-1260 °C) and much higher than equilibration temperatures for the protogranular peridotites (down to 660-760 °C). The maintenance of such high temperatures, combined with the high degree of textural disquilibrium confirms that the secondary texture formation was a relatively recent event, associated with modern magmatic activity beneath the island arc.

The Ritter suite thus provides a remarkably detailed insight into the broad diversity of melt/fluid compositions and fluid-rock reaction processes of oceanic sub-arc mantle. Several of these features can be found both in other samples of sub-arc mantle and also cratonic mantle, demonstrating the ubiquity of such processes beneath modern arcs and also the potential genetic relationship between subduction zone processes and the formation of cratons. In this way, sub-arc xenoliths such as the Ritter suite, whilst presently under-sampled, can provide crucial insights for understanding the relationship between the mechanisms by which modern arc systems are generated and evolve, and the nature of the upper mantle once subduction processes have ceased.

2.15

Garnet chemical and oxygen isotope zoning and accessory mineral investigation to constrain the evolution of subducted continental crust (Sesia Zone, Italy)

Alice Vho[1], Daniela Rubatto[1,2], Pierre Lanari[1], Francesco Giuntoli[3] & Daniele Regis[4]

[1] *Institut für Geologie, University of Bern, Baltzerstrasse 1+3, CH-3012 Bern (anlice.vho@geo.unibe.ch)*
[2] *Institut des sciences de la Terre, University of Lausanne, Géopolis, CH-1015 Lausanne*
[3] *School of Geography, Earth and Environmental Sciences, Plymouth University, PL4 8AA, Portland Square, Plymouth UK*
[4] *Geological Survey of Canada, 601 Booth Street, K1A 0E8 Ottawa, Ontario Canada*

Garnet is a key mineral in metamorphic petrology for constraining pressure and temperature (P-T) paths. Garnet can preserve multiple growth stages due to its wide P-T stability field and the relatively slow diffusivity for major and trace elements at sub-solidus temperatures. P-T-t-fluid paths of the host rock may be reconstructed by combining metamorphic petrology with microscale trace element and oxygen isotope measurements in garnet and accessory mineral in situ dating. Subduction zones represent relevant geological settings for geochemical investigation of element exchanges during aqueous fluid-rock interactions. The Sesia Zone consists of a continental sequence containing a variety of mono- and poly-metamorphic lithologies such as metagranitoids, sediments and mafic boudins.

The Varisican-Permian granulite to amphibolite-facies basement (6-9 kbar 650-850°C; Lardeaux & Spalla 1991) experienced HP metamorphism (15–22 kbar 500–550°C; Regis et al. 2014) during Alpine subduction. In different lithologies of the Internal Complex (Giuntoli & Engi 2016), including metabasites from Ivozio Complex, Ti-rich metasediments from Val Malone, micaschists from Lys Valley and pre-Alpine Mn-quartzites associated to metagabbros from Cima Bonze, garnet is abundant and shows a variety of textures that can be related to resorption, replacement and possible metasomatism. Internal zoning in zircon in these samples preserves information about the age of the protolith (ca. 350 Ma gabbro at Ivozio), Permian (Val Malone) and Alpine metamorphism (Ivozio and Lys Valley).

In-situ microscale oxygen isotopes analysis of garnet zones was performed by ion microprobe with the SwissSIMS Cameca at University of Lausanne and SHRIMP-SI at the Australian National University. Each sample has a distinct $\delta^{18}O$ composition and shows different degrees of variation between domains. Homogeneously values of <5‰ are measured in the garnets from Ivozio metagabbro. Intragrain variations up to ~3.5‰ in the porphyroblasts from Val Malone metasediments, and up to ~6.5‰ in Cima Bonze garnets suggest significant metasomatic replacement from external fluids. The combination of oxygen isotopes, trace element geochemistry and geochronology, and P-T modelling allows reconstructing the major stages of metasomatism, as well as identifying the nature of the fluid interacting with the rock at each metamorphic stage.

REFERENCES

Lardeaux, J. M., & Spalla, M. I. 1991: From granulites to eclogites in the Sesia zone (Italian Western Alps): A record of the opening and closure of the Piedmont ocean. Journal of Metamorphic Geology, 9, 35–59.

Regis, D., Rubatto, D., Darling, J., Cenki-Tok, B., Zucali, M., & Engi, M. 2014: Multiple metamorphic stages within an eclogite-facies terrane (Sesia Zone, Western Alps) revealed by Th–U–Pb petrochronology. Journal of Petrology, 55, 1429-1456.

Giuntoli, F., & Engi, M. 2016: Internal geometry of the central Sesia Zone (Aosta Valley, Italy): HP tectonic assembly of continental slices. Swiss Journal of Geosciences, 109, 445-471.

2.16

Epidosite alteration of the oceanic crust: cumulative water–rock ratios derived from reactive-transport modelling

Samuel Weber[1], Larryn W. Diamond[1], Peter Alt-Epping[1]

[1] *Rock–Water Interaction, Institute of Geological Sciences, University of Bern, Baltzerstrasse 1+3, CH-3012 Bern, Switzerland (samuel.weber@geo.unibe.ch)*

Oceanic crust is subject to extensive fluid-rock interaction soon after formation. Driven by hot, shallow intrusives, recharging seawater is heated and chemically modified by chemical reactions with basaltic wall-rocks. The rocks in turn are pervasively altered to ‹spilites› consisting of chlorite + albite + quartz + hematite + titanite ± actinolite. Along the discharge path of these convective systems, the fluid is thought to alter pre-existing spilites to ‹epidosites›, i.e. rocks consisting of epidote + quartz + Fe-oxides + titanite (e.g. Richardson et al., 1987; Alt, 1995). When the fluid reaches the seafloor at focussed vents, it may form black smokers, eventually producing volcanogenic massive suphide (VMS) deposits. Insights into these hydrothermal processes are primarily gained from active seafloor vents (e.g. Von Damm, 1995), studies of fossil oceanic crust, i.e. ophiolites (e.g. Harper et al., 1988; Gilgen et al., 2016) and hydrothermal experiments (e.g. Seyfried et al., 1988). However, owing to insufficient knowledge of the hydrothermal reactions involved, the significance of epidosites as markers of fluid discharge paths and their link to VMS deposits are debated (e.g. Jowitt et al., 2012; Gilgen et al., 2016). In the present study we use quantitative reactive-transport modelling to provide a new perspective on this issue.

The first question we have addressed is the volume of fluid that has infiltrated each cubic metre of rock (water–rock ratio) during epidotisation. This is an important variable to quantify, as it sets constraints on the total fluid recycled through the oceanic crust and on the capacity of the fluid to transport metals to the VMS deposits. Differing estimates of cumulative water–rock (W/R) ratios required to form epidosites have been made in the past (e.g. Richardson et al., 1987; Seyfried et al., 1988; Bettison-Varga et al., 1995). Depending on the method used (e.g. stable isotopes, strontium isotopes, base-metal balance calculations, experimentally determined magnesium solubility or batch reaction modelling), these mass-ratios vary from 10:1 to over 1000:1.

Using the reactive-transport code Flotran (Lichtner, 2007), we have performed isothermal, isobaric simulations of the spilite-to-epidosite transformation at subseafloor conditions (350 °C, 40 MPa, 0.5 mol/kg Cl^-), as determined by fluid inclusions in epidosites in the Semail Ophiolite, Oman (Richter and Diamond, 2017). The results reproduce the changes in mineralogy, whole-rock composition and rock porosity observed in the Semail epidosites (Gilgen et al., 2016; Brett et al., 2017).

We have found that epidosites can be formed by fluids with a range of initial aqueous Ca/Na concentrations and *pH* values. The modelling results confirm that large volumes of fluid are required to achieve complete epidotisation. The main reason is the requirement that magnesium, which has a low solubility at elevated temperatures, must be completely leached from the precursor spilite. Minimum W/R volume ratios of 500:1 are necessary to achieve complete epidotisation at a *pH* of 4. Much larger volumes are needed if the fluid has a higher *pH*, owing to the *pH*-dependence of the Mg concentration in equilibrium with the rock. While these results do not necessarily limit epidotisation to low-*pH* fluids, complete epidotisation becomes increasingly unlikely at neutral *pH* because of the enormous amounts of fluid required.

REFERENCES

Alt, J. 1995: Subseafloor Processes in Mid-Ocean Ridge Hydrothermal Systems. Seafloor Hydrothermal Systems: Physical, Chemical, Biological and Geological Interactions, Geophysical Monograph 91, 85-114.

Brett, A. C., Diamond , L. W., and Gilgen, S. 2017: Deep flow paths in VMS systems: Porosity and permeability of epidosite alteration in the Semail ophiolite, Oman, in Proceedings SGA Annual Conference, Quebec City, Quebec, Canada, 2017. Abstracts Volume, p. 661-664.

Bettison-Varga, L., Schiffman, P. and Janecky D. 1995: Fluid-rock interaction in the hydrothermal upflow zone of the Solea graben, Troodos ophiolite, Cyprus. Geological Society of America Special Paper, 296, 81-100.

Gilgen, S., Diamond , L. W., and Mercolli, I., 2016: Sub-seafloor epidosite alteration: Timing, depth and stratigraphic distribution in the Semail Ophiolite, Oman: Lithos, v. 260, p. 191–210.

Harper, G., Bowman, J. and Kuhns, R. 1988: A field, chemical and stable isotope study of subseafloor metamorphism of the Josephine ophiolite, California-Oregon. Journal of geophysical research, 93, 4625-4656.

Jowitt, S. M., Jenkin, G. R. T., Coogan, L. A., and Naden, J., 2012: Quantifying the release of base metals from source rocks for volcanogenic massive sulfide deposits: Effects of protolith composition and alteration mineralogy: Journal of Geochemical Exploration, v. 118, p. 47-59.

Lichtner, P. C., 2007: FLOTRAN User's Manual: Two-phase non-isothermal coupled thermal-hydrologic-chemical (THC) reactive flow and transport code, Version 2, Los Alamos National Laboratory, Los Alamos, New Mexico.

Richardson C., Cann, J. Richards, H. and Cowan, J. 1987: Metal-depleted root zones of the Troodos ore-forming hydrothermal systems, Cyprus. Earth and Planetary Science Letters, 84, 243-253.

Richter, L., and Diamond, L. W. 2017; Epidotization of the oceanic crust: products of hydrothermal alteration caused by brines or by modified seawater?, in Proceedings European Current Research on Fluid Inclusions ECROFI, Nancy, France, July 2017, Abstracts Volume, p. 108.

Seyfried, W., Berndt, M. and Seewald, J. 1988: Hydrothermal alteration processes at mid-ocean ridges: constraints from diabase alteration experiments, hot-spring fluids and composition of the oceanic crust. Canadian Mineralogist, 26, 787-804.

Von Damm, K. 1995: Controls on the Chemistry and Temporal Variability of Seafloor Hydrothermal Fluids. Seafloor Hydrothermal Systems: Physical, Chemical, Biological and Geological Interactions, Geophysical Monograph 91, 222-247.

2.17

Metal enrichment in granitic melts: the role of protolith chemistry and partial melting conditions

Mathias Wolf[1], Rolf L. Romer[1] & Leander Franz[2]

[1]German Research Centre for Geoscience GFZ, Telegrafenberg, D-14473 Potsdam (mwolf@gfz-potsdam.de)
[2]Institute of Mineralogy and Petrography, University of Basel, Bernoullistrasse 30, CH-4056 Basel

The mobilization of ore elements during partial melting of metasedimentary rocks critically influences the potential of granitic melts to develop mineralizations. We present data from migmatite samples together with thermodynamic modeling results to highlight the importance of protolith chemistry, melting conditions and mode of melt extraction during the generation of Sn-enriched granitic melts.

The distribution of elements between melt and restite is controlled by the stability of element-sequestering minerals during melt generation. The stability of a phase with high affinity for a certain element in the restite prevents enrichment of the corresponding element in the melt and leads to its enrichment in the restite. For Sn, muscovite, biotite, titanite and magnetite represent such sequestering phases in metasedimentary rocks. As muscovite and biotite are involved in dehydration melting at different conditions, those two minerals play a key role for the distribution and mobilization of Sn during partial melting. Release of Sn during the breakdown of muscovite at lower temperatures does not necessarily lead to Sn-rich melts, as large quantities of Sn can be redistributed into restitic biotite, leading to Sn-enrichment in the restite. Further heating, eventually resulting in biotite dehydration melting of Sn-enriched restitic rocks leads to Sn-rich melts, if no other Sn-sequestering phase is stable. Biotite dehydration melting starts at elevated temperatures (>800 °C). Crust internal heat production alone is not sufficient to reach such high temperatures. Therefore, there must be additional advective heat input to reach biotite stability limits. Such heat input may originate from input of mantle melts in subduction zones (e.g. South China, Malaysia), crustal extension (e.g. Cornwall) or the emplacement of UHT metamorphic units in settings of continental collision (e.g. Variscan orogen, in particular the Erzgebirge).

Strongly weathered Paleozoic shales represent an ideal protolith for the generation of Sn-enriched granitic melts. Due to the intense weathering they show a depletion in the feldspar-bound elements Ca, Na, Sr and Pb and a relative enrichment in Al, K, Rb and Sn. The distinct chemical composition (low Ca, Na and high Al, K) leads to a very specific mineral assemblage with high modal amounts of hydrous minerals during prograde metamorphism. These high amounts of muscovite and biotite lead to high amounts of melt during partial melting. The concentration of Sn in the melt is not only a function of Sn concentration in the protolith but also of the melt volume and removal of low-T melts. If Sn is released into large amounts of low Sn-melt from muscovite dehydration melting, the overall concentrations will remain low. Thus, melt extraction prior to the decomposition of biotite and the resulting release of Sn enhances Sn concentration in late melts. The high modal abundance of muscovite leads to high melt volumes at low temperatures, which facilitates the extraction of melt before the breakdown of biotite. Partitioning of Sn into small melt volumes results in elevated concentrations in the melt, even before further enrichment by fractional crystallization starts.

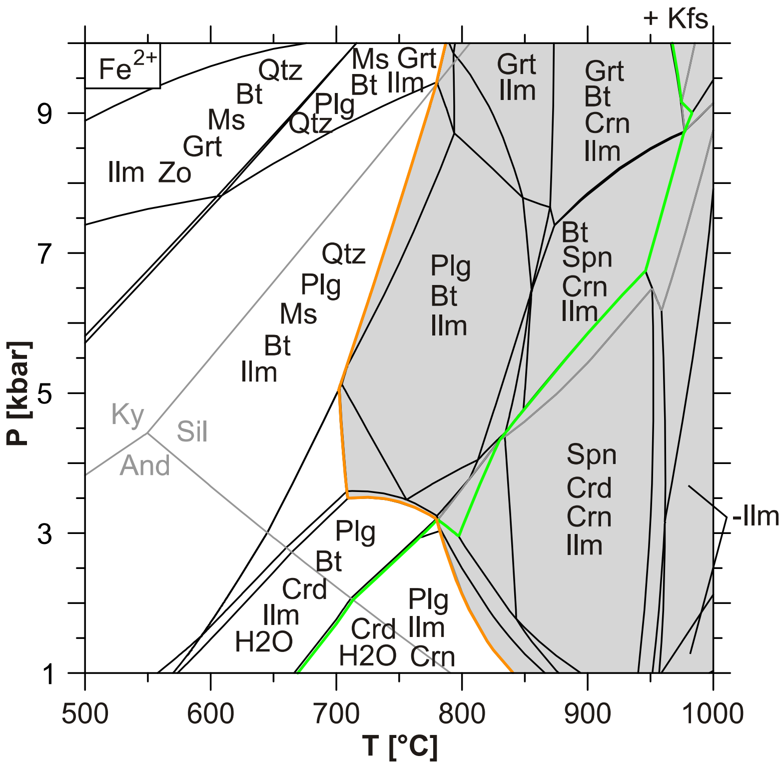

Figure 1. Equilibrium phase diagram for a deeply weathered shale. The red line represents the solidus of the system and the melt generation by muscovite breakdown at elevated pressures. The green line denotes the biotite stability limit. Melts generated before the breakdown of biotite are unlikely to be Sn-enriched as much of it is redistributed into restitic biotite.

P 2.1

High-precision zircon dating of miocene magmatism in the Apuseni Mountains (Romania) with TIMS

Manuel Brunner[1] & Lukas Müller[1]

[1]Institute of Geochemistry and Petrology, Department of Earth Science, ETH Zurich, Clausiusstrasse 25, CH-8092 Zurich (mbrunner@student.ethz.ch)

Most of the calc-alkaline and alkaline magmatic rocks in the southern Apuseni Mountains (SAM) are Neogene in age. They mainly crop out along the NW-SE oriented Zarand-Brad-Zlatna intra-mountain basin. The graben like structure is a consequence of a translational and rotational movement of the Tisia block (Harris et al. 2013). Roşu et al (2004a) showed that the intrusives were emplaced between 14.7 and 7.4 Ma (K-Ar ages) and also proposed the involvment of fluids to explain a “subduction signature” in the extensional magmatism in the area. The SAM is characterized by numerous porphyry copper(-gold) deposits and is known as the “Golden Quadrangle” due to some of Europe’s biggest Au-Ag deposits. Three main time intervals for the mineralization ages are 13.6 Ma for the Rosia Montana area, the second in regional scale between 12.5-10 Ma and the third between 9.5-8.5 Ma at Baia de Aries (Roşu et al. 2004b).

With a thermal ionization mass spectrometry on zircons (von Quadt et al. 2015) we try to confine the old K-Ar ages. Some of the intrusions in deposit scale are too similar to see a trend in the area (e.g. basin opening, mineralization ages).

Samples of intrusions (outcrops and boreholes) were collected in and around the basin. At Rovina Valley and Certej exploration sites we were able to gather material of pre-, syn- and post mineralization dykes.

REFERENCES

Harris, C. R., Pettke, T., Heinrich, C. A., Roşu, E., Woodland, S. & Fry, B. 2013, Tethyan mantle metasomatism creates subduction geochemical signatures in non-arc Cu–Au–Te mineralizing magmas, Apuseni Mountains (Romania). Earth and Planetary Science Letters, v. 366, p. 122-136.

Roşu, E., Seghedi, I., Downes, H., Alderton, D.H.M., Szakács A., Pécskay, Z., Panaiotu, C., Panaiotu, C.E., & Nedelcu, L. 2004:

Extension-related Miocene calc-alkaline magmatism in the Apuseni Mountains, Romania: origin of magmas. Swiss Bull. Miner. Petrol., 84/1–2, pp. 153-172

Roşu, E., Udubaşa, G., Pécskay, Z., Panaiotu, C., & Panaiotu, C.E. 2004:

Timing of Miocene–Quaternary Magmatism and Metallogeny in the South Apuseni Mountains, Romania. Economic Geology “Gold in Metaliferi Mountains”, Alba Iulia, Romania, Plenary Lectures, Rom. J. Miner. Depos., vol. 81, pp. 33-38

von Quadt, A., Wotzlaw, J.-F., Buret, Y., Large, S. J. E., Peytcheva, I. & Trinquier, A. 2016, High-precision zircon U/Pb geochronology by ID-TIMS using new 1013 ohm resistors. Journal of Analytical Atomic Spectrometry, v. 31, no. 3, p. 658-665.

P 2.2

Heterogeneities in natural $^{40}Ar/^{39}Ar$ flux monitors and pristine magmatic micas

Maria Naumenko-Dèzes[1], Yann Rolland[1], Sylvain Gallet[1], Igor M. Villa[2]

[1] *Geoazur, Université Nice Sophia Antipolis, France (marie@geosphere.ch)*
[2] *Geologisches Institut, Universität Bern, Switzerland*

The K-Ar geochronometer, and the $^{40}Ar/^{39}Ar$ technique deriving from it, are amongst the most widely used tools for dating geological samples. Since its invention, the accuracy and reproducibility $^{40}Ar/^{39}Ar$ dating technique plays an important role in determining the age of planets, constraining the durations of geological processes and establishing their sequence of occurrence. The reliability of studies addressing Earth's history and dynamics, in particular in terms of rates, cycles and periodicities closely depends on our ability to calculate these ages with the best possible precision and accuracy. Currently the total uncertainty of the $^{40}Ar/^{39}Ar$ method due to uncertainty contributions of the ^{40}K decay constant, the branching ratio and the flux monitor ages is estimated to be larger than 1.5% (Dèzes, 2016). However, modern Ar mass-spectrometry can produce ages with the laboratory in-run statistical dispersion of the measurements of 0.2%, that gives the opportunity to ascertain the intragrain age distributions on relative scale with permil precision. In this study two types of minerals were investigated: (1) sanidine flux monitors (Fish Canyon (FCs) and Yulinshan (YBCs)) and (2) pristine micas (Palaborwa plutonic complex and Rubikon pegmatite).

In literature, step-heating of sanidine flux monitors, such as FCs and Alder Creek (ACs), resulted in discordant age spectra, which were attributed to a combination of mass fractionation, inherited Ar and minor recoil effects (Phillips and Matchan, 2013; Phillips et al, 2017). Hall (2014) extensively discussed the influence of impurity phases on recoil of Ar isotopes during irradiation. We investigated FCs and YBCs with a precision of 0.2%, additionally measuring all five Ar isotopes. We observed that most of the age discordance is accounted for by heterochemical impurities. The discordance of the age spectrum is similar to that of the literature data (which, however, do not discuss the heterochemical Ca/Cl/K systematics). It can also be noted that more discordant age spectra were obtained on ARGUSVI mass-spectrometers equipped with CO_2 laser system, whereas step-heating of the YBCs in a resistance furnace connected to a VG5400 mass spectrometer did not produce discordant age spectra (Wang et al., 2014).

The second type of samples, pristine micas from retrogression-free magmatic complexes (such as the Phalaborwa carbonatite) were studied to observe the intragrain age distribution as well as step-heating behavior (see Fig.1). Intra-grain age variations are well known for samples recording retrogression reactions (Hames & Cheney, 1997; Villa & Hanchar, 2017). Especially when chemical alteration patches deviate by less than 1 % from stoichiometry, they escape detection by electron microprobe analysis, but can be detected by $^{40}Ar/^{39}Ar$ analyses, which can achieve a 0.2 % precision. Thus, investigation of intra-grain K-Ar age distributions is crucial for systematic calibration work.

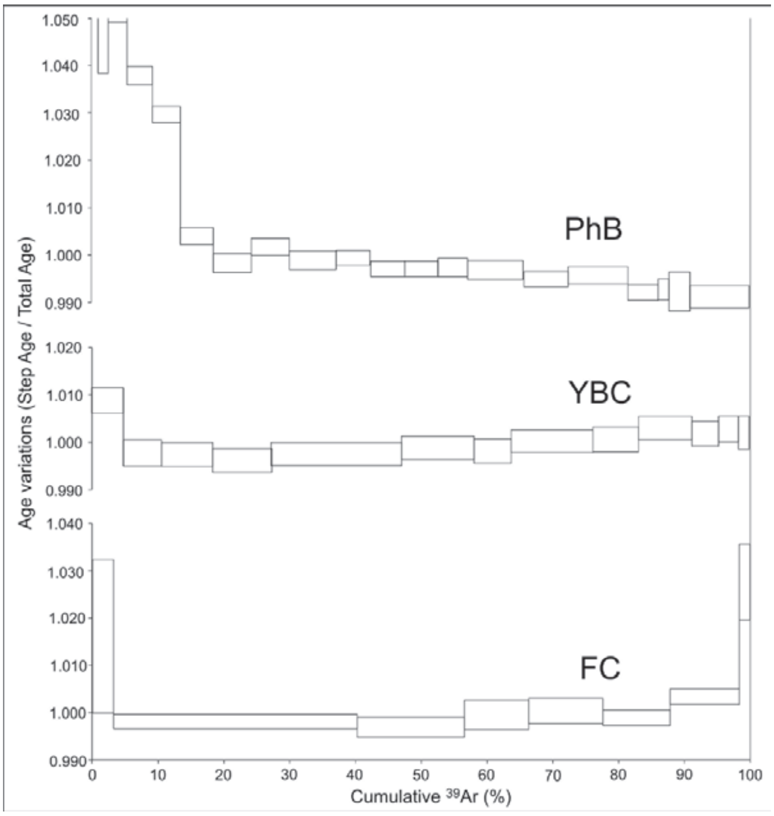

Figure 1. Comparison of step-heating age spectra for Fish Canyon sanidine (FC), Yulinshan sanidine (YBC), Phalaborwa phlogopite (PhB).

REFERENCES

Dèzes M (2016). Refined isotopic compositions of K, Ca and a complementary comparison of the ^{40}K-^{40}Ca, ^{40}K-^{40}Ar and ^{87}Rb-^{87}Sr chronometers. PhD thesis. Institut für Geologie. Universität Bern. 160pp.

Hall, Ch.M. (2014). Direct measurement of recoil effects on ^{40}Ar/ ^{39}Ar standards. Geol. Society, London, Special Publications, 378, 53–62.

Hames, W.E. and Cheney, J.T. (1997). On the loss of $^{40}Ar^*$ from muscovite during polymetamorphism. Geochim. et Cosmochim. Acta, 61(18), pp. 3863-3872

Phillips D. and Matchan E. L. (2013) Ultra-high precision $^{40}Ar/^{39}Ar$ ages for Fish Canyon Tuff and Alder Creek Rhyolite sanidine: New dating standards required? Geochim. Cosmochim. Acta 121, 229–239.

Phillips D., Matchan E. L., Honda M. and Kuiper K. F. (2017) Astronomical calibration of $^{40}Ar/^{39}Ar$ reference minerals using high-precision, multi-collector (ARGUSVI) mass spectrometry. Geochim. Cosmochim. Acta.

Villa I.M., Hanchar J.M., 2017. Age discordance and mineralogy. American Mineralogist

Wang F., Jourdan F., Lo C. H., Nomade S., Guillou H., Zhu R., Yang L., Shi W., Feng H., Wu L. and Sang H. (2014) YBCs sanidine: A new standard for $^{40}Ar/^{39}Ar$ dating. Chem. Geol. 388, 87–97

P 2.3

Oxygen isotopes in white mica from the Larderello geothermal field – a potential tool to trace fluid flow in complex magmatic – hydrothermal systems

Florian Bulle[1], Daniela Rubatto[1], Giovanni Ruggieri[2]

[1]Institut für Geologie, Universität Bern, Baltzerstrasse 1+3, CH-3012 Bern (florian.bulle@geo.unibe.ch)
[2]CNR-Instituto di Geoscienza e Georisorse, Via La Pira 4, I-50121 Firenze

The Larderello geothermal field in southern Tuscany is underlain by a series of shallow intrusions of isotopically and geochemically distinct two-mica granites belonging to the Miocene-Pleistocene Tuscan Magmatic Province (Dini et al. 2005). Their emplacement in already thinned contintental crust produced an extensive geothermal anomaly that has been commercially exploited for over 100 years. Muscovite is ubiquitous in the granites, the contact metamorphic aureole and the deep pre-Alpine metasedimentary units that constitute the lower reservoir. Texturally and chemically distinct generations of muscovite record stages of magmatic crystallization, thermometamorphic/hydrothermal replacement and fluid/rock interaction (Petrucci et al. 1994, Cavaretta & Puxeddu, 2001).

Existing O isotope data of whole rock and mineral separates indicates that granite and contact metamorphic rocks have been gradually depleted in d^{18}O (+5-12‰; Gianelli & Ruggieri 2002). Although some secondary minerals, such as muscovite, proved highly retentive and retained its pre-alteration signature (+8-10‰), biotite can have d^{18}O values as low as +1.5‰ (Petrucci et al. 1994). Bulk rock and mineral oxygen isotope values thus show evidence of both hydrothermal stages, especially in the deeper part of the reservoir. However, the complex textural and chemical characteristics of single muscovite grains (Fig.1) may record several individual episodes of fluid-rock interaction. An *intra-grain* variation in the muscovite O isotope signature is thus expected based on lithology, spatial distribution, hydrothermal alteration grade and formation age. To investigate that we will perform in-situ O isotope microanalyses with Secondary Ion Mass Spectrometry (SIMS) on muscovite from granite, contact metamorphic micaschist and phyllite, and metasediments from the upper and lower reservoir rocks from geothermal wells.

We have identified at least two muscovite generations that show textural and chemical differences. Preliminary data for muscovite in granite indicates an early fine-grained, Na-bearing (0.09-0.19 apfu), Mg- and Fe-poor (<0.15 Mg+Fe$_{tot}$ apfu) generation and a late, complex-zoned, coarse-grained Mg-Fe-rich (0.3-0.8 Mg+Fe$_{tot}$ apfu) population (Fig.1A). Muscovite from the thermometamorphic units is chemically variable (3.0-2.3 Al apfu, 3.0-3.3 Si apfu, 0.0-0.4 Mg apfu) and texturally complex (Fig.1B-C). The lone meta-arkose sample from the upper reservoir has one chemically homogeneous muscovite generation (2.7-2.4 Al apfu, 3.3-3.2 Si apfu, 0.2-0.4 Mg apfu, Fig.1D) and one slightly heterogeneous generation with an intra-grain Na variation of 0.0 to 0.2 apfu. We expect that the O isotope signature varies within the different muscovite generations and/or chemical domains in response to fluid-induced re-crystallization and O isotope exchange.

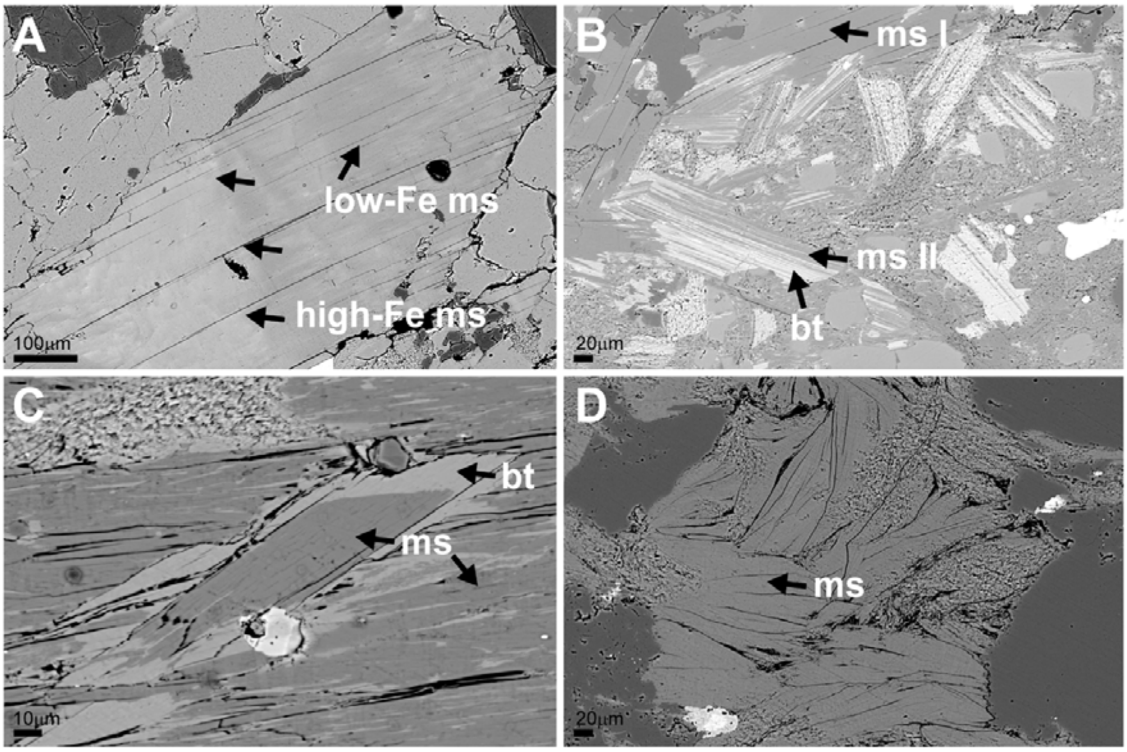

Figure 1. Back-scatter electron (BSE) images of representative muscovite grains in A – granite, B-C – contact aureole micaschist, D – meta-arkose from upper reservoir (ms – muscovite, bt – biotite)

REFERENCES

Cavarretta, G., Puxeddu, M., 2001: Two-mica F–Li–B-rich monzogranite apophysis of the Larderello batholith cored from 3.5km depth. N. Jb.Miner.Abh. 177, 77–112.

Dini, A., Gianelli G., Puxeddu M., Ruggieri G., 2005: Origin and evolution of Pliocene-Pleistocene granites from the Larderello geothermal field (Tuscan Magmatic Province, Italy). Lithos 81, 1 – 31.

Gianelli, G., Ruggieri, G., 2002: Evidence of a contact metamorphic aureole with high-temperature metasomatism in the deepest part of the active geothermal field of Larderello, Italy. Geothermics 31, 443– 474.

Petrucci, E., Gianelli, G., Puxeddu, M., Iacumin, P., 1994: An oxygen isotope study of silicates at Larderello, Italy. Geothermics 23, 327–337.

P 2.4

Quality criteria for municipal solid waste incineration bottom ash with regard to recycling and deposition without aftercare

Andreas Glauser[1], Urs Eggenberger[1], Gisela Weibel[2], Urs K. Mäder[1]

[1] *Institut für Geologie, Universität Bern, Baltzerstrasse 1+3, CH-3012 Bern (andreas.glauser@geo.unibe.ch)*
[2] *Zentrum für nachhaltige Abfall- und Ressourcennutzung ZAR, Wildbachstrasse 2, CH-8340 Hinwil*

Switzerland has a long tradition of waste incineration. Municipal solid waste (MSW) that cannot be recycled has to be thermally treated in one of the 30 MSW incinerators. The main objectives of thermal waste treatment are mass and volume reduction, destruction of organic compounds, energy recovery and transformation into inert incineration residues. At present about 750'000 tons of bottom ash are produced annually in Switzerland which are deposited in landfills of type D. These large quantities and environmental concerns caused the Federal Office of the Environment, Forestry and Landscape to elaborate guidelines for waste management in 1986. These guidelines encouraged the investigation of bottom ash composition and treatment methods (Belevi et al. 1992; Bunge 2010; Eggenberger & Mäder 2010). As a result, the recently revised Swiss Waste Ordinance (VVEA, Swiss Confederation 2016) dictates improved metal recovery rates. Consequently, new processes for the recovery of metals in finer fractions have been developed and implemented in individual MSWI plants.

Despite these improvements ca. 90 wt-% of bottom ash remain after metal separation, predominantly as a sand fraction. At present, little is known about the properties and composition of this residue. The aim of this study is to evaluate the quality of bottom ash residues with regard to deposition or use as secondary raw material. Assessment criteria are defined by the VVEA explicitly for deposition. They are moreover limited to threshold values for TOC and particulate non-ferrous metal content.

In order to assess bottom ash integrally with regard to recycling and deposition without aftercare, further criteria for the quality have to be defined. These criteria have to focus on contaminant and emission potential for deposition or recycling. A promising first approach to do this in Switzerland is to compare bottom ash fractions from different processes with data from similar materials published in the European reference database LeachXS (van der Sloot et al. 2012). The interpretation of bottom ash in a European context will help to define key parameters for an improved quality assessment.

REFERENCES

Belevi, H., Stämpfli, D.M. & Baccini, P. 1992: Chemical behaviour of municipal solid waste incinerator bottom ash in monofills. Waste Management & Research, 10, 153-167.

Bunge, R. 2010: Wertstoffgewinnung aus KVA-Rostasche - KVA-Rückstände in der Schweiz. Der Rohstoff mit Mehrwert. BAFU, 170-184.

Eggenberger, U., & Mäder, U. 2010: Charakterisierung und Alterations-reaktionen von KVA-Schlacken - KVA-Rückstände in der Schweiz. Der Rohstoff mit Mehrwert. BAFU, 116-134.

Swiss Confederation. 2016: Verordnung über die Vermeidung und die Entsorgung von Abfällen (VVEA), 1-46.

Van der Sloot, H. A., Kosson, D., Hjelmar, O., Comans, R., Seignette, P., Garrabrants, A., & van Zomeren, A. 2012: A reference database in LeachXS™ Lite for release of substances from construction products including alternative materials. Waste Materials in Construction Wascon 2012, Proceedings of the 8th International conference on Sustainable management of waste and recycled materials in construction.

P 2.5

Hydrothermal Epidosite Formation in the Oceanic Crust

Lisa Richter & Larryn W. Diamond

Water−Rock Interaction Group, Institute of Geological Sciences, University of Bern, Baltzerstr. 3, CH-3012 Bern (lisa.richter@gmx.net)

Hydrothermal seafloor alteration is best preserved in obducted oceanic lithosphere. Among the alteration types in the basaltic crustal section of ophiolites are rocks which have been completely altered to epidote + quartz ± titanite ± Fe-oxides, so-called epidosites. These rocks have been interpreted to form within the base of hydrothermal discharge zones that ultimately feed black-smoker seafloor vents (Richardson et al., 1987). Cowan and Cann (1988) and Juteau et al. (2000) observed high-salinity liquid + low-salinity vapor fluid inclusions in epidotized trondhjemites in the Troodos and Oman ophiolites, respectively, and concluded that these boiling fluids transformed the adjacent sheeted dikes into massive epidosites.

We have sampled massive epidosites in pillow lavas in the Semail ophiolite of Oman, as described by Gilgen et al. (2016). For comparison we have also sampled the same trondhjemites at the base of the sheeted dike complex as studied by Juteau et al. (2000). Epidote in the massive epidosites hosts primary, homogeneously trapped L–V inclusions with final ice melting temperatures, T_m(Ice), between -2.7 and -1.6 °C, implying salinities from 2.7 to 4.6 wt.% $NaCl_{eq}$ or 3.5 to 5.4 wt.% $CaCl_{2eq}$. The inclusions homogenize into the liquid state between 300 and 315 °C. Coeval quartz crystals host pseudosecondary, homogeneously trapped fluid inclusion assemblages with T_m(Ice) from -1.8 to -1.5 °C (corresponding to 2.6 to 3.1 wt.% $NaCl_{eq}$ or 3.3 to 3.9 $CaCl_{2eq}$) and homogenization into the liquid phase between 275 and 290 °C. In the igneous quartz crystals within the trondhjemites we found primary melt inclusions and secondary healed fractures containing coexisting brine + vapor fluid inclusions, in agreement with the work of Juteau et al. (2000).

As only single-phase fluids are present in the massive epidosites, the observed homogenization temperatures correspond to minimum trapping temperatures, i.e. the epidosites formed at T > 275–315 °C. Using the stratigraphic depth constraints provided by Gilgen et al. (2016) and assuming hydrostatic pressure gradients, the fluid inclusion densities imply that the massive epidosites formed at T = 305–355 °C and P_{fluid} = 28–42 MPa.

In contrast to previous models, our results show that the metasomatism that produces massive epidosites in pillow lavas of the oceanic crust is caused by a homogeneous aqueous liquid with chlorinity similar to that of seawater. The hydrothermal fluid was originally seawater that has been enriched in Ca and depleted in Na and Mg by water–rock reactions during hydrothermal circulation. We conclude that the brine + vapor inclusions trapped in quartz within the trondhjemites are magmatic fluids which play no role in formation of the massive epidosites in the pillow lavas. Accordingly, low-salinity fluids, rather than brines, should be the basis of any genetic model that includes epidosites in the hydrothermal circulation path leading to seafloor vents and their associated volcanogenic massive sulfide deposits.

REFERENCES

Cowan, J.G. & Cann, J. 1988: Supercritical two-phase separation of hydrothermal fluids in the Troodos ophiolite, Nature, 333, 259–261.

Gilgen, S., Diamond, L.W. & Mercolli, I. 2016: Sub-seafloor epidosite alteration: Timing, depth and stratigraphic distribution in the Semail ophiolite, Oman, Lithos 260, 191-210.

Juteau, T., Manac'h, G., Moreau, O., Lecuyer, C. & Ramboz, C. 2000: The high temperature reaction zone of the Oman ophiolite: new field data, microthermometry of fluid inclusions, PIXE analyses and oxygen isotopic ratios, Marine Geophysical Researches 21 (3–4), 351–385.

Richardson, C.J., Cann, J.R., Richards, H.G. & Cowan, J.G. 1987: Metal depleted root zones of the Troodos ore-forming hydrothermal systems, Cyprus. Earth and Planetary Science Letters, 84 (2–3), 243–253.

P 2.6

The fossilization potential of gypsum and its relevance to the search for life on Mars

Simon E. Rouwendaal[1], Timothy I. Eglinton[1], Negar Haghipour[1], Hamad A Al-Saad Al-Kuwari[2] & Tomaso Renzo Rezio Bontognali[1,2,3]

[1] Erdwissenschaftliches Departement, ETH Zurich, Sonnegstrasse 5, CH-8092 Zurich (simonro@student.ethz.ch)
[2] Environmental Science Center, Qatar University, Doha, Qatar
[3] Space-X, Fbg de l'Hôspital 68, 2000 Neuchâtel, Suisse

The existence of hydrated sulfate minerals on Mars, such as kieserite, polyhydrated sulfate and gypsum, has been confirmed with satellite data (e.g. Arvidson et al. 2005; Gendrin et al. 2005; Langevin et al. 2005) and observations from the Mars Exploration Rover Opportunity (Squyres et al., 2004). On Earth, such minerals form through evaporation of liquid water, in shallow saline lakes and coastal inland lagoons (sabkha's), and in association with hydrothermal environments (Warren, 2016, and references therein). Recent studies show that gypsum crystals on Earth have the capacity to permineralize micro-organisms, (Benison & Karmanocky, 2014; Schopf et al., 2012) and even preserve organic molecules for millions of years (Aubrey et al., 2006). Thus, gypsum proves to be an exciting target for the search of signs of life on Mars. To get a better understanding of the potential of gypsum in perserving signs of past life, we have analyzed gypsum samples from a site that is considered a good analogue to Mars, namely the Dohat Faishakh sabkha in Qatar. Our analysis revealed the presence of bacterial phospholipid fatty acids and archael glycolipids with biomarker analysis, beta-carotene with Raman spectroscopy and possibile microbial textures with scanning electron microscopy inside the gypsum crystals.

REFERENCES

Arvidson, R.E., Poulet, F., Bibring, J.-P., Wolff, M., Gendrin, A., Morris, R. V., … Bellucci, G. 2005: Spectral reflectance and morphologic correlations in eastern Terra Meridiani, Mars. Science, 307(5715), 1591-1594.

Aubrey, A., Cleaves, H.J., Chalmers, J.H., Skelley, A.M., Mathies, R.A., Grunthaner, F.J., … Bada, J.L., 2006: Sulfate minerals and organic compounds on Mars. Geology, 34(5), 357-360.

Gendrin, A., Mangold, N., Bibring, J.-P., Langevin, Y., Gondet, B., Poulet, F., LeMouelic, S. 2005: Sulfates in Martian Layered Terrains: The OMEGA/Mars Express View. Science, 307(5715), 1587-1591.

Langevin, Y., Poulet, F., Bibring, J.-P., Gondet, B. 2005: Sulfates in North Polar Regions of Mars Detected by OMEGA/Mars Express View. Science, 307(5715), 1584-1586.

Schopf, J.W., Farmer, J.D., Foster, I.S., Kudryavstev, A.B., Gallardo, V. a. & Espinoza, C. 2012: Gypsum-Permineralized Microfossils and Their Relevance to the Search for Life on Mars. Astrobiology, 12(7), 619-633.

Squyres, S.W., Grotzinger, J.P., Arvidson, R.E., III, J.F.B., Calvin, W., Christensen, P.R., … Soderblom, L.A. 2004: In Situ Evidence for Ancient Aqueous Environment at Meridian Planum. Science, 306(5702), 1709-1714.

Warren, J.K., 2016: Evaporites (2nd ed.). Springer International Publishing.

Benison, K.C., & Karmanocky, F.J. 2014: Could microorganism be preserved in Mars gypsum? Insights from terrestial examples. Geology, 42(7), 615-617.

P 2.7

Determining the physical and chemical processes behind four caldera-forming eruptions in rapid succession in the San Juan caldera cluster, Colorado, USA

Adam Curry[1], Luca Caricchi[1], Thomas Sheldrake[1], Guy Simpson[1], & Peter Lipman[2]

[1] *Department of Earth Sciences, University of Geneva, Rue des Maraîchers 13, CH-1205 Geneva (adam.curry@unige.ch)*
[2] *U.S. Geological Survey, 345 Middlefield Road, Menlo Park, California 94025, USA*

A primary goal of volcanology is to understand the frequency and magnitude of large, explosive volcanic eruptions to mitigate their impact on society. Recent studies show that the average magma flux and the time between magma injections into a given magmatic-volcanic system fundamentally control the frequency and magnitude of volcanic eruptions, yet these parameters are unknown for many volcanic regions on Earth. We focus on major and trace element chemistry of individual phases and whole-rock samples, cross-correlation of zircon zonation profiles, initial zircon ID-TIMS analyses, and zircon SIMS oxygen isotope analyses of four caldera-forming ignimbrites from the San Juan caldera cluster in the Southern Rocky Mountain volcanic field, Colorado, to determine the physical and chemical processes leading to large eruptions.

We collected outflow samples along stratigraphy of the three caldera-forming ignimbrites of the San Luis caldera complex: the Rat Creek Tuff (~150 km^3), Cebolla Creek Tuff (~250 km^3), and Nelson Mountain Tuff (>500 km^3); and we collected samples of both outflow and intracaldera facies of the Snowshoe Mountain Tuff (>500 km^3), which formed the Creede caldera. Single-crystal sanidine $^{40}Ar/^{39}Ar$ ages show that these large eruptions occurred in rapid succession between 26.91 ± 0.02 Ma (Rat Creek Tuff) and 26.87 ± 0.02 Ma (Snowshoe Mountain Tuff), providing an opportunity to investigate the temporal evolution of magmatic systems feeding large, explosive volcanic eruptions. Major and trace element analyses show that the first and last eruption of the San Luis caldera complex (Rat Creek Tuff and Nelson Mountain Tuff) are rhyolitic to dacitic ignimbrites, whereas the Cebolla Creek Tuff and Snowshoe Mountain Tuff are crystal-rich, dacitic ignimbrites.

Trace elements show enrichment in light rare-earth elements (LREEs) over heavy rare-earth elements (HREEs), and whereas the trace element patterns are similar for each caldera cycle, trace element values for each ignimbrite show variability in HREE concentrations. This variability indicates that these large eruptions sampled a magmatic system with some degree of internal heterogeneity. These results have implications for the chemical and physical processes, such as magmatic flux and injection periodicity, leading to the formation of large magmatic systems prior to large, explosive eruptions.

P 2.8

Mafic magma fragmentation and eruption dynamics of the May 2016 Etna eruption

Matt Edwards[1], Laura Pioli[1], Daniele Andronico[2], Antonio Cristaldi[2] & Simona Scollo[2]

[1]Department of Earth Sciences, University of Geneva, 1205 Geneva, Switzerland (Matthew.Edwards@unige.ch)
[2]Istituto Nazionale di Geofisica e Vulcanologia, Sezione di Catania-Osservatorio Etneo, Italy

Fragmentation of low viscosity mafic magmas has largely been overlooked on the assumption that such magmas have very limited explosivity and low potential to undergo brittle fragmentation. As such, fragmentation of low viscosity magmas remains a poorly understood process despite the recognised occurrence of highly explosive, ash-forming eruptions at some mafic volcanoes. The specific mechanism governing mafic fragmentation, the primary factors controlling fragmentation efficiency, and a link between eruption style and fragmentation efficiency are currently unknown.

In addressing this gap in mafic fragmentation knowledge, we have first examined the May 2016 eruption of Mount Etna, a type example basaltic volcano with frequent eruptions of variable magnitude, intensity and explosivity. Within this complex 10-day eruption, a vent within the Voragine crater went through three cycles of explosive activity (pulsating lava jets) alternating with effusive activity (lava flows). The three associated plumes which were produced deposited tephra along narrow axes to the east and south east. Tephra deposits associated with 1) the first two plumes and 2) the third plume were sampled.

We characterise the May 2016 eruption by assessing plume heights, eruption phases, total erupted masses and fallout boundaries and comparing them to previous eruptions. We also analyse the total grainsize distribution (TGSD) of the scoria particles formed in the jets. Conventional methods for obtaining grainsize and total distributions of an eruption are based on mass and provide limited information on fragmentation though. For this reason, the TGSD was assessed by coupling particle analyser data and conventional sieving data to assess both particle size and number of particle distributions with better precision. This allowed for more accurate testing of several existing models describing the shape of the TGSD. Coupled further with observations on eruption dynamics and eruption phase durations obtained from the network of fixed INGV cameras, early insight into possible links between fragmentation and eruption conditions are identified. A link between fragmentation and magma properties is also examined and we discuss the relationship between the conventional and new analytical methods and their potential in unravelling key information on the fragmentation process.

Additionally, geochemical analyses on melt inclusions and their host olivine, clinopyroxene and plagioclase phenocrysts, along with groundmass glasses give insight into the May 2016 magma ascent. We propose the explosive activity resulted from the arrival of fresh magma, which triggered the effusive eruption of an older, shallow magma.

P 2.9

Monitoring local-scale igneous underplating crystallization and interactions with country-rocks by garnet Y+REE chemistry.

Arnaud Devoir[1], Othmar Müntener[1]

[1] *Institut des Sciences de la Terre, Universtity of Lausanne, UNIL-Mouline, CH-1015 Lausanne*

The Ivrea-Verbano zone in northwestern Italy is a well-known almost complete section through the permian lower crust. Due to the 90° tilting during the Alpine orogeny, this section is now exposed. Bordered in the north-west by the Insubric line and in the south-east by the Cossato-Mergozzo-Brissago (CMB line) and the Pogallo lines, it mainly consists of (1) supracrustal rocks of the kinzigite and stronalite formation, (2) the mafic complex and (3) the mantle peridotite of Balmuccia. The kinzigites and stronalites formation include metapelitic, metabasic, metacarbonatic and metapsammitic rocks from lower amphibolite to granulite facies with a north-west metamorphic gradient direction. In the mafic complex, metasedimentary units called septa have been incorporated. In the litterature, many studies have shown that the gabbroic rocks were contaminated by the surrounding country rocks and the so-called septas. Since this effect is poorly constrained at a very local scale, the first goal of the present work is to study the spatial chemical evolution of the contaminated gabbro using major and trace elements whole-rock geochemistry on a sample showing the contact between a metapelitic septa and a gabbro.

Garnet, a very common mineral in the Ivrea-Verbano mafic complex, is one of the most promising asset for monitoring the cristallization and the temperature-time evolution of the mafic complex. As the diffusivities of rare earth elements (REE) in garnet are 0.5 to 1.5 order of magnitude smaller than those for the major cations (Carlson, 2012), REE can monitor the geochemical evolution of the surrounding rocks. A the base of the mafic complex some gabbros display large garnet crystals, up to 5 cm, some show numerous small garnets of 1 to 2 mm and some show no garnet. The septas are divided in several layers corresponding to the original metapelite, the restitic part after melting and mobilization of the melt, and the in-situ cristallized melt, also called charnockite. In those septas, garnets are mainly located in the restitic part but also in the charnockite layer. The garnets from the gabbros and the septas show different shapes and geochemistries and seem to have crystallized from different processes. The second goal of this work is the study of the garnet in the septa and the gabbro with 3D tomography grain size quantification and chemical maps on major cations (Fe, Mg, Ca, Mn), traces element (Ti, V, Cr, Y) and rare earth elements in order to understand its and to investigate the processes by which they crystallized.

REFERENCES

Carlson, W. D. 2012: Rates and mechanisms of Y, REE, and Cr diffusion in garnet. Am. Min. 97, 1598-1618.

Quick, J.E., Sinigoi, S., Snoke, A.W., Kalakay, T.J., Mayer, A., Peressini, G. 2003: Geologic map of the southern Ivrea-Verbano zone , northwestern Italy. U.S. Geological Survey.

Sinigoi, S., Quick, J.E., Mayer, A., Budahn, J. 1996: Influence of stretching and density contrast on the chemical evolution of continental magmas : an example from the Ivrea-Verbano zone. Contrib. Mineral. Petrol. 123, 238-250.

Sinigoi, S., Quick, J.E., Demarchi, G., Klötzli, U., 2011: The role of crustal fertility in the generation of large silicic magamtic system triggered by intrusion of mantle magma in the deep crust. Contrib. Mineral. Petrol. 162, 691-707.

Voshage, H., Hofmann, A.W., Mazzuchelli, M., Rivalenti, G., Sinigoi, S., Raczek, I., Demarchi, G. 1990: Isotopic evidence form the Ivrea zone for a hybrid lower crust formed by magmatic underplating. Nature 347, 731-736.

P 2.10

Lithium partitioning and isotope fractionation in the Limousin ophiolite (Massif Central, France)

Afifé El Korh[1,2], Etienne Deloule[2], Marie-Christine Boiron[3], Béatrice Luais[2]

[1] *Unité des Sciences de la Terre, Département des Géosciences, Université de Fribourg, Chemin du Musée 6, CH-1700 Fribourg, Suisse (afife.elkorh@unifr.ch)*
[2] *Centre de Recherches Pétrographiques et Géochimiques (CRPG), UMR 7358 CNRS–Université de Lorraine, 15 rue Notre Dame des Pauvres, BP 20, F-54501 Vandœuvre-lès-Nancy, France*
[3] *GeoRessources, UMR 7359 Université de Lorraine–CNRS, BP 70239, F-54506 Vandoeuvre-lès-Nancy, France*

Lithium is an alkaline fluid mobile light element that can be used as a tracer of (sub-)seafloor hydrothermal alteration in oceanic crust and lithospheric mantle. Fresh MORB have low Li and δ^7Li values (< 8 ppm and +3.4 ± 1.4 ‰ at 2σ, respectively; Tomascak et al., 2008 and references therein). High Li enrichments and high δ^7Li of altered MORB result from low-temperature (low-T) hydrothermal alteration prior to subduction by interaction with heavy Li-rich seawater (+32‰; Chan et al., 1988, 2002). By contrast, serpentinites may display variable δ^7Li values (Decitre et al., 2002; Wunder et al., 2010). In-situ SIMS analyses were employed to investigate Li mobility and isotope fractionation during low-T and high-temperature (high-T) hydrothermal alteration in a series of Variscan basic and ultrabasic rocks from the Limousin ophiolite.

The Limousin ophiolite is located in the upper part of the Middle Allochthon domain of the Variscan belt. Serpentinisation of dunites and harzburgites, as well as amphibolitisation of the gabbros and mafic dykes, result from intensive seafloor hydrothermal alteration under low-P conditions (~0.2 GPa) and temperatures from high-T late-magmatic conditions to low-T greenschist–zeolite metamorphic facies, following magma emplacement (Berger et al., 2005). Because of the absence of talc, serpentinisation is thought to have occurred below 500°C, while amphibolitisation took place at 570–750°C (Berger et al., 2005). Serpentine in the serpentinised harzburgites follows a retrograde reaction with a rimward Mg# increase related to the formation of a chrysotile/lizardite generation, suggesting a decrease of temperature during hydrothermal alteration (e.g. Mével, 2003; Wunder et al., 2010). In the serpentinised dunites, serpentine is mostly magnesian, but its Mg# ratio decreases in altered zones.

Li concentrations were determined by AA Spectrometry (± 2–10%; 1σ) for whole rocks, and by SIMS (external 2σ SE ± 0.7–1.8%) for minerals. High-temperature hydrothermal alteration of oceanic ultrabasic rocks produced serpentinites with low whole rock Li abundances (0.9–4.6 ppm), as commonly observed for ocean floor serpentinites and serpentinised peridotites (e.g. Decitre et al., 2002). Amphibolites display typical Li contents (3.1–8.2 ppm) of hydrothermally altered sheeted dykes and gabbros.

In ultrabasic rocks, serpentine is the main host for Li, with higher contents in Fe-richer serpentine (1.2–8.2 ppm) than in Mg-rich serpentine (0.3–3.6 ppm). The less abundant olivine and amphibole display similar Li contents as serpentine (1.5–3.0 and 1.1–3.5 ppm, respectively), while chlorite have low Li abundances (0.2–1.0 ppm). In amphibolites, Li abundances are higher in Mg-hornblende (1.3–10.7 ppm) than in plagioclase (0.1–1.0 ppm).

Li isotopes were analysed by SIMS using a Cameca ims1280-HR (external 2σ SE ± 1.1‰). In the serpentinised dunites, serpentine has a δ^7Li varying from -12.4 to -3.5 ‰. In the serpentinised harzburgites, δ^7Li values of serpentine range from -9.56 to +6.95‰, and show a rimward increase from Fe-richer to Fe-poorer generations. Co-existing amphibole has a δ^7Li of +4.5 to +9.4 ‰, while relicts of olivine have a δ^7Li of +3.1 to +8.8‰. Hornblende in amphibolitic dykes has MORB-like δ^7Li of -0.15 to +6.9‰, which increases up to +9.4 to +10.1‰ in alteration zones. In metagabbros, hornblende has higher δ^7Li values (+2.9 to 18.2‰).

The δ^7Li decrease and only weak Li increase from olivine to the replacing Fe-rich serpentine during the early stage of hydrothermal alteration suggest that serpentinisation probably results from fluid-induced kinetic fractionation caused by the higher diffusivity and preferential incorporation of ^{6}Li in serpentine compared to ^{7}Li (Decitre et al., 2002). By contrast, in the second generation of serpentine (Mg-richer serpentine) and cogenetic amphibole, the Li abundances decrease and the δ^7Li increases. Those variations reflect changes in temperature and/or fluid composition, such as more evolved hydrothermal fluids, the latter becoming heavier during their way through the oceanic crust (Decitre et al., 2002). Our results also agree with Wunder et al. (2010), who show that chrysotile is generally heavier than antigorite.

The δ^7Li values in amphibolitic dykes are typical of the Li signatures of hydrothermally altered deep oceanic basic rocks (sheeted dykes and gabbros: -1.7 to +7.9 ‰; Chan et al., 2002). However, the δ^7Li increase in alteration zones and metagabbros indicates an interaction with heavy-Li fluids – seawater or upwelling hydrothermal fluids – under high-temperature conditions.

Even if dehydrating serpentinites play a major role in the fluid-mobile element recycling during subduction and generate high amounts of fluids (e.g. Kodolányi et al., 2012), our results show that subduction and subsequent dehydration of abyssal serpentinites with Li-poor MORB-like abundances would release Li-poor fluids with variable δ^7Li in subduction zones.

REFERENCES
Berger, J., Féménias, O., Mercier, J.C.C. & Demaiffe, D. 2005: Journal of Metamorphic Geology, 23, 795-812.
Chan, L.H., Alt, J.C. & Teagle, D.A.H. 2002: Earth and Planetary Science Letters, 201, 187-201.
Chan, L.H. & Edmond, J.M. 1988: Geochimica et Cosmochimica Acta, 52, 1711-1717.
Decitre, S.E., Deloule, E., Reisberg, L., James, R., Agrinier, P. & Mevel, C. 2002: Geochemistry Geophysics Geosystems 3, doi:10.1029/2001GC000178
Kodolányi, J., Pettke, T., Spandler, C., Kamber, B.S. & Gméling, K. 2012: Journal of Petrology, 53, 235-270.
Mével, C. 2003: Comptes Rendus Geoscience, 335, 825-852.
Tomascak, P.B., Langmuir, C.H., Le Roux, P.J. & Shirey, S.B. 2008: Geochimica et Cosmochimica Acta, 72, 1626-1637.
Wunder, B., Deschamps, F., Watenphul, A., Guillot, S., Meixner, A., Romer, R. & Wirth, R. 2010: Contributions to Mineralogy and Petrology, 159, 781-790.

P 2.11

Iron isotope fractionation in the Limousin ophiolite (Massif Central, France)

Afifé El Korh[1,2], Béatrice Luais[2], Marie-Christine Boiron[3], Etienne Deloule[2], Damien Cividini[2]

[1] *Unité des Sciences de la Terre, Département des Géosciences, Université de Fribourg, Chemin du Musée 6, CH-1700 Fribourg, Suisse (afife.elkorh@unifr.ch)*
[2] *Centre de Recherches Pétrographiques et Géochimiques (CRPG), UMR 7358 CNRS–Université de Lorraine, 15 rue Notre Dame des Pauvres, BP 20, F-54501 Vandœuvre-lès-Nancy, France*
[3] *GeoRessources, UMR 7359 Université de Lorraine–CNRS, BP 70239, F-54506 Vandoeuvre-lès-Nancy, France*

Ophiolites are remnants of ancient oceanic lithosphere, consisting of an association of ultrabasic, basic and sedimentary rocks. Before being embedded in tectonic processes, the oceanic lithosphere undergoes various stages of (sub-) seafloor hydrothermal alteration, mainly: 1) high-temperature (high-T; > 350°C) hydrothermal alteration along mid-oceanic ridges; 2) low-temperature (low-T; < 350°C) hydrothermal alteration on the seafloor.

Fe stable isotope fractionation may fractionate significantly during low-T hydrothermal processes, as well as during high-T magmatic processes. During hydrothermal processes, Fe isotope fractionation strongly depends on Fe redox state, the heavier Fe isotopes being preferencially incorporated into the Fe^{3+}-phases. However, Fe isotopes also fractionate if the chemistry of Fe-bearing solutions changes (e.g. chlorinity, Fe speciation, relative abundance and coordination number of Fe^{2+} and Fe^{3+}; Hill et al., 2010). The hydrothermally altered basaltic oceanic crust may display variable Fe isotopic composition, depending on the nature of hydrothermal products: Fe^{2+}-rich sulfides (low δ^{56}Fe) or Fe^{3+}-rich clays (e.g. celadonite) or Fe-hydroxides (high δ^{56}Fe) (Rouxel et al. 2003).

In this study, we have measured Fe isotopes in series of metagabbros and serpentinites from the Limousin ophiolite (French Massif Central) to investigate Fe isotope fractionation during low-T and high-T hydrothermal alteration. We aim to determine whether subducted serpentinites may inherit Fe isotope signature of pre-subduction hydrothermal alteration (abyssal serpentinites).

The Limousin ophiolite belongs to the upper part of the Middle Allochthon domain of the Variscan belt. Serpentinisation of the ultrabasic rocks (dunites and harzburgites) and amphibolite facies metamorphism of gabbros and mafic dykes occurred during intensive seafloor hydrothermal alteration that followed magma emplacement. Alteration took place under low-pressure conditions (~ 0.2 GPa) and temperatures from high-T late-magmatic conditions to low-T greenschist–zeolite metamorphic facies (serpentinisation: < 500°C; amphibolitisation: 570–750°C; Berger et al., 2005).

Fe isotopes ($\delta^{56}Fe_{IRMM-014} \pm 0.01–0.04$ ‰ at 2σ SE) were measured in bulk samples using a Neptune*Plus* MC-ICPMS (ThermoFisher Scientific) after sample dissolution and Fe separation through ion exchange chromatography column at the CRPG (Liu et al., 2014). The $Fe_2O_3^{tot}$ and FeO contents were measured at the SARM (CRPG) by ICP-AES and by volumetric method, respectively, and allowed calculation of the $Fe^{3+}/\Sigma Fe$ ratios.

Amphibolite facies metagabbros and basaltic dykes from the Limousin ophiolite have $Fe_2O_3^{tot}$ (5.3–8.6%) similar to oceanic gabbros (Kaczmarek et al., 2008) and basalts (Jenner and O'Neill, 2012). Their $Fe^{3+}/\Sigma Fe$ ratios (0.11–0.14) and $\delta^{56}Fe$ values (+0.12 to +0.18‰) are generally within the range of MORB values ($Fe^{3+}/\Sigma Fe$: 0.07–0.16; $\delta^{56}Fe$: +0.06 to +0.18‰; see El Korh et al., 2017; and references therein). Only one metagabbro show a lower $\delta^{56}Fe$ of 0.03‰. These results suggest that Fe was relatively immobile during high-T hydrothermal alteration, which prevented Fe isotopes fractionating. Serpentinites have higher $Fe_2O_3^{tot}$ contents (7.4–11.3%) and $Fe^{3+}/\Sigma Fe$ ratios (0.6–0.7), which are typical for greenschist facies serpentinites in ophiolites (Debret et al., 2014). However, serpentinites display heavier $\delta^{56}Fe$ values (+0.15 to +0.18‰) than abyssal serpentinites (–0.098‰ to +0.108‰; Craddock et al., 2013; Debret et al., 2016). Fe isotope fractionation occurred concomitantly with Fe oxidation during seafloor hydrothermal alteration under lower T conditions, and probably results from the precipitation of Fe^{3+}-rich secondary products (magnetite, Fe-hydroxydes).

The $\delta^{56}Fe$ composition of the Limousin serpentinites is comparable to the highest $\delta^{56}Fe$ values measured in some blueschist-facies Alpine serpentinites (from -0.011 to +0.142‰; Debret et al., 2016), which are thought to result from the release of sulfate-rich or hypersaline Fe^{2+}-bearing fluids during serpentinite dehydration. However, the high $\delta^{56}Fe$ values of the Limousin serpentinites suggest that Fe isotopes may already fractionate towards heavier values in highly oxidised abyssal serpentinites before subduction of the oceanic lithosphere.

REFERENCES

Berger, J., Féménias, O., Mercier, J.C.C. & Demaiffe, D. 2005: Journal of Metamorphic Geology, 23, 795-812.
El Korh, A., Luais, B., Deloule, E. & Cividini, D. 2017: Contributions to Mineralogy and Petrology, 172:41.
Kaczmarek, M.A., Müntener, O. & Rubatto, D. 2008: Contributions to Mineralogy and Petrology, 155, 295-312.
Craddock, P.R., Warren, J.M. & Dauphas, N. 2013: Earth and Planetary Science Letters, 365, 63-76.
Debret, B., Andreani, M., Muñoz, M., Bolfan-Casanova, N., Carlut, J., Nicollet, C., Schwartz, S. & Trcera, N. 2014: Earth and Planetary Science Letters, 400, 206-218.
Debret, B., Millet, M.A., Pons, M.L., Bouilhol, P., Inglis, E. & Williams, H. 2016: Geology, 44, 215-218.
Jenner, F.E., O'Neill, H.S.C., 2012: Analysis of 60 elements in 616 ocean oor basaltic glasses. Geochemistry Geophysics Geosystems 13, Q02005.
Hill, P.S., Schauble, E.A. &Young, E.D. 2010: Geochimica et Cosmochimica Acta, 74, 6669-6689.
Liu, P.P., Zhou, M.F., Luais, B., Cividini, D. & Rollion-Bard, C. 2014: Earth and Planetary Science Letters,399, 21-29.
Rouxel, O., Dobbek, N., Ludden, J. & Fouquet, Y. 2003: Chemical Geology, 202, 155-182.

P 2.12

Morphological Features of Chkheri (the Great Caucasus) and Khertvisi (Southern Georgia) Lava Flows

Ketevan Gabarashvili[1], Koba Lobzhanidze[1], Tamar Beridze[1], Giorgi Vashakidze[1], Manana Kavsadze[1], Manana Togonidze[1]

[1] Al. Janelidze Institute of Geology, Iv. Javakhishvili Tbilisi State University, A. Politkovskaya 31, 0186 Tbilisi, Georgia (qgabarashvili@yahoo.com)

Studies of lava flows physical volcanology on the example of two Neogene-Quaternary volcanic provinces of Georgia have been recently established for the first time by the group of presented work authors. Two distinct localities of lava flows exposures have been selected on this purpose: basalt (known before as dolerites) flows from the vicinities of the village Khertvisi (Javakheti Highland, Southern Georgia) and andesite flows from the river Chkheri gorge (Kazbegi, the Greater Caucasus). Morphological features of these lava flows have been recorded on the basis of detailed field observations. Preliminary results of these studies are introduced here.

Khertvisi lava flows have been ascribed to the river Mtkvari (Kura) dolerite flow in previous publications (Skhirtladze1958; Maisuradze1981). According to these data several relics of this flow are exposed within the River Mtkvari gorge. The recently studied cliff section of lavas in the immediate vicinity of the village Khertvisi is represented by compound pahoehoe, rubbly pahoehoe and ‘a’ā units forming flow fields with hummocky and sheet flows morphologies (Duraiswami 2014; Self 1998). The lower and upper flows are separated by prominent pillow breccia unit.Thin section petrographic analysis of these flows shows, that these are olivine basalts. Various types of alteration minerals are represented by carbonate, illite-seladonite-chlorite, goethite, iddingsite.

The Chkheri lava flows are exposed on the both slopes and in the valley of the same named river (the left tributary of the river Tergi) and form four flows separated by breccia horizons. The flows correspond to andesites by composition and constitute thick entablature ‘a’ā flows. Some of them preserve breccia core rosettes.

Surface morphology and internal structures of the Khertvisi flow field are indicative for low viscosity lavas, whereas the Chkheri lava flows represent highly viscous lava flows.

REFERENCES

Self, S., Thordarson, Th., & Keszthelyi, L. 1997: Emplacement of continental flood basalt lava flows. In: Mahoney, J.J., Coffin, M.F. (Eds.), Large Igneous Provinces: Continental, Oceanic, and Planetary Flood Volcanism. Am. Geophys. Union Geophy. Monogr 100, 38-410.

Skhirtladze, N. 1958: Postpaleogene effusive volcanism of Georgia. Proceedings of the Institute of geology of the Academy of Science of GSSR. Tbilisi, 8, 368.

Maisuradze, G. 1981: About the stratigraphy of the young volcanites of southern Georgia. Bulletin of the commission of Quaternary period studies, 51, 74-84.

Duraiswami, R., Gadpallu, P., & Tahira, S., Cardin, N. 2014: Pahoehoe–aa transitions in the lava flow fields of the western Deccan Traps, India-implications for emplacement dynamics, flood basalt architecture and volcanic stratigraphy. Journal of Asian Earth Sciences, 84, 146-166.

P 2.13

Cenozoic subduction to post-collision magmatic evolution of the Lesser Caucasus: new constraints from the Tejsar and Amulsar areas, Armenia

Marion Grosjean[1], Robert Moritz[1], Rafael Melkonyan[2], Samvel Hovakimyan[1,2] & Alexey Ulianov[3]

[1]*Department of Earth Sciences, University of Geneva, CH-1205 Geneva, Switzerland*
[2]*Institute of Geological Sciences, National Academy of Sciences, Yerevan, Armenia*
[3]*Institute of Earth Sciences, University of Lausanne, 1015 Lausanne, Switzerland*

The Lesser Caucasus, located in the Central Tethyan orogenic belt, extends from the Black Sea to the Caspian Sea across Georgia, Armenia and Azerbaidjan. It resulted from the Neotethys ocean closure during the Late Cretaceous and the Cenozoic as a consequence of NNE-verging convergence of Arabia, Gondwana derived microplates and Eurasia. Timing of the collision onset remains uncertain (Rezeau et al., 2017) and recent studies, including this one, focused on constraining the geodynamic and metallogenic evolution from the subduction to post-collision stage in this part of the Tethyan orogenic belt.

The Lesser Caucasus is divided in three main tectonic domains, including from NE to SW (Fig. 1): 1) the magmatic and sedimentary Somkheto-Karabagh belt and the Kapan Zone belonging to the Eurasian plate, 2) the ophiolitic Amasia-Sevan-Akera suture zone, and 3) the Gondwana-derived South Armenian block (SAB) (Sosson et al., 2010). Long lived Cenozoic magmatic activity took place along the Pambak-Sevan-Sunik and Garni faults zones (see PSSF and GF in Figure 1, after Philip et al., 2001), as well as intermittent emplacement of Eocene to Miocene porphyry and epithermal deposits (Moritz et al., 2016). Our knowledge concerning the geodynamic, magmatic and metallogenic evolution of the Lesser Caucasus remains fragmentary.

The Cenozoic geodynamic, magmatic and metallogenic evolution of the Lesser Caucasus has been relatively well constrained by recent studies in its southermost part (see MOP in Figure 1; Rezeau et al., 2016, 2017). Three distinct magmatic events of different ages and compositions have been recorded in this area, varying from calc-alcaline mid-Eocene to shoshonitic/adakitic early Miocene magmatism. Each magmatic episode being associated with the formation of porphyry copper and/or epithermal deposits and prospects (Rezeau et al., 2016, 2017).

This study focuses on the Tejsar and Amulsar areas in Armenia (Fig. 1). They present a similar geodynamic, magmatic and metallogenic context to the MOP, but which remains poorly documented. Both study areas include epithermal deposits spatially associated with Cenozoic magmatism, as well as porphyry occurrences in the case of Tejsar. Field mapping has highlighted chronological relationships among distinct magmatic intrusions with different compositions similar to the MOP area. New geochemical and petrogenetic data of the different Cenozoic intrusions surrounding the epithermal and porphyry deposits combined with U-Pb zircon dating will improve our understanding about the geodynamic, magmatic and metallogenic evolution of the Lesser Caucasus.

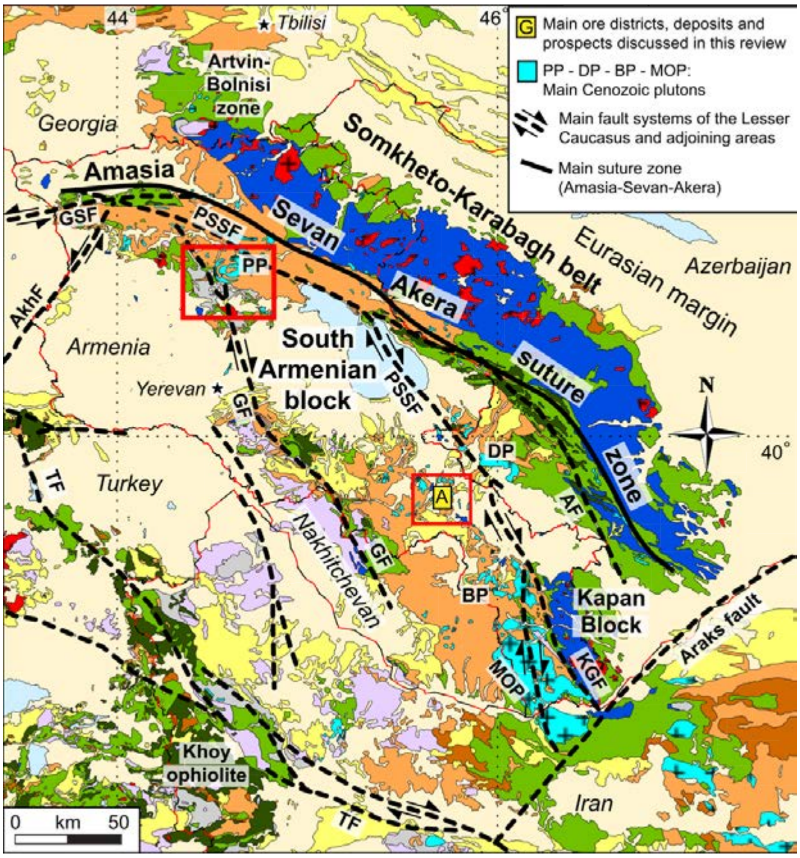

Figure 1. Geology and major regional faults of the Lesser Caucasus (Philip et al., 2001; Moritz et al., 2016). The northern red box outlines the Tejsar study area including the Cenozoic Pamback pluton (PP) and Meghradzor gold deposit. The southern red box outlines the Amulsar study area (A). Both study areas are located along the Pamback – Sevan – Sunik and Garni Faults (PSSF and GF, respectively) and are part of the South Armenian Block (SAB).

REFERENCES

Moritz, R., Melkonyan, R., Selby, D., Popkhadze, N., Gugushvili, V., Tayan, R., and Ramazanov, V. 2016: Metallogeny of the Lesser Caucasus: From arc construction to postcollision evolution. Society of Economic Geologists Special Publication 19, 157–92.

Philip, H., Avagyan, A., Karakhanian, A., Ritz, J.-F., Rebai, S., 2001: Estimating slip rates and recurrence inervals for strong earthquakes along an intracontinental fault: example of the Pambak-Sevan-Sunik fault (Armenia). Tectonophysics 343, 205–232.

Rezeau, H., Moritz, R., Leuthold, J., Hovakimyan, S., Tayan, R., and Chiaradia, M. 2017: 30 Myr of Cenozoic magmatism along the Tethyan margin during Arabia–Eurasia accretionary orogenesis (Meghri–Ordubad pluton, southernmost Lesser Caucasus). Lithos 288–289, 108–24.

Rezeau, H., Moritz, R., Wotzlaw, J.-F., Tayan, R., Melkonyan, R., Ulianov, A., Selby, D., d›Abzac, F.-X., Stern, R.A., 2016. Temporal and genetic link between incremental pluton assembly and pulsed porphyry Cu-Mo formation in accretionary orogens. Geology 44, 627–630.

Sosson, M., Rolland, Y., Müller, C., Danelian, T., Melkonyan, R., Kekelia, S., Adamia, Sh. et al. 2010: Subductions, obduction and collision in the Lesser Caucasus (Armenia, Azerbaijan, Georgia), New insights. Geological Society of London Special Publication 340, 329–52.

P 2.14

Cross correlation of magmatic crystals: intepreting correlations and identifying families

Tom Sheldrake[1], Luca Caricchi[1], Martin Gander[2], Glen Wallace[3] & Guy Simpson[1]

[1] *Department of Earth Sciences, University of Geneva, 13 rue des Maraîchers, 1205 Geneva, Switzerland (thomas.sheldrake@unige.ch)*
[2] *Section of Mathematics, University of Geneva, 4 rue du Lièvre, 1205 Geneva, Switzerland*
[3] *Pacific Groundwater Group, 2377 Eastlake Ave E, Seattle, USA*

Crystals growing in magma record thermal and chemical variations within a reservoir. Linking the chemical zoning of minerals to magmatic processes can serve to identify the sequece of events leading to a volcanic eruption. Correlating the pattern of zonation between multiple crystals allows the similarities and differences between suites of crystals to be quantified, both within the same sample and between different samples. This offers an opportunity to quantify the chemical and/or thermal structure of a magmatic reservoir and the magmatic processes that precede a volcanic eruption.

We are advancing a method that has been designed to rapidly and objectively correlate crystal profiles based on chemical and grayscale profiles of magmatic crystals including zircon, clinopyroxene and plagioclase. An important component of this method is its ability to account for the misalignement of crystals (i.e. if from a thin section), or if profiles are taken from different crystal axes and thus vary in length. The critical aspect of this methodology, however, is determining when two crystals are significantly correlated. This varies, depending on whether the correlation of crystals is in the exterior or interior of the crystal, and on the complexity of the zonation that is observed. We approach this issue using two examples (zircons and clinopyroxene), and the identify the large potential of this quantitative approach, which provides an automatic method to identify correlation in different portions of crystal profiles, for many hundreds of profiles.

P 2.15

Magma dynamics and long-term evolution of Nevado de Toluca volcano, Mexico

Gregor Weber[1], Luca Caricchi[1], Tom Sheldrake[1] & José Luis Arce[2]

[1] Department of Earth Sciences, University of Geneva, Rue des Maraîchers 13, 1205 Geneva (Gregor.Weber@unige.ch)
[2] Departamento de Geología Regional, Instituto de Geología, UNAM, Cd. Universitaria, Coyoacán, México D.F., 04510, Mexico

Linking pre-eruptive processes to the frequency at which eruptions of different magnitudes occur is essential to understand the underlying factors controlling the behaviour of volcanoes. To attempt to establish this link it is necessary to study in detail the long-term evolution and dynamics of magmatic systems.

For this study we sampled the entire about 1.5 Ma spanning eruptive history of Nevado de Toluca in Mexico, a subduction-related volcano with well documented effusive and explosive eruptions. We use a combination of whole rock and mineral chemistry, as well as cross-correlation of plagioclase and zircon crystal zoning profiles to compare eruptions of different magnitude, size and style. The first results show that Nevado de Toluca is characterized by a remarkably homogeneous dacitic major element composition, even for contrasting eruptive styles, throughout its eruptive history.

This indicates that similar processes in favour of production and extrusion of this magma type must operate on long timescales beneath the volcano. Trace element patterns are also rather restricted in variability for eruptions of different style through time and show enrichment of LREE over HREE. Larger variability is observed for monogenetic cones in the vicinity of the volcano.

Interestingly, Nevado de Toluca is characterized by high Sr/Y of up to 90 showing an adakite-like signature. Further work will provide quantitative insights on petrogenetic processes and on the frequency at which intensive parameters changed within the magma reservoir before the eruptions. Our results will be integrated in a global database including other volcanic systems and literature data in an attempt to identify similarities and differences between magmatic reservoirs feeding volcanic eruptions of different magnitudes. The final target of this project is to constrain the physical factors controlling the recurrence rate of volcanic eruptions at regional and global scale.

P 2.16

The Temporal Evolution of an Arc Volcano through Thermobarometry and Petrography of Intrusive and Volcanic Products

Max J. Jensen, Luca Caricchi, Jon Blundy, Lena Melekhova George Cooper

Eruptible magma (magmas with <50 vol.% of crystals) represents a variable but generally small fraction of the total amount of magma in subvolcanic reservoirs. Therefore, the exclusive analysis of volcanic products may provide a biased picture of the temporal evolution of the thermal and chemical structure of magma reservoirs. Consequently, the study of coeval volcanic and intrusive products is better suited to unravel the processes controlling the chemical evolution of volcanic systems.

The volcanic islands of St. Martin, St Kitts and Nevis, situated in the northern part of the Lesser Antilles Volcanic Arc in the Caribbean Sea, offers a rare opportunity to study coeval plutonic and volcanic rocks from the same magmatic system. On St. Martin, volcanic quiescence has prevailed since ~ 26 Ma, allowing erosion to expose the intrusive parts of the volcanic system. While on the younger islands of St. Kitts and Nevis, where no intrusive rocks are exposed, cumulates are present in the volcanic products, which indirectly sample the intrusive rocks and can be utilized to further investigate the plumbing system at depth.

We focus on petrography combined with recent Al-in-hornblende geobarometry (Mutch et al. 2016), and amphibole–plagioclase thermometry (Putirka 2008), from the volcanic and intrusive products (plutonic + cumulates) to trace the temporal evolution of the islands magmatic systems. Analysis of major and trace element compositions of bulk rock and minerals will be determined using XRF, EPMA and LA-ICP-MS. The results will be used to compare the geochemistry of coeval deposits from volcanic and intrusive products to determine if the results, when integrated, provide a complementary picture of the temporal evolution of magmatic systems.

P 2.17

Differentiation of intermediate calc-alkaline magmas at 2 kbar

Felix Marxer[1], Peter Ulmer[1]

[1]*Institute of Geochemistry and Petrology, ETH Zürich, Clausiusstrasse 25, CH-8092 Zürich (felix.marxer@erdw.ethz.ch)*

To improve the understanding of the geochemical and petrophysical evolution of magmas forming intermediate calc-alkaline batholiths after emplacement at shallow crustal levels, phase equilibria relations were established for a tonalitic/andesitic system at a pressure of 2 kbar and under water-saturated conditions.

Melting experiments were performed at temperatures between 700 and 1000 °C in externally heated HCM pressure vessels, with oxygen fugacity controlled close to the Ni-NiO buffer equilibrium (NNO) employing an argon-methane mixture as pressure medium and Co-Pd redox sensors to verify fO_2 conditions.

Natural rock powder of a Medium-K tonalite from the Adamello Batholith in Northern Italy served as experimental starting material. Recovered charges were first analysed by Scanning Electron Microscopy coupled with Energy Dispersive X-ray Spectroscopy (SEM-EDS) and subsequently remeasured with an Electron Probe Micro Analyser (EPMA) allowing the determination of an isobaric crystallisation sequence for an upper crust hosted tonalitic intrusion.

Based on compositional data of stable phases, mass balance calculations were performed in order to investigate the evolution of the crystal/melt ratio with respect to temperature. Furthermore, compositional trends of minerals as well as the liquid line of descent of residual melts were obtained. Orthopyroxene, clinopyroxene and plagioclase were identified as near-liquidus phases (below 990 °C). At 900 °C, amphibole joins the solid phase assemblage at the expense of clinopyroxene, indicating the existence of a peritectic relation between the two phases.

With subsequent cooling, clinopyroxene completely disappears and amphibole becomes the dominant mafic mineral phase (875 °C). Crystallisation proceeds continously to 825 °C with a linear decrease of residual melt fractions reaching a plateau of 40 % at 800 °C with only minor additional crystallisation upon further cooling. Quartz and biotite saturate at 775 °C coevally with orthopyroxene approaching its stability limit.

Residual liquids compositionally evolve along a typical calc-alkaline differentiation trend with decreasing temperature (increasing SiO_2 and decreasing Al_2O_3, CaO, MgO and FeO contents) and become peraluminous at temperatures below 900 °C.

P 2.18

U-Pb age constraints on skarn formation in the Madan Pb-Zn district, Bulgaria: zircon evidence from Tertiary magmatism

Aaron L. Hantsche[1], Kalin Kouzmanov[1], Andrea Dini[2], Rossitsa Vassileva[3], Marcel Guillong[4] & Albrecht von Quadt[4]

[1] *Department of Earth Sciences, University of Geneva, Rue des Maraîchers 13, 1205 Geneva, Switzerland ([1]correspondence: aaron.hantsche@unige.ch)*
[2] *Instituto di Geoscienze e Georisorse, CNR - Pisa, Via Moruzzi 1, 56124 Pisa, Italy*
[3] *Geological Institute, Bulgarian Academy of Sciences, Acad. G. Bonchev Str. 24, 1113 Sofia, Bulgaria*
[4] *Institute of Geochemistry and Petrology, ETH Zürich, Clausiusstrasse 25, 8092 Zürich, Switzerland*

The Madan district, located in the Central Rhodopes in southern Bulgaria, is renowned for its Pb-Zn skarn, vein, and carbonate replacement ore bodies (Vassileva et al., 2009). The deposits are controlled by 6 district-scale northwest trending structures that cut across the Mesozoic amphibolite-grade gneissic host rocks. These structures extend up to 2.5 km in length and are thought to be the primary fluid conduit for Pb-Zn sulfide mineralization. The highest metal concentrations are found where these structures intersect marble lenses within the gneiss, where much of the ore is hosted in pyroxene skarn bodies that predate the mineralization event (Vassileva et al., 2009). The geneteic relationship between the skarns and the Pb-Zn mineralization is still controversial.

The timing of sulfide mineralization has been constrained using Ar-Ar dating on hydrothermal sericite at 29-30.5 Ma (Kaiser-Rohrmeier et al., 2004, 2013). Since the skarn mineralization predates the Pb-Zn mineralization, this is a minimum age limit for skarn formation in Madan. The prograde mineralogy of the skarns consists only of Mn-rich pyroxene, and no geochronometer has been utilized to constrain the maximum age of skarn formation. Regional Tertiary magmatism that predates the mineralization has previously been proposed as the source of heat and fluid for skarn formation (Marchev, et al., 2005). In this study, we present new field relationships between a skarn body and rhyolite dike which help constrain the upper age limit of skarn formation based on LA-ICP-MS zircon dating and trace element analyses from the rhyolite.

Regional magmatic activity in the Tertiary is found across the Madan district, and has been a focus of other tectonic and economic studies (Figure 1). The Smilian Granite, previously dated at 42.29 ± 0.08 Ma (TIMS U-Pb on zircon, Kaiser-Rohrmeier et al., 2013), is interpreted as a crustal melt that was generated during a post-orogenic extension event in the Rhodopes (Kaiser-Rohrmeier et al., 2013), resulting in the formation of low-angle normal fault structures in the region. Pegmatite intrusions in the vicinity have been dated at 35.31 ± 0.25 Ma (Rb-Sr on Kfs; Peytcheva et al., 2003). Post-collisional extension was followed by the emplacement of pre-mineralization east-west oriented rhyolite dike swarm in the northern part of the district and regional ignimbrite deposits to the northwest that have been previously dated between 30 and 32 Ma (Harkovska et al., 1998; Kaiser-Rohrmeier et al., 2013).

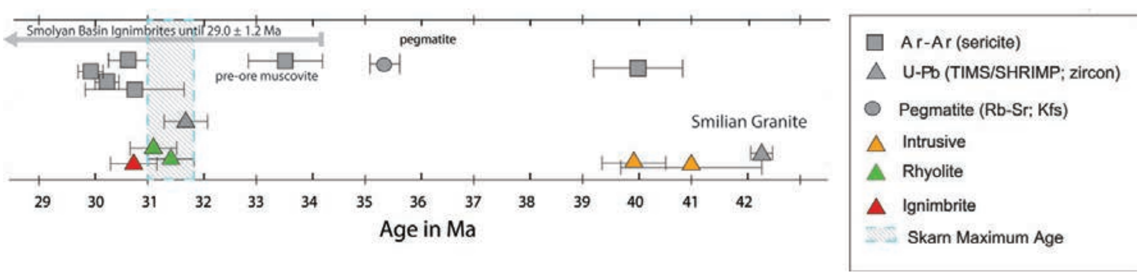

Figure 1. LA-ICP-MS weighted mean ages (WMA) for concordant zircon dates from this study. Error bars reflect 2σ error. Samples in gray - from Peytcheva et al. (2003) [Rb-Sr] and Kaiser-Rohrmeier et al. (2013) [U-Pb TIMS; Ar-Ar]. Ignimbrite age range - from Harkovska et al. (1998) [K-Ar; Ar-Ar].

Five samples from the Madan district have been dated and analyzed for trace elements in zircon. Two samples of the E-W trending rhyolite dikes produced ages of 31.41 ± 0.39 Ma (16-MN-13; n = 35) and 31.15 ± 0.39 Ma (16-MN-03; n = 15). Sample 16-MN-13 is from a subsurface rhyolite dike at the Mogilata deposit which predates the skarn body, as skarn-forming fluids exploited the contact between the dike and the marble. One sample from an ignimbrite from the Smolyan basin (16-LA-02) was dated at 30.71 ± 0.40 Ma (n = 27).

Two intrusive samples from the Smilian granite body in the western part of the Madan district, 16-MN-20 and 16-MN-21, produced crystallization ages of 39.85 ± 0.50 Ma (n = 18) and 41 ± 2.6 Ma (n = 3) respectively. The presence of inherited cores and zircon xenocrysts supports interpretations of crustal melting during extension and exhumation of the Central Rhodopes.

REFERENCES

Harkovska, A., Marchev, P., Machev, P., Pecskay, Z, 1998: Paleogene magmatism in the Central Rhodope Area , Bulgaria - A review and new data: Acta Vulcanologica, v. 10 p. 199-216.

Kaiser-Rohrmeier, M., Handler, R., von Quadt, A., Heinrich, C., 2004: Hydrothermal Pb–Zn ore formation in the Central Rhodopian Dome, south Bulgaria: Review and new time constraints from Ar–Ar geochronology. Schweizerische Mineralogische und Petrographische Mitteilungen, 84,.37–58.

Kaiser-Rohrmeier,von Quadt, A., Driesner, T., Heinrich, C., Handler, R., Ovtcharova, M., Ivanov, Z., Petrov, P., Sarov, S., Peytcheva, I., 2013: Post-Orogenic Extension and Hydrothermal Ore Formation: High-Precision Geochronology of the Central Rhodopian Metamorphic Core Complex (Bulgaria-Greece), Economic Geology, 108, 691-718.

Peytcheva, I., von Quadt, A., Ovtcharova, M., Handler, R., Neubauer, F., Salnikova, E., Kostitsyn, Y., Sarov, S., Kolcheva, K., 2003: Metagranitoids from the eastern part of the central Rhodopian Dome (Bulgaria): U-Pb, Rb-Sr, and 40Ar/39Ar timing of emplacement and exhumation and isotope geochemical features, Mineralogy and Petrology, 81, 1-32.

Marchev, P., Kaiser-Rohrmeier, M., Heinrich, C., Ovtcharova, M., von Quadt, A., Raicheva, R., 2005: 2: Hydrothermal ore deposits related to post-orogenic extensional magmatism and core complex formation: The Rhodope Massif of Bulgaria and Greece. Ore Geology Reviews, 27, 53-89.

Vassileva, R. D., Atanassova, R., Bonev, I., 2009: A review of the morphological varieties of ore bodies in the Central Rhodopes, Geochemistry, Mineralogy, and Petrology, 47, 31–49.

P 2.19

Lhasa Block partial melt zones: matching geophysical characteristics and petrological origin

György Hetényi[1], Mattia Pistone[1], Peter Nabelek[2] & Lukas Baumgartner[1]

[1] *University of Lausanne, Institute of Earth Sciences, UNIL-Mouline Géopolis, 1015 Lausanne (gyorgy.hetenyi@unil.ch)*
[2] *Geological Sciences, University of Missouri, Columbia, USA*

Zones of partial melt in the middle crust of Lhasa Block, Southern Tibet, have been geophysically observed as seismically reflective “bright spots” in the past 20 years. These batholiths bear important relevance for geodynamics as they serve as the principal observation at depth supporting channel-flow models in the Himalaya-Tibet orogen.

Here we assess the spatial abundance of and partial melt volume fraction within these crustal batholiths, and establish lower and upper estimate bounds using a joint geophysical-petrological approach.

Geophysical imaging constrains the abundance of partial melt zones to 5 ± 2 km^3 per surface-km^2 on average. Physical properties detected by field geophysics and interpreted by laboratory measurements constrain the amount of partial melt to be between 15 ± 5 percent.

We evaluate the compatibility of these estimates with petrological modeling based on geotherms, crustal bulk rock compositions and water contents consistent with the Lhasa Block. These simulations determine: (a) the physico-chemical conditions of melt generation at the base of the Tibetan crust and its transport and emplacement in the middle crust; (b) the melt percentage produced at the source, transported and emplaced to form the observed “bright spots”.

Two main mechanisms are considered: (1) melting induced by fluids produced during mineral dehydration reactions in the underthrusting Indian lower crust; (2) dehydration-melting reactions caused by heating within the Tibetan crust. We find that both mechanisms demonstrate first-order match in explaining the formation of the partially molten “bright spots”.

Thermal modelling of their cooling shows that these Lhasa Block batholiths are fated to crystallize within geologically short times (few Myr). This, together with their small size compared to the Tibetan Plateau, suggests that these partially molten zones are ephemeral and local features of the geodynamic evolution. Their transience excludes both long-distance and long-lasting channel flow transport in Tibet.

P 2.20

Archaean Barite: Strontium Isotopes as a tracer of early crust-mantle evolution

Arathy Ravindran[1], Klaus Mezger[1], S. Balakrishnan[2], Michael M. Raith[3]

[1] Institut für Geologie, Universität Bern, Baltzerstrasse 1+3, 3012 Bern, Switzerland
[2] Department of Earth Sciences, Pondicherry University, Puducherry, India-605014
[3] Mineralogisch-Petrologisches Institut, Universität Bonn, Poppelsdorfer Schloss, D-53115 Bonn, Germany

Strontium-rich Archaean barites ($Ba[Sr]SO_4$), depleted in ^{18}O, can potentially preserve primary $^{87}Sr/^{86}Sr$ ratios and thereby give information on the extent and timing of crust-mantle evolution during Earth's earliest preserved history. Barite precipitated formed from hydrothermal solutions during the Archaean included Sr from both seawater and surrounding basalts and provide an upper limit for the composition of the mantle and a lower limit for early Archaean seawater (e.g., McCulloch, 1994).

Early Precambrian stratiform barite deposits have been reported from a small number of places including the Pilbara Block of Western Australia, the Fig Tree and the Onverwacht Groups of Swaziland Supergroup of South Africa and the Sargur Group in Karnataka, India (Deb,M et al., 1991). The barite-bearing zone in the Ghattihosahalli Schist Belt (GSB) occurs as minor, conformable and discontinuous bands and lenses, largely confined to the fuchsite quartzite horizon and lie directly above the older mafic-ultramafic units. The sulphate-sulphide association and the significant Cr content in the layers prove a hydrothermal origin for the barites. The barites from the Sargur greenstone belt were first studied for their isotopic signatures by Deb at al. who report an average for $^{87}Sr/^{86}Sr$= 0.7018±7 (their preferred value) with the lowest value of 0.70128±5 and 4.02‰ for $\delta^{34}S$. In the present study, $^{87}Sr/^{86}Sr$ values from 0.70157±4 to 0.70182±6 were determined (with negligible Rb). This range is similar to the values from the ~3.2Ga Barite Valley barites in the Barberton Greenstone Belt, South Africa (Henshall et al., 2017). These values are in the range of the least radiogenic, coeval mantle values defining less production of crustal material and can give information on Sr evolution. The measured Sr-isotope values are similar to seawater Sr evolution curve (proposed by Veizer, 1989) and imply a 'mantle-buffered' ocean during the Archaean.

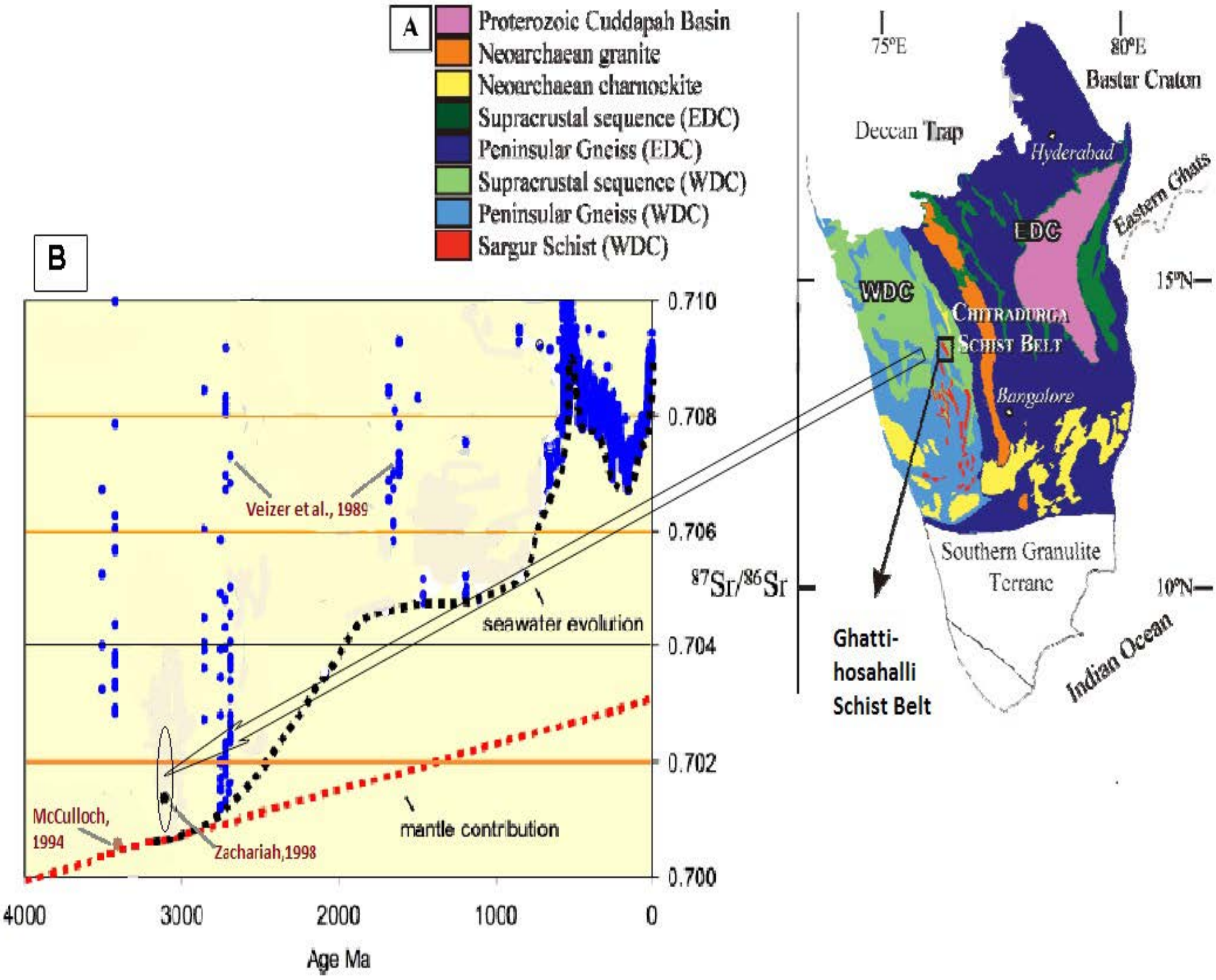

Figure: (A) Simplified model of the Dharwar Craton, modified after E. Muller et al., 2017 (B) Strontium isotopic evolution, modified after Veizer, 1989. The poorly time-constrained values are removed. The ellipse gives the range of values measured for the Archaean Sargur barites.

REFERENCES

Deb, M., et al. 1991: Isotopic composition of two Precambrian stratiform barite deposits from the Indian shield, Geochim. Cosmochim. Acta 55, 303-308.

Henshall, Tom. 2017: The volatile element evolution of the solar system constrained by the Strontium isotopic composition of Archaean barite and Calcium-Aluminium-rich inclusions (Doctoral Thesis).

Mc Culloch, M.T. 1994: Primitive $^{87}Sr/^{86}Sr$ from an Archaean Barite and Conjecture on the Earth's Age and Origin, Earth and Planetary Science Letters, 126, 1-13.

Muller, E. et al. 2017: Primary sulfur isotope signatures preserved in high-grade Archean barite deposits of the Sargur Group, Dharwar Craton, India, Precambrian Research, 295, 38-47.

Veizer, J. 1989: Strontium isotopes in seawater through time, Ann. Rev. Earth Planet. Sci. 17: 141-167

P 2.21

Neogene retro-arc basaltic magmatism in southern Patagonia: magmatic arc connection and alternatives to subslab models

Davide Roggero[1], Othmar Müntener[1], Sébastien Pilet[1]

[1] *Institute of Earth Sciences, University of Lausanne, Quartier UNIL-Mouline, Géopolis, CH-1015 Lausanne (davide.roggero@unil.ch)*

The southern Patagonian (South America) Neogene retro-arc magmatism has been associated to the opening of slab windows and/or slab tearing beneath the South American plate (Gorring et al. 1997, Guivel et al. 2006), as a consequence of the Chile ridge subduction and the melting of OIB-type asthenospheric mantle. This retro-arc magmatic activity produced alkaline to subalkaline transitional lavas – magmas with geochemical characteristics intermediate between intra-plate alkaline and arc calc-alkaline geochemistry – yet the spatial and temporal evolution of their geochemical signatures remain largely unconstrained.

New geochemical data and detailed field investigations from the retro-arc lavas of Sierra Baguales and Cerro del Fraile-Tres Lagos area (southern Patagonia), located about 100-150 km east of the active volcanic front, are used to test the potential relationships between the geochemical signature and the dynamics of the southern Patagonian subduction system during the last 20 million years. Results show that basaltic magmas from the Sierra Baguales plateau lavas are primitive magmas with subalkaline signature. Their positive Pb and negative Nb anomalies are hallmarks of calc-alkaline magmas, but the enriched incompatible trace element patterns differ from typical arc volcanoes. In contrast, less voluminous and similar spatially located basaltic lavas from Cerro del Fraile, Tres Lagos and Sierra Baguales as well, have an alkaline and OIB-like signature, suggesting a geochemically different mantle source without a slab-related component.

Experimental results have demonstrated that melting of amphibole-rich metasomatic veins or cumulates located in the lithospheric mantle are a viable mechanism for the origin of intra-plate alkaline volcanism (e.g. Pilet et al. 2008). Likewise melting amphibole-rich lithologies in the sub-arc mantle might produce the trace element signatures of arc-related transitional to alkaline magmas and are directly related to the metasomatic process induced by mobile components that form the amphibole-rich rocks. These amphibole-rich cumulates could be produced by calc-alkaline arc magma differentiation at depth, and their potential delamination (e.g. Müntener & Ulmer, 2006) and partial melting on a Ma time-scale could represent an alternative mantle source. Our goal is to test the various hypothesis to produce transitional magmas, characterized by low Nb high Pb content, and spatially related OIB-like magmas, by linking arc and retro-arc geodynamic and magmatism by cumulate melting with mantle melting. Slab window and/or slab tearing models are not required to explain the chemical characteristics of arc-rear arc associations.

REFERENCES

Gorring, M.L., Kay, S.M., Zeitler, P.K., Ramos, V.A., Rubiolo, D., Fernandez, M.I.,Panza, J.L. 1997: Neogene Patagonian plateau lavas: Continental magmas associated with ridge collision at the Chile Triple Junction. Tectonics, 16, 1-17.

Guivel, C., Morata, D., Pellete r, E., Espinoza, F., Maury, R. C., Lagabrielle, Y., et al. 2006: Miocene to Late Quaternary Patagonian basalts (46–47°S): Geochronometric and geochemical evidence for slab tearing due to active spreading ridge subduction. Journal of Volcanology and Geothermal Research, 149(3-4), 346-370.

Müntener, O. & Ulmer, P. 2006: Experimentally derived high-pressure cumulates from hydrous arc magmas and consequences for the seismic velocity structure of lower arc crust. Geophysical Research Letters, 33(21), L21308.

Pilet, S., Baker, M. B., & Stolper, E. M. 2008: Metasomatized lithosphere and the origin of alkaline lavas. Science (New York, N.Y.), 320(5878), 916–919.

P 2.22

Water content of Nominally Anhydrous Mineral in mantle xenoliths from Southern Patagonia: Spatial variability and implications

Alexandra Demers-Roberge[1], Peter Tollan[2]and Othmar Müntener[1]

[1] *Earth Sciences Institute, University of Lausanne, CH-1015, Lausanne (alexandra.demers-roberge@unil.ch)*
** Institute of Geological Sciences, University of Bern, Baltzerstrasse 3, 3012 Bern

Several decades of studies have shown that Nominally Anhydrous Minerals (NAMs) in Earth's mantle may contain a substantial amount of water incorporated in defects in the mineral structure, making the mantle a significant "water" reservoir (Bell and Rossman, 1992a). Water in minerals, even in small concentrations, has an influence on mechanical strength, melting behavior, diffusion rate, electrical conductivity, viscosity and rheology (Beran and Libowitzky, 2006). The influence is even greater in a large volume of rocks such as the mantle where it has important implications for geodynamics and mantle processes. The main NAMs in which water is incorporated are olivine, orthopyroxene, clinopyroxene and garnet. A very good proxy to measure water contents in the upper mantle is peridotite xenoliths. This study focuses on measuring water contents in peridotite xenoliths coming from several different localities throughout Southern Patagonia, using Fourier Transformation Infrared Laser (FTIR). The final goal of the work would be to understand the relationship and influence between water concentrations in the samples and different mantle processes such as depletion, metasomatism or water loss during magma ascent. The presence of mantle xenoliths in Southern Patagonia is related to Miocene to Pleistocene alkaline volcanism in the back-arc region (Rivalenti, G. et al. 2004). The source of this alkaline volcanism is debated, but one of the hypotheses is upwelling of the asthenosphere, related to the opening of a slab window which is due to the subduction of the active Chile spreading ridge (between the Nazca and the Antarctica plates) beneath the South American plate (Gorring, M. L et al. 1997). The dispersion of mantle xenoliths occurrences from west to east make Southern Patagonia a good location to study spatial variability of water contents in the mantle wedge. Three main areas have been chosen: Tres Lagos, Cerro del Fraile and Estancia Las Cumbres. The peridotite samples were collected in different lavas flow and scoria cones. Their shape, size and alteration degree vary from one locality to the other. The samples are spinel-lherzolites, harzburgites, dunites and pyroxenites. The measurements using FTIR were taken on single crystals of olivine (ol), clinopyroxene (cpx) and orthopyroxene (opx) mounted in epoxy and doubly polished. 400 microns doubly polished sections were also made to investigate a potential link between textures, minerals and the water measurements in the samples. The preliminary results on the Las Cumbres xenoliths show very low concentration of water in ol, cpx and opx in dunites and harzburgites. Absence of water may signify water loss during ascent or depletion. Future work will investigate whether water contents vary from core to rim, in which case it would be possible to model diffusion profiles of hydrogen to extract rates of magma ascent.

REFERENCES

Bell, D.R., Rossman, G.R. 1992: Water in Earth's Mantle : The Role of Nominally Anhydrous Minerals, Science, 255, No 5050, 1391-1397.

Beran, A. and Libowitzky E. 2006: Water in Natural Mantle Minerals II: Olivine, Garnet and Accessory Minerals, Reviews in Mineralogy & Geochemistry, vol. 62, 169-191.

Gorring, M. L et al. 1997: Neogene Patagonian plateau lavas: continental magmas associated with ridge collision at the ChileTriple Junction,Tectonics, 16, 1-17.

Rivalenti, G. et al. 2004:The backarc mantle lithosphere in Patagonia, South America, Journal of South America Earth Sciences, 27, 121-152.

P 2.23

Water incorporation and site-specific hydrogen diffusion in garnets

Julien Reynes[1], Jörg Hermann[1], Michael Jollands[2]

[1]Institut für Geologie, Universität Bern, Baltzerstrasse 1+3, 3012 Bern (julien.reynes@geo.unibe.ch)
[2]Institut des Sciences de la Terre, Université de Lausanne, Quartier UNIL-Mouline Bâtiment Géopolis, CH-1015 Lausanne

Garnet is an anhydrous mineral but water can be incorporated in the form of OH groups, replacing cations in the lattice, known as point defect. Garnet is of particular interest, because it is present in many metamorphic rocks. If water features are preserved in garnet through metamorphism, hydrogen diffusion in garnet could be used as a geo-speedometer. For this purpose, we need to know how retentive water is, how fast the diffusion of hydrogen is and how many point defects incorporating water there are in garnet.

To address these questions, we performed diffusion experiments on natural gem-quality spessartine (300 ppm H_2O) and grossular (800 ppm H_2O). The chemical composition of garnet influences the peak positions in infrared spectra, which are lower in wave numbers for spessartine than for grossular. The experiments were conducted on cubes of 1.5*1.5*1.5 mm^3, at 1 atm over a temperature range of 750-1050°C under both air and various lower oxygen fugacities buffered by CO/CO_2 gas mixes (ΔQFM+8 to ΔQFM-3). Water diffusion profiles were measured by FTIR with 3 µm step in a slice through the center of the cube.

Water diffusion is fast in air, slows down with oxygen fugacity and is absent at our experimental timescales at low (ΔQFM -3) indicating that hydrogen diffusion is coupled to the very fast oxidation reaction

, where M is Fe or Mn. The activation energy (Ea) of this exchange has been determined with experiments at 950, 850 and 750°C. Ea is low, (158kJ/mol) consistent with a diffusion mechanism that doesn't involve metal vacancies. Figure 1 shows that a change of colour (darkening) at the edge of the grossular garnet slice (a) is linked with a water loss (b), consistant with an iron oxidation related mechanism. We noticed that the water concentration at the interface of the slice is not zero, meaning that when all iron get oxidised, this fast mechanism stops. An automated deconvolution program was developed to resolve the relative contributions of each FTIR band in the measured diffusion profiles. Absorption bands decrease at different rates during H diffusion allowing identification of "families" of bands that belong to the same point defects. Some bands even grow during the experiment. Our data provide evidence for up to four different water incorporation mechanisms in garnet. Apart from H in silicon vacancies, our results suggest water related to trivalent cations, water in dodecahedral vacancies as well as water associated with minor Ti.

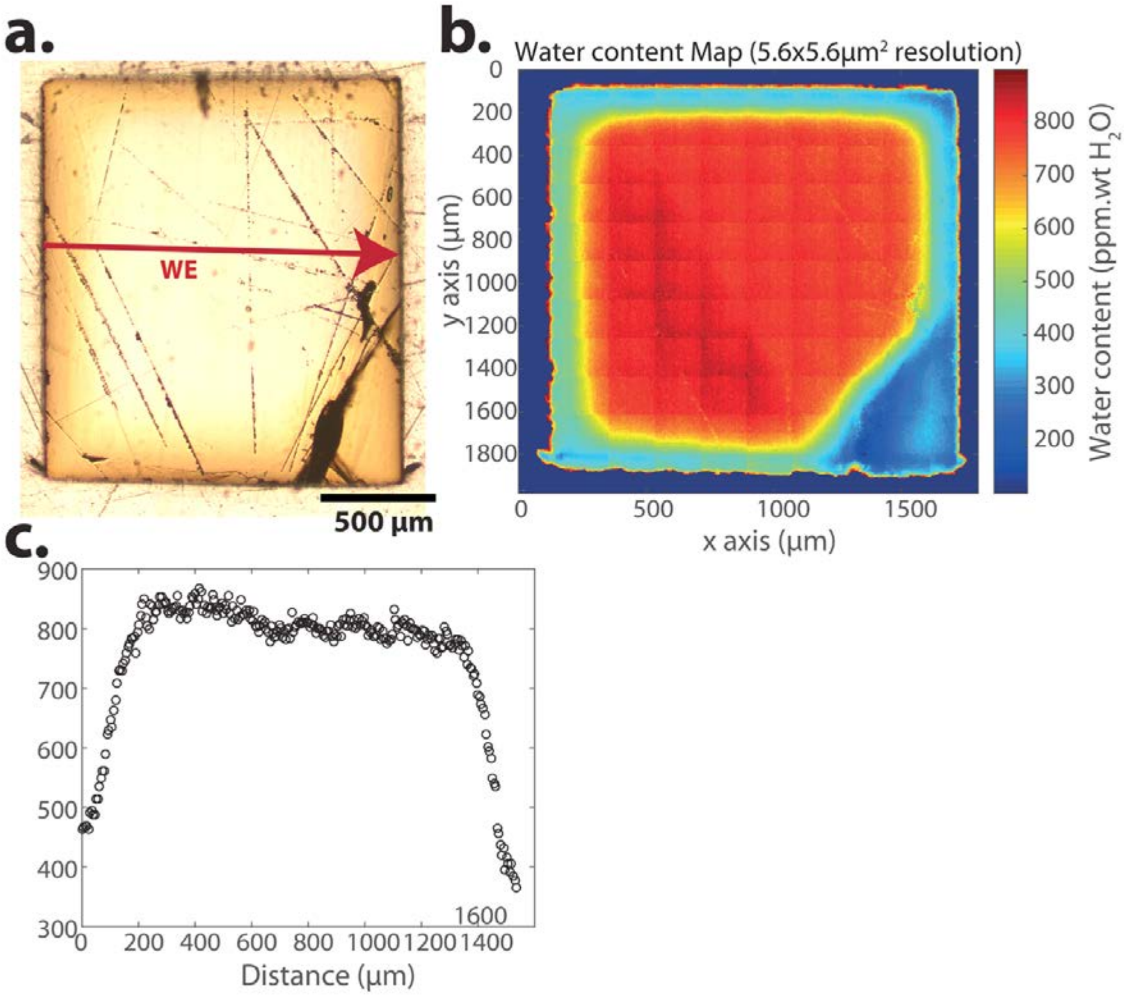

Figure 1. Slice of a grossular garnet cube after a diffusion experiment in air at 850°C for 5 days and related water map and profile. a) Picture of the slice taken with a light microscope in transmission mode. b) Water map aquired using FTIR with a Focal Planned Array detector. Pixel size is 5.6 x 5.6µm². Conversion of total absorbance to water content is made using the calibration of Maldener et al. 2003 for grossular. c) Profile of water content measured with high resolution (3µm step) along the WE line drawn on a). Calibration used is identical as the one used for the map.

REFERENCES

Maldener, J., Hösch, A., Langer, K., & Rauch, F., 2003: Hydrogen in some natural garnets studied by nuclear reaction analysis and vibrational spectroscopy, Phys Chem Minerals, 30, 337-344.

P 2.24

Permian magmatism and metamorphism in the Dent Blanche nappe: constraints from field observations and geochronology

Paola Manzotti[1], Daniela Rubatto[2], Afifé El Korh[3], Michel Ballèvre[4], Benedicte Cenki-Tok[5], Michele Zucali[6] & Martin Engi[2]

[1] *Institute of Earth Sciences, University of Lausanne, Géopolis, Quartier Mouline, Lausanne 1015, Switzerland (paola.manzotti@gmail.com)*
[2] *Institute of Geological Sciences, University of Bern, Baltzerstrasse 1+3, 3012 CH-Bern*
[3] *Unit of Earth Sciences, Department of Geosciences, University of Fribourg, Chemin du Muse 6, CH-1700 Fribourg, Switzerland*
[4] *Géosciences Rennes, UMR CNRS 6118, Université Rennes1, Campus de Beaulieu, Rennes Cedex 35042, France*
[5] *Géosciences Montpellier, Université Montpellier 2, Place E. Bataillon, 34095 Montpellier cedex 5, France*
[6] *Dipartimento di Scienze della Terra "Ardito Desio", Università degli Studi di Milano, Via Mangiagalli 34, 20133 Milano, Italy*

In the Dent Blanche Tectonic System, the Mont Morion biotite-bearing granite is a km-scale intrusion preserved in a low-strain volume. Zircon saturation thermometry suggests that it crystallised from a melt that reached about 800°C. U-Pb zircon and allanite geochronology indicates crystallization of the magma in the Permian (290 ± 3 Ma; 280 ± 8 Ma, respectively). Migmatitic biotite-gneiss and amphibolite are found as xenoliths within the Mont Morion granite and constitute its country-rocks. In two samples of migmatitic biotite-gneiss zircon has metamorphic overgrowths that yield U-Pb ages of 285 ± 3 Ma and 281 ± 4 Ma, and are thus contemporaneous with the intrusion of the granite. The Mont Morion granite with its country-rocks of migmatitic biotite-bearing gneiss and amphibolite was thus emplaced at middle crustal levels while amphibolite facies metamorphism affected its country rocks. The magmatic and metamorphic record in the Mont Morion area reflects the high-temperature regime and lithospheric thinning of the Adriatic continental margin during Permian (Manzotti et al., in press).

REFERENCES

Manzotti, P., Rubatto, D., Zucali, M., El Korh, A., Cenki-Tok, B., Ballèvre M. & Engi M. In press: Permian magmatism and metamorphism in the Dent Blanche nappe: constraints from field observations and geochronology. Swiss Journal of Geosciences.

P 2.25

Th-U-Pb cleft monazite crystallization ages linked to exhumation history and shear zone activity in the Tauern Window

Emmanuelle Ricchi[1], Edwin Gnos[2], C. Bergemann[1], M. Whitehouse[3]

[1] *Department of Earth Sciences, University of Geneva, Rue des Maraîchers 13, 1205 Geneva, Switzerland (Emmanuelle.Ricchi@unige.ch)*
[2] *Natural History Museum Geneva, 1 Route de Malagnou,1208 Geneva, Switzerland*
[3] *Swedish Museum of Natural History, Stockholm, Sweden*

Monazite-(Ce) is a light rare earth element phospate (LREE,Th)PO_4 of major interest for geochronology in hydrothermal systems because the Th-U-Pb system is not affected by diffusion at temperatures below ~450°C at which they form (Cherniak et al., 2004). Even though it is very resistant to radiation damage, its isotopic system can be reset by recrystallization or dissolution/reprecipitation in presence of hydrous fluid (e.g., Seydoux-Guillaume et al., 2012; Grand'Homme et al., 2016) at relatively low temperatures (<400°C; Grand'Homme et al, 2016).

Hydrothermal monazites are found in alpine fissures that formed during tectonic movement under peak to retrograde metamorphic conditions. Retrograde mineral reactions at temperatures below 350°C are common in clefts due to the presence of fluid while this is rarely observed in the surrounding rocks. Monazite-(Ce) dissolution/precipitation at such low temparatures is mainly caused by tectonic events. This means that the tectonic activity can be dated (Berger et al., 2013; Bergemann et al., 2017).

SIMS Th-U-Pb dates were obtained for different monazite growth domains in grains from the western and central Tauern window, Austria. Growth domains were identified by BSE images and corresponding to trace element variations (REE+Y, Th, U and Pb). Dating of these domains revealed that stepwise growth (and dissolution) occurred mainly at 20 and between 17 and 13 Ma in the western part and between 13 and 11, 11 and 10 Ma in the central part. Field observations confimed that in some cases the repeated tectonic activity resulted in cleft deformation and formation of a second set of fissures with different orientation. Interestingly, recent studies in the eastern Tauern have shown that crystallization of monazite occurred in a temperature range of ~200-300°C and started in most cases at the closure temperature of the zircon fission track system and ceased at higher temperatures than those recorded by the zircon (U-Th)/He system (e.g., Gnos et al., 2015). In the central and western Tauern monazite-(Ce) crystallization in fissures seems to be controlled by the tectonic movement along the major faults (e.g. Greiner Shear Zone (GSZ), Ahrntal Shear Zone (AhSZ), Ahorn Shear Zone (ASZ)). Whereas the major tectonic activity is recorded at around 13 Ma, the youngest domain ages show movement as late as 10 Ma.

REFERENCES

Bergemann, C., Gnos, E., Berger, A., Whitehouse, M., Mullis, J., Wehrens, P., Pettke, T. and Janots, E., 2017. Th-Pb ion probe dating of zoned hydrothermal monazite and its implications for repeated shear zone activity: An example from the Central Alps, Switzerland. Tectonics, 36(4), pp.671-689.

Berger, A., Gnos, E., Janots, E., Whitehouse, M., Soom, M., Frei, R. and Waight, T.E. (2013). Dating brittle tectonic movements with cleft monazite: Fluid-rock interaction and formation of REE minerals. Tectonics 132: 1-14.

Cherniak, D.J., Watson, E.B., Grove, M. and Harrison, T.M. (2004). Pb diffusion in monazite: A combined RBS/SIMS study. Geochimica and Cosmochimica Acta 68: 829-840.

Gnos, E., Janots, E., Berger, A., Whitehouse, M., Walter, F., Pettke, T and Bergemann, C. (2015). Age of cleft monazites in the eastern Tauern Window: constraints on crystallization conditions of hydrothermal monazite. Swiss Journal of Geosciences 108: 55-74.

Grand'Homme, A., Janots, E., Seydoux-Guillaume, A. M., Guillaume, D., Bosse, V., & Magnin, V. (2016). Partial resetting of the U-Th-Pb systems in experimentally altered monazite: Nanoscale evidence of incomplete replacement. Geology, 44(6), 431-434.

Seydoux-Guillaume, A.M., Montel, J.M. , Bingen, B., Bosse, V., de Perseval, P., Paquette, J.L., Janots, E., and Wirth, R. (2012). Low-temperature alteration of monazite: Fluid mediated coupled dissolutionprecipitation, irradiation damage, and disturbance of the U-Pb and Th-Pb chronometers. Chemical Geology, 330-331: 140-158.

P 2.26

Veining and mineralizaton history of Bor (Serbia)

Dina Klimentyeva[1], Christoph Heinrich[1] & Albrecht Von Quadt[1]

[1] *Institute of Geochemistry and Petrology, ETH Zurich, Clausiusstrasse 25, 8092 Zurich (dina.klimentyeva@erdw.ethz.ch)*

The Bor metallogenic zone contains world-class porphyry copper, high- and low-sulphidation epithermal deposits of Bor, Veliki Krivelj and a newly discovered Cukaru Peki with over 20 million tons of Cu and 1000 tons of Au (Jelenković et al., 2016). The deposits are located at the Eastern margin of the Timok magmatic complex, in the Serbian part of the Apuseni-Banat-Timok-Srednogorie belt (ABTS). The Bor deposit is overlain by epiclastic layers of andesitic and dacitic composition intercalated with pelites (Đorđević, 2005) and is truncated on the Eastern side by reverse Bor fault and Bor conglomerates (Jankovic et al., 2002).

A complete range of mineralization types from porphyry (pyrite-chalcopyrite veins at lower levels of T and T1 orebodies, quartz-pyrite and quartz-chalcopyrite veins as well as pyrite paint veins at Borska reka) to high-sulfidation epithermal (anhydrite-pyrite-covellite veins at upper levels of Borska reka and at Tilva Ros) and massive sulfide orebodies (T and T1) is present at Bor. The extreme high-sulfidation assemblage occurs within the L orebody with native sulfur and massive sulfide ore.

Massive sulfide mineralization is contained in veins and in 30 to 50 m isometric to lens-like massive sulfide orebodies (Tilva Ros, T, T1 and T2). At the bottom of the T orebody, matrix-supported breccias occur with clasts of vuggy silica, bornite and chalcopyrite in a silicified matrix, and quartz with minor pyrite mineralization. These breccias are mineralized, sometimes to a degree where quartz clasts are embedded in pure covellite matrix.

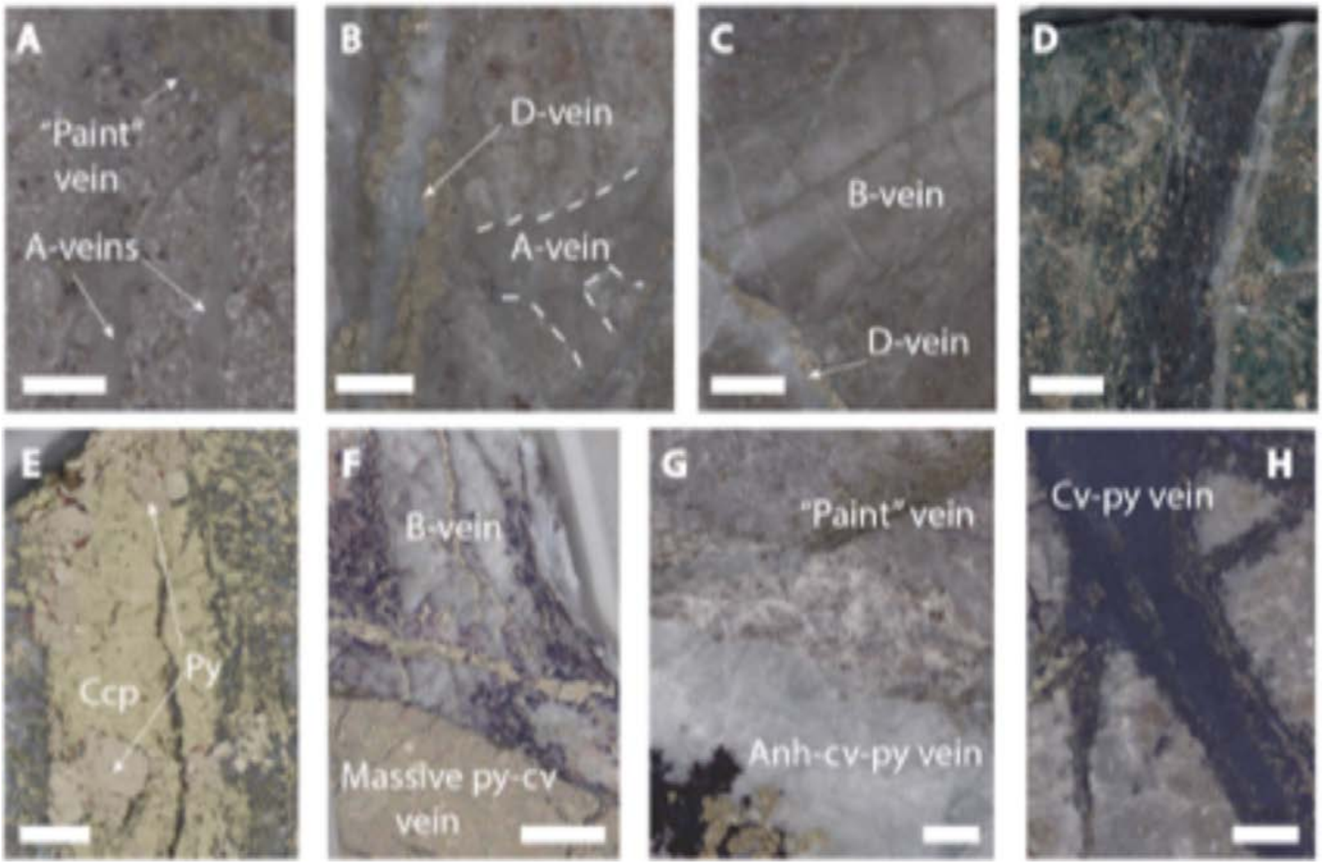

Figure 1. Porphyry and epithermal type mineralization at Bor. A) Sinuous quartz vein cut by a pyrite paint vein. B) Sinuous quartz veins cross-cut by anhydrite-pyrite vein with euhedral pyrites. C) Anhydrite-pyrite D type vein cross-cuts earlier quartz-pyrite vein with thread-like pyrite aggregates. D) Magnetite-chalcopyrite-quartz vein, deep levels of Borska Reka porphyry. E) Pyrite + chalcopyrite equilibrium texture, lower part of T1 massive sulfide orebody. F) Massive pyrite vein with covellite x-cutting C-type pyrite-quartz vein with pyrite central line, transition from Borska Reka porphyry to Tilva Ros epithermal orebody. G) Epithermal anhydrite-covellite-pyrite vein cross-cutting pyrite paint vein, Borska Reka porphyry. H) Epithermal covellite-pyrite vein cross-cutting quartz A-vein. Scale bar = 1 cm.

Cross-cutting relationships between different types of veins suggest the following time sequence of vein emplacement:

1. Earliest barren stage is accompanied by the formation of sinuous quartz veins, practically free of sulfides and cross-cut by all other vein types.
2. Porphyry-style B-veins, either with pyrite/chalcopyrite stringers, or with euhedral pyrite crystals, crosscut early sinuous quartz veins and are cross-cut by epithermal veins.
3. Epithermal pyrite-anhydrite veins, which cut early sinuous quartz veins and are in turn cross-cut by pyrite paint veins and anhydrite-covellite veins, are of transitional nature between porphyry and epithermal mineralization styles.
4. Pyrite paint veins, cross-cut by the latest vein assemblage. However, this cross-cutting relationship is occasionally reversed. This generation of veins is coeval with massive pyrite mineralization.
5. Latest anhydrite-covellite veins with some pyrite and solid sulfur. Solid sulfur forms and equilibrium texture with anhydrite; this assemblage overgrows early covellite-anhydrite assemblage. Anhydrite-covellite veins represent the late stage of mineralization, as well as covellite-enargite assemblage within massive sulfide orebodies.

One of the pecularities of late-stage veins and advanced argillic alteration assemblage is ubiquitous presence of anhydrite, which might indicate that the formation of massive sulfide ore coincided in time with transition from subaerial to submarine conditions.

REFERENCES

Đorđević, M., 2005. Volcanogenic Turonian and epiclastics of senonian in the Timok magmatic complex between Bor and the Tupižnica mountain, eastern Serbia. Geoloski anali Balkanskoga poluostrva, 66: 63-71

Jankovic, S., Jelenković, R., and Kozelj, D., 2002. The Bor copper and gold deposit. QWERTY, Bor. 298

Jelenković, R., Milovanović, D., Koželj, D., and Banješević, M., 2016. The Mineral Resources of the Bor Metallogenic Zone: A Review. Geologia Croatica, 69(1): 143-155

P 2.27

Recovery Potential of Heavy Metals from Swiss Fly Ash

Wolfgang Zucha[1], Urs Eggenberger[1], Gisela Weibel[1,2]

*Institut für Geologie, Universität Bern, Baltzerstrasse 1+3, CH-3012 Bern (wolfgang.zucha@students.unibe.ch)
**Zentrum für nachhaltige Abfall- und Ressourcennutzung ZAR, Wildbachstrasse 2, CH-8340 Hinwil

In Switzerland the disposal of untreated waste has been prohibited for 17 years. At present non-recyclabe waste must be thermally treated in Municipal Solid Waste Incineration plants (MSWI). Ca. 73 kt of fly ashes are the annual by-product of the combustion process. The fly ashes are enriched with volatile heavy metals and cannot be disposed of without further treatment. Today's state of the art treatment in Switzerland is the FLUWA process (Schlumberger et al., 2007), during which heavy metals are extracted by acidic leaching. Nowadays around 50 % of the fly ashes are treated in this way. All other ashes are either mixed with concrete prior to disposal or exported and deposited underground. However, as from 2021, the new Ordinance on Waste and Disposal (VVEA, Swiss Confederation 2016) requires not only the removal but also the recovery of heavy metals by a "state of the art" process. Such a state of the art solution would be the FLUREC process (Schlumberger et al., 2007) that allows the recovery of Zn, Cu, Pb and Cd.

Since the VVEA is not specific on how this is done, so that the upcoming guidelines need further elaboration and assessments. In collaboration with the Federal Office for the Environment and all MSWI plant operators, a detailed study of all MSWI fly ash in Switzerland has been initiated: Chemical and composition of the solid state have already been analyzed with XRF and XRD.
The recovery potential of heavy metals in Swiss fly ashes measured during this study (Table 1) is very promising and confirms the results from previous unpublished investigations by the ZAR (Zentrum für nachhaltige Abfall- und Ressourcennutzung).

Table 1. Recovery potential of Zn, Cu, Pb and Cd in t/a. The yield corresponds to the current state of the FLUREC process.

Metal	Concentration in fly ashes	Yield	Amount [t/a]
Zn	4.60%	80%	~2'850
Cu	0.26%	40%	~80
Pb	0.99%	85%	~650
Cd	0.03%	100%	~26

Metal recovery is not only required because of environmental aspects. It is also interesting from an economic point of view due to the retrieval of pure zinc (99.99 %). This study study will help to assess the economical impact of the FLUREC process on a national scale.

REFERENCES

Schlumberger, S., Schuster, M., Ringmann, S., Koralewska, R., 2007. Recovery of high purity zinc from filter ash produced during the thermal treatment of waste and inerting of residual materials. Waste Management & Research 25, 547-555.
Swiss Confederation. 2016: Verordnung über die Vermeidung und die Entsorgung von Abfällen (VVEA), 1□46.

P 2.28

Lithogeochemical classification of hydrothermally altered Paleoproterozoic plutonic rocks associated with gold mineralisation: examples from South Greenland and Northern Sweden

Denis M. Schlatter[11], Katerina Schlöglova[2], Réginald Fettweis[3], Glenn Bark[3] and Joshua W. Hughes[4]

[1] *Helvetica Exploration Services GmbH, Carl-Spitteler-Strasse 100, CH-8053 Zürich*
([1] denis.schlatter@helvetica-exploration.ch; http://www.helvetica-exploration.ch)
[2] *Institute of Geochemistry and Petrology, ETH Zürich, Clausiusstr. 25, CH-8092 Zürich*
[3] *Division of Geosciences and Environmental Engineering, Luleå University of Technology, Sweden*
[4] *Department of Earth Sciences, Durham University, Science Labs, DH1 3LE, UK*

Lithogeochemical techniques using immobile elements are widely described in the literature and such methods have been successfully applied in mineral exploration for the classification of variably (hydrothermally) altered host rocks and for more advanced chemostratigraphy (e.g. Barrett and McLean, 1994). Although lithogeochemical rock classifications are well established for volcanic rocks (including those which have experienced intense alteration), suitable rock classification diagrams for altered plutonic rocks, particularly granitoids, are lacking, with the literature heavily biased to the least altered examples.

Rock classification diagrams based on major oxides (e.g. Debon & Le Fort, 1982; De la Roche *et al*., 1980) are useful for unaltered rocks, however are wholly inappropriate for altered rocks due to the mobility of major elements during alteration. For example, K, Na, Ca, Si, Fe, Mg are recognised to be mobile during alteration and can be added or removed during metasomatism (Barrett and McLean, 1994). The addition of K is observed within highly altered granitoids located in proximal sericite alteration zones at the Vagar gold prospect in South Greenland (Fig. 1a; Schlatter *et al*., 2013). This alteration style is widely reported from other orogenic gold deposits of various ages.

In this contribution we discuss how altered plutonic rocks can be classified based on immobile elements. This has the potential to be used in distinguishing favourable granodiorite compositions associated with gold mineralisation within the study areas thus providing a useful vector for future gold exploration. We present new preliminary classification diagrams from 94 granitoid samples from Vagar gold prospect in the Nanortalik Gold Belt of South Greenland (Schlatter *et al*., 2013) and from the Svartliden (Schlöglova *et al*., 2013) and Fäbodtjärn (Fettweis, 2015) deposits of the Gold Line in Northern Sweden.

The plutonic rocks of both areas host auriferous quartz veins deposited at ca.1.8 Ga (e.g. at Vagar and Fäbodtjärn) or are spatially associated with the gold mineralisation (Schlatter *et al*., 2016; Fettweis, 2015). The preliminary classification diagrams based on the immobile elements Zr and Y discriminate the calc-alkaline Vagar granodiorite samples from the Svartliden and the Fäbodtjärn samples (Fig 1b), and classification based on the immobile element ratios Al/Ti and Zr/Al (Fig. 1c) allow the discrimination of granitoids of different areas and two geochemically discrete granodiorites at Vagar, a feature which is not apparent from major oxides diagrams (Fig. 1a).

It is conceivable that the granodiorites predate the orogenic gold, and thus “fertile” granodiorites reflect the fact they are suitable chemical or structural traps. Perhaps the composition of the Vagar granitoid, hosting significant gold mineralisation (e.g. quartz veins up to 2533 ppm and granodiorite up to 14.4 ppm) and with high Al/Ti ratio (Fig. 1c), is more reactive with an auriferous fluid than other granitoids, and thus represent a more favourable host for gold mineralisation.

High field strength elements bearing phases e.g. synchesite, allanite and monazite identified in SEM-BSE images and EDS analyses of gold bearing samples from Vagar (Schlatter *et al*., 2013), suggests that the hydrothermal fluid introduced REE elements together with the gold, making REE a possible pathfinder for gold exploration.

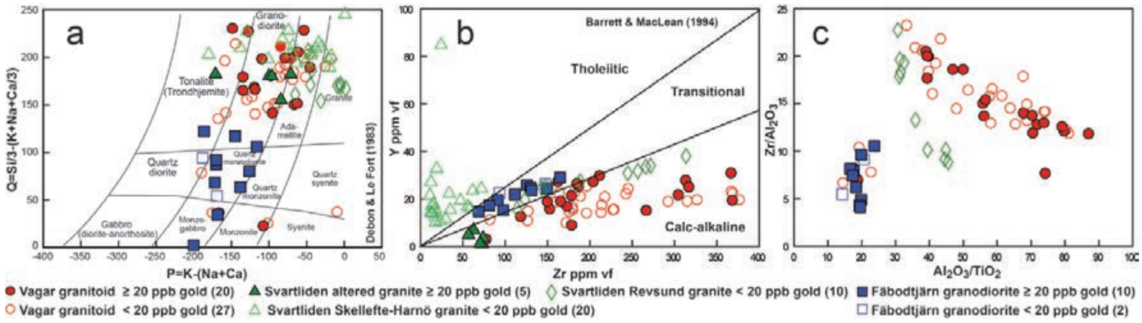

Figure 1. Lithogeochemical plots based on (a) major oxides (b) immobile elements assessing the affinity (c) immobile element ratios fingerprinting different granitoid types. Granitoids carrying gold are discriminated (filled symbols) from those barren (non-filled symbols). vf = volatile free basis.

REFERENCES

Barrett, T.J. & MacLean, W.H. 1994: Chemostratigraphy and hydrothermal alteration in exploration for VHMS deposits in greenstones and younger volcanic rocks. In: Lentz, D.R. (editor) Alteration and alteration processes associated with ore-forming systems. Short Course Notes, Volume 11. Geological Association of Canada: 433-467

Debon, F. & Le Fort, P. 1982: A chemical-mineralogical classification of common plutonic rocks and associations. Transactions of the Royal Society of Edinburgh: Earth Sciences 73: 135-149

De la Roche, H., Leterrier, J., Grandclaude, P. & Marchal, M. 1980: A classification of volcanic and plutonic rocks using R1R2-diagram and major-element analysis - its relation with current nomenclature. Chemical Geology, 29: 183-210

Fettweis, R. 2015: Geology of the Fäbodliden C Lode Gold Deposit in Northern Sweden. Implications for Gold Process Mineralogy. Master’s thesis, Luleå University of Technology. 45 pages including 7 appendices.

Schlatter, D.M., Hughes, J.W. & Schlöglova, K. 2016: Comparison of Paleoproterozoic orogenic gold deposits/occurrences of Nalunaq and Vagar in South Greenland and Svartliden in Northern Sweden. 14th Swiss Geoscience Meeting, Geneva, 18th – 19th November 2016. Abstract Volume: 102-103

Schlatter, D.M., Berger, A. & Christiansen, O. 2013: Geological, petrographical and geochemical characteristics of the granitoid hosted Amphibolite Ridge gold deposit in South Greenland. Conference proceedings, “Mineral deposit research for a high-tech world.” 12th Biennial SGA Meeting: 1189-1192

Schlöglova, K., Gordon, C., Hanes, R., Ask, H. & Broman, C. 2013: Svartliden gold mine: shear zone and BIF-hosted orogenic gold deposit, Gold Line, northern Sweden. Conf. Proceed. 12th Biennial SGA Meeting: 1193-1196

P 2.29

Trace element geochemistry of pyrites from porphyry systems in Elatsite ore field, Bulgaria: a reliable tool for exploration of porphyry (Cu-Au-Mo) and epithermal base metal-Au deposits

Elitsa Stefanova[1], Peter Marchev[1], Stoyan Georgiev[1], Irena Peytcheva[1], Raya Raicheva[1]

[1]*Geological Institute, Bulgarian Academy of Sciences, Acad. G. Boncgev street 24, 1113 Sofia (stefanova_e@geology.bas.bg)*

The pyrite is one of the the most abundant sulfide minerals in hydrothermal ore deposits which is also a part of hydrothermal alteration haloes formed at great distance from the main mineralization. During the last few decades the development of high sensitivity and excellent spatial resolution microbeam techniques, such as LA-ICP-MS, allowed determination of many trace elements in pyrites and other hydrothermal minerals like magnetite, titanite, rutile, chlorite and epidote. The geochemistry of these hydrothermal minerals makes them an efficient tool for provinance studies and mineral exploration. The most commonly studied trace element in pyrites is gold, due to its great economic importance. Recent studies of pyrite, arsenian pyrite and arsenopyrite revealed that they can contain significant amount of the so called “invisible” Au and others trace metals such as: Ag, As, Cu, Pb, Zn, Co, Ni, Sb, Se, Te, Hg, Tl and Bi (Cook and Chryssoulis, 1990; Large et al., 2009; Reich et al., 2013). We have analyzed pyrite and arsenopyrite (where present) from different types of mineralisazations in Elatsite ore field using a combination of SEM-EDS and LA-ICP-MS techniques. The LA-ICP-MS system consists of Perkin Elmer ELAN DRC-e ICP quadrupole mass spectrometer coupled with New Wave UP-193 nm ArF excimer laser, based at the Geological Institute of the Bulgarian Academy of Sciences. The aim of the study is to determine the trace element composition of pyrites and to test weather their geochemistry can be a reliable exploration tool for destingtion of porphyry copper and base metal-gold mineralizations in the region.

Elatsite-Chelopech ore field is an excellent area for such a study, because it comprises numerous porphyry copper and epithermal gold deposits and occurences. It is situated at the northern end of the Panagyurishte ore district of the Central Srednogorie Zone, Bulgaria. The Srednogorie Zone is part of the Apuseni-Banat-Timok-Srednogorie Magmatic and Metallogenic Belt of the Alpine-Balkan-Carpathian-Dinaride orogenic system. A number of important ore deposits, mainly porphyry Cu-Au-(Mo) and epithermal Au deposits with Late Cretaceous age, are associated with this belt. In the present study we have analysed pyrites from three porphyry copper systems: The first one comprises Elatsite porphyry Cu-Au (PGE) deposit, the proximal base metal-Au occurence Negarshtitsa and the distal base metal- and Au-bearing veins of Kapalu, Kordunsko Dere and Svishti Plaz; The second one consists of Gorna Kamenitsa porphyry Cu-Mo deposit and Dolna Kamenitsa base metal occurence; The third one comprises a porphyry copper occurence of Etropole and barite-base metal mineralization of Kiselitsa.

The LA-ICP-MS data reveiles that the pyrites from the three porphyry copper deposits have similar trace element compositins. They have low As and Au contents and relatively high concentrations of Se. Typical characteristics of these pyrites are the high Co and Ni concentrations and low Ag, Cu, Pb and Sb contents. The pyrites from the base metal and base metal-gold veins have higher As content and elevated concentrations of Au than these from the porphyry copper deposits . The concentrations of Au are highly variable (from few ppm up to 100 ppm) and show positive correlation with As content of the pyrite. They have also higher Cu, Pb and Sb and lower Se concentrations compared to the pyrtite from the porphyry copper deposits. The pyrite from these types of mineralizations is often formed together with arsenopyrite, that has also high gold concentrations, reaching up to 160 ppm Au. Two elements that behave differently in pyrites from base metal and base metal-gold veins and allow to destinguish among them are Co and Ni. In pyrites from the base metal deposits, these elements have concentrations comparable to the pyrites from the porphyry copper deposits. On the other hand the pyrites from the base metal-gold veins comprise lower concentrations of Co and Ni.

Our results show that pyrites from the different types of deposits from Elatsite ore filed have specific geochemical characteristics that can be used as an exploration tool in the region. The best option will be their combination with the geochemistry of some hydrothermal alteration minerals (e.g. chlorite, epidote, rutile from propylitic zones), which are recognized good indicators of the distance from the ore body in porphyry systems (e.g. Wilkinson et al., 2015).

REFERENCES

Cook, N.J., & Chryssoulis, S.L. 1990: Concentrations of “invisible gold” in the common sulphides: Canadian Mineralogist, 28, 1–16.

Large, R.R., Danyushevsky, L., Hollit, C., Maslennikov, V., Meffre, S., Gilbert, S., Bull, S., Scott, R., Emsbo, P., Thomas, H., Singh, B. & Foster, J. 2009: Gold and trace element zonation in pyrite using a laser imaging technique: Implications

for the timing of gold in orogenic and Carlin-style sediment-hosted deposits. Economic Geology, 104, 635–668
Reich, M., Deditus, A., Chryssoulis, S., Li, J., Ma, Ch., Parada, M.A., Barra, F. & Mittermayr, F. 2013: Pyrite as a record of hydrothermal fluid evolution in porphyry copper system: A SIMS/EMPA trace element study. Geochimica et Cosmochimica Acta, 104, 42-62
Wilkinson, J., Chang, Z., Cooke, D., Baker, M., Wilkinson, C., Inglis, S., Chen, H. & Gemmell, J. 2015: The chlorite proximitor: A new tool for detecting porphyry ore deposits. Journal of Geochemical Exploration, 152, 10-26.

P 2.30

Shirimi – Georgian Travrtine

Manana Kavsadze[1], Otar Dudauri[1], Manana Togonidze[1], Giorgi Vasahkidze[1], Ketevan Gabarashvili[1], Tamar Beridze[1]

[1] Al. Janelidze Institute of Geology, Iv. Javakhishvili Tbilisi State University, Politkovskaya str. 31, 0186 Tbilisi, Georgia (mananakavsadze@yahoo.com)

The term “Shirimi” is widely used in Georgian Architecture and art history science to define the building material which is generally named travertine or calcareous tufa (calcareous sinter).It can be found in Georgian toponymy as well. In particular - Shirimi Mountain located on the Mtiuleti-Gudamakari range (the Great Caucasus) and the river Shirimiskhevi which begins from the northern slope of the same named mountain. Historically in the river Shirimiskhevi gorge, in the vicinity of the village Tsinamkhary was distinguished the exposure of travertine deposit (Mineral resources of Georgia, 1933; Natural resources of Georgian SSR. 1959).

The reason of our interest to shirimi was conditioned by conspicuous inconsistencies between the architectural and geological data. The great majority of Georgian architectural monuments either completely (Alaverdi, Fudznari, Kvetera, Zemo Krikhi, Tvibi, Mutsdi, BevreTi and etc.) or to a certain degree (Dzveli Shuamta, Veres Gvtismshobeli, Atenis Natlismtsemeli, Tskheta and etc.) are built by shirimi. These monuments are scattered in different regions of Georgia and therefore the source areas for the building stone (shirimi) should be more numerous and proximal to the monuments’ locations, than it has been recorded so far. In geological sources presence of travertine (shirimi) deposits exposures is indicated only in the Truso, Gudamakari, Mestia and Khashuri environs. It is also well-known, that during the historical period constructions in Georgia the building stones from remote areas were not used. The idea, that travertine deposits are more widespread on the territory of Georgia, than it is recorded in historical geological data inspired our research group to find out new occurrences of these rocks. Consequently, outcrops of thick sequences of travertine deposits in the environs of villages Makarta, Dumatskhomde and in the river Boseli gorge have been recently detected (fig. 1, 2, 3). We present the results of petrographic and X-ray analysis of eight shirimi deposits. According to these data, recently found in Gudamakari area shirimi occurrences completely meet the requirements for the use of these rocks as a building stone. Further investigations aiming to define and study more occurrences of shirimi are planned in the nearest future.


Figure 1: Calcareous tufas – shirimi near the v. Makarta.


Figure 2: Makarta shirimi - calcareous tufas (close view).


Figure 3: Shirimi - calcareous tufa in the river Boseli bed.

On the basis of our field observations and analytical data, we assume that Gudamakari calcareous tufas – shirimi correspond to the rocks which generally are known as travertine. As the word "travertine" is derived from Italian toponym, we consider that it will be fair to establish using of the name "shirimi" in Georgian geological terminology to denote calcareous tufas of the local origin. It is especially topical as this name has been already widely introduced in Georgian architectural-art history sciences. This will bring closer research communities of national natural and art history sciences and will contribute in active exchanging of the related to this issue information.

REFERENCES

Mineral resources of Georgian SSR. 1933: Aditor Godabrelidze S.A., pub.by. Gostekhizdatelstvo Gruzii "Teqnika da shroma". Tiflis, Georgia, 293, 263.
Natural resources of Georgian SSR. 1959: pub. the USSR AS, volume II, Moscow.

P 2.31

Hemoilmenite from andesite of the Late Cretaceous Timok Magmatic Complex, Serbia

Aleksandar Luković[1], Janez Zavašnik[2], Predrag Vulić [4], Miodrag Banješević[3] , Kristina Šarić[4], Vladica Cvetković[4] & Aleksandar Pačevski[4]

[1] Nature History Museum, Njegoševa 51, 11000 Belgrade (aca.lukovic@nhmbeo.rs)
[2] Centre for Electron Microscopy and Microanalysis, Jozef Stefan Institute, Jamova 39, Ljubljana 1000, Slovenia
[3] Balkan Exploration and Mining d.o.o. 11000 Belgrade, Serbia
[4] University of Belgrade, Faculty of Mining and Geology, Đušina 7, 11000 Belgrade, Serbia

During the examination of Fe-Ti oxides from andesites of the Late Cretaceous Timok Magmatic Complex in East Serbia (hereafter TMC), special attention was paid to the appearance of hemoilmenite. Hemoilmenite was discovered exclusively in hornblende-biotite andesite of the first volcanic phase, which is known to host the large Bor and Veliki Krivelj porphyry copper deposits [Karamata et al., 2002].

This mineral was discovered on three out of four investigated outcrops, namely in Majdanpek, Krivelj and Nikoličevo, whereas it was absent at the Brestovac locallity. This is to the best of our knowledge the first time that the presence of hemoilmenite is reported in TMC andesites. It is comprehensively studied by reflected light microscope, electron microprobe analysis (EMPA), X-ray diffraction (XRD) and transmission electron microscope (TEM).

The study found that only grains from the Krivelj locality are homogeneous. According to the EMPA and WRD results, it is established that the studied hemoilmenite generally corresponds to the intermediate member of the series with 53.34 mole% ilmenite.

The grains of hemoilmenite from the Majdanpek site show very fine exsolutions of the hematite-ilmenite phase, along the (0001) direction The average chemical composition of this decomposed hemoilmenite corresponds to the composition of the homogeneous hemoilmenite from the Krivelj site, probably because the host rocks belong to the same volcanic phase, but due to slower cooling of andesite from Majdanpek, the breakdown of initial hemoilmenite has occurred Hemoilmenite from the Nikoličevo site exhibits distinctive exsolutions of rutile, most likely, as a result of subsequent hydrothermal activity.

The absence of hemoilmenite in the Brestovac locality implies that this mineral is not ubiquitously present in all andesites of the first phase. Furthermore, we suggest that presence/absence of hemoilmenite could serve for further subdivision of volcanic rocks of the first phase, which may potentially have large significance for mineral prospecting, i.e. for distinguishing volcanic rocks that are genetically related to porphyry and other mineralization processes in the TMC in a most direct way.

REFERENCES

Brown, N.E., Navrotsky, A., Nord, G.L., and Banerjee, S.K. 1993: Hematite (Fe_2O_3)-Ilmenite ($FeTiO_3$) solid solutions: Determinations of Fe-Ti order from magnetic properties. American Mineralogist, 78, 941–951.

Karamata S., Knežević - Đorđević V., Milovanović D., 2002. : A review of the evolution of Upper Cretaceous-Paleogene magmatism in the Timok magmatic complex and associated mineralization. In: Koželj, D., Jelenković, R., (eds). International Symposium –Geology and metallogeny of copper and gold deposits in the Bormetallogenic zone – Bor 100 years, Special issue, Bor, 15-28.

Robinson, P., Harrison, R.J., McEnroe, S.A., and Hargraves, R.B. 2002: Lamellar magnetism in the haematite-ilmenite series as an explanation for strong remanent magnetization. Nature, 418, 517-520.

P 2.32

Upper Cretaceous Kachagiani (Sakdrisi) Ore deposit host rocks analysis, Bolnisi ore field, Georgia

Nino Sadradze[1], Tamar Beridze[2], Guga Sadradze[3]

[1] *Tbilisi State University, M. Nodia Institute of Geophysics, Alexidze str.1. 0161, Tbilisi, Georgia. ninosadradze@gmail.com*
[2] *Tbilisi State University, A. Janelidze Institute of Geology, Polytcovskaya str. 31, 0186, Tbilisi, Georgia*
[3] *Tbilisi State University, Department of Geology, Faculty of Exact and Natural Sciences, University str. 13, 0186, Tbilisi, Georgia*

The Bolnisi ore field is located in the northwest part of the Lesser Cavcasioni (Lesser Caucasus) and is the part of the Artvin-Bolnisi tectonic unit. It was developing as a relatively uplifted Mesozoic island-arc type unit with suprasubduction magmatic events and related Late Cretaceous ore mineralization. Volcanogenic complexes are characterized by variable lateral and vertical regional stratigraphic relationships and are subdivided into several formations due to their petrological features. The depositional environments of Upper Cretaceous volcanic formations vary from submarine (marine micro and macro fauna data (Tsagareli et al. 1965; Migiheishvili & Gavtadze 2010; Popkhadze et al. 2014) to subaerial (lithofacies analysis data). Mafic to intermediate volcanic rocks are in subordinate amount. Felsic formations are the major hosts of numerous ore deposits (Madneuli, Kachagiani (Sakdrisi), Bertakari, Bneli Khevi etc.) within the ore field.

Within the Bolnisi ore district, Kachagiani deposit host lithofacies and spatial distribution of associated mineralization has been recently studied within the large-scale geological mapping framework. Kachagiani deposit is the part of Sakdrisi group of deposits, which is the hosted by Upper Cretaceous felsic Mashavera formation. Based on deposit host rocks analysis (outcrops, drill cores, thin section microscopy) several lithofacies units have been identified.

The deposit is hosted by volcanic (rhyo-dacite lava flows and domes) and volcaniclastic rocks. Primary volcanic (pyroclastic) deposits are represented by
ignimbrites (columnar jointed in places), crystal, lithic and pumice rich lapilli tuffs. Resedimented syn-eruptive volcaniclastic rocks are introduced by volcaniclastic turbidites.

Here as well as in nearly all deposits of the Bolnisi ore field has been distinguished the link of mineralization to various types of breccias (phreatic, phreatomagmatic and hydrothermal). Epigenetic hydrothermal breccias (Fig.1) have become good criteria in mineral deposits exploration within Bolnisi ore field (Lavoie 2014; Sadradze et al. 2017).

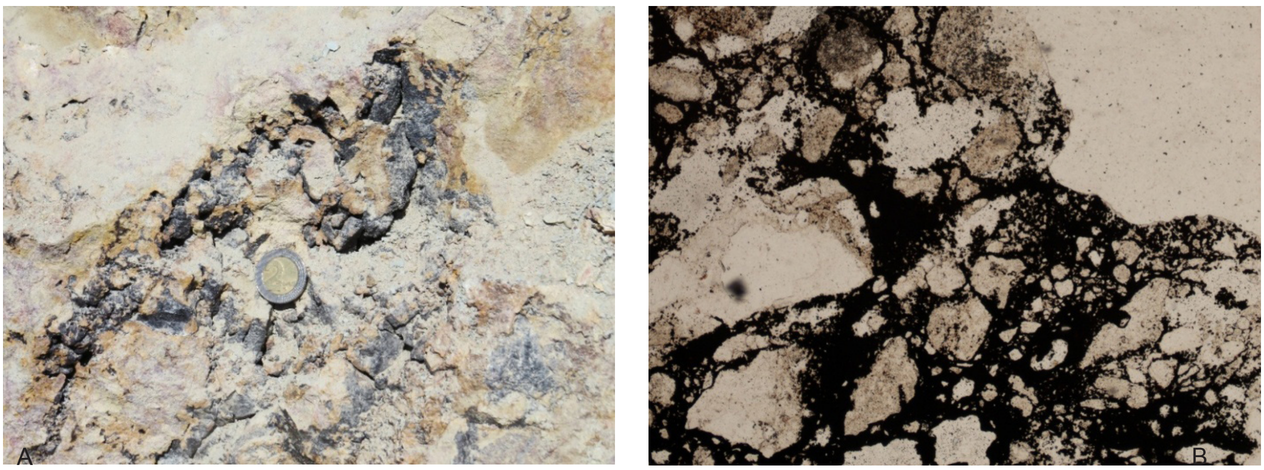

Figure 1. Epigenetic mineralized hydrothermal breccia, (A) in outcrop, (B) in thin section.

REFERENCES:

Lavoie, J. 2015: Genetic constraints of the Late-Cretaceous Epithermal Beqtakari prospect, Bolnisi Mining District, Lesser Caucasus, Georgia. University of Geneva, Department of Earth Sciences, Master of Geology Thesis, 82.

Migineishvili, R., & Gavtadze, T. 2010: Age of the Madenuli Cu-Au deposit, Georgia: evidence from new nannoplankton data: Bulletin of the Georgian National Academy of Sciences, 4, 85-91.

Popkhadze, N. Moritz, R. & Gugushvili, V. 2014: Architecture of Upper Cretaceous rhyodacitic hyaloclastite at the polymetallic Madneuli deposit, Lesser Caucasus, Georgia: Central European Journal of Geoscience, 6, 308–329.

Sadradze N., Adamia Sh, & Beridze T. 2017: Magmatizm and Ore Formation in the Bolnisi Ore Field on the example of Bertakari and Bneli Khevi Deposits. Book of abstracts, 3rd international scientific practical conference on up-to date problems of Geology. Technical University, Tbilisi, Georgia, 120-122.

Tsagareli, A., Zesashvili, V., Javakhishvili, Sh., Adamia, Sh., & Gambashidze, R. 1965: Cretaceous system, *in* Geological structure and metallogeny of south-eastern Georgia: Proceedins of the Geological Institute of the Academy of Sciences of Georgian SSR, new series, 1, 52-78 (In Russian).

P 2.33

Cenozoic magmatic/metalogenic activity of distinct areas of SW Bulgaria, FYR of Macedonia and Northern Greece

Georgiev S.[1], Peytcheva I.[1,2], von Quadt A.[2], Grozdev V.[1], Marchev P.[1], Serafimovski T.[3]

[1] *Geological Institute, Bulgarian Academy of Sciences, 1113 Sofia, Bulgaria (kantega@abv.bg)*
[2] *ETH Zürich, Rämistrasse 101, 8092 Zürich, Switzerland;*
[3] *Faculty of Natural and Technical Sciences, "Gotse Delčev" University of Štip, FYR of Macedonia*

The present research is focused on the Cenozoic magmatic-metalogenic activity along a NNE–SSW transect and covers rejuvenating magmatic episodes (40–6 Ma) in 7 distinct areas of SW Bulgaria, FYROM and Northern Greece. Although it postdates the main Late Cretaceous subduction event, the magmatism preserves subduction-related features as sourced in the subcontinental mantle lithosphere and lower crust that were enriched during the previous subduction. The rocks from the distinct magmatic areas show specific geochemistry and petrological characteristics and can be assigned to five evolving geodynamic episodes:

1. Paleocene to Early–Middle Eocene. The Late Cretaceous subduction-related magmatism (93–68 Ma) is followed by a magmatic gap of ≈ 10–14 Ma, related to compressional regime and crustal thickening. Afterwards the magmatic activity was rejuvenated forming a Late Paleocene to Early – Middle Eocene magmatic belt (56–40 Ma). It is represented by scattered felsic plutons in the Rhodope Massif, dyke swarms in the Kraishte Zone and asthenosphere alkaline basalts in NE Serbia. The ***Visoka Elha paleovolcano*** is part of that magmatic activity. The rocks are medium-K calk-alkaline and exhibit adakite-like features that most probably are due to that the garnet was residue in their source. The $^{87}Sr/^{86}Sr_{(i)}$ ratio of 0.70565–0.70579 and $\varepsilon Nd_{(i)}$ (–2.16/–2.44). The Concordia U-Pb zircon age of the rhyolite is determined at 40.38±0.48 Ma.

2. Eocene-Oligocene. The later magmatic activity was followed by 5–7 Ma regional uplift, exhumation of the Late Cretaceous and Paleocene to Early-Mid-Eocene granitoids, migmatisation (at ≈ 38 Ma) and core-complex formation in the Rhodopes. The magmatic activity resumed over the entire Rhodope Massif at 35 to 28 Ma forming a Late Eocene–Early Oligocene magmatic belt. The composition of the rocks correlates with the present-day crustal thickness. Studied areas: North Pirin pluton, Ilovitsa, Kratovo-Zletovo: The ***North Pirin pluton and related subvolcanic rocks in Padesh, Kresna and Karnalovo area*** are predominantly intermediate to acid in composition, high-K calc-alkaline, metaluminous to peraluminous. The $^{87}Sr/^{86}Sr_{(i)}$ (0.71010–0.71448) and $\boldsymbol{\varepsilon Nd}_{(i)}$ (–6.47/–8.34) ratios of the magmatic rocks correspond to that of the upper continental crust. A clear tendency of decreasing $^{87}Sr/^{86}Sr_{(i)}$ and encreasing $\varepsilon Nd_{(i)}$ with crustal depth (Moho discontinuity) is found. The U-Pb zircon geochronological data suggest Late Alpine plutonic and volcanic-subvolcanic activity at 35 to 31 Ma. Subvolcanic bodies (stocks), numerous dikes and related ***Ilovitsa*** Cu-Au deposit are formed during the Oligocene in the area of Ilovitsa village, SE FYROM. The granodiorite-porphyry stock that hosts the Cu-Au mineralisation is formed in two magmatic phases, dated by ID–TIMS at 30.31±0.054 Ma and 30.13±0.032 Ma, respectively. The ages of the post-mineralisation dykes are in the interval of 29.6–28.8 Ma. The $^{87}Sr/^{86}Sr_{(i)}$ ratio of 0.70791–0.70883 and $\varepsilon Nd_{(i)}$ (–5.25/–7.14) is in accordance to the thinner crust (compared with N Pirin) and is most probably due to mantle derived magma affected by crustal assimilation, fractionation and mixing. ***Kratovo – Zletovo*** is a large volcanic area located at the border of Serbo-Macedonian Massif and Vardar Zone. It is presented by several main volcanic phases with intermediate to dacitic – trachydacitic, rarely more mafic in composition, high K calc-alkaline to shoshonitic rocks. The $^{87}Sr/^{86}Sr_{(i)}$ ratio is in the range of 0.705859–0.708647 and $\varepsilon Nd_{(i)}$ (–1.57/–6.7). The volcanic activity, based on the zircon U-Pb geochronology is dated at 32.5 to 27 Ma, nevertheless a few subvolcanic bodies with ages around 25 Ma are observed. Au-epithermal, basemetal and porphyry copper mineralisations are related to that magmatic activity.

3. Early Miocene. Since ca. 24–18 Ma, the Aegean region has been the site of pronounced late orogenic crustal extension, which is considered to be a result of the rollback of the Hellenic slab and formation of the Aegean Sea basin. This time coincides with the onset of the formation of the metamorphic core complexes in the Mediterranean region such as Southern Rhodopes, Cyclades and Menderes Massif. Studied area: ***Buchim – Borov dol – Doyran – Vathi*** magmatic area is presented by several subvolcanic bodies and epiclastics and pyroclastics, predominantly with latite-trachydacitic, rarely rhyolitic composition and high-K calc-alkline to shoshonitic seriality. Mingling and mixing is often observed. The $^{87}Sr/^{86}Sr_{(i)}$ ratio is in the range of 0.70634–0.70739 and $\varepsilon Nd_{(i)}$ (–2.30/–3.80). The U–Pb zircon ages are very close 24.5–24.0 Ma with just a few rare xenocrystyc zircons found. The Buchim porphyry copper deposit and the Vathi porphyry copper occurance are related to this magmatic activity.

4. Middle to Early Miocene. During the Middle to Late Miocene the region was a site of variable magmatism. The formation of those magmatic rocks can be directly linked to the Miocene extensional tectonic regime and formation of the curvature of the Hellenide orogeny. Studied area: Limited occurrences of small and scattered subvolcanic bodies crop out along ***Strimon River valley (Kozhuh and Neo Petritsi) and Doyran region*** **(*Stoyakovo)*.** The rocks are fractionated high-K trachyte to trachydacites, which exhibit adakite-like signatures most probably due to amphibole fractionation in a crustal chamber. The relatively high $^{87}Sr/^{86}Sr_i$ ratios (0.70616–0.70648) and negative **$\varepsilon Nd_{(i)}$** (–3.29/–3.46) are observed. The rocks are dated by ID–TIMS at 12.24±0.03 Ma (Kozhuh cryptodome) and LA–ICPMS at 11.32±0.10 Ma (subvolcanic body near Stoyakovo village) respectively.

5. Late Miocene to Pleistocene. The last magmatic episode in the region is represented by Late Miocene to Pleistocene extensional magmatism (6–1.8 Ma) in the Vardar zone in FYROM, and in southern Serbia. Studied rocks are the trachytes that represent one of the most widespread phases of ***Kozhuf paleovolcano***. The trachytes show adakite-like charackteristics (due to amphibole fractionation) and are dated by ID–TIMS at 5.988±0.026 Ma. The $^{87}Sr/^{86}Sr_{(i)}$ (0.709048–0.709145) and $\varepsilon Nd_{(i)}$ (–6.77/–6.96). In the Kozhuf area, the Sb–As–Tl–Au Allchar deposit and Au Duditsa mineralisation are well known and are related to this magmatic activity.

Acknowledgements: The study is supported by SNF-SCOPES Projects IZ73Z0–128089 and IZ74Z0–160512.

P 2.34

Spinel formation by sulphur-rich saline brines from Mansin (Mogok area, Myanmar)

Adolf Peretti[1], Josef Mullis[2], Leander Franz[2], Detlef Günther[3]

[1] *GRS Gemresearch Swisslab AG, Baldismoostr. 14, CH-6043 Adligenswil (adolf@peretti.ch)*
[2] *Instute of Mineralogy and Petrography, University of Basel, Bernoullistrasse 32, CH-4056 Basel*
[3] *ETH Zürich, Laboratory of Inorganic Chemistry, Wolfgang-Pauli-Str. 10, CH-8093 Zürich*

During the last 2 decades, one of the authors has mapped the mineral occurrences in the Mogok valley and registered the mineral assemblages of approximately 100 spinel mines in a profile of 30 km length (first part published in Peretti et al., 2007 and Peretti & Tun 2016).

The map of the mineral occurrences shows the co-existence of spinel with ruby and sapphire in various types of marble rocks. Different colour varieties of spinel were found including fancy spinel, vivid red spinel and vibrant pinkish-red spinel. The variable colours of spinel may be due to the influence of trace elements from different types of metasedimentary or intrusive rocks in the environment of the marbles and changes in fluid compositions and formation conditions.

Detailed investigations with different methods (microthermometry, Raman spectroscopy, stable isotope and LA-ICP-MS geochemistry) are ongoing on spinel of one of the commercially most important mine, the Mansin mine. Its rock suite was investigated and sampled by detailed field work. The Mansin spinels formed in an impure layered dolomitic marble with layers of olivine, sulfides and spinel. There are indications for the influx of fluids that created halos in the marble forming Fe-rich dolomite.

To characterize the growth conditions of the Mansin spinels, fluid and solid inclusions were investigated in detail. At least two types of fluid inclusion assemblages are distinguished. Based on the actual knowledge, they were more or less simultaneously trapped as immiscible fluids (Giuliani et al. 2015) in the system Na? - K? - Ca - Mg - Al - Fe - Zn – SO_4 - Cl - H_2S - H_2O, with traces of some volatiles. These fluid inclusions may contain accidentally trapped minerals like phlogopite, calcite and retrograde precipitated daughter mineral phases, i.e. native sulphur, different salts, diaspore, brucite, calcite, goethite, pyrite, marcasite, sphalerite, fluorapatite, etc. One fluid inclusion assemblage is characterized by an H_2S bubble of 10 to 35 vol.% and a series of daughter minerals. In contrast, the H_2S bubble of the second fluid inclusion assemblage is markedly smaller (3-5 vol.%), but nearly totally filled with daughter minerals. A striking feature of the first inclusion assemblage is the presence of two immiscible yellowish liquid phases (L1 and L2 at room temperature) and a vapour bubble (Fig. 1). The homogenization temperature of the L1 with the vapour phase lies at 101 ± 2 °C, close to the critical temperature of H_2S, which has been verified by Raman spectroscopy. An additional striking feature is the presence of large rounded, Raman inactive solids which are interpreted as salts.

Based on these preliminary results we conclude that the formation of spinel from Mansin was triggered by a very sulphur-rich, highly saline brine.

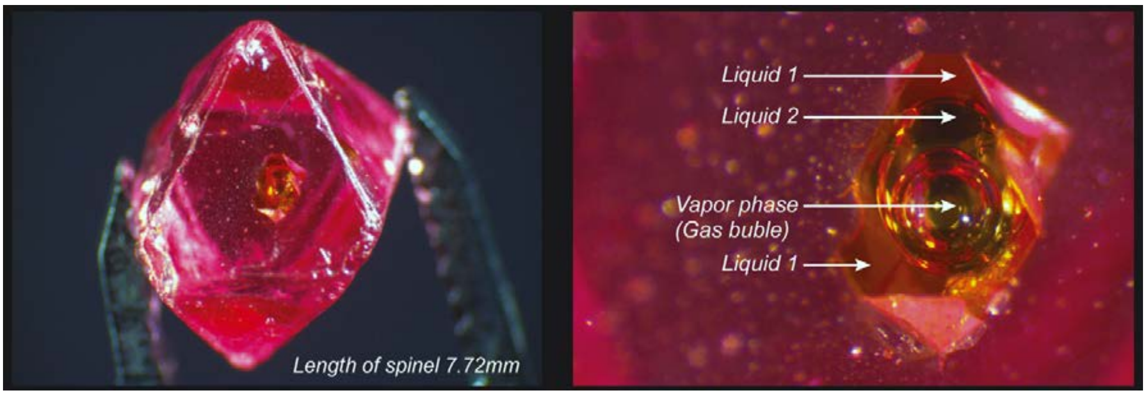

Figure 1. Multiphase fluid inclusion within a spinel from Mansin (East Mogok) at room temperature. There are two immiscible liquid phases and a vapor phase (gas bubble).

REFERENCES

Giuliani, G., Dubessy, J., Banks, D.A., Lhomme, T. & Ohnenstetter, D. 2015: Fluid inclusions in ruby from Asian marble desposits: genetic implications. European Journal of Mineralogy, 27, 393-404.

Peretti, A., Peretti, F., Tun, N.L., Günther, D., Hametner, K., Bieri, W., Reusser, E., Kadiyski, M. & Armbruster, T. 2007: Gem quality johachidolite: occurrence, chemical composition and crystal structure. Contributions to Gemology, 5, 1-53.

Peretti, A. & Tun, N.L. 2016: Mapping of minerals, corundum color varieties, collector, gems, mining and market activities prior to 2008 in Mogok. Contributions to Gemology, Abstract volume.

3. Palaeontology +
4. Stratigraphy

Christian Klug, Torsten Scheyer, Lionel Cavin +
Alain Morard, Reto Burkhalter, Oliver Kempf & Ursula Menkveld-Gfeller

Swiss Palaeontological Society (SPG/SPS)
Kommission des Schweizerischen Paläontologischen Abhandlungen (KSPA)
Swiss Commitee for Stratigraphy (SKS/CSS)

TALKS:

3.1 **Adams Arthur**, Diamond L.W.
Meteoric diagenesis of a carbonate ramp: a reinterpretation of the Upper Muschelkalk, Switzerland

3.2 **Argyriou Thodoris**
Paleobiology and interrelationships of Saurichthys (Actinopterygii, Saurichthyidae), and the importance of the Swiss fossil record

3.3 **Bagherpour Borhan**, Bucher H., Vennemann T., Chiaradia M., Schneebeli-Hermann E., Schaltegger U., Yuan Dx., Leu M., Zhang C., Shen Sz.
C and Sr isotope chemostratigraphy and the extension of Emeishan volcanism to early Wuchiapingian time: new insights from the Middle–Late Permian transition in South China

3.4 **Drage Harriet**, Vandenbroucke T.R.A., Roy V.P., Daley A.C.
Freshly-moulted nileid trilobites from the Fezouata lagerstätte of Morocco

3.5 **Fau Marine**, Villier L.
Comparative anatomy and phylogeny of the Forcipulatacean starfish (Asteroidea, Echinodermata

3.6 **Ferrante Christophe**, Furrer H., Martini R., Cavin L.
Coelacanths from the Middle Triassic of Switzerland: Stratigraphic distribution and diversity

3.7 **Friesenbichler Evelyn**, Hautmann M., Nützel A., Urlichs M., Bucher H.
Palaeoecology of Late Ladinian (Middle Triassic) benthic faunas from the Schlern and Seiser Alm (South Tyrol, Italy)

3.8 **Gaillard Charlène**, Vasylian D., Maridet O., Lu X.-Y., Prieto J.
Fossil fauna of Glovelier karstic pocket

3.9 **Garbin Rafaella C.**, Böhme M., Joyce W.G.
New geoemydid material (Cryptodira: Testudinoidea) from the Eocene of Vietnam and its implication for geoemydid systematics

3.10 **Garefalakis Philippos**, Schlunegger F.
Late Oligocene megafan progradation and shifts in depositional style driven by higher concentrations of supplied sediment – the Rigi conglomerates

3.11 **Jattiot Romain**, Brayard A., Bucher H., Vennin E., Caravaca G., Jenks J.F., Bylund K.G., Escarguel G.
Distribution and abundance of Smithian (Early Triassic) ammonoid faunas within the western USA basin and their controlling parameters

3.12 **Klug Christian**, Fuchs D., Landman N.H, Mapes R.H.
On the origin of the Coleoidea

3.13 **Lebanidze Zurab**, Beridze T., Koiava K., Khutsishvili S., Chagelishvili R., Khundadze N.
Trace Fossils from Deep Sea Sediments of the Palaeocene-Lower Eocene Borjomi Suite Exposed in the Eastern Part of the Achara-Trialeti Fold-Thrust Belt, Georgia

3.14 **Pates Stephen**, Daley A.C.
Diversity of USA Radiodonta

3.15 **Pohle Alexander**, Klug C.
Body size of orthoconic cephalopods from the late Silurian and Devonian of the Anti-Atlas (Morocco)

3.16 **Scheyer Torsten M.**, Jaquier V.P., Fraser N.C., Furrer H.
A new specimen of Macrocnemus (Archosauromorpha: Tanystropheidae) from the Middle Triassic of Monte San Giorgio, Switzerland: implications for species recognition and palaeogeography of the group

3.17 **Schneebeli**-Hermann Elke, Looser N., Hochuli P.A., Furrer H., Reisdorf A.G., Wetzel A., Bernasconi S.M.
Palynology of Triassic–Jurassic boundary sections in Northern Switzerland

3.18 **Veitschegger Kristof**
Reconstructing life history from the fossil record – the case of Pleistocene cave bears

3.19 **Wohlwend Stephan**, Bernasconi S., Deplazes G.
A new high-resolution C-isotope chemostratigraphic correlation through the Aalenian Opalinus Clay – from Mont Terri to Northeastern Switzerland

POSTERS:

P 3.1 **Bailey Lydia**, Picotti V., Schenker F., Fellin G.
Cretaceous Stratigraphic and Tectonic Evolution of the Eastern Margin of the Pelagonian Zone, Northern Greece

P 3.2 **Djeffal Rami**, Chadi M., El Hadj B.Y.
Tectono-Stratigraphy of The Cretaceous Shelf (Constantinois Platform- NE Algeria)

P 3.3 **Koiavqa Kakhaber**, Kvaliashvili L., Maissuradze L., Mauvilly J., Mosar J.
Species of the genus Porosononion from Sarmatian deposits of Georgia and their stratigraphic significance

P 3.4 **Lefort Apolline**, Yilmaz T.
Reconstruction of a Late Jurassic marine environment

P 3.5 **Lesniak Barbara**, Blattmann T.M., Wessels M., Eglinton T.I., Gehring A.U.
Bio-magnetic feedback to eutrophication

3.1

Meteoric diagenesis of a carbonate ramp: a reinterpretation of the Upper Muschelkalk, Switzerland

Arthur Adams[1], Larryn W. Diamond[1]

[1] *Rock–Water Interaction, Institute of Geological Sciences, Baltzerstrasse 1+3, 3012 Bern, Switzerland (arthur.adams@geo.unibe.ch)*

Carbonate ramps provide excellent settings to observe the effects of overprinting diagenesis. Their low-angle geometries make them susceptible to marine, mixing-zone, meteoric and burial diagenetic environments. However, the resulting diagenetic textures are seldom diagnostic of any single environment and a combination of petrographic and isotopic analyses are required for any positive interpretation.

The paleoenvironment of the Middle Triassic Upper Muschelkalk provides a distinct setting to identify multiple overprinting diagenetic events, including dolomitization, over a geologically short period of time. Previous studies suggested that diagenesis took place entirely within marine pore fluids, with possible later meteoric recrystallization of dolomites. Diagenetic analyses in this study (cathodoluminescence, UV-fluorescence microscopy, isotope geochemistry and point counting) of calcitic bioclastic beds show that marine fluids were in fact only minor components of early diagenesis (pre-stylolitization) and the accompanying porosity evolution of the Upper Muschelkalk.

Four sequential diagenetic stages have been identified: marine, mixing-zone, meteoric and dolomitization. Marine diagenesis produced brightly fluorescing bladed and inclusion-rich syntaxial cements that occlude a mean 6 vol.% of bioclastic bed porosity. Mixing-zone diagenesis induced the precipitation of fluorescent dog-tooth cements, silicification, aragonite–calcite transformation and the formation of mouldic porosity. These processes reduced porosity by 9 vol.% in bioclastic beds. Meteoric diagenesis has been identified by the low average δ18OVPDB (-9.36‰) of blocky, inclusion-free and dog-tooth cements. Meteoric cements do not exhibit any recrystallization. Approximately 9 vol.% porosity in bioclastic beds was occluded by meteoric cements. We attribute the incursion of meteoric groundwaters to hydraulic gradients on the Vindelician High, which induced percolation through tens of kilometres of the ramp during early Ladinian sealevel low-stands. Finally, following this meteoric diagenesis, the upper-half of the Upper Muschelkalk was dolomitized by refluxing brines.

Early diagenesis accounts for the low porosity in Upper Muschelkalk calcitic bioclastic beds (average = <5%) and higher porosities in dolomitized rocks (up to >20%). This study emphasizes the impacts of early diagenesis on present-day reservoir properties and demonstrates the importance of combined isotopic and petrographic analyses to decipher pore-fluid evolution.

3.2

Paleobiology and interrelationships of *Saurichthys* (Actinopterygii, Saurichthyidae), and the importance of the Swiss fossil record

Thodoris Argyriou[1]

[1]Paläontologisches Institut und Museum, Universität Zürich, Karl-Schmidt-Strasse 4, CH-8006, Zürich (thodoris.argyriou@pim.uzh.ch)

Saurichthyiformes (latest Permian–Middle Jurassic) is an emblematic group of carnivorous actinopterygians, characterized by a torpedo-like body. *Saurichthys*, the iconic representative of this group, is a common member of Triassic ichthyofaunas and has a particularly rich and almost cosmopolitan fossil record. The middle Triassic locality of Monte San Giorgio (MSG), Ticino, has produced hundreds of *Saurichthys* specimens, some of which are exceptionally well-preserved, allowing the study of the aspects of anatomy and paleobiology that are otherwise unapproachable in other fossil fishes.

The rare preservation of fossilized digesta within the intestine (cololites) of *Saurichthys*, provides a unique insight into the gastrointestinal (GIT) anatomy of this long extinct clade, and constitutes an excellent basis for the study of the evolution of the actinopterygian GIT. *Saurichthys* possessed a straight, but greatly distensible stomach, a short and likely unconvoluted anterior intestine, and a spiral intestine with a markedly high turn count (~30), unusual for actinopterygians. A comparison between the spiral intestine of *Saurichthys* and that of extant animals with a spiral valve (chondrichthyes, piscine sarcopterygians and non-teleosten actinopterygians), shows that phylogeny and/or an energetically expensive lifestyle are the main factors explaining the increase in spiral valve turn counts.

The recovery of delicate fossils of embryonic and perinatal *Saurichthys* from MSG allowed for the description of new anatomical markers of early ontogenetic stages, which can aid in the distinction between juveniles versus adults of small-sized species in the fossil record. These markers include: i) the presence of a large fontanelle between the frontals and the dermopterotics; ii) the delayed ossification of parietals; and iii) the presence of open sensory grooves and pit organs on top of dermal bones. In addition, the study of gravid, live-bearing *Saurichthys* provided glimpses into the reproductive biology of the genus. Embryos were likely accommodated in ovarian structures, similar to those of modern live-bearing sharks. The embryonic presence of rostrum and dentition suggests that *Saurichthys* gave birth to fully formed neonates, capable of exogenous feeding.

Despite the wealth of research focused on *Saurichthys*, our knowledge of the phylogenetically important endoskeletal anatomy of the genus rests on works conducted decades ago, with the use of less accurate analog techniques. Based on previous knowledge, saurichthyiforms are often considered as relatives of the Chondrostei (sturgeons and paddlefishes), but this view is not universally accepted. Using µCT on undistorted fossils from the Early Triassic of East Greenland and Nepal, I reinvestigated the endoskeletal anatomy of the genus, uncovering an array of anatomical features previously unknown. Key new features include: i) a poorly developed lateral cranial canal; ii) perichondrally lined pockets opening to the fossa bridgei, similar to those of modern sturgeons; iii) well-developed nasobasal canals; iv) a grooved ceratohyal; etc. Moreover, additional evidence from other Early Triassic, as well as Swiss, Middle Triassic fossils, suggests that the bone historically referred to as operculum, is a suboperculum. Novel data from this work provide further support for a chondrostean affiliation of saurichthyiforms.

With such an unparalleled wealth of paleobiological information available, *Saurichthys* can be considered as one of the best known early actinopterygians, and constitutes a much needed model for comparison between living and fossil forms. Furthermore, the reassessment of the systematic position of saurichthyiforms is a small advance towards reconstructing the tree of life of fossil, non-teleostean actinopterygians.

REFERENCES

Argyriou, T., Clauss, M., Maxwell, E.E., Furrer, H. & Sánchez-Villagra., M.R. 2016: Exceptional preservation reveals gastrointestinal anatomy and evolution in early actinopterygian fishes, Scientific Reports, 6:18758.

Argyriou, T., Friedman, M., Giles, S., Romano, C., Kogan, I. & Sánchez-Villagra., M.R. in prep.: µCT-aided investigation of the internal cranial anatomy of *Saurichthys* and its bearing on tracing the interrelationships of the genus.

Maxwell, E.E., Argyriou, T., Stockar, R. & Furrer, H. submitted.: Re-evaluation of the ontogeny and reproductive biology of the Triassic fish *Saurichthys* (Actinopterygii: Saurichthyidae).

Stensiö, E.A., 1925: Triassic fishes from Spitzbergen, part II, Kungl. Svenska Vetenskapsakademiens Handligar, 2:1, Stockholm.

3.3

C and Sr isotope chemostratigraphy and the extension of Emeishan volcanism to early Wuchiapingian time: new insights from the Middle–Late Permian transition in South China

Borhan Bagherpour[1], Hugo Bucher[1], Torsten Vennemann[2], Massimo Chiaradia[3], Elke Schneebeli-Hermann[1], Urs Schaltegger[3], Dong-xun Yuan[4], Marc Leu[1], Chao Zhang[4] & Shu-zhong Shen[4]

[1] *Paleontological Institute, University of Zurich, Karl Schmid-Strasse 4, 8006 Zürich, Switzerland (borhan.bagherpour@pim.uzh.ch)*
[2] *Institute of Earth Surface Dynamics, University of Lausanne, Géopolis, 1015 Lausanne, Switzerland*
[3] *Department of Earth Sciences, University of Geneva, Geneva, 1205, Switzerland*
[4] *Nanjing Institute of Geology and Palaeontology, Chinese Academy of Sciences, Nanjing 210008, China*

In South China the volcanic activity of the Emeishan Large Igneous Province (ELIP) near the Guadalupian–Lopingian boundary (GLB) (ca. 260 ma) is associated with several paleoenvironmental changes such as facies changes, carbon cycle perturbation and a temperature rise. A substantial facies change from shallow-marine bioclastic limestone to deep-marine radiolarian siliceous limestone followed by ELIP volcanic or volcaniclastic rocks in the mid-Capitanian has been considered as the consequence of a pre-eruption rapid subsidence in South China (Sun et al. 2010). This drowning event was associated with a large negative Carbon Isotope Excursion (CIE), which has been attributed to the release of thermogenic C from ELIP (Wignall et al. 2009).

Here we present a new but younger drowning event (here named "Mapojiao Event") documented in the Pingtang syncline, Mapojiao section in southern Guizhou province, whose sedimentary signature is similar to older events. Based on conodont biostratigraphic age control, the age of the Mapojiao Event is early Wuchiapingian. Carbonate carbon isotope data ($\delta^{13}C_{carb}$) document a drastic 3.5‰ negative CIE concomitant with this drowning event. Oxygen isotope data ($\delta^{18}O_{carb}$) from this section do not show signs of diagenetic alteration of the $\delta^{13}C_{carb}$ values. Organic carbon isotope values ($\delta^{13}C_{org}$) display a positive 2‰ shift across the drowning event, decoupled from the $\delta^{13}C_{carb}$. Rock-Eval and palynofacies analyses reveal the terrestrial origin of the concomittant peak of OM burial into the drowned basin. Hence, the decoupling of $\delta^{13}C_{carb}$ and $\delta^{13}C_{org}$ records could be explained by a modification of $\delta^{13}C_{org}$ due to mixing of different organic carbon pools rather than diagenetic alteration of $\delta^{13}C_{carb}$. Strontium isotope data ($^{87}Sr/^{86}Sr$) also show a transient negative shift (from 0.70715 to 0.70694), during the negative CIE, interrupting the prolonged global positive trend in the Wuchiapingian. This short-lived excursion argues in favor of enhanced hydrothermal flux related to a short pulse of LIP-related volcanism.

Data compilation around the GLB indicates that the similar drowning events occurred in three short time-intervals;1- mid-Capitanian, 2- latest Capitanian, 3- early Wuchiapingian and suggest a similar driving mechanism. Our new finding indicates that the similarities between the drowning events in S. China is not only manifested by a convergence of facies changes but also is expresed by analog chemostratigraphic signals. The coupling of negative shifts in C and Sr isotopes during the "Mapojiao Event" strongly suggest a genetic relation with bursts of ELIP eruptive activity, which spanned mid Capitanian to early Wuchiapingian times (*Clarkina guangyuanensis* Interval Zone). The comparison of the Chinese C-isotope records with the contemporaneous records from the other parts of the Tethys (e.g. Iran and Turkey) reveals obvious discrepancies. These cast some profound restrictions for the use of C-isotope records as a correlation tool during Capitanian-Wuchiapingian times. Comparative timing of the ELIP-related events with fluctuations of species richness shows that only the oldest C-isotope excursion, which is only documented in S. China, was associated with a prolonged extinction event. Hence, this study questions simplistic causal relations between excursions of the C-isotope record and GLB changes of marine diversity.

REFERENCES

Sun, Y., Lai, X., Wignall, P.B., Widdowson, M., Ali, J.R., Jiang, H., Wang, W., Yan, C., Bond, D.P.G. & Vedrine, S. 2010: Dating the onset and nature of the Middle Permian Emeishan large igneous province eruptions in SW China using conodont biostratigraphy and its bearing on mantle plume uplift models. Lithos, 119, 20–33.

Wignall, P.B., Sun, Y., Bond, D.P.G., Izon, G., Newton, R.J., Védrine, S., Widdowson, M., Ali, J.R., Lai, X., Jiang, H., Cope, H. & Bottrell, S.H. 2009: Volcanism, mass extinction, and carbon isotope fluctuations in the Middle Permian of China. Science, 324, 1179–1182.

3.4

Freshly-moulted nileid trilobites from the Fezouata lagerstätte of Morocco

Harriet B. Drage[1,2], Thijs R. A. Vandenbroucke[3], Peter Van Roy[4], Allison C. Daley[5]

[1] *Department of Zoology, University of Oxford, Tinbergen Building, South Parks Road, Oxford, UK, OX1 3PS (harriet.drage@zoo.ox.ac.uk)*
[2] *Oxford University Museum of Natural History, Parks Road, Oxford, UK, OX1 3PW*
[3] *Ghent University, Department of Geology, Ghent, Belgium*
[4] *34Yale University, Department of Geology & Geophysics, New Haven, Connecticut, USA*
[5] *Faculty of Geosciences and Environment, University of Lausanne, Sorge Géopolis, CH-1015 Lausanne, Switzerland*

Arthropods, including trilobites, must moult their protective exoskeleton for growth, development, and repair (Daley & Drage, 2016). The process of moulting involves the separation of the exoskeletal cuticle from the epidermis, secretion of new cuticle and transferral of structures (muscle attachment, sensory and circulatory systems), then splitting and shedding of the old cuticle (exuviation). Post-moulting, the new larger exoskeleton is soft and must be expanded before it stiffens, and is fully mineralised in some groups.

At this 'soft-shell' freshly-moulted stage, prior to expansion and hardening, the individual remains extremely vulnerable to predation, and thus the stage tends to be very short-lived. The brevity of this stage in the arthropod moult process is reflected in the rarity of preserved soft-shelled specimens. However, freshly-moulted individuals likely also have a lower preservation potential owing to their incomplete exoskeletal mineralisation. Very few trilobite specimens to-date have been described as preserved immediately post-moulting in their soft-shell stage (Miller & Clarkson, 1980; Speyer & Brett, 1985). These are distinguished based on clear wrinkling and flattening of the exoskeleton. However, deformation may also produce this appearance, and thus possible freshly-moulted specimens must be considered in the context of preservation. We describe a rare example of preservation of this short-lived period in the arthropod life cycle.

Ten specimens of a nileid trilobite species (referred to *Symphysurus* sp., following Ebbestad, 1999) were collected from the Burgess shale-type Lower Ordovician Fezouata biota of Morocco. These illustrate the moulting sequence, including two probable moulted exoskeletons, several fully mineralised and hardened carcasses, and others showing variable degrees of soft-shell exoskeletons. The latter show differing amounts of characteristic longitudinal wrinkling, and flattening. Several specimens have been thin-sectioned to explore differences in cuticle composition (e.g. Miller & Clarkson, 1980). Preservational bias is excluded, as other arthropods from the same locality do not show wrinkling or deformation, and nor do the putative nileid moults. The co-occurrence of moults, typical carcasses, and soft-shelled carcasses (also seen on a wider scale from the locality) represent one of the only existing examples of a preserved in-the-act mass moult assemblage.

Figure 1. Putative moulted exoskeleton of the Fezouata nileid trilobite species (left) with the cephalon angled dorsally, and soft-shelled carcass preserved immediately post-moulting (right) displaying the characteristic flattening and longitudinal wrinkles. Scale bars=5mm. Photographs: HBD.

REFERENCES

Daley, A.C. & Drage, H.B. 2016: The fossil record of ecdysis, and trends in the moulting behaviour of trilobites. Arthr. Str. Dev., 45, 71-96.

Ebbestad, J.O.R. 1999: Trilobites of the Tremadoc Bjorkasholmen Formation in the Oslo Region, Norway. Fossils & Strata, 47, 1-112.

Miller, J. & Clarkson, E.N.K. 1980: The post-ecdysial development of the cuticle and the eye of the Devonian trilobite *Phacops rana milleri* Stewart 1927. Phil. Soc. Trans. B, 288, 461-480.

Speyer, S.E. & Brett, C.E. 1985: Clustered trilobite assemblages in the Middle Devonian Hamilton Group. Lethaia,18, 85-103.

3.5

Comparative anatomy and phylogeny of the Forcipulatacean starfish (Asteroidea, Echinodermata)

Marine Fau[1] & Loïc Villier[2]

[1] Department of Geosciences, University of Fribourg, Switzerland (marine.fau@unifr.ch)
[2] Université Pierre & Marie Curie. Centre de Recherche sur la Paléobiodiversité et les Paléoenvironnements, 4, place Jussieu, Tour 46-56, case 104, F-75005 Paris, France

Among echinoderm groups, the use of both molecular and morphological data favoured the emergence of a comprehensive and operational systematics in Echinoidea and Ophiuroidea. Unfortunately we are far from reaching such a consensus in the Asteroidea, despite a background of 30 years of modern phylogenetic analyses. Debates on starfish phylogeny still oppose various hypotheses, each supported by both molecular data and morphological characters. Recent researches demonstrate that a large set of morphological characters can be defined from comparative anatomy of skeletal elements (ossicles) for phylogenetic purposes, describing ossicle shapes, articulations among ossicles, marks of soft tissues on the skeleton (e.g. tube feet or muscle insertions). Both extant and extinct taxa can be analysed conjointly in phylogenetic studies of ossicle characters, which may help with tree rooting and consideration of fossils.

The superorder Forcipulatacea is one of the major monophyletic groups with about 400 extant species, morphologically well-delimited, and for which a few phylogenetic hypotheses are available for its internal relationships. We explored the diversity of morphological features expressed in the group, considering 30 extant species and at least 5 fossil forms. The anatomy was investigated from progressive dissection of specimens from the zoological collections of the Muséum National d'Histoire Naturelle, Paris and the Yale Peabody Museum. The comparative work allowed definition of about 130 characters, a majority being new or reconsidering previous homology hypothesis. Four distinct taxon of each major clade of living forms (Velatida, Valvatida, Paxillosida and Spinulosida) were tested as outgroup for rooting.

3.6

Coelacanths from the Middle Triassic of Switzerland: Stratigraphic distribution and diversity

Christophe Ferrante[1,3], Heinz Furrer[2], Rossana Martini[1] & Lionel Cavin[3]

[1] *Department of Earth Sciences, University of Geneva, Rue des Maraîchers 13, 1205 Genève (christophe.ferrante@ville-ge.ch)*
[2] *Institute and Museum of Palaeontology, University of Zurich, Karl Schmid-Strasse 4, 8006 Zurich*
[3] *Department of Geology and Palaeontology, Natural History Museum of Geneva, CP 6434, 1211 Genève 8*

Middle and Upper Triassic deposits from Switzerland have yielded a rich fossil record of marine vertebrates. Nevertheless, coelacanth fossils are scarce and known mostly from the Middle Triassic sites of Monte San Giorgio (canton Ticino) with *Ticinepomis peyeri* Rieppel, 1980, and of the Ducan–Landwasser mountains (canton Graubünden) with cf. *Ticinepomis peyeri* (Cavin *et al*., 2013), together with an odd-looking new taxon (Cavin *et al*., in prep.). The presence of a third taxon referred with caution to cf. *Holophagus picenus*, was reported from Monte San Giorgio by Rieppel (1985). An ongoing study (Ferrante *et al*., 2017) has pointed out that this taxon is part of a large collection of 80 specimens kept in the Institute and Museum of Palaeontology, University of Zurich.

At Monte San Giorgio, *Ticinepomis peyeri* is represented by a subcomplete specimen found in the upper part of the Besano Formation ("Grenzbitumenzone") and cf. *Holophagus picenus* (Rieppel, 1985) by fragmentary specimens found in the middle part of that formation. This late Anisian – earliest Ladinian formation (Furrer *et al*., 2008) is a 16 m thick sequence of alternating black shales and finely laminated organic matter-rich dolomites. These sediments were deposited below maximal storm base in a 30-130 m deep intraplatform basin with anoxic bottom water conditions.

Coelacanth remains from the Prosanto Formation, in the Ducan–Landwasser mountains near Davos, consist of two nearly complete individuals of a new genus and new species (Cavin *et al.,* in prep.), as well as an isolated caudal fin and a subcomplete specimen referred to cf. *Ticinepomis peyeri* (Cavin *et al*., 2013). The last was found in the middle part of the formation near the Ducanfurgga (DF10) and the caudal fin in its upper part at the locality Strel. Both fossils of the new genus and new species were excavated in the most fossiliferous upper part of the formation at another site near the Ducanfurgga (DF4). The Prosanto Formation is a 120 m thick sequence of dark limestones, marls and dolomites deposited in a deeper intraplatform basin with normally oxygen-depleted bottom water conditions.

The vertebrate assemblages of the Prosanto Formation show similarities with the assemblage of the Monte San Giorgio sites. U-Pb zircon age determinations of volcanic ash layers have yield ages of 240.91 ± 0.26 My for the most fossiliferous upper part of the Prosanto formation and 241.2 ± 0.8 My for the middle part of the Besano Formation (Furrer *et al*., 2008). The Prosanto Formation corresponds to the early Ladinian fossiliferous levels of the lower Meride Limestone at Monte San Giorgio (Furrer *et al*., 2008).

Coelacanths are characterized by a very conservative morphology since the Devonian to such a point that the only extant taxa, *Latimeria*, became the iconic example of a "living fossil". Most studies demonstrate that this clade has a relatively slow evolving morphologic rate, but this view is questioned by other studies (e.g. Casane & Laurenti, 2013). Thus, the recent discovery of a new taxon (Cavin *et al*., in prep.) and the ongoing study of the unidentified coelacanth taxon (Ferrante *et al*., 2017), both presenting unusual morphologies, are an excellent opportunity to study how morphologically deviant coelacanth taxa have evolved, possibly through heterochronic evolution between systematically and stratigraphically closely related taxa.

REFERENCES

Casane, D. & Laurenti, P. 2013: Why coelacanths are not 'living fossils': a review of molecular and morphological data. Bioessays 35, 332-338.

Cavin, L., Furrer, H., Obrist, C. 2013: New coelacanth material from the Middle Triassic of eastern Switzerland, and comments on the taxic diversity of actinistans. Swiss Journal of Geosciences 106, 161-177.

Ferrante, C., Martini, R., Furrer, H., Cavin, L. 2017: Coelacanths from the Middle Triassic of Switzerland and the pace of actinistian evolution. Research & Knowledge, vol. 3, (2), 59-62.

Furrer, H., Schaltegger, U., Ovtcharova, M. and Meister, P. 2008: U-Pb zircon age of volcanic layers in Middle Triassic platform carbonates of the Austroalpine Silvretta Nappe (Switzerland). Swiss Journal of Geosciences 101, 595-603.

Rieppel, O., 1985: A second actinistian from the Middle Triassic of Monte San Giorgio, Kt. Tessin, Switzerland. Eclogae Geologicae Helvetiae 78, 707-713.

3.7

Palaeoecology of Late Ladinian (Middle Triassic) benthic faunas from the Schlern and Seiser Alm (South Tyrol, Italy)

Evelyn Friesenbichler[1], Michael Hautmann[1], Alexander Nützel[2] Max Urlichs[3], Hugo Bucher[1]

[1] *Paleontological Institute and Museum, University of Zurich, Karl-Schmid-Strasse 4, 8006 Zurich (evelyn.friesenbichler@pim.uzh.ch)*
[2] *SNSB-Bayrische Staatssammlung für Paläontologie und Geologie, Department of Earth and Environmental Sciences, Palaeontology & Geobiology, Geo-Bio-Center LMU, Richard Wagner Straße 10, 80333 Munich*
[3] *Staatliches Museum für Naturkunde Stuttgart, Rosenstein 1, 70191 Stuttgart*

The rich benthic fauna of the Schlern and Seiser Alm area, which is one of the few places in the world where the platform-slope-to-basin transitional zone is preserved in its primary setting (Keim 2008; Brander et al. 2016), is known for more than 100 years but its palaeoecology has been insufficiently known. We present a detailed palaeoecological study based on quantitative faunal data of the fauna from the Schlernplateau beds (late Ladinian to early Carnian) and the more or less time-equivalent Pachycardientuffe (late Ladinian).

The Schlernplateau beds yield a diverse fauna with more than 50 species. The ecology of the fauna, which is dominated by shallow infaunal suspension feeders, epifaunal grazers/detritivores and free-lying epifaunal suspension feeders, as well as the geological context leave no doubt that the Schlernplateau beds represent lagoonal sediments. The unusually high diversity for this environment and the locally restricted fossil occurences indicate an open lagoonal setting palaeogeographically close to an oceanic inlet. The high evenness of the fauna is best explained with time averaging.

The fauna of the Pachycardientuffe is highly diverse, with more than 220 species; however, in contrast to the Schlernplateau beds, it is clearly dominated by two species of the eponymous bivalve genus *Pachycardia*. Several lines of evidence, such as the lack of fossils that were preserved in life position, the lack of bivalves that are preserved with conjoined valves, frequent fragmentation of fossils and poorly sorted sediment, indicate that the fauna of the Pachycardientuffe is allochthonous. By means of ecological features of the fauna and palaeogeographic reconstructions three possible source areas for the fauna of the Pachycardeintuffe were identified; (1) the lagoon of the Schlernplateau beds, (2) the reef fringing the lagoon of the Schlernplateau beds and (3) a shallow clastic coast of a nearby volcanic island and/or submarine high dominated by *Pachycardia*.

The different context of the faunas requires different interpretations of their diversities: whereas the Schlernplateau fauna provides an estimation of the alpha-diversity in shallow-marine tropical seas ca. 15 Ma after the end-Permian mass extinction, the fauna of the Pachycardientuffe represents an integral of the diversity from different environmental settings and as such an approximation of the gamma-diversity of the region. Apart from the sheer increase in richness in comparison to Early Triassic benthic faunas, where alpha-diversity seldom exceeds 15-20 species and gamma diversity is usually lower than 30-40 species even at the end of this epoch, a larger variety of modes of life and a significantly higher proportion of gastropod species are notable features of the more fully recovered faunas of the late Middle Triassic.

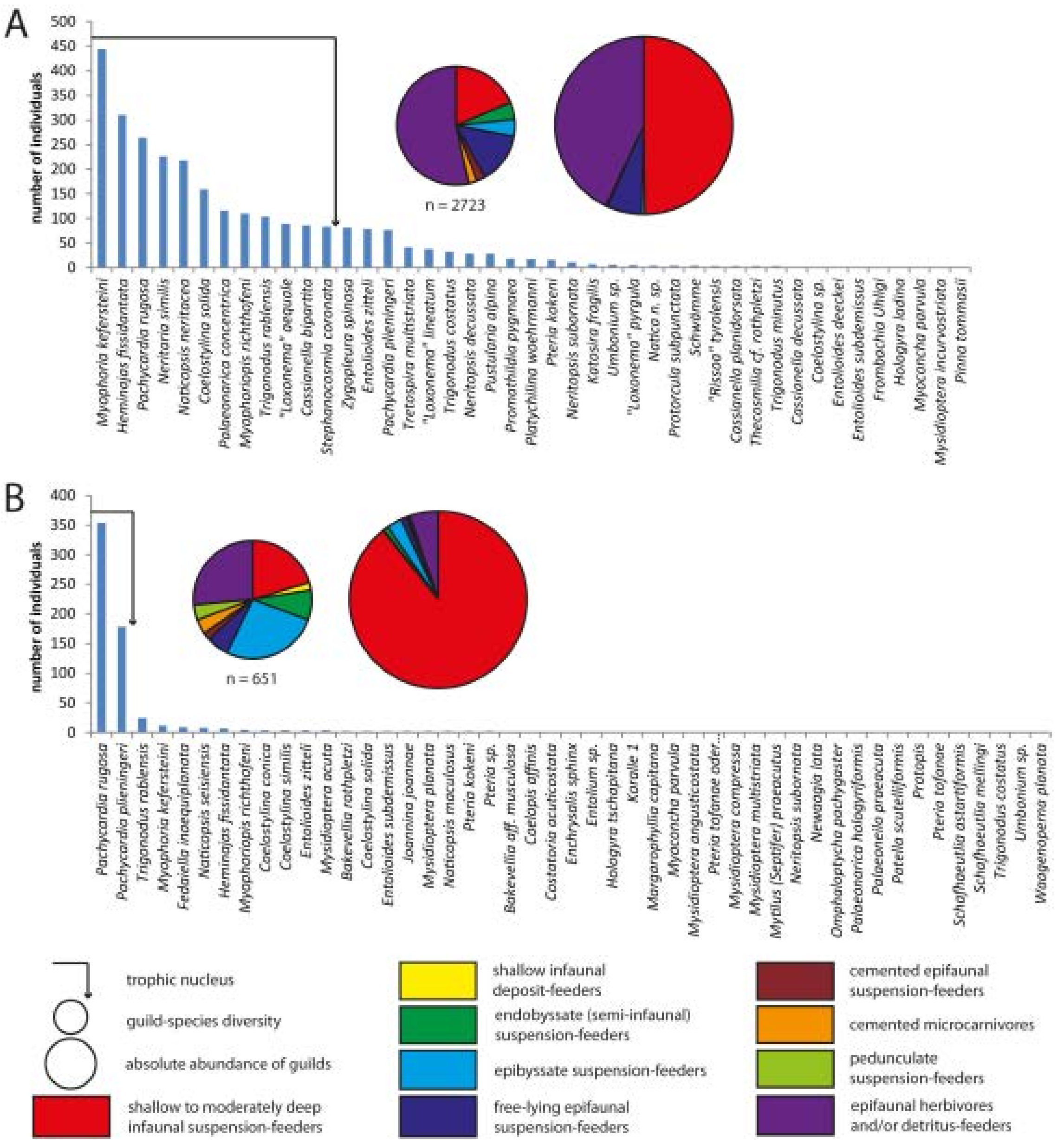

Figure 1. Rank-abundance distributions and guild-structure of the fauna of the Schlernplateau beds (A) and Pachycardientuffe (B). n = total number of individuals.

REFERENCES

Brandner, R., Gruber, A., Morelli, C., Mair, V. 2016: Pulses of Neotethys-Rifting in the Permomesozoic of the Dolomites. Geo. Alp., 13, 7-70.

Keim, L. 2008: Geologie im Gebiet Schlern-Seiser Alm: vom Tethysmeer zum Gebirge. Gredleriana, 8, 25-46.

3.8

Fossil fauna of Glovelier karstic pocket

Gaillard Charlène[1], Vasylian Davit[1,2], Maridet Olivier[1,2] Xiao-Yu Lu[1,2] & Prieto Jérôme[3]

[1] *Department of Geosciences, University of Fribourg, Chemin du Musée 6, CH-1700 Fribourg*
[2] *JURASSICA Museum, Route de Fontenais 21, CH-2900 Porrentruy*
[3] *Department for Earth and Environmental Sciences, Ludwig-Maximillians-University, Geschwister-Scholl-Platz 1, D-80539 Munich*

The karstic fillings of Glovelier, known as “La Petite Morée”, are located in the Swiss Jura, near the town of Glovelier. The pocket 1, of two meters in height, is placed in the Oxfordian limestone (Hug *et al*., 1997). The fossil remains of that pocket indicate sedimentary influence both from continental and marine environments. The small mammal assemblage indicates a MN4a age, whereas the marine foraminifers and shark point at a Burdigalian age. Thus, the pocket was deposited during the transgression phase of the Upper Marine Molasse and represents one of the rare continental records of that time. In fact, the north coast of the OMM Sea was at its northernmost location at that time and the Aquitanian tectonic uplift did not allow the deposition of sediments in the Jura. With both terrestrial and marine fossils, Glovelier is already a unique deposit. Moreover, it was set as the reference locality for the “*Democricetodon franconicus – Megacricetodon collongensis*” interval zone (Kälin & Kempf, 2009). Thus, the aim of this study is to provide more data on faunistic assemblage and the palaeoenvironment.

Among all Glovelier fissure fillings the most fossiliferous is the pocket 1, which is the focus of the present study. The karstic pocket of two meters height is filled with clay and sandy sediments. The upper 60 cm of the sediments is represented by thin laminated sands with reworked clays from the underlying layers.

New samples of the horizon have been screen-washed and provided more fossil material. The continental fauna of vertebrates is represented by salamanders, frogs, lizards, snakes, turtle, glirids, lagomorphs, cricetids, eomyds and artiodactyls. Aside from them, marine taxa such as fish teeth, shark teeth and benthic foraminifera have been found as well. The fossiliferous layer provides also reworked Mesozoic invertebrate, especially echinoderms and mollusks remains. With the rodent fauna, Glovelier can be considered as one of the first few Early Miocene localities with two cricetid species, after the Early Miocene so-called “cricetid-vacuum”. Among the reptiles, a *Varanus* sp. is present in the fossil assemblage and represents one of the earliest occurrences of the genus in Europe. The rare glirid genus *Simplomys,* considered as an endemic genus from Spain, suggests the presence of a connection with the west.

The terrestrial and marine fossils of Glovelier provide a window of terrestrial and marine fossils from the Early Miocene of the Central Europe especially for the Jura region. Among the faunistic elements, Glovelier contains both taxa with Asian affinities (e.g. cricetids, *Varanus*) as well as truly European forms (*Simplomys*). Moreover, a comparison between Glovelier and other European localities of MN4 age will enable a better understanding of the Early Miocene faunistic interchanges and palaeoenvironmental condition. In addition to this, the fossil locality will enlighten the history of the Swiss Molasse Basin during the OMM-OSM transition. Importantly, the presence of some key species also provides an opportunity for the reconstruction of the paleoenvironment and climatic parameters of the late Early Miocene of the North Alpine Foreland Basin.

REFERENCES

Hug, W.A., Berger, J.-P., Clement, I., Kälin, D. & Weidmann, M. 1997: Miocene fossiliferous paleokarst (MN4) and OSM deposit (MN5-?) near Glovelier (Swiss Jura Mountains). Fifth Meeting of Swiss Sedimentologists, Abstract from January 25th, 1997 in Fribourg.

Kälin, D. & Kempf, O. 2009: High-resolution stratigraphy from the continental record of the Middle Miocene Northern Alpine Foreland Basin of Switzerland. Neues Jahrbuch für Geologie und Paläontologie, 241, 208-225.

3.9

New geoemydid material (Cryptodira: Testudinoidea) from the Eocene of Vietnam and its implication for geoemydid systematics

Rafaella C. Garbin[1], Madelaine Böhme[2] & Walter G. Joyce[1]

[1] *Department of Geosciences, University of Fribourg, 1700 Fribourg, Switzerland*
[2] *Senckenberg Center for Human Evolution and Paleoenvironment, University of Tübingen, 72074 Tübingen, Germany*

Aquatic testudinoid turtles have a particularly rich fossil record in the Tertiary of the northern hemisphere, but little is known about the evolutionary history of the group, as the phylogenetic relationships of most fossils have not been established with confidence, in part due to high levels of homoplasy and polymorphism.

We here focus on a sample of approximately 100 geoemydid skeletons, mostly shell material, collected from the mid to late Eocene (35–39Ma) Na Duong Formation, Vietnam, a continental swamp deposit that has yielded abundant remains of aquatic and terrestrial faunas and floras (Böhme *et al*., 2011, 2014). All turtle material was collected from a single stratigraphic horizon and is therefore thought to represents a true population.

Although two size classes can be distinguished among our sample, a larger one ranging from 28 to 38 cm and a smaller from 13 to 17 cm of carapace length, we believe that the smaller morph represents the juvenile stage of the other, as it presents a three-keeled carapace, a diagnostic character for juvenile geoemydids. Our material shares many characters with two recently described geoemydids from the Eocene of China, *Isometremys lacuna* and *Guangdongemys pingii* (Claude *et al.* 2012), in particular by exhibiting anteriorly short-sided neurals with exception of an octagonal fourth neural and square or rounded fifth neural, by lacking a nuchal emargination, and by possessing a notched pygal bone completely divided by the intermarginal sulcus, an entoplastron anteriorly and posteriorly intersected by the humerogular and humeropectoral sulcus, respectively, and a deep anal notch.

A phylogenetic analysis using an updated character matrix consisting of 87 morphological characters of the shell and seven molecular loci, reveals that this Vietnamese turtle material is located at the base of Geoemydinae, suggesting at least an Eocene age for the crown group.

REFERENCES

Böhme M, Prieto J, Schneider S, Hung NV, Quang DD, Tran, DN. 2011: The Cenozoic on-shore basins of Northern Vietnam: Biostratigraphy, vertebrate and invertebrate faunas, Journal of Asian Earth Sciences, 40(2), 672–687.

Böhme M, Aiglstorfer M, Antoine P-O, Appel E, Havlik P, Métais G, Phuc LT, Schneider S, Setzer F, Tappert R, Tran DN, Uhl D, Prieto J. 2014: Na Duong (northern Vietnam) – an exceptional window into Eocene ecosystems from Southeast Asia, Zitteliana A, 53, 120–167.

Claude J, Zhang J-Y, Li J-J, Mo J-Y, Kuang X-W, Tong H. 2012: Geoemydid turtles from the Late Eocene Maoming basin, southern China. Bulletin de la Société Géologique de France, 183, 641–651.

3.10

Late Oligocene megafan progradation and shifts in depositional style driven by higher concentrations of supplied sediment – the Rigi conglomerates

Philippos Garefalakis[1] & Fritz Schlunegger[1]

[1] *University of Bern, Institute of Geological Sciences, Baltzerstrasse 1+3, CH-3001 Bern, Switzerland (philippos.garefalakis@students.unibe.ch)*

The Late Oligocene large-scale coarsening and thickening upward megasequences situated in the North Alpine foreland basin have conventionally been used to infer a depocenter progradation. This was also the case for the c. 4 km-thick suite of the Rigi megafan conglomerates situated in central Switzerland (Stürm, 1973), where megafan progradation was associated with an increase in sediment accumulation rates. Here, we present new sedimentological evidence to document that fan progradation was mainly driven by an increase in the flux and the concentration of the supplied sediment in response to mantle scale processes.

Depositional mechanisms are derived from the stacking patterns and the fabric of the conglomerates. We additionally measure shifts in grain size distributions and channel depths recorded by the conglomerates. In this context, channel depths are measured by estimating the palaeo water depth at the situation during bankfull discharge. Accordingly, we measure either the top of a conglomerate bank as well as the lowest point of it, or the thickness of foresets and longitudinal bars. We choose the condition of bankfull discharge, as the largest sediment particles are likely to be transported at these high-water stages. As a consequence, we simultaneously measure the grain size of the 4-6 largest clasts at the base of each channel. These field based data about channel depth and the largest grain size are then used to calculate the fan surface slope, which can be computed by combining the measured data with the Shields criteria for bedload transport. We additionally measure the sizes of a total of approximately 4500 grains. We finally combine slope and bulk grain size data with the Bagnold equation for sediment transport to infer changes in the flux and concentrations of the supplied sediment.

The field-based observations reveal, that the lowermost conglomerates are made up of individual and amalgamated stacks of 2 – 3 m-thick beds with a clast-supported, massive-bedded fabric. Individual conglomerate beds scour severals meters deeply into the underlying mudstones. Towards the top of the section, the conglomerates are arranged as clast-supported and massive-bedded deposits with imbrications in places. Interbedded mudstones are mostly absent. These changes in stacking patterns and sedimentary fabrics reflect a shift in depositional style from channelized, confined flow at the base of the section, to braided and thus non-confined flow in a more proximal environment towards the top. Simultaneously the largest grain size increases from <15cm to >20cm towards the top of the suite, while the augmentation in bulk grain size is less (<20%). Channel depths, however, reveal an opposite trend and decrease from >2m to <1m from the base to the top of the conglomerate suite. Using these constraints, we calculate (Shields criteria) a steepening of the fan surface slopes from originally <0.3° to >1.0° through time. We use these shifts in depositional mechanisms, fan surface slopes and bulk grain size to infer (Bagnold equation) an increase in both the flux and the concentrations of the supplied sediment (Church, 2006). In addition, the ensemble of these changes points towards the occurrence of faster erosion in the Alpine hinterland where the sediment sources were situated. These mechanisms most likely reflect a surface response of the Alpine landscape to fast rock uplift, which occurred in response to slab break-off and thus to mantle-scale processes underneath the Central Swiss Alps.

As implications, the inferred increase in erosion rates points towards a change of the shape of the Alpine landscape, which evolved from a diffusive, slowly eroding topography to an incised, fast eroding Alpine hinterland, where mass failure processes were dominant (fig. 1). The study thus shows that changes in conglomerate deposition chronicle an explicit surface response to dynamic processes within the mantle.

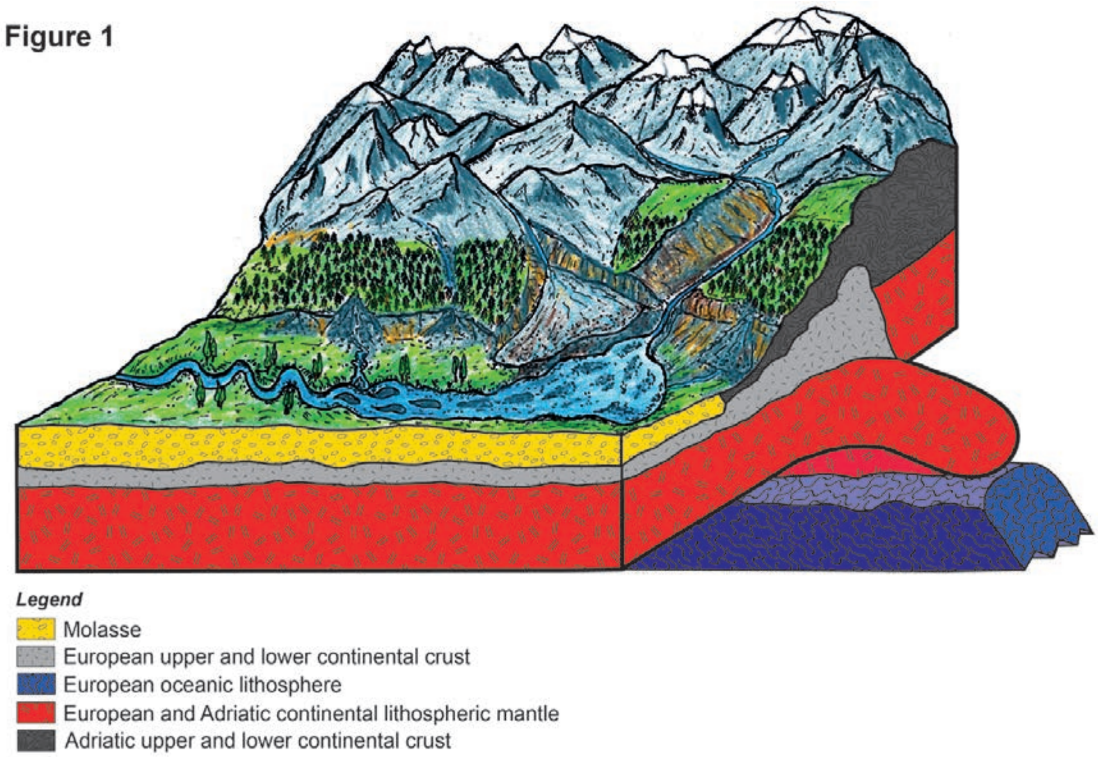

Figure 1. Rigi megafan with the underlying ongoing subduction of the European lithosphere and the slab break-off. These processes induced fast rock uplift in the Alpine hinterland, which resulted in higher erosion rates and thus larger volumes and concentrations of the supplied sediment.

REFERENCES

Stürm, B. 1973: Die Rigischüttung. Sedimentpetrographie, Sedimentologie, Paläogeographie, Tektonik. PhD thesis, Univ. Zürich. Switzerland, 98 p.

Church, M. 2006: Bed material transport and the morphology of alluvial river channels. Ann. Rev. Earth Planet. Sci. 34, 325-354.

3.11

Distribution and abundance of Smithian (Early Triassic) ammonoid faunas within the western USA basin and their controlling parameters

Romain Jattiot[1,2], Arnaud Brayard[2], Hugo Bucher[1], Emmanuelle Vennin[2], Gwenaël Caravaca[2], James F. Jenks[3], Kevin G. Bylund[4] & Gilles Escarguel[5]

[1] *Paläontologisches Institut der Universität Zürich, Karl Schmid-Strasse 4, 8006, Zürich, Switzerland (romain.jattiot@pim.uzh.ch)*
[2] *Biogéosciences, UMR 6282, CNRS, Université Bourgogne Franche-Comté, 6 boulevard Gabriel, 21000 Dijon, France*
[3] *1134 Johnson Ridge Lane, West Jordan, Utah 84084, United States of America*
[4] *140 South 700 East, Spanish Fork, Utah 84660, United States of America*
[5] *Univ. Lyon, Université Claude Bernard Lyon 1, CNRS, ENTPE, UMR 5023 Laboratoire d'Ecologie des Hydrosystèmes Naturels et Anthropisés, 27-43 boulevard du 11 novembre 1918, 69622 Villeurbanne Cedex, France*

The aim of this paper is to quantitatively investigate the biogeography of Smithian ammonoids within the western USA basin. The faunal dataset consists of a taxonomically homogenized compilation of the spatial and temporal occurrences and abundances of ammonoid taxa in 39 Smithian localities within the western USA basin. Two complementary multivariate techniques were applied to identify the main biogeographical structuring recorded in the analyzed presence/absence data: additive Cluster Analysis using the Neighbor-Joining algorithm (NJ) and Non-metric Multidimensional Scaling (NMDS). Regarding abundance data, a taxonomic diversity (sensu evenness) analysis was coupled with graphical comparisons of the relative abundances of selected taxa. The identified relationships indicate that middle Smithian ammonoids of the western USA basin were geographically organized in terms of both distribution and abundance, with the biogeographical distinction of a southern and a northern cluster. Some taxa are indeed confined to a single sub-basin, and many taxa display a geographical abundance gradient whose maximum is centered either on the southern or northern cluster. This N/S dichotomy in the distribution and abundance of middle Smithian ammonoids echoes pronounced spatial differences identified for the same time interval based on the sedimentary and geochemical records. In some cases, a link between depositional environment parameters (e.g., terrigenous inputs and hydrodynamism) and local abundances of certain taxa is suggested. Regarding the late Smithian, our results show a non-significant difference of faunal assemblages. This absence of ecological partitioning, independent of the depositional environments, is here interpreted as the hallmark of the late Smithian extinction, as a cosmopolitan faunal distribution is well recognized at that time.

3.12
On the origin of the Coleoidea

Christian Klug[1], Dirk Fuchs[2], Neil H. Landman[3] & Royal H. Mapes[4]

[1] *Paläontologisches Institut und Museum, Universität Zürich, Karl Schmid-Strasse 4, CH-8006 Zürich (chklug@pim.uzh.ch)*
[2] *Freie Universita¨t Berlin, Institute of Geological Sciences, Branch Palaeontology, Malteserstrasse 74-100, 12249 Berlin, Germany*
[3] *Division of Paleontology (Invertebrates), American Museum of Natural History, 79th Street and Central Park West, 10024 New York, USA*
[4] *North Carolina Museum of Natural Sciences, West Jones St., Raleigh, NC, USA*

The origin of major clades is often blurred by the scarcity of fossils and by the pattern of plesiomorphic and apomorphic traits of the very early members of the corresponging clade. In the case of the Coleoidea, which contains squids, octopuses, cuttlefish etc., many aspects of their origin remains blurred (e.g., House 1988). For example, the supposedly earliest coleoids were described from the Early Devonian Hunsrück Slate (Bandel et al. 1983). The coleoid affinity is still under debate. From the Carboniferous, however, a greater number of unequivocal taxa have been described (e.g., Landman & Davis 1988; Doguzhaeva et al. 1999, 2007, 2010; Mapes et al. 2010). Some of these materials are remarkably well preserved including ink sacs, jaws, radula etc. (Clements et al. 2016).

Examinations of Carboniferous specimens illustrated in the literature appeared promising for a re-examination because some structures visible in the illustrations were not examined in greater detail. We studied some of these materials using various sorts of light. These re-examinations revealed a number of anatomical details that shed light on both morphology and the early evolution of the Coleoidea. In addition to these new anatomical details, we discuss the processes that might have led to the internalisation of the coleoid phagmocone, which coincides with the formation of the rostrum.

REFERENCES

Bandel, K., Reitner, J., & Stürmer, W. 1983: Coleoids from the Lower Devonian black slate (“Hunsrück-Schiefer”) of the Hunsrück (West Germany). Neues Jahrbuch für Geologie und Paläontologie Abhandlungen, 165, 397-417.

Clements, T., Colleary, C., De Baets, K. & Vinther, J. 2016: Buoyancy mechanisms limit preservation of coleoid cephalopod soft tissues in Mesozoic lagerstätten. Palaeontology, 60, 1–14.

Doguzhaeva, L.A., Mapes, R.H., & Mutvei, H. 1999: A Late Carboniferous spirulid coleoid from the Southern Mid-continent (USA). In: Oloriz, F. & Rodriguez -Tovar, F.J. (eds.), Advancing Research on living and fossil cephalopods, p. 47-57. Kluwer Academic/ Plenum, New York.

Doguzhaeva L.A., Mapes, R.H., & Mutvei, H., 2007: A late Carboniferous coleoid cephalopod from the Mazon Creek (USA), with a radula, arm hooks, mantle tissue, and ink. In: Landman, N.H., Davis, R.A., & Mapes, R.H. (eds.), Sixth International Symposium, Cephalopods – Present and Past, p. 121-143. Springer, Netherlands.

Doguzhaeva L.A., Mapes, R.H., & Mutvei, H., 2010: A Carboniferous radiation in evolution of coleoid cephalopods as indicated by their the morphological plasticity. Seventh International Symposium, Cephalopods - Present and Past.

House, M. R. 1988: Major features of cephalopod evolution. In, Wiedman, J. and Kulmann, J. eds, Cephalopods Past and Present, 2nd International Cephalopod Symposium, p. 1-16. Schweizerbart, Stuttgart.

Landman, N.L. & Davis, R.A., 1988: Jaw and crop preserved in an orthoconic nautiloid cephalopod from the Bear Gulch Limestone (Mississippian, Montana). New Mexico Bureau of Mines and Mineral Resources, Memoir, 44, 103-107.

Mapes, R.H., Weller, E.A., & Doguzhaeva, L. A., 2010: Cephalopods showing a tentacle with arm hooks and and ink sac from Montana, USA. In: Tanabe, K., Shigeta, Y., Sasaki, T. & Hirano, H. (eds.) Cephalopods - Present and Past. Tokai University Press, Tokyo, p. 155-170.

3.13

Trace Fossils from Deep Sea Sediments of the Palaeocene-Lower Eocene Borjomi Suite Exposed in the Eastern Part of the Achara-Trialeti Fold-Thrust Belt, Georgia

Zurab Lebanidze[1], Tamar Beridze[2], Kakha Koiava[1], Sophio Khutsishvili[2], Rusudan Chagelishvili[3], Nino Khundadze[4].

[1] *Department of Geology, Faculty of Exact and Natural Sciences, Iv.Javakhishili Tbilisi State University, University str. 13, 0186, Tbilisi, Georgia, zurab.lebanidze@tsu.ge*
[2] *Al. Janelidze Institute of Geology, Iv. Javakhishvili Tbilisi State University, Politkovskaya str. 31, 0186, Tbilisi, Georgia*
[3] *Department of Geology and Paleontology, Georgian National Museum, Purtseladze str. 3, 0105, Tbilisi, Georgia*
[4] *Alexander Tvalchrelidze Caucasian Institute of Mineral Resources, Iv. Javakhishvili Tbilisi State University, Mindeli str. 11, 0186, Tbilisi, Georgia*

The Palaeocene-Lower Eocene Borjomi suite is an exemplary for the Achara_Trialeti fold-thrust mountain belt lithostratigraphic unit and is exposed in the anticline structures of the central and eastern parts of the belt. In the eastern part 900-1100 meters thick turbidites (flysch deposits) of the Borjomi suite are extended as a continuous line along the northern slope of the Trialeti Range and are made up by the alternation of calcareous quartz-greywacke sandstones, marls and clays. Constructing the suite sandstones are grouped into three packages with average thickness 30-50 m each. According observed in the field sedimentary features (our fieldwork data) these sandstones record sedimentation in a turbidite system. The 500 meters thick upper part of the entire section comprises *Globorotalia aragonensis* zone microfauna and *Nummulites planulatus*, as for the lower part – it contains *Globorotalia aequa* zone micro fossils. The boundary between these two zones matches with the top of the medium package of sandstones. The 100-150 meters thick lowermost part of the section is attributed to the *Globorotalia pseudomenardii* zone.

The ichnofauna occurrence is located within the facing stone quarry on the southern periphery of the village Kvemo Nichbisi. Here, according to historical (Papava et. al., 1971) and our recently obtained data about 50 meters thick sandstone package without visible unconformity overlies the faunistically dated Danian varicolored suite.

The medium to fine grained, massive and laminated quartz-greywacke sandstones are thin - and rarely medium-bedded. They show abundant intercalations of plant debris along with wood fragments and carbonaceous remains which is considered as a diagnostic criterion for the recognition of extrabasinal (hyperpycnal) turbidites (Zavala C. et. al., 2012). Couplets of very thin siltstones and fine grained sandstones beds are observed as well.

In the studied sandstones beds abundant pre- and postdepositional trace fossils have been recently detected. Predepositional assemblage is rich in graphoglyptids and grazing traces preserved as secondary impressions in the bases of turbidite beds and comprise following ichnogenera: *Belocosmorhaphe, Helminthopsis, Helminthorhaphe, Megagrapton, Paleodictyon, Rotundusichnium, Scolicia (Sc. strozzii), Spirophycus, Spirorhaphe* and *Urohelminthoida*. The postdepositional assemblage - *Avetoichnus, Chondrites, Gyrophillites, Ophiomorpha, Phycosiphon, Phymatoderma, Planolites, Polykampton, Scolicia (Sc. prisca, Sc. isp.), Taenidium, Trichichnus* and *Zoophycos* is represented by dwelling, resting and grazing traces. They are mainly preserved at the tops of the beds and rarely at the bottoms and inside the beds. The wood fragments show presence of allochtonous *Teredolites*. Taking into account trace fossils morphology, the studied ichnocomplex is typical for deep-sea *Nereites* ichnofacies, whereas the majority of graphoglyptids are indicative of thin bedded sandy turbidites *Paleodictyon* ichnosubfacies (Uchman & Wetzel 2012). We suppose that studied turbidites formed in the basin plane or lower slope, apparently in fan fringe. Abundance of postdepositional forms reflects rapid colonization of the substrate (Buatois et al. 2001), whereas trace fossils (*Planolites, Phycosiphon, Scolicia*) formed without permanent link to the sea floor show good oxiganation of pore waters (Demircan & Uchman 2016).

REFERENCES:

Buatois, L., Gabriela Mangano, M. & Sylvester, Z. 2001: A diverse deep-marine ichnofauna from the Eocene Tarcau sandstone of the Eastern Carpathians, Romania. Ichnos 8(1), 23-62.

Demircan, H. & Uchman, A. 2016: Trace fossils from deep sea sediments of the Ceylan Formation (SW Thrace, Turkey). Bull. Min. Res. Exp. 153, 91-111.

Papava, D., Devdariani, E. & Ageev, V. 1971: The results of geological survey and structural drilling within the eastern subsidence zone of the Achara-Trialeti folded system. Funds of Geological Department of Georgia

Uchman, A. & Wetzel, A. 2012: Deep-sea fans. In: Bromley, R. G. & Knaust, D. (Eds.), Trace Fossils as Indicators of Sedimentary Environments. *Developments in Sedimentology* 64, 643-671. Elsevier, Amsterdam.

Zavala C., Arcuri, M., Blanco Valiente, L., 2012. The importance of plant remains as a diagnostic criteria for the recognition of ancient hyperpycnites. Revue de Paléobiologie 11, 457–469.

3.14
Diversity of USA Radiodonta

Stephen Pates[1], Allison C. Daley[2]

[1] *Department of Zoology, University of Oxford, Oxford, OX2 6GG, United Kingdom (stephen.pates@zoo.ox.ac.uk)*
[2] *Faculty of Geosciences and Environment, University of Lausanne, Sorge Géopolis, CH1015, Lausanne, Switzerland*

Our understanding of large Cambrian pelagic predators, including radiodontans such as *Anomalocaris, Hurdia, Peytoia* and *Caryosyntrips* has increased greatly over recent years (e.g. Daley et al. 2009). The bodyplan of a radiodontan includes a segmented frontal appendage specialised for feeding, a circular mouthpart made of radial plates, a segmented body with lateral flaps for movement, a pair of compound eyes, and an anterior sclerite. Recent work has identified radiodontans as stem group arthropods, and shed light on the origin of the biramous limb, the compound eye and arthropod brain structure (Paterson et al. 2011; Cong et al. 2014; Van Roy et al. 2015).

Radiodontans are often preserved disarticulated: as isolated frontal appendages, mouthparts, or carapace elements. Frontal appendage morphology is often used to differentiate different species and genera, as well as to infer feeding style.

Most recent studies have focussed on the Chengjiant Biota (China), Emu Bay Shale (Australia) and Burgess Shale (Canada). Radiodontans are also an important component of soft-bodied faunas from the Great Basin (Utah, Nevada, and California) and the Kinzers Formation (Pennsylvania). These deposits offer an opportunity to study the evolution and distribution of radiodontans at a local and regional level, and at high temporal resolution. These sites have also increased our knowledge of the diversity of Radiodonta. Amongst other radiodontans, three species of *Anomalocaris*, one species of *Caryosyntrips*, the youngest representative of *Staneycaris* and *Tamisiocaris*, and a new genus of hurdiid (Figure 1) are only known from USA deposits.

Radiodontans from the USA show a trend that Anomalocarididae dominate in older sites, and Hurdiidae in younger sites. Interpretation of the functional morphology of these radiodontans suggests that these taxa possessed a range of ecologies, mirroring other, more famous, Cambrian Lagerstätten.

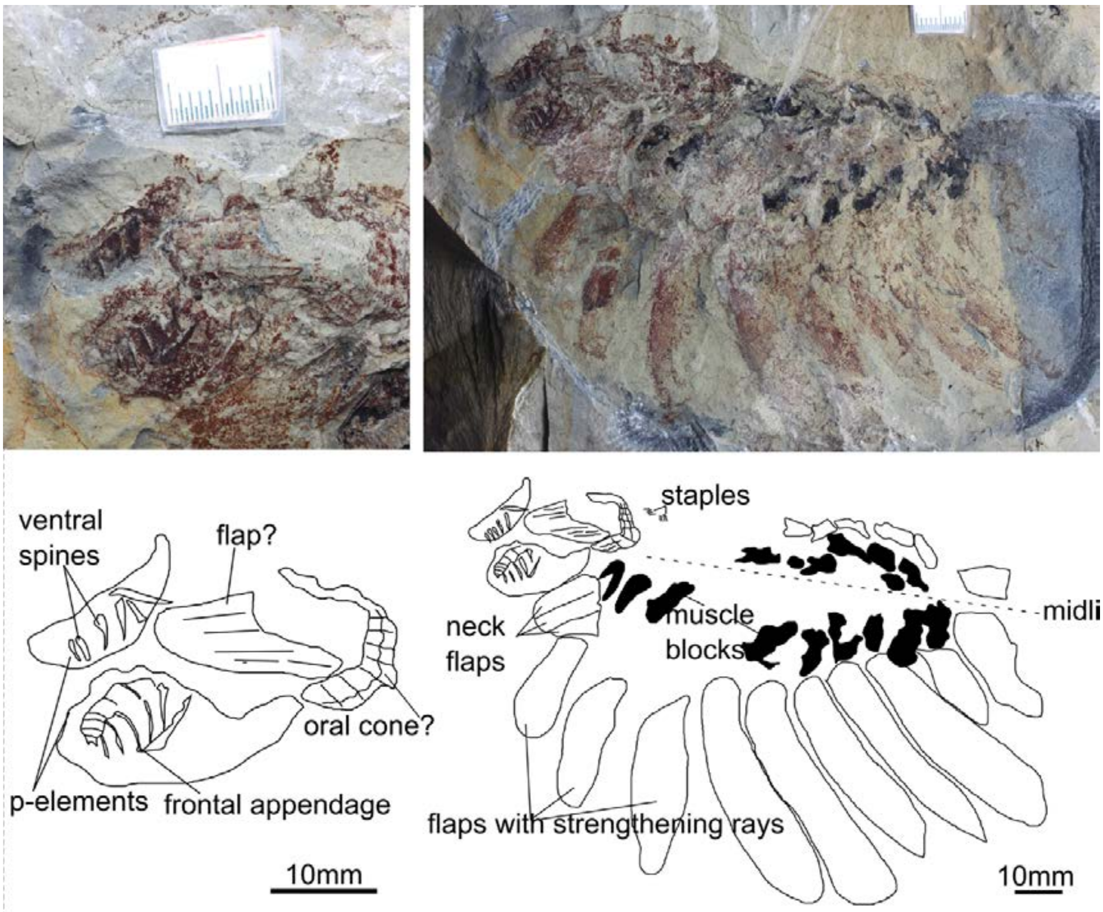

Figure 1. Hurdiid radiodontan from the Spence Shale Member, Langston Formation, Utah (Cambrian Series 3, Stage 5). Left: Closeup of mouthparts with two frontal appendages and P-elements. Right: Complete specimen, showing elongated flaps, muscle blocks, midline, neck flaps and head region.

REFERENCES

Cong, P., Ma, X., Hou, X., Edgecombe, G. D., & Strausfeld, N. J. 2014: Brain structure resolves the segmental affinity of anomalocaridid appendages, Nature 513, 538.

Daley, A. C., Budd, G. E., Caron, J-B., Edgecombe, G. D., & Collins, D. 2009: The Burgess Shale anomalocaridid Hurdia and its significance for early euarthropod evolution, Science, 323,1597-1600.

Paterson, J. R., García-Bellido, D. C., Lee, M. S., Brock, G. A., Jago, J. B., & Edgecombe, G. D. 2011: Acute vision in the giant Cambrian predator *Anomalocaris* and the origin of compound eyes, Nature, 480, 237-240.

Van Roy, P., Daley, A. C., & Briggs, D. E. 2015: Anomalocaridid trunk limb homology revealed by a giant filter-feeder with paired flaps, Nature, 522, 77.

3.15

Body size of orthoconic cephalopods from the late Silurian and Devonian of the Anti-Atlas (Morocco)

Alexander Pohle[1] & Christian Klug[1]

[1] Paläontologisches Institut und Museum, Universität Zürich, Karl-Schmid-Strasse 4, 8006 Zürich (alexander.pohle@pim.uzh.ch)

Orthoconic cephalopods are very common, sometimes even dominant elements of marine Palaeozoic strata. As such, they can be used to statistically adress palaeontological questions based on large numbers of specimens (e.g., Wendt 1995). Some orthocones are known to have reached very large sizes of up to 6 meters in length (Teichert & Kummel 1964, Klug et al. 2015). However, usually only the extreme sizes are reported, so it is not possible to tell from the literature, whether the average conch size increased as well. In our study we examined size distributions by measuring a large number of specimens in consecutive layers in several locations in the Anti-Atlas of Morocco (Pohle & Klug 2017). Most of the included specimens belong to the Orthocerida, a couple of them to the Pseudorthocerida and only very few to the Actinocerida, Bactritida and Lituitida.

The results show that body size of orthoconic cephalopds was subject to considerable fluctuations in late Silurian to Late Devonian sediments of the study area. The combination of measurements of diameters and apical angles allows the reconstruction of their total conch size (length and volume), which revealed a strongly right-skewed size distribution with an average length of 278 mm, while the largest Devonian actinocerids exceeded 2 m in length. Within the examined groups, there is no uniform trend, but rather frequent fluctuations with maximum sizes in the late Lochkovian and early Emsian. Body size decreased in times of global transgressions or extinction events (House 2002), while more stable periods are mostly associated with a size increase. The relationship between body size and these events is further corroborated by the strong correlation of conch size with gamma diversity and global $\delta^{13}C$ values (Figure 1). A more enigmatic result is the negative correlation between apical angle and septal diameter of orthocones, but this relationship is only observed when their mean values are compared across beds.

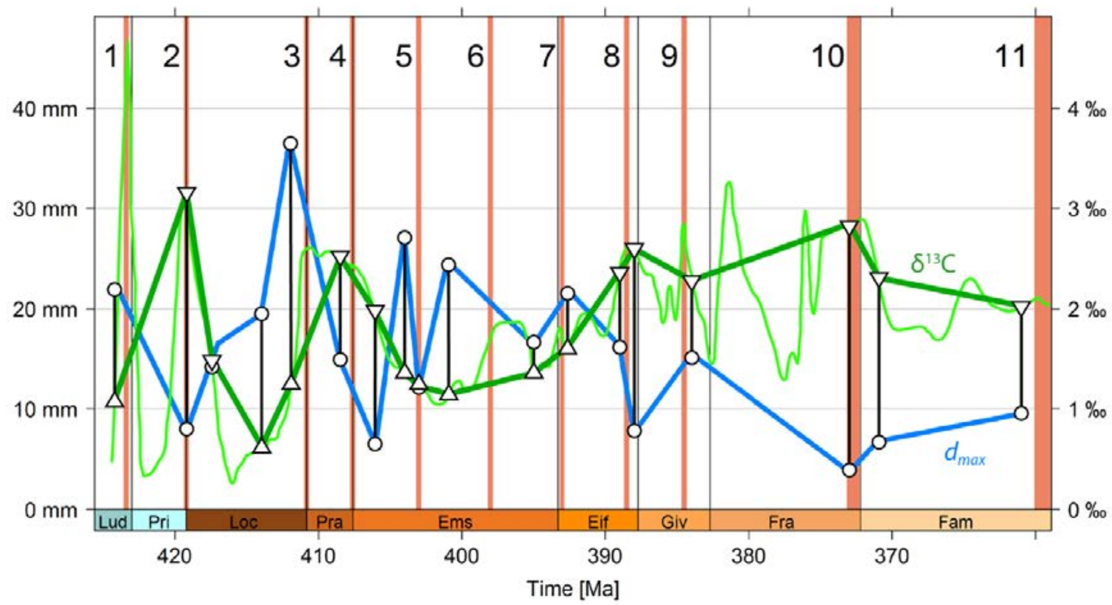

Figure 1. Mean phragmocone diameter (d_{max}) of orthoconic cephalopods, showing its strong correlation to global $\delta^{13}C$ values (Spearman's rank correlation r_s = -0.76, P = 0.0003) and extinction events (vertical bars). Circles: samples of orthocones. Triangles: approximate global mean $\delta^{13}C$ –value at the same point in time. 1. Lau event., 2. Klonk event, 3. End-*pesavis* event, 4. Zlíchov event, 5. Chebbi event, 6. Daleje event, 7. Choteč event, 8. Kačák event, 9. Taghanic event, 10. Kellwasser event, 11. Hangenberg event. Source: Pohle & Klug (2017).

REFERENCES

House, M.R. 2002: Strength, timing, setting and cause of mid-Palaeozoic
extinctions. Palaeogeography, Palaeoclimatology, Palaeoecology 181, 5-25.

Klug, C., De Baets, K., Kröger, B., Bell, M.A., Korn, D. & Payne, J.L. 2015: Normal giants? Temporal and latitudinal shifts of Palaeozoic marine invertebrate gigantism and global change. Lethaia 48, 267-288.

Pohle, A. & Klug, C. 2017: Body size of orthoconic cephalopods from the late Silurian and Devonian of the Anti-Atlas (Morocco). Lethaia, https://doi.org/10.1111/let.12234.

Teichert, C. & Kummel, B. 1960: Size of endoceroid cephalopods. Breviora Museum of Comparative Zoology 128, 1-7.

Wendt, J. 1995: Shell directions as a tool in palaeocurrent analysis. Sedimentary Geology 95, 161-186.

3.16

A new specimen of *Macrocnemus* (Archosauromorpha: Tanystropheidae) from the Middle Triassic of Monte San Giorgio, Switzerland: implications for species recognition and palaeogeography of the group

Torsten M. Scheyer[1], Vivien P. Jaquier[1], Nicholas C. Fraser[2] & Heinz Furrer[1]

[1] *Universität Zürich, Paläontologisches Institut und Museum, Zurich, Switzerland (tscheyer@pim.uzh.ch)*
[2] *National Museums Scotland, Edinburgh, UK*

During the past two decades, a wealth of marine and terrestrial reptiles, including protorosaurian archosauromorphs, has been described from Triassic shales and limestones in southern China. Recovered from the eastern margin of the Tethys Ocean, these forms often show remarkable similarities to taxa that were previously known and described only from Europe, i.e., the western Tethyan margin. One protorosaurian taxon that is known from both the western (two species) and eastern Tethyan province (one species) is the genus Macrocnemus with currently three recognized species. M. bassanii has been found in the Middle Triassic Besano Formation and Meride Limestone (Late-Anisian – Early Ladinian) from the UNESCO World Heritage Site Monte San Giorgio, Ticino, Switzerland (Peyer 1937; Rieppel 1989). The second species, M. fuyuanensis, is so far known only from the Falang Formation (Ladinian), Yunnan Province, southern China (Li et al. 2007), and the third species, M. obristi, was recently described from the Prosanto Formation (Early Ladinian) of the Ducan area, Grisons, Switzerland (Fraser & Furrer 2013). At the moment, the forelimb (humerus/radius) and hind limb (tibia/femur) ratios are the only criteria used for species recognition, whereas previously recognised discrete morphological characters were found to be ambiguous and thus not able to separate the species (see discussion in Jiang et al. 2011 and Fraser & Furrer 2013).

Recently a new specimen, PIMUZ T 1559, from the upper Besano Formation at Meride, Ticino, Switzerland, was prepared, revealing a disarticulated skeleton which includes most of the cranium and lower jaw, pre-caudal vertebral column and ribs, the forelimbs, and girdle elements. Unambiguously assignable to the genus Macrocnemus, it has particularly gracile elongated cervical ribs, as well as a humerus/radius ratio that is comparable only to that of the specimens of M. fuyuanensis from southern China, but not to the specimens from Europe. It thus implies the first recognition of the eastern Tethyan species in Europe. The position and exquisite preservation of the clavicle and interclavicle in this specimen allows a revision of the shoulder girdle of Macrocnemus when articulated, which also has implications for closely related protorosaurian taxa, such as the long-necked Tanystropheus. Furthermore, differences in the shape and morphology of the interclavicle might represent rare discrete characters that allow separation of the species M. bassanii and M. fuyuanensis.

In accordance with previous palaeogeographic scenarios we further propose that during the late Early Triassic, tanystropheid reptiles first evolved from their Late Permian and Early Triassic ancestors in central Pangaea and then dispersed along the western margin of the Tethys Ocean, before spreading to the eastern margins of the Tethys during the Middle Triassic. The dispersal to what is now North America started only later, during the early Late Triassic.

REFERENCES

Fraser, N., & Furrer H. 2013: A new species of Macrocnemus from the Middle Triassic of the eastern Swiss Alps. Swiss Journal of Geosciences, 106, 199-206.

Jiang, D.-Y., Rieppel, O., Fraser, N. C., Motani, R., Hao, W.-C., Tintori, A., Sun, Y.-L. & Sun, Z.-Y. 2011: New information on the protorosaurian reptile Macrocnemus fuyuanensis Li et al., 2007, from the Middle/Upper Triassic of Yunnan, China. Journal of Vertebrate Paleontology, 31, 1230-1237.

Li, C., Zhao, L. & Wang L. 2007: A new species of Macrocnemus (Reptilia: Protorosauria) from the Middle Triassic of southwestern China and its palaeogeographical implication. Science in China Series D: Earth Sciences, 50, 1601-1605.

Peyer B. 1937: Die Triasfauna der Tessiner Kalkalpen. XII. Macrocnemus bassanii Nopcsa. Abhandlungen der schweizerischen Paläontologischen Gesellschaft, 59, 1-140.

Rieppel O. 1989: The hind limb of Macrocnemus bassanii (Nopcsa) (Reptilia, Diapsida): development and functional anatomy. Journal of Vertebrate Paleontology, 9, 373-387.

3.17

Palynology of Triassic–Jurassic boundary sections in Northern Switzerland

Elke Schneebeli-Hermann[1], Nathan Looser[2], Peter A. Hochuli[1], Heinz Furrer[1], Achim G. Reisdorf[3], Andreas Wetzel[3], Stefano M. Bernasconi[2]

[1] *Institute and Museum of Palaeontology, University of Zurich, Karl Schmid-Str. 4, CH-8006 Zurich, Switzerland*
[2] *Department of Earth Sciences, ETH Zurich, Sonneggstrasse 5, CH-8092 Zurich, Switzerland*
[3] *Geologisch-Paläontologisches Institut, Universität Basel, Bernoullistrasse 32, CH-4056 Basel, Switzerland*

Palynological associations are used to refine the dating of Upper Triassic deposits of northern Switzerland. Spore-pollen and dinoflagellate records are documented from the upper part of the Upper Triassic Klettgau Formation and the lower part of the Lower Jurassic Staffelegg Formation.

Several Triassic–Jurassic boundary sections (drill cores, outcrops) were studied and five informal palynological associations are described. The correlation of these associations with successions in the Central European Epicontinental Basin and the Tethyan realm provides a biostratigraphic framework for the uppermost Triassic sediments in northern Switzerland.

Throughout the uppermost Triassic to Jurassic sections a remarkable prominence of *Classopollis* spp. is observed. Besides *Classopollis* spp. the three palynological associations of the upper part of the Klettgau Formation (Gruhalde and Belchen Member) include typical Rhaetian spore-pollen and dinoflagellate taxa (e.g., *Rhaetipollis germanicus*, *Geopollis zwolinskae*, *Rhaetogonyaulax rhaetica*, and *Dapcodinium priscum*).

The relative abundance of the sporomorph taxa such as *Perinopollenites* spp. differs significantly in these three Rhaetian associations. Spore diversity is highest in the late Rhaetian palynological association and relative abundance of spores is also increased. In contrast to the Rhaetian palynological associations the Hettangian to Sinemurian associations include *Pinuspollenites* spp., *Trachysporites fuscus*, and *Ischyosporites variegatus*.

The changes in relative abundances of prominent sporomorph taxa indicate palaeoenvironmental changes throughout the studied succession. These are interpreted applying the sporomorph ecogroup model by Abbink et al. (2004).

REFERENCES

Abbink, O.A., Van Konijnenburg - Van Cittert, J.H.A. & Visscher, H., 2004. A Sporomorph Ecogroup Model for the Northwest European Jurassic – Lower Cretaceous I: concepts and framework. Netherlands Journal of Geosciences 83: 17-28.

3.18

Reconstructing life history from the fossil record – the case of Pleistocene cave bears

Kristof Veitschegger[1]

[1] *Palaeontological Institute and Museum, University of Zurich, Karl-Schmid-Strasse 4, CH-8006 Zürich (kristof.veitschegger@pim.uzh.ch)*

The understanding of the biology of past life is one of the main goals of paleontology. Cave bears are an especially suitable subject to use diverse approaches to reconstruct the biology of extinct vertebrates, due to their abundance in the fossil record and their exceptionally well preserved remains of many ontogenetic stages. Here, I present a comprehensive dataset of 412 skulls, 95 teeth, 77 bones, and tooth eruption data used to infer different aspects of life history evolution of cave bears in a phylogenetic context.

The endocranial volume and body size inferred from the skulls of ten extant and extinct ursid species clearly evidence the small relative brain size of cave bears. By incorporating diet and dormancy data for the investigated bear species, I discovered a significant effect of these two variables on brain size. An ancestral stage reconstruction based on a Brownian motion model of evolution resulted in a decoupled pace of brain and body size in the evolution of cave bears (Veitschegger 2007).

Data collected from tooth cementum lines evidences the long life span of cave bears up to 30 years, which is longer than most extant bear species can reach in the wild. The relative emergence pattern of replacement teeth compared to molar tooth eruption shows a heterochronic shift in the eruption of p4. This tooth emerges later in cave bears than in brown bears, which indicates a faster life history in the former (Veitschegger and Sánchez-Villagra in prep.).

Bone histology can be used to directly infer the growth rate of cave bears by investigating the microstructure as well as measuring the distance between lines of arrested growth (LAGs), which are produced yearly (Figure 1). Cave bears show a high growth rate comparable to polar bears and reached skeletal maturity late in life, around the age of 12 years. They likely reached sexual maturity between the age of 4 – 6 years. By binning the growth rate data according to the entrance altitute of the 23 cave sites represented in the dataset, I showed that the growth rate of cave bears is not influenced by body size trends found in high-alpine populations. Thus, the smaller high-alpine cave bears exhibit the same growth rate as their lowland counterparts (Veitschegger et al. submitted).

The life history implications based on brain size are that cave bears had a small birth and weaning mass as well as a long gestation time and large litter sizes. Bone histology and relative replacement tooth emergence additionally evidence a fast paced growth for this species. Finally, by investigating the tooth cementum of cave bears, I established a minimum longevity for this species (Veitschegger 2007, Veitschegger et al. submitted, Veitschegger and Sánchez-Villagra in prep.)

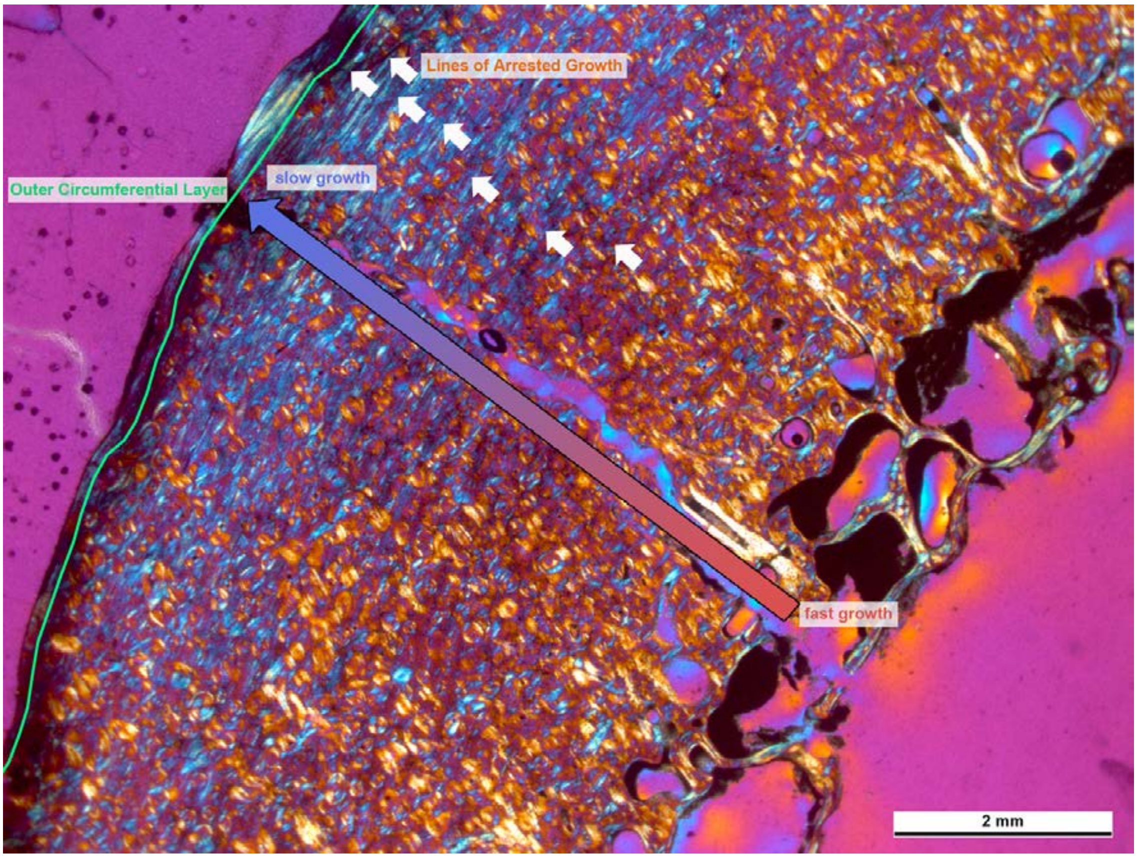

Figure 1. Histology of the anterior part of the femur midshaft of cave bears from Gamssulzen cave, Austria. Warm colours indicate fast growth, cold colours slow growth. Growth slows down from interior to outer part of the cortex. Indicated with white arrows are lines of arrested growth, which are deposited in yearly cycles. In green the boarder to outer circumferential layer, which indicates skeletal maturity and thus the cessation of growth (photograph by Kristof Veitschegger).

REFERENCES

Veitschegger, K. 2007: The effect of body size evolution and ecology on encephalization in cave bears and extant relatives, BMC Evolutionary Biology, 17, 124.

Veitschegger, K., Kolb, C., Amson, E., Scheyer, T.M. & Sánchez-Villagra, M.R. submitted: Palaeohistology and life history evolution in cave bears, *Ursus spelaeus* s.l., PLoS One.

Veitschegger, K. & Sánchez-Villagra M.R. in prep: An overview of the life history and growth of cave bears. Historical Biology (invited contribution).

3.19

A new high-resolution C-isotope chemostratigraphic correlation through the Aalenian Opalinus Clay - from Mont Terri to Northeastern Switzerland

Stephan Wohlwend[1], Stefano M. Bernasconi[1] & Gaudenz Deplazes[2]

[1] *Geological Institute, ETH Zurich, Sonneggstrasse 5, CH-8092 Zürich (stephan.wohlwend@erdw.ethz.ch)*
[2] *Nagra, Postfach 280, Hardstrasse 73, CH-5430 Wettingen*

The formation Opalinus Clay, mainly deposited during the Early Aalenian (Opalinum Zone), consists of dark grey to black calcareous and sandy claystone and has a relatively homogeneous composition. Based on the mineralogy and grain-size, the Opalinus Clay, however can be further divided into sub-units. The extent of these sub seismic-scale sub-units can be investigated by comparing the records of different outcrops and drill cores. To predict potential lateral facies changes within the Opalinus Clay, the depositional environment must be investigated and for that not only a compositional but also a chronological differentiation is needed.

Biostratigraphy based on ammonites and palynomorphs is a frequently applied method to establish a chronology in these clay rich Mesozoic sediments (e.g. Feist-Burkhardt & Pross 2010, Hostettler et al. 2017). However, the resolution of these biostratigraphic tools is mostly not high enough to differentiate the sub-units of different drill cores within the Opalinus Clay.

Therefore we established a high-resolution carbon isotope stratigraphy measured on carbonates as well as on organic matter. The newly established C-isotope chemostratigraphy shows several distinct negative and positive excursions during the latest Toarcian (Aalensis Zone) to Early Aalenian (Opalinum Zone) time interval which can be followed throughout the drill cores from Mont Terri, Schafisheim, Riniken, Beznau, Weiach, Benken to Schlattingen-1 over about 120 km.

A stepwise negative excursion can be seen in the lowermost Opalinus Clay in the Opalinum Subzone of the Opalinum Zone. A second excursion with an increase of values can be seen in the uppermost part of the Opalinus Clay succession in the Comptum Subzone of the Opalinum Zone. The newly established high-resolution C-isotope correlation allows to investigate the timing of several calcareous intervals and hardgrounds within the Opalinus Clay.

REFERENCES

Feist-Burkhardt, S. & Pross, J. 2010: Dinoflagellate cyst biostratigraphy of the Opalinuston Formation (Middle Jurassic) in the Aalenian type area in southwest Germany and north Switzerland. Lethaia, 43, 10-31.

Hostettler, B., Reisdorf, A. G., Jaeggi, D., Deplazes, G., Bläsi, H., Morard, A., Feist-Burkhardt, S., Dietze, D. & Menkveld-Gfeller, U. 2017: Litho-and biostratigraphy of the Opalinus Clay and bounding formations in the Mont Terri rock laboratory (Switzerland). Swiss Journal of Geosciences, 110, 23-37.

P 3.1

Cretaceous Stratigraphic and Tectonic Evolution of the Eastern Margin of the Pelagonian Zone, Northern Greece

Lydia Bailey[1], Vincenzo Picotti[1], Filippo Schenker[2] & Giuditta Fellin[2]

[1] Geologisch Institut, ETH Zürich, Sonneggstrasse 5, CH-8092 Zürich
[2] Institute of Earth Sciences, SUPSI, Campus Trevano, CH-6952 Canobbio

Conventional geological mapping and stratigraphic analysis was applied to the eastern margin of the Pelagonian Zone in order to unravel the Late Creteceous detrital record of the newly discovered Kallipetra Basin. Illite crystallinity, low-temperature thermochronology, and fluid inclusion analysis helped provide new constraints on the tectonic evolution of the Vardar Zone and the eastern Pelagonian Zone, as well as deciphering how these tectonics influenced the development of the Kallipetra Basin.

Following ophiolitic obduction of the Vardar oceanic lithosphere at 155-130 Ma, and exhumation of the Pelagonian Gneiss Dome at 116 Ma, the Kallipetra Basin was formed as a hybrid forearc- to foreland-type basin resting on the eroded Vardar Ophiolitic Complex (VOC) and Pelagonian basement. The basin was elongated NW-SE, parallel to the suture of the colliding Adriatic and European plates.

Subaerial erosion and fluvial transport provided the first sediments, serpentinite-rich conglomerates, to the initially shallow sedimentary basin. As the basin progressively deepened, the slopes underwent frequent soft-sediment slumping, and mass flows and Pelagonian olistoliths were deposited on the bottom slopes during instability. The Pelagonian continent was positioned on the north-werstern flank of the basin, providing more quartz-rich material to the north-western slopes. The basin experienced peak depths at the Cenomanian – Turonian boundary when distinct red and green marly limestones were deposited, corresponding to OAE2 and peak global transgression. Shallowing of the Kallipetra Basin occurred in the Turonian due to sedimentation, an increasing input of serpentinite-rich material from an approaching Vardar source in the south, and global sea level fall.

Rudist mounds were constructed on shallow slopes that were sloping towards the north, away from the approaching VOC. The bioherms have a core made principally of micrite and whole floating rudists *(Hippurites),* and the core is built on a bioclastic breccia containing rudists, sponges, echinoderm fragments, serpentinite and quartz. The mounds are asymmetric with steeper slopes on the southern flank. Flank deposits on the northern flank of the mounds consist of marls, or a series of breccias and sandstones displaying an increasing content of serpentinite. Serpentinite breccias, originating from the VOC positioned upslope, stack up against the steep southern flanks of the mound. *Helvetoglobotruncana helvetica* place deposition of flank deposits around ~ 93 Ma and upwards.

After ~91 Ma, the VOC tectonically overrides the Kallipetra Basin. Shear heating and circulation of hot fluids created greenschist conditions at the contact, and an inverted thermal profile in the Kallipetra Basin below the tectonic contact. Apatite ages were reset. Extension occurred during the Oligocene to early Miocene, documented by a reset AFT age of 32.7 Ma, WNW-ESE trending normal faults, and NE-SW trending dextral strike slip faults.

P 3.2

Tectono-Stratigraphy of The Cretaceous Shelf (Constantinois Platform-NE Algeria)

Rami Djeffal[1], Mohammed Chadi[2], & El Hadj Youcef Brahim[3]

[1] Geologic sciences department Constantine 1 University, (djeffal.rami@umc.edu.dz).
[2] Management of urban technics department Constantine 3 University, chadi43@yahoo.fr
[3] Department of Geology, Université of Batna 2, Fisdis (wahidyb@yahoo.fr)

The synthesis of stratigraphic and structural data of Constantinois limestone massifs has allowed the refining of the southern Tellian series at nummilites stratigraphy and proposing a structural model. The most significant sites and less disturbed by tectonics, are the Taxas syncline and southern flank of Guerioun massif, exactly at the Djebel Ras Rihane. Also, at the level of Taxas syncline, and surmounting the hard ground which ended the Aptian neritic limestone, the marly levels had provided Cenomanian microfauna: *Favusella washitensis*, *Rotalipora appenninica*, *R. cushmani*, *R. brotzeni*, *Hedbergella* sp., and *Praeglobotruncana stephani*.

On the southern reverse of Djebel Ras Rihane, at the level of Chaabet Ras Chiboub notch, we can observe, on the hard ground that terminates the Aptian nerititic limestones, a clayey Cenomonian over one hundred meters of thickness.
The samples from these clays have provided many *Hedbergella*, *Rotalipora brotzeni*, *R. cushmani*, *R. globotruncanoides* and *Praeglobotruncana* gr. *Stephani*.

The top of these clays has provided Coniacian foraminifera and revamped Cenomanian *rotalipora.* The study of the stratigraphic series of s neritic massifs allowed the refining of our predecessor's results.
Also the yellow marls stratigraphically surmounting the terminal Aptian- basal Albian through a hard ground, represents the Cenomanian-Turonian.

Microscopic analysis of samples from this hard ground highlights sedimentological phenomena that attest the emersion of Constantinois platform during the terminal Aptian- basal Albian.

In the Constantinois limestone massifs, ‘’the southern Tellian units at Nummilites ‘’ represent the normal marly cover of neritic limstones.

REFERENCES

Chadi, M., 1991 : Géologie structurale des monts d›AïnM'lila (Algérie orientale). Thèse de Doctorat de l'Université de Nancy I.191 pp., 1 carte géol. h. t.
Chadi, M., 2004 : Cadre géologique et structural des séries crétacées néritiques du constantinois (Est-Algérien).Thèse de Doctorat d'Etat, Université de Constantine, 229 pp.
Coiffait,P.E., 1992 : Un bassin post-nappe dans son cadre structural : l'exemple du bassin de Constantine. Thèse de Doctorat d'Etat, Université de Nancy I, 502 pp.

P 3.3

Species of the genus *Porosononion* from Sarmatian deposits of Georgia and their stratigraphic significance

Kakhaber Koiava[1], Lika Kvaliashvili[2], Lamara Maissuradze[3], Jeremiah Mauvilly[4] & Jon Mosar[4]

[1] *Ivane Javakhishvili State University, Alexandre Janelidze Institute of Georgia, A. Politkovskaia str. 5, GEO-0186 Tbilisi (koiava_ka@yahoo.com)*
[2] *LTD "GeoEngService", Ambrolauri str. 5, GEO-0160 Tbilisi (lkvaliashvili@yahoo.com)*
[3] *Georgian National Museum, Institute of Paleobiology, GEO-0108 Tbilisi (lamaramaissuradze@gmail.com)*
[4] *Department de Géosciences – Sciences de la Terre, Université de Fribourg, Chemin du Musée 6, CH-1700 Fribourg (mosar@unifr.ch)*

Prolonged study of foraminifers in the Sarmatian sediments of Georgia (Maissuradze, 1971; Koiava, 2006; Maissuradze & Koiava, 2011), made it possible to collect a rather rich factual data set indicating diversity, stratigraphic distribution and significance of species of the genus *Porosononion* (Figure 1).

Analysis of the data indicates that in the Sarmatian basin of Georgia, genus *Porosononion* is represented by five species and one subspecies. Three species: *Porosononion granosum* (d'Orbigny), *Porosononion subgranosum subgranosum* (Eggery) and *Porosononion martkobi* (Bogdanowicz) are typical both to the Konkian and Sarmatian basins, which reduces their stratigraphic value. The remaining two species: *Porosononion aragviensis* (O. Djanelidze), *Porosononion hyalinum* (Bogdanowicz) and one subspecies *Porosononion subgranosum umboelata* (Gerke), however, are playing the significant role in thebiostratigraphic subdivision of the region (Koiava et al., 2008; Koiava et al., 2016).

The subspecies *Porosononion subgranosum umboelata* (Gerke) occurs at the boundary between Veseliankian and Volhynian regional substages and presents one of the index species in foraminifer complex, typical for the mentioned stratigraphic level. Biozones, corresponding to the middle part of Bessarabian and upper part of Bessarabian, are known as *Porosononion aragviensis* and *Porosononion hyalinum*. The first of them is defined according to the first appearance of the species *Porosononion aragviensis* (O. Djanelidze) in foraminifer complexes, while the second is defined on the basis of the dominance of *Porosononion hyalinum* (Bogdanowicz) in foraminifer complexes.

Therefore, it can be conlcuded that representatives of species of the genus *Porosononion* are rather numerous in the Sarmatian sediments of Georgia and are playing the significant role in biostratigraphic subdivision of the Sarmatian sediments of the region.

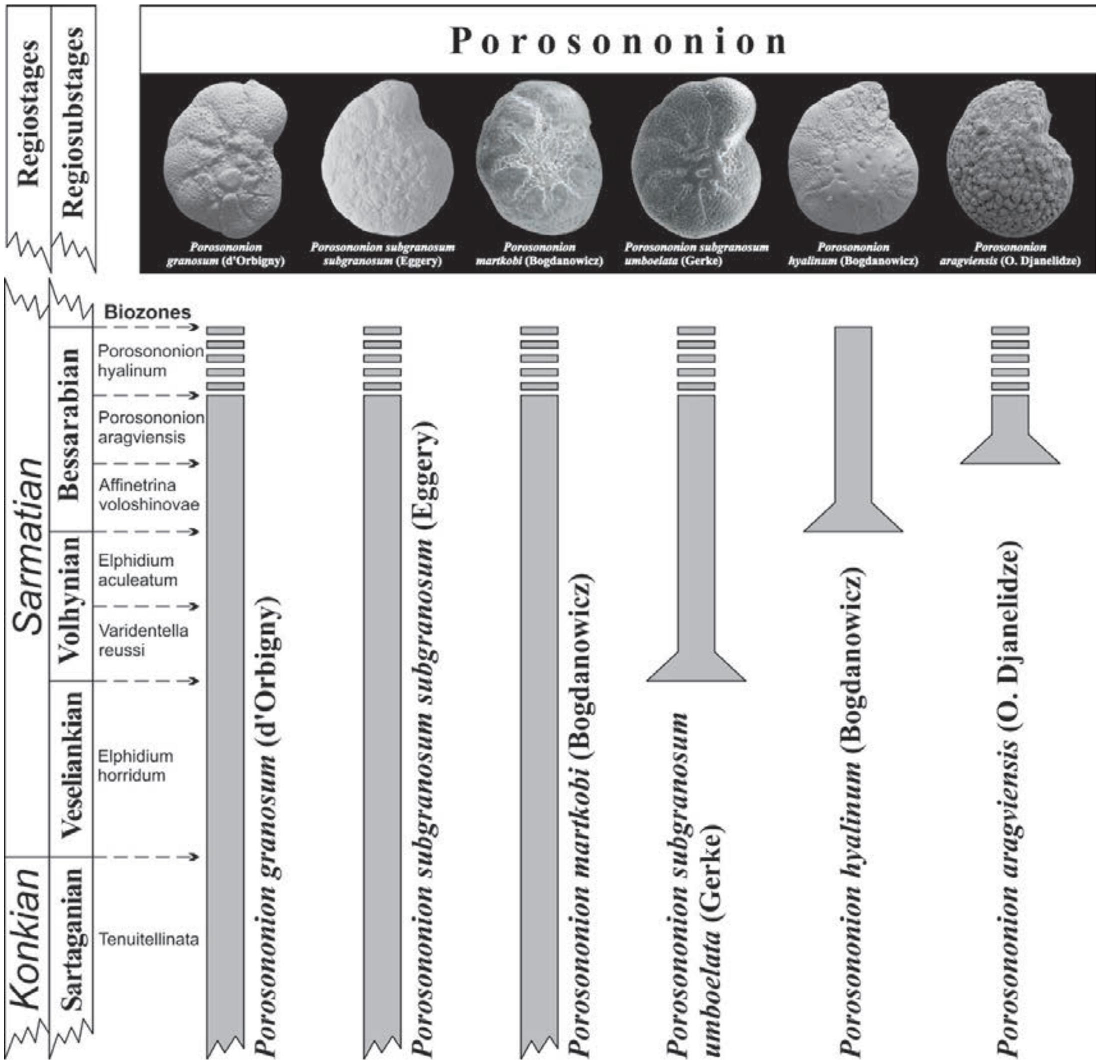

Figure 1. The stratigraphic distribution of species of the genus *Porosononion* in the Sarmatian sediments of Georgia.

REFERENCES

Koiava, K. 2006: The Biostratigraphy of Sarmatian Deposits of Eastern Georgia Based on Foraminifera, PhD thesis, Alexandre Djanelidze Institute of Geology, Tbilisi, 1-163. (In Georgian)

Koiava, K., Maissuradze, L., Shatilova, I., Spezzaferri, S., Strasser, A. 2008: The subdivision of Sarmatian deposits of Eastern Georgia based on foraminifera, The Fifth International Conference “Environmental Micropaleontology, Microbiology and Meiobenthology”, Chennai, India, February 17-25, 150-153.

Koiava, K., Mosar, J., Kvaliashvili, L., Mauvilly, J. 2016: About Konkian/Sarmatian Boundary of Georgia Based on Foraminifera, Swiss Geoscience Meeting, Geneva, Switzerland, November 18-19, 224-225.

Maissuradze, L. S. 1971: Sarmatian Foraminifera of the West Georgia, “Mecniereba”, Tbilisi, 1-120. (In Russian)

Maissuradze, L., Koiava, K. 2011: Biodiversity of Sarmatian Foraminifera of the Eastern Paratethys, Bulletin of the Georgian National Academy of Sciences, 5(1), 143-151.

P 3.4

Reconstruction of a Late Jurassic marine environment

Apolline Lefort[1] & Tayfun Yilmaz[1]

[1] *Section d'archéologie et paléontologie, Office de la Culture, République et Canton du Jura, Porrentruy (apolline.lefort@jura.ch)*

Good pictures of palaeoenvironmental reconstructions are very in demand and useful for teaching, scientific publications or popularization. Until recently, classical fossils or environments were mainly illustrated in two-dimensional pencil drawings. The construction of the highway A16 in the Canton of Jura allowed us to collect a lot of fossils (~ 40.000) between 2000 and 2012, and to have a better understanding of the excavated strata. The Late Kimmeridgian (~155 Ma) beds were extensively documented and studied (e.g. Comment et al. 2015; Püntener et al. 2017; Leuzinger et al. 2017). Thanks to this rich palaeontological, sedimentological and geochemical data we are attempting to build and draw as faithfully as possible a shallow marine carbonate platform environment.

We present a reconstruction of the palaeoenvironment of the Lower Virgula Marls (or "Marnes à *virgula* inférieures") drawn using high-resolution modern tools and taking into account scientific details.

Three pictures built with Blender software will be exhibited : A: fauna of the benthic domain, B: nekton in the epipelagic zone and C: nekton on the top of the water column. These photographic snapshots are possible thanks to the overlapping of all the intermediate studies made at the Paléontologie A16.

All environmental parameters take their meaning in the drawing. For example the depth: the highly diversified invertebrate fauna indicates a soft substrate subtidal environment. The faunal assemblage indicates relatively deep water of more than 10 m water depth. At a depth of 10 m, the red and orange colors are already absorbed. The trophic level and turbidity of the water also influence visibility. Then, each organism requires a preparatory work before its introduction into the final palaeoenvironment. Let us exemplify the process by a well identified bivalve: *Nanogyra (Palaeogyra) virgula*. This small ostreid is well described in the litterature (e.g. Koppka 2015). We need to find the best preserved specimen in our collection. For the 3D picture, we scan several objects, smooth, sculpt and correct the digitalized fossil. We need to understand their ecology: *Nanogyra* are epifaunal suspensivore feeders, gregareous and encrusters. It is necessary to observe several specimens to understand their way of life. Finally, the designer imagines the animal's soft parts and the color of the shell.

The interest of digital drawing in three dimensions is to be able to modify, retouch and improve as science advances. The perspectives of the marine environment are respected and the point of view of the camera can be moved. Organisms can be reconstituted with high accuracy and may also be reused on their own or in other contexts.

Figure 1. The reconstruction of the sea floor of the well known Lower Virgula Marls deposits in the Swiss Jura (Late Kimmeridgian): semi-faunal, infaunal organism and nekton. (Design not finished).

REFERENCES

Comment, G., Lefort, A., Hantzpergue, P., & Koppka, J., 2015: Le Kimméridgien d'Ajoie (Jura, Suisse): lithostratigraphie et biostratigraphie de la Formation de Reuchenette. Revue de Paléobiologie, 34(2), 195–233.

Koppka, J. (2015). Revision of the Bivalvia from the Upper Jurassic Reuchenette Formation, Northwest Switzerland – Ostreoidea. Zootaxa, 3927(1), 001–117.

Leuzinger, L., Cuny G., Popov, E. & Billon-Bruyat J.-P., 2017: A new Chondrichthyan fauna from the Late Jurassic of the Swiss Jura (Kimmeridgian) dominated by hybodonts, chimaeroids and guitarfishes. Papers in Palaeontology, 1-41.

Püntener, C., Anquetin J., & Billon-Bruyat J.-P. 2017: The comparative osteology of *Plesiochelys bigleri* n. sp., a new coastal marine turtle from the Late Jurassic of Porrentruy (Switzerland), PeerJ 5, e3482.

P 3.5

Bio-magnetic feedback to eutrophication

Barbara Lesniak[1], Thomas M. Blattmann[2], Martin Wessels[3], Timothy I. Eglinton[2], Andreas U. Gehring[1]

[1] *Institute of Geophysiscs, ETH Zurich, 8092 Zurich, Switzerland (barbara.lesniak@erdw.ethz.ch)*
[2] *Geological Institute, ETH Zurich, 8092 Zurich, Switzerland*
[3] *ISF Langenargen, Argenweg 50/1, D-88085 Langenargen*

Anthropogenically induced eutrophication is a well-known phenomenon in lakes where the uncontrolled input of sewage and fertilizers causes enhanced primary productivity which subsequently leads to oxygen depletion in the water column upon degradation of settling organic matter. Bacteria adapted to anaerobic conditions flourish in such environments. Magnetotactic Bacteria (MTB) are among these bacteria and they are often found in lakes.

MTB synthesize intracellular chains of nearly uniform particles that generally consist of magnetite (Fe_3O_4). The chain arrangement generates a strong magnetic dipole like a compass needle that is used by MTB to navigate along the Earth's magnetic field. The magnetite particles, however, are relatively stable in comparison to surrounding cellular material, and therefore, magnetite chains and their remains, denoted magnetofossils, have high preservation potential and can be used as proxies for oxygen-depleted aquatic environments in geological systems.

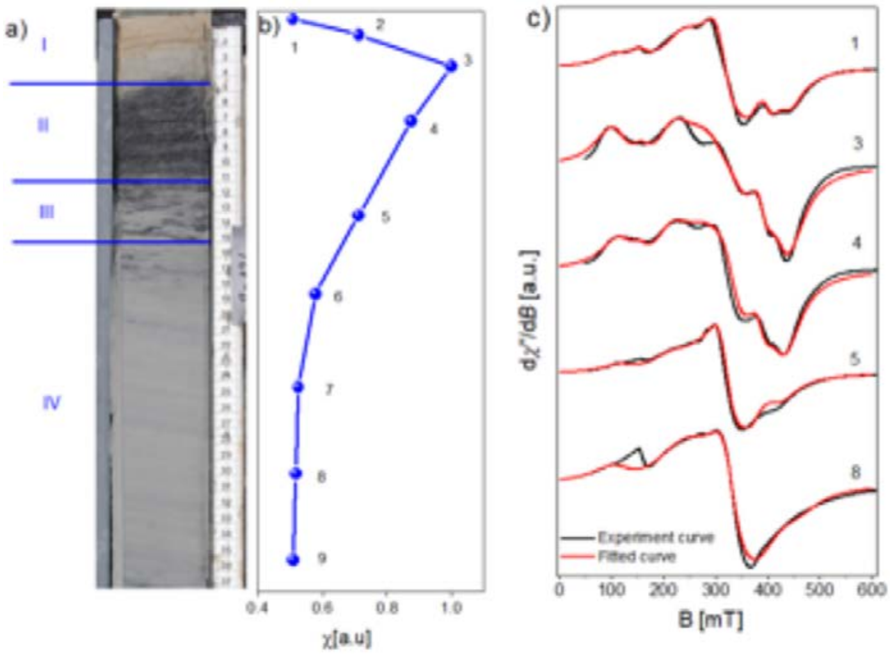

Figure 1. a) Depth profile from Lake Constance subdivided into four distinct sections, b) magnetic susceptibility (), c) measured FMR spectra (black curve) and their simulations (red curve).

In order to test if MTB can be an indicator of eutrophication and low oxygen conditions, we used a sediment core from Lake Constance, where anthropogenic eutrophication is historically well documented. The sediment profile can be subdivided into four sections (Fig.1). The black sediments of section II indicate the peak eutrophic state. Sections I and IV represents deposition under a prevailing aerobic environment and section III records the transition from oligotrophic to eutrophic. Corresponding magnetic susceptibility of the profile shows a maximum in the magnetic content close to the boundary between sections I and II, followed by a continuous decrease with depth.

For the characterization of the magnetic content we use ferromagnetic resonance (FMR) spectroscopy, which is a powerful tool to detect magnetic particles in a chain configuration, which is a feature unique to MTB. The FMR spectrum of a sediment sample records the total magnetic content comprising different components which can be disentangled by spectral separation (see Fig. 2). The experimental curve can be modelled with the superposition of three simulated spectra that represent isolated magnetite particles and particles in chains differing in their length (Charilaou et al. 2011). The two pronounced maxima of a simulated spectrum due to the uniaxiality of the chains, is the characteristic feature to identify MTB.

The measured spectra from sections I and II exhibit the characteristic MTB features, whereas the FMR signals from section IV can be attributed to magnetite particles dispersed in the sediment (Fig.2). This suggests that simultaneously to the onset of eutrophication, MTB began to flourish in Lake Constance. Considering the susceptibility data, the maximum concentration of magnetofossils is found in the sediments that marking the onset of re-oligotrophication. This indicates that the eutrophication driven bloom of MTB is time-delayed.

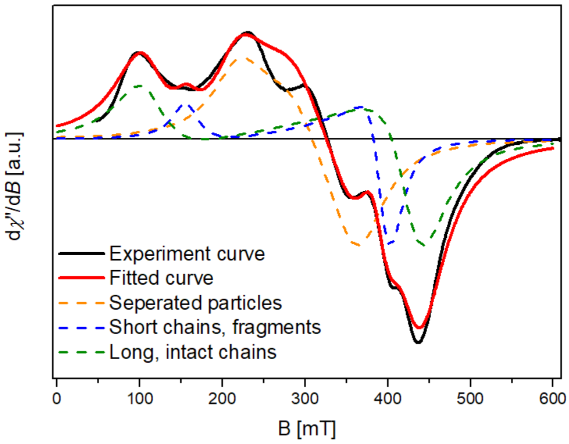

Figure.2. Comparison of the experimental with the fitted curve consisting of three simulated spectral components.

In summary, the occurrence of MTB remains in sedimentary archives has the potential to be used as inorganic magnetic biomarker to infer environmental conditions in depositional environments.

REFERENCES

Charilaou, M., Winklhofer, M., & Gehring, A. U. 2011: Simulation of ferromagnetic resonance spectra of linear chains of magnetite nanocrystals. Journal of Applied Physics, 109(9), 093903.

5. Shale-Gas, CO_2 Storage and Deep Geothermal Energy

Lyesse Laloui, Larryn Diamond, Paul Bossart

Swiss Geothermal Society
Swiss Association of Energy Geoscientists (SASEG)

TALKS:

5.1 **Afshari Moein M.J**., Tormann T., Valley B., Wiemer S., Evans K.F.
Constraining the stochastic fracture network using induced microseismicity in the Basel geothermal reservoir

5.2 **Doetsch J.**, Amann F., Gischig V. , Jalali R., Krietsch H., Villiger L., Evans K., Valley B., Dutler N., Brixel B., Klepikova M., Kittilä A., Wiemer S., Saar M.O., Loew S., Driesner T., Maurer H., Giardini D.
Overview of the hydraulic stimulation experiments at the Grimsel Test Site

5.3 **Dutler N.**, Valley B., Villiger L., Krietsch H., Jalali R., Gischig V., Doetsch J., Amann F.
Injection Protocol and First Results of Hydraulic Fracturing Experiments at the Grimsel Test Site

5.4 **Egli D.**, Baumann R., Küng S., Berger A., Baron L., Herwegh M.
Fault structure and porosity distribution in an active hydrothermal system

5.5 **Fryer**, B., Laloui, L.
The stochastic modelling of large basement seismicity during fluid injection in sedimentary horizons

5.6 **Gawenda P.**
A decade of unconventional exploration in Europe – where are we now

5.7 **Gischig V.**, Jalali M., Doetsch J., Krietsch H., Villiger L., Amann F.
Pressure propagation during decameter-scale hydraulic stimulation experiments in crystalline rock at the Grimsel Test Site

5.8 **Kong X.-Z.**, Ma J., Saar M.O.
Alteration of hydrogeochemical properties during reactive flow-through experiments on sandstone specimen using CO_2-charged brine

5.9 **Krietsch H.**, Gischig V., Doetsch J., Valley B., Amann F.
Mechanical response of a decameter-scale reservoir during an in-situ hydraulic stimulation experiment

5.10 **Lavanchy J.M**. (Keynote speaker)
AGEPP – First Swiss hydrothermal well for electricty and heat production

5.11 **Minardi A.**, Ferrari A., Ewy R., Laloui L.
Experimental study on the swelling behaviour of a gas shale

5.12 **Moradian Z.**
Acoustic Emission Monitoring of Fractures in Opalinus Clay Shale

5.13 **Nussbaum C.**, Guglielmi Y., Jeanne P., Birkholzer J.
In-situ observations of fault leakage during a semi-controlled fault activation (FS) experiment, Mont Terri rock laboratory, Switzerland

5.14 **Van Den Heuvel D.B**., Gunnlaugsson E., Gunnarsson I., Stawski T.M., Diamond L.W., Benning L.G.
Two pathways of silica scaling inside a high-enthalpy geothermal power plant

5.15 **Wanner C.**, Diamond L.W., Alt-Epping P.
Quantification of the 3D thermal anomaly in the orogenic geothermal system at Grimsel Pass, Switzerland

POSTERS:

P 5.1 **Alt-Epping P.**, Diamond L.W., Wanner C.
Regional-scale reactive transport models of the orogenic hydrothermal system at Grimsel Pass, Switzerland

P 5.2 **Aschwanden L.**, Adams A., Diamond L.W.
Effect of progressive burial on matrix porosity and permeability in Muschelkalk dolostones, Swiss Molasse Basin

P 5.3 **Carvalho I**, Meylan F., Piguet F., Erkman S.
An overview of CO_2 storage and utilization

P 5.4 **Blasco M.**, Auqué L.F., Gimeno M.J., Acero P., Asta M.P.
Geothermometrical calculations and the influence of the mobile elements in a low temperature thermal system hosted in carbonate-evaporitic rocks

P 5.5 **Jansen G.**, Valley B., Miller S.A.
A MATLAB package for thermo-hydraulic modeling and fracture stability analysis in fractured reservoirs

P 5.6 **Liu D.**, Lecampion B., Benedetti L.
Modelling the propagation of hydraulic fracture using cohesive zone models

P 5.7 **Makhloufi Y.**, Samankassou E., Rusillon E., Brentini M., Meyer M.
Dolomitization of the Upper Jurassic Carbonate Rocks in the Geneva Basin, Switzerland and France

P 5.8 **Räss L.**, Duretz T., Podladchikov Y.
Fluid flow in porous rocks: drastic localisation due to time-dependent deformation of the matrix

P 5.9 **Sohrabi R.**, Omlin S., Miller S.A.
BATMAN – 3D Numerical simulator for mass and heat transport with porosity change using GPUs technology

P 5.10 **Wenning Q.C**., Madonna C., Joss L., Pini R.
Measuring pressure dependent aperture heterogeneity in rough-walled fractures using X-ray computed tomography

P 5.11 **Zhang W.**, Wang Q., Zappone A. , Madonna C., Burg J.
Comparison between permeability and seismic velocity anisotropy of shales

5.1

Constraining the stochastic fracture network using induced microseismicity in the Basel geothermal reservoir

Mohammad Javad Afshari Moein*, Thessa Tormann**, Benoit Valley[3], Stefan Wiemer**, Keith F. Evans

[1] Geological Institute, ETH Zurich, Sonneggstrasse 5, CH-8092 Zurich (mohammad.moein@erdw.ethz.ch)
[2] Swiss Seismological Service (SED), ETH Zürich, Sonneggstrasse 5, CH-8092 Zürich
[3] Centre for Hydrogeology and Geothermics, University of Neuchâtel, Rue Emile-Argand 11, CH-2000 Neuchâtel

Hydraulic stimulation is key to the creation of a commercially exploitable Enhanced Geothermal System (EGS) reservoir. The operation commonly generates a relatively large numbers of microseismic events, some of which may be large enough to be felt by the community and hinder further developments (e.g. 2006 Basel geothermal project). The task of designing reservoir stimulation protocols that are effective in creating suitably-connected linkage of flow-paths in the reservoir without producing damaging seismic events requires satisfactory characterization of the reservoir, particularly with regard to the distribution and properties of natural fractures and faults. Typically, insufficient information is available to develop fully-deterministic discrete fracture network (DFN) models that are adequately-constrained. Thus, stochastically-generated fracture networks, supplemented by deterministic information, are usually used to generate realizations of the discontinuity distribution.

In this analysis, we investigate the use of microseismicity patterns to constrain attributes of the natural fracture network. Since the injection of fluid into a reservoir can induce microseismicity from the earliest stages when conditions in the reservoir are relatively undisturbed, we prefer to use those observations to calibrate our DFNs. For small magnitudes, we can assume that the earthquake hypocenters correspond to the centers of circular fracture planes. We applied fractal geometry to relate the existing fracture network to the fractal patterns observed in relocated Basel microseismicity data (Kraft & Deichmann 2014). The spatial organization of induced microseismicity can be characterized by computing the correlation function and its slope (i.e. the correlation dimension). The correlation function of the earthquake hypocenters also provides some information about the underlying network geometry (e.g. the presence of a fracture zone if the correlation dimension is around *2*) and the potential presence of repeating events (multiple ruptures of individual fractures if there is a sudden drop in the local slope) (Figure 1a).

In order to generate fractal DFNs, we choose a statistical model presented by Davy *et al.* involving fractal clustering of fractures and power-law size distribution given by $n(l,L).dl = c.L^{D}\, l^{-a}.dl$, where n is the number of fractures whose size is in the range $[l,l + dl]$ and whose center belongs to a volume in L^3 with c being a constant). The spatial and size distributions of fractures in a given DFN model are related by a new scaling law, relating size and average distance from a fracture to the closest nearest neighbour having a larger size (distance function) (Bour & Davy 1999). We implement a similar concept to extract the statistical distribution of fracture size in Basel, assuming fractal spatial and size relations govern the distributions. We include the uncertainty of hypocentral locations in computing the size distributions, producing a large number of possible realizations and different estimates of the size exponent (a) (Figure 1b). A probabilistic analysis of the available data reveals a normal distribution of size exponent ($a=2.08\pm0.09$). Current results bring additional insight to the key reservoir characteristics and they are expected to provide more reliable inputs for reservoir simulations.

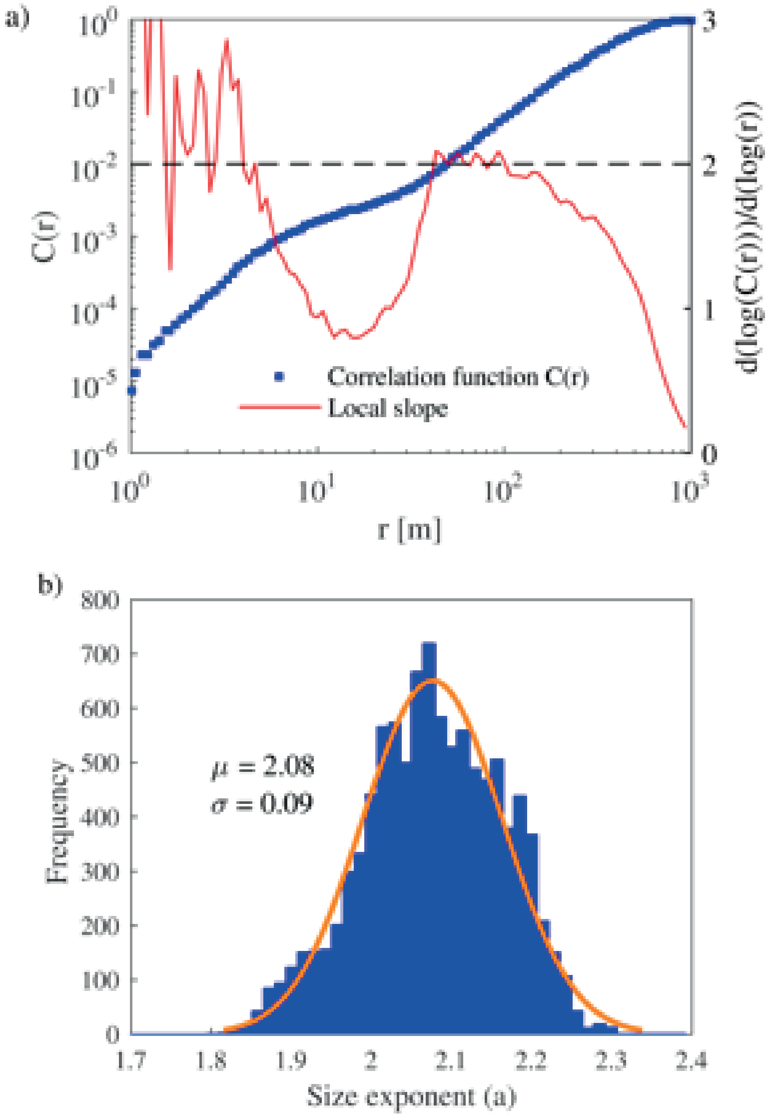

Figure 1 a) Spatial distribution (correlation function) of relocated earthquake hypocenters in the Basel geothermal reservoir. b) Probabilistic distribution of fracture size exponents considering the hypocentral uncertainties.

REFERENCES

Bour, O. & Davy, P. 1999: Clustering and size distributions of fault patterns: theory and. *Geophys Res Lett* 26, 2001-2004.

Davy, Sornette, A. & Sornette, D. 1990: Some consequences of a proposed fractal nature of continental faulting. *Nature* 348, 56-58.

Kraft, T. & Deichmann, N. 2014: High-precision relocation and focal mechanism of the injection-induced seismicity at the Basel EGS. *Geothermics* 52, 59-73.

5.2

Overview of the hydraulic stimulation experiments at the Grimsel Test Site

Joseph Doetsch[1], Florian Amann[1], Valentin Gischig[1], Reza Jalali[1], Hannes Krietsch[1], Linus Villiger[1], Keith Evans[1], Benoît Valley[2], Nathan Dutler[2], Bernard Brixel[1], Maria Klepikova[1], Anniina Kittilä[1], Stefan Wiemer[1], Martin O. Saar[1], Simon Loew[1], Thomas Driesner[1], Hansruedi Maurer[1], Domenico Giardini[1]

[1] ETH Zurich, Department of Earth Sciences, Sonneggstrasse 5, 8092 Zurich, Switzerland (joseph.doetsch@erdw.ethz.ch)
[2] University of Neuchatel, Laboratory of Geothermics and Reservoir Geomechanics, 2000 Neuchâtel, Switzerland

Within the In-situ Stimulation and Circulation (ISC) project at the Grimsel Test Site (GTS), twelve hydraulic stimulation experiments have been performed to address questions related to the stimulation and production phases of geothermal reservoirs (Amann et al., 2017). The stimulations were prepared by detailed geological and geophysical characterization (Doetsch et al., 2017) and extensive measurements of the in-situ stress state and its spatial variation (Krietsch et al., 2017; Gischig et al., 2017). Two sets of shear zones dissect the rock mass, but apart from these persistent large-scale structures, the rock mass contains exceptionally few small-scale fractures. In order to study hydraulic stimulation, both hydraulic shearing (HS) and hydraulic fracturing (HF) experiments were performed. Six injection intervals were chosen to cover pre-existing structures, to generate slip on the pre-existing structures (HS). The other six injection intervals were chosen in intact rock to create new fractures (HF). Both water and a high-viscosity fluid were injected with the aim of studying toughness and viscosity-dominated hydraulic fracture growth.

The rock volume of interest is accessed by a total of twelve boreholes, one of which is used for high-pressure water injection into a 1-m-long interval and four boreholes are used for pressure monitoring. Longitudinal strain along three boreholes is monitored using fibre-optic technology and 26 sensors in tunnels and four boreholes are used to record micro-seismicity (Figure 1). Borehole positions and the sensor locations are optimized for monitoring the pressure propagation and deformation of the rock volume during the HS and HF experiments. A high spatial coverage of sensors from a distances of 3.5 to 30 m with respect to the injection interval provide great detail in observations.

All twelve experiments have been successfully performed in Feb. and May 2017 and all monitoring systems have recorded high-quality data. Data processing is ongoing, but preliminary results already show the exceptional scientific value of the acquired data. The permeability enhancement shows strong variability, ranging from 1 to >1000 fold, with the final injectivities all being within one order of magnitude. Several thousand micro-seismic events have been detected during some of the injections, much fewer in others. Although there is strong variability in the number of events between injections, no apparent link to the change in permeability has been observed. Pressure data show indications of both non-linear pressure diffusion and heterogeneous flow channeling, and rock deformation data clearly show slip on some pre-existing structures and opening of new fractures during the experiments.

The aim of the ISC project was to create a new benchmark data set for the seismic and hydro-mechanical response of hydraulic stimulations. After preliminary analysis of the recordings, we are confident that our data have the potential to act as such a benchmark.

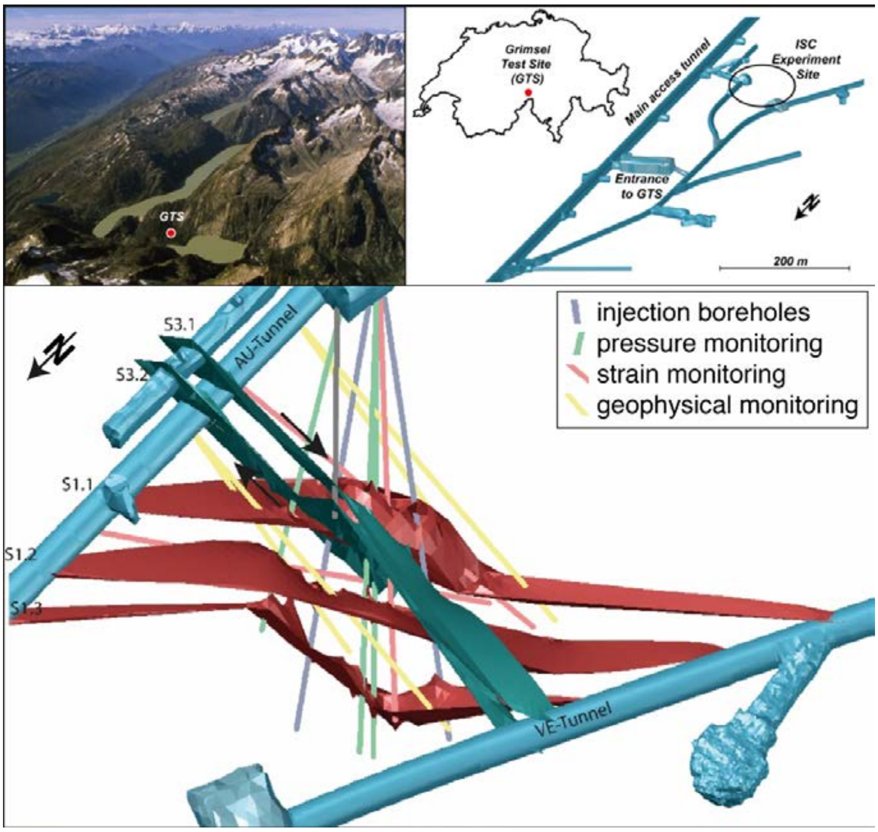

Figure 1: Location of the Grimsel Test Site (GTS), the ISC experiment within the GTS and on overview of the experimental volume. Two sets of shear zones (S1.x and S3.x) dissect the rock mass and have been stimulated. Twelve boreholes access the volume for high-quality monitoring.

REFERENCES

Amann, F., Gischig, V., Evans, K., Doetsch, J., Jalali, R., Valley, B., Krietsch, H., Dutler, N., Villiger, L., Brixel, B., Klepikova, M., Kittilä, A., Madonna, C., Wiemer, S., Saar, M.O., Loew, S., Driesner, T., Maurer, H., Giardini, D., 2017. The seismo-hydro-mechanical behaviour during deep geothermal reservoir stimulations: open questions tackled in a decameter-scale in-situ stimulation experiment. Solid Earth Discuss. 1–55. doi:https://doi.org/10.5194/se-2017-79

Doetsch J, Krietsch H, Lajaunie M, Schmelzbach C, Maurer H, Amann F. GPR imaging of shear zones in crystalline rock. InAdvanced Ground Penetrating Radar (IWAGPR), 2017 9th Inter. Workshop on 2017 Jun 28 (pp. 1-5). IEEE.

Gischig, V.S., Doetsch, J., Maurer, H., Krietsch, H., Amann, F., Evans, K.F., Nejati, M., Jalali, M., Valley, B., Obermann, A., Wiemer, S., Giardini, D., 2017. On the link between stress field and small-scale hydraulic fracture growth in anisotropic rock derived from microseismicity. Solid Earth Discussions 1–40. doi:https://doi.org/10.5194/se-2017-78

Krietsch, H., Gischig, V., Jalali, M.R., Amann, F., Evans, K.F., Doetsch, J. and Valley, B., 2017. Stress measurements in crystalline rock: Comparison of overcoring, hydraulic fracturing and induced seismicity results. In Proceedings of 51st US Rock Mechanics/Geomechanics Symposium.

5.3

Injection Protocol and First Results of Hydraulic Fracturing Experiments at the Grimsel Test Site

Nathan Dutler[1], Benoît Valley[1], Linus Villiger[2], Hannes Krietsch[3], Reza Jalali[3], Valentin Gischig[3], Joseph Doetsch[3] & Florian Amann[3]

[1] *Centre for Hydrogeology and Geothermics, University of Neuchâtel, Rue Emile-Argand 11, CH-2000 Neuchâtel*
[2] *Swiss Seismological Service, ETH Zurich, Sonneggstrasse 5, CH-8092 Zurich*
[3] *Department of Earth Sciences, ETH Zurich, Sonneggstrasse 5, CH-8092 Zurich*

Hydraulic fracturing (HF) is a common method to create artificial fractures and increase the bulk permeability of a rock mass. We aim to study injection parameters, such as injection flow rate and fluid viscosity, and their influence on fracture propagation, fracture geometry and micro-seismicity in crystalline rock.

The HF experiments are part of the in-situ stimulation and circulation project (Amann et al., 2017), which is recently carried out at the Grimsel Test Site. The preceding characterization phase includes a stress characterization campaign (refs).

For the actual experiment, a total of six HF experiments were executed in two boreholes. The injection protocoll consists of three cycles. Prior to testing the integrity of the packed interval was tested with a pressure pulse (i.e. assessment of the pressure decay following the pressure pulse). The measured transmissivity in intact rock ranges from 1e-13 to 1e-14 m^2/s. The objective of the first cycle was to break down the formation (i.e. to initiate a hydraulic fracture) using small flow rates (i.e. 5 l/min injections for 60 s). The second cycle aimed to propagate the hydraulic fracture away from the wellbore and connect it to the pre-existing fracture network using progressively increasing flow rates (up to 100 l/min with an interruption due to pump switch). A shut-in and venting period followed. Finally, a third cycle was utilized to quantify the final injectivity and jacking pressure of the created structure, using a pressure step injection (Amann et al., 2017).

For fracture propagation two different types of fluid were used (Figure 1 A): pure water and a water-xanthan-salt-mixture with 0.025 weight percent of Xanthan and 0.1 weight percent of salt with a viscosity between 35 and 40 cPs (Figure 1 B). Using the xanthan-mixture, cycle 2 is extended with a flushing sequence. Figure 1 shows two injection protocols and pressure response in the injected interval for two different experiments. During stimulation, the monitoring includes pressure observation in boreholes and tunnel surface, micro-seismicity, strain and temperature in boreholes and at the tunnel surface, tilt at the tunnel surface, electric conductivity measurement, gas analysis on fault zone and sampling back-flow. After stimulation, the dislocation was measured in active injection borehole using an acoustic televiewer.

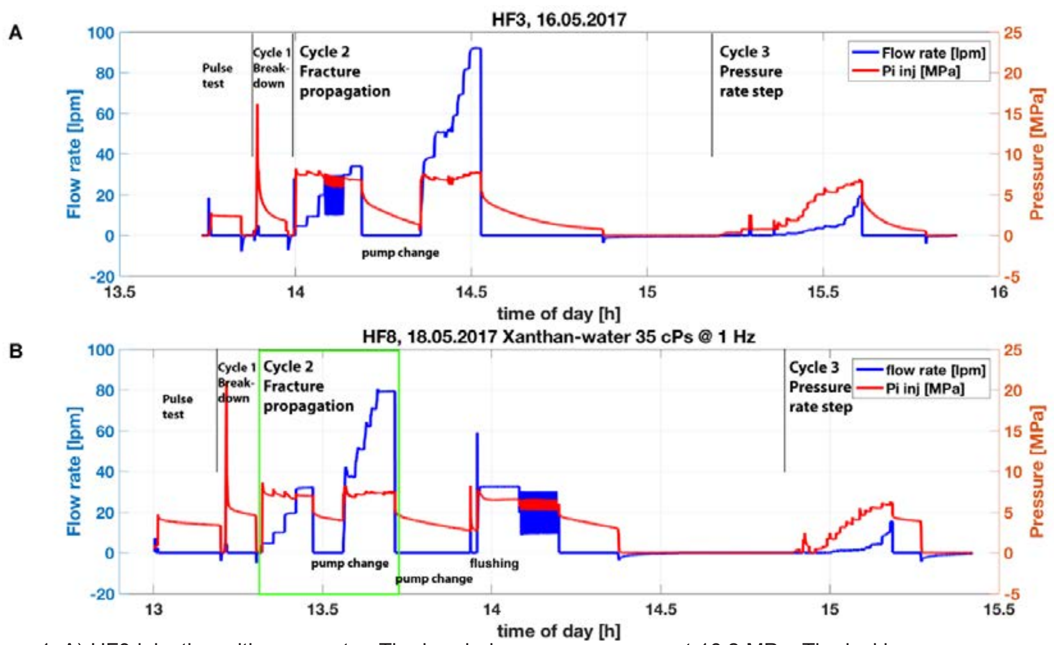

Figure 1: A) HF3 injection with pure water. The break down pressure was at 16.2 MPa. The jacking pressure measures 5.8 MPa and the final injectivity measures 0.88 l/min/MPa. B) HF8 injection with Xanthan-salt-water (green window). The break down pressure was at 21.1 MPa. The jacking pressure measures 5.0 MPa and the final injectivity measures 0.20 l/min/MPa.

REFERENCES

Amann, F., et al. (2017), The seismo-hydro-mechanical behaviour during deep geothermal reservoir stimulation: open questions tackled in a decameter-scale in-situ stimulation experiment. Solid Earth Discuss., https://doi.org/10.5194/se-2017-79

Krietsch, H., Gischig V., Jalali R., Amann F., Evans K. F., Doetsch J., and Valley B. (2017), Stress measurements in crystalline rock: Comparison of overcoring, hydraulic fracturing and induced seismicity results, in *ARMA 51st US Rock Mechanics / Geomechanics Symposium*, edited, San Francisco, California, USA.

Gischig, V.S., Doetsch, J., Maurer, H., Krietsch H., Amann F., Evans, K.F., Nejati, M., Jalali, M., Valley, B., Obermann, A., Wiemer, S. and Giardini, D. (2017), On the link between stress field and small-scale hydraulic fracture growth in anisotropic rock derived from microseismicity. Solid Earth Discuss., https://doi.org/10.5194/se-2017-78

Jalali M.R., Gischig, V., Doetsch, J., Krietsch, H., Amann, F., and Klepikova, M., (2017), Mechanical, Hydraulic and Seismological Behavior of Crystalline Rock as a Response to Hydraulic Fracturing at the Grimsel Test Site, in *ARMA 51st US Rock Mechanics / Geomechanics Symposium*, edited, San Francisco, California, USA.

5.4

Fault structure and porosity distribution in an active hydrothermal system

Daniel Egli[1], Rahel Baumann[1], Sulamith Küng[1], Alfons Berger[1], Ludovic Baron[2] & Marco Herwegh[1]

[1] *Institute of Geological Sciences, University of Bern, Baltzerstrasse 1+3, CH-3012 Bern (daniel.egli@geo.unibe.ch)*
[2] *Institute of Earth Sciences, University of Lausanne, Bâtiment Géopolis, CH-1015 Lausanne*

The geometry of fracture networks and matrix porosity of fault rocks are key parameters controlling the permeability and ultimately the fluid flux along fault zones. On the example of a long-lived and still active fault-bound hydrothermal system, i.e. the Grimsel breccia fault (Hoffmann et al., 2004; Belgrano et al., 2016) in the crystalline basement of the Aar Massif (Swiss Alps), this study aims at understanding the extent, occurrence, dynamics and evolution of natural fluid pathways along faults and their characteristics in hydrothermal zones in particular. Better understanding of such naturally porous and permeable rocks is of prime importance for the successful exploration of natural hydrothermal systems. This study shows continuous structural data and matrix porosity measurements collected from a cored drillhole across the Grimsel breccia fault. A central fault core showing large amounts of fault breccia and gouge material of increased porosity of up to >25% is adjoined by several large subsidiary faults and interconnected by a intensly fractured damage zone. Fracturing is controlled by regularly spaced variations in ductile deformation intensity ranging from granite to ultramylonite. The variable degree of ductile precursory deformation shows a range of matrix porosity values between <0.1 and 7% and thus forms a succession of subparallel sealing and high-porosity structures bridged by a dense fracture network. Fluid flow is therefore directly related to the combined effect of fractures and enhanced fault-related matrix porosity. In this specific setting, the width of the damage zone exceeds the distance between the large scale faults that can be observed on the surface and which are characterized by a regular increase in fracture density. However, of several such parallel fault zones, the Grimsel breccia fault is the only one showing enhanced heat flow. This suggests a key importance of matrix porosity within fault core rocks (breccia & fault gouge) for the transport of hydrothermal fluids as an enhanced fracture network alone is not providing sufficient permeability in the case of this natural hydrothermal system.

REFERENCES

Belgrano, T.M., Herwegh, M. & Berger, A. 2016: Inherited structural controls on fault geometry, architecture and hydrothermal activity: an example from Grimsel Pass, Switzerland. Swiss J. Geosci. 1-20.

Hoffmann, B.A., Helfer, M., Diamond, L.W., Villa, I.M., Frei, R. & Eikenberg, J. 2004: Topography-driven hydrothermal breccia mineralization of Pliocene age at Grimsel Pass, Aar massif, Central Swiss Alps. Schweiz. Mineral. Petrogr. Mitt., 84, 271–302.

5.5

The stochastic modelling of large basement seismicity during fluid injection in sedimentary horizons

Barnaby Fryer[1], Lyesse Laloui[1]

[1] *Soil Mechanics Laboratory – Chair "Gaz Naturel" Petrosvibri, Station 18, Swiss Federal Institute of Technology in Lausanne, Route Cantonale, 1015 Lausanne, Switzerland (barnaby.fryer@epfl.ch)*

In the last few years, earthquakes which have been attributed to waste-water injection have been felt at the surface in the continental United States. These earthquakes have been primarily occurring in the crystalline basement rock located below the injection interval and not the injection interval itself. As waste-water injection is fairly analogous to CO_2 storage in deep saline aquifers, this kind of seismicity could potentially become an issue for large-scale CO_2 storage; indeed, minor seismicity in crystalline basement rock during CO_2 storage has already been seen (Goertz-Allmann et al., 2017).

Previous studies have modelled fluid injection above crystalline basement rock and shown that seismicity can occur in the basement, at times even without fluid pressurization (Chang and Segall, 2016). This study, however, quantifies the relative chance of large events occurring in the basement rock. The premise is essentially that basement rocks typically have larger shear moduli and shear strength allowing them to support larger differential stresses (Vilarrasa and Carrera, 2015).

Because differential stress is inversely proportional to the Gutenberg-Richter b-value (Schorlemmer et al., 2005), this means that seismicity in basement rocks has the potential to exhibit much lower b-values than in typical reservoir rocks.

Further, because crystalline basement is also more likely to be critically stressed than sedimentary layers (Vilarrasa and Carrera, 2015), a much smaller change in effective stress is required to induce seismicity in the basement than in the reservoir. The larger differential stresses in the basement rock and its stress criticality mean that seismicity is not only predicted to occur in the basement rock, it is predicted to have a disproportionately high number of large seismic events.

In order to test this hypothesis, the theory of linear poroelasticity was used to produce pore pressure and stress perturbations for a typical injection scheme before a semi-analytical variant of the seismicity model originally presented by Layland-Bachmann et al. 2012 was used to quantify the potential of large events in both the reservoir and basement rock.

This work has been supported by a research grant (SI/500963-01) of the Swiss Federal Office of Energy. The authors are also grateful for the helpful input of Dr. Gunter Siddiqi.

REFERENCES

Chang, K. and Segall, P. 2016: Injection-induced seismicity on basement faults including poroelastic stressing. Journal of Geophysical Research, 121:2708–2726. doi:10.1002/2015JB012561

Goertz-Allmann, B., Gibbons, S., Oye, V., Bauer, R., and Will, R. 2017: Characterization of induced seismicity patterns derived from internal structure in event clusters. Journal of Geophysical Research - Solid Earth, 122:3875–3894. doi:10.1002/2016JB013731

Layland-Bachmann, C., Wiemer, S., Goertz-Allmann, B., and Woessner, J. 2012: Influence of pore-pressure on the event-size distribution of induced earthquakes. Geophysical Research Letters, 39. doi:10.1029/2012GL051480

Schorlemmer, D., Wiemer, S., and Wyss, M. 2005: Variations in earthquake-size distribution across different stress regimes. Nature, 437:539–542. doi:10.1038/nature04094

Vilarrasa, V. and Carrera, J. 2015: Geologic carbon storage is unlikely to trigger large earthquakes and reactivate faults through which CO2 could leak. Proceedings of the National Academy of Sciences, 112:5938–5943. doi:10.1073/pnas.1413284112

5.6

A decade of unconventional exploration in Europe – where are we now

Piotr Gawenda

IHS Markit Ltd, 24 chemin de la Mairie, CH-1258 Perly (GE)
(piotr.gawenda@ihsmarkit.com)

An unprecedented rise of oil and gas production from unconventional reservoirs in the US has radically changed the view of the hydrocarbon prospectivity of petroleum provinces in Europe. As many European basins were found to be promising for unconventional exploration, a licensing boom occurred between 2006 and 2011: operators of all sizes, from majors through mid-size independents to niche players acquired acreage in the region - valid contracts covered the entire area believed to be prospective (Fig. 1a).

Resulting, pursuits of “shale gas“ and coal-bed methane commenced in Austria, Bulgaria, Czech Republic, France, Germany, Lithuania, Poland, Romania, Spain, Sweden and Switzerland. Shale oil operations started in France, heavy oil project continued in Albania, while Estonia kept mining oil shales. New projects exploring “tight“ sandstones were started in Hungary and Poland.

The primary targets of operation covered the Lower Palaeozoic successions, the Carboniferous coal series and the Mesozoic organic-rich mudstone units.

The first wells for unconventional purposes were drilled in 2008 in northern Germany, attesting potential of the Jurassic Posidonia series. Some 90 wells were subsequently completed. Of this number, more then 60 wells targeted the Lower Palaeozoic series along the edge of the East European Platform in Sweden, Denmark and Poland.

Operations in Sweden, aiming at the Cambrian Alum series, have shown that the succession holds residual gas, while a well in Denemark intercepted a poor quality reservoir. The Baltic Basin in Poland, seen as one of Europe’s most promising areas of unconventional exploration, attracted the bulk of attention. Over 50 wells were spudded during 2010-2015 to evaluate the Upper Cambrian-Lower Ordovician Piasnica Formation (Alum equivalent), the Middle-Upper Ordovician Sasino Formation, the Lowermost Silurian Jantar Member (Paslek Formation) and their lateral equivalents in the Lublin Basin to southeast. The results of the wells have proven that the prospective successions are hydrocarbon-bearing and extraction could be feasible in places. However, multiple fracture stimulations and tests conducted even in the horizontal sections failed to deliver commercial flow rates.

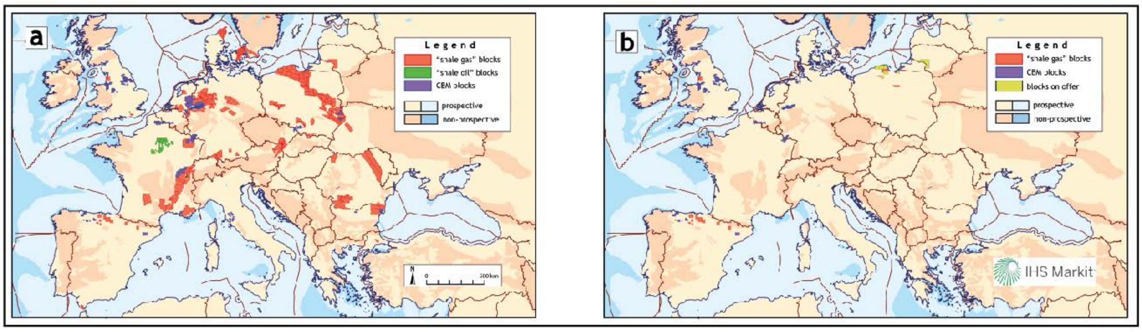

Figure 1. Map of Europe displaying (a) contracts/applications for unconventional exploration in early 2011 and (b) in 2017.

As the exploration efforts unfolded, the legislators in several European countires enacted new rules for unconventional activities: the search for “shale gas” was banned in France and Bulgaria, while moratoriums on operations were imposed in Switzerland and the Netherlands. Many projects were discontinued in Austria, Czech Republic and Spain, while in Germany the use of hydraulic fracture stimulation in hydrocarbon exploration was barred pending future revision.

Owing to disappointing results of the early exploration phase, growing fiscal and environmental uncertainty triggered by the legal actions impairing or prohibiting operations, as well as due to devastating results of prolongued low commodity price, coupled with structural transformations in the larger energy market, virtually all active players pulled out of European unconventional exploration by mid-2016 (Fig. 1b).

Although a few contracts with the relevant targets still remain valid, the plans to unlock their potential are either abandoned or suspended. In mid-2017, the only developments in the unconventional scene were reported in Poland and the UK.

Notwithstanding the operational and commercial setbacks, exploration activities of the years 2006-2016 have delivered a new scientific input into the geological development of several European basins, some of which were dormant for decades. Newly acquired seismic and well data provided key insight into the structure of the subsurface, prompting in places a major redefinition of the vintage geological and petroleum models. Ongoing hydrocarbon exploration progressively focuses on the low-porosity/low-permeability zones.

Applying new geological facts, the authorities in e.g. Poland and Lithuania have selected acreage with unconventional targets for licensing that may commence in 2018. Assuming favourable macroeconomic environment, a new round of unconventional exploration in Europe could be envisioned.

5.7

Pressure propagation during decameter-scale hydraulic stimulation experiments in crystalline rock at the Grimsel Test Site

Valentin Gischig[1], Mohammadreza Jalali[1], Joseph Doetsch[1], Hannes Krietsch[1], Linus Villiger[1], Florian Amann[1]

[1]Swiss Competence Center for Energy Research, ETH Zurich, Sonneggstrasse 5, 8092 Zurich (gischig@erdw.ethz.ch)

The nature of pressure propagation in fractured rock during hydraulic stimulations is being debated in the context of enhanced geothermal systems and induced seismicity. It has been suggested that flow is non-linear due to permeability enhancement during stimulation (Murphy et al., 2004) and channelized due to the heterogenous nature of rock fractures (e.g., Nicol and Robinson, 1990). The In-situ Stimulation and Circulation experiment (ISC) recently performed at the Grimsel Test Site (Amann et al., 2017) gives new insights into these and other flow processes on a decameter scale due to numerous pressure monitoring locations surrounding the injection borehole interval. We present and compare pressure evolution across a series of six hydraulic stimulation experiments. We observe that for most experiments the pressure response at distances of only few meters from the injection point reached only a fraction of the maximum injection pressure unlike expected from a pulse-like pressure propagation typical for non-linear pressure diffusion (Murphy et al., 2004). Injectivity estimates before and after the stimulations show that permeability has changed by two to three orders of magnitude, which indicates that non-linear pressure diffusion must have occured in the rock mass but has not been detected during most experiments. Seismic velocity changes gained from active seismic experiments show a linear relationship between pressure variations and seismic slowness changes at the pressure monitoring intervals. Thus, time-lapse 3D images of seismic velocity changes reveal the spatial and temporal evolution of pressure changes that are much below the actual injection pressure. In contrast, high-pressure pulses are not detected from slowness images. Additionally, insights into pressure evolution are obtained from a comparison with the distribution of induced microseismicity. Seismic events are strongly grouped in clusters associated with asperities that might illuminate preferntial flow channels. We suspect that non-linear pressure diffusion occurs along strongly localized channels that are often not sampled by the pressure monitoring points. The results of an extensive hydraulic characterization before and after the stimulation confirm the existance of such distinct preferential flow paths and possibly new ones created by stimulation. Our observations indicate that flow during stimulation in a natural fracture system may be both strongly heterogenous and non-linear. Such a degree complexity has to be anticitpated for designing and modeling full-scale hydraulic stimulations in deep geothermal reservoirs.

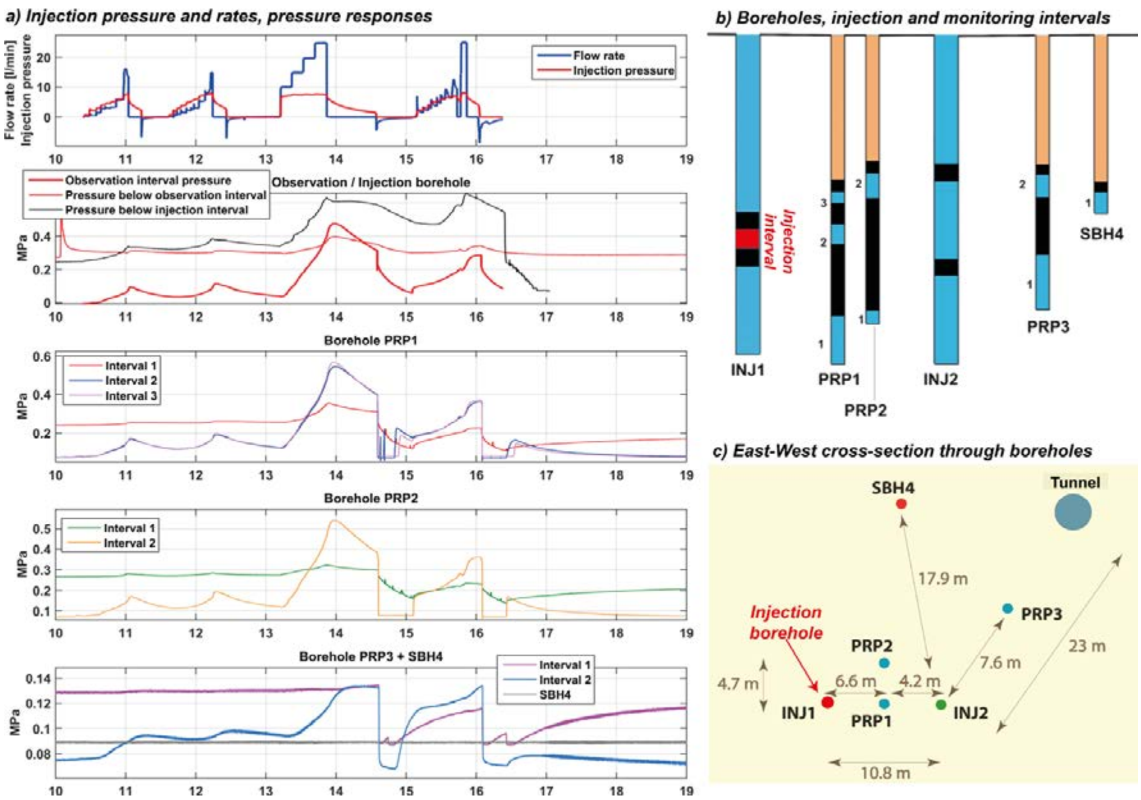

Figure 1: a) Time series of pressure monitoring during hydraulic stimulation at an interval at 27.2 - 28.2 m depth of borehole INJ1. b) Injection and pressure monitoring concept in six boreholes. c) Geometrical relatioship between boreholes along a vertical cross section in EW direction.

REFERENCES

Amann, F, et al. (2017), The seismo-hydro-mechanical behaviour during deep geothermal reservoir stimulation: open questions tackled in a decameter scale in-situ stimulation experiment. Solid Earth Discuss., http://doi.org/10.7194/se-2017-79

Murphy H., C. Huang, Z. Dash, G. Zyvoloski, A. White (2004). Semi-analytical solutions for fluid flow in rock joints with pressure-dependent openings. Water Resources Research 40, W12506.

Nicol, D. A. C., and B. A. Robinson (1990), Modelling the heat extraction from the Rosemanowes HDR reservoir, Geothermics, 19, 247-257.

5.8

Alteration of hydrogeochemical properties during reactive flow-through experiments on sandstone specimen using CO_2-charged brine

Xiang-Zhao Kong[1,1], Jin Ma[1], Martin O. Saar[1]

[1] Institute of Geophysics, ETH-Zurich, Sonneggstrasse 5, 8092 Zurich, Switzerland
([1]Corresponding author's email: xkong@ethz.ch)

Utilization of underground reservoirs for geothermal energy extraction, particularly using CO_2 as a working fluid, requires an in-depth understanding of fluid, solute (e.g., dissolved CO_2 and minerals), and energy (heat, pressure) transport through geologic formations. Such operations necessarily perturb the chemical, thermal, and/or pressure equilibrium between native fluids and rock minerals. The involved physico-chemico-thermo-mechanical processes often lead to modifications of permeability and cause immense consequences for fluid, solute, and energy transport, injectivity, and/or withdrawal in/from such reservoirs. Here we report evolutions of permeability and water chemistry observed in core-flood experiments using CO_2-charged fluids under formation conditions. During the experiments, fluids were injected at constant flow rates in a recycling mode where outlet fluids were re-injected into the specimen. This allows us to examine geochemical reactions from far-from-equilibrium to equilibrium. We also analysed the outlet fluid chemistry samples throughout the experiments and imaged our rock cores before and after the flow-through experiments using X-Ray Computed Tomography (XRCT). Water chemistry indicates precipitation of secondary minerals during the experiments. Together with SEM and XRCT data, we are able to interpret the changes in permeability, porosity, and (reactive) surface area at the core scale. Moreover, we will present numerical modelling results of 1D reactive transport through the same setup as the experiments to faciliate the understanding of alteration of hydrogeochemical properties.

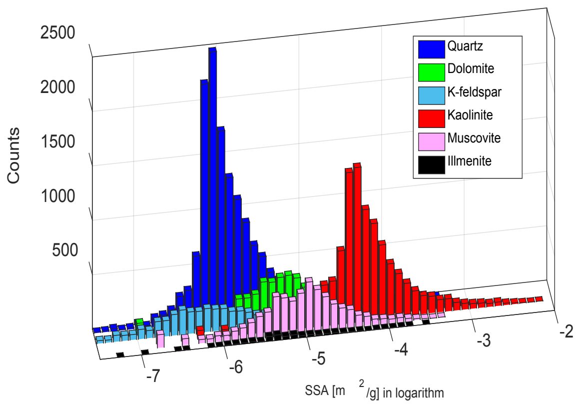

Figure 1. Mass-specific surface area (SSA) distributions of six minerals in a sandstone sample. Here the SSA distribution is pore-wised.

5.9

Mechanical response of a decameter-scale reservoir during an in-situ hydraulic stimulation experiment

Hannes Krietsch[1], Valentin Gischig[1], Joseph Doetsch[1], Benoit Valley[2] & Florian Amann[1]

[1] *Swiss Competence Center for Energy Research, ETH Zurich, Sonneggstrasse 5, 8092 Zurich (hannes.krietsch@erdw.ethz.ch)*
[2] *Center for Hydrogeology and Geothermics, University of Neuchâtel, Emile-Argand 11, 2000 Neuchâtel.*

The decameter-scale In-situ Stimulation and Circulation (ISC) experiment has been recently carried out at the Grimsel Test Site (GTS) (Amann et al, 2017). In February 2017, six hydraulic shearing experiments were conducted on pre-existing shear zones and fractures. To measure the spatial mechanical response of the rock mass and fractures distributed in the experimental volume, a total of 60 Fibre-Bragg Grating (FBG) sensors with baselengths of 1 m were distributed in three differently orientated boreholes. The FBG sensors have a resolution of 0.1 µstrains and an accuracy of 1 µstrain. Additionally, three tiltmeters, measuring the deviation from horizontal in two axes with a sensitivity of 0.1 µradians, are positioned in a tunnel west of the test volume. In this contribution, we present first results from the data analysis of the strain and tilt measurements.

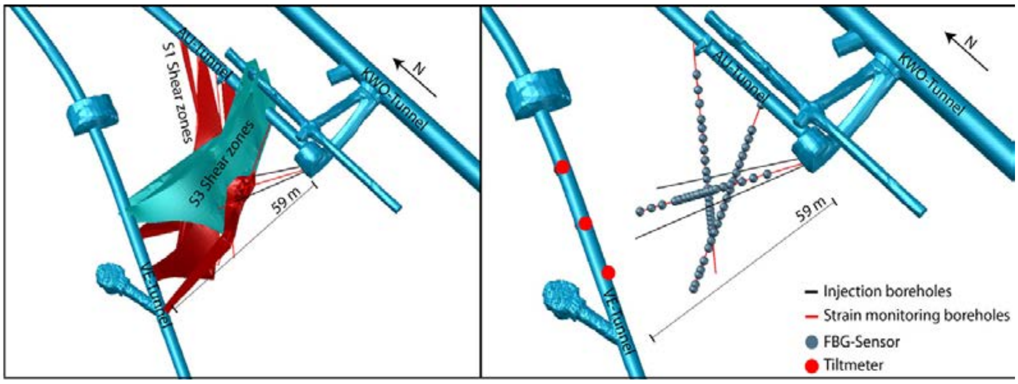

Figure 1. Three dimensional model of the experimental volume. Left: Main shear zones are shown with strain monitoring and injection boreholes. Right: The FBG-sensor and tilt meter locations are indicated along the boreholes and in the tunnel.

The strain data captured by the FBG system shows a strong dependence of the strain magnitude on the distance to the injection point (Figure 2). Closest to the injection point (around 4 m away), strains of 400 to 500 µstrain have been reached (Figure 2). Besides the distance, also the number of fractures across the base length of the FBG sensors influences the measured strain magnitude. The transient 3D strain field is analyzed by visualizing the maximum (compressional or tensional) and permanent strains observations. Additionally, the ratio between maximum and permanent strains are used to qualitatively infer the relative importance of normal opening or slip along the monitored fractures.

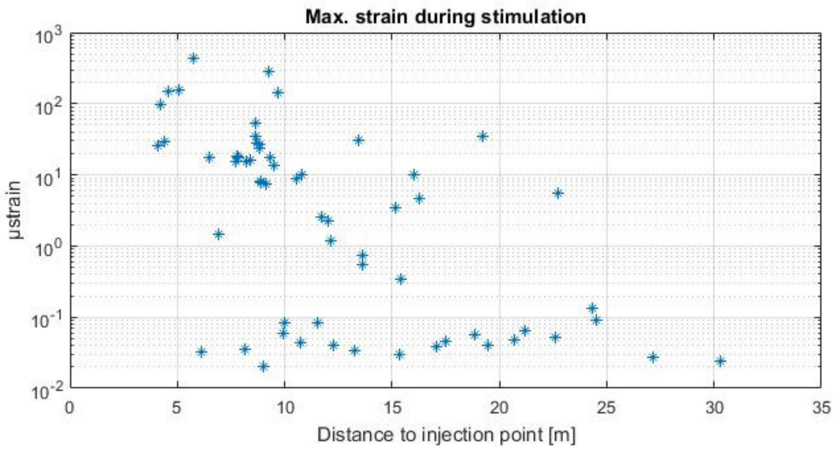

Figure 2. Maximum strains during stimulation experiment. A decrease of strain with increasing distance to injection point can be observed.

The mechanical response of the fractures due to high pressure fluid injection is strongly dependent on the in-situ stress field. Therefore, the dilation and slip tendency were calculated for each fracture based on the estimated in-situ stress field (Krietsch et al, 2017). These tendencies may give additional hints on whether a fracture was reactivated by dilation or slip movement.

During most of the experiments the tiltmeters indicate an expansion of the test volume with increasing injected fluid volume, as they all show a general tilt towards west. Considering the NS tilt component we find two distinct behaviors possible related to reactivation of different shear zones (S1 or S3, Figure 1). We are able to infer the orientation of the stimulated structure, by modelling the expected tilt associated with a normal opening across faults with different orientation using a three dimensional finite element model, in which normal opening is uniformly distributed across penny-shaped faults.

As a next step the mechanical response will be analyzed in greater detail by considering the measured pressure propagation as source.

REFERENCES

Amann, F, et al. (2017), The seismo-hydro-mechanical behaviour during deep geothermal reservoir stimulation: open questions tackled in a decameter scale in-situ stimulation experiment. Solid Earth Discuss., http://doi.org/10.7194/se-2017-79

Krietsch, H., Gischig, V., Jalali, R., Amann, F., Evans, K.F., Doetsch, J., and Valley, B. (2017), Stress measurement in crystalline rock: Comparison of overcoring, hydraulic fracturing and induced seimicity results. ARMA 51st US Rock Mechanics/Geomechanics Symposium, San Francisco, California, USA.

5.10
AGEPP – First swiss hydrothermal well for electricty and heat production

Jean-Marc Lavanchy[1]

[1]CSD Ingénieurs SA, Chemin de Montelly 78, 1007 Lausanne (jm.lavanchy@csd.ch)

The AGEPP project consists in a single 2'300 to 3'000 m deep geothermal well. It aims at exploiting the renewable geothermal energy present in Lavey (canton of Vaud), one of the best known sites in Switzerland in terms of geothermal potential. Indeed, a geothermal resource was discovered in Lavey during the 19th century. The geothermal water is currently pumped via two wells of 200 and 600 m deep and feeds the thermal complex of Les Bains de Lavey.

For the AGEPP project, water will be pumped from the aquifer located in highly permeable naturally fractured cristalline rocks (gneiss). Water at 110°C (at the drill head) is expected to be pumped at a rate of 40 l/s. These conditions will enable the production of 4.2 GWh of electricity and 15.5 GWh of heat. In the long run, the residual energy could be used for district heating, greenhouses, fish farming, etc.

The main milestones of 2015 to 2017, in extension of the former studies performed several years before, consisted in the realisation of additional technical studies, the actualisation of the business plan, the confirmation of private and public financing, the funding from the OFEN and the Canton of Vaud, the creation of AGEPP SA, the review process by the authorities to obtain the authorizations for the drilling and operation phases, according to partly new requirements.

This presentation will highlight the current state of the project as well as the results of geoscientific studies conducted with a panel of experts (structural geology, hydrogeological conceptual model and hydromodeling results, natural sismicity as well as risk analysis and risk management concerning possible induced sismicity, etc.).

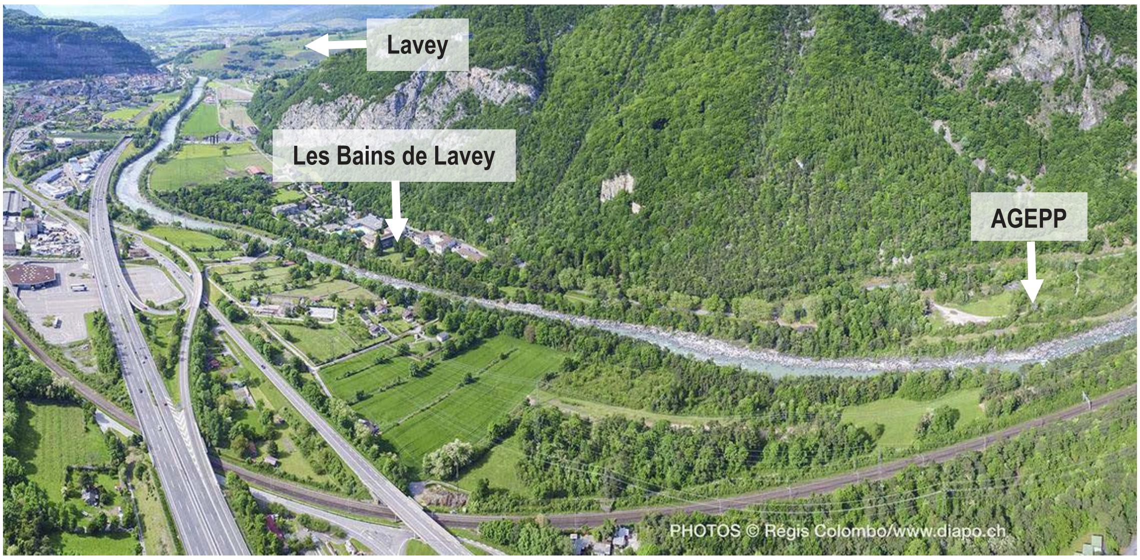

Figure 1 : Localisation of the AGEPP project within the Rhône Valley

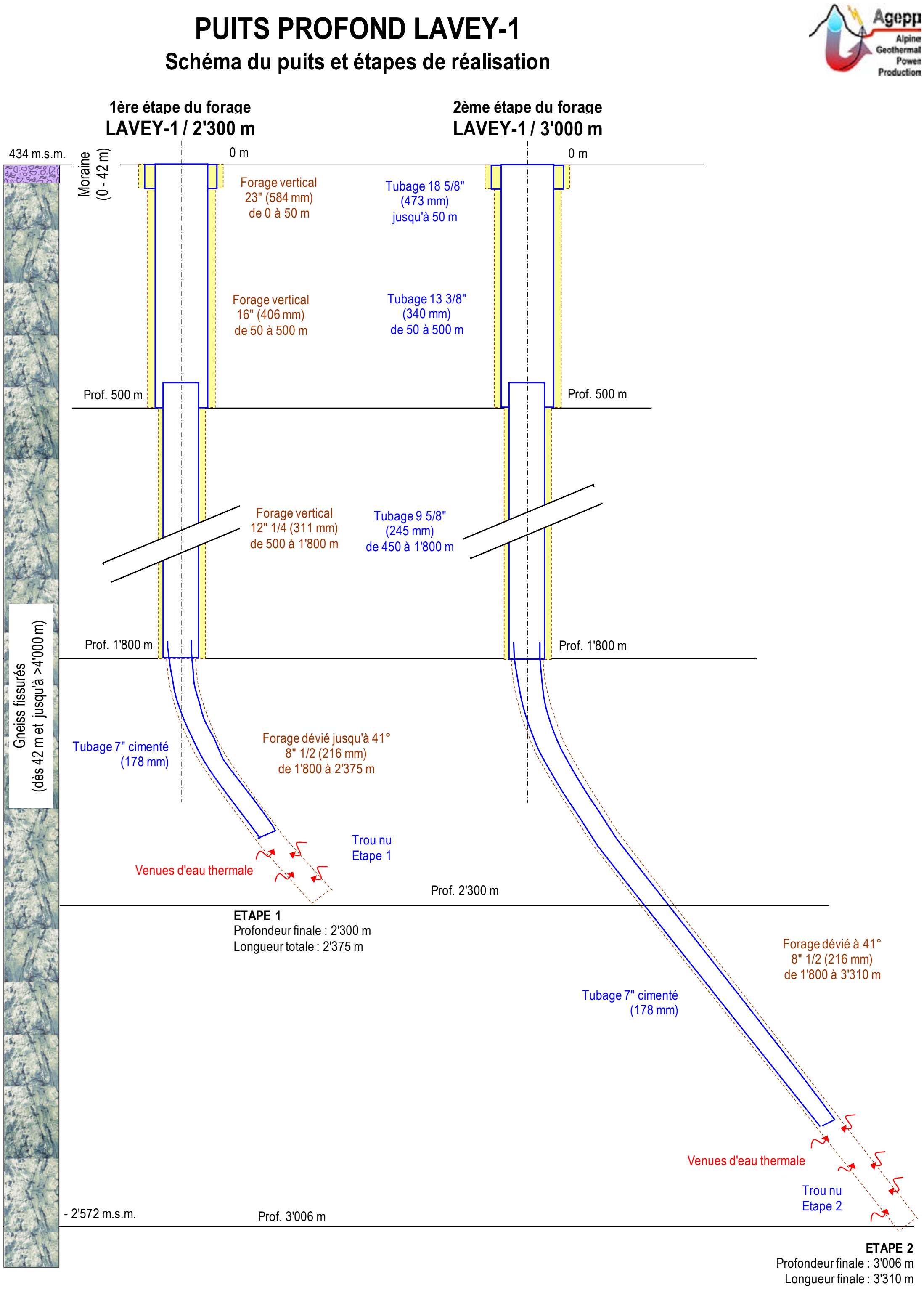

Figure 2 : AGEPP – Sectional drawings of the hydrothermal well (2 scenarii: 2'300m and 3'000m)

5.11

Experimental study on the swelling behaviour of a gas shale

Alberto Minardi[1], Alessio Ferrari[1], Russell Ewy[2], Lyesse Laloui[1]

[1] *Laboratory for Soil Mechanics – Chair "Gaz Naturel" Petrosvibri, Swiss Federal Institute of Technology, EPFL, Station 18, Lausanne, Switzerland (alberto.minardi@epfl.ch)*
[2] *Chevron Energy Technology Co., Richmond, CA, USA*

Water loss during flowaback operations represents one of the main environmental concerns related to the use of hydraulic stimulation to exploit unconventional shale gas reservoirs. Among the main involved causes, the water uptake by the rock reservoirs plays a major role. The presence of clay minerals in the composition of gas shales makes these geomaterials capable to absorb a great amount of the injected fracturing fluids. To quantify the water uptake in gas shales, imbibition tests are typically performed at the laboratory scale. These tests foresee the immersion of gas shale specimens in water (or other fluids) with the following assessment of the amount of imbibed water through the measurement of the weight variation of the specimen.

Despite the importance of imbibition tests for the upscaling of imbibition data at the reservoir scale, two fundamental aspects are usually neglected. Firstly, as typical of shales (Ferrari et al. 2014; Minardi et al. 2016), also gas shales might exhibit a significant expansion during the imbibition process which may significantly affect the amount of imbibed water. Secondly, the swelling observed in the laboratory might not be representative of the response experienced by the material under reservoir conditions; indeed, the presence of the in-situ stress is expected to play a major role in controlling the expansion of the material. Hence, running imbibition tests without accounting for these two aspects may lead to a misleading quantification of the amount of imbibed water by the shale gas reservoir.

This work aims to show the different swelling response of a gas shale when subjected to an imbibition process under free and stressed conditions. A testing set-up and an experimental methodology have been developed to assess the volumetric response of the tested gas shale duirng the imbibition process with and without the application of a mechanical stress. Imbibition process is performed through the exposition of the tested specimens to a controlled relative humidity air and the direct contact with deionized water.

Obtained experimental results show clearly the impact of the volumetric swelling on the imbibed amount of water when the tests are performed without any mechanical tress. Neglecting the volumetric expansion of the tested material leads to a significant excess of imbibed water (up to 40%). Moreover, even if the volumetric swelling is properly considered, an overestimation of the amount of imbibed water is obtained in free stress conditions. Indeed, experimental results from imbibition tests performed under stress highlight a significant lower swelling response of the material with respect to free stress conditions. Figure 1 shows an example of experimental results where the volumetric behaviour exhbited by two specimens which undergone the same imbibition process but in different stress conditions is compared; the application of an axial stress of 7 MPa to the tested specimen reduces its volumetric swelling by more than 50% with respect to the specimen tested without mechanical stress. As a consequence of this different response, a lower amount of imbibed water is expected when an imbibition process is performed under stress.

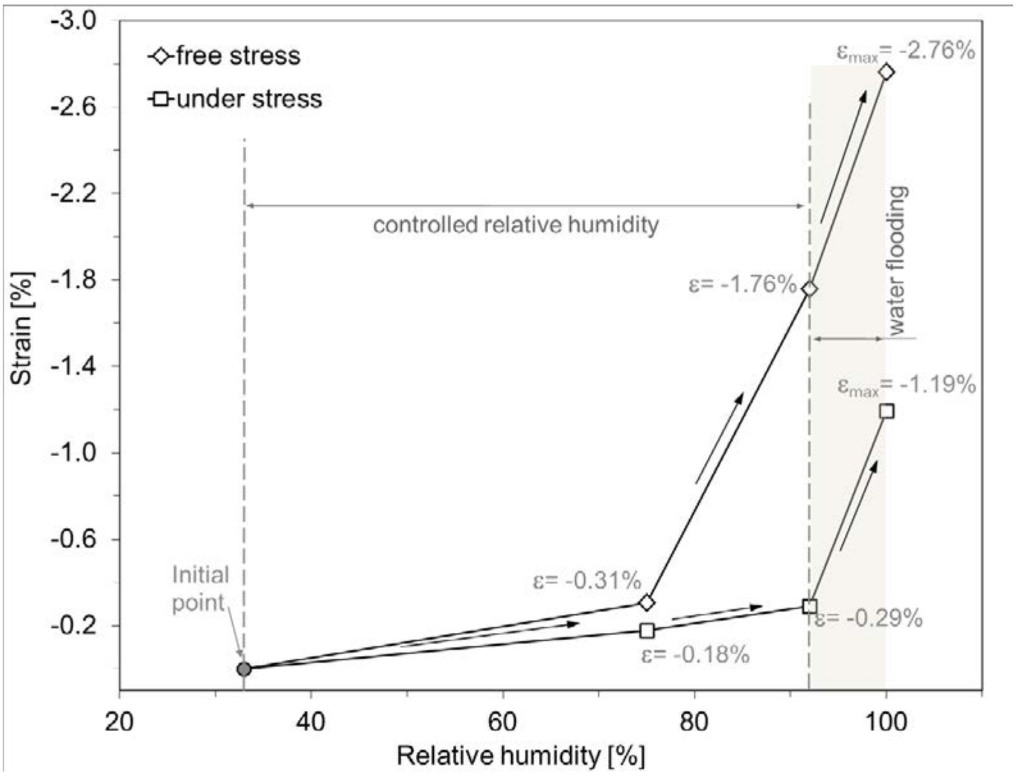

Figure 1. Comparison of the swelling behaviour under free and stressed conditions of two gas shale specimens.

REFERENCES

Ferrari A, Favero V, Marschall P, Laloui L, (2014). Experimental analysis of the water retention behaviour of shales. International Journal of Rock Mechanics and Mining Sciences. 72, pp. 61–70.

Minardi, A., Crisci, E., Ferrari, A. and Laloui, L., 2016. Anisotropic volumetric behaviour of Opalinus clay shale upon suction variation. Géotechnique Letters, 6(2), pp.144-148.

5.12

Acoustic Emission Monitoring of Fractures in Opalinus Clay Shale

Zabihallah Moradian[1,2]

[1] *Department of Civil and Environmental Engineering and Earth Resources Lab (ERL), Massachusetts Institute of Technology (MIT), Cambridge, MA, USA*
[2] *Engineering Geology, Institute of Geology, Swiss Federal Institute of Technology (ETH), Zurich, Switzerland (zabihallah.moradian@erdw.ethz.ch)*

Cracking and failure behavior of Opalinus clay shale (OPA), as a candidate for hosting nuclear wastes, have been highly investigated over last years. Microseismic monitoring of the fractures provides a good estimation of the cracking processes, as well as the produced fracture network. However, data obtained from different experimental studies on OPA illustrats that the cumulative microseismic events only reflect a small fraction of the rock damage. In addition, this small portion of the microseismic data shows a very wide and dispersed zone of activity instead of imaging the actual fracture network. An essential task is to understand whether the silence in the microseismic activity and the scatter in the microseismic locations are real and therefore must be taken into account, or they are due to uncertainties associated with the microseismic technique.

Several factors such as fracture processes (tensile splitting, sliding along bedding, stress perturbation in pores), wave propagation (attenuation, anisotropy in the velocity model) and data collection (sensor array, sensitivity, frequency range) are responsible for these behaviors. Using scanning electron microscopy (SEM), acoustic emissions (AE) and stress-strain data, the nucleation and propagation of fractures in OPA were investigated in micro- and macro scales. The objective was to see how fracture processes are responsible for aforementioned issues with the microseismic response of OPA.

The results demonstrated that OPA is seismically silent because 1) it contains high clay content, around 75% (the more clay content, the less it produces seismicity), 2) cracking is mostly intergranular, in the clay matrix with lower energy rather than intragranular through grains such as pyrite or calcite, 3) fracturing mostly happens along bedding planes with gradual AE release and low breakdown pressures which create less number of AEs with low energies.

Source locations were found to be dispersed because 1) many events are generated from reactivating natural fractures and bedding planes that are distributed throhout the rock, 2) stress perturbations in the pores and fossil locations produce disperse seismic events, 3) a complex fracture network is created due to bedding angles and heterogeneity and finally, 4) process zones at the tip of the fractures produce a disperse cloud of microseismic events.

Using a denser sensor array with a good geometric coverage of the fracture zone, employing sensors with higher sensitivity (higher signal to noise ratio (SNR)), attaching sensors closer to the fracture point, taking into account the attenuation and using an anisotropic velocity model for source locations can improve the results considerably.

5.13

In-situ observations of fault leakage during a semi-controlled fault activation (FS) experiment, Mont Terri rock laboratory, Switzerland

C. Nussbaum[1], Y. Guglielmi[2], P. Jeanne[2] and J. Birkholzer[2]

[1]*Federal Office of Topography, Swisstopo, Seftigenstrasse 264, CH-3084 Wabern (Switzerland)*
[2]*Lawrence Berkeley National Laboratory, Earth and Environmental Science Area, 1 Cyclotron road, M/S 74R316C, Berkeley, CA 94720*

Underground carbon dioxide (CO_2) injection and storage may result in enhanced fault permeability, potentially inducing fluid leakage from the injection zone through overlying caprock, and possibly triggering shallow earthquakes. Fault slip can also be triggered by fluid injection inducing seismicity and an increase in fault-zone permeability. Therefore, it is crucial to better understand the processes of fault reactivation with in-situ experiments. Here we present measurements of fault rupture, permeability variation, and seismicity induced by fluid injection in a mature fault affecting the low-permeable Opalinus Clay (Mont Terri underground rock laboratory, Switzerland) at an overburden depth of 300 m. We monitored the fault zone to detect potential displacement and estimated the associated fault leakage and induced seismicity. We used two probes for this experiment: one on the Main Fault slip surface and one at the injection source. The latter was moved to four different locations to test the fractured host rock above and below the fault, the fault fracture damage zone, and the fault core that is composed of scaly-clay fabric. We applied the step-rate injection method and synchronously monitored pressure, flow rate, and 3D fault displacements. From these measurements, we estimated changes in elastic modulus, permeability, and local variations in the effective stress state through time.

Inside the fault, shear-slip occurred and a magnitude ~-2.5 seismic event was triggered following an aseismic slip period. Outside the fault zone, we detected normal aseismic openings. All tests displayed a sharp increase in permeability from 10^{-16} to 10^{-12} m^2 above the water-entry pressure, which was significantly less (~-0.8MPa) inside the fault core compared to outside the fault. This different reactivation behaviour is related neither to the state of stresses nor to the orientation of pre-existing discontinuities relative to the direction of local effective stress, which is almost the same in all four tests. We explain this behaviour as reflecting strong contrasts in rock-type properties. Indeed, we calculate a decrease in Young's modulus from the host rock to the damage zone by a factor 5 and from the damage zone to the fault core by a factor 2. In the host rock, our results are in reasonable agreement with laboratory data showing a strong elastic anisotropy characterized by the direction of the plane of isotropy parallel to the laminar structure of the shale formation. In the fault zone, we observe strong rotations of the direction of anisotropy. The plane of isotropy can be oriented either parallel to bedding (when few discontinuities are present), parallel to the direction of the main fracture family intersecting the zone, and possibly parallel or perpendicular to the fractures that are critically oriented for shear reactivation.

From the results of this experiment we infer that large fault permeability variations are associated with infra-mm dilatant slip pulses. The aseismic component induced by fluid pressure drives low-level seismicity within the pressurised zone. However, we note that passive seismic monitoring may give an incomplete picture of a fault's status. Implementation of complex permeability monitoring in comparison with a critical shear relationship could help to refine the analyses. In addition, complementary monitoring of pressure difference transients and active seismic imaging appear to be promising ways to advance research and to better assess potential for fault leakage.

5.14

Two pathways of silica scaling inside a high-enthalpy geothermal power plant

Daniela B. van den Heuvel[1,2], Einar Gunnlaugsson[3], Ingvi Gunnarsson[3], Tomasz M. Stawski[2,4], Larryn W. Diamond[1], Liane G. Benning[2,4]

[1] *Institut of Geological Sciences, University of Bern, Baltzerstrasse 1+3, CH-3012 Bern (daniela.vandenheuvel@geo.unibe.ch)*
[2] *School of Earth & Environment, University of Leeds, Leeds, LS2 9JT, United Kingdom*
[3] *Reykjavik Energy, Baejarhals 1, 110 Reykjavik, Iceland*
[4] *German Research Center for Geosciences, GFZ, 14473, Potsdam, Germany*

Amorphous silica (SiO_2) precipitation or scaling has been identified as one of the most common problems in high-enthalpy geothermal systems and is a major issue limiting the efficiency of geothermal energy production. Despite the impact of silica scaling, no universally applicable solution to prevent silica precipitation is available yet. In order to improve mitigation techniques, the understanding of the pathways and mechanisms of amorphous silica precipitation inside geothermal power plants has to be advanced.

In this study we describe the microtextures of amorphous silica scale from the Hellisheiði power station (SW-Iceland) in order to evaluate the precipitation mechanism. Our results revealed that there are two independent mechanisms of silica precipitation occurring concurrently: (1) direct deposition of monomeric silica onto equipment surfaces (= heterogeneous nucleation) resulting in the formation of a dense, botryoidal layer which grows in thickness over time and (2) the formation of silica particles through homogeneous nucleation in the fluid, growth and subsequent aggregation and cementation to form mm-sized fan- and ridge-shaped structures growing towards the flow. Direct deposition was found to primarily depend on the concentration of dissolved silica as well as temperature. The precipitation rates were found to be up to 1 g day^{-1} m^{-2} at 120°C and nearly 800 ppm SiO_2. While homogeneous nucelation and particle growth were controlled by the same parameters, particle deposition was contolled by the number of particles in the fluid and by the flow rate. No rate could be determined. In addition to number of particles and flow rate, the salinity of the fluid has a major impact on the aggregation behaviour. Thus it is expected that the homogeneous pathway of particle formation and aggregation will be dominant in the saline geothermal systems of the European sedimentary basins. In order to mitigate this problem, more research into the transport and deposition behaviour of silica particles is necessary as well as the development of disperging agents.

5.15

Quantification of the 3D thermal anomaly in the orogenic geothermal system at Grimsel Pass, Switzerland

Christoph Wanner[1], Larryn W. Diamond[1] & Peter Alt-Epping[1]

[1]*Institute of Geological Sciences, University of Bern, Baltzerstrasse 3, CH-3012 Bern (wanner@geo.unibe.ch)*

Hydrothermal springs with temperatures up to 28 °C are present ~250 m beneath Grimsel Pass, where they discharge into a tunnel hosting a major European gas pipeline (Pfeifer et al., 1992). The springs occur over a narrow tunnel section of <100 m where it intesects the WSW–ENE-striking Grimsel Breccia Fault (GBF). Beside the occurrence of warm springs, hydrothermal activity is also manifested by the occurrence of a 3 Ma old hydrothermal breccia, which is widely exposed at and near Grimsel Pass and represents the fossil manifestation of the same hydrothermal system. Oxygen isotopes in quartz and adularia, combined with fluid inclusion data, indicate a breccia formation temperature of about 165 °C and reveal a meteoric fluid origin (Hofmann et al., 2004).

For this contribution we present results from solute geothermometry and from coupled thermal-hydraulic simulations aimed at elucidating the penetration depth of the meteoric water and at quantifying the shape, dimensions and magnitude of the subsurface thermal anomaly of such fracture-flow hydrothermal systems, which we refer to as “orogenic geothermal systems”. The Na-K geothermometer (Giggenbach, 1988) applied to the thermal spring waters provides strong evidence that the circulating meteoric water reaches a temperature of at least 250 ℃, corresponding to a remarkable penetration depth of ~10 km, given that the background geothermal gradient of 25 °C/km is the only source of heat in the area.

Simulation results suggest that a steady-state temperature distribution is attained in less than 5000 years, which is much shorter than the 3 Ma minimum lifetime of the Grimsel-Pass system. Moreover, they demonstrate that the extent of temperature anomalies induced by orogenic geothermal systems are mainly controlled by (i) the upflow rate, i.e., by the fault zone permeability as well as the hydraulic head gradient driving hydrothermal circulation, and (ii) the 3D extent of the flow system. Calibrating the model against discharge temperatures and flow rates of thermal springs and against the temperature anomaly measured along the tunnel wall has allowed us to quantify the current thermal anomaly of the Grimsel Pass system to about 10^{11} MJ per km depth, which corresponds to a theoretical power output of 10–20 MW (Fig. 1). Conversely, our simulations predict that the fluid upflow rate and heat anomaly of the fossil system 3 Ma ago were about double the current values.

We conclude that orogenic geothermal systems are promising plays for geothermal power production. Based on our modelling, exploration should focus on high topography areas such as those in the Vallais and in surrounding valleys of the Central Alps where hydraulic head gradients and hence upflow rates are at maximum values.

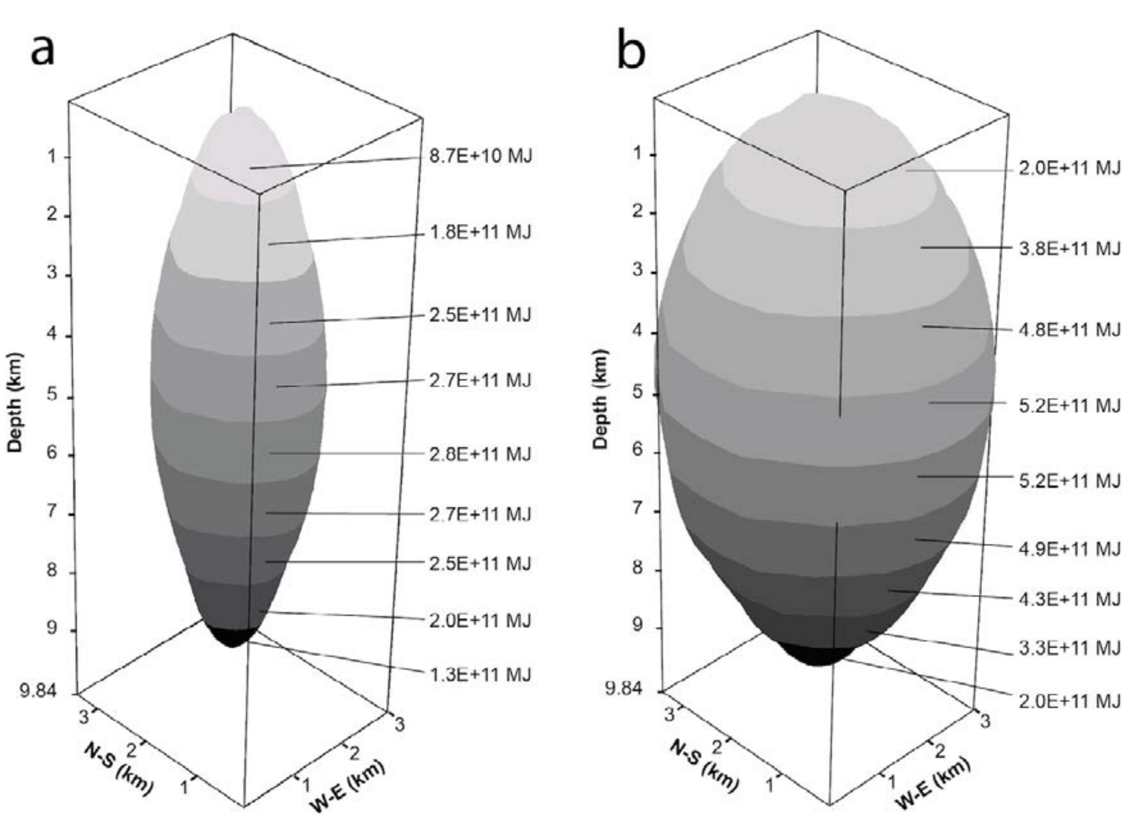

Figure 1. Anomalous heat (i.e. that exceeding the background regional geothermal gradient) per km depth predicted for: (a) the calibrated model simulating the current flow system and (b) the model simulating the temperature of the fossil system (i.e., 165 °C at a depth of ~3 km).

REFERENCES

Hofmann, B. A.; Helfer, M., Diamond, L. W.; Villa, I. M.; Frei, R.; Eikenberg, J. 2004. Topography-driven hydrothermal breccia mineralization of Pliocene age at Grimsel Pass, Aar massif, Central Swiss Alps. Schweizerische Mineralogische und Petrographische Mitteilungen, 84(3), 271–302.

Giggenbach W. F. (1988) Geothermal solute equilibria. Derivation of Na-K-Mg-Ca geoindicators. Geochimica Et Cosmochimica Acta 52, 2749-2765.

Pfeifer, HR; Sanchez A.; Degueldre, C. Thermal springs in granitic rocks from the Grimsel Pass (Swiss Alps): The late stage of a hydrothermal system related to Alpine Orogeny. In: Kharaka YK & Maest AS, editors, Proceedings of Water-Rock Interaction WRI–7, Park City, Utah, A.A. Balkema, Rotterdam, The Netherlands; 1992. p. 1327-1330

P 5.1

Regional-scale reactive transport models of the orogenic hydrothermal system at Grimsel Pass, Switzerland

Peter Alt-Epping, Larryn W. Diamond & Christoph Wanner

Institute of Geological Sciences, University of Bern, Baltzerstrasse 3, CH-3012 Bern (alt-epping@geo.unibe.ch)

Thermal fluids at temperatures in the range of 17 – 28 °C discharge into a tunnel underneath Grimsel Pass (2164 m) in the Central Alps. Discharge occurs at low rates (≤ 10 L/min) along the Grimsel Breccia Fault (GBF), which extends some 100 m along the tunnel. Geochemical evidence suggests that the water is a mixture of old geothermal water and younger cold water components. Both components are meteoric in orgin. Residence times have been estimated to be at least 30 ky and about 7 years, respectively (Waber et al., 2017).

A hydrothermal breccia in the Grimel Pass area, which formed ~3 Ma years ago, is fossil evidence for a long lived activity of the system. Oxygen isotope and fluid inclusion data from this breccia reveal a formation temperature of about 165 °C and a meteoric origin (Hofmann et al., 2004). Constraints from the Na-K geothermomenter (Giggenbach, 1988) suggest a maximum temperature of the hydrothermal fluid of at least 250 °C. Given the local geothermal gradient and the absence of a thermal anomaly at depth, this corresponds to a circulation depth of about 10 km.

The hydrothermal system is clearly confined to the GBF, which provides a permeable pathway for fluids recharging at high altitude, infiltrating the rock to great depths and discharging as thermal fluids at lower altitude. The GBF strikes approximately WSW-ENE (Belgrano et al., 2016) which suggests that recharge to the hydrothermal system could be associated with the glaciated mountains exceeding altitudes of 3000 m some 10 km to the WSW. The difference in elevation head between recharge and discharge zones thus could be up to 1000 m. This head difference constitutes the main driving force for fluid circulation in the fault zone. Little is known about the permeability distribution and the geometry of the flow pattern within the fault zone. Local permeability measurements in the upflow zone below the discharge site at Grimsel Pass indicate fault permeabilities on the order of 1e-13 m^2.

We use the high performance reactive-transport code PFLOTRAN to model the hydrothermal system in its entirety (i.e. the recharge zone, the reaction zone at depth and the upflow and discharge zones below Grimsel Pass) and use it to integrate geological, hydrological, thermal and geochemical observations. The geometry of the model copies the topography around Grimsel Pass. The GBF is modelled as a 100 m wide zone of elevated permeability. We assume that recharge of meteoric water occurs over an arbitrary length of the fault trace. As the properties of the deep flow path are unknown, we perform simulations that obey the chemical and thermal constraints of the discharging water and the mineralogy of the fossil site to explore feasible permeability distributions and flow patterns in the deep fault zone. Preliminary results reproduce the observed intense silicification of the hydrothermal breccia (Figure 1A) only if the infiltration of meteoric water to 10 km depth occurs via discrete permeable zones, rather than via a long, diffuse zone of homogeneous permeability. If the latter were the case we predict that, after initial circulation through the system (including discharge at Grimsel Pass) has been established, the fluid would migrate through the overlying low permeability rock, slowly establishing a secondary circulation system. Discharge of the fluid would then occur over a long segment of the GBF-trace at higher altitude, collapsing the previously established upflow at Grimsel Pass (Figure 1B), which is contrary to observations.

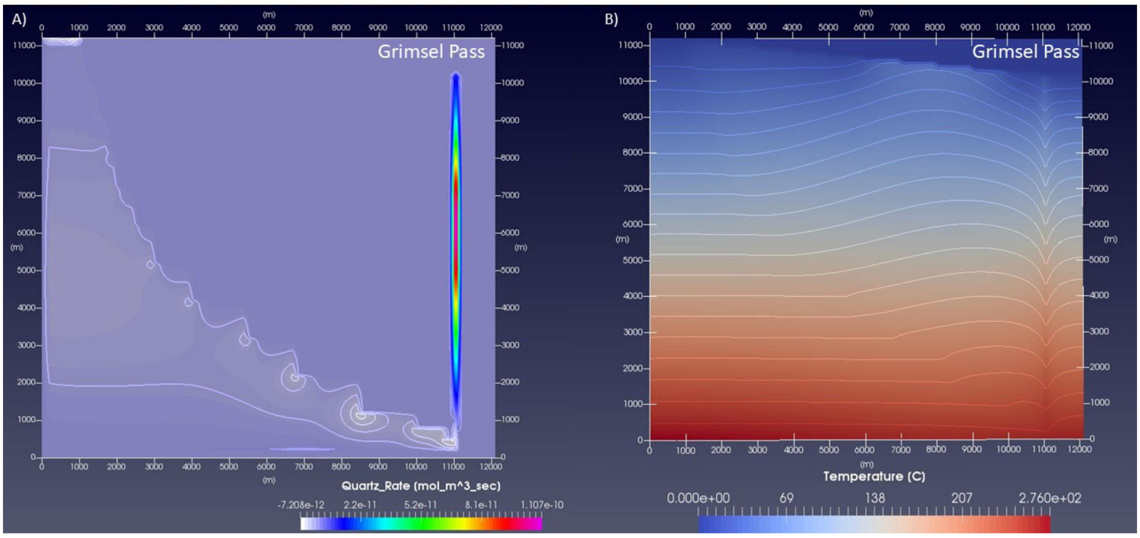

Figure 1. Panel A: Quartz dissolution (< 0) and precipitation (> 0) rates along the vertical cross-section comprising the GBF. The fluid attains equilibrium with quartz during infiltration to 10 km depth as quartz dissolves. Upflow and cooling of the hydrothermal fluid leads to quartz re-precipitation in the upflow zone. Panel B: Temperature distribution illustrating a simulation case where diffuse recharge has led to the formation of a secondary convective system through the low permeability rock and the collapse of the upflow zone at Grimsel Pass.

REFERENCES

Belgrano, T. M., Herwegh, M. & Berger A. 2016: Inherited structural controls on fault geomttry, architectureand hydrothermal activity: an example from Grimsel Pass, Switzerland, Swiss J Geosci, 109, 345-364.

Giggenbach, W. F. 1988: Geothermal solute equilibria. Derivation of Na-K-Mg-Ca geoindicators. Geochimica Et Cosmochimica Acta 52, 2749-2765.

Hofmann, B. A., Helfer, M., Diamond, L. W., Villa, I., Frei, R., and Eikenberg, J. 2004: Topography-driven hydrothermal breccia mineralization of Pliocene age at Grimsel Pass, Aar massif, Central Swiss Alps: Schweizerische Mineralogische und Petrographische Mitteilungen, v. 84, no. 3, p. 271–302.

Waber, H.N., Schneeberger, R., Mäder, U.K., Wanner, C. 2017: Constraints on evolution and residence time of geothermal water in granitic rock at Grimsel (Switzerland). 15th Water-Rock Interaction Syposium, WRI-15, Procedia Earth and Planetary Science 17, 774-777.

P 5.2

Effect of progressive burial on matrix porosity and permeability in Muschelkalk dolostones, Swiss Molasse Basin

Lukas Aschwanden[1], Arthur Adams[1], Larryn W. Diamond[1]

[1]Institute of Geological Sciences, University of Bern, Baltzerstrasse 1+3, CH-3012 Bern (lukas.aschwanden@geo.unibe.ch)

Carbonate rocks are currently being investigated worldwide, especially owing to their economic importance as hydrocarbon reservoirs or potential reservoir rocks for subsurface gas storage (methane or CO_2) and geothermal energy or electricity production. Especially dolostones, which tend to have higher porosity and permeability at great depth than associated limestones are of particular interest. Despite the enormous research interest in carbonate reservoirs, their burial compaction trends, i.e. rock-matrix porosity and permeability versus depth curves, are not completely understood. However, for exploration campaigns, it is essential to understand how the porosity and permeability of carbonates decrease with compaction and how to predict the magnitudes of these properties at depth. The present study examines the effect of progressive burial on two dolostone units belonging to the Middle Triassic Muschelkalk (Trigonodus Dolomit and Dolomit der Anhydritgruppe) within the Swiss Molasse Basin and aims at providing conceptual understanding to support the assessment of dolomite reservoirs in similar tectonic and sedimentary settings elsewhere.

Our investigations aim at providing compaction trends and insight into the compactional modification of crystal textures, pore sizes, pore geometries, the respective roles of chemical and mechanical compaction, diagenetic processes, as well as the impact of these parameters on matrix porosity and permeability. We have constructed compaction trends by interpreting wireline porosity logs retrieved from up to 5 km depth in wells throughout the Molasse Basin. The porosity deduced from these logs is calibrated against our new drill core analyses, which include plug measurements of porosity and permeability, as well as pseudo-logs of porosity calculated from density logs acquired by using a Geotek Multi-Sensor Core Logger. Examinations of the compactional modification of the rocks is based on thin-section petrography by standard optical, UV-fluorescence and scanning electron microscopy, digital image-analysis and visual logging of the geometry and frequency of macroscopic features related to burial compaction (e.g. stylolites). The role of diagenetic processes is investigated based on fluid inclusion studies and stable and radiogenic isotope analyses of rock forming and pore- and fracture-filling minerals.

The results show that average matrix porosity and permeability within the Trigonodus Dolomit decrease rapidly within the first 1.5 km below surface (from 23% to 9% and 2 to 0.02 mD). At depths of more than 2000 m, porosity and permeability maintain virtually constant values of 1–7% and <0.008 mD, respectively. These trends go along with distinct changes in dolomite crystal textures, pore sizes, pore geometries and stylolite frequency and amplitude. At the shallow well of Bözberg (i.e. 58 m) the rock matrix is composed of a relatively “loose” framework of euhedral dolomite crystals, which show straight and regular crystal faces and it contains considerable amounts of intercrystalline pore space. All the intercrystalline pores of the dolostones have nearly equant geometries, regardless of size. Pores larger than 100 μm^2 constitute between 40 and 92% of the total pore space of the rock. The frequency of diagenetic stylolites is 3.4/m with average amplitudes of 1.3 mm.

At the deep Lindau well (i.e. 2225 m) the rock matrix shows a dense packing of anhedral dolomite crystals, which show curved, lobate, serrated, sutured or otherwise irregular boundaries. Intercrystalline pores <100 μm^2 are nearly equant too, whereas larger pores are increasingly elongated. However, the quantity of pores larger than 100 μm^2 is nominal (1–11% of the total pore space). A major portion of the interparticle and separate-vug pores are clogged by saddle dolomite showing $^{87}Sr/^{86}Sr$ ratios of 0.7122–0.7134, which significantly exceed the rock matrix values of <0.7105. Primary fluid inclusions in these dolomites show homogenization temperatures of 138–147 °C, which is distinctly higher than the maximum burial temperatures derived from basin modelling (~120 °C, Nagra, 2002; Mazurek et al., 2006). The frequency of diagenetic stylolites is 9.4/m with average amplitudes of 2.4 mm.

The results demonstrate that compactional modification of matrix porosity and permeability in the Muschelkalk dolostones is largely determined by (1) mechanical compaction by which particles are rearranged and pores are squeezed, (2) chemical compaction and associated pressure solution, which expresses itself either by dissolution along dolomite crystal-to-crystal contacts or by dissolution along stylolites. The increase in the frequency and amplitude of diagenetic stylolites with burial depth indicates an increasing impact of pressure solution with burial depth and thus an increasing potential of cementational loss of porosity and permeability. (3) Pore clogging by the precipitation of saddle dolomite at the deep well of Lindau is interpreted to result from the influx of water from the underlying crystalline basement and/or the Buntsandstein as these units are the only feasible sources of radiogenic strontium in the local stratigraphy. This hypothesis is further supported by the high fluid inclusion homogenization temperatures, which significantly exceed the maximum burial temperatures derived from basin modelling. To date, it is not exactly known to what extent pore clogging by the precipitation of saddle dolomite contributes to the overall compactional loss of porosity and permeability in these dolostones at great depth.

REFERENCES

Mazurek, M., Hurford, A.J. & Leu, W. 2006: Unravelling the multi-stage burial history of the Swiss Molasse Basin: integration of apatite fission track, vitrinite reflectance and biomarker isomerisation analysis. Basin Research, 18, 27–50.

Nagra 2002. Projekt Opalinuston, Synthese der geowissenschaftlichen Untersuchungsergebnisse – Nagra Technischer Bericht NTB 02-03. Wettingen, Nagra.

P 5.3

An overview of CO_2 storage and utilization

Ignes A. C. C. de Carvalho[1], Frédéric Meylan[2], Fréderic Piguet[3] & Suren Erkman[4]

[1] *Institute of Earth Surface Dynamics, University of Lausanne, Géopolis, CH-1015 Lausanne (ignes.contreiras@unil.ch)*
** Institute of Earth Surface Dynamics, University of Lausanne, Géopolis, CH-1015 Lausanne (frederic.meylan@unil.ch) - Department of Environment, United Nations Industrial Development Organization, Vienna International Centre, P.O. Box 300, 1400 Vienna, Austria (f.meylan@unido.org)
[3] *Institut Biosphère, 16 B route de Jussy, CH-1226 Genève (fppiguet@institutbiosphere.ch)*
[4] *Institute of E*arth Surface Dynamics, University of Lausanne, Géopolis, CH-1015 Lausanne (suren.erkman@unil.ch)

This study aims to understand the integration of two different approaches for the use of carbon dioxide (CO_2). The close link between economic growth, energy consumption, carbon dioxide emissions and depletion of fossil resources demands new strategies able to dramatically reduce atmospheric greenhouse gas concentration.

The Carbon Capture and Storage (CCS) is a technique that allows the geologic sequestration of the CO_2 that is separated and captured as a by-product from industrial processes. Another complementary strategy is the Carbon dioxide Capture and utilization (CCU), which allows (quasi) circular material flows by considering the CO_2 as valuable feedstock (Meylan et al., 2015). This is aligned with the industrial ecology strategies, taking into consideration material and energy constraints, enabling the industrial utilization of the carbon dioxide to provide various final products as shown in the figure 1.

The geological sequestration is an important option that can be economically interesting when using CO_2 for enhanced oil recovery (EOR), a technique between sequestration and utilization. Currently, the proportion of CO_2 used by industrial activities (approximately 0.2 Gt/yr) is considerably small comparing to the anthropogenic emissions (more than 30 Gt/yr). However, new processes are being developed to increase this proportion and reduce the environmental impact.

This approach faces challenges in multiple domains. With regard to the legal aspects, the European Union has recently shown interest in CO_2 recycling as an alternative and complementary approach for CO_2 geological sequestration, which is already regulated by the Carbon Storage Directive 2009/31/ EU (CSD) (Piguet et al., 2017).

In this context, the CCS and the CCU can be combined (Carbon Capture, Utilization and Storage, CCUS) to respond to environmental concerns (Oldenburg, 2012). This combination can potentially close carbon cycles according to industrial ecology and circular economy principles. A way to merge this is to re-think and re-design business models able to deliver economic, environmental and social values, considering financial resilience and long-term viability and stability.

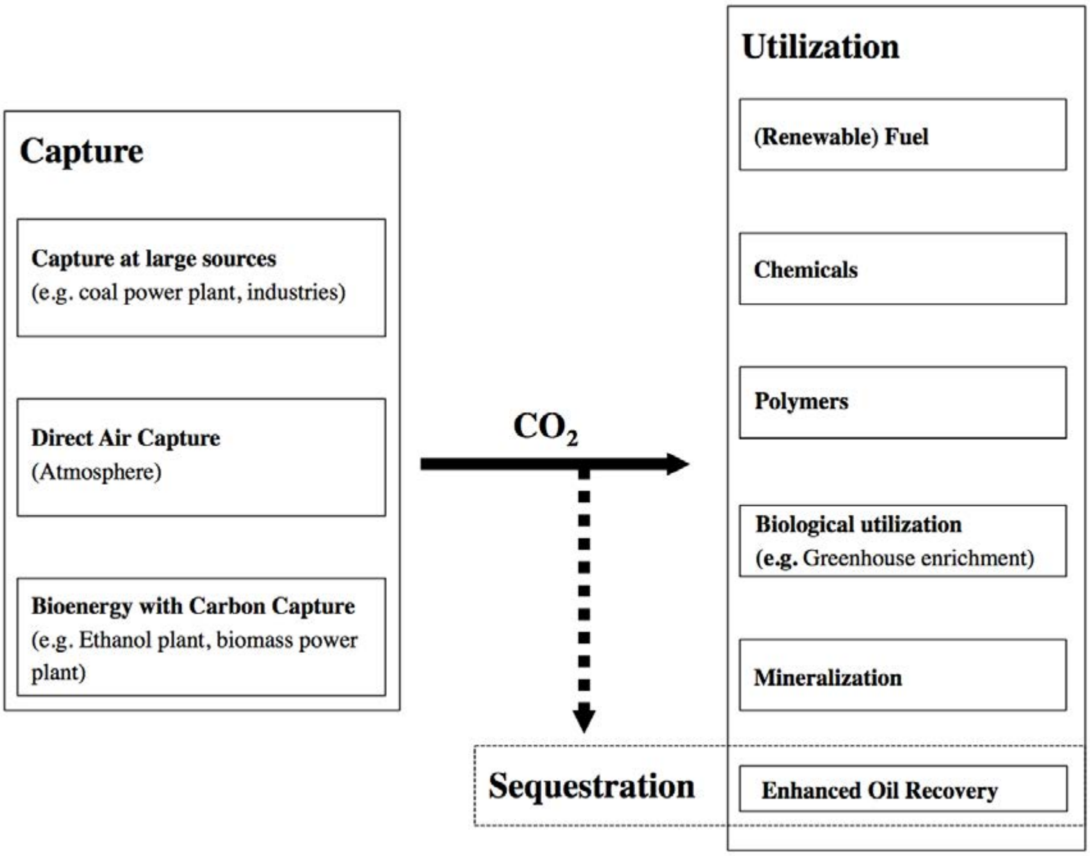

Figure 1. Integration of CCS and CCU processes (based on Meylan *et al*., 2015).

REFERENCES
Erkman, S. 2004: Vers une écologie industrielle, Paris: Éditions Charles Léopold Mayer.
Meylan, F., Moreau, V. & Erkman, S. 2015: CO2 utilization in the perspective of industrial ecology, an overview, Journal of CO2 Utilization,12, 101–108.
Oldenburg, C. 2012: Why we need the “and” in CO2 utilization and storage, Greenhouse Gases-Science and Technology, 2(1), pp.1–2.
Piguet, F., Meylan, F., Largey, T., Erkman, S. 2017: Recycling and Utilisation of Carbon Dioxide in the European Union’s Directives, European Energy and Environmental Law Review, 26(1), pp. 2-12

P 5.4

Geothermometrical calculations and the influence of the mobile elements in a low temperature thermal system hosted in carbonate-evaporitic rocks

Mónica Blasco[1], Luis F. Auqué[1], Maria J. Gimeno[1], Patricia Acero[1] & Maria P. Asta[2]

[1] *Petrology and Geochemistry Area, Earth Sciences Department, University of Zaragoza, Spain C/ Pedro Cerbuna 12, 50009 Zaragoza, Spain (monicabc@unizar.es)*
[2] *Environmental Microbiology Laboratory (EML), École Polytechnique Fédérale de Lausanne (EPFL). EPFL-ENAC-IIE-EML. Station 6, 1015, Lausanne, Switzerland.*

In this work the carbonate evaporitic and low temperature Tiermas geothermal system (northern Spain) has been studied. The main geochemical characteristics and the water temperature in the deep reservoir have been assessed. The thermal waters, hosted in a Paleocene carbonate aquifer in contact to the Triassic evaporites,are of chloride-sodium type and emerge with a temperature close to 37 ºC and pH about 7. In a small area (about 50 m^2) several springs respresenting two different hydrogeochemical groups have been identified, one with lower sulphate content (≈ 1200 ppm) and TDS values (≈ 7500 ppm) and the other with higher sulphate (≈ 3700 ppm) concentration and TDS values (≈ about 11000 ppm).

The reservoir temperature has been calculated by combining chemical geothermometers (SiO_2-quartz, Na-K, K-Mg, Na-K-Ca and Ca-Mg), isotopic geothermometres ($\delta^{13}C_{CO2-HCO3}$, $\delta^{18}O_{CO2-H2O}$, $\delta^{18}O_{CaSO4-H2O}$) and geothermometrical modelling performed with the PHREEQC geochemical code (Parkhurst and Appelo, 2013) and the LLNL thermodynamic database provided with the code (Figure 1).

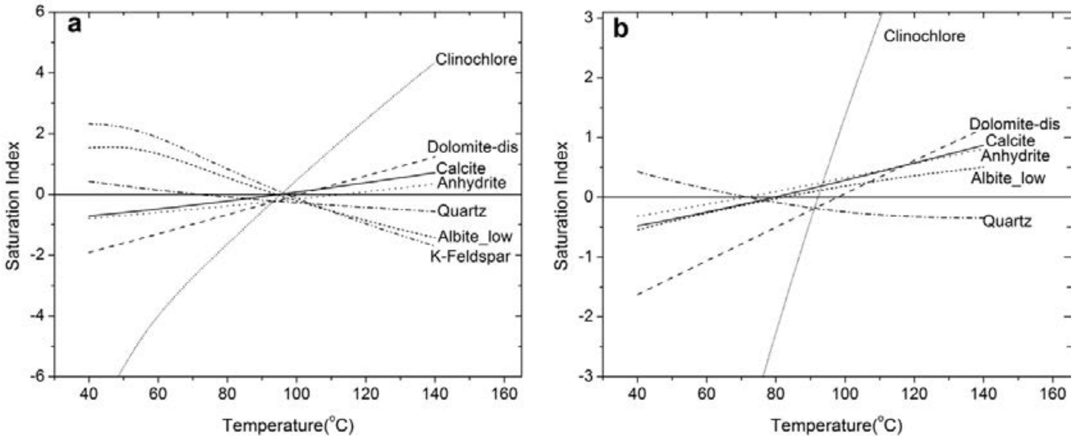

Figure 1. Evolution with temperature of the saturation indices of the different minerals supposed to be in equilibrium with the low sulphate water (panel a) and high sulphate water (panel b). In panel b the aluminium concentration has been fixed by performing the modelling maintaining the equilibrium with K-feldspar. Dolomite-dis: disordered dolomite; Albite_ low: low temperature albite.

The deduced temperature is slightly different for the two identified groups. In the case of the low-sulphate waters the temperature range established is 90 ± 20 ºC while in the high-sulphate waters is somewhat lower, 82 ± 15 ºC. However, the mineral equilibria at depth is the same for both groups of waters: anhydrite, calcite, dolomite, quartz, K-feldspar, albite and other aluminosilicates. Therefore, the differences found between both groups of waters are attributed to the existence of two different flow paths that, although hosted in the same rocks, undergo different intensities of water-rock interaction processes and present slightly different temperatures.

It is remarkable the good agreement between the results obtained with the different geothermometrical techniques, even with the cationic geothermometers which are usually considered unsuitable for low temperature carbonate-evaporitic systems. This unusual situation may be attributed to the presence of some detrital rocks (silicate minerals) in the carbonate-evaporitic aquifer, which provides the equilibrium between albite and K-feldspar, as found in the geothermometrical modelling and also suggested by the Giggenbach diagram (Giggenbach, 1988)

The influence of halite dissolution in the aquifer has also been evaluated and the results indicate that this process (and the increase in the chloride concentration) conditions the overall chemical characteristics (SO_4, Na, K, Ca and Mg contents) of the waters throught its effects on the mineral equilibrium situations in the reservoir.

Finally, a favourable structure for CO_2 storage has recently been identified in the Paleocene-Eocene carbonates (ALGECO2 Project; IGME, 2010), which is the probable aquifer of the Tiermas geothermal system and, therefore, the groundwaters studied here could be used as analogues to the waters in that site. The results obtained in this work help to understand the main processes associated to the CO_2 injection in this type of water. Near the injection wells, the waters will desiccate and calcite, dolomite and anhydrite would precipitate, since the waters are in equilibrium with respect to these phases in the reservoir. In the long term, the water will acidify leading to the carbonate dissolution and sulphate precipitation. These processes would lead to changes in the porosity and permeability of the rocks.

REFERENCES

Giggenbach, W.F. 1988: Geothermal solute equilibria. Derivation of Na-K-Mg-Ca geoindicators. Geochim Cosmochim Acta 52, 2749-2765.

IGME (2010). Selección y caracterización de áreas y estructuras geológicas favorables para el almacenamiento geológico de CO_2 en España. http://info.igme.es/algeco2/ (accessed 21-03-2016).

Parkhurst, D.L. & Appelo, C.A.J. 2013: Description of Input and Examples for PHREEQC Version 3. A Computer Program for Speciation, Batch-Reaction, One-Dimensional Transport, and Inverse Geochemical Calculations. In: U.S. Geological Survey (Ed.). Techniques and Methods, book 6, chap. A43. U.S.Geological Survey., Denver, Colorado, available only at http://pubs.usgs.gov/tm/06/a43.

P 5.5

A MATLAB package for thermo-hydraulic modeling and fracture stability analysis in fractured reservoirs

Gunnar Jansen[1], Benoît Valley,[1] Stephen A. Miller[1]

[1] *CHYN - Centre for Hydrogeology and Geothermics, Laboratory of Geothermics and Geodynamics, University of Neuchâtel, Rue Emile-Argand 11, CH-2000 Neuchâtel (gunnar.jansen@unine.ch)*

A large fraction of the world‘s water and energy resources are located in naturally fractured reservoirs within the earth‘s crust. Understanding the dynamics of such reservoirs in terms of flow, heat transport and fracture stability is crucial to successful application of engineered geothermal systems (also known as enhanced geothermal systems, EGS) for geothermal energy production in the future. The reservoir development characteristics such as permeability creation and induced seismicity largely depend on the traits of preexisting fractures such as porosity, permeability and orientation within the local stress field. One of the primary driving mechanisms for permeability creation in EGS involves shear failure induced by fluid injection at high pressures. In environments with low differential stress, tensile fractures may develop if the injection pressure exceeds the minimal principal stress (e.g. fracking). Clearly, preexisting, critically stressed and optimally oriented fractures provide the most favorable conditions for enhancing permeability of EGS. Reservoir stimulation itself changes the local stress field due to thermo- and poro-elastic effects as well as slip induced stress transfer. Thus fracture stability is likely to be very heterogeneous in space and time. Therefore understanding the stress state and its changes in the fractured reservoir is of major importance in order to understand reservoir development and mitigate the risk of induced seismicity.

We present an open source implementation of an embedded discrete fracture model for single phase flow and heat transport. The fractured reservoir modelling framework is implemented in MATLAB. It can be used as a standalone simulation package for TH(M) applications in geothermal reservoirs or as a blue print for the reimplementation of of the method e.g. in a high performance computing (HPC) framework. In addition to flow and heat transport modelling we also adress fracture stability by an analytical approach. In combination with an irreversible permeability increase in case of failure the modelling framework is suited to adress common problems of reservoir stimulation. We evaluate the perfomance and accuracy of the model by comparing it with a widely used package in several test cases.

P 5.6

Modelling the propagation of hydraulic fracture using cohesive zone models

Dong Liu[1], Brice Lecampion[1] & Lorenzo Benedetti[1]

[1] *Laboratory of Geo-energy (GEL), École Polytechnique Fédéral de Lausanne (EPFL), EPFL - ENAC – GEL Station 18 CH-1015 Lausanne (d.liu@epfl.ch)*

Hydraulic fracturing (HF) is widely used in the oil and gas industry to enhance production from tight reservoirs. The process involves the injection of fluid at a given flow rate into a wellbore in order to propagate a fracture in rocks and thus increase their permeability. Some studies (Chudnovsky et al. 2008; Papanastasiou 1999) have shown that linear elastic fracture mechanics (LEFM) tends to underestimate the hydraulic fracturing propagating pressure compared to some in-situ measured data. Rocks are typically known to exhibit a quasi-brittle fracture behavior which is characterized by the fact the fracture energy is spent over a material lengthscale, i.e. the process zone size may not be necessarily negligible compared to other lengthscales (e.g. wellbore size). This quasi-brittle behavior can be well described by a softening traction-separation law in cohesive zone models (Bazant & Planas 1997).

Here, we revisit the problem of a plane-strain hydraulic fracture driven by the injection of a Newtonian fluid in a tight rock (at the time-scale of the injection). We model the quasi-brittle nature of the rock with a cohesive zone model using different traction separation laws while keeping the material fracture energy constant (Figure 1). We investigate numerically both the toughness and viscosity dominated propagation regime (Detournay 2004), and compare our results with semi-analytical solutions based on LEFM. We show that –although the numerical results obtained with a cohesive zone model differs at early time (where the cohesive zone is large compared with the crack), they tend to the semi-analytical HF propagation solutions based on LEFM at large time. We also discuss the difference between different traction separation laws and the numerical oscillations that can occur on too coarse meshes.

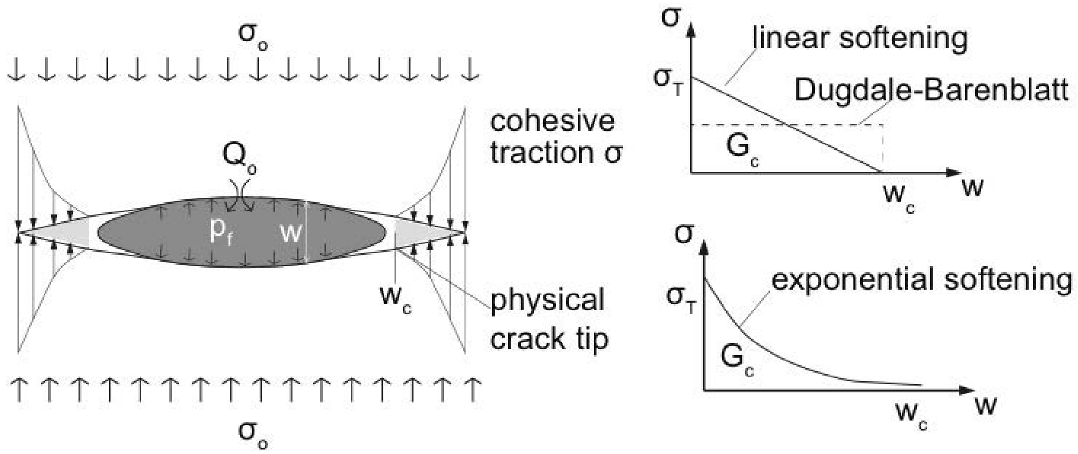

Figure 1. Schema of the formulation of the problem and different traction-separation laws

REFERENCES

Bazant, Z. & Planas, J. 1997: Fracture and size effect in concrete and other quasibrittle materials. Vol. 16. CRC press.

Chudnovsky, A., Fan, F., Shulkin, Y., Zhang, H., Dudley, J. & Wong, G. 2008: Hydraulic Fracture Simulation Revisited, In: 42nd US Rock Mechanics Symposium and 2nd US-Canada Rock Mechanics Symposium. ARMA.

Detournay, E. 2004: Propagation regimes of fluid-driven fractures in impermeable rocks. Int J Geomech, 4(1), 35-45.

Lecampion, B. 2012: Hydraulic Fracture Initiation From an Open-hole: Wellbore Size, Pressurization Rate And Fluid-solid Coupling Effects, In: 46th U.S. Rock Mechanics/Geomechanics Symposium and 6th US-Canada Rock Mechanics Symposium. ARMA.

Papanastasiou, P. 1999: The effective fracture toughness in hydraulic fracturing. Int J Fracture, 96.2,127–147.

P 5.7

Dolomitization of the Upper Jurassic Carbonate Rocks in the Geneva Basin, Switzerland and France

Yasin Makhloufi[1], Elias Samankassou[1], Elme Rusillon[1], Maud Brentini[1], & Michel Meyer[2]

[1] *Department of Earth Sciences, University of Geneva, Rue des Maraîchers 13, CH-1205 Geneva*
[2] *Service Industriels de Genève (SIG), CP 2777, 1211 Geneve 2.*

The Upper Jurassic carbonate rocks represent an important potential targeted reservoir for geothermal energy in the Geneva Basin, Switzerland and France. Horizons affected by dolomitization, the focus of the present study, are of particular interest because they proved to be productive in time-equivalent deposits currently exploited in Southern Germany. The study is based on samples from the sub-surface and outcrops in the Geneva Basin and surroundings. Data originated from petrography (optical microscopy, cathodoluminescence, scanning electron microscopy, calcite staining) with the aim to constrain the paragenesis for each stratigraphic unit concerned (Calcaires de Tabalcon, Calcaires Récifaux and Calcaires de Landaize) prior to discussing the cause(s) and effect(s) of dolomitization.

Data reveal that the three units underwent common bio-chemical and physical diagenetic stages, typical of carbonate sediments. All samples show at least two stages of burial blocky calcite cementation with the exception of the sub-surface samples of the Calcaires Récifaux. Dolomitization is a major event that affected all units. Our results and interpretations point to an early dolomitization, in the form of replacement planar dolomite rhombs. Furthermore, dedolomitization, through calcitization and/or dissolution, is an important process in the Upper Jurassic carbonate rocks of the Geneva Basin, leading to creation of secondary pore space.

Results of the present study favor rather a reflux model for dolomitization than the mixing-zone model suggested in earlier studies in this area. However, due to the geodynamical context of the Geneva Basin and the active aquifer, passive margin and post-orogenetic burial diagenesis models are not discarded for the subsurface. The creation of secondary pore space might contribute to connect the intraparticular and interparticular microporous networks and, thus, provided enhanced reservoir properties that are suitable for geothermal energy exploitation.

These results are a first step towards a better understanding of the diagenetic history of the Upper Jurassic in the Geneva Basin. Moreover, it provides a reasonable framework for further geochemical and petrophysical analyses in order to pinpoint the nature and timing of fluid migration trough the basin while providing a better understanding and exploitation of the Geneva Basin subsurface. The diagenetic path established and the dolomitization scenario favored hold the potential to help in ongoing exploration for geothermal energy beyond the Geneva Basin.

P 5.8

Fluid flow in porous rocks: drastic localisation due to time-dependent deformation of the matrix

Ludovic Räss[1], Thibault Duretz[2] & Yury Podladchikov[1]

[1] *Scientific Computing Group, Institute of Earth Sciences, University of Lausanne, Quartier Mouline, CH-1015 Lausanne (ludovic.raess@unil.ch)*
[2] *Geosciences Rennes, Université de Rennes 1, CNRS UMR 6118, France.*

Evidences of fluid flow in porous rocks are numerous on Earth. In the deep interior, metasomatism and dehydration reactions generate fluid excess which then migrates in self-arranging preferential pathways. At shallower depths, numerous seismic surveys in sedimentary basins unveil vertical pipe-like structures. These high-permeability pipes show elevated concentration of gas or buoyant liquid and are strong evidences of flow localisation. However, there is a current lack in understanding the formation process of vertical pipes leading to flow localisation in porous rocks.

Within this work, we investigate the formation and evolution of self-developing pipes in two and three dimensions. We use high-resolution and predictive numerical modelling to solve two-phase flow equations at optimal performance on supercomputers.

We demonstrate that drastic localisation of the pore liquid occurs due to time-dependent deformation of the porous matrix. Recent laboratory experiments confirm the creep behaviour of saturated porous reservoir rocks (sandstone, limestone, shale) and unveil a strong dependence on fluid pressure minus total pressure.

We developed robust 2D and 3D numerical solvers based on an enhanced iterative method. We performed predictive numerical simulation on very high resolution and show that drastic localisation of liquids in porous rocks occurs due to localised viscous creep of the porous matrix.

P 5.9

BATMAN - 3D Numerical simulator for mass and heat transport with porosity change using GPUs technology

Reza Sohrabi[1], Samuel Omlin[2], Stephen A. Miller[1]

[1] *CHYN – Centre for Hydrogeology and Geothermics, Laboratory of Geothermics and Geodynamics, University of Neuchâtel, Rue Emile-Argand 11, CH-2000 Neuchâtel (reza.sohrabi@unine.ch)*
[2] *ISTE - Institute of Earth Sciences, University of Lausanne, Géopolis, CH-1015 Lausanne*

BATMAN is a **B**iph**A**sic **T**hermo**M**ech**A**nical **N**umerical simulator for fluid dynamics in fractured geological media. The simulator considers mass and heat transport with porosity changes in response to dehydration of hydrous minerals. *BATMAN* utilises a finite difference scheme to solve the governing PDEs associated with 3D large-scale hydrothermal systems or geothermal reservoirs.

The simulator can be run on GPU workstations or GPU clusters. The physical processes implemented into the code are those associated with deep hydrogeological complexes where high fluid pressures generated by dehydration reactions can be sufficient to induce hydro-fracture that significantly influences the porosity and permeability structures within geological formation. The conceptual and numerical model couple the mechanical and thermodynamic effects of fluid pressure in 3D, with application to understanding mass and heat transport through fractured networks. Possible applications include geothermal resource development and CO_2 sequestration.

We present results of the model applied to the Lusi (Java, Indonesia) hydrothermal system where it is hypothesised that a magmatic intrusion at depth induced large-scale dehydration of clay sediments that added substantial additional water.

P 5.10

Measuring pressure dependent aperture heterogeneity in rough-walled fractures using X-ray computed tomography

Quinn C. Wenning[1], Claudio Madonna[1], Lisa Joss[2] & Ronny Pini[2]

[1] *Geological Institute, Department of Earth Sciences, ETH Zurich, Switzerland (quinn.wenning@erdw.ethz.ch)*
[2] *Department of Chemical Engineering, Imperial College London, UK*

Significant interest in the Swiss and international geothermal energy communities revolves around quantifying the rate of fluid-rock heat transfer, which is directly linked with the transport properties of fractures, underscoring the importance of fracture aperture characterization for achieving optimal heat production. In this context, coupled core-flooding experiments with non-invasive imaging techniques (e.g., X-Ray Computed Tomography – X-Ray CT) provide a powerful method to make observations of hydromechanical properties of fractured rocks under representative geologic conditions.

This study utilizes a recently developed calibration-free CT method to quantify the three-dimensional fracture aperture distribution in a fractured Westerly granite core [Huo et al., 2016]. A porosity estimate is also assessed with the X-ray saturation technique using the contrast between highly transmissible helium and krypton gases [e.g., Vega et al., 2014]. A single through-going rough-walled fracture was induced in the Westerly granite sample (diameter: 5 cm, length: 10 cm) before being mounted in a high-pressure aluminum core-holder and placed inside a medical CT scanner for imaging. The pore fluid pressure was undrained and constant during scanning, while the confining pressure was regulated to the desired effective pressure (0.5, 5, 7, and 10 MPa) under loading and unloading conditions. 3D fracture aperture and porosity reconstructions have been prepared at a maximum resolution of $(0.24\times0.24\times1)\ mm^3$. In addition to the 3D heterogeneity, fracture transmissivity from CT scan methods are verified using traditional core flow pressure analysis.

Confining pressure dependent fracture aperture maps obtained independently using helium and krypton for the whole core depict a similar heterogeneous aperture field. Estimates of the average hydraulic aperture from CT scans are in quantitative agreement with our own fluid flow experiment results and typical behavior in literature. However, the latter lack the observational detail degree achieved through imaging, which further evidence the presence of strong heterogeneities in fracture aperture at the mm-scale. These results highlight the ability of non-destructive imaging to determine fracture aperture heterogeneity, which can be used to study fluid flow channelization and heat transfer that cannot be obtained from core-flooding experiments alone.

REFERENCES

Huo, D., Pini, R., & Benson, S. M. 2016: A calibration-free approach for measuring fracture aperture distributions using X-ray computed tomography. *Geosphere*, *12*(2), 558-571.

Vega, B., Dutta, A., & Kovscek, A. R. 2014: CT imaging of low-permeability, dual-porosity systems using high X-ray contrast gas. *Transport in porous media*, *101*(1), 81-97.

P 5.11

Comparison between permeability and seismic velocity anisotropy of shales

Wen Zhang[1], Qin Wang[1], Alba Zappone[2,3] , Claudio Madonna[2], Jean-Pierre Burg[2]

[1] School of Earth Sciences and Engineering, Nanjing University, 163 Xianlin Avenue, Nanjing 210046, China
[2] Department of Earth sciences, Geological Institute, ETH Zurich, Sonneggstrasse 5, 8092, Zurich, Switzerland
[3] Department of Process Engineering, ETH Zurich, Sonneggstrasse 3, CH-8092 Zurich, Switzerland

Permeability and seismic velocity are critical parameters in shale gas production and exploration. Clay-rich shales show strong permeability and seismic anisotropy. We collected shale samples from the Lomgmaxi Formation in Upper Yangtze Area (China), in which a high-yield shale gas field was explored. Cylindrical samples of 25.4 mm diameter and about 30 mm length were acquired in the directions both parallel and perpendicular to beddings to measure the permeability and velocity anisotropy. Permeability measurements were conducted using transient pulse decay method under different effective pressure (up to 13.8 MPa) and room temperature. On the same core plugs we measured ultrasonic compressional wave velocity (Vp) and shear wave velocity (Vs) at 1 MHz frequency at increasing confining pressure up to 225 MPa. Modal composition was determined through X-ray diffraction (XRD) analysis. SEM imaging and low temperature nitrogen adsorption were performed to characterize the pore size distribution. Results show that permeability decrease exponentially with increasing effective pressure, and velocities increase nonlinearly with increasing effective pressure. In contrast, permeability anisotropy increase with increasing effective pressure, and velocity anisotropy decrease with increasing effective pressure. Because there are more micropores (< 2 nm) and mesopores (2-50 nm) in organic matter, a positive relation between total organic carbon (TOC) content and velocity was observed. Our results indicate that influence of pore size on velocity is much pronounced than on permeability, while permeability depends more on the development of fractures and the pore connectivity.

6. Progress in assessment of hazards and risks in mountain regions

Michael Bründl, Linda Zaugg, Markus Stoffel

TALKS:

6.1 **Aye Z.C**., Artigue V., Jaboyedoff M., Derron M., Gerber C., Lévy S.
An open-source webGIS platform for risk management of natural hazards in Canton Vaud

6.2 **Brunner M.I**., Viviroli D., Sikorska A.E., Seibert J., Favre A.-C.
Synthetic design hydrographs for gauged and ungauged catchments in Switzerland

6.3 **Derron M.-H**., Rouyet L., Guerin A., Lefeuvre C., Jaboyedoff M.
Imaging of non-gravitationnal movements in rock faces

6.4 **Evers F.M**., Frank P., Hager W.H., Boes R.M.
Outburst floods triggered by impulse wave overtopping

6.5 **Fäh D.**, Cauzzi C.
Towards rapid likelihood estimation of earthquake-triggered mass-movements in Switzerland based on the calibration to historical observations

6.6 **Franz M.**, Rudaz B., Jaboyedoff M., Podladchikov Y.
Coupling SLBL with shallow water model to assess landslide-generated tsunami hazard at Oeschinensee

6.7 **Jaboydedoff M.**, Artigue V., Aye Z.C., Derron M.-H., Gerber C., Lévy S.
From the average velocities of deep seated landslides to intensity-frequency scenarios

6.8 **Leonarduzzi E.**, Molnar P., Mcardell B.W.
How much rain does it take to cause a landslide?

6.9 **Noël F.**, Wyser E., Jaboyedoff M., Derron M.
Real-size rockfall experiment: How different rockfall simulation impact models perform when confronted with reality?

6.10 **Nurtaev B.**, Inatov N., Nurtaev D., Kurbanova D., Bühler Y.
Numerical simulations of mudflow movements using RAMMS:HILLSLOPE Software: a case study from Uzbekistan

6.11 **Semakova E.**, Popov A., Bühler Y.
Experience of snow avalanche numerical simulation in Uzbekistan

POSTERS:

P 6.1 **Tonini M.**, Cama M.
Detection and analysis of space-time landslides pattern in Switzerland

P 6.2 **Glueer F.**, Manconi A., Loew S.
Kinematic Analysis of the September 2016 Moosfluh Landslide Acceleration

P 6.3 **Meier C.**, Derron M., Jaboyedoff M., Gerber C., Artigue V.
Inventory of shallow landslides in regards to their frequency in the Canton of Vaud (Switzerland).

P 6.4 **Vouillamoz N.**, Rothmund S., Joswig M.
Characterizing active clayey landslides dynamics by microseismic monitoring

P 6.5 **D’almeida C.**, Guerin A., Jaboyedoff M., Hantz D.
Model and cartography of the Saint-Eynard cliff erosion by rockfalls

P 6.6 **Wyser E.**, Jaboyedoff M.
Dramatic granular impact(s): a plastic- or friction-dominated transition phase

P 6.7 **Noël F.**, Wyser E., Jaboyedoff M., Derron M.
Real-size rockfall experiment: A relatively simple method to acquire 3D impact characteristics from video footage

P 6.8 **Nduwayezu E.**, Jaboyedoff M., Derron M.-H, Nsengiyumva J.-B., Twarabamenye E.
Pression démographique et outils analyse d’aléas et risques gravitaires au Rwanda.

P 6.9 **Ben Hammouda M.**, Jaboyedoff M., Derron M.H., Bouaziz B.
Rockfall hazard evaluation in a touristic area of northern Tunisia using SFM photogrammetry in a zero data site

P 6.10 **Matti B.**, Beffa F., Salvadè A., Pellegrini D., Gardenghi R., Monleone R, Marti U.
A revolutionary Array Synthetic Aperture Radar (ASAR) and methodology for landslide, unstable slope and manmade structure measurement

P 6.11 **Nigg V.**, Girardclos S., Kremer K., Anselmetti F.
Tsunami deposits in coastal areas surrounding perialpine lakes in Switzerland

P 6.12 **Schimmel A.**, Hübl J.
Automatic detection of debris flows based on infrasound and seismic data

P 6.13 **Voumard J.**, Derron M.-H., Jaboyedoff M.
Characterization of natural hazard events affecting the Swiss transportation networks from 2012 to 2016

6.1

An open-source webGIS platform for risk management of natural hazards in Canton Vaud

Zar Chi Aye[1], Veronica Artigue[1,2], Michel Jaboyedoff[1], Marc-Henri Derron[1], Christian Gerber[2], Sebastien Lévy[2]

[1] *Institute of Earth Sciences, University of Lausanne, Quartier UNIL-Mouline, Bâtiment Géopolis, CH-1015 Lausanne (zarchi.aye@unil.ch)*
[2] *Direction Générale de L'Environnement DGE, Etat de Vaud, CH-1014 Lausanne*

Following changes in Swiss subsidy system in 2008, different protection projects were needed to prioritize in terms of their cost-effectiveness, as a response to limited financial resources (Bründl et al. 2009). According to the legislation of Canton Vaud, municipalities are responsible for managing risks by taking into account the provided hazard maps, and relevant issues must be included in their spatial planning policies. For the funding of protection measures and analyses, tools such as EconoMe (BAFU 2017a) and Valdorisk (DGE 2017) have been developed for risk evaluation and prioritization of mitigation projects, serving as decision-making instruments to the responsible authorities for risk management of natural hazards. However, these tools lack, in particular, the spatial representation of natural hazards and risks. Since natural hazards are location dependent, risk management activities can benefit from geographical representations.

Therefore, in this study, based on the same principles established, we developed an interactive webGIS platform for Canton Vaud, using open-source software and technologies. This platform aims for: 1) the risk evaluation of buildings and roads for different types of natural hazards, 2) the rapid evaluation of risk before and after protection measures, and 3) testing the efficiency of measures using a simple cost-benefit analysis. Different types of hazards are considered in this study (such as avalanches, floods, debris flows, rock falls and landslides) and intensity maps for different scenarios (such as 30, 100 and 300 years of return periods based on Swiss guidelines) are used for risk analysis. To adapt the tool of the Swiss Confederation (i.e., EconoMe) at the level of Canton Vaud, cantonal register of buildings (RCB) data are used by making a correspondance between building classes of RCB and EconoMe. For the roads, SwissTopo data are used as a starting point. Then, the corresponding vulnerability data of EconoMe (BAFU 2017b) are used accordingly to calculate different types of risk (objects and persons) for a combination of hazard and object types. Compared to EconoMe and Valdorisk, one of the main advantages of this platform is that it offers the possibility to perform rapid risk analysis at various study scales, depending on the user requirements.

The platform is composed of various components for data upload, risk calculation, formulation, cost calculation and selection of protection measures. The user can upload necessary input maps and configure additional parameters for risk calculation. Based on the given inputs, risk is calculated dynamically and the user can visualize results in the map interface. It also allows the user to calculate risk only for an interested zone by drawing a polygon in the map. Based on risk outcomes, the user can propose (draw) measures before realizing the actual design and dimensions of such protective measures in the area. Or can upload the measure map if available (Fig. 1). For the re-calculation of risk after protection measures, the user can upload new intensity and object maps or can update these maps manually by editing features in the platform. For the selection of measures, the user can calculate annual cost of measures and can compare them using a simple cost-benefit analysis tool.

This platform will be demonstrated with a study area in Canton Vaud, and this research work is performed within a project funded by Canton Vaud.

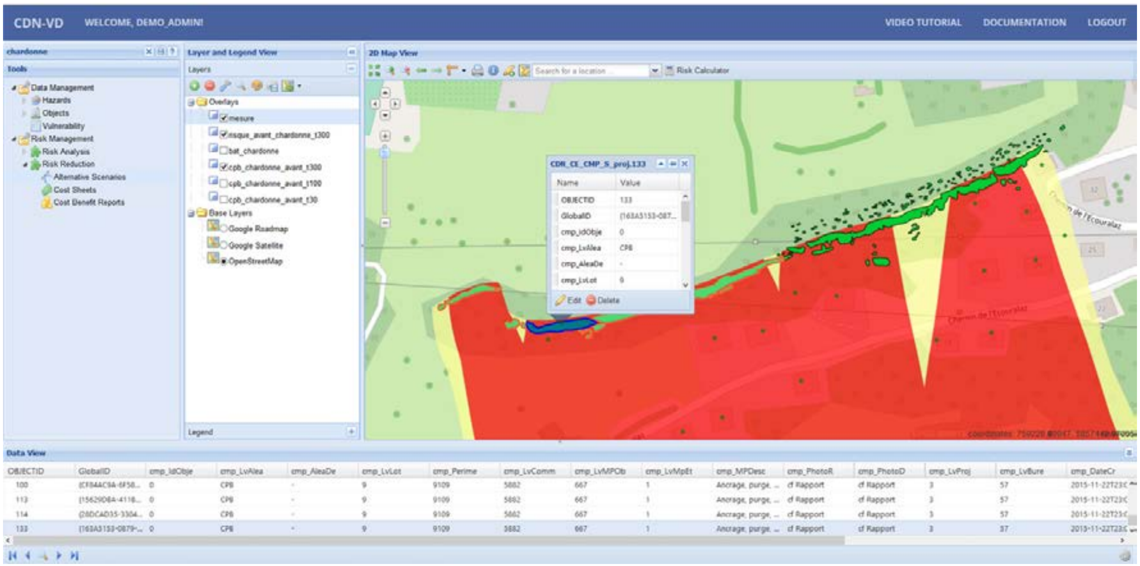

Figure 1. Visualization of an existing measure (uploaded by the user) for the rock falls hazard at the study area of Chardonne.

REFERENCES

BAFU. 2017a: EconoMe 4.0: Wirtschaftlichkeit von Schutzmassnahmen gegen Naturgefahren, Bundesamt für Umwelt, http://www.econome.admin.ch/, last access: 24.08.2017.

BAFU. 2017b: EconoMe 3.0 Objektparameter, http://www.econome.admin.ch/doc/Objektparameter_generate.php, last access: 24.08.2017.

Bründl, M., Romang, H. E., Bischof, N., & Rheinberger, C. M. 2009: The risk concept and its application in natural hazard risk management in Switzerland, Nat. Hazards Earth Syst. Sci., 9, 801-813.

DGE. 2017: Calculateur de risque Valdorisk - Direction Générale de l'Environnement, http://www.vd.ch/index.php?id=61124, last access: 24.08.2017.

6.2

Synthetic design hydrographs for gauged and ungauged catchments in Switzerland

Manuela I. Brunner[1,2], Daniel Viviroli[1,3], Anna E. Sikorska[1,4], Jan Seibert[1,5] & Anne-Catherine Favre[2]

[1]*Department of Geography, University of Zurich, Zurich, Switzerland*
[2]*Univ. Grenoble Alpes, CNRS, IRD , Grenoble INP1, IGE, Grenoble, France*
[3]*belop gmbh, Sarnen, Switzerland*
[4]*Department of Hydraulic Engineering, Warsaw University of Life Sciences SGGW, Warsaw, Poland*
[5]*Department of Earth Sciences, Uppsala University, Uppsala, Sweden*

Design hydrographs for a defined return period are necessary for hydraulic design tasks such as the construction of dams and retention basins as well as for flood management tasks such as drawing flood hazard maps [*Klein et al.*, 2010]. Traditionally, design floods have been specified by peak discharge within the univariate flood frequency framework which neglects hydrograph volume and its relation to peak discharge. Design hydrographs that also represent hydrograph volume and shape in addition to peak discharge provide a more complete picture of the flood behavior of a catchment. We thus propose a method for the construction of a set of event-type specific synthetic design hydrographs (SDHs), characterized by peak discharge, hydrograph volume, and shape, which represents the flood-process variability within a gauged catchment. In addition, we also introduce a bivariate regional index flood approach to regionalize such SDH sets to ungauged catchments based on a dataset of 163 medium-size Swiss catchments.

Gauged catchments

The SDH construction approach in gauged catchments is based on observed runoff time series. On the one hand, it models the hydrograph shape via a probability density function which is fitted to a representative hydrograph shape. On the other hand, the magnitude of the event is estimated in a bivariate flood frequency analysis taking into account the dependence between peak discharges and hydrograph volumes via a copula function. This approach can be used to construct a single catchment-specific SDH that summarizes the flood behavior of a specific catchment [*Brunner et al.*, 2017]. In addition, it can be applied to construct several flood-type or event-type specific SDHs that represent the different event types and the runoff variability associated to them. We found that three event-types, a fast, intermediate, and slow event, are sufficient in most catchments to describe the hydrograph shape variability induced by different flood mechanisms.

Ungauged catchments

We propose a regional index flood approach to regionalize event-type-specific SDHs that account for process variability to ungauged catchments (Figure 1). In a first step, we identified regions of catchments with a similar reaction to flood triggering precipitation events. We found that three regions, a quickly reactive, a slowly reactive, and a uniformly reactive region, well described the different reaction types in our dataset. In a second step, we assigned an ungauged catchment to one of the three reactivity regions based on its catchment characteristics. In a third step, we used a bivariate regional index flood model to estimate the magnitude of the design event in the ungauged catchment based on the pooled data in the corresponding reactivity region.

We found that the bivariate regional index flood model is suitable for the regionalization of event-type-specific SDH sets to ungauged catchments. Using different event-type specific SDHs, the engineer or practitioner will get a more complete picture than from just one design estimate which does not represent process variability in sufficient detail.

1 Institute of Engineering Univ. Grenoble Alpes

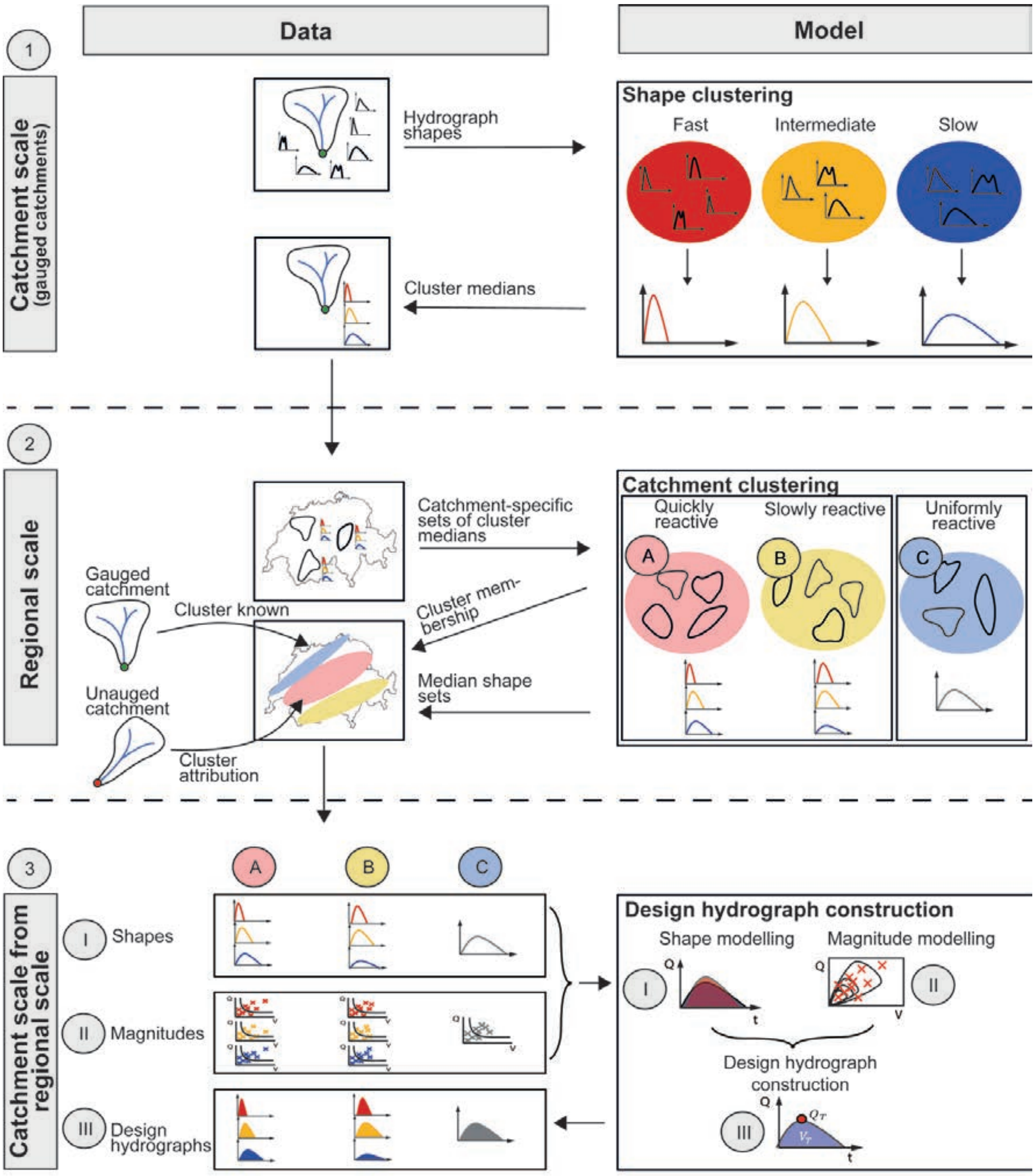

Figure 1. Illustration of the regionalization framework. The data input and output for the models are indicated for the three different steps of the approach: 1) hydrograph shape clustering, 2) catchment clustering, and 3) design hydrograph construction. Hydrograph shape clustering was done on the catchment scale, catchment clustering on the regional scale, and design hydrograph construction used regional data to derive estimates on the catchment scale. Design hydrographs were constructed based on three regions: quickly reactive (A), slowly reactive (B), and uniformly reactive (C). The hydrograph shape (I) and magnitude (II) were modelled and combined to a synthetic design hydrograph (III).

REFERENCES

Brunner, M.I., Viviroli, D., Sikorska, A.E., Vannier, O., Favre, A.-C. & Seibert, J. 2017: Flood type specific construction of synthetic design hydrographs. *Water Resources Research*, 53, 1390-1406, doi:10.1002/2016WR019535.

Klein, B., Pahlow, M., Hundecha, Y. & Schumann, A. 2010: Probability analysis of hydrological loads for the design of flood control systems using copulas. *Journal of Hydrologic Engineering*, 15(5).

6.3

Imaging of non-gravitationnal movements in rock faces

Derron Marc-Henri[1], Rouyet Line[1,2], Guerin Antoine[1], Lefeuvre Caroline[1], Jaboyedoff Michel[1]

[1] *Groupe Risk, Institut des Sciences de la Terre, Geopolis, Université de Lausanne (marc-henri.derron@unil.ch)*
[2] *Norut - Northern Research Institute, Tromsø, Norway*

Two remote sensing techniques have significantly contributed to a better understanding of gravitational movements these last twenty years: radar interferometry (InSAR) and laser scanning (LiDAR). Because of their high spatial and time resolutions, these techniques are also able sometimes to capture movements which are not gravitational. Here "non-gravitational" is used to describe movements which "go up the slope", part of the time at least. Such movements had already been recognized from punctual measurements by differential GNSS or extensometers for instance. The recent and original contribution of InSAR and LiDAR is that it is now possible to get images from these non-gravitational movements, with some surprising results sometimes. Non-gravitational movements are important to understand gravitational ones. These periodical deformations contribute to rock mass weakening and material fatigue. Two cases are presented hereafter.

1. Daily thermal fluctuations of a granite flake

In the Yosemite National Park (California), the daily variation of rock surface temperature can easily reach 40°C (Collins & Stock 2016). A granite flake has been monitored for 24 hours with terrestrial LiDAR, crackmeters, contact temperature sensors and thermography (Guerin et al., 2016). The amplitude of daily deformation exceeds 5mm in some places (Figure 1).

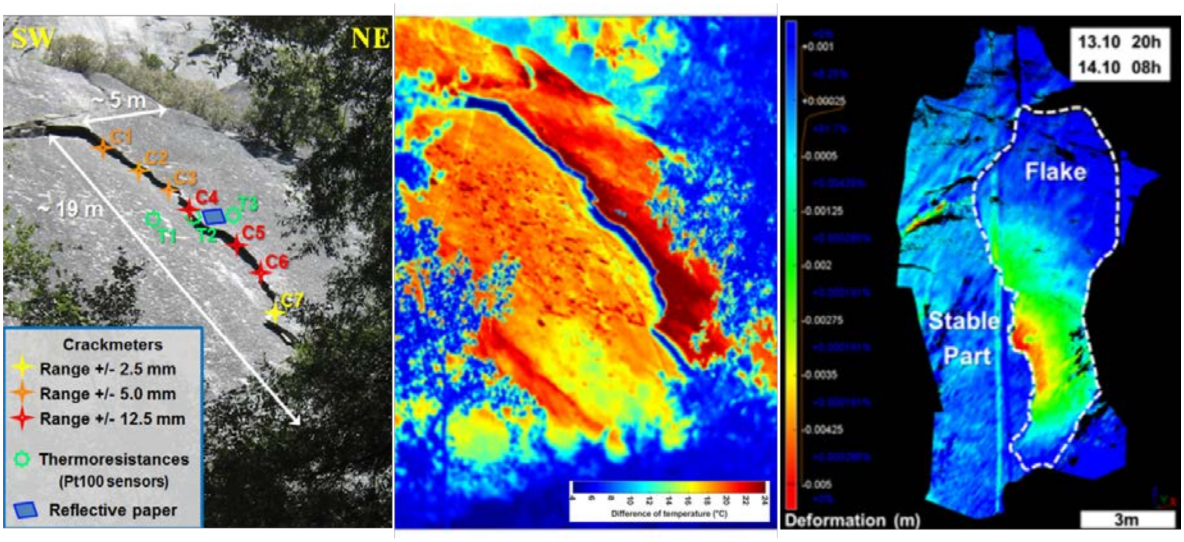

Figure 1. Granite flake in the Rhombus wall (Yosemite Park). Left: locations of devices. Middle: temperature difference between 8:00 and 11:40. Right: deformation recorded during an interval of 12 hours. From Guerin et al., 2016.

2. Seasonal breathing in the Børa valley side (Norway)

Two groundbased InSAR have been set up at the bottom of the valley of Romsdalen (Western Norway) to monitor the rockslide of Mannen (Rouyet et al. 2017). The area covered by those two radars is much larger than the rockslide itself, and an unsuspected displacement pattern was recorded in the neighbouring area, by both devices and during two consecutive years. The Børa valley side is a 1 km high steep rock face of fractured gneiss. Every year, a 300m by 800m zone in the middle of this slope start to inflate at the end of June. The distance of the surface to the radar is reduced by about 1cm (going down). Near mid-August this displacement is reversed, the rock surface "moving up" away from the radar (Figure 2). These movements have been confirmed by satellite InSAR (Rouyet et al. 2017). They are interpreted as a change of water pressure in the valley side due to an interplay between snow melt at the top and frozen fractures in the rock face.

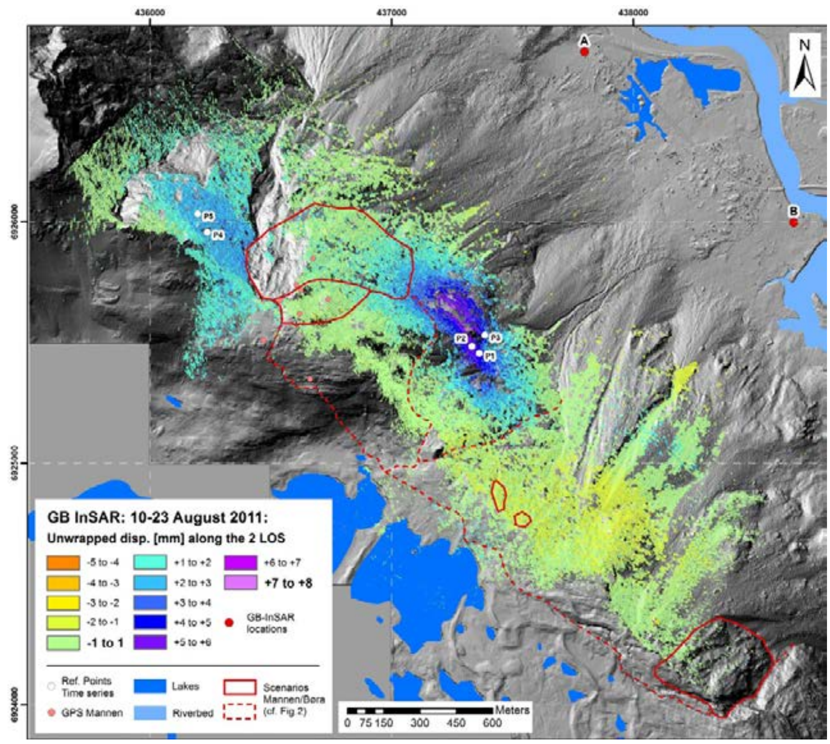

Figure 2. Displacements recorded by groundbased InSAR during the deflating phase of mid-August 2011. Displacements are in mm, positive values indicating that the rock surface is moving away from the radar, up the slope (from Rouyet et al. 2017).

REFERENCES

Collins B. & Stock G. (2016). Rockfall triggering by cyclic thermal stressing of exfoliation fractures. Nature Geoscience 9, 395–400.

Guerin A., Derron M.-H., Jaboyedoff M., Abellán A., Dubas O., Collins B. & Stock G. (2016). Exfoliation sheets detection with terrestrial laser scanning and thermal imaging (Yosemite Valley, California, USA). Proceedings of the Virtual Geoscience Conference, Bergen 2016, 55-56 (online).

Rouyet L., Kristensen L., Derron M.-H., Michoud C., Blikra L., Jaboyedoff M. & Lauknes T. Evidence of rock slope breathing using ground-based InSAR. Geomorphology 289 (2017): 152-169.

6.4

Outburst floods triggered by impulse wave overtopping

Frederic M. Evers[1], Pierre-Jacques Frank[2], Willi H. Hager[1] & Robert M. Boes[1]

[1]*Laboratory of Hydraulics, Hydrology, and Glaciology (VAW), ETH Zurich, CH-8093 Zürich (evers@vaw.baug.ethz.ch)*
[2]*Axpo Power AG, Parkstrasse 23, CH-5401 Baden (formerly VAW, ETH Zurich)*

Outburst floods are characterized by a sudden water release from a standing water body to downstream regions of lower geodetic elevation and therefore representing a serious hazard in mountain regions. Potential water bodies include e.g. artificial reservoirs for hydropower generation, lakes impounded by a landslide dam, or moraine-dammed proglacial lakes.

Water masses overtopping the dam crest are a major load for the dam faces, eventually causing a complete failure of the structure due to erosion. The transport of water mass over the dam structure is initiated either by a water level rise exceeding the dam crest elevation, or by wave impact. While the former process is gradual allowing for monitoring and a temporal estimation of the instant of overtopping, the latter is subject to larger uncertainty. Impulse waves generated by substantial mass wasting into the water body pose a particular threat to the stability of embankment dams, even under conditions of sufficient freeboard to withstand the load of wind waves. Westoby et al. (2014) classify impulse wave generation by landslides or avalanches as a major triggering mechanism for outburst floods from moraine-dammed lakes.

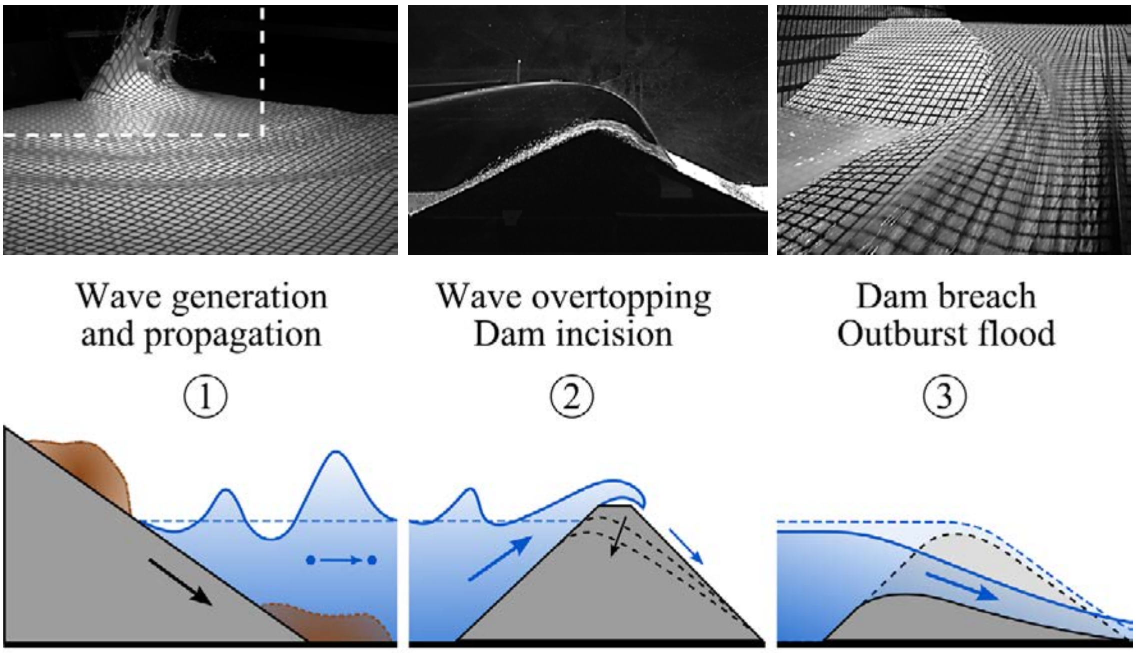

Figure 1. Hydraulic model setups in VAW laboratory corresponding to three stages of outburst flood event triggered by impulse wave overtopping.

Although outburst flood events are widely simulated by means of numerical models (Westoby et al. 2014), the physical principles of the triggering mechanisms related to impulse wave overtopping are still lacking detailed understanding and are a source of substantial uncertainties. Hydraulic experimentation allows for gaining a deeper insight into the individual stages of the overall process chain. Therefore, three different hydraulic model setups were operated: impulse wave generation and spatial propagation in a 3D wave basin, wave overtopping in a 2D wave channel, and spatial dam breach in a 1 m wide flume (Figure 1). The height of the impulse waves generated by a landslide or an avalanche in 3D is mainly governed by the following slide parameters: slide impact velocity, slide mass, slide thickness, slide width, and slide impact angle as well as the stillwater depth (Evers & Hager 2017). The propagation distances in impounded mountain lakes are commonly short and the waves are still comparatively large upon impact onto the shore or a dam. As to wave overtopping at a dam, the eroded crest depth is defined as the vertical distance between the initial dam crest and the highest dam elevation after erosion. It is mainly governed by the freeboard, followed by the wave height and the dam shape (Huber et al. 2017).

Another important quantity is the overtopping volume: even if the dam crest withstands the wave loading and the entire structure is not subject to failure, small overtopping volumes can already create severe downstream flooding. If the eroded crest depth after multiple wave overtopping is larger than the initial freebord, an incision for initiating a dam breach is created. The peak breach discharge of the outflow hydrograph is mainly governed by the maximum headwater level, the reservoir water surface area, the cross-sectional dam area, and the inflow discharge if the drainage discharge is assumed to be negligible (Frank 2016, Boes et al. 2017). The results indicate that the reservoir water surface area represents a more practical parameter to describe peak breach discharge as compared with the often-used reservoir volume. In addition, it is directly extracted from ortho-images so that no information of the reservoir bathymetry is needed for estimating the peak discharge.

The experimental data are crucial to develop integrated numerical schemes covering all stages of an outburst flood event, offering the potential to model prototype settings including downstream reaches. In addition, model tests provide the basis for generally applicable equations serving for an overall hazard assessment as well as a prediction of reservoir outflow hydrographs as the decisive input parameter for numerical simulations of the flood wave propagation in the downstream valley and floodplain and its impact.

REFERENCES

Boes, R., Frank, P.-J. & Hager, W.H. (2017). Spatial breach development of homogeneous non-cohesive levees and embankment dams due to overtopping. Proc. 85th ICOLD Annual Meeting, Prague, Czech Republic, Paper 344, 10 pages.

Evers, F.M. & Hager, W.H. 2017: Spatial generation and propagation of landslide generated impulse waves, Coastal Engineering Proceedings, 35. DOI: 10.9753/icce.v35.currents.13

Frank, P.-J. 2016: Hydraulics of spatial dike breaches, Doctoral Thesis 23938, ETH Zurich, Switzerland. DOI: 10.3929/ethz-a-010803310

Huber L.E., Evers F.M., & Hager W.H. (2017). Solitary wave overtopping at granular dams, J. Hydraul. Res. (in press).

Westoby, M.J., Glasser, N.F., Brasington, J., Hambrey, M.J., Quincey D.J. & Reynolds, J.M. 2014: Modelling outburst floods from moraine-dammed glacial lakes, Earth-Sci. Rev., 134, 137-159. DOI: 10.1016/j.earscirev.2014.03.009

6.5

Towards rapid likelihood estimation of earthquake-triggered mass-movements in Switzerland based on the calibration to historical observations

Donat Fäh[1] & Carlo Cauzzi[1]

[1] *Schweizerischer Erdbebendienst, ETH Zürich, Sonneggstr. 5, CH-8092 Zürich (donat.faeh@sed.ethz.ch)*

In Switzerland, nearly all historical *Mw* ~ 6 earthquakes have induced damaging landslides, rockslides and snow avalanches that, in some cases, also resulted in damage to infrastructure and loss of lives. We describe herein the customisation to Swiss conditions of globally calibrated statistical approaches originally developed to rapidly assess earthquake-induced landslide likelihoods worldwide. Since the valuable Swiss historic dataset of earthquake-induced phenomena is not rich enough to develop Swiss specific prediction models, we chose to develop recipes for optimal adaptation of global models to Switzerland. We adopted the model of Nowicki et al. (2014) and adjusted the predictive equations to capture the distribution of mass movements associated to the historical earthquakes.

We tuned the model to capture the observations from past historical events in Switzerland in 1295, 1356, 1584, 1601, 1755, 1774, 1855 and 1946, for which information on earthquake-triggered mass-movements have been collected and interpreted (e.g. Fritsche et al., 2012). This also includes the discussion about the expected incompleteness of the historical dataset. We recalibrated the coefficients of the global model to output likelihoods larger than 0.75 at location of known historical mass-movements. The customised predictions are based on: (i) seismic input from Swiss ShakeMap, (ii) high-resolution geomorphology, (iii) local mass-movement susceptibility data, and (iv) the calibrated model for historical earthquake-induced mass-movements. We also propose a simplified representation of mass-movement likelihoods for stakeholders. The predictive model is optimised for near-real-time estimates based on USGS-style ShakeMaps routinely produced by the Swiss Seismological Service (Cauzzi et al., 2014).

This study has a high practical relevance to many Swiss-ShakeMap stakeholders, especially those managing lifeline systems, and to other global users interested in conducting a similar customisation for their region of interest. Even if calibrated on historic events with moderate-to-high magnitudes, the methodology presented in this paper yields sensible results also for low-magnitude recent events

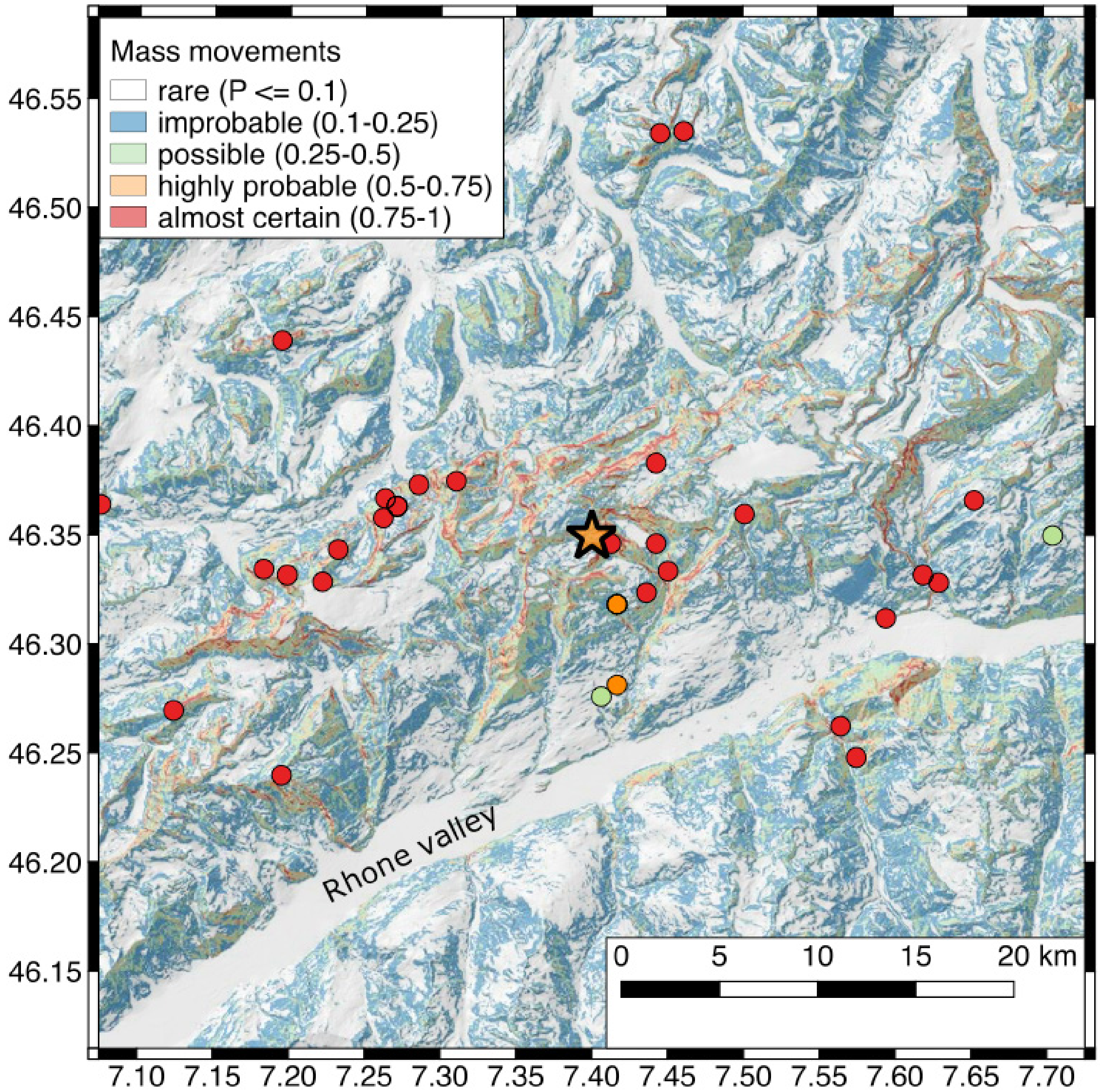

Figure 1. Mass-movement likelihood and known mass-movement observations (circles; Fritsche et al., 2012) of the 1946 Mw 5.8 Sierre mainshock and largest Mw 5.5 aftershock. The epicentral location of the mainshock according to ECOS-09 is shown by the orange star. Known mass-movements are colored according to the maximum predicted likelihood within 500 m of the mapped location.

REFERENCES

Cauzzi, C., Edwards, B., Fäh, D., Clinton, J., Wiemer, S., Kastli, P., Cua, G., & Giardini, D. 2014: New predictive equations and site amplification estimates for the next-generation Swiss ShakeMaps, Geophys. J. Int., 200, 421–438.

Fritsche, S., Fäh, D., & Schwarz-Zanetti, G. 2012: Historical intensity VIII earthquakes alongthe Rhone valley (Valais, Switzerland): primary and secondary effects, Swiss J. Geosci.,105, 1–18.

Nowicki, M.A., Wald, D.J., Hamburger, M.W., Hearne, M., & Thompson, E.M. 2014: Development of a globally applicable model for near real-time prediction of seismically induced landslides, Eng. Geol., 173, 54–65.

6.6

Coupling SLBL with shallow water model to assess landslide-generated tsunami hazard at Oeschinensee

Martin Franz, Benjamin Rudaz, Michel Jaboyedoff, Yury Podladchikov

Institut des sciences de la Terre, University of Lausanne, CH-1015 Lausanne (martin.franz@unil.ch)

Water bodies located in mountainous regions are susceptible to be reached by mass movement, which could lead to an impulse wave. Because of the concentration of the population in valleys and on the shores, such phenomenon could lead to catastrophic consequences. In order to assess comprehensively this phenomenon together with the induced risks, we have developed a 2.5D numerical model which aims to simulate the propagation of the landslide, the generation and the propagation of the wave and eventually the spread on the shores or the associated downstream flow.

The whole process is done in three steps implying different methods. Firstly, the geometry of the sliding mass is constructed using the Sloping Local Base Level (SLBL) concept. Secondly, the propagation of this volume is performed using a model based on the shallow water equations (SWE) with Bingham and granular flow rheologies. Finally, the wave generation and propagation are also simulated using the SWE stabilized by the Lax-Friedrichs scheme. The transition between wet and dry bed is performed by the combination of SWE and the viscous flow equations.

The ability of the model to simulate the complex sequence of mass movement, wave generation and propagation, run-up and floods is demonstrated with the case study of Oeschinensee (Bern, Switzerland). Indeed, the lake is surrounded by cliffs and glaciers and is prone to landslide-generated tsunami in case of rock or ice avalanches. A potential overtopping may lead to a downstream flood that threatens the city of Kandersteg.

6.7

From the average velocities of deep seated landslides to intensity-frequency scenarios

Michel Jaboydedoff[1], Veronica Artigue[1,2], Zar Chi Aye[1], Marc-Henri Derron[1], Christian Gerber[2], Sébastien Lévy[3]

[1] *Risk-group - ISTE – Institut des sciences de la terre - GEOPOLIS – 3793 University of Lausanne, CH-1015 Lausanne – Suisse*
[2] *DGE - Division GEODE-DN – Section Dangers naturels – Canton de Vaud, Avenue de l'Université 5 - 1014 Lausanne – Suisse*
[3] *DGE – Division FORET - Chemin de la Vulliette 4, CH – 1014 Lausanne – Suisse*

Hazard maps (Lateltin, 1997) indicate degrees of danger that qualify the potential of events according to their intensity and their return period, usually set at 30, 100 and 300 years. For landslides, intensities are determined on the basis of their average annual displacement velocity. These velocities are in most cases derived from expert opinion based on observations. They are not sufficient to establish scenarios associated with the usual return periods. Therefore, we present here a method allowing to deduce intensities on the basis of the negative exponential distribution of the landslides velocities for the three return periods. These intensities correspond to the differential movements potentially induced by the landslides. The deformation thresholds are a function of the landslide surface and its estimated average velocity. This approach leads to three scenarios that provide data for a risk analysis.

This method is implemented in a WEBGIS platform (Aye et al., 2016a, 2016b), which automatically calculates the risks using the buildings register - including their values and assignments, and an inventory of landslides as polygons with three velocity classes attributed to the three return periods.

We consider here the impact of the intensity level on the building as a new hazard scale. Therefore, we use the average displacement velocity (v) and the landslide surface (A) to get a differential motion. Based on A and v the differential strain $\dot{\mathcal{E}}$ $\dot{\mathcal{E}}$ in cm / (m × an) or in% per year is given by:

$$\dot{\varepsilon} = 2\frac{v}{\sqrt{A/_2}}$$

Where it is assumed that the ratio of the length to the landslide width is 2, and that the distribution across the width $\sqrt{A/2}$ $\sqrt{A/2}$ is an isosceles triangle. This value of $\dot{\mathcal{E}}$ is the characteristic of each landslide (polygon in a GIS). The results will depend on the thresholds for intensities and therefore on the calibration of the potential damages. We assume that a building of width w = 10 m is affected by a deformation during a period of time Δt. This makes it possible to calculate the differential displacement dd on w during this period:

$$dd = w \times \dot{\varepsilon} \times \Delta\mathrm{t}$$

The event frequency is calculated on the basis of the velocities indicated in the inventory, fixing w = 10 m and Δt = 30, 100 and 300 years. The results are classified into four intensity classes (Table 1).

This method has been applied to a region of the inventory of the canton of Vaud (VD, 2017) in Diablerets. It allows intensity maps to be drawn up for three different return periods and to assess the total risk of these three scenarios (Figure 1). This approach makes possible to implicitly integrate extreme events, which is relevant for a risk analysis. The first risk calculations with this method provide results corresponding to our knowledge of the local context.

Intensity	Limits for dd [cm / 10 m]
High	I ≥ 100
Medium	50 ≤ I < 100
Low	10 ≤ I <50
Negligible	I<10

Table 1. Value of selected intensity thresholds.

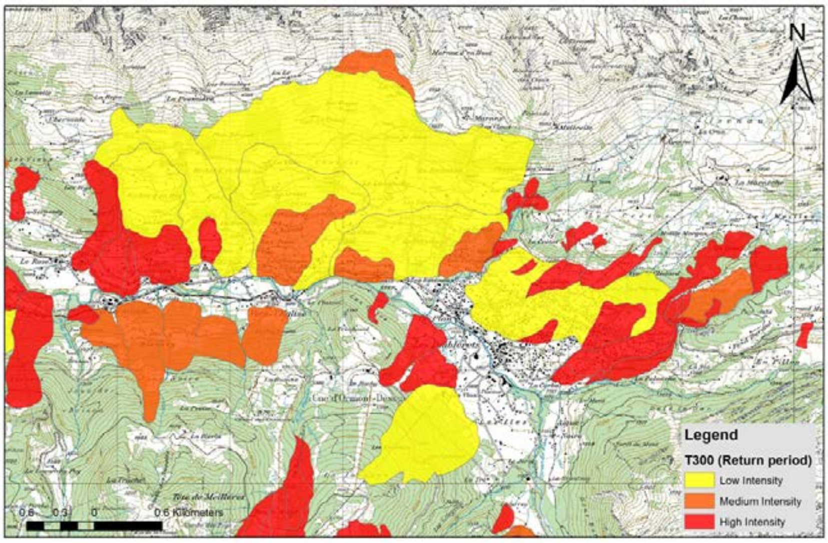

Figure 1. Example of intensity classification according to the proposed method for the return period of 300 years for deep seated landslide (GPP) (based on VD, 2017).

REFERENCES

Aye, Z.C., Jaboyedoff, M., Derron, M-H., van Westen, C.J., Hussin, H.Y., Ciurean, R.L., Frigerio, S., Pasuto, A. (2016a). An interactive web-GIS tool for risk analysis: a case study in the Fella River Basin, Italy. Nat. Hazards Earth Syst. Sci., 16, 85–101. doi:10.5194/nhess-16-85-2016.

Aye Z. C., Nicolet P., Jaboyedoff M., M.-H. Derron, Gerber C., and Lévy S. (2016b): A prototype web-GIS application for risk analysis of natural hazards in Switzerland. In General Assembly 2016 - V. 18 -4356.

Lateltin, O. (1997): Prise en compte des dangers dus aux mouvements de terrain dans le cadre des activités de l'aménagement du territoire. Recommandations, OFEFP, 42p.

Raetzo, H. & Loup, B.(2016): Protection contre les dangers dus aux mouvements de terrain : aide à l'exécution concernant la gestion des dangers dus aux glissements de terrain, aux chutes de pierres et aux coulées de boue / auteurs: Hugo Raetzo et Bernard Loup ; traduction: Cristian Marro. Office fédéral de l'environnement OFEV, 98 p.

VD (2017) : http://www.geo.vd.ch/theme/dangers_nat_thm, consulté le 12.05.2017.

6.8

How much rain does it take to cause a landslide?

Elena Leonarduzzi[1,2], Peter Molnar[1], Brian W. McArdell[2]

[1] *Institute of Environmental Engineering, ETH Zurich, Switzerland (leonarduzzi@ifu.baug.ethz.ch)*
[2] *Swiss Federal Institute for Forest, Snow and Landscape Research WSL, Birmensdorf, Switzerland*

In Switzerland floods are responsible for most of the damage caused by rainfall-triggered natural hazards (89%), followed by landslides (6%, ca. 520 M Euros) as reported in Hilker et al. (2009) for the period 1972-2007. The prediction of landslide occurrence is particularly challenging because of their wide distribution in space and the complex interdependence of predisposing and triggering factors. One of the most popular approaches for the definition of regional early warning systems for landslides is that of precipitation thresholds.

Here we propose an objective and robust framework for their definition (Leonarduzzi et al., 2017). We analysed rainfall triggering thresholds for landslides from a new gridded daily precipitation dataset (RhiresD, MeteoSwiss) for Switzerland combined with landslide events recorded in the Swiss Damage Database (Hilker et al.,2009). The high-resolution gridded precipitation dataset allows us to avoid problems concerning the selection of representative raingauges and allows a spatially explicit assesment of rainfall as a triggering factor.

Each of the 1670 rainfall triggered landslides in the database in the period 1972-2012 was assigned to the corresponding 2x2 km precipitation cell based on its location. For each of these cells, precipitation events were defined as series of consecutive rainy days and the following event parameters were computed: duration (d), maximum and mean daily intensity (mm/d), total rainfall depth (mm) and maximum daily intensity divided by Mean Daily Precipitation (MDP). The events were classified as triggering if a landslide happened during them and non-triggering otherwise. This classification of observations was compared to predictions based on a simple threshold model for each of the parameters. The predictive power of each parameter and the best threshold value were assessed by ROC curve analysis and statistics such as AUC and True Skill Statistic (TSS).

Event parameters containing intensity were found to have similarly high predictive power (TSS=0.59-0.65, AUC=0.87-0.90), with the exception of duration (TSS=0.23 and AUC=0.65). Slightly better performances were obtained when considering a typical power law intensity-duration curve (TSS=0.67). The analysis was repeated for sub-regions of the country based on erosivity and climate, using local climate (MDP) and erodibility (Kuehni and Pfiffner, 2001), or a combination thereof, in the classification. When defining regional maximum intensity thresholds, the performances were further improved in all cases although marginally (TSS + 0.7-2.5%). The regional maximum daily intensity thresholds varied greatly among classes, with differences of up to 33 mm/day, and they increased with decreasing erodibility and increasing wetness (MDP). The range of best threshold values are even greater when considering variables divided by the local MDP value (Fig.1, for maximum daily intensity). The trend of increasing thresholds required to generate landslides in wetter climates suggests the existence of a landscape balance between climate, erosion and soil formation. In order to demonstrate the quality and robustness of the results, we also analysed ROC reference cases obtained by randomization of landslides in space and time, and resampling to equal sample size between triggering and non-triggering events (prevalence).

From these results, we conclude that the rainfall threshold identification method defined here is robust, the True Skill Statistic is an adequate optimization criterion for the definition of rainfall thresholds, that erodibility and local climate (Mean Daily Precipitation) provide additional information with predictive skill for landslide generation, and finally that daily precipitation, although insensitive to the strongest convective events is still very useful in providing insights on the occurrence of lanslides.

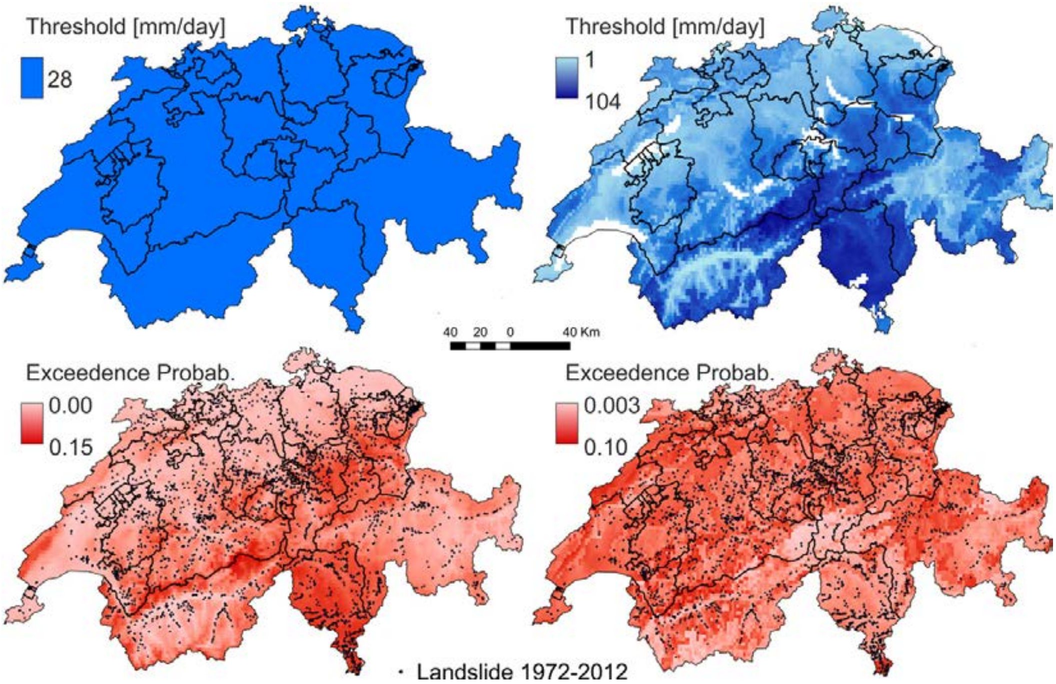

Figure 1. Best rainfall thresholds and the correspondent exceedance probability computed for 1972-2012. Recorded landslides are shown as black dots. a) best country-wide maximum daily intensity threshold, c) corresponding exceedance probability, b) best threshold computed using local Mean Daily Precipitation and best maximum intensity/MDP thresholds for each of the 16 MDP-erodibility region and d) the corresponding exceedance probability.

REFERENCES

Hilker, N., Badoux, A., & Hegg, C. (2009). The swiss flood and landslide damage database 1972-2007. Natural Hazards and Earth System Science, 9(3), 913–925. https://doi.org/10.1002/asl.183

Kuehni, A., & Pfiffner, O. A. (2001). The relief of the Swiss Alps and adjacent areas and its relation to lithology and structure: Topographic analysis from a 250-m DEM. Geomorphology, 41(4), 285–307. https://doi.org/10.1016/S0169-555X(01)00060-5

Leonarduzzi, E., P. Molnar, and B. W. McArdell (2017), Predictive performance of rainfall thresholds for shallow landslides in Switzerland from gridded daily data, Water Resour. Res., 53, https://doi:10.1002/2017WR021044.

6.9

Real-size rockfall experiment: How different rockfall simulation impact models perform when confronted with reality?

François Noël[1], Emmanuel Wyser[1], Michel Jaboyedoff[1] & Marc-Henri Derron[1]

[1] Risk Analysis Group, Institute of Earth Sciences (ISTE), University of Lausanne, CH-1015 Lausanne (francois.noel@unil.ch)

To manage rockfall hazards, it is important to correctly estimate the reach distances and velocities of rock blocks. For that, characteristics of 103 impacts from a real-size rockfall experiment were added to a visualization tool to facilitate the analysis of empirical data and the comparison with numerous rockfall simulations impact models (Noël et al., 2017a, in this conference). In this presentation, the particle impact behaviour from the empirical data is first explored and the developed tool described (Figure 1, 1st line). We observe that the normal apparent coefficient of restitution R_n clearly increases with decreasing incident angle θ_1 and normal velocity V_{n1}. The restituted tangential velocity V_{t2} shows a linear increase with increasing incident tangential velocity V_{t1}, so a constant apparent tangential coefficient of restitution R_t. The apparent total coefficient of restitution R seems to decrease linearly with the angular deviation of the trajectory. This could be explained like this: the more work the ground has to provide to change the course of the particle, the more kinetic energy is lost through plastic deformation. The output values of the different models at their default parameters corresponding to the terrain materials are then compared. Finally, the effect some input parameters have on the models is explored using real-time updates of the output values. (Figure 1 follows the References section due to its full page format)

REFERENCES

Azimi, C. & Desvarreux, P., 1977. Calcul de chutes de blocs et vérification sur modèle réduit.

Dorren, L., 2015. Rockyfor3D (v5.2) revealed - Transparent description of the complete 3D rockfall model. ecorisQ paper, p.31.

Noël, F. et al., 2017a. Real-size rockfall experiment: A relatively simple method to acquire 3D impact characteristics from video footage. In 15th Swiss Geoscience Metting. Davos.

Noël, F. et al., 2017b. Development of a 3D rockfall simulation model for point cloud topography. In European Geosciences Union General Assembly 2017. Vienna, Austria.

Pfeiffer, T.J. & Bowen, T.D., 1989. Computer Simulation of Rockfalls. Environmental & Engineering Geoscience, 26(1), pp.135–146.

Stevens, W.D., 1998. RocFall, a tool for probabilistic analysis, design of remedial measures and prediction of rockfalls. University of Toronto.

Wyllie, D.C., 2014. Rock fall engineering: development and calibration of an improved model for analysis of rock fall hazards on highways and railways. The University of British Columbia.

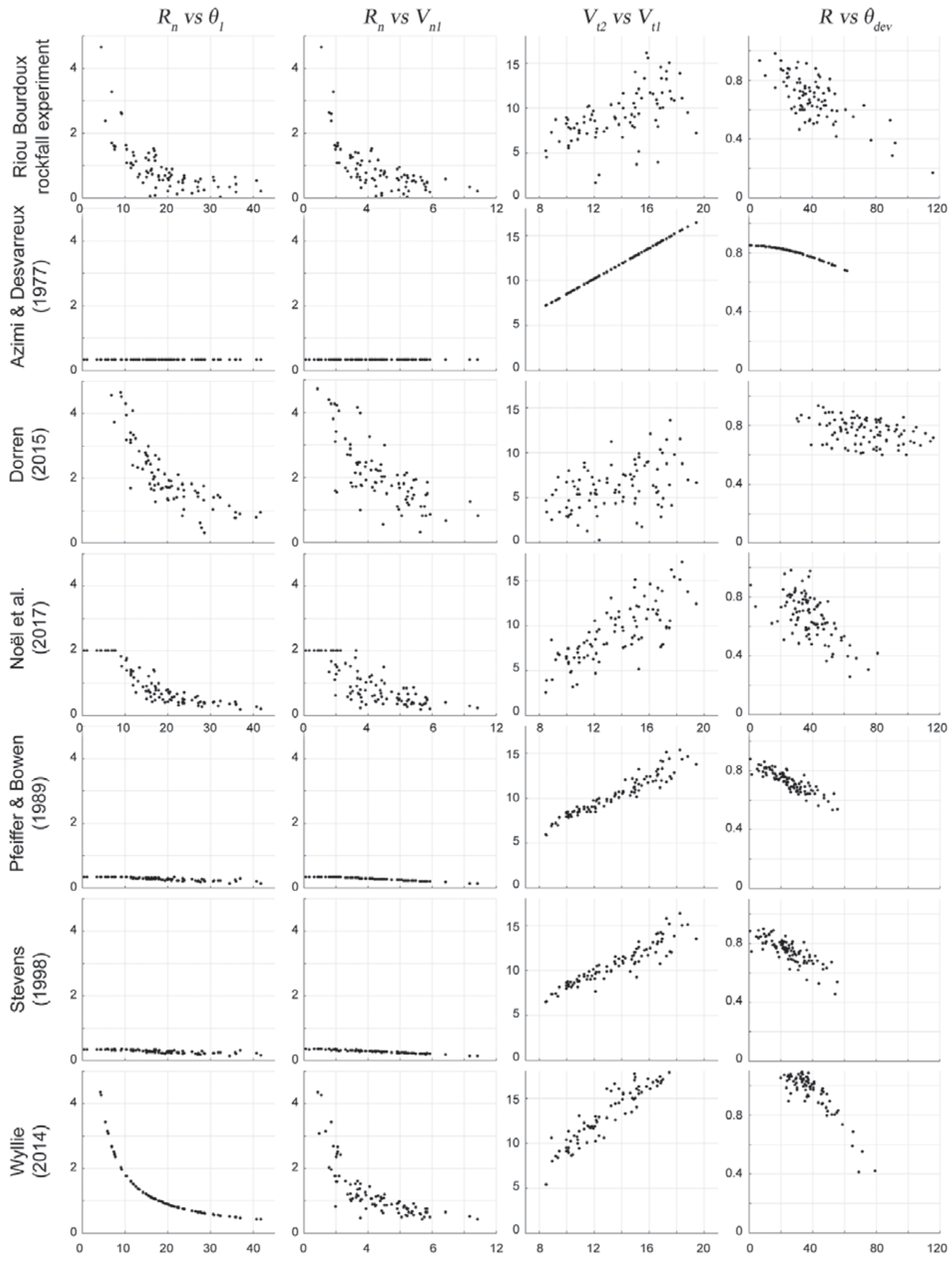

Figure 1. Comparison of different rockfall impact models with real-size rockfall values using all the same 94 impact's incident values. Column 1 (C1) shows the apparent normal coefficient R_n in relation with the incident impact angle θ_I. C2 shows R_n vs. the incident normal velocity V_{nI}. C3 shows the restituted tangential velocity V_{t2} vs. the incident tangential velocity V_{tI}. C4 shows the total apparent coefficient R vs. the angular deviation θ_{dev}.

6.10

Numerical simulations of mudflow movements using RAMMS:HILLSLOPE Software: a case study from Uzbekistan

Bakhtiar Nurtaev[1], Nurbek Inatov[1], Diyor Nurtaev[1], Dilshoda Kurbanova[1] & Yves Bühler[2]

[1] Institute of geology and geophysics, Olimlar 49, 100041 Tashkent, Uzbekistan (nurtaevb@gmail.com)
[2] WSL Institute for Snow and Avalanche Research SLF, Davos Dorf, 7260,Switzerland

In Central Asian Uzbekistan, 100 up to 300 active debris flows and landslides occur every year. The occurrence these disasters has great negative impact for the local communities and their economy. In the framework of Swiss National Science Foundation (SNF) supported project “Improving Hazard Assessment for debris flows, rockfalls and snow avalanches in Uzbekistan applying numerical models”, the Institute of Geology and Geophysics Uzbekistan and the Swiss WSL Institute for Snow and Avalanche Research SLF foster their partnership to exchange knowledge in the application of numerical models for hazard mapping and mitigation measure planning.

Numerical simulations of landslides/debris flow movements are difficult because the dynamical behaviour of each process is governed by different flow regimes and impact mechanics in interaction with the terrain. The present study focuses on the simulation and analysis of three selected landslides/mudflow events occurring during the past years at different regions in Uzbekistan applying the RAMMS:HILLSLOPE Software (Christen et al., 2011). The basins chosen for this study differ considerably in their geological-structural and geomorphological aspect in order to represent the present variability of typical alpine environments. The main emphasis was to understand how closely numerical simulation predicted the flow paths, runout distances, velocities and impact pressures of such processes in alpine terrain.

The landslide a) Djauz is located in the basin of the river Djinidarya in South Uzbekistan where it produced a mudflow with volume of 0.3 million m^3. The beginning of the landslide movement was recorded on March 11, 2015. During 6 hours a mass of rocks with height up to 10 m moved for a distance of 600 m. The flow width varied from 20 m in the upper, 45-50 m in the middle and up to 17 m in the lower zone. The mudflow b) Baybaksay is located close to Charvak water reservoir in Tashkent region where mudflow with a volume of 1.4 million m^3 occurred. The beginning of the landslide movement was recorded on April 7, 2005 and during 2.5 hours the mass of rocks with a height up to 10 m moved for a distance of 800 m. Within next 3 days it moved another 250 m, destroying a important road, a bridge and some old facilities.

The landslide c) Khandiza is in the basin of the river Khursandarya in South Uzbekistan close to village Khandiza, at the same place where a previous landslide occurred in 2015. The beginning of the landslide movement was recorded on March 31, 2017, when mudflow with volume of 1.8 million m^3 occurred. During 22 hours the mass of loess soil with a height of 3 to 5 m moved for a distance of 110 m. 257 persons living in the expected hazard zone (66 houses) were temporarily evacuated.

Within the next 3 days (April 3)the landslide moved for a distance of 230 m, with heights up to 10m, destroying a school building. Within another 3 days (April 6) the landslide reached the river and covered half of it‘s bed. The landslide soil was partially washed away by the the main river and was moved by excavators in order to prevent the full blocking of the river bed. The overall runout of the mudflow within 18 days was 2200 m (Fig.1).

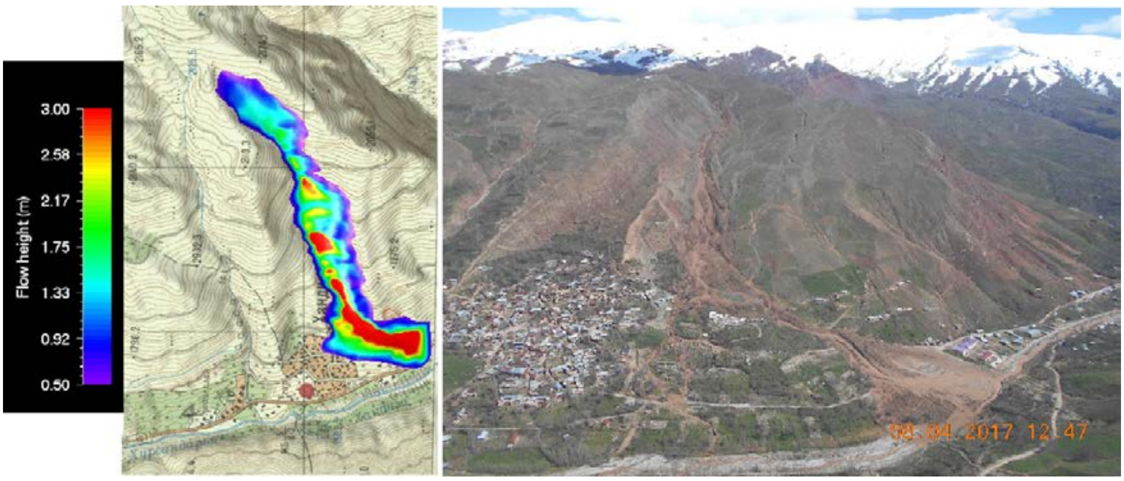

Figure 1. Best-fit results of the mudflow event Khandiza, simulated with RAMMS: HillSlope.

A prerequisite for meaningful numerical calculation is an accurate digital elevation model. The available resolution of the digital elevation models is often given by the products of national mapping agencies. Bühler et al. (2011) demonstrated that digital elevation models with poor spatial resolution (on the order of 25 m and more) may miss important terrain features while too accurate elevation models (on the order of 1 m or less) may lead to extensive computation times and even incorrect simulation results. We selected a 5m digital elevation model as the optimal spatial resolution for our cases.

Three documented mudflows in Uzbekistan were backcalculated with RAMMS: HILLSLOPE simulation tools. These results are based on the assumption that the entire landslide fails instantaneously and not progressively as a sequence of smaller landslides with barriers over a longer period of time. Therefore we can predicted the flow paths and runout distances, but not the real velocities of such processes. Generally the runout prediction of simulation models for the three mudflow events show plausible results when comparing to the observed deposition zones. These vital output parameters can very helpful to predict runout zones of potential future flows. However, more case studies have to be conducted to develop a more comprehensive recommendation for modeling the runout of mudflows in natural terrain.

REFERENCES

Christen, M., Bühler, Y., Bartelt, P., Leine, R., Glover, J., Schweizer, A., Graf, C., McArdell, B. W., Gerber, W., Deubelbeiss, Y., Feistl, T., and Volkwein, A. (2012). Integral hazard management using a unified software environment: numerical simulation tool “RAMMS” for gravitational natural hazards, edited by: Koboltschnig, G., Hübl, J., and Braun, J., 12th Congress INTERPRAEVENT, 23–26 April 2012 Grenoble, France, Proceedings, Vol. 1, Klagenfurt, International Research Society INTERPRAEVENT, 77–86.

Bühler Y., Christen M., Kowalski J. and Bartelt P. (2011). Sensitivity of snow avalanche simulations to digital elevation model quality and resolution. Ann. Glaciol., 52(58), 72–80.

6.11

Experience of snow avalanche numerical simulation in Uzbekistan

Eleonora Semakova[1], Albert Popov[2] & Yves Bühler[3]

[1] Ulugh Beg Astronomical Institute of the Uzbekistan Academy of Sciences, Department of Applied Space Technologies, 33 Astronomicheskaya str., Tashkent, 100052, Uzbekistan (ella9sem@gmail.com)
[2] Centre of Hydrometeorological Service at Ministry of Emergency Situations of the Republic of Uzbekistan, 72, 1 st Bodomzor yuli str., Tashkent, 100052, Uzbekistan
[3] WSL Institute for Snow and Avalanche Research SLF, Flüelastrasse, 11, 7260 Davos Dorf, Switzerland

Progress in Uzbekistan's economic development predetermines the future active development of the republic's mountain territories and these include adventure tourism, road-building and electric power line construction. The development and recreational activities in the mountains are threatened because of frequent avalanche activity, which is widespread over the mountain ranges of Uzbekistan (Semakova et al. 2009). Numerical avalanche simulation is a helpful tool to tackle this hazard. It can calculate runout distances and impact pressures and therefore estimate potential damage. Accordingly avalanche dynamics calculations are important for decision making about risk assessment, the engineering of protection structures, and the forecasting and monitoring of snow avalanches.

By the example of selected avalanche catchments, located in the Western Tien-Shan mountains and with economic importance and recreation activities, we considered observed snow avalanches that are different by genesis types, volumes, and runout distances. To simulate them we used the RAMMS software, developed by the WSL Institute for Snow and Avalanche Research SLF (Bühler et al. 2011). This modeling software can calculate the flow height, velocity, and impact pressure in complex three-dimensional terrain for snow avalanches, rockfalls, debris flows, and shallow landslides, from initiation to runout. Thanks to calibration and verification using full-scale tests at various sites, the model can be applied to study hazards in any mountain area where observations exist to adapt the model parameters to local conditions. Calculation of the dynamic characteristics at every point in the flow will enable risk assessments to be performed for objects located in the hazard area.

The experience of the dynamic modeling of snow avalanche in the first study area (Kamchik pass region, Fig. 1) showed the difference in avalanche runout distance and affected area when different digital elevation models (DEMs) were used (Semakova & Bühler 2017). These DEMs were generated using various data (remote sensing and topographical data) and techniques (optical stereo-photogrammetry, radar interferometry, and laser altimetry) with specific spatial resolution and acquisition date. In this case the input parameters such as friction coefficients, release zone height, snow density, avalanche category, numerical calculation schemes were the same. We found the DEM with which the calculated avalanche parameters corresponded to real observations.

Figure 1. Location of study area: (a) - Kamchik pass region, (b) - Chimgan valley.

The second study area (Chimgan valley, Fig. 1) is one of the most popular mountain resorts in Uzbekistan and well known for downhill skiers, snowboarders and hikers. We compared the trends in annual and winter values for average air temperature and precipitation sum in these study areas as well as in snow and avalanche characteristics. The numerical simulation for extreme dry snow avalanches with maximal volume and rare frequency in the Chimgan valley showed good agreement between observed and calculated runout distances. Automatically calculated friction parameters for small wet snow avalanches revealed inconsistency with real cases but this analysis will be repeated with new DEM data and the scientific version RAMMS, which takes snow temperature, density variation and snow erosion into account.

Moreover, one of the future tasks is to assess the influence of new snow fences and protective anti-avalanche constructions on the change in the dynamic characteristics of snow avalanches and debris flows in given catchments of the study areas to increase the safety for highways and economic objects in an avalanche prone area of Uzbekistan.

REFERENCES

Bühler Y. et al. 2011: Sensitivity of snow avalanche simulations to digital elevation model quality and resolution. Annals of Glaciology 52(58), 72-80.

Semakova, E. & Bühler, Y. in press: TerraSAR-X / TanDEM-X data for natural hazards research in mountainous regions of Uzbekistan. JARS, SPIE.

Semakova E. et al. 2009: The current state of avalanche risk analysis and hazard mapping in Uzbekistan. Proc. of ISSW, 509-513, Davos, Switzerland.

P 6.1

Detection and analysis of space-time landslides pattern in Switzerland

Marj Tonini[1], Mariaelena Cama[2]

[1]Institute of Earth Surface Dynamics, Faculty of Geosciences, University of Lausanne (Switzerland)
[2] Institute of Geography, Department of Geosciences, University of Tuebingen (Germany)

Landslides represent a major hazard in the mountainous regions, causing extensive erosion and being responsible of fatalities and high economic losses. In particular, in the Swiss territory landslides are related to the geological, geomorphological and glacial history of the country and are influenced by preparatory factors, such as climate or human activities. It is estimated that more than 6% of the area in Switzerland is exposed to landslides causing damages for about CHF 19.46 million per year (mean 1972-2016 - source WSL). Therefore, the Swiss Federal Institute for Forest, Snow and Landscape Research (WSL,Hilker et al. 2009) implemented a multitemporal landslide damage database at the national scale. This catalogue is based on the analysis of historical information and covers a period of 45 years (1972 up to nowadays).

A vast literature exists on landslides, especially concerning susceptibility mapping aimed at evaluating the probability of having or not a landslide in a given area. These maps are the result of sophisticated stochastic approaches based on the relatioships between the landslide events and a set of known predisposing factors (e.g. slope, aspect, lithology, land cover, precipitations). These techniques normally assume that landslides are uncorrelated in space and in time: however, recent studies demonstrated that this assumption is false. In particular, two recent studies focused on the pattern distribution and the cluster behaviour of landslides in Switzerland applied a global cluster indicator, namely the Ripley's K-function, to demonstrate that the analysed events were spatially clustered at well identified distance ranges (Pedrazzini et al. 2015; Tonini et al. 2014). Results showed also that the spatial distribution of landslides was mainly conditioned by the tectonic activity and by climatic processes (i.e. the action of glaciers on the formation of over deepened valleys). As regards the temporal distribution of landslides, Witt et al. (2010) analysed temporal correlations and temporal clustering of a proxy historical landslide time series, demonstrating that the assumption that landslides are uncorrelated in time is false.

The present research analyses the spatio-temporal pattern distribution of landslide events with the aim of detecting whether space and time are independent variables of the overall phenomena or if, conversely, neighbouring events are also closer in time, generating clusters. More in detail, both global and local cluster indicators were applied to estimate the degree of clustering and to detect overdensities. This approach was successufully applied to analyse the pattern distribution of wildfires in Portugal (Tonini et al. 2017). Finally, possible relationships among spatio-temporal clusters of landslides and environmental variables were investigated. Specifically, a multivariate analysis, including associated variables such as the type of landslide, the rainfall distribution, the affected objects was applied to characterise the detected clusters and to infer about the independency of different classes of events.

The results revealed the presence of significant clustering of all analysed structures at different scales, measured in terms of distances (in space) and frame periods (in time). The comparison of the detectable spatio-temporal clusters and the surrounding spatial variables (rainfall records, land use changes, presence of new infrastructure, increase in wild fires, and abandonment of agricultural terraces) led to the identification of events which predisposed the slope instability or, conversely, which stabilized a previously active areas.

In conclusion, thanks to the application of spatio-temporal cluster analysis, we have been able to identify framing periods where the hazard is more likely to occur and, finally, valuing the huge effort it costs to create multitemporal landslide inventories.

REFERENCES

Hilker, N., Badoux, A. & Hegg, C., 2009. The Swiss flood and landslide damage database 1972-2007. *Natural Hazards and Earth System Science*, 9(3), pp.913–925.
Pedrazzini, A. et al., 2015. Characterisation and spatial distribution of gravitational slope deformation in the Upper Rhone catchment (Western Swiss Alps). *Landslides*, (February).
Tonini, M. et al., 2017. Evolution of forest fires in Portugal: from spatio-temporal point events to smoothed density maps. *Natural Hazards*, 85(3), pp.1489–1510.
Tonini, M. et al., 2014. Spatial pattern of landslides in Swiss Rhone Valley. , pp.97–110.
Witt, A. et al., 2010. Temporal correlations and clustering. , 1156(June), pp.1138–1156.

P 6.2

Kinematic Analysis of the September 2016 Moosfluh Landslide Acceleration

Franziska Glueer*, Andrea Manconi* & Simon Loew*

[1]*ETH Zurich, Institute of Geology, Earth Sciences, Zurich, Switzerland*

The Great Aletsch Glacier is experiencing a remarkable retreat with rates in the order of 50 meters every year. During the last 150 years, several pre-existing landslides have been partially or completely unloaded from the glacier ice mass and reacted by showing relevant surface deformation. In particular, a large slope instability located in the area called "Moosfluh" has shown evidences of slow but progressive increase of surface displacement during the past 20 years. The toppling mode instability of the Moosfluh affects an area of about 2 km^2 and entails a total volume estimated in 150-200 Mm^3.

We monitored the evolution of the Moosfluh instability with two robotized total stations and time-lapse cameras. Comparison with surface displacement vector fields derived from total station measurements and digital image correlation allows to assess and explain local variations in strain fields and to develop a semi-quantitative kinematic model.

In late summer 2016 the Moosfluh instability experienced a large acceleration in particular at the toe of the instability (ca. 8 Mm^3). Compared to previous years when annual ground deformations were in the order of few centimeters or decimeters, during September-October 2016 maximum velocities have reached locally 1 m/day. Displacement rates decelerated between middle of September and middle of October, however, they have reached a steady state level of around 5 cm/day and remained constant during the winter period. In the 2017 spring season surface displacments have increased again and sectors of the slope were displaced by up to 50-60 meters. Currently (August 2017), displacements at the toe of the Moosfluh are in the order of 30 cm/day and still accelerating.

Our monitoring results show a remarkable change in the current displacement pattern compared to previous years. A secondary headscarp was generated and the majority of displacements are now concentrated in the last 200 m of altitude towards the glacier. Moreover, areas located close to the secondary headscarp show a larger vertical displacement compared with areas closer to the toe (see Figure 1). This can be intepreted as the formation of a basal sliding plane with maximum depth of 50 m.

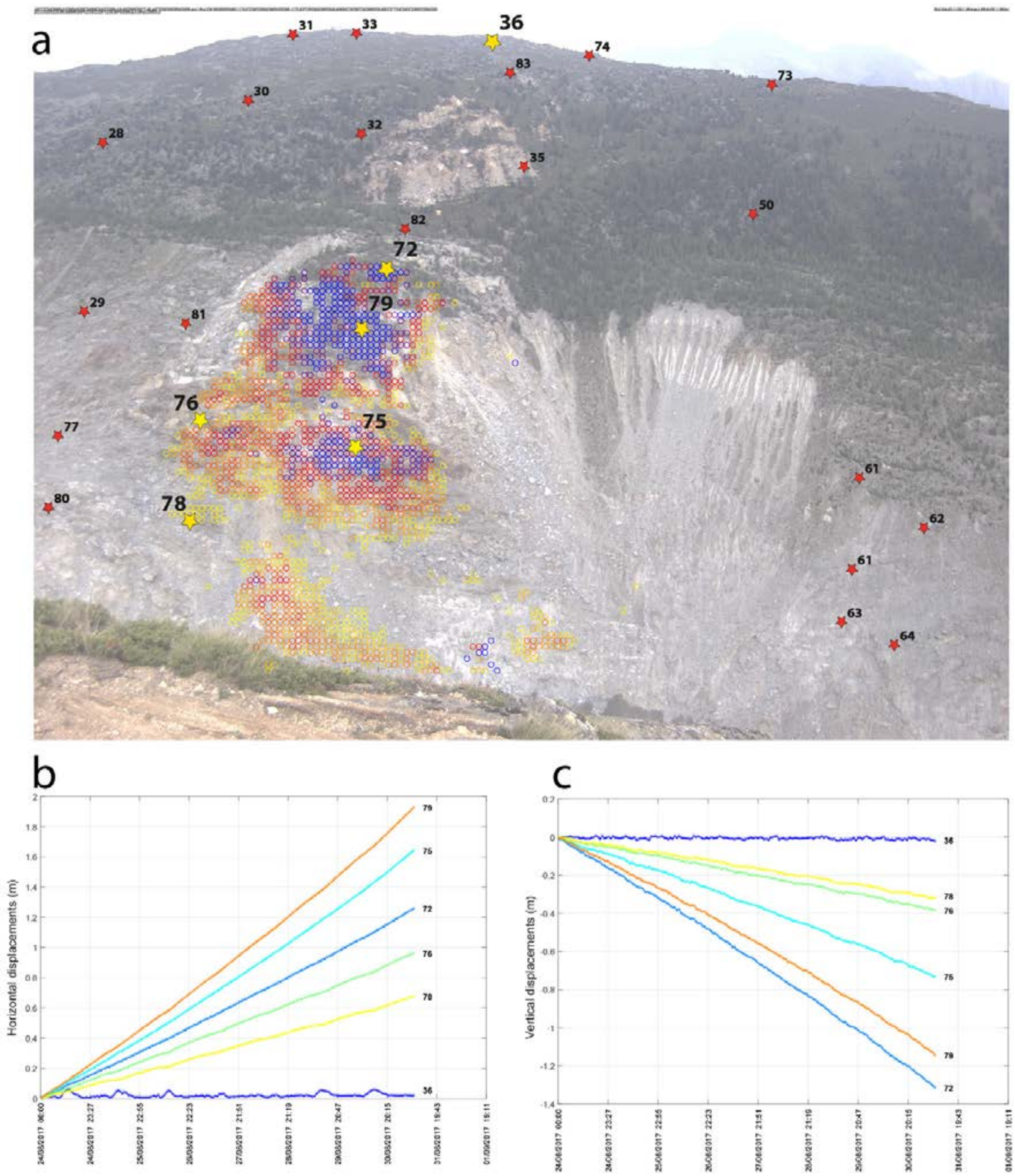

Figure 1. (a) Digital image correlation results relevant to the period 24/08/2017 – 30/08/2017 over the Moosfluh slope instability. Images acquired from the webcam located in Driest. The color scale shows the deformation in pixels. Numbered stars show the location of reflectors monitored via the Robotized Total Station (RTS) located on the other side of the valley (Driest). (b-c) Horizontal and vertical surface displacements of selected RTS monitoring points for the same time period shown in (a).

P 6.3

Inventory of shallow landslides in regards to their frequency in the Canton of Vaud (Switzerland).

Cedric Meier[1], Marc-Henri Derron[1], Michel Jaboyedoff[1], Christian Gerber[2], Veronica Artigue[2]

[1] Group RISK – ISTE, University of Lausanne, CH 1015 Lausanne, Switzerland.
[2] Natural Hazard group, UDN-DGE-DIRNA-GEODE, Rue de l'Université 5, CH-1014 Lausanne, Switzerland.

The study consists in making a new inventory of shallow landslides in the Canton of Vaud in Switzerland, including volumes and occurrences. The Canton of Vaud has been very active in developing approaches for natural hazard mapping over the last years (VD, 2017). It includes gravitational hazards such as: permanent landslides (deep), spontaneous landslides (shallow), rockfalls, subsidence or collapse. Although shallow landslides are typically small in volume, they are frequently located close to populated areas, have often high velocities and impact energies, and then can be very damaging for persons and infrastructures.

In 2015, the whole Canton de Vaud territory was covered by a new airborne LiDAR acquisition with an unprecedented density of points (up to 80 points / m^2). This new dataset offers an excellent opportunity to make a new inventory of shallow landslides including volumes estimations.
Main datasets used for this project are: 1) a digital elevation model (DEM) at 0.5 m grid cell size. The full LiDAR point clouds datasets are available too; 2) a former inventory including more than 610 events from years 1889 to 2013, 3) present phenomena and danger maps, 4) basic documents such as: geological and topographical maps, airphotos, ….

Main part of the work is to identify and map shallow landslides on hillshaded representations of the new DEM, for various geological, soils and sites conditions (Prealps, Plateau and Jura). The volume of each landslide is then assessed using the Sloping Local Base Level (SLBL) method (Jaboyedoff & Derron 2005). The SLBL method is based on the base level concept, typically the lowest level that the erosion can reach in sedimentology but applied here to shallow landslides. It is able to address a large number of landslides automatically. In a first step, in order to test the method, shallow landslides whose volumes are known from independent technical reports or inventories are used.

The goal is to get an inventory of shallow landslides representative of the various geological / sites conditions of the Canton. The preliminary results indicate that the volume follows power law like distributions, which depends on the geological context. In addition, in several cases, the reach-angle can be observed, allowing a first to assess the probability of propagation. All these results will improve significantly hazard and risk assessment maps for shallow landslides.

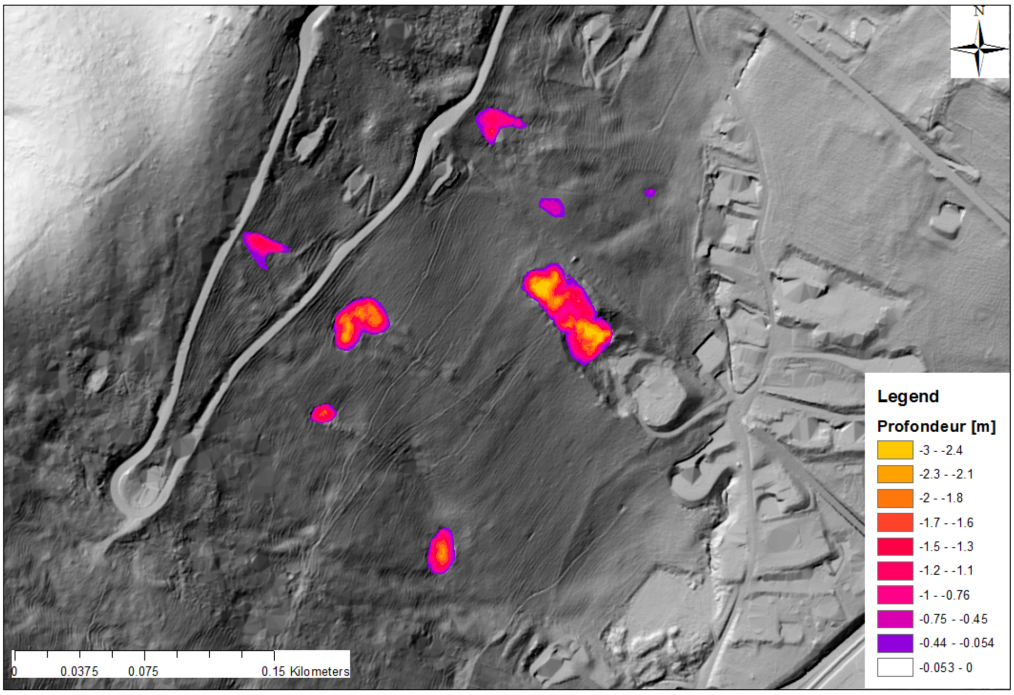

Figure 1. Map of shallow landslides at the site "Les Avants". The thickness has been estimated using the SLBL method.

REFERENCES

Jaboyedoff M., & Derron M.-H. 2005: A new method to estimate the infilling of alluvial sediment of glacial valleys using a Sloping Local Base Level, Geogr.Fis.Dinam. Quat., 28, 37-46.
VD (2017) : http://www.geo.vd.ch/theme/dangers_nat_thm, consulté le 12.05.2017.

P 6.4

Characterizing active clayey landslides dynamics by microseismic monitoring

Naomi Vouillamoz[1], Sabrina Rothmund[1], & Manfred Joswig[2]

[1] Institut für Geophysik, Universität Stuttgart, Azenbergstrasse 16, 70174 Stuttgart, Deutschland (naomi.vouillamoz@geophys.uni-stuttgart.de)

Landslides developed in clay-rich formations are characterized by unpredictable reactivation. In recent years, seismic monitoring of active landslides detected a variety of - generally weak – seismic signals which are inferred to be triggered by the slope deformation. Evaluating the landslide seismicity and characterizing its occurrence in space and time enable thus to monitor and map dynamics of the landslide in near real-time. Thus, passive seismic monitoring present a good approach to complement surveillance of active landslides. If precursor events are detected and recognized, it will suport early-warning systems and slope failure anticipation. However, extreme scattering and attenuation of the waveforms in the heterogeneous material composing the instabilities, combined to the inherent difficulty of operating seismic networks with optimal geometry in rugged terrains severely challenge standard approaches to event location and consequently impedes source processes interpretation.

In this study, we investigate continuous seismic data of the well-instrumented Super-Sauze landslide (Southeastern France) and compare observations with newly acquired seismic data at the Pechgraben landslide (Upper Austria). We apply the nanoseismic monitoring methodology to detect and evaluate seismicity patterns (Sick et al. 2012; Vouillamoz et al. 2016). Despite varying displacement rates (mm d^{-1} – 10’s of cm d^{-1}) and hydrological conditions, comparable signals that range from impulsive earthquake-like signals to minute-long tremor sequences are detected at both landslides. In addition to beam forming methods (Joswig, 2008), we use waveform attenuation patterns to evaluate the signal source location.

Source sizing is then benchmarked with calibration shots carried out at the two landslides. First results indicate that endogenous seismicity rates correlate positively with higher displacement rates. Signals seem to be preferentially originated at shearing boundaries of the slides, which in turn suggests creeping processes to be the main source of seismic energy release.

REFERENCES

Joswig, M. (2008): Nanoseismic monitoring fills the gap between microseismic networks and passive seismic, special topic, Leveraging Technology, first break, 26, 117–124.

Sick, B., Walter, M. & Joswig, M. (2012): Visual Event Screening of Continuous Seismic Data by Supersonograms, Pure and Ap-plied Geophysics, doi:10.1007/s00024-012-0618-x.

Vouillamoz, N., Wust-Bloch, G.H., Abednego, M., & Mosar, J. (2016). Optimizing Event Detection and Location in Low-Seismicity Zones: Case Study from Western Switzerland. Bulletin of the Seismological Society of America, 106(5), 2023-2036. doi: 10.1785/0120160029.

P 6.5

Model and cartography of the Saint-Eynard cliff erosion by rockfalls

Cécile d'Almeida[1], Antoine Guerin[1], Michel Jaboyedoff[1] & Didier Hantz[2]

[1]Institute of Earth Sciences, University of Lausanne, Geopolis, CH-1015 Lausanne (cecile.dalmeida@unil.ch)
[2]University of Grenoble Alpes, ISTerre, FR-38000 Grenoble

Rockfall hazard is a major threat in mountainous area. The Saint-Eynard limestone cliff in the north of Grenoble, France, is prone to rockfalls. As the Grenoble agglomeration extends to the Saint-Eynard footcliff, a proper characterization of the rockfall hazard is required to set suitable safety measures for these high exposed areas.

In order to evaluate the erosive dynamic of the Saint-Eynard cliff, a rockfall detection based on the Lidar method has been performed from 2015 to 2017. Over 900 rockfalls have been detected with a resolution of 0.001 m^3 (Figure 1).
This method provides the location, the volumetric and the temporal (annual accuracy) information of rockfall.

Several studies propose the use of a power law to model the frequency-magnitude distribution of rockfalls and its use for diffused hazard assessment of future rockfall events.
The use of a power law for the purpose of hazard assessment is based on the assumption of its temporal stability. The Saint-Eynard is one of the longest Lidar monitored site with 8 years of Lidar records. Benefiting from this long-time set of data, the temporal stability of the power law is evaluated.
The result showed that the power law is stable over years and quite sensitive to the quality of the database considered. However, it is a suitable method for the short time prediction of rockfall.

The Lidar detection method allows to establish a consistent rockfall database but suffers from some limitations such as superimposition of rockfalls and large temporal dating (annual accuracy).
The exploitation of weekly photographs of the cliff for rockfall detection allows to get rid of superimposition issues and to refine the temporal information of the rockfall.

An automatic method of change detection using heterogeneous and medium resolution photographs is an ongoing development of this study. The method should detect changes in homogeneous media just like the cliff surface of the Saint-Eynard site, and handle differences in illumination, shadowing, resolution, scale and framing. Currently, the method allows to detect rockfalls in case of relatively same scale, and permits to detect smaller rockfall than the ones detected with the lidar method (Figure 1). Nevertheless, it importantly suffers from noise due to an insufficiently fine registration in case of different scales. It prevents the detection of small rockfalls that the Saint-Eynard cliff experiments the most.

The temporal information retrieved from the photographs are intended to be used to evaluate the fluctuation of the erosion dynamic in a year and to evaluate correlations with meteorological fluctuations. This study will lead to the computer modelling of rockfall process, cliff retreat and talus debris accumulation.

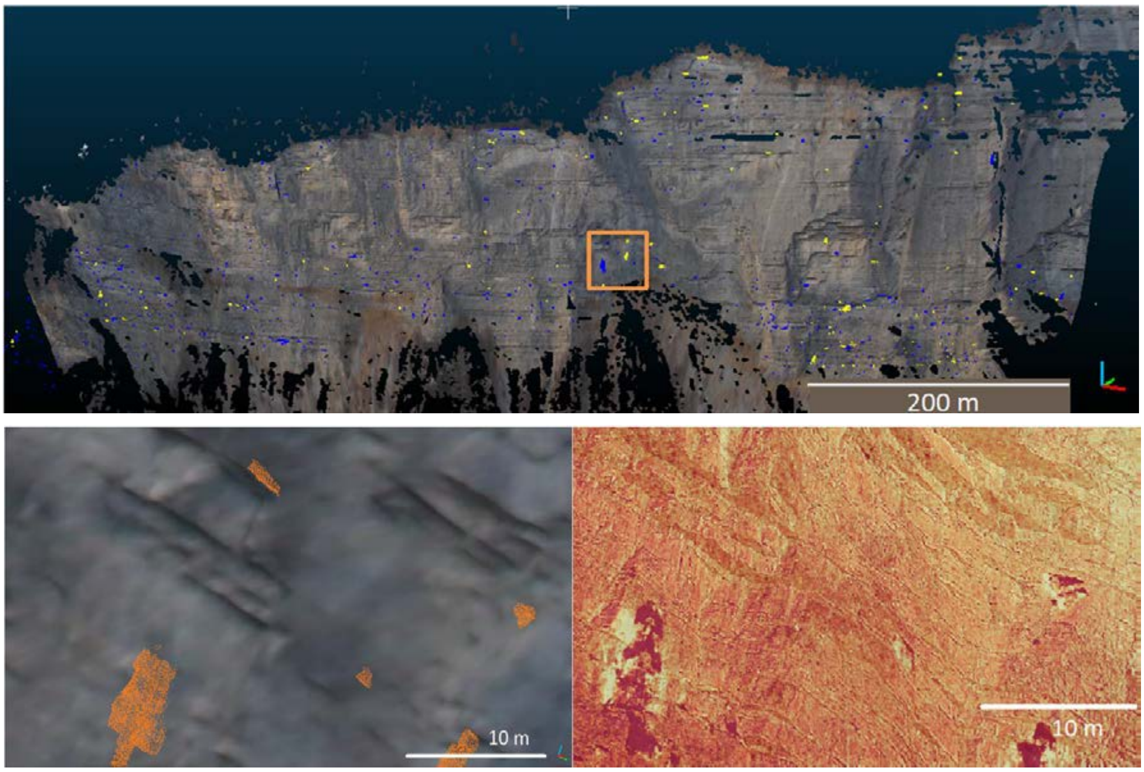

Figure 1. Top: Rockfalls detected with the Lidar method for the site of Saint-Eynard where blue rockfalls occurred between 2015 and 2016, and yellow rockfalls occurred between 2016 and 2017. Bottom images are blow-ups of the orange rectangle of the top one: result of the rockfall detection from the lidar point cloud (left) and from the photography method (right).

REFERENCES

Barlow, J., & al. 2012: Modelling cliff erosion using negative power law scaling of rockfalls, Geomorphology, 139-140, 416-424.

Hantz, D., Vengeon, J-M. & Dussauge-Peisser C. 2003: An historical and probabilistic approach to rockfall hazard assessment. Natural hazards and Earth System sciences, 3, 693-701.

Carrea, D., Abellan, A., Derron, M-H. & Jaboyedoff, M. 2015: Automatic rockfalls volume estimation based on terrestrial laser scanning data. Engineering Geology for Society and Territory,2, 425-428

P 6.6

Dramatic granular impact(s): a plastic- or friction-dominated transition phase

Emmanuel Wyser[1], Michel Jaboyedoff[1]

[1]*Institute of Earth Science, University of Lausanne, Quartier Mouline (emmanuel.wyser[at]unil.ch)*

Over the last decade, typical responses of impacted surface receive an increasing interest. Rockfall dynamic is mainly governed by 1) rock mass motion during both free fall phase and impact phase (e.g. velocity, angular momentum, restitution coefficient) and by 2) various parameters related to terrain deformation properties (e.g. grain size distribution, void fraction, cohesion and friction angle). We investigated different bed response over the impactor dynamic, i.e. how would the rock mass behave when considering a friction-dominated or plastic-dominated regime within the impacted medium.

We established our own 2D distinct element algorithm to solve impact problems of low to intermediate impact velocity, i.e. typically ranging from 1 to 10 m/s, onto granular media (for a detailed overview of DEM, refer to Poschel & Schwager, 2005). The latter is written in a C programming language environment to ensure fast calculation cycles. Our visco-elastic model (often referred as a nonlinear spring-dashpot system) solves a set of equations of motion (translational and rotational) for the granular behavior of the medium. Non-linear normal response (i.e. based on the Hertz-Mindlin theory for spherical impact) and linear shear response are addressed as well as normal cohesive ductile bonds between particles (e.g. plastic deformations occur when the tensile strength or normal strain at the contact reaches a critical value leading to breakages of cohesive bonds, see Langlois et al. 2015, for further details).

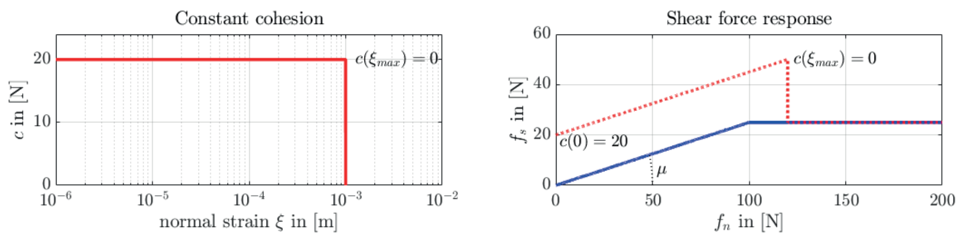

Figure 1: Illustration of a simplistic constant cohesive force (left) and a linear cohesive shear force within the granular medium. Bonds breakage becomes irreversible (no new bonds can be formed) as soon as the normal strain exceeds a critical threshold.

Since impact dynamic is mainly governed by both initial impactor and bed conditions, we conducted a set of preliminary numerical investigations related to differential responses of the bed. The latter are due to variable initial bed conditions regarding constant initial impactor conditions.

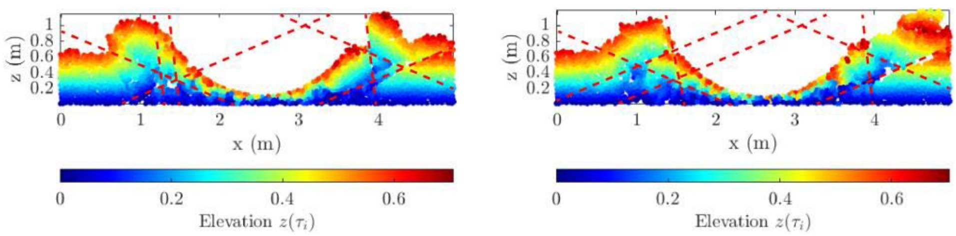

Figure 2: Initiation of shear zones induced either by a regular (left) or plastic (right) shear stress response of the granular medium. The initial granular medium properties (i.e. geometry of the assembly, grain size and mechanical parameters) are invariant. Impact conditions assume an initial impact velocity of 10 m/s for an impact projectile radius 20 times greater than the average medium's particle radius. The Bond number is 200.

These preliminary investigations suggest that within a cohesive medium, the frictional response mainly prevails as a governing strain mechanism (e.g. shear strain). In addition, the impactor's rebound appears to be clearly governed by an elastoplastic response of the medium. This suggests a combination of both friction (large shear strain) and elastoplastic influences over the impactor dynamic.
As prospective suggestions, we will carry on many numerical experiments to better establish the respective influences to propose a quantitative description of the impactor's rebound.

REFERENCE

Langlois, V., Quiquerez, A., Allemand, P. (2015) Collapse of a two-dimensional brittle granular column: Implication for understanding dynamic rock fragmentation in a landslide. Journal of Geophysical Research: Earth Surface. 120. 1866-1880.

Poschel, T., Schwager, T. “Computational Granular Dynamics: Models and Algorithms” Springer-Verlage Berlin Heidelberg. 2005.

P 6.7

Real-size rockfall experiment: A relatively simple method to acquire 3D impact characteristics from video footage

François Noël[1], Emmanuel Wyser[1], Michel Jaboyedoff[1] & Marc-Henri Derron[1]

[1] *Risk Analysis Group, Institute of Earth Sciences (ISTE), University of Lausanne, CH-1015 Lausanne (francois.noel@unil.ch)*

To manage rockfall hazards, it is important correctly estimate the reach distances and velocities of rock blocks. When rockfall is primarily composed of freefall and rolling rebound phases, free-flight velocities and reach distances are mainly the result of energy transfers that occur at impacts against the ground. So, it is better to focus directly on impacts for calibration of simulation models. For this, accessible and shareable empirical data with which models can be tested are needed. Since steep terrains are difficult to access, we developed a fast acquisition method that does not require measurement of impact positions using survey methods, precision GPS or trajectory tracking algorithms. The impact position is rather visually noted on high resolution digital terrain model, like we did for the Riou Bourdoux site (Figure 1). The time interval between the impacts is then used to reconstruct the 3D trajectories with their velocities:

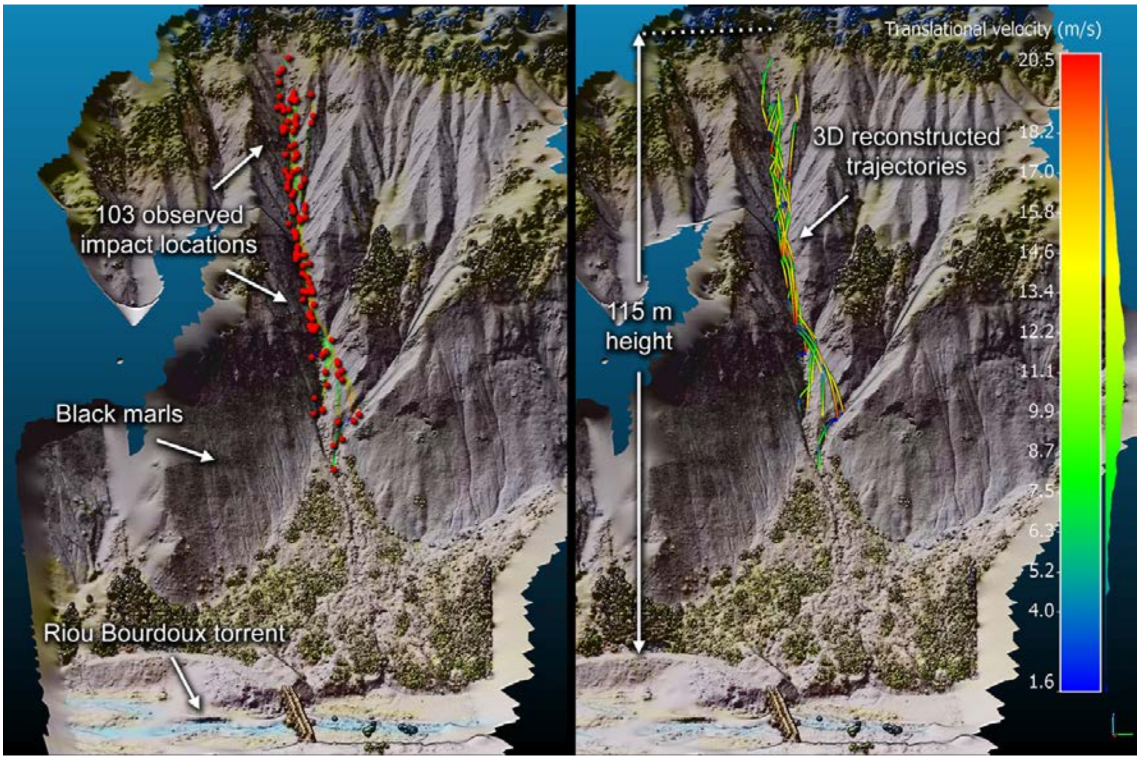

Figure 1. The high resolution TLS meshed 3D point cloud of the Riou Bourdoux site. The scene is shaded with computed hillshade & Eye Dome Lighting values based on the local terrain orientation and not by wrapping a high resolution photo over low resolution elevation data (Hue & Saturation from LiDAR camera, Value from hillshade & EDL). This is important to specify because here the detailed terrain we observe is directly linked to the good quality of the TLS data.

The high resolution digital terrain model can be generated by SFM or LiDAR methods. The rockfall trajectories must ideally be filmed with more than one point of view. Those reconstructed in 3D can then be compared with those in the videos to validate the location of the points of impact. For the Riou Bourdoux site, 103 impacts were noted from 11 trajectories of blocks of about 0.35 m (0.04 m^3). Characteristics such as 3D terrain orientation, incident and restituted velocities, incident angle and 3D deviation of 103 impacts were added to a visualization tool (Figure 2). It has been developed to facilitate the analysis of empirical data and to help making an informed choice of the parameters to be used with some rockfall simulation models. Ultimately, as the tool is easily shared, it should improve practice and facilitate the teaching of rockfall hazards.

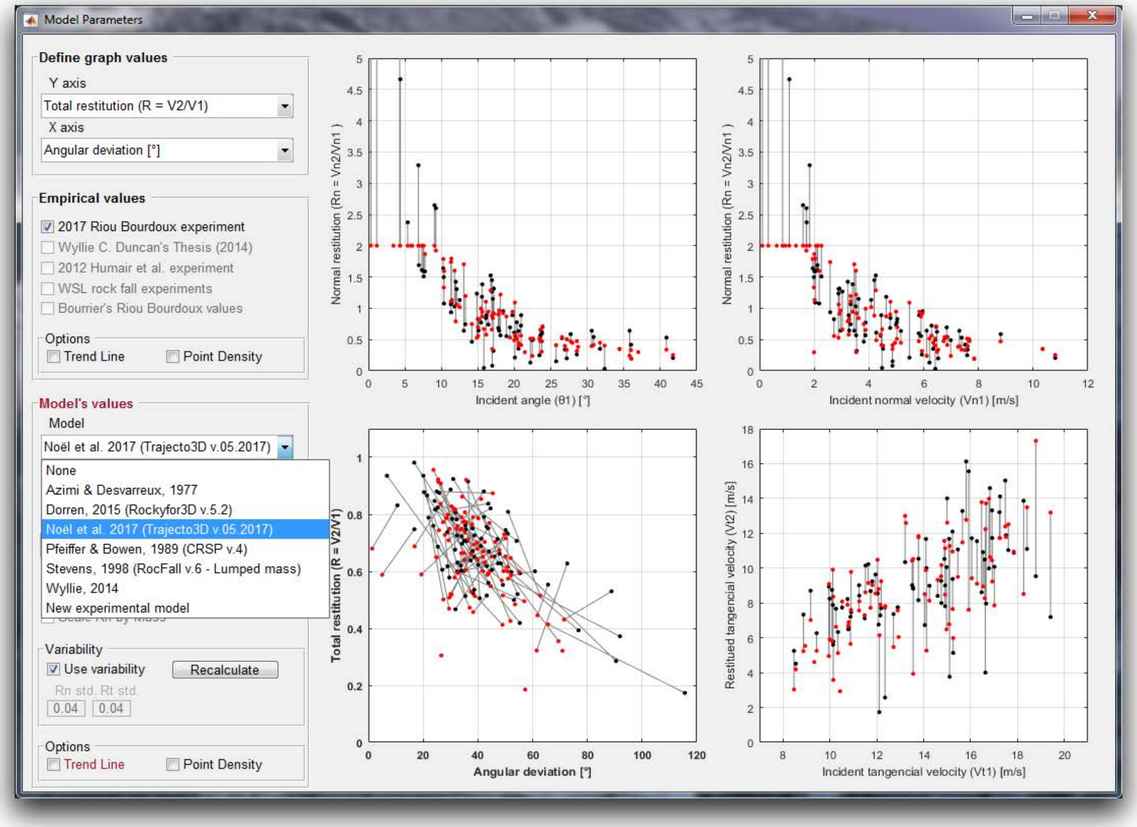

Figure 2. The tool we developed in which the empirical values of the real-size rockfall experiment are embedded and shown as black dots on the graphs. User can click on each graph and chose which variables he wants do display while trying to find correlations. We also added at the core of the tool numerous existing rockfall simulation models. Their outputs values computed in 3D from the input empirical values can be displayed in red, linked to their corresponding empirical values with grey lines. Some of their parameters can be adjusted (eg. Rn, Rt, soiltype, the slope surface roughness, etc.), while seeing the effect on the outputted values in real-time. This should help finding the right set of parameters for a given study site, especially if more than one rockfall simulation program is used. Of course, the given study site should be similar to the one from which the empirical values comes from. So feel free to contact us if you have empirical values to share!

P 6.8

Pression démographique et outils d'analyse de dangers et risques gravitaires au Rwanda.

Emmanuel NDUWAYEZU[1], Michel JABOYEDOFF[1], Marc-Henri DERRON, Jean-Baptiste NSENGIYUMVA[2] & Emmanuel TWARABAMENYE[3]

[1]*Risk Group. INSTITUTE OF EARTH SCIENCE .UNIVERSITY OF LAUSANNE FGSE. UNIL MOULINE GEOPOLIS CH- 1015 LAUSANNE (emmanuel.nduwayezu@unil.ch)*
[2] *DIRECTOR OF RISK REDUCTION AND PREPAREDNESS UNIT, MIDIMAR KIGALI RWANDA.*
[3] *Departement of Geography, SCHOOL OF SCIENCE UNISERSITY OF RWANDA.*

Le territoire occupé par le Rwanda a été soumis à de nombreuses contraintes dont l'acuité et l'intensité ont varié dans le temps, en fonction de la variation des densités sur d'innombrables formes heurtées du relief (G. ROSSI 1991). Tout l'espace est exploité et l'habitat y est dispersé (BART F. 1993, CAMBREZY L. 1911), y compris parfois des zones avec des pentes très abruptes et les bas-fonds (CHARLERY DE LA MASSELIERE B. 1993; G.RWANYINZIRI 2008).

Cela a pour conséquence que, pendant la saison pluvieuse, les pentes avec les activités humaines sont affectées par les processus gravitationnels, principalement des glissements et des coulées de boue et de inondations. Les événements de cette dernière décennie (MIDIMAR 2012 et 2013) illustrent ces glissements de terrain et inondations fréquents comme principaux aléas de la montagne rwandaise. Mais les travaux déjà effectué sur l'espace Rwandais en l'état actuel des données illustrent une diversité des dangers et des risques (MIDIMAR : 2015, National Risk Atlas of Rwanda) dans cette espace dite des mille collines avec des altitudes qui y varient de 900 m à plus de 4500m.

Selon UWIZEYIMANA L (1991) il existerait une certaine périodicité d'occurrence des pics d'impacts sur les nombreux versants et vallées d'un territoire surpeuplé à faible taux d'urbanisation (17% selon le National Institute of Statistics of Rwanda, 2012). Et l'objectif de notre poster faire un aperçu sur l'évolution des méthodes d'études problèmes de la montagne au Rwanda tout en essayant de faire des essaie d'évaluation d'applicabilité de méthodes modernes (HORTON P. et alii 2013) eu égard à la qualité de données disponibles afin de mieux cerner les aléas pour mieux évaluer les risques (JABOYEDOFF M. et alii 2008 et 2012) relatifs à la montagne rwandaise.

REFERENCES

Bart , Fr., Montagnes d'Afrique, terres paysannes. Le cas du Rwanda. Bordeaux : CEGET, Presses Universitaires de Bordeaux, 1993.

Cambrezy, L. Conquête des marais au Rwanda et dynamique de population. In: Études rurales, n°83, 1981. pp. 45-67; doi : 10.3406/rural.1981.2664

Charlery de la Masseliere, B., « Versants du Rwanda: la gestion de l'incertitude ».in *Cahiers d'Outre-mer, n°185 de janv. Mars 1994*. pp. 7-22.

Charlery de la Masseliere, B. et alii, « La répartition régionale des cultures vivrières au Rwanda. Analyse statistique ». in *Cahiers des Sciences Humaines Vol.22, n° 3-4*. 1986 pp453-496.

Horton et alii.: Flow-R, un modèle de cartographie de la susceptibilité des flux de débris et d'autres dangers gravitationnels à l'échelle régionale, Nat. Hazards Earth Syst. Sci., 13, 869-885, doi: 10.5194 / nhess-13-869-2013, 2013.

JABOYEDOFF M. et alii; "Preliminary mass movement susceptibility mapping using DEM and Lidar DEM" In B. PRADHAN and BUCHROITNER (eds), *Terrigenous Mass Movements*. DOI: 10.1007/978-3-25495-6_5, Springer-Verlag, Berlin Heidelberg, 2012 pp.109-170.

MIDIMAR; National Disaster Risk Management Plan, Kigali, September 2013.

ROSSI, G., Croissance de la population, mise en valeur et équilibre des versants: quel avenir pour le Rwanda?» in Les Cahiers d'Outre-mer n°174 janvier- mars 1991. Bordeaux 1991.

P 6.9

Rockfall hazard evaluation in a touristic area of northern Tunisia using SFM photogrammetry in a zero data site

Mariam Ben Hammouda[1], Michel Jaboyedoff[1], Marc-Henri Derron[1], Samir Bouaziz[2]

[1] *University of Lausanne, ISTE-FGSE, Group Risk, Géopolis-Quartier Mouline 1015, Lausanne, Switzerland (mariam.benhammouda@unil.ch, +41 78 711 38 37)*
[2] *University of Sfax, ENIS Sfax, Laboratory 3E Tunisia (samir.bouaziz@enis.rnu.tn, +216 23 517 061)*

The study area is located in the north-west of Cap Bon, northern Tunisia, where the issues of landslides hazards have recently emerged. Despite the multitude, the complexity and the high degree of dangerousness of these instabilities, the region remains virgin without any previous numerical support or basic data for a risk study.

Djbel Korbous is an important relief dominating the southeastern edge of the Gulf of Tunis and presents a special site of tourism and therapy. The main road, which is the only access to it, is a coastal road passing along a damaged cliff and suffers of several instabilities and rockfall of different sizes reaching the sea and destroying the protection measures.

Structure for motion photogrammetry, being a simple, practical and inexpensive monitoring tool, was an efficient choice to initiate the modeling of a very vulnerable and inaccessible cliff. The present study aims at defining a multi-risk assessment methodology that fits to the characteristics of a touristic area where there were no pre-existing digital field data.

The first part aims at the development of a high quality digital terrain model for the entire site, about 12km2, which required photogrammetric acquisitions from the sea and GPS surveys to realize the georeferencing. Thus the mapping of phenomena and the characterization of potential and fallen volumes allow the consitution of the first instabilities inventory for the zone. In addition, many terrestrial LiDAR scans were realized to complete the first model as well as several local photogrammetric acquisitions were done to capture the spatio-temporal instabilities' evolution and to understand the mechanism of rupture and the cliff degradation.

The second part of the study is to constitute a quantitative and qualitative rockfall hazard zoning based on 2D and 3D trajectory modelling (RocFall, RockyFor 3D and Trajecto 3D).

As a result, SFM photogrammetry enabled the reconstruction of a high spatial resolution data support, providing a reliable and detailed 3D model for a site where there was no numerical data. Subsequently we define the main structurally controlled failure types and we could detect and map all potential instability sources from steep slopes.
Combining different rockfall numerical models all together allowed a complete and comparative analysis methodology to predict the rockfall runout distance and the propagation areas and to estimate velocities and energies of fallen blocks.

P 6.10

A revolutionary Array Synthetic Aperture Radar (ASAR) and methodology for landslide, unstable slope and manmade structure measurement

Boris Matti[1], Floriano Beffa[1], Andrea Salvadè[2], Damiano Pellegrini[2], Roberto Gardenghi[3], Ricardo Monleone[4], Urs Marti[5]

[1] *Muttoni & Beffa SA (main industrial partner), Via Cantonale 15, 6760 Faido, Switzerland (boris.matti@mebsa.ch)*
[2] *SUPSI – DTI – ISEA – TTHFLab, Dipartimento tecnologie innovative Istituto sistemi e elettronica applicata, Galleria 2, Via Cantonale 2c, CH-6928 Manno, Switzerland (andrea.salvade@supsi.ch)*
[3] *New Celio Electronics GmbH, Via Pedemonte 5, 6715 Dongio, Switzerland*
[4] *Meet Electronics Sagl, Via San Giorgio 7, 6877 Coldrerio, Switzerland*
[5] *Huggenberger AG, Tödistrasse 68, 8810 Horgen, Switzerland*

The continuous expansion of human habitats, the presence of transport routes in remote valleys, melting of alpine permafrost as a consequence of global warming, and exceptional climatic events are amplifying the risk of catastrophic mountain-slope failures, landslides and, more in general, hydro-geological instability.

Among the many natural hazards in mountainous regions, rockfalls are frequently occurring processes that are characterized by their suddenness and difficulty of prediction. Urbanization development and growth imply higher and higher impacts on the territory. In civil engineering, excavation works are becoming routine and thus increasing destabilization and slope failure risks on the dug out areas. The investigation of potentially unstable mountain cliffs and slopes is today a primary need to increase natural and anthropic risk prevention and forecasting.

Slope Monitoring Radar

The use of slope monitoring radar such as **Synthetic-Aperture Radar** (**SAR), InSAR (Interferometric Synthetic-Aperture Radar) or TInSAR (Terrestrial Interferometric SAR)** is now the most advanced practice for the active monitoring of slope for safety critical landslide monitoring; with the aim of providing alerts in the event of progressive movements which could potentially lead to slope failure. If not yet systematically used, these devices are already well operated in situation of particular necessity; only mentioning Valegion landslide in Ticino, Aletschgletscher, Sörenberg, Bondo, etc.

Safely “around-the-clock” long-term monitoring slopes is therefore a necessity. With early detection, accidents can be prevented, with long-term analysis general knowledge and geological processes can be better understood and mitigated. **Even tough the end results are always good and useful, the tedious mobilization of such instruments in addition to their behavior and reliability under harsh environments**, as well the higher investment costs, **have always been the main limitations**.

The interest of a new development of this kind of instrument, with less mechanical mobile elements, lighter and financially more approachable, but still providing a good degree of accuracy and reliability, is therefore tangible. Actual instruments (**Figure 1B**) are often very bulky, and require particular conditions to guaranty an acceptable utilization, present a certain complexity of utilization, the obtained precision is not always sufficient and are definitely very expensive.

Environmental and Operation Conditions and Constraints

For a large part of the existing radar systems, environmental conditions is a main limitation. These devices are not able to operate in all weather conditions (rain, fog, snow,…), and even less, in extreme conditions such as in strong thunderstorms and wind.
Most of the actual SARS are very bulky, heavy (over 200 kg!) and work on rails. The complexity of the assembly is strongly decreasing the flexibility and the mobility of such devices.

SAR Monitoring devices should be, due to usual problematic transport conditions and difficult accesses of the monitoring sites (e.g. to remote and/or mountainous areas), constituted by elements which are easily transportable, shock resistant, waterproof and light. The installation and the assembly of such devices shouldn’t involve complex operations.

Objectives and Perspectives of A New Development

The revolutionary **Array Synthetic Aperture Radar (ASAR)** (see **Figure 1A**) developed meets the following objectives and characteristics:

- Realization of a complete GB-SAR **based on modular antenna array** (**Figure 1A)**
- **Operational range: 20 – 3000** [m]
- Range resolution: 0.75 [m]
- **Measurement threshold : 4mm (at 3'000 m a.s.l. and optimal environmental conditions)**
- Cross-range resolution: 14 [mrad] (improvable to 4.3 mrad)
- Acquisition time: 30 [s] … 5 [min]
- **Compact system, robust, lightweight and portable to simplify the transport and set-up: 12…30 kg (depending of cross-range resolution)**
- Automatic alarm system
- **Real time results and logging possibility**
- **Cost reduction compared to actual GB-SAR on the market**

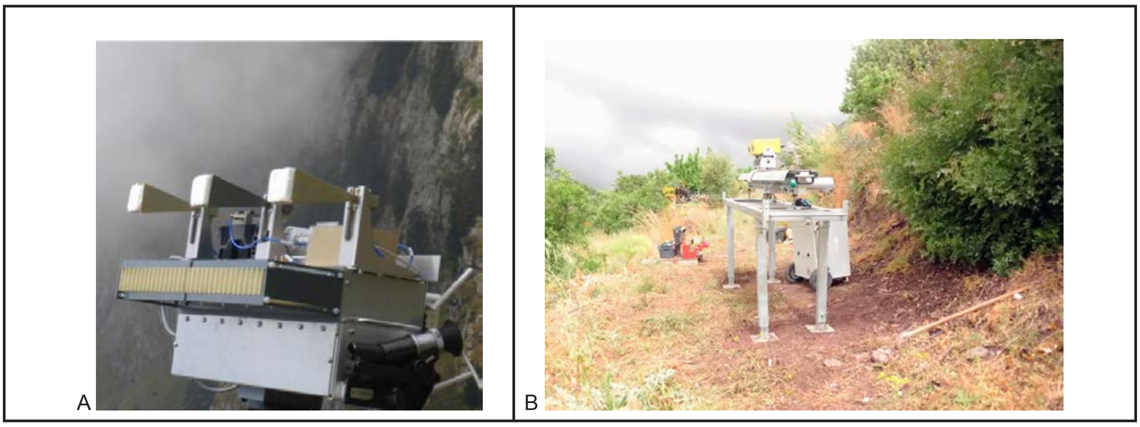

Figure 1. A) The new revolutionary Array Synthetic Aperture Radar (on the left) vs (B) the actual existing systems (on the right).

P 6.11

Tsunami deposits in coastal areas surrounding perialpine lakes in Switzerland

Nigg Valentin[1], Girardclos Stéphanie[2], Kremer Katrina[3], Anselmetti Flavio[4]

[1] *Institute of Geological Sciences, University of Bern, Switzerland (valentin.niggeo.unibe.ch)*
[2] *Department of Earth Sciences and Institute for Environmental Sciences, University of Geneva*
[3] *Swiss Seismological Service, ETH Zurich, Switzerland*
[4] *Institute of Geological Sciences and Oeschger Centre for Climate Change Research, University of Bern, Switzerland*

On the basis of historical reports, multibeam bathymetric datasets, seismic reflection surveys and numerical wave modelling, previous studies have shown that devastating tsunamis occurred in perialpine lakes in Switzerland. These events have diverse trigger mechanisms such as earthquakes, rockfalls or spontaneous subaquatic mass movements displacing large amounts of water. For instance, a tsunami with a height of 4 m occurred in Lake Lucerne after an earthquake (Mw 5.9) in 1601 AD. (Cysat, 1969; Schnellmann et al., 2002; Fäh et al. 2011; Hilbe and Anselmetti, 2015). At Lake Geneva, a major subaerial rockfall triggered a partial subaquatic collapse of the Rhone delta in 536 AD causing a tsunami with a height of several meters (Montandon, 1925; Kremer et al., 2012).

This study uses cross-sections based upon sediment cores to identify historic tsunami deposits in coastal settings of Swiss lakes. It will provide the foundation to confirm and quantify historic tsunami events and to extend the event catalogue to the prehistoric period. We will investigate in which way lacustrine tsunami deposits differ from their marine counterparts, how they can be discerned from terrestrial flood deposits and infer run-up height, inland penetration distance and flow regime. Results will establish a tsunami chronology that will be correlated with major mass-transport deposits observed in various lake basins (Schnellmann et al., 2002; Kremer et al., 2015). This study is part of an interdisciplinary project addressing the causes, controls, frequency of this to date underrated lacustrine tsunami hazard and also includes numerical modelling of tsunami propagation and inundation. Furthermore the information gained from historic tsunami deposits will serve to ground truth results yielded by numerical models.

REFERENCES

Cysat, R., (1969). Collectanea Chronica und denkwürdige Sachen pro Chronica Lucernensi et Helvetiae. Erste Abteilung, Stadt und Kanton Luzern. Erster Band, Zweiter Teil. Collectanea Chronica und denkwürdige Sachen zur Geschichte der Stadt Luzern. Bearbeitet von Dr. phil. Josef Schmid.

Fäh, D., Giardini, D., Kästli, P., Deichmann, N., Gisler, M., Schwarz-Zanetti, G., ... & Bethmann, F. (2011). ECOS-09 earthquake catalogue of Switzerland release 2011 report and database. Public catalogue, 17. 4. 2011. Swiss Seismological Service ETH Zurich. RISK.

Hilbe, M. and Anselmetti, F.S., (2015). Mass movement-induced tsunami hazard on perialpine Lake Lucerne (Switzerland): Scenarios and numerical experiments: Pure and Applied Geophysics 172, 545-568.

Kremer, K., Simpson, G., & Girardclos, S., (2012). Giant Lake Geneva tsunami in ad 563. Nature Geoscience, 5(11), 756-757.

Kremer, K., Hilbe, M., Simpson, G., Decrouy, L., Wildi, W., & Girardclos, S., (2015). Reconstructing 4000 years of mass movement and tsunami history in a deep peri-Alpine lake (Lake Geneva, France-Switzerland). Sedimentology, 62(5), 1305-1327.

Montandon, F., (1925). Les Eboulements de la Dent du Midi et du Grammont (Examen critique de la question de Tauredunum). Le Globe. Revue genevoise de géographie, 64(1), 35-91.

Schnellmann, M., Anselmetti, F. S., Giardini, D., McKenzie, J. A., & Ward, S. N., (2002). Prehistoric earthquake history revealed by lacustrine slump deposits. Geology, 30(12), 1131-1134.

P 6.12

Automatic detection of debris flows based on infrasound and seismic data

Andreas Schimmel[1], Johannes Hübl[1]

[1] Institute of Mountain Risk Engineering, University of Natural Resources and Life Sciences, Vienna, Austria

Due to the fast socio-economic development of mountain areas, processes like debris flows, debris floods, or bed load transport, constitute an increasing hazard to lives and property. Monitoring debris flow torrents is essential for warning issues and gaining more knowledge about the processes. Debris flows and debris floods induce, by the collision of stones and by the friction of the flow to the channel, waves in the low-frequency infrasonic spectrum and seismic waves. The fact that debris flows have a characteristically pattern in the time-frequency range for the infrasound and seismic signals, permits an early detection and identification of these events, even before a surge passes the sensor location.

Several approaches to detect debris flows with infrasonic (e.g. Chou et al. 2010) or seismic sensors (e.g. Arattano et al. 2014) are already existing but so far no warning system based on a combination of seismic and infrasound sensors has been developed and no approach for identifying mass movement processes in respect to their process-type, and – magnitude based on this both signals has been considered.

This work aims to build up a warning system for detecting and identifying alpine mass movements by analysing the seismic and infrasound waves. The developed system is build up on a minimum of one seismic and one infrasound sensor which are co-located and a microcontroller which runs a detection algorithm to detect debris flows and debris floods with high accuracy in real time directly on-site (Schimmel et al. 2016). The developed detection algorithm analyses the evolution in time of the frequency content from the infrasonic and seismic mass movement signals. Therefore three different frequency bands are used to analyze the infrasound signal, whereby a 3 to 15 Hz band characterizes debris flows and a 15 to 45 Hz band is used for debris floods. The frequency bands below (manly dominated by wind) is used to eliminate false alarms due to wind and there is also a criteria using the variance of the amplitudes to eliminate artificial false alarms. Figure 1 shows an example of the seismic and infrasound signals and the amplitudes of the frequency bands of a debris flow occurred at the Tyrolese test site Lattenbach on 16.08.2015. The time between detection and passing of the main surge for this event was 40 s which is an adequate time for early warning.

The System has been installed at eleven different test sites in Austria, Italy and Switzerland. All 22 debris flow events which occurred since 2013 has been detected and also the most of smaller debris floods and bedload transport processes has been identified. During the whole operation time only six false alarms were registered.

Further work will compare the data of recorded events with information of other measurement systems, to define a common set of identification rules for event-type and magnitude identification. The detection system will be extended by this identification rules and the developed process identification system will then be tested on several test sites.

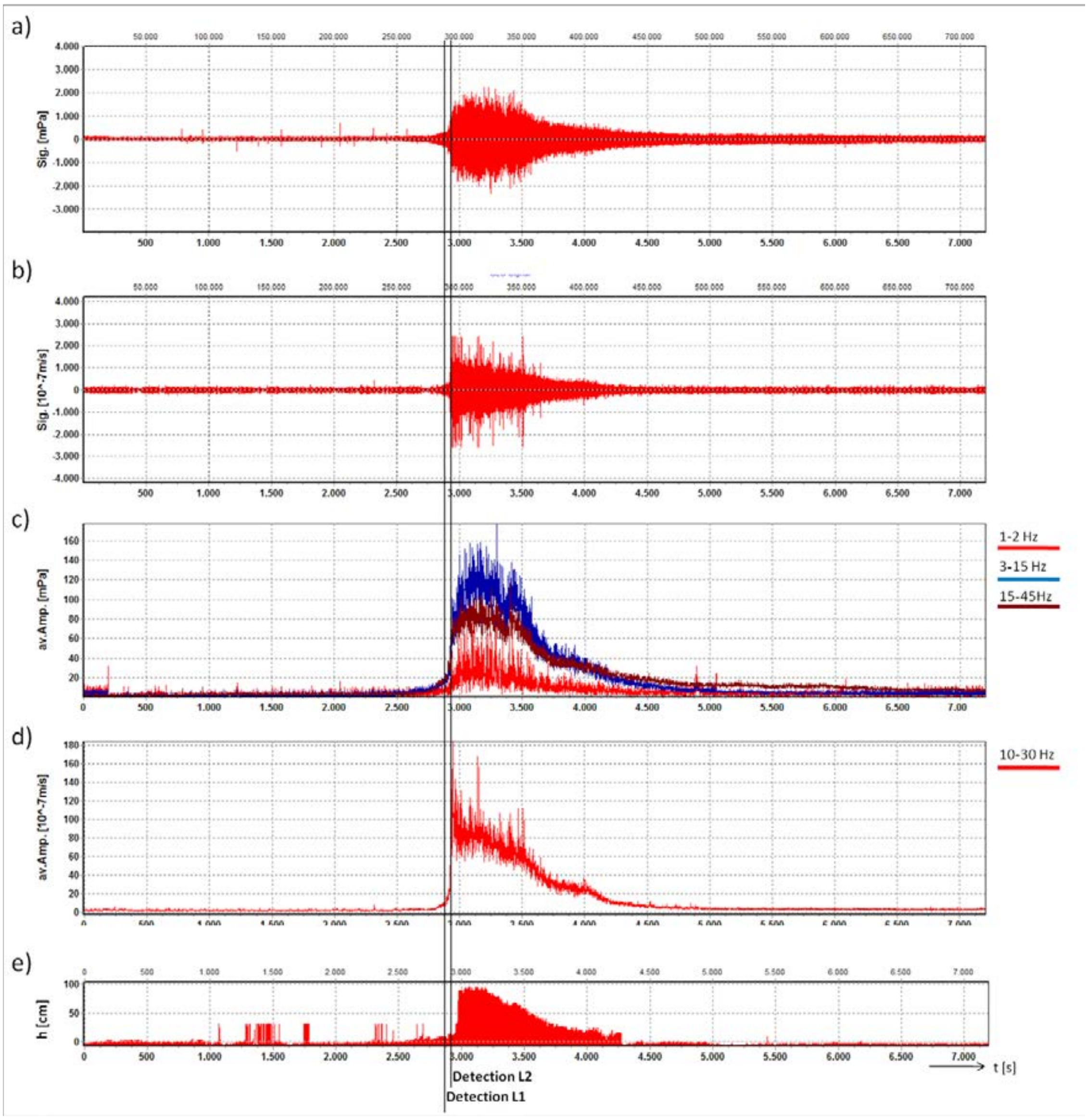

Figure 1. Infrasound and seismic data of the debris flood monitored at the test site Lattenbach on 16.08.2015. Signals are represented with a common base of time. (a) Infrasound time series; (b) Seismogram; (c) Average amplitude of the three frequency bands of the infrasound signal; (d) Average amplitude of the frequency band of the seismic signal; (e) (g) Flow hight; Line: time of first detection based on infrasound and seismic data for two alarm levels.

REFERENCES

Arattano, M., Abancó, C., Coviello, V., Hürlimann, M. (2014): Processing the ground vibration signal produced by debris flows: the methods of amplitude and impulses compared, Computers & Geosciences, Vol. 73,17-27

Chou, H.T., Chang, Y.L. and Zhang, S.X. (2010): Acoustic signals and geophone response of rainfall-induced debris flows. J. of Chinese Institute of Engineers.

Schimmel, A., Hübl, J. (2016): Automatic detection of debris flows and debris floods based on a combination of infrasond and seismic signals. Landslides Vol. 13(5), 1181--1196, ISSN 1612-510X, doi: 10.1007/s10346-015-0640-z.

P 6.13

Characterization of natural hazard events affecting the Swiss transportation networks from 2012 to 2016

Jérémie Voumard[1], Marc-Henri Derron[1] & Michel Jaboyedoff[1]

[1] *Risk analysis group, Institute of Earth Sciences, University of Lausanne, Switzerland, Géopolis UNIL-Mouline, CH-1015 Lausanne (jeremie.voumard@unil.ch)*

As many transportation networks around the world, roads and railways in Switzlerand are regularly affected by natural hazard especially due to its mountainous topography. Consequences of communication chanel closures due to natural hazard events affect several human activities linked to the economy, the tourism, the emergency services or the everday life of the people living close to the closures.

While large natural hazard events affecting roads and railways are generally well studied (i.e. La Frasse VD, Gurtnellen UR, Valparghera GR), this is not the same for minor and medium-sized events ranging from a few cubic decimeters to a few thousand of cubic meters. This is especially because their direct consequences are often rapidly fixed (i.e. the road can be re-opened few hours after the event or is only partially closes). There is thus not much interest to study minor events instead of large natural hazard events that concern scientists, administration and politicans for years. Although there are different databases dedicated to natural hazards in Switzerland, they are not enough focused on small events affecting roads and railways to study features and damages of affected transportation network tracks by natural hazard events. To reduce this lack of knowledge, we began to collect all natural hazard events affecting road and railways repported in newspapers from 2012 to 2015 with a view to better knowing them and to try to evaluate their consequences.

Nearly 850 natural hazard events classified into six classes (landslide, debris flow, rockfall, flood, snow avalanche and others) were collected during the five years considered. Data come from Swiss online press articles sorted by Google Alerts with over fifty keywords in German, French and Italian. Then, for each event, over as 160 attributes were given to describe the event and its damages.

The following is a summary of some events caracteristics. The half of the colletected events are floods (50% of all events, 84 yearly), followed by rockfalls (11%, 19 yearly), debris flows (8%, 14 yearly), remaining landslides (23%, 19 yearly), other events including snowdrifts (6%, 11 yearly) and snow avalanches (2%, 3 yearly). 44% of events occurred in spring, 32% in summer, 13% in winter and 11% in autumn. June (30% of all events) and July (25%) are the months with the most events occurrence. Most events occurend in the afternoon (38%) or in the evening (27%). 44% of the events occurred in the Alps and on the Swiss Plateau while the remaning 12% occurred in the Jura area. 12% of events occurred in the canton of Bern, 11% in the canton of Vaud, 10% in the canton of Valais and 9% in the canton of Grisons. 28% of events occurred in villages followed by 25% in the countryside and 22% in forest. 88% of events affected roads and 12% railways. Considering the damages, 55% of events generated track closures, 18% no closure (only trafic restriction during a short time), and 17% generated partial dommages on the track embankment.

With the low number of considered year, it is not possible to give statistic of the real impact of natural hazard on the Swiss transportation network. This study must be considered as a picture made in the mid 2010s giving idea of the number of natural hazard events on roads and railways and their damages. This study allows to consider the bakground noise of the small events affecting the Swiss transportation network which is not insignificant. Indeed, the summed distance of all deviations for road closures is 8’500 km (average of 20 km for the 418 proven road deviations) and the sum of closure duration is almost 48’000 hours which represent neat to 5.5 years of closure duration (average close to one week track closure for the 296 known closure durations).

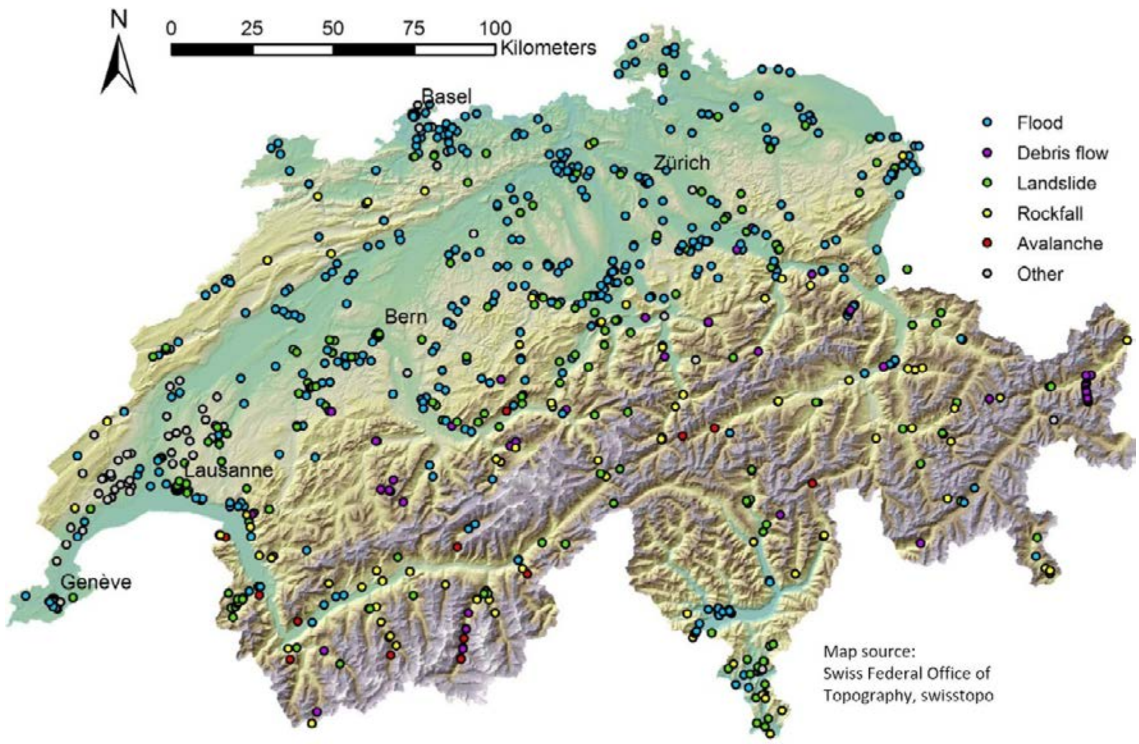

Figure 1. Spatial distribution of the natural hazard events affecting roads and railways in Switzerland (2011-2016).

7. Geomorphology

Nikolaus Kuhn, Christoph Graf, Isabell Kull, Geraldine Regolini,
Isabelle Gärtner-Roer, Sébastien Castelltort, Margreth Keiler, Christophe Lambiel,
Christian Scapozza, Reynald Delaloye, Christine Levy

Swiss Geomorphological Society (SGS)
Swiss Association of Geographers (ASG)

TALKS:

7.1 **Bakker M.**, Costa A., Silva T.A., Stutenbecker L., Girardclos S., Loizeau J.-L., Molnar P., Schlunegger F., Lane S.N.
Combined climate and flow abstraction impacts on an aggrading Alpine river

7.2 **Costa A.**, Molnar P., Schmitt R.J. P.
River network bedload model: a tool to investigate the impacts of flow regulation on bed load and grain size in a large Alpine basin

7.3 **King G.E**., Tsukamoto S., Sueoka S., Herman F., Ahadi F., Gautheron C., Delpech G., Tagami T.
Low-temperature thermochronometry of the Japanese Alps

7.4 **Lehmann B.**, Valla P.G., King G.E. , Ivy-Ochs S., Kronig O., Herman F.
Constraining paleo-glacier extent and local erosion using OSL and ^{10}Be surface exposure dating

7.5 **Mertin M.**, Ramirez J.A., Zimmermann M., Peleg N., Skinner C., Keiler M.
Simulating the effect of check dams on landscape evolution at centennial time scales

7.6 **Mettra F.**, Antoniazza G., Lane S.
Sediment transport in a small alpine river: hysteresis and seasonal behaviour

7.7 **Morgenthaler J.**, Frehner M.
Bulldozer-like soil erosion at the front of a rockglacier indicates change in advance dynamics: Case study from the Furggentälti, Vallais, Switzerland

7.8 **Schide K.**, Gallen S., Lupker M., Märki L., Willett S., Cook K., Gajurel A.
Evaluating the role of coseismic landsliding on cosmogenic nuclides, erosion rates, and topographic evolution in mountainous landscapes. A case study of the Mw 7.8 Gorkha Earthquake.

7.9 **Walter F.**, Marchetti E., Clinton J.
Monitoring alpine mass movement with seimology and infraosund

POSTERS:

P 7.1 **Abbassi M.**, Ouezdou B.H., Fraj B.T., Reynard E., Moussa M.
Geohistorical analysis of the evolution of the hydraulic system of Jessour in Southeast Tunisia

P 7.2 **Ambrosi C.**, Castelletti C., Czerski D., Scapozza C, Schenker F.L.
The new landslide and rock glacier inventory map of Canton Ticino

P 7.3 **De Palézieux L.**, Leith K., Loew S.
Incorporation of hillslope morphology into an analysis of river profile development in NW Bhutan

P 7.4 **Goldman N.**, Mayer M., Fister W., Kuhn N.J.
A methodological approach to improve erosion experiments on biochar by using a high precision rainfall simulator and photogrammetry

P 7.5 **Greenwood P.**, Kuhn N.J.
Impatiens glandulifera (Himalayan Balsam) and increased soil loss: causation or association? Case studies from Switzerland and the UK

P 7.6 **Huber M.L.**, Gallen S.F., Lupker M., Haghipour N., Christl M., Gajurel A.P.
Assessing the origins, timing and transport distances of large exotic boulders in trans-Himalayan rivers

P 7.7 **Larsen A.**, Larsen J., Lane S.N.
Dam busy: beavers and their influence on the structure and function of river systems

P 7.8 **Salehipour Milani A.**, Mohammadi A., Kaveh A.
Active Tectonic Faults and Their Effects on Quaternary Shorelines of the Malekan Regions (Northwestern Iran)

P 7.9 **Schläfli S.**, Ruiz-Villanueva V., Schlunegger F., Stoffel M.
Regulated flows influence on river morphodynamics: the Spöl River (Swiss National Park)

P 7.10 **Winterberg S.**, Willett S, Picotti V.
Paleo drainage networks of the Alpine region

P 7.11 **Zaki A.S**., Castelltort S.
Saharan networks and the Martian networks: a key analogue to extract response of surface to past, present and future climatic changes

P 7.12 **Kuhn N.**, Kuhn B., Maendli D., Schaub D.
UAV based soil erosion monitoring for soil protection

7.1

Combined Climate and Flow Abstraction Impacts on an Aggrading Alpine River

Maarten Bakker[1], Anna Costa[2], Tiago A. Silva[3,4], Laura Stutenbecker[5], Stéphanie Girardclos[4,6], Jean-Luc Loizeau[3,4], Peter Molnar[2], Fritz Schlunegger[5] & Stuart N. Lane[1]

[1] *Institute of Earth Surface Dynamics, University of Lausanne, Géopolis, CH-1205 Lausanne (maarten.bakker@unil.ch)*
[2] *Institute of Environmental Engineering, ETH Zürich*
[3] *Department F.-A. Forel for Environmental and Aquatic Sciences, University of Geneva*
[4] *Institute for Environmental Sciences, University of Geneva*
[5] *Institute of Geological Sciences, University of Bern*
[6] *Department of Earth Sciences, University of Geneva*

Widespread temperature increase has been observed in the Swiss Alps and is most pronounced at high elevations. Alpine rivers are very susceptible to such change where large amounts of sediments are released from melting (peri)glacial environments and potentially become available for transport. These rivers are also impacted on a large scale by hydropower exploitation, where flow is commonly abstracted and transferred to a hydropower scheme. Whilst water is diverted, sediment is trapped at the intake and intermittently flushed down the river during short duration purges. Thus, these rivers are impacted upon by both climate and human forcing. In this study we quantify their relative and combined impacts upon the morphological evolution of an aggrading Alpine river.

Our study focusses on the development of a sequence of braided reaches of the Borgne River (tributary of the Rhône) in south-west Switzerland. A unique dataset forms the basis for determining sediment deposition and transfer: (1) a set of high resolution Digital Elevation Models (DEMs) of the reaches was derived through applying Structure from Motion (SfM) photogrammetry to archival aerial photographs available for the period 1959-2014; (2) flow intake management data, provided by Grande Dixence SA, allowed the reconstruction of (up- and downstream) discharge and sediment supply since 1977. Subsequently we used climate data and transport capacity calculations to assess their relative impact on the system evolution over the last 25 years.

Not surprisingly, considerable aggradation of the river bed (up to 5 meters) has taken place since the onset of flow abstraction in 1963. The initial morphologic response was however modest, generally associated with channel narrowing and vegetation encroachment. Major, widespread aggradation did not commence until the onset of glacier retreat in the late 1980s and the notably warm (and dry) period in the early 1990s. The river reaches showed a common, synchronous development, steepening in response to altered flow sediment supply conditions.

Where the aggradation coincided with a phase of increased sediment supply, it accounts for only circa 25% of supplied material and the remainder was transferred through the reaches downstream. Estimations of bed load transport capacity indicate that flow abstraction reduces transport capacity by an order of magnitude but that the residual transport rates are close to sediment supply rates, which is why significant transport remains. However, the reduction in transport capacity makes the system much more sensitive to changes in climate-driven hydrological variability and climate-induced changes in intake management and sediment delivery rates.

In the Borgne River we find that despite the considerable impact of flow abstraction, it is still possible to identify a climate change signal that propagates through the system and drives river morphological response. This signal is associated with a critical climate control upon upstream sediment supply coupled with the effects of combined climate and human impact on the operation of the hydroelectric power scheme.

7.2

River network bedload model: a tool to investigate the impacts of flow regulation on bed load and grain size in a large Alpine basin

Anna Costa[1], Peter Molnar[1], Rafael J. P. Schmitt[2]

[1] Institute of Environmental Engineering, ETH Zurich, Stefano Franscini Platz 3, CH-8093, Zurich (costa@ifu.baug.ethz.ch)
[2] Center for Environmental Design Research, University of California Berkeley, CA-94720, Berkeley

The balance between transport capacity and sediment supply determine bedload and the grain size distribution (GSD) of water courses. Altered climatic conditions as well as human activities may impact both transport capacity and sediment supply, ultimately affecting bedload and the GSD. Climate change shifts the timing of runoff and affects its magnitude by modulating basin evapotranspiration, snow cover and snowmelt, glacier melt, etc. Glacier retreat may also enhance sediment supply by exposing to erosion loose sediment in proglacial areas. Human activities in Alpine basins affect runoff by water withdrawals, water impoundment and flow regulation due to hydropower operation. In addition, the effects on sediment supply of reservoir sedimentation, channelization of rivers and gravel mining activities may also be significant in Alpine regions.

In this work, we focus on the effects of flow regulation on bedload and GSD of the upper Rhone basin, a large Alpine catchment, heavily affected by hydropower operations since 1960s. Substantial changes in discharge, mainly an increase in winter and decrease in summer flows (Fig. 1), have occurred at multiple locations in the catchment, potentially leading to alterations of the sediment regime. However, the spatial distribution and the magnitude of these changes are not easily inferable due to the non−linear, threshold−based nature of sediment transport.

To address the effect of streamflow regulation on bedload fluxes, we developed a network−scale, fractional sediment transport model. Following the approach of Schmitt et al. (2016), we conceptualize the river network as a dendritic tree of connected links (river reaches). We derive the geometric characteristics of links from a digital elevation model and from satellite images. Surface roughness is assigned on the basis of the channel bed GSD, while we estimate bed shear stress for each link under the assumptions of normal flow and a rectangular prismatic cross section. Finally, we estimate transport rates of multiple grain size classes and the resulting GSD by balancing sediment supply and transport capacity, computed with the Wilcock and Crowe surface−based transport model. The model is forced with time series of daily discharge simulated with a spatially distributed physically-based hydrological model for pre and post hydropower scenarios. Under the assumption that coarse grains (d_{90}) are mobilized only during mean annual maximum flows, we initialize GSD on the basis of ratios between d_{90} and characteristic diameters estimated from field measurements.

Results indicate that effects of flow regulation in this Alpine catchment vary significantly in space and in time and are grain size dependent. They show that hydropower operations led to an overall reduction of sediment transport, especially in summer and predominantly for coarser grains. We propose that the network approach is a useful tool to quantify the spatially−variable impacts of changes in flow conditions on sediment dynamics, driven by hydropower or by any other driving factor, including climate change.

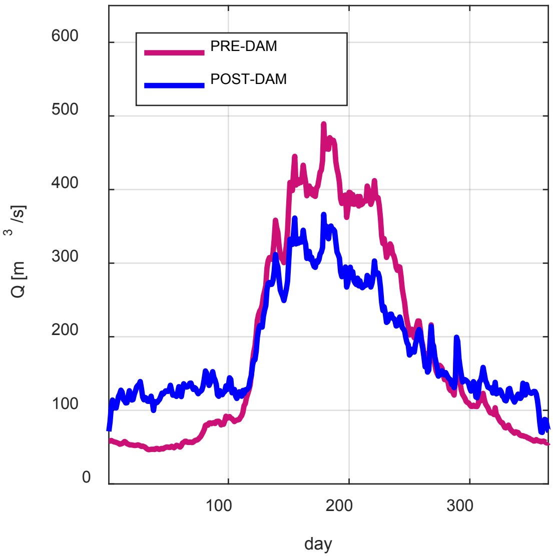

Figure 1. Mean daily discharge at the outlet of the catchment under pre and post dam conditions.

REFERENCES

Schmitt, R. J. P., Bizzi, S., Castelletti, A. 2016: Tracking multiple sediment cascades at the river network scale identifies controls and emerging patterns of sediment connectivity, Water Resources Research, 52, 3941-3965.

7.3

Low-temperature thermochronometry of the Japanese Alps

Georgina E. King[1], Sumiko Tsukamoto[2], Shigeru Sueoka[3], Frédéric Herman[4], Floriane Ahadi[5], Cécile Gautheron[5], Guillaume Delpech[5] and Takahiro Tagami[6]

[1] *Institute of Geological Sciences, University of Bern (georgina.king@geo.unibe.ch)*
[2] *Leibniz Institute for Applied Geophysics, Hannover, Germany*
[3] *Japan Atomic Energy Agency, Toki, Japan*
[4] *Institute of Earth Surface Dynamics, University of Lausanne*
[5] *Université de Paris Sud, France*
[6] *University of Kyoto, Japan*

Japan is one of the most tectonically active locations on Earth, situated adjacent to two triple junctions between four tectonic plates. Within this convergent zone, the Hida, Kiso and Akaishi ranges of the Japanese Alps are thought to have been uplifted within the last 1 to 3 Myr. Whilst predominantly tectonically driven, this mountain-building may also have been coincident with the onset of the Quaternary period, and the associated global climatic transition to ice-house conditions. Extremely high rates of precipitation (>3,000 mm/yr) coupled with earthquake enhanced landsliding potentially make the Japanese Alps one of the most rapidly exhuming places on Earth. However the rate of exhumation and the topographic evolution of this significant tectono-climatic setting remain poorly constrained. Quantifying exhumation rates will provide insights into the tectonic evolution of the Japanese Alps as well as an improved understanding of the coupling between tectonics and climate through erosion processes.

Thermochronometry enables exhumation rates to be determined from the measurement of rates of rock cooling. Conventional low temperature thermochronometers such as (U-Th-Sm)/He in apatite are unable to resolve rates of cooling within parts of the Japanese Alps, because of their recent exhumation (Suoeka et al., 2016). Instead here we use a combination of two new very-low temperature thermochronometry techniques based upon the trapped-charge dating methods of optically stimulated luminescence (OSL) and electron spin resonance (ESR) dating. We collected 19 samples from the Hida range of the Japanese Alps, including 4 samples from a high-temperature tunnel which has a present day temperature of ~40-50 °C, but experienced temperatures of up to 166 °C prior to excavation in the 1930s. The high-temperature samples have apparent ages of zero when measured using OSL and ESR-thermochronometry, providing a local control on the performance of these recently established techniques. Measurement of the remaining 15 samples will complement previous (U-Th-Sm)/He in apatite (Ahadi et al., In Prep.), zircon fission track (Yamada and Harayama, 1999; Ito and Tanaka, 1999) and zircon U-Pb (Ito et al., 2013) measurements which have been made on the same sample suite. Once analyses are complete, we will be able to invert the different thermochronometric data together, to determine the exhumation of the Hida range over the past 3 Myr.

REFERENCES

Yamada, R., Harayama, S., 1999, Fission track and K-Ar dating on the Hida Mountain Range, some granitic rocks of. Central Japan. Geochemical Journal 33, 59-66.

Ito, H., Tanaka, K., 1999. Radiometric age determination on some granitic rocks in the Hida Range, central Japan: Remarkable age difference across a fault. Journal of Geological Society of Japan 105, 241-246.

Ito, H., Yamada, R., Tamura, A., Arai, S., Horie, K., Hokada T., 2013. Earth's youngest exposed granite and its tectonic implications: the 10-0.8 Ma Kurobegawa Granite. Scientific Reports 3: 1306.

Suoeka, S., Tsutsumi, H., Tagami, T., 2016, New approach to resolve the amount of Quaternary uplift and associated denudation of the mountain ranges in the Japanese Islands. Geoscience Frontiers 7, 197-210.

Yamada, R., Ito, H., Tamura, A., Morishita, T., Arai, S., 2012. Thermochronologic analysis of granitic rocks in the Japanese Northern Alps (Hida mountain range). Abstract of the 13th International Conference on Thermochronology.

7.4

Constraining paleo-glacier extent and local erosion using OSL and ^{10}Be surface exposure dating

Benjamin Lehmann[1], Pierre G. Valla[2], Georgina E. King[2], Susan Ivy-Ochs[3], Olivia Kronig[3] and Frédéric Herman[1]

[1] Institute of Earth Surface Dynamics, Faculty of Geosciences and Environment, University of Lausanne, CH-1012 Lausanne (benjamin.lehmann@unil.ch)
[2] Institute of Geological Sciences and Oeschger Center for Climate Research, University of Bern, 3012 Bern
[3] Laboratory of Ion Beam Physics, ETH Zurich, 8093 Zurich, Switzerland

In this study, we present a new approach to evaluate post-glacial bedrock erosion in mountainous environments by combining ^{10}Be and optically stimulated luminescence (OSL) surface exposure dating (Haberman et al., 2000; Sohbati et al., 2011). It relies on the idea that both OSL-signal bleaching and ^{10}Be concentration within a rock sample depend on the exposure time and the surface erosion rate. We developed an iterative approach that enables us to invert OSL bedrock and ^{10}Be concentration into exposure time and erosion rate.

We then apply our approach to a well-constrained glacial environment: the Mer de Glace glacier (Mont Blanc massif, France). Samples were collected on granitic bedrock surfaces between the LGM ice surface (~2505 m a.s.l, Coutterand et al., 2006) and the present-day glacier (1920 m a.s.l), covering ~600 m of elevation over which the ice has fluctuated since the LGM. Our results exhibit increasing exposure age with sample elevation, from 0.2 ± 0.1 to 21.0 ± 1.4 ka, and an integrated erosion rate varying from 0.5 to 5 $mm.ka^{-1}$ since the Last Glacial Maximum. We thus propose that combining OSL and ^{10}Be surface exposure dating would allow to constrain both paleo-glacier fluctuations and weathering processes during the Lateglacial to Holocene times.

REFERENCES

Habermann, J., Schilles, T., Kalchgruber R., Wagner, G.A. 2000: Steps towards surface dating using luminescence. Radiation Measurements 32(5): 847-851.

Sohbati, R., Murray, A.S., Jain, M., Buylaert J-P., Thomsen K.J. 2011: Investigating the resetting of osl signals in rock surfaces. Geochronometria, 38(3).

Coutterand, S. and J.-F. Buoncristiani. 2006: Paléogéographie du dernier maximum glaciaire du Pléistocène récent de la région du massif du Mont Blanc, France. Quaternaire. Revue de l’Association française pour l’étude du Quaternaire, 17(1): 35-43.

7.5

Simulating the effect of check dams on landscape evolution at centennial time scales

Mirjam Mertin[1], Jorge Alberto Ramirez[1], Markus Zimmermann[1], Nadav Peleg[2], Chris Skinner[3], Margreth Keiler[1]

[1] *Institute of Geography, University of Bern, Hallerstrasse 12, CH-3012 Bern*
[2] *Institute of Environmental Engineering, ETH Zurich, Stefano-Franscini-Platz 5, CH-8093 Zürich*
[3] *Energy and Environment Institute, University of Hull, Cottingham Rd, UK-HU6 7RX Hull*

Check dams are structures to stabilize mountain rivers by decreasing flow velocity and reducing channel erosion. Over long time scales (100 yrs) a series of check dams constructed in a particular river reach can have significant effects on sediment and water dynamics and river channel responses. Over time the maintenance and repairing or even the replacement of check dams is costly. Given the drawbacks of check dam maintenance, the question then arises: what would happen geomorphologically if check dams were not maintained and allowed to structurally deteriorate? Herein we apply a landscape evolution model (CAEASAR-Lisflood) to the Guerbe catchment containing 80 check dams that stabilize the main river (Figure 1). These longstanding structures afford a sense of security for downstream communities by mitigating small- and mid-scale flood and debris flow hazards. High spatial and temporal resolution rainfall data driving the landscape evolution model is generated by a stochastic spatially distributed rainfall generator (STREAP). Using CAESAR-Lisflood we simulate future scenarios of the river development at centennial time scales. Scenarios consider the quantity and location of check dams that are neglected, subsequently collapse, and release large amounts of sediment. By doing this we are better able to understand how the neglect of check dams cascades through the catchment and provides information about optimal check dam placement and amount.

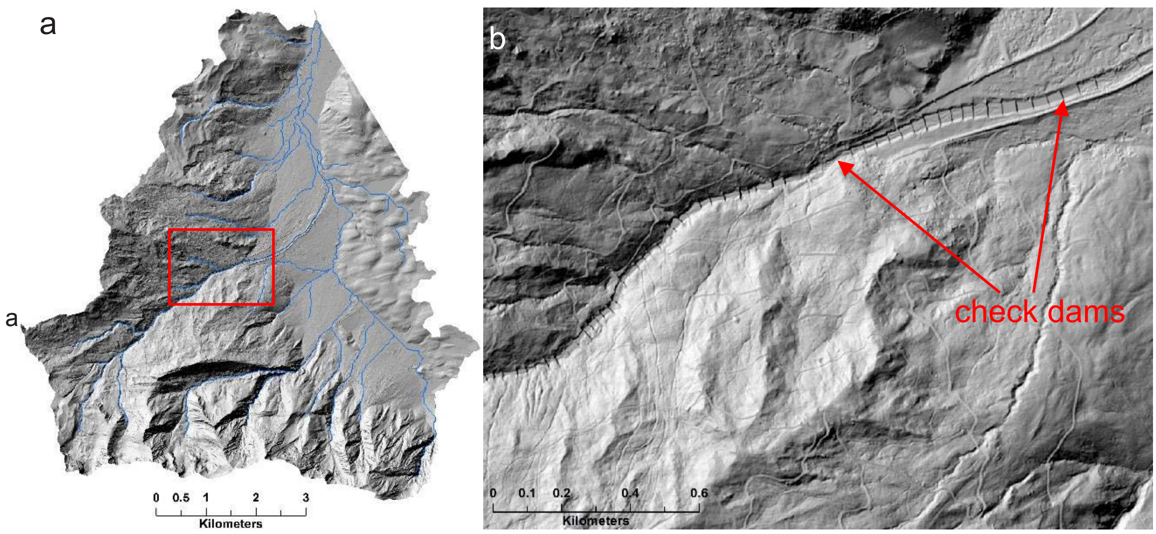

Figure 1. (a) Guerbe catchment and (b) reach containing check dams.

7.6

Sediment transport in a small alpine river: hysteresis and seasonal behaviour

François Mettra[1], Gilles Antoniazza[1] & Stuart Lane[1]

[1] *IDYST, University of Lausanne, CH-1015 Lausanne (francois.mettra@unil.ch)*

This study aims to understand the behaviour of sediment transport in a small alpine river. Sediment transport is known to show large fluctuations, particularly in mountainous catchment. Using continuous sediment transport data from a new measurement station (WSL-UNIL) in Vallon de Nant, VD, Switzerland, we analyse the hysteresis behaviour of the relation between water and sediment discharges. Here, we focus on the main floods that occurred during the summer season, as the catchment is coverred by snow in the winter.

Interestingly, we observe a shift in the hysteresis during summer 2016, with sediment transport maximum occuring before water discharge maximum for early summer storms, and inversely in late summer. To explain this behaviour, we hypothesize, first, that sediments come from the river channel in early summer, as the upper-part of the catchment is still covered by snow. Secondly, in late summer, sediments seem to come from further upstream, as the sediment transport maximum at the station occures generally after the flood peak (sediment sources are further from the catchment outlet).

The observation of a limited sediment supply in early summer, and a sediment delivery approaching transport capacity in late summer could confirmed this hypothesis. The effects of strong convective storms, as the one observed in the first of August 2017, will be also discussed.

7.7

Bulldozer-like soil erosion at the front of a rockglacier indicates change in advance dynamics: Case study from the Furggentälti, Vallais, Switzerland

Joël Morgenthaler[1] & Marcel Frehner[1]

[1] *Geological Institute, Department of Earth Sciences, ETH Zurich, Sonneggstrasse 5, CH-8092 Zurich (mjoel@student.ethz.ch, marcel.frehner@erdw.ethz.ch)*

Several active rockglaciers in the Alps have increased their creep velocity in the last few decades. An example for such a rockglacier is the well-studied Furggentälti rockglacier near the Gemmi Pass in the Valais Alps in Switzerland. If a rockglacier flows onto soil, erosion can occur forming peculiar landforms. At the Furggentälti, a bulldozer-like soil erosion takes place and therefore a bulge is developing in front of the rockglacier (Figure 1a).

The aim of our study was to simulate the dynamical creep behavior of the Furggentälti rockglacier and in particular to reproduce the erosional process at the rockglacier front. For this, we used the finite-element code presented in Frehner et al. (2015). We assume the rockglacier movement to be governed by purely viscous creep behavior, which is driven downhill by gravity. To design a realistic model representing the Furgentälti rockglacier as well as possible, we used the swissALTI3D digital elevation model for the rockglacier topography and the interpreted seismic refraction data of Nussbaum (2008) for the internal structure (i.e., thickness of active layer and depth to bedrock). In addition, we added a 1 m thick soil layer in front of the rockglacier and beneath the frontal 30 m of the rockglacier. The extent and dimensions of this soil layer are based on local observations and areal images.

Figure 1. a) Bulldozer-like soil erosion at the front of the Furggentälti rockglacier. People for scale. b)–d) Progressive snapshots of numerical simulation. Shown in color is the total horizontal normal stress. The bulge in the soil forms immediately in front of the advancing rockglacier.

The numerical simulation (Figure 1b–d) results in the development of a bulge in the soil in front of the rockglacier. Several key observations from the Furggentälti rockglacier are very well reproduced by the model:

- (i) The position and shape of the bulge.
- (ii) The amplitude of the bulge.
- (iii) The fact that only one bulge forms in the soil, and not several with a distinct wavelength (as compared to the furrow-and-ridge morphology on top of the rockglacier, see Frehner et al., 2015).

Our study also led to various new thoughts and speculations, which we summarized in a conceptual model of a rockglacier moving onto soil (Figure 2). At the rockglacier front, we observe several discrete packages of soil that are incorporated into the rockglacier. Therefore, we assume that a bulge can only reach a certain size (Figure 2b) before it is sheared off and incorporated into the rockglacier (Figure 2c), after which a new bulge forms. This cycle repeats continuously while the sheared-off soil packages are transported up the rockglacier front (Figure 2d). This observation contradicts the commonly accepted caterpillar-like dynamics of a rockglacier, which is characterized by a frontal movement downwards, not upwards.

Therefore, we propose that the entire frontal dynamics changes when a rockglacier moves from bedrock onto soil, from caterpillar-like (Figure 2a) to sliding (Figure 2d).

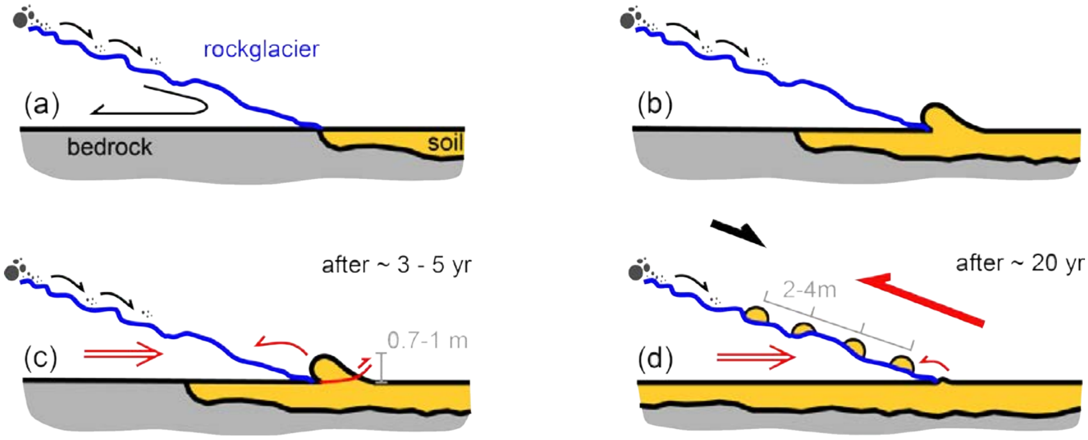

Figure 2. Schematic model of a rockglacier moving from bedrock onto soil. The frontal dynamics changes from caterpillar-like to sliding.

It is interesting to note that the point in time when the Furggentälti rockglacier increased its creep velocity coincides with the moment it moved from bedrock onto soil. Therefore, we also propose that the two different movement dynamics have two different speeds. The increase in creep velocity might be triggered by the change in substrate and the corresponding change in movement dynamics of the rockglacier front, from caterpillar-like movement to sliding.

REFERENCES

Frehner, M., Ling, A.H.M. & Gärtner-Roer, I. 2015: Furrow-and-ridge morphology on rockglaciers explained by gravity-driven buckle folding: A case study from the Murtèl rockglacier (Switzerland), Permafrost and Periglacial Processes, 26, 57–66.

Nussbaum, A. 2008: Geophysikalische Untersuchungen am Blockgletscher Furggentälti, Gemmi (VS), Diplomarbeit, Geografisches Inst., Universität Bern.

7.8

Evaluating the role of coseismic landsliding on cosmogenic nuclides, erosion rates, and topographic evolution in mountainous landscapes. A case study of the Mw 7.8 Gorkha Earthquake.

Katherine Schide[1], Sean Gallen[1], Maarten Lupker[1], Lena Märki[1], Sean Willett[1], Kristen Cook[2], Ananta Gajurel[3]

[1] *Geologisches Institut, ETH Zürich, Sonneggstrasse 5, CH-8093 Zürich (katherine.schide@erdw.ethz.ch)*
[2] *GFZ German Centre for Geosciences, Telegrafenberg, DE-14473 Potsdam*
[3] *Department of Geology, Tribhuvan University, Tri-Chandra Campus, NP-44605 Kathmandu*

The M_w 7.8 2015 Gorkha earthquake presents a unique opportunity to study the effects of coseismic landsliding on sediment transport and landscape response in the years immediately following a large earthquake. The effects of these infrequent mass wasting events on longer-term erosion rates is still not fully understood. In addition, recent studies question whether these large earthquakes build or destroy topography at the orogen-scale (Marc et al.,2016; Parker et al., 2008). In this on-going project, we repeatedly sample river sediments in effected valleys for terrestrial cosmogenic nuclides (TCN) to look for changes in concentrations in the years after the Gorkha earthquake. Assuming landslides mobilize deeper material with lower TCN concentrations, we expect an "earthquake signal" as sediment is excavated from hillslopes and moves downstream. In addition, we measure landslide geometries using high resolution digital surface models created by camera-equipped unmanned aerial vehicles (UAVs) and terrestrial lidar. Comparing landslide volumes with the amount of landslide material in the river channel will allow us to quantify storage on hillslopes and understand the relationship between channel connectivity and export. This project investigates how large, infrequent events effect basin-averaged erosion rates on both long and short timescales.

REFERENCES

Marc, O., Hovius, N., Meunier, P., 2016. The mass balance of earthquakes and earthquake sequences. Geophys. Res. Lett. 43, 1–9. doi:10.1002/2016GL068333

Parker, R.N., Densmore, A.L., Rosser, N.J., de Michele, M., Li, Y., Huang, R., Whadcoat, S., Petley, D.N., 2011. Mass wasting triggered by the 2008 Wenchuan earthquake is greater than orogenic growth. Nature Geoscience 4, 449–452. doi:10.1038/ngeo1154

7.9

Monitoring Alpine Mass Motion with Seismology and Infrasound

Fabian Walter[1,2], Emanuele Marchetti[3], John F. Clinton[4]

[1] Laboratory of Hydraulics, Hydrology and Glaciology, ETH Zurich, CH-8093 Zurich
[2] Swiss Fed. Inst. for Forest, Snow and Landscape Res. WSL, CH-8903 Birmensdorf
[3] Dipartimento di Scienze della Terra, Univ. degli Studi di Firenze, I-50121 Firenze
[4] Swiss Seismological Service, ETH Zurich, CH-8092 Zurich

Gravity-driven mass movements constitute a severe natural hazard in Alpine regions. Ranging from small rock falls to landslides involving millions of cubic meters of material, the impact and trigger of mass movements are highly variable and difficult to constrain with predictive models. Recent large-scale events such as the 23 August 2017 Bondo landslide in the Bergell (GR) as well as smaller-scale recurring debris flows in various torrents throughout Switzerland underline the need for early warning measures.

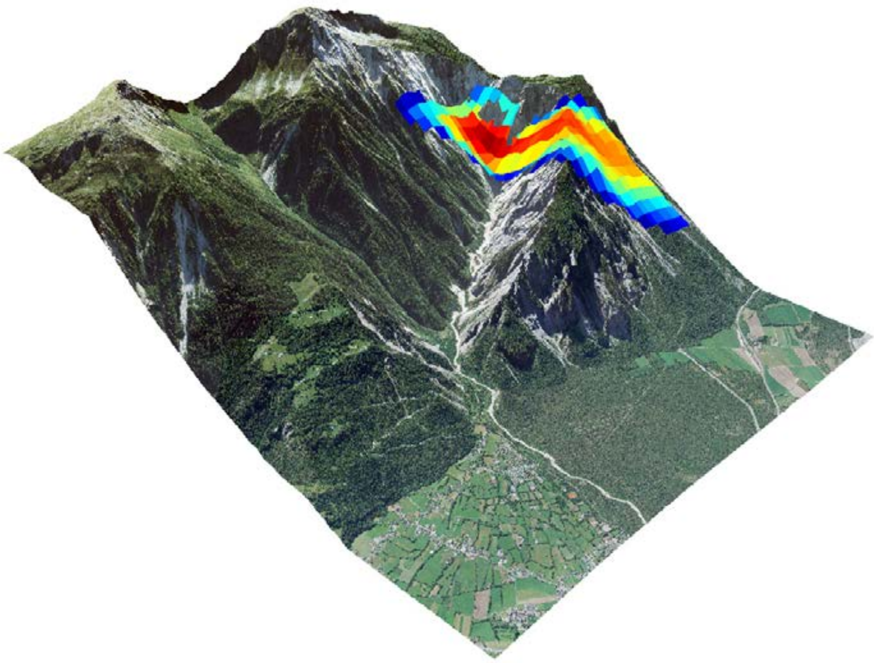

Figure 1. Seismic location (red color) of debris flow front at Illgraben (Valais).

We discuss monitoring and early warning schemes, which exploit the propagation of seismic and infrasound waves induced by mass movements. Focusing on the Bondo landslide and debris flows at Illgraben (VS) we show the potential of these signals for rapid event detection and post-event analysis. Other techniques such as interferometric radar, in situ rock deformation measurements and detection of critical precipitation amounts are often indespensable. Yet seismic and infrasound monitoring has its own advantages and can provide additional information for event detection and process studies.

P 7.1

Geohistorical analysis of the evolution of the hydraulic system of *Jessour* in Southeast Tunisia

Mohamed Abbassi[1,2], Hédi Ben Ouezdou[1], Tarek Ben Fraj[1], Emmanuel Reynard[2] & Mohamed Moussa[3]

[1] Laboratoire de cartographie géomorphologique des milieux, des environnements et des dynamiques (CGMED), FLSH, Université de Tunis, 94, BD du 9 avril 1938, 1007 - Tunis (abassi.med84@gmail.com)
[2] Institut de géographie et durabilité, Université de Lausanne, Géopolis, CH–1015 Lausanne
[3] Institut des Régions Arides, Route du Djorf Km 22.5, Médenine

Jessour (singular: *Jesr*) are a traditional hydro-agricultural system in Southeast Tunisia aimed at collecting water and sediments from the wadis of this arid region (average <120 mm per year) and thus to improve the water and sediment balance of the agricultural plots (notably allowing the cultivation of the olive tree well beyond its ecological limits). These structures are both hydro-agricultural installations and a hydraulic heritage. They are currently subjected to different issues related to climate change (aridification) and socio-economic changes (agricultural abandonment, which reduces the possibilities of maintenance of structures). A project of the universities of Tunis and Lausanne and of the Institute of Arid Regions of Médenine aims at better characterizing these structures (typology, water balance) and at proposing solutions for their sustainable maintenance and their cultural popularization (tourism).

In this poster, a geohistorical analysis of the evolution of *Jessour* over a period of one century in a specific sub-watershed is proposed. Historical aerial photographs and maps are processed withing a GIS environment to detect changes in the *Jessour* system (development of *Jessour* in new talwegs, abandonment, changes in the vegetation cover, erosional features, etc.).

The objective is to propose a map of current situation of *Jessour* in their geomorphological context and diachronic maps of changes over one century.

P 7.2

The new landslide and rock glacier inventory map of Canton Ticino

Christian Ambrosi[1], Claudio Castelletti[2], Dorota Czerski[1], Cristian Scapozza[1] and Filippo L. Schenker[1]

[1] Institute of Earth Sciences, University of Applied Sciences and Arts of Southern Switzerland (SUPSI), Campus Trevano, 6952 Canobbio, Switzerland
[2] CSD Ingegneri SA, Via Lucchini 12, 6901 Lugano, Switzerland

The landslide inventory map of Canton Ticino was recently upgraded thanks to 2D and 3D digital photo-interpretation. This mapping allowed the inventory of 2035 landslides (covering a surface of 184.4 km^2), 4376 shallow landslides (covering a surface of 133.7 km^2) and 188 Deep Seated Gravitational Slope Deformations (DSGSD). Landslides are composed by 1494 slides, 86 flows, 390 falls (comprised between 100 and 1’000’000 m^3) and 65 rock avalanches (> 1’000’000 m^3). 334 landslides were considered as active (238 slides, 17 flows and 79 falls). Shallow landslides includes: erosion areas; talus slopes, scree slopes, coarse-scree slopes and rockfall deposits (< 100 m^3); debris flow deposits; mixed cones (both rockfall and debris flow deposits).

Based on this mapping, the regional rock glacier inventory was also updated. Actually, 279 rock glaciers were recognised in the Ticino Alps, comprising 48 ice-cemented active rock glaciers, 17 ice-cored active rock glaciers, 51 ice-cemented inactive rock glaciers, 3 ice-cored inactive rock glaciers, 157 relict rock glaciers and 3 push-moraines.

P 7.3

Incorporation of hillslope morphology into an analysis of river profile development in NW Bhutan

Larissa de Palézieux[1], Kerry Leith[1], Simon Loew[1]

[1] *Geological Institute, ETH Zurich, Sonneggstrasse 5, CH-8092 Zurich (larissa.depalezieux@erdw.ethz.ch)*

With large alluvial plains, narrow gorges, prominent knick points, and chains of terraces or cut-off ridges, the deeply-incised valleys in Bhutan reflect an environment of diverse erosional activity. Topography ranges from 97 m to 7570 m, with characteristic postglacial landscapes typically located above ca 4200 m. The lower latitudes below ca 3000 m show high relief and terraced or linear hillslopes indicative of a fluvial origin.

Although full channel analyses in the region suggest significant local tectonic contributions to longitudinal river profiles (Adams et al., 2016), we develop a method to isolate rivers in an apparently homogeneous tectonic block in the mid to upper- elevations. Profiles of rivers in this region show a consistent pattern with a marked topographic step covering 2000 m of elevation change within 10 km. Field observations of knick points, terraces, inner gorges, and cut-off ridges associated with the step suggest a regionally consistent signal resulting from changes in relative uplift or erosion rate. Chi plots correlate well for all channels when the base level is chosen to isolate rivers below the main alluvial plain, suggesting similar fluvial erosion histories in upstream regions.

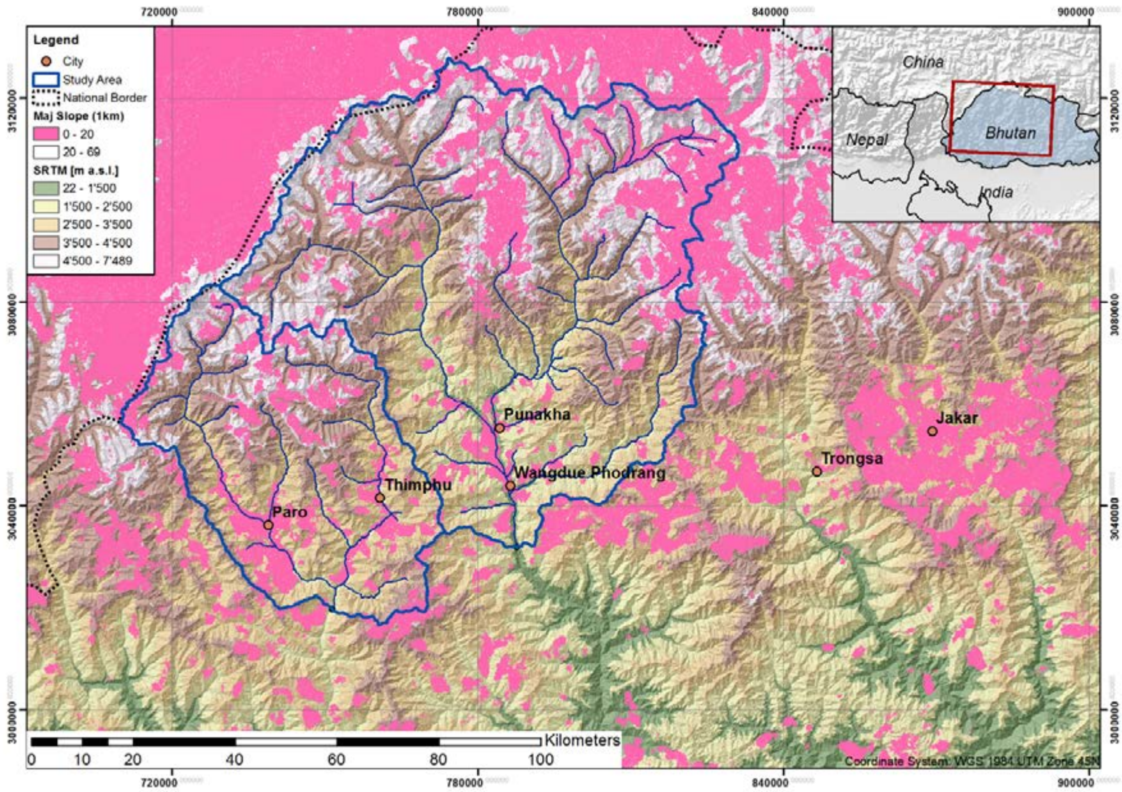

Figure 1. Topographic map with elevation (color scale), study area, and areas of low slope angle (pink: the majority of cells within a distance of 1km are <20°).

Employing third order topographic derivatives (Minár et al., 2013), we identify low angle slope sections/plateaus corresponding to terraces and/or extrapolated ridges that project onto former valley floor levels. With ridges projected to the present-day channels (Fig. 2), this allows us to treat them in a similar manner as fluvial knickpoints, providing a means of testing for regionally consistent changes in coupled fluvial and hillslope activity that may be tied to major structural, tectonic, or climatic changes.

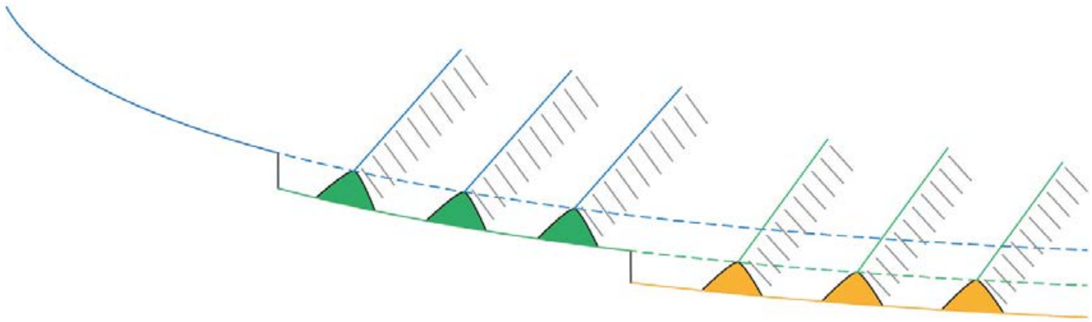

Figure 2. Schematic representation of links between ridges and paleo river profiles.

REFERENCES

Adams, B., Whipple, K. X., Hodges, K. V. & Heimsath, A. M. (2016), In situ development of high-elevation, lowrelief landscapes via duplex deformation in the Eastern Himalayan hinterland, Bhutan. Journal of Geophysical Research: Earth Surface, 925–938.

Minár, J., Jenˇco, M., Evans, I. S., Minár, J., Kadlec, M., Krcho, J., Pacina, J., Burian, L., and Benová, A., (2013), Third-order geomorphometric variables (derivatives): definition, computation and utilization of changes of curvatures. International Journal of Geographical Information Science, v. 27, no. 7, p. 1381-1402.

P 7.4

A methodological approach to improve erosion experiments on biochar by using a high precision rainfall simulator and photogrammetry

Nina Goldman, Marius Mayer, Wolfgang Fister & Nikolaus J. Kuhn

University of Basel, Physical Geography and Environmental Change, Environmental Sciences, Basel, Switzerland (wolfgang.fister@unibas.ch)

Biochar is termed a soil amendment, which could have a positive effect on the anthropogenic climate change by sequestering carbon in the ground. However, these positive effects can only arise if the biochar is not eroded during the first rainfall events. Initial experimental results indicate that a large quantity of the applied biochar is lost, but soil erosion is also reduced by incorporating biochar into the soil. The overall objectives of this study are to gain insights into the process knowledge of erodibility of soils with incorporated biochar, and to develop new techniques for their observation. A drip type rainfall simulator is used on a microscale flume (0.2m2) to be able to precisely control and monitor the thin surface flows and rainfall characteristics. In order to reduce the complexity of the experiments and to be able to differentiate between biochar and sediment loss, only pure sand and biochar mixtures have been used so far. Since a clear differentiation between soil and biochar is not feasible without the use of heavy acids, we aim on developing a new method, which will be of use for future experiments with biochar-soil mixtures. For this purpose we combine photogrammetry with information on the vertical distribution of biochar within the sand colums before and after an experiment. Together, this should enable a more accurate quantification of the residual amount of biochar and hence, enable us to calculate the net biochar loss. The results of this study could provide guidelines for the types of methods that can be used to assess biochar erosion as well as to calculate the potential monetary loss due to biochar discharge through rainfall events.

P 7.5

Impatiens glandulifera (Himalayan Balsam) and increased soil loss: causation or association? Case studies from Switzerland and the UK

Philip Greenwood & Nikolaus Kuhn

University of Basel, Basel-4056, Switzerland

The annual invasive plant, *Impatiens glandulifera* (Himalayan Balsam), is now well established in most temperate European countries. It is also common across east and west regions of North America and is increasingly being recorded on some Australasian islands. As a ruderal species with a preference for damp, fertile and frequently disturbed soils, riverbanks and the riparian zone represent prime habitat. Whilst I. glandulifera is able to crowd-out most perennial vegetation, as an annual plant with an intolerance to cold weather, its death over the winter period leaves invaded areas devoid or depleted in surface vegetation and at an increasing risk of erosion when compared against uninvaded areas supporting perennial vegetation. Despite these claims, attempts to quantify its role have only recently been undertaken during erosion monitoring research conducted over the autumn dieback of 2012 to the spring germination period of 2013 along a section of watercourse in northwest Switzerland. The investigation, which is still ongoing, now benefits from additional data covering four consecutive die-off to germination periods, from 2012-16, from the same watercourse as above, as well as data from a second river in southwest UK, which covers three consecutive die-off to germination periods, from 2013-16. Statistical analysis of each data-set indicates that soil loss from areas invaded with I. glandulifera was significantly greater than soil loss from spatially and topographically comparable reference areas over six out of the seven measurement periods. Reinterpreting all erosion data has led us to rethink whether I. glandulifera causes high erosion, or is merely associated with areas where high erosion regularly occurs. We now explore whether I. glandulifera may preferentially colonise low-lying areas where the frequent deposition of flood-derived sediment (and seeds) may perpetuate poorly developed soil structure, low cohesion and limited ability to resist erosion; all of which may be responsible for high rates of soil loss.

P 7.6

Assessing the origins, timing and transport distances of large exotic boulders in trans-Himalayan rivers

Marius L. Huber[1], Sean F. Gallen[1], Maarten Lupker[1], Negar Haghipour[1], Marcus Christl[2] & Ananta P. Gajurel[3]

[1]*Geological Institute, Department of Earth Sciences, ETH Zurich, Sonneggstrasse 5, CH-8092 Zurich, (humarius@student.ethz.ch)*
[2]*Laboratory of Ion Beam Physics (LIP), Institute for Particle Physics, Department of Physics, ETH Zurich, Otto-Stern-Weg 5, CH-8093 Zurich*
[3]*Department of Geology, Tri-Chandra Campus, Tribhuvan University, Ghantaghar, Kathmandu, Nepal*

Tectonically active landscapes develop equilibrium topographies by balancing rock uplift and erosion over long time-scales (>1 Myr) (e.g. Burbank et al. 1996). On shorter timescales (≤ 10^5 yr) landscape evolution is complex and characterized by phases of erosion and aggradation within drainage systems (e.g. Schumm 1973). Periods of erosion and aggradation in fluvial systems can be caused by changes in climate and tectonic forcing or by stochastic processes, such as landsliding or catastrophic outburst floods. While the role of climate and tectonics in shaping landscapes is relatively well understood (e.g. Whipple & Tucker 1999), the impact of stochastic, catastrophic events, which rarely occur on human time-scales, on landscape evolution remains unclear.

In trans-Himalayan river valleys, i.e. rivers sourced on the Tibetan plateau and crossing the entire range, numerous large boulders of >10 m in diameter can be found in the modern river channel or on and within river terraces alongside (Figure 1). The gneissic lithology of some of these large boulders differs from the local, Lesser Himalaya, phyllites and schists present on the adjacent hillslopes and suggests a Higher Himalaya origin 10's of kilometers upstream. The large boulders show evidence of fluvial rounding and are located 2000 m below the last glacial maximum ice extent (Owen & Benn 2005), implying that glacial transport is unlikely. The exact transport mechanism responsible for such exceptionally large grain sizes remains unknown, but may represent the sedimentological expression of reoccurring catastrophic events such as outburst floods or mountain-scale slope failures.
There is clear evidence for rapid sediment infill thought to be associated with catastrophic events in trans-Himalayan river valleys followed by very fast downcutting of rivers (extremely high incision rates) in the central Himalayan region (Pratt-Sitaula et al. 2004; Schwanghart et al. 2016).

In this study we focus on boulders of exeptional sizes (>10 m diameter), found in the Trishuli and Sun Kosi/Bhote Koshi valleys in central Nepal (Figure 1). The location, lithology and ^{10}Be exposure ages of these boulders in combination with paleohydrological and flow path modeling will shed new light on possible emplacement mechanisms of these enagmatic large boulders. This ongoing research will allow us to test different hypothesis of transport processes including extensive mass wasting in combination with landslide dammed or glacier lake outburst floods or large scale synchronuous destabilisation of hillslopes during earthquakes. At the time of presentation results, interpretations, discussion and conclusions will be available.

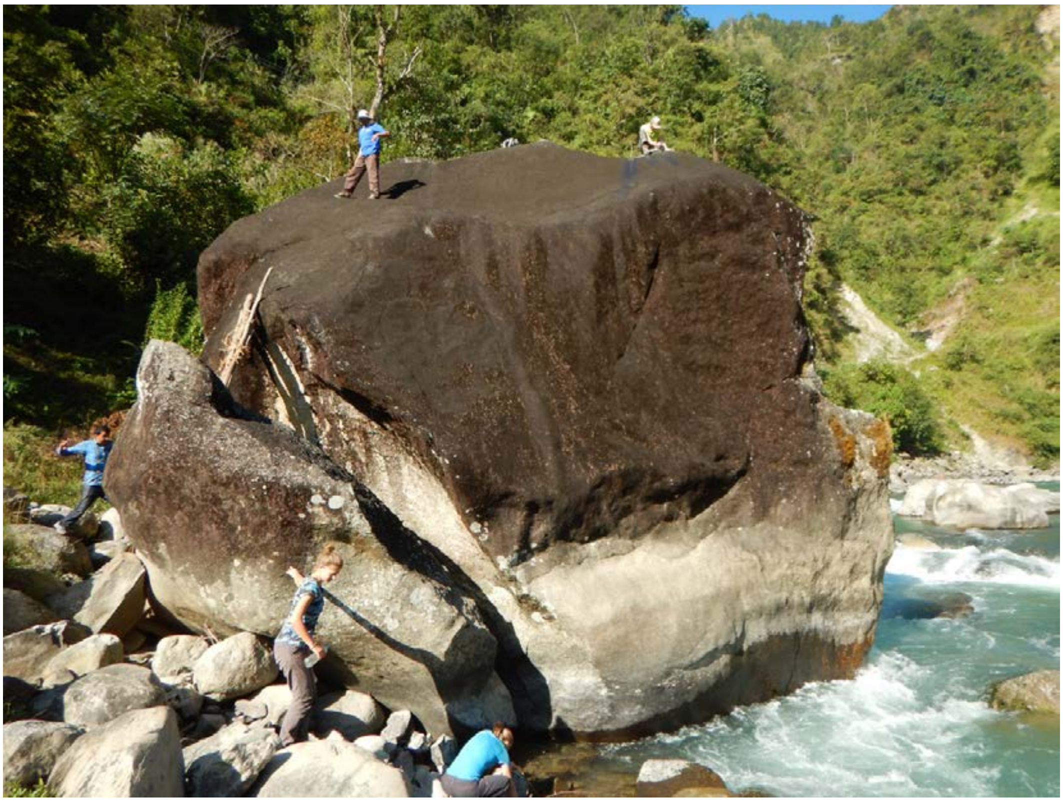

Figure 1. Large gneiss boulder in a tributary of the Sun Kosi river. Higher Himalayan lithology differs from local hillslopes and indicate travel distance minimum about 20 km (14 m diameter, up to 4'000 t).

REFERENCES

Burbank, D.W., Leland, J., Fielding, E., Anderson, R.S., 1996: Bedrock incision, rock uplift and threshold hillslopes in the northwestern Himalayas. Nature, 379(6565), 505.

Owen, L.A. & Benn, D.I., 2005: Equilibrium-line altitudes of the Last Glacial Maximum for the Himalaya and Tibet: an assessment and evaluation of results. Quaternary International, 138, 55-78.

Pratt-Sitaula, B., Burbank, D.W., Heimsath, A., Ojha, T., 2004: Landscape disequilibrium on 1000–10,000 year scales Marsyandi River, Nepal, central Himalaya. Geomorphology, 58(1), 223-241.

Schumm, S., 1973: Geomorphic thresholds and complex response of drainage systems. Fluvial geomorphology, 6, 69-85.

Schwanghart, W., Bernhardt, A., Stolle, A., Hoelzmann, P., Adhikari, B.R., Andermann, C., Tofelde, S., Merchel, S., Rugel, G., Fort, M., 2016: Repeated catastrophic valley infill following medieval earthquakes in the Nepal Himalaya. Science, 351(6269), 147-150.

Whipple, K.X. & Tucker, G.E., 1999: Dynamics of the stream-power river incision model: Implications for height limits of mountain ranges, landscape response timescales, and research needs. Journal of Geophysical Research: Solid Earth, 104(B8), 17661-17674.

P 7.7

Dam busy: beavers and their influence on the structure and function of river systems

Annegret Larsen[1], Joshua Larsen[1,2] Stuart N. Lane[1]

[1] *Institute of Earth Surface Dynamics, Université de Lausanne, 1015 Lausanne, Switzerland*
[2] *School of Earth & Environmental Sciences, University of Queensland, Australia*

Beavers (*castor fiber, castor canadensis*) are the most influential mammalian ecosystem engineer, heavily modifying rivers and floodplains and influencing the hydrology, geomorphology, carbon and nutrient cycling, and ecology. They do this by constructing dams, digging canals and burrows, felling trees and introducing wood into streams, which in turn impounds water, raises shallow water tables, and alters the partitioning of the water balance, sediment transport and channel patters, biogeochemical cycling, and aquatic and terrestrial habitats. However, largely in the absence of predators, beaver numbers have been rapidly increasing throughout Europe since the 1980s, but also in parts of the US and South America, prompting a need to comprehensively review the current state of knowledge on how beavers influence the structure and function of river systems. Here, we synthesize the overall impacts on hydrology, geomorphology, biogeochemistry, and aquatic and terrestrial ecosystems. We then examine the key feedbacks and overlaps between these changes induced by beavers, finding that modifications to the longitudinal connectivity drive many key process feedbacks. However, the magnitude of these feedbacks is also heavily dependent on the landscape and climatic context, with the ability to promote lateral connectivity determining the extent of beaver impacts as stream order increases. Crucially, beavers shape a river corridor, introducing distinct processes and feedbacks that would have existed prior to the historical collapse of beaver populations. There is thus a need to adapt current river management and restoration practices such that they can accommodate and enhance the ecosystem engineering services provided by beavers. We summarize key knowledge gaps that remain in our understanding of beaver impacts, which help map an interdisciplinary future research agenda.

P 7.8

Active Tectonic Faults and Their Effects on Quaternary Shorelines of the Malekan Regions (Northwestern Iran)

Alireza Salehipour Milani* ,Ali Mohammadi**, Amaneh Kaveh[3]

* Department of Physical Geography, Faculty of Earth Science, Shahid Beheshti University, Tehran, Iran (Ar_Salehipour@sbu.ac.ir) .
** ETH Zurich,Geological Institute ,Secretariat ,Sonneggstrasse 5.,8092 Zurich, Switzerland
[3] ETH Zurich,Geological Institute ,Secretariat ,Sonneggstrasse 5.,8092 Zurich, Switzerland

Introduction

The Urmia Lake are located in northwest of Iran between the provinces of East Azerbaijan and West Azerbaijan, and west of the southern portion of the Caspian Sea. It was the largest lake in the Middle East and the sixth-largest saltwater lake on Earth, with a surface area of approximately 5,200 km^2 (2,000 sq. mi), a length of 140 km (87 mi), a width of 55 km (34 mi), The Urmia Lake area is surrounded by several major active oblique-slip faults with dextral and normal offsets. Study area are located in southeast part of this lake in near Malekan City.

Methodology

Interpretation obtained by qualitative and quantitative data. The quantitative data includes satellite image interpretation and digital elevation models, alluvial fan morphometric, channel displacement and rate of sediments uplift. Longitudinal and cross profile and gradient analysis used to detect quaternary fault and lineation in study area. For such interpretation, ArcGIS, Erdas Imagine were utilized. The detection of main tectonic lineaments in the study area was firstly carried out by classical procedures: image sharpening of Landsat 8 images, directional filters applied to ASTER, medium resolution Digital Elevation Models analysis (SRTM and ASTER GDEM) and hill shades interpretation. In addition, a new approach in fault zone identification, based on multispectral satellite images classification, has been tested in Malkean area. Field studies were performed for the identification and measurement of parameters such as the dip and direction of fault, displacements of river and pale shorelines. Age of Quaternary shorelines determined by C14 analysis and elevation of lake terraces obtain by Dual-Frequency RTK GPS. Finally, the data obtained during field studies are compared and analyzed through quantitative and descriptive methods. Plaeo shoreline were identified during field work according to sedimentological characteristics, and presence of lacustrine shell fragment like as gastropod in sediments.

Discussion

According to C14dating from biological content of this shoreline ages of these shoreline are determined for 36500BP.
The main Quaternary tectonic activity is represented by Reverse movement faults along the malekan region that found for the first time in this Research. The Plaeo shorelines elevation and sedimentation is strongly influenced by tectonic processes in north part of Malekan Region. In malekan region we found 6 quaternary shorelines. Three shorelines including Malekan3 shoreline in 1324m.s.l. (54 meter above present lake level), Malekan –bonab3 shoreline in 1339.6m.s.l. (69 meter above present lake level) and Malekan –bonab2 shoreline in 1330m.s.l. (60 meter above present lake level) are located on slope of this fault.

Conclusion

We can detect Uplift rate along this fault based on elevation of lake terraces that located in slope of these faults compare to elevation of another quaternary shorelines including Malekan-Bonab 5, 6, 4 that found near malekan fault (malekan fault had not affected them). results shows we are faces to active fault in north of Malekan City and during 36500 years ago, in different parts of this fault uplift was between 4 meter to 24 meter.

Keywords—, Quaternary Shoreline, Active Tectonic ,Remote Sensing, the Urmia Lake, Malekan

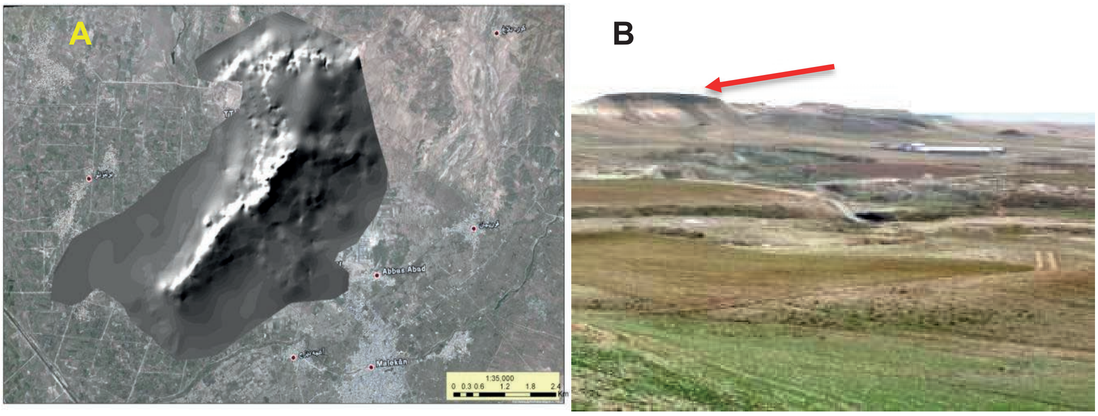

Figure1. A:Hillshade of Malekan Fault, B: Malekan fault

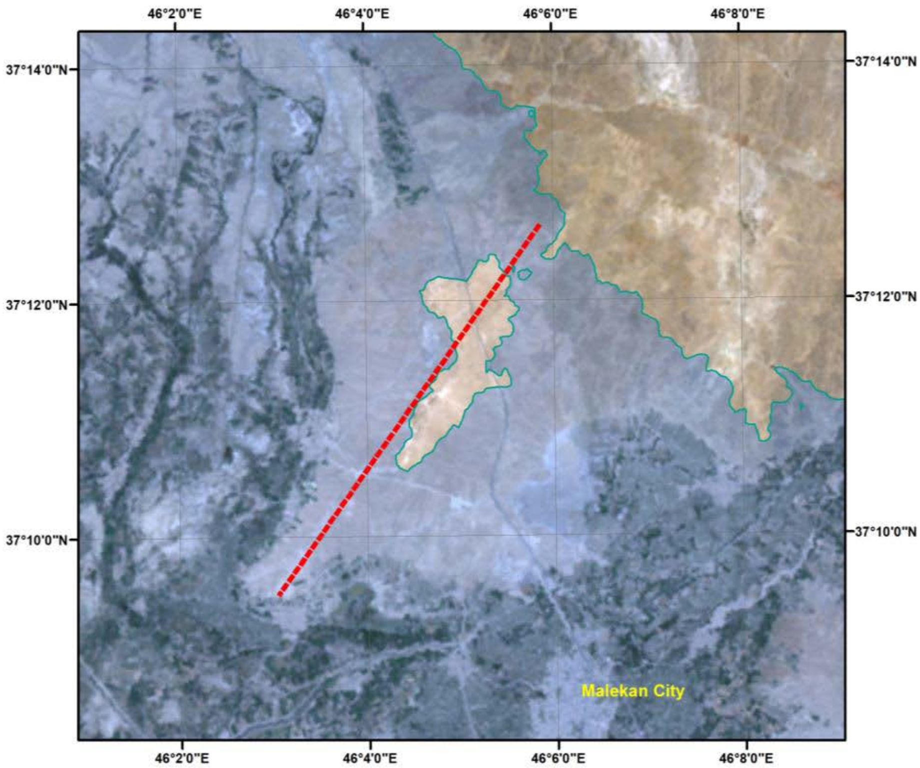

Figure2.Lake level rise in Malekan in 36500 years ago(Blue Water Level, Red Malekan Fault

P 7.9

Regulated flows influence on river morphodynamics: the Spöl River (Swiss National Park)

Salome Schläfli[1], Virginia Ruiz-Villanueva[2], Fritz Schlunegger[1], Markus Stoffel[2]

[1]Institut für Geologie, University of Bern, Baltzerstrasse 1+3, CH-3012 Bern (salome.schlaefli@students.unibe.ch)
[2]Institute for Environmental Science (ISE), University of Geneva, 66 Boulevard Carl-Vogt, CH-1205 Genève

Natural morphodynamics of rivers have been altered for centuries through the regulation of their flow regimes. This paradigm in river management has changed over the course of the last few years, and in some cases pioneering regime-based criteria have been applied to partially recover river integrity. One benchmark example is the Spöl River in the Swiss National Park (SNP), where a long-term artificial flood program started in 2000 (with the release of 15 high flows during the last 8 years). One of the main purposes of this program was to improve morphological and therefore habitat heterogeneity in the river. After 16 years of the starting of this project, many studies showed that the river recovered part of its mountain river character, and the artificial floods mitigated some of the effects of the river regulation. However, the morphodynamic effects of such effects are still not fully understood and to date there is not a detailed morphological map of the Spöl available. The aim of this research project is to fill this gap and to improve the understanding of regulated flow effects on river morphodynamics. The research questions are: (1) How heterogeneous is the current morphology of the Spöl after several years of the regulated floods program? (2) How can drones help to identify, classify, and map fluvial features and to monitor geomorphic changes in a mountain river? (3) How does the Spöl River´s morphodynamics respond to flow regulation? To answer these questions field and laboratory investigations are combined. Field surveys consist of field observations and unmanned aerial data to gather hyperspatial imagery, which will then allow construction of high-accuracy digital surface models (DSM). The unmanned aerial surveys were carried out in summer 2017 using the AscTec Falcon 8 available at the SNP equipped with the RGB camera Sony Alpha NEX-7. The approach contains the following three steps: (1) a sediment connectivity analysis on the watershed scale, (2) a historical analysis of aerial pictures back to 1946 and (3) a high-resolution characterization of the current morphology. The hyperspatial imagery together with the DSM will allow the identification, classification and mapping of the main fluvial features (i.e., morphometry) (see figure 1). This approach has been rapidly spread in the field of fluvial geomorphology (Bangen et al., 2014). Main fluvial landforms will be identified, classified and mapped along the Spöl. The geomorphic classification will be based on consistent and the most updated guidelines (Buffington & Montgomery, 2005; Grunell et al., 2014; Rinaldi et al., 2015; Wheaton et al., 2015). The better understanding of the spatial distribution of fluvial landforms or geomorphic features will shed light to the fluvial processes occurring in the river (i.e., erosion and deposition of sediment). Therefore, the expected results will provide an important analytical tool for the SNP and the artificial flood program in particular. Moreover, results will be of interest for the research community in general, as they are expected to improve knowledge about the use of unmanned aerial systems, hyperspatial imagery and the high-resolution topography to monitor fluvial processes; but, outcomes will also contribute to the biological and ecological monitoring of the Spöl (e.g. characterizing physical habitats) and other river restoration programs.

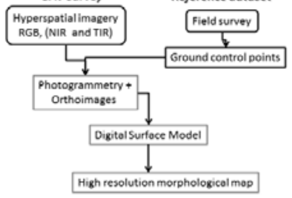

Figure 1. General flow chart with the framework

ACKNOWLEDGMENTS
Swiss academies of arts and science, ICAS, Thomas Scheurer
Swiss National Park, Ruedi Haller, Samuel Wiesmann, Christian Rossi
HYDRA Büro für Gewässerökologie Mürle und Ortlepp, Johannes Ortlepp
University of Geneva, Marjorie Perroud
Gabriela Schär

REFERENCES

Bangen, S. G., Wheaton, J. M., Bouwes, N., Bouwes, B., & Jordan, C. (2014). A methodological intercomparison of topographic survey techniques for characterizing wadeable streams and rivers. Geomorphology, 206(February), 343–361.

Buffington, J. M., & Montgomery, D. R. (2005). Geomorphic Classification of Rivers and Streams. In Treatise on Geomorphology (Vol. 9, pp. 171–204). https://doi.org/10.1002/0470868333.ch7

A.M. Gurnell, M. Bussettini, B. Camenen, M. González Del Tánago, R.C. Grabowski, D. Hendriks, A. Henshaw, A. Latapie, M. Rinaldi and N. Surian (2014) A hierarchical multi- scale framework and indicators of hydromorphological processes and forms. Deliverable 2.1, Part 1, of REFORM (REstoring rivers FOR effective catchment Management), a Collaborative project (large-scale integrating project) funded by the European Commission within the 7th Framework Programme under Grant Agreement 282656.

Rinaldi, M., Surian, N., Comiti, F., & Bussettini, M. (2015). A methodological framework for hydromorphological assessment, analysis and monitoring (IDRAIM) aimed at promoting integrated river management. Geomorphology, 251(November), 122–136. https://doi.org/10.1016/j.geomorph.2015.05.010.

Wheaton, J. M., Fryirs, K. A., Brierley, G., Bangen, S. G., Bouwes, N., & O'Brien, G. (2015). Geomorphic mapping and taxonomy of fluvial landforms. Geomorphology, 248(August 2016), 273–295. https://doi.org/10.1016/j.geomorph.2015.07.010.

P 7.10

Paleo drainage networks of the Alpine region

Sascha Winterberg[1,*], Sean Willett[1], Vincenzo Picotti[1]

[1]*Geological Institute, ETH Zürich, Sonneggstrasse 5, 8092 Zürich, Switzerland*
**email: sascha.winterberg@erdw.ethz.ch*

The topography of the Alps formed through the interaction between convergent tectonic and surface processes, yet the contribution of different drivers of Alpine topography remain an ongoing controversy. Mantle processes, lithospheric structure, and unloading by erosion have variously been suggested to account for vertical motions in the Alps (Robl et al. 2017).

During the active convergence phase, crustal shortening and thickening was the main driver for surface evolution (Handy et al. 2014). However, since the Miocene, most of the Alps have entered a post-tectonic stage, in which shortening has almost ceased, and erosion and subsequent isostatic adjustment dominate vertical motions (Fox et al. 2016). Excepting the glacial periods of the late Quarternary, erosional processes and rates are governed by fluvial systems. The river profiles and drainage basins of the Alps are both the recorders of the tectonic history and active players in the erosional processes and we present a geomorphic and geographic analysis of river basins in the Alps in order to demonstrate these processes. Analysis reveals historic and recent river captures that strongly influence catchment size and horizontal movement of water divides. These adjustment indicate and drive spatial variability in erosion rates.

We also attempt to apply geomorphic principles on paleo river networks as an interpretation tool. Paleogeographic models in combination with tectonic models demonstrate the interaction between surface and deep processes. We construct a series of paleo geographic maps using sedimentology and provenance data from the literature, and correct these features for paleo location based on tectonic reconstructions. The resulting paleo drainage maps demonstrate how spatial variations in erosion and exhumation can be extended back in time.

From the interpreted river network the predicted erosion rate variability is compared with the modern erosion rates and fit to long-term exhumation rates derived from thermochronometry (Fox et al. 2016).

We found disequilibria in the river networks that is related to events in regions well outside the Alpine orogen, including the Carpathians and the Rhine Graben, where geomorphic perturbations in steepness, erosion rate or network geometry have propagated upstream into the Alps. Systematic changes in the river network have therefore continued into the post-tectonic stage of the mountain belt, inducing temporal changes in exhumation rate that are non-tectonic in origin.

REFERENCES

Fox, M., Herman, F., Willett, S.D., Schmid, S.M., 2016: The Exhumation history of the European Alps inferred from linear inversion of thermochronometric data. American Journal of Science 316, 505-541.

Handy, M.R., Ustaszewski, K., Kissling, E., 2014: Reconstructing the Alps–Carpathians–Dinarides as a key to understanding switches in subduction polarity, slab gaps and surface motion. International Journal of Earth Sciences, 1-26.

Robl, J., Heberer, B., Prasicek, G., Neubauer, F., Hergarten, S., 2017: The topography of a continental indenter: The interplay between crustal deformation, erosion and base level changes in the eastern Southern Alps. Journal of Geophysical Research: Earth Surface.

P 7.11

Saharan networks and the Martian networks: a key analogue to extract response of surface to past, present and future climatic changes

Abdallah S. Zaki[1], Sébastien Castelltort[1]

[1] *Earth Surface Dynamics, Department of Earth Sciences, University of Geneva (abdallah.s.zaki@outlook.com).*

The discovery of seemingly water-worn valleys on Mars remains one of the most transforming events in the history of our exploration of the solar system. Images from the Mariner 6 and 7 revealed small valley networks on the Martian surface in 1969. However, these landforms were not recognized as fluvial until Mariner 9 images were obtained in 1970 (McCauley et al., 1972). Most valley networks developed during earlier warmer and wetter climatic environments, this interpretation based on data collected from Mariner 9 (1971) and the Viking orbiters (1976-1980) (e.g., Mars Channel Working Group, 1983). New details of the valley networks were obtained by High-resolution images from the Mars Orbiter Camera (MOC) abroad the Mars Global Surveyor (1997-2006), the Thermal Emission Imaging System (THEMIS) abroad the Mars Odyssey (2002-present), and finally, Curiosity Rover which landed on the floor of the 150-km-diameter Gale Crater by Mars Science Laboratory on 6 August 2012. Fluvial-like landforms such as river channels, alluvial fans and deltas, and sedimentary rocks testifying sediment transport under the influence of water have been observed in numerous regions on Mars (Fig. 1). Fluvial activity on Mars has been assigned to ages as old as Noachian and as young as Amazonian (<3.0 Ga) (Howard et al., 2005). Wilson et al. (2016) recently suggested that flowing water, perhaps from snowmelt, formed mid-latitude valleys between 2 to 3 billion years ago.

Drainage systems in the eastern Sahara such as valley networks, buried drainage systems, and inverted drainage systems exist because they have been formed during several previous Paleogene and Neogene periods of humid climate (Issawi and McCauley, 1993; Zaki and Giegengack, 2016). Such relict landforms thus constitute a natural repository of possible analogues for fluvial and fluvial-like landforms on Mars, which can be readily studied in order to provide new insights on surface response at past, present, and future climatic changes.

We will systematically characterize the mosaic of paleodrainage systems in the eastern Sahara, using quantitative metrics with specific focus on paleohydrology, and study the earth surface response to a drying climate. Using this analogue, we will carry out an attempt to constrain paleohydrological conditions of early Mars.

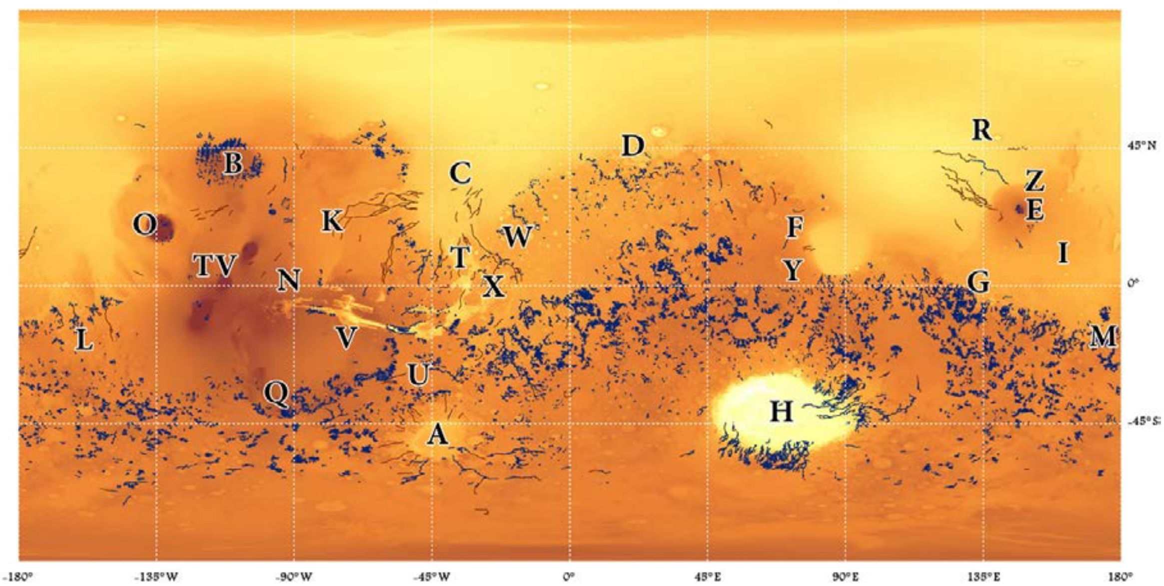

Figure 2. Map of Mars showing the distribution of valley network; blues are valley networks from (Hynek et al., 2010) and browns are channels and valleys from (Tanaka et al., 2014). Other features indicated by letters are volcanoes, B-Alba Patera, E-Elysium Mons, O-Olympus Mons, TV-Tharsis volcanoes, Y-Syrtis Major Planitia, and Z-Hecates Tholis; impact basins and craters, A-Argyre, C-Chryse, F-Jezero Crater, G-Gale Crater, H-Hellas; deltas, F-Jezero, U-Eberswalde; tectonic features, N-Noctis Labyrinthus, V-Valles Marineris; channels and valleys, D-Okavango Vallis, I-Athabasca Vallis, J-Maja Vallis, K-Kasei Vallis, L-Mangala Vallis, M-Ma'adim Vallis, P-Marte Vallis, Q-Warrego Vallis, R-Hrad Vallis, S-Shalbatana Vallis, T-Tiu and Simud Valles, U-Uzboi Vallis, W-Mawth Vallis, X-Aram Chaos and channel. Background extracted from Mars Orbiter Laser Altimeter (MOLA-DTM).

REFERENCES

Howard, A.D., Moore, J.M., Irwin, R.P.I.I.I. (2005). An intense terminal epoch of widespread fluvial activity on early Mars: 1. Valley network incision and associated deposits. J. Geophys. Res. 110, E12S14?.

Hynek, B. M., Beach, M., Hoke, M. R. T. (2010). Updated global map of Martian valley networks and implications for climate and hydrologic processes, J. Geophys. Res., 115, E09008, doi: 10.1029/2009JE003548.

Issawi, B., McCauley, J. F. (1993). The Cenozoic landscape of Egypt and its river systems, Ann. Geol. Survey of Egypt,- 19, - 357-384.

Tanaka,K.L., J.A. Skinner, Jr., J.M. Dohm, R.P. Irwin, III, E.J. Kolb, C.M. Fortezzo, Thomas Platz, G.G. Michael, and T.M. Hare (2014). Geologic Map of Mars, Scale 1:20,000,000, U.S. Geological Survey Scientific Investigations Map SIM 3292.

Mars Channel Working Group (1983). Channel and valleys on Mars. Geological Society of America Bulletin, 94, 1035-1054.

McCauley, J. F., M. H. Carr, J. A. Cutts, W. K. Hartmann, H. Masursky, D. J. Milton, R. P. Shaarp, and D. E. Wilhelms (1972). Preliminary Mariner 9 report on the geology of Mars. Icarus, 17, 289-327.

Wilson, S. A., A. D. Howard, J. M. Moore, and J. A. Grant (2016). A cold-wet middle-latitude environment on Mars during the Hesperian-Amazonian transition: Evidence from northern Arabia valleys and paleolakes, J. Geophys. Res. Planets, 121, 1667–1694.

Zaki, A. S., R. Giegengack (2016). Inverted topography in the southeastern part of the Western Desert of Egyp. Journal of African Earth Sciences 121, 56-61.

P 7.12

UAV based soil erosion monitoring for soil protection

Nikolaus Kuhn[1], Delia Mändli[1], Brigitte Kuhn[1], Daniel Schaub[2]

[1] *Physical Geography & Environmental Change, University of Basel, Klingelbergstrasse 27, CH-4056 Basel (nikolaus.kuhn@unibas.ch)*
[2] *Kanton Aargau, Departement Bau, Verkehr und Umwelt, Entfelderstrasse 22, CH-5001 Aarau*

Since 2017, regional governments in Switzerland have to monitor soil erosion and take action when non-sustainable rates of erosion are exceeded. UAV acquired imagery offers the potential to support this task. In this study, a small UAV was used to map rills and crusted areas after a snowmelt/rainfall event in February 2017. In total, four fields were mapped at resolutions ranging from 0.4 cm to 2.61 cm. DEMs generated from the acquired images illustrated the potential of UAVs to document erosion, including rough estimates of soil loss in rills.

The study also raises several questions regarding the legal and administrative framework of erosion monitoring using UAVs. Most obviously, DEMs have limited accuracy what affects the associated estimation of soil loss. Furthermore, when a long-term average loss is seen as a limit, a single observation, even when above the limit for one year, may not be legally sufficient to take action. The occurrence of rills alone was also not necessarily a sign of non-sustainable soil management in our study because runoff often appears to be generated outside cropland. A further issue is the frequency of the monitoring, ranging from regular mapping of all areas at risk, to just documenting erosion after it occurred. The difference between the two would presumably lead to different technical approaches when images are acquired, with the former requiring larger UAVs and at least a partially automated rill detection algorithm. The latter, on the other hand, relies on a network of observers.

Overall, our study showed that UAVs have a great potential in applied soil erosion monitoring. However, procedures that enable a legally sound use still require further definition to complete the assessment of the potential of this new tool.

8. Quaternary environments: landscapes, climate, ecosystems, human activity during the past 2.6 million years

Naki Akçar, Christine Pümpin, Stéphanie Girardclos, Gaudenz Deplazes, Stephanie Wirth, Jean Nicolas Haas, René Löpfe, Loren Eggenschwiler

Swiss Society for Quaternary Research (CH-QUAT)

TALKS:

8.1 **Deák J.**, Magny M.M., Wüthrich S.S.
Late Neolithic to Middle Bronze Age (ca 4900-3100 cal. BP) lake-level and palaeoclimatic fluctuations revealed by the sediment sequence of the Colombier/Les Plantées de Rive site (Neuchâtel, Switzerland).

8.2 **Glaus N.C**., Vogel H., Anselmetti F.S.
Flood-event reconstruction and land-use history in Alpine Lake Grosssee (Flumserberg, Switzerland)

8.3 **Guillemot T.**, Stockhecke M., Bechtel A., Schubert C.
Paleo-humidity reconstruction around Lake Van (Turkey) between MIS 5 to 7 based on alkenones assemblages and δD measurements

8.4 **Ordóñez L.**, Ariztegui D., Chiaradia M., Vogel H., Melles M., Russell J.M., Bijaksana S. & The Tdp Scientific Team
Investigating Fe-phases as potential recorders of past environmental changes

8.5 **Zwahlen P.**
Klimageschichte der späten Würm-Eiszeit im hinteren Prättigau

POSTERS:

P 8.1 **Abbott P.**, Jaccard S., Barker S., Gottschalk J.
Constraining the timing of deep-water ventilation changes and the marine reservoir effect in the Southern Ocean between 40-10 kyr BP: A tephrochronological and radiocarbon approach

P 8.2 **Amsler H.E**., McCave I.N., Ikehara M., Jaccard S.L.
Variations in near-bottom flow of ACC during the past glacial cycle in SW Indian Ocean

P 8.3 **Blattmann F.R**., Eglinton T.I., Haghipour N., Bernasconi S.M., Dittrich M., Al-Kuwari A.H.A., Bontognali T.R.R.
Assessing the Biogenicity and Fossilization Potential of Polygonal Sedimentary Structures

P 8.4 **Boxleitner M.**, Maisch M., Brandova D., Egli M., Ivy-Ochs S., Christl M.
Going beyond the YD – The difficulty of dating early Lateglacial stadials in central Switzerland

P 8.5 **Camperio G.**, Lloren R., Ladd N.S., Prebble M., Dubois N.
Tracing human arrival and ecosystem modification in the Pacific archipelago of Vanuatu

P 8.6 **Czerski D.**, Adatte T., Humane S.
Sedimentary record of the Naleshwar Lake (Maharastra, India): a witness of climate change and influence of human activity during the last 100 years

P 8.7 **Grischott R.**, Kober F., Ivy-Ochs S., Hippe K., Lupker M., Christl M., Vockenhuber C., Maden C.
Determination the age of Swiss Deckenschotter with cosmogenic isochron burial dating

P 8.8 **Haas M.**, Belkina N., Subetto D., Dubois N.
How politics shape agricultural landscapes: The plant wax record of Lake Lavijärvi, Russia Karelia

P 8.9 **Kaveh Firouz A.**, Burg J.-P., Haghipour N., Mandal S.K., Elyaszadeh R., Christl M.
Spatial variability of 10Be-derived erosion rates in Ghezel-Ozan Basin, NW Iran

P 8.10 **Lloren R.**, Augustinus P., Dubois N.
Multiproxy approach in assessing the downcore variations of Lake Pupuke, North Island, New Zealand during the last 1700 cal yr BP

P 8.11 **Makri S.**, Grosjean M., Rey F., Gobet E.
Long-term productivity and meromixis dynamics on the Swiss Plateau (Lake Moossee, Switzerland) inferred from Hyperspectral Imaging

P 8.12 **Mettler K.**, Fredin O., Romundset A., Christl M., Vockenhuber C., Akçar N.
Reconstruction of deglaciation chronology and relative sea level change in northern Norway using cosmogenic nuclides

P 8.13 **Morlock M.A**., Vogel H., Hadi J., Foubert A., Ariztegui D., Melles M., Russell J.M., Bijaksana S. & The Tdp Science Team
A novel 4D-view on sediments: insights to sedimentation processes and post-sedimentary mineral formation

P 8.14 **Normand R.**, Simpson G., Biswas R.H., Herman F., Bahroudi A.
Optically stimulated luminescence dating of the Western Makran marine terraces (Iran)

P 8.15 **Pregler A.**, Werthmüller S.
Uranium accumulation and leaching in Swiss plateau wetlands

P 8.16 **Salehipour Milani A.**
Mangrove Forest Sedimentary Environments along Iranian Coasts of The Persian Gulf (Bushehr to Naybad Bay)

P 8.17 **Silva T.A.**, Costa A., Girardclos S., Stutenbecker L., Bakker M., Schlunegger F., Lane S. N., Molnar P., Loizeau J.-L.
Sediment input fluctations to Lake Geneva – climate and human impact

P 8.18 **Zwahlen P.**
Würmeiszeit und die Rückzugsstadien im Alpenrheintal

8.1

Late Neolithic to Middle Bronze Age (ca 4900-3100 cal. BP) lake-level and palaeoclimatic fluctuations revealed by the sediment sequence of the Colombier/Les Plantées de Rive site (Neuchâtel, Switzerland).

Judit Deák[1], Michel Magny[2] § Sonia Wüthrich[1]

[1] *Office du Patrimoine et de l'Archéologie du Canton de Neuchâtel, Laténium, Espace Paul Vouga 7, 2068 Hauterive, Suisse (judit.deak@ne.ch)*
[2] *CNRS, Laboratoire Chrono-environnement, UFR Sciences et Techniques, 16 Route de Gray, 25030 Besançon, France*

The site of Colombier/Les Plantées de Rive (hereafter COL-PR) is located on the north-west shore of Lake Neuchâtel, in the bay of Auvernier. The latter is well-known for its numerous prehistoric lake settlements covering discontinuously the time span of 3790-850 BC, i.e. 5740-2800 cal. BP (Arnold, 2009).

Recent archaeological investigations in 2013 at the site of COL-PR revealed an exceptional concentration of anthropic structures spanning from the Late Neolithic to the Late Bronze Age (Wüthrich, 2014) interbedded within an alternation of terrestrial and lacustrine deposits. Thanks to its relatively elevated topographic position compared to the long-term mean water-level of Lake Neuchâtel, the site of COL-PR offered an unique opportunity to observe the sedimentary imprints of major rises in lake-level over the period of spanning ca. 4900-3100 cal. BP.

Using a sedimentological and pedological approach based on various proxies and with the support of radiocarbon dates from terrestrial material and additional chronological information provided by archaeological structures and artefacts, the study of the COL-PR sediment sequence allows the reconstruction of past changes in lake level of Lake Neuchâtel and leads to the following conclusions (Deák et al., 2017).

- Three major lake-level highstands occurred at ca 4900, 3650 and 3400 cal. BP which appear to be in agreement with the regional pattern of lake-level fluctuations (Magny, 2013). They also show synchronicities with increases in flood activity documented by deep cores from Lake Le Bourget in the French Pre-Alps and Lake Bodensee in southwestern Germany, changes in length of the glacier of Mer de Glace in the French Alps, or variations in latewood density from Swiss subalpine zone. The available data indicate that these climatic deteriorations are related with the variations of solar activity sometime reinforced by volcanic forcing.

- More particularly, the COL-PR sediment sequence provides new robust data to document phases of climatic deteriorations responsible for the general abandonment of lake-dwellings north of the Alps during the Middle Bronze age.

- Finally, it is worth to note the interbedding of rests of successive monuments within terrestrial and lacustrine deposits. This indicate a relative continuity of the ritual utilisation of the area at the interface between lacustrine and terrestrial domains, despite interruptions provoked by major lake-level rises and associated flooding in response to periods of climatic deterioration. All these suggest a significant role played over hundreds years by the collective memory in the perpetuation of the ceremonial and funeral vocation of the site.

REFERENCES

Arnold, B. 2009: A la poursuite des villages lacustres neuchâtelois: un siècle et demi de cartographie et de recherche. Archéologie Neuchâteloise 45. Neuchâtel: Office et musée cantonal d'archéologie.

Deák, J., Magny, M., Wüthrich, S. 2017: Late Neolithic to Middle Bronze Age (around 4900-3100 cal. BP) lake-level fluctuations at Lake Neuchâtel (Switzerland) as reflected by the sediment sequence of the site of Colombier/Les Plantées de Rive: palaeoclimatic and archaeological implications. The Holocene, online. doi.org: 10.1177/0959683617714598

Magny, M. 2013: Orbital, ice sheet, and possible solar forcing of Holocene lake-level fluctuations in west-central Europe: A comment on Bleicher. The Holocene, 23(8), 1202-1212.

Wüthrich, S. 2014: Colombier NE, Plantées de Rive. Chronique archéologique 2013. Annuaire d'Archéologie Suisse 97, 207.

8.2

Flood-event reconstruction and land-use history in Alpine Lake Grosssee (Flumserberg, Switzerland)

Nicole C. Glaus[1], Hendrik Vogel[1] and Flavio S. Anselmetti[1]

[1] Oeschger Centre for Climate Change Research and Institute of Geological Sciences, University of Bern, Baltzerstrasse 1+3, CH-3012 Bern (nicole.glaus@students.unibe.ch)

Flood-events are amongst the most frequent and destructive natural hazards. As it is still highly uncertain how the occurrence of floods especially in mountain regions, will change in our era of climate change, it is essential to study controls and occurrences of such past events over long time scales. In this study, the lake sediments of Lake Grosssee (Flumserberg, Switzerland) are targeted to provide a several thousand years long record of flood-events. Grosssee is an Alpine lake at an elevation of 1617 m a.s.l. The lake has a surface area of 0.05 km2 and a maximum water depth of 11.5 m. The lake catchment of 2.2 km2 lies in the Helvetic Alpine nappes and consists partly of the Permian volcanoclastic Verrucano and the Triassic Quarten formations, which together provide the characteristic reddish colour of many parts of the catchment. During a flood event, these sediments are mobilized from the catchment and carried into the lake where they are expected to build distinct reddish flood layers providing thus ideal conditions for a flood-event reconstruction.

In February 2017, five short sediment cores with lengths between 70 and 100 cm have been recovered from the lake basin. In a second field campaign in June 2017, a long sediment core has been retrieved allowing to establish a composite section of 773 cm containing 3 major lithostratigraphic units. The uppermost 4 meters generally show dark, organic matter-rich and partly laminated sediments intercalated by reddish beds that are primarily composed of detrital siliciclastics and show normal gradation from sand to clay (Unit I). The dark sediment sections are interpreted as hemi-pelagic background sediments. The reddish siliciclastics beds are interpreted as turbidites deposited during flood-events. At least 30 flood-event layers ranging from 1-15 cm in thickness have been identified in this unit, the upper ones coinciding with some documented flood events of the area. In the next lithostratigraphic unit II, from 3.9 m to 5.7 m, homogenous, blackish sediments with fewer turbidites are present. At 5.7 m, a significant change from the overlaying organic matter-rich, dark sediments to predominantly clastic, greyish sediments occurs (Unit III). The unity Unit II / Unit III boundary is interpreted as the Late Glacial/Holocene transition. The greyish to beige bedding of the Late Glacial sediments also shows intercalation with reddish turbidite beds. A 5 cm-thick layer of small gravel marks the bottom of this lithostratigraphic unit forming the base of the composite section.

This sediment record will help to improve the understanding of triggers, magnitudes and frequency of flood-events recorded in Lake Grosssee in the past 10’000 years. The aim is to gain insights not only in the local flood frequency but also the flood intensity. In order to distinguish between a human-induced change in sediment availability and erodibility in the catchment due to grazing or ski-slope activities and a climate signal recorded in the lake sediments, an estimation of erodibility and its change over time is necessary. Volumetric and possibly palynologic analysis of the sediments are expected to provide the required information.

8.3

Paleo-humidity reconstruction around Lake Van (Turkey) between MIS 5 to 7 based on alkenones assemblages and δD measurements

Typhaine Guillemot[1], Mona Stockhecke[2,3] Achim Bechtel[4] & Carsten Schubert[1]

[1] *Swiss Federal Institute of Aquatic Science, Eawag, Kastanienbaum, Switzerland. (typhaine.guillemot@eawag.ch)*
[2] *Swiss Federal Institute of Aquatic Science, Eawag, Dübendorf, Switzerland.*
[3] *Large Lakes Observatory, University of Minnesota Duluth, Duluth, USA.*
[4] *Montan University, Chair in Petroleum geology, Leoben, Austria.*

Long chain alkenones are biosynthesized by haptophyte algae and generally use as a biomarker to reconstruct paleo-temperatures in marine and lacustrine environments (*Brassell et al., 1986*). Coupled with hydrogen isotope measurements, they provide information on salinity changes in the water column (*Schouten et al., 2006*).

Eastern Mediterranean paleoclimatic reconstructions during glacial/interglacial cycles are scarce and their resolution rather poor. Due to its key climatic position and morphometry, Lake Van (38.5°N, 43°E) was chosen in 2010 as the site of an International Continental Scientific Drilling (*Litt et al., 2014*). Located close to the border of Iran in Turkey, it is situated at the crossroad of the atmospheric south-western jet stream and the northern branch of the subtropical high-pressure belt. With a volume of 607 km^3, Lake Van is considered the fourth largest terminal lake and the largest soda lake of the world (pH_{water} of 9.8 and salinity of 22 g/kg). Before 500 ka, a tectonic event isolated the until then endorheic lake. Hence, its water level reflects the local precipitations to evaporation ratio (p/e ratio), offering a unique opportunity for reconstructing rainwater availability.

A long sediment record was retrieved in 350 m water depth at Ahlat Ridge (AR; 38˚40’N; 42˚40’E), spanning the last 600 kyrs or 15 Marine Isotopic Stages (MIS; *Stockhecke et al., 2014*).

Previous studies inventorying alkenone assemblages were already realized on Lake Van sediments (*Randlett et al., 2014*). Unfortunately, the important diversity of haptophyte species avoids a reliable reconstruction of paleo-temperatures and humidity, using classical protocols for isolating alkenones. Indeed, quantifications and hydrogen isotope measurements on these biomarkers can be difficult and error prone when they are present in trace amount or co-eluting with other compounds.

We therefore developed an efficient procedure to identify each individual alkenone, changing and combining previous protocols (*D’Andrea et al., 2007; Rontani et al., 2011; Longo et al., 2013*). This procedure allows us to identify and quantify clearly each alkenone compounds in order to reconstruct with more reliability paleo-temperatures and humidity around Lake Van.

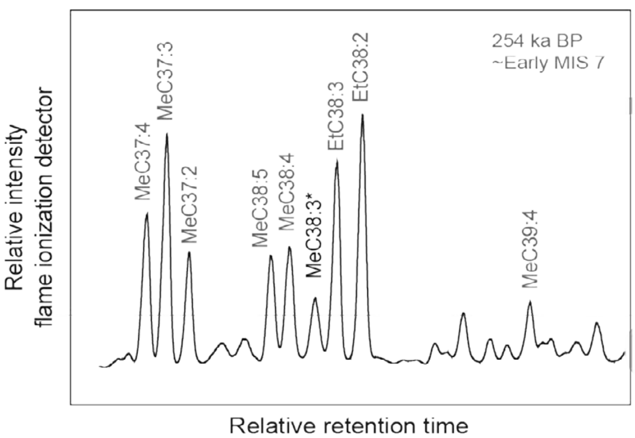

Figure 1 : Alkenone assemblage in Lake Van sediments

REFERENCES

Brassell, S.C., Brereton, R.G., Eglinton, G., Grimalt, J., Liebezeit', G., Marlowe, I.T., Pflaumann, U., Sarnthein, M., 1986. Palaeoclimatic signals recognized by chemometric treatment of molecular stratigraphic data. Organic Geochemistry, 10, 649–660.

D'Andrea, W. J., Liu, Z., Alexandre, M. D. R., Wattley S., Herbert, T. D., Huang, Y., 2007. An efficient method for isolating individual alkenones for coumpound-specific hydrogen isotope analysis. Analytical Chemistry, 9, 3430-3435.

Litt, T., Anselmetti, F. S., 2014. Lake Van deep drilling project PALEOVAN. Quaternary Science Reviews 104: 1-7.

Longo, W. M., Theroux, S., Giblin, A. E., Zheng, Y., Dillon, J. T., Huang, Y., 2016. Temperature calibration and phylogenetically distinct distributions for freshwater alkenones: evidence from northern Alaskan lakes. Geochimica et Cosmochimica Acta, 180, 177-196.

Randlett, M.-È., Coolen, M.J.L., Stockhecke, M., Pickarski, N., Litt, T., Balkema, C., Kwiecien, O., Tomonaga, Y., Wehrli, B., Schubert, C.J., 2014. Alkenone distribution in Lake Van sediment over the last 270 ka: influence of temperature and haptophyte species composition. Quaternary Sciences Reviews, Special Issue 104, 53–62.

Rontani, J-F., Wakeham, S.G., Prahl, F.G, Vaultier, F., Volkman, J.K., 2011. Analysis of trace amounts of alkenones in complex environmental samples by way of NaBH4/NaBD4 reduction and silylation. Organic Geochemistry, 42, 1299-1307.

Schouten, S., Ossebaar, J., Schreiber, K., Kienhuis, M. V. M., Langer, G., Benthien A., Bijma, J., 2006. The ffect of temperature, salinity and growth rate on the stable hydrogen isotopic composition of long chain alkenones produced by Emiliania huxleyi and Gephyrocapsa oceanic. Biogeosciences, 3, 113-119.

Stockhecke, M., Kwiecien, O., Vigliotti, L., Anselmetti, F. S., Beer, J., Namik Cagatay, M., Channell, J. E. T., Kipfer, R., LAchner, J., Litt, T., Pickarski, N., Sturm, M., 2014a. Chronostratigraphy of the 600 ka old continental record of Lake Van (Turkey). Quaternary Science Reviews, 104: 8-17.

8.4

Investigating Fe-phases as potential recorders of past environmental changes

Luis Ordóñez*, Daniel Ariztegui*, Massimo Chiaradia*, Hendrik Vogel**, Martin Melles[3], James M. Russell[4], Satria Bijaksana[5] & the TDP scientific team

[1] *Department of Earth Sciences, University of Geneva, 1205 Geneva, Switzerland (luis.ordonez@unige.ch)*
** Institute of Geological Sciences and Oeschger Centre for Climate Change Research, University of Bern, 3012 Bern, Switzerland
[3] *Institute of Mineralogy and Geology, University of Cologne, 50674 Köln, Germany*
[4] *Department of Geological Sciences, Brown University, Providence, RI 02912*
[5] Faculty of Mining and Petroleum Engineering, Institut Teknologi Bandung, Bandung 40132, Indonesia

Lake Towuti (East-Sulawesi Ophiolite belt, island of Sulawesi, Indonesia) provides an excellent archive, from orbital to millennial time-scales, for hydroclimate changes during the Quaternary, allowing the reconstruction of environmental and climate dynamics in the western equatorial Pacific region (Russell et al., 2014). Run-off waters drain the strongly weathered ultramafic catchment and anomalously enrich the basin with iron and other redox sensitive elements. Today, the lake is ultra-oligotrophic, S-depleted, and has anoxic bottom waters. However, previous studies focusing on the last 60 kyr sediments reveal water column mixing during dry periods, leading to the deposition of higher amounts of Fe(III)-phases (Costa et al., 2015).

Iron is a redox sensitive element widely used to track redox conditions at the moment of sediment deposition. Therefore, iron speciation has been explored through different analytical methods with the aim of characterizing past environmental changes. In this study, we test iron speciation obtained by sequential extraction of sediments of the ferruginous Lake Towuti, following the method of Poulton and Canfield (2005). Although the modal distribution of Fe-phases provides a good indication of oxic and reduced stratigraphic horizons, it does not necessarily indicate the redox conditions in the water column. Fast sedimentation rates and post-depositional processes like diagenesis and microbial respiration could respectively mask or replace authigenic phases which usually would record water oxygenation levels.

Positive δ56Fe values of magnetite and Fe-oxyhydroxides usually reflect water bodies-redox conditions since they can precipitate at the chemocline by the oxidation of aqueous Fe2+ during stratified lake episodes (Busigny et al., 2014). However, also magnetite constitutes, like siderite, an end product of microbial respiration under reducing conditions (Zachara et al., 2002)sediments, and groundwater. Two-line ferrihydrite is a bioavailable Fe(III. We performed Fe-isotopes analyses in a selection of Fe-phases (siderite, magnetite, Fe-oxihydroxides and Fe-oxides) of endmember samples. The negative δ56Fe values of magnetites (-0.5‰) suggest microbial processes in oxic horizons whereas in extremely reducing horizons magnetite has δ56Fe values near the detrital isotope background (0 ‰) and elevated Ti-contents suggesting a detrital origin. Siderite Fe isotope data behaves antithetically, indicating a duality between magnetite and siderite. Reducing horizons have negative δ56Fe values (-0.5‰) suggesting higher Fe-reduction rates probably due to the high contents of organic matter available for microbial respiration.

With this study we aim to provide important insight into climatically/environmentally induced processes and mechanisms capable of producing characteristic Fe-isotope footprints in sedimentary records and determine how Fe-fractionation relates to the dominant redox reactions taking place in this particular environment.

REFERENCES

Costa, K.M., Russell, J.M., Vogel, H., Bijaksana, S., 2015. Hydrological connectivity and mixing of Lake Towuti , Indonesia in response to paleoclimatic changes over the last 60 , 000 years. Palaeogeography, Palaeoclimatology, Palaeoecology 417, 467–475.

Russell, J.M., Vogel, H., Konecky, B.L., Bijaksana, S., Huang, Y., Melles, M., Wattrus, N., Costa, K., King, J.W., 2014. Glacial forcing of central Indonesian hydroclimate since 60,000 y B.P. Proceedings of the National Academy of Sciences of the United States of America 111, 5100–5.

Poulton ,S. & Canfield, DE, 2005: Development of a sequential extraction procedure for iron: implications for iron partitioning in continentally derived particulates. Chemical Geology 214 (2005) 209–221.

Busigny, V., Planavsky, N., Jézéquel, D., Crowe, S., Louvat, P., Moureau, J., Viollier, E., Lyons, T., 2014: Iron isotopes in an Archean ocean analogue. Geochimica et Cosmochimica Acta 133, 433-462.

Zachara, J., Kukkadapu, R., Fredrickson, J., Gorby, Y., Smith, S., 2002 : Biomineralization of Poorly Crystalline Fe(III) Oxides by Dissimilatory Metal Reducing Bacteria (DMRB). Geomicrobiology Journal, vol. 19, Iss. 2.

8.5

Klimageschichte der späten Würm-Eiszeit im hinteren Prättigau – Funde von fossilen Hölzern aus den Baugruben der A28a Prättigauerstrasse zwischen Küblis und Serneus 1980 bis 2009,^{14}C-Datierungen und Holzartbestimmungen

Peter Zwahlen

BTG Büro für Technische Geologie AG, Grossfeldstrasse 74, Postfach 78, CH-7320 Sargans

Zum Neubau der A28a Prättigauerstrasse zwischen Küblis Dalfazza und Serneus Bad (Kanton Graubünden, Schweiz) wurden zwischen 1982 und 1992 im Auftrag des Tiefbauamtes Graubünden geologische Sondierungen, u. A. Kernbohrungen und seismische Profile, und ab 2002 bis 2010 die entsprechenden Vortriebsarbeiten ausgeführt (BTG-Berichte Kap. 10.3). In vielen Baugruben und Lockergesteinsstrecken der Tunnelvortriebe entlang des ganzen Projektabschnittes wurden immer wieder fossile Hölzer (7 m lange Arvenstämme, Wurzelstöcke, Wurzeln, Äste, vermodertes Holz und Rinde) ausgegraben oder angebohrt. 17 Proben davon wurden an Alterslabors ^{14}C-datiert, an 7 Proben davon zudem die Baumart bestimmt.

Untersuchungsresultate: Die Altersdatierungen decken einen Altersbereich von Bölling (um 14‘500 cal.J.BP) bis Atlantikum (6‘600 bis 7‘800 cal.J.BP) ab. Dabei waren die ältesten (alle Bölling) Ast- und Wurzelstücke wenige Meter über der Felsoberfläche in der Grundmoräne des Kübliser Stadiums eingelagert und bestanden nachgewiesenermassen ausschliesslich aus Wacholder- (Juniperus 3 von 4 Proben) und Weidengehölzen (1 fleischroter Ast). Dies waren Funde aus der östlichen (oberen) Lockergesteinsstrecke des Saasertunnels. Auf der Obermoräne der Stadien von Serneus und Küblis lagerten die grossen Stämme und Wurzelstöcke von mind. 50 Jahre alten Arven (pinus cembra, Präboreal, 2 Stämme) und Föhren (pinus mugo oder sylvestris, Präboreal, 2 Stämme mit Stockansatz). Entlang der Basis des Saaser Rutsches, wenig über den Obermoränen, wurden nicht weiter identifizierte Aststücke und Holzfasern von vermutlich Koniferen und Weiden oder Erlen aus dem Präboreal bis Boreal (11‘500 bis 9‘200 cal.J.BP, 6 Proben) erbohrt. Die jüngsten Stämme, Ast- und Rindenstücke (3 Proben, Fichte, picea abies, Atlantikum) lagerten bei Küblis Dalfazza in und seitlich zu einem mächtigen Murgangkegel aus dem Schanielatobel, d.h. dem nördlichen Seitental aus St. Anthönien.

Interpretation: Kurz nach der massiven Klimaerwärmung Älteste Dryas/Bölling (GS-2/GI-1 oder DO1-event, Rasmussen et al. 2014) schmolz die Eiszunge des Landquartgletschers im Bölling (Spätwürm) so weit in den Talabschnitt Saas-Serneus zurück, dass sich in den tieferen Talflanken eine Wacholder-Weiden-Buschvegetation etablieren konnte. Im Talboden breitete sich vermutlich gleichzeitig eine mehr oder weniger mächtige Eiszunge aus, jedenfalls wurden die Buschgehölze durch temporäre Wiedervorstösse in die Grund- und Seitenmoränen eingewalzt. Die Verteilung von asymmetrischen Bergsturzablagerungen bei Serneus spricht ebenfalls für die Existenz einer verbleibenden Eiszunge im Talgrund. Auf entsprechenden Bergsturzfächern und/oder Randmoränen wuchsen im Präboreal hochstämmige Arven und Föhren. Diese lichten Pionierwälder wurden unter spätestglazialen Klimarückschlägen bzw. den Egesen-Vorstössen (Präboreal) aus den höheren Talflanken niedergewalzt oder überschottert aber wie die Stockansätze und Stammlängen zeigen, wohl nie weit verschleppt. Kurz darauf, noch im Präboreal, destabilisierten sich die Talhänge innerhalb des Prättigau-Flysches (Saaser Rutsch im NE, Conterser Rutsch im SW) vermutlich unter dem Porenwasserdruck von zunehmend abschmelzendem Permafrost. Die Grundgleitung des Saaser Rutsches war dabei noch bis ins Boreal aktiv und überwälzte fortwährend die aufwachsenden Buschwälder, wie sie typisch sind für aktive Rutschgebiete. Die Grossrutsche beider Talflanken gleiten heute noch, aber in um 10 m bis 100 m höheren Niveaus. Beim Murgangereignis aus dem Schanielatobel bei Küblis handelt es sich um ein, evtl. auch mehrere, unabhängige Niedergänge im feucht-warmen Älteren Atlantikum d.h. wohl unter dem Einfluss der starken Klimaschwankungen innerhalb des „Neolithischen Optimums“.

P 8.1

Constraining the timing of deep-water ventilation changes and the marine reservoir effect in the Southern Ocean between 40-10 kyr BP: A tephrochronological and radiocarbon approach

Peter Abbott[1,2], Samuel Jaccard[1], Steve Barker[2], Julia Gottschalk[1]

[1] *Institute of Geological Sciences and Oeschger Center for Climate Change Research, University of Bern, Baltzerstrasse 1-3, Bern 3012, Switzerland (peter.abbott@geo.unibe.ch)*
[2] *School of Earth and Ocean Sciences, Cardiff University, Park Place, CF10 3AT, Cardiff, UK*

Establishing tighter constraints on phase relationships between sedimentary evidence for deep-water ventilation of carbon dioxide (CO_2), and ice-core evidence for past atmospheric CO_2 variations can help in determining the future response of the Earth system to rising CO_2 levels. The rate and timing of deep-water ventilation can be determined through paired ^{14}C dating of planktonic and benthic foraminifera in marine sequences, however, uncertainty still exists regarding the temporally variable marine reservoir effect, the age offset between the atmosphere and surface waters. Providing independent age control for marine sequences and/or directly synchronising the marine and ice-core records can provide constraints on the reservoir effect and aid comparisons between these records. This can be achieved using tephrochronology, with common horizons of volcanic ash traced between palaeoclimatic sequences acting as time-synchronous tie-lines due to their rapid deposition. This allows ages unaffected by the reservoir effect (e.g. terrestrial ^{14}C, Ar/Ar, ice-core) to be transferred into the marine chronologies.

We are applying this approach within the Atlantic sector of the Southern Ocean, a key area for the release of CO_2 via deep-water ventilation during the deglaciation that has several upwind volcanic systems known to have deposited volcanic ash over the region. Two marine cores with pre-existing ventilation age estimates (MD07-3076Q and TN057-21) are currently under investigation using recently developed methods for the identification of marine cryptotephras, ash horizons not visible upon core inspection. Following their identification attempts will be made to trace them within the Antarctic ice-core records and/or proximal sequences to provide independent age control. Focused ^{14}C dating of planktonic foraminifera around any tephra horizons will help constrain the marine reservoir effect and in addition dating of benthic foraminifera will provide new ventilation age estimates that are independent of reservoir age uncertainties, which have previously complicated ventilation age reconstructions.

P 8.2

Variations in near-bottom flow of ACC during the past glacial cycle in SW Indian Ocean

Helen Eri Amsler[1], Samuel L. Jaccard[1], Ian Nicholas McCave[2] & Minoru Ikehara[3]

[1] *Institute of Geological Sciences and Oeschger Centre for Climate Change Research, University of Bern, Baltzerstrasse 1+3, CH-3012 Bern, Switzerland (helen-eri.amsler@geo.unibe.ch)*
[2] *Department of Earth Sciences, University of Cambridge, Downing Street, Cambridge, Cambridgeshire, CB2 3EQ, United Kingdom*
[3] *Center for Advanced Marine Core Research, Kochi University, 200 Monobe-otsu, Nankoku, 783-8502 Japan*

The meridional overturning circulation of the ocean plays a key role in global climate variability by storing and redistributing heat, fresh water, carbon and nutrients. In the North Atlantic surface water sinks to the abyss, but a major part of this cycle is the return path from the ocean's interior through upwelling in the Southern Ocean. This upwelling is largely regulated by the latitudinal position of the Southern westerly winds associated with the deep-reaching Antarctic Circumpolar Current (ACC) (Rintoul et al. 2001).

Observations in the last few decades show progressively poleward intensifying winds and climate models suggest a possibly related increase in ACC transport and southward shifting of its mean position and increased upwelling. However, a number of recent numerical studies have shown that the sensitivity of the large-scale circulation in the Southern Ocean may be reduced by eddy-effects (Böning et al 2008).

As there remains significant uncertainty regarding the degree of sensitivity of the Southern Ocean circulation to wind stress and the response of the Antarctic circumpolar transport, our aim is to investigate the temporal and latitudinal evolution of the ACC dynamics over the last glacial cycle.

Previous studies suggested a stronger ACC during glacials in the Indian Ocean (Mazaud et al. 2010), but more recent studies in the Drake Passage and Scotia Sea indicate less throughflow during glacials and lateral differences in current speeds (McCave et al. 2014, Lamy et al. 2012). Here we present the sortable silt mean-size of a series of cores across the ACC in the SW Indian Ocean, the mean-size of the re-deposited silt fraction being proportional to the near-bottom flow velocity.

REFERENCES

Böning C.W., Dispert A., Visbeck M., Rintoul S. R., Schwarzkopf F. U. (2008) Nature Geoscience, 1, 864-869.
Lamy F., Arz H. W., Kilian R., Lange C. B., Lembke-Jene L., Wengler M., Kaiser J., Baeza-Urrea O., Hall I. R., Harada N., Tiedemann R. (2015) PNAS, 112, 13496–13501.
Mazaud A., Michel E., Dewilde F., Turon J. L. (2010) G3, 11, doi:10.1029/2010GC003033.
McCave I. N., Crowhurst S. J., Kuhn G., Hillenbrand C-D., Meredith M. P. (2014) Nature Geoscience, 7, 113-116.
Rintoul S. R., Hughes C., Olbers D. (2001) in Siedler, G., Church, J., Gould, J. (eds). Ocean Circulation and Climate, Academic Press, 271-302.

P 8.3

Assessing the Biogenicity and Fossilization Potential of Polygonal Sedimentary Structures

Franziska R. Blattmann[1], Timothy I. Eglinton[1], Negar Haghipour[1], Stefano M. Bernasconi[1] , Maria Dittrich[2], Hamad A Al-Saad Al-Kuwari[3] & Tomaso R.R. Bontognali[1,3,4]

[1] *Erdwissenschafltiches Departement, ETH Zürich, Sonneggstrasse 5, 8092 Zürich (blattmaf@student.ethz.ch)*
[2] *Department of Physical and Environmental Sciences, University of Toronto Scarborough, Toronto, Canada*
[3] *Environmental Science Center, Qatar University, Doha, Qatar*
[4] *Space-X, Fbg de l'Hôpital 68, 2000 Neuchâtel, Suisse*

Around the globe, macroscopic polygonal structures are commonly found in the intertidal zone of sabkhas and other evaporitic environments. However, it is unclear whether their formation is purely abiotic (i.e., caused by desiccation) or due to a microbial process. Proving the biogenicity and the fossilization potential of these structures is relevant not only for the study of early life on Earth, but also for the search of signs of life on Mars. On Mars, exploration is currently being done by rovers equipped with cameras that do not have the resolution for identifying single microfossils, but could easily spot a cm-size morphological biosignature.

Here, we studied the occurrence and mechanism of formation of polygonal structures in two sabkhas of Qatar (i.e., the Dohat Faishakh and the Khor al Adaid), as well as an outcrop in the area of Al-Ruwais, Qatar that includes putative fossil equivalents of the modern polygons. We described the macro- and microscopic sedimentological structures and petrography of the polygons, determined growth rates using radiocarbon dating, investigated the mineralogical composition by XRD and conducted stable isotope analyses. We have subsequently evaluated the preservation potential of these features by demonstrating that the fossilized polygonal structures found at Al-Ruwais are lithified remnants of the same structures found in the intertidal zone of the modern sabkhas. This was assessed by comparison with the modern features, changes in mineralogy and shifts in stable isotope composition.

We conclude that the studied polygons are not simply the result of desiccation, but rather a microbially-influenced structure that formed by trapping of detrital particles (mainly carbonate and quartz sand) within extracellular polymeric substances and lithification through precipitation of a micrite made of High-Mg calcite, dolomite, and authigenic clay minerals of various compositions. The overall geometry of the structure is mainly determined by the presence of a microbial mat that has an average growth rate of 1.05 to 1.29 mm/year. Although our investigations of the fossil polygons show that no microfossils or visible biomass are preserved after 2800 years of diagenesis, the micrite stabilizes the polygonal structures, which can potentially be preserved in the geological record –on Earth and on Mars– providing evidence of past microbial life.

P 8.4

Going beyond the YD - The difficulty of dating early Lateglacial stadials in central Switzerland

Max Boxleitner[1], Max Maisch[1], Dagmar Brandova[1], Markus Egli[1], Susan Ivy Ochs[2], Marcus Christl[2]

[1] *Geographisches Insititut, Universität Zürich, Winterthurerstrasse 190, CH-8050 Zürich*
[2] *Labor für Ionenstrahlphysik, ETH Zürich, Otto-Stern-Weg 5, CH-8093 Zürich*

The glacier development in the Alps after the Last Glacial Maximum has been of interest for researchers in the field of Quaternary geology and climatology for more than a century. But still our understanding of the overall ice retreat from the alpine foreland into the valleys and cirques is fragmentary. Series of end moraines show that the deglaciation happened stepwise: The remnants outlining former glacier extents bear witness to climate-driven halts or re-advances called stadials. A first subdivision of the Alpine Lateglacial into stadials was established by Penck & Brückner (1909). Since then this concept was repeatedly widened and modified. At present it includes the phase of ice-decay, the Gschnitz, the Clavadel/ Senders, the Daun and the Egesen (e.g. Heiri et al., 2014 and references therein).

Especially due to new results from surface exposure dating our knowledge about the timing of these stadials has markedly increased during the last decades. Studies from all-over the Alps show that the, in many places multi-phased, Egesen re-advances can be assigned to the Younger Dryas (12,8 - 11,7 ky). However, for the older stadials, in particular for the Daun and Clavadel, age constraints are still rare (Ivy-Ochs et al., 2008).

In our studies of the Lateglacial landscape evolution and glacier development in the Meiental and Göscheneralp in central Switzerland we could show that moraines that were formerly attributed to the Daun (based on morpho-stratigraphy and glacier equilibrium line depressions (ΔELA)) were most likely deposited during the Younger Dryas (Boxleitner et al., 2017). While this questions the equilibrium line approach and/or the definition of the Daun-stadial (see also: Reitner et al., 2016), it does not question the existence of significantly older moraines in the area.

Geomorphologic witnesses of glacier stages preceding the Younger Dryas can be found further down the Reuss-valley to which both the Meiental and the Göscheneralp at that time contributed as ice streams. With the aim of going beyond the Younger Dryas we took 9 rock samples from different key locations along the main valley for ^{10}Be-surface exposure dating and retrieved an additional peat core.

With our new results we hope to be able to improve our knowledge of this time period despite the role that human activity and the ravages of time, i.e. natural depositional and erosional processes in the area, play for the preservation of glacial landforms selected for dating.

REFERENCES

Boxleitner, M., Musso, A., Waroszewski, J., Malkiewicz, M., Maisch, M., Dahms, D., Brandová, D., Christl, M., de Castro Portes, R., Egli, M., 2017. Late Pleistocene – Holocene surface processes and landscape evolution in the central Swiss Alps. Geomorphology 295, 306–322. doi:10.1016/j.geomorph.2017.07.006

Heiri, O., Koinig, K.A., Spötl, C., Barrett, S., Brauer, A., Drescher-Schneider, R., Gaar, D., Ivy-Ochs, S., Kerschner, H., Luetscher, M., Moran, A., Nicolussi, K., Preusser, F., Schmidt, R., Schoeneich, P., Schwörer, C., Sprafke, T., Terhorst, B., Tinner, W., 2014. Palaeoclimate records 60–8 ka in the Austrian and Swiss Alps and their forelands. Dating Synth. Interpret. Palaeoclim. Rec. Model-Data Integr. Adv. Intim. Proj. Ice Core Mar. Terr. Rec. COST Action ES0907 106, 186–205. doi:10.1016/j.quascirev.2014.05.021

Ivy-Ochs, S., Kerschner, H., Reuther, A., Preusser, F., Heine, K., Maisch, M., Kubik, P.W., Schlüchter, C., 2008. Chronology of the last glacial cycle in the European Alps. J. Quat. Sci. 23, 559–573.

Penck, A., Brückner, E., 1909. Die Alpen im Eiszeitalter, 1199 S. Tauchnitz Leipzig

Reitner, J., Ivy-Ochs, S., Drescher-Schneider, R., Hajdas, I., Linner, M., 2016. Reconsidering the current stratigraphy of the Alpine Lateglacial: Implications of the sedimentary and morphological record of the Lienz area (Tyrol/Austria) E&G Quaternary Science Journal. 65. 113-144. doi:10.3285/eg.65.2.02

P 8.5

Tracing human arrival and ecosystem modification in the Pacific archipelago of Vanuatu

Giorgia Camperio[1,2], Ronald Lloren[1,2], Nemiah S. Ladd[1,2] , Matthew Prebble[3] & Nathalie Dubois[1,2]

[1] *Department of Earth Science, ETH Zürich, Sonneggstrasse 5, 8092 Zürich*
[2] *Department of Surface Waters, Research & Management, eawag, Überlandstrasse 133, 8600 Dübendorf*
[3] *Department of Archaeology and Natural History, Research School of Asia Pacific Studies, The Australian National University, Canberra*

It is widely recognized that our species is causing irreversible ecological impacts through intensive land use and primary resources exploitation. Although these activities are deemed necessary to feed the increasing human population, major attention is drawn to the consequences of such activities in terms of climate change and biodiversity loss. Reconstructing past human activities can help retrieving information on the environmental responses to different rates and degrees of change. These responses are likely to be reflected in the present and in future scenarios.

Small islands, where resources are scarce and space is by definition limited, are paradigmatic cases of anthropogenic impact on ecosystems. First successful settlements in Remote Oceanic Islands came along with major landscape modifications (e.g. land clearance, introduction of allochthonous species) which allowed long-term demographic success by the establishment of extensive agriculture. However, not all the pacific islands testified a successful human establishment.

Which factors led to the failure or the establishment of a sustainable human-ecosystems interaction remains an open question. Through the multi-proxy analysis of lakes and swamps sediment cores, we can trace past human arrival and identify consequent landscape modifications in the Pacific archipelago of Vanuatu. We use an integrated approach, combining geochemical tools based on biomarkers (fossil molecules of known origin) with traditional sedimentological, archaeological, and paleoecological methods.

Variations in coprostanol (faecal biomarker) and bile acid are used to trace the arrival of humans and subsequent evolution of population size.

Here we present the preliminary results from the data collected during the last field campaign in the archipelago of Vanuatu (June-August 2017).

Tracing past anthropogenic impacts on these islands not only can provide information on the environmental changes that occurred with human arrival, but can also contribute to identify key factors related to the ecological resilience and the adaptive capacity of socio-ecological systems in changing environments.

P 8.6

Sedimentary record of the Naleshwar Lake (Maharastra, India): a witness of climate change and influence of human activity during the last 100 years

Dorota Czerski[1], Thierry Adatte[2] and Sumedh Humane[3]

[1] *Institute of Earth sciences (IST), University of Applied Sciences and Arts of Southern Switzerland (SUPSI), Campus Trevano, CH-6952 Canobbio, Switzerland*
[2] *Institute oof Earth Sciences, Faculty of Geosience and Environment, University of Lausanne (UNIL), Unil-Mouline, CH-1015 Lausanne, Switzerland*
[3] *Post Graduate Deaprtment of Geology, Rashtrasanr Tukadoji Maharaj Nagpur University, Rao Bahadur D. Laxminarayan Campus, Law College Square, Nagpur, MS 440 001, India*

In the present study a multiproxy approach including sedimentological, mineralogical and geochemical analyses was carried out on two cores sampled in a lake in Maharastra, central south India.

The aim is to provide a reconstruction of the recent history of the small reservoir lake. First, the sedimentary record was analyzed, in order to correlate the weathering of the catchment and the detrital supply due to climate variations, seasonal or over a larger scale. Secondly, the anthropogenic influence on the sedimentary regime of the lake was evaluated.

The Naleshwar Lake is located on a basement composed of metamorphic sedimentary rocks. Forest and some small villages surround the area and the local people main livelihood consists in animal breeding, fishing and agriculture activities. The semi-arid climate affected annually by the monsoon cause important yearly water level fluctuations with a consistent variation of the surface covered by the lake. In 1914 a dam was built in order to constitute a reservoir, control the water level and extract it for irrigation. When the lake level drops during the dry season, the exposed lakeside portions rich in nutrients are used for cultivation. Pesticides and fertilizers are spread on the soil and this, combined with the other human activities, may infer a signature in the lake sediments.

The monsoon plays a very important role for the existence of lakes in the region. Some studies illustrate how lake sediments can record the Holocene climate variations linked to the monsoonal system. Our project takes into consideration a much shorter period of time, nevertheless, variations related to the climate seasonality could still be observed.

The analyses were focused on two one-meter cores sampled with a gravity corer in the deepest part of the lake (4.9 meters depth). The cores were analyzed with a resolution of one centimeter and 0.5 centimeters in the upper 20 centimeters of the cores. A comparison with soil profiles and rock samples collected around the lake was carried out, in order to better understand the record of the lacustrine sediments. Thus, a precise chronostratigraphy was carried out for the first time on central India lakes using the method of ^{137}Cs activity within the sediments.

The ^{137}Cs dating showed that studied sediments approximately cover the last seventy years, with sedimentation rates of 1.7 cm/year. The data revealed very fine sediments with cyclical variations between a silty and clayey deposit, which could be mainly related to climate and seasonal variation (magnetic susceptibility, granulometry, mineral fraction (%)). In the upper part a positive excursion of clay minerals, iron and phosphorus is observed. Suggesting that some change in sedimentation or supplies is registered for this level, which could be natural or human induced.

The increase of phosphorus in the upper part of the core reflects an eutrophication of the basin, resulting in an increment of primary productivity in the lake. Both TOC (%) and N_{tot} increase towards the top of the core, this combined with a higher HI shows an enhancement of the algae proliferation in the basin. Moreover, the organic carbon isotope record also shows a slight increase in the last part of the record, confirming the increase in productivity and the subsequent depletion of lighter carbon isotope in the basin. The data mainly revealed an allochtonous source of organic matter to the lake. The HI and OI records showed a vascular plant origin or a very degraded organic matter. However, the TOC/N_{tot} ratio showed an OM signature of lacustrine origin. This can be explained with the results of the soil profiles around the lake, which show similar values. Intense bacterial activity within the soil and subsequent leaching during the rainy season represent in fact a good explanation.

Additionally, a uranium rich layer corresponding to the increase of primary productivity suggests the setting of anoxic/ suboxic conditions in the lake basin. This observation is coherent with the resulting depletion of phosphorus towards the top of the core. Unfortunately no pyrite framboids were observed at SEM. Finally, the main weathering product of the catchment is kaolinite. This clay mineral is very common in warm and humid regions and is often a product of quartzitic rocks. The clay minerals as well as the CIA (around 85%) remain constant all over the record.

To conclude, the recorded eutrophication could result from human activity and the surrounding cultivated fields. But except this, the sedimentological record seems to be related to natural variations as climate. Nevertheless, the sedimentary record shows a decrease of the organic carbon isotopic composition from bottom to top of the cores. This could be the result of the global and human induced environmental change.

P 8.7

Determination the age of Swiss Deckenschotter with cosmogenic isochron burial dating

Reto Grischott*, F. Kober**, S. Ivy-Ochs*, K. Hippe*, M. Lupker[3], M. Christl*, C. Vockenhuber*, C. Maden[3]

[1] *Labor für Ionenstrahlphysik, ETH Zürich, Otto-Stern-Weg 5, CH-8093 Zürich*
[2] *NAGRA, Hardstrasse 73, 5430 Wettingen*
[3] *Geologisches Institut, ETH Zürich, Sonneggstrasse 5, CH-8092 Zürich*

The evolution of landscape change during the Quaternary time epoch merits particular importance in modelling the long-term safety of the deep geological repositories for nuclear waste disposal in the northern Alpine Foreland (NAGRA, 2014). In this context, the timing of the deposition and incision of glaciofluvial gravels, that form high elevated terraces and plateaus in the northern Swiss Foreland – the so called Swiss Deckenschotter (amongst others) - is of special interest. They signify the onset and persistence of glacial or glacially related landscape forming processes since the Pliocene/ Pleistocene boundary. Knowing the depositional ages of these spatially extensive paleosurfaces and the subsequent incision of them is crucial in order to establish incision and erosion scenarios, river drainage patterns and related base-level reconstructions.

Working with cosmogenic nuclides in a isochron burial dating approach (Balco and Rovey, 2008) has shown to be feasible also for glaciofluvial gravels with low nuclide inventories (e.g. Akçar et al., in press). The differential decay of a nuclide pair in a mineral target (here: ^{26}Al and ^{10}Be in quartz) is used to determine the depositional age of the sediment. Whereas determination of the ^{10}Be content in sediment is a common task, extraction and measurement of ^{26}Al has still been a challenge. The low inheritance of glaciofluvial sediments and a subsequent long burial time result in low ^{26}Al concentrations and therefore a low ^{27}Al background is required. Accordingly, careful cleaning of the samples is needed. Samples with a sufficiently low total Al content were further processed for the analysis of cosmogenic ^{10}Be and ^{26}Al.

In this study, we aim to reconstruct the chronology of the Deckenschotter units along a transect in space and time at two locations: the gravel pit Tromsberg in Kirchdorf (AG) which represents the Higher Deckenschotter (HDS) of the Dürn-Gländ region and a nearby gravel pit at Bärengraben in Würenlingen (AG) being the Lower Deckenschotter (TDS) of the Iberig region. Previous age estimates for HDS suggest an age range of 1.5 ±0.2 Myr based on isochron burial dating at the nearby site Siglistorf (Akcar et al. 2017) and 1.8 to 2.5 Myr based on mammalian faunal assemblages (MN17) at site Irchel (Bolliger et al. 1996). At both sites, pebbles from various lithologies, sand lenses and amalgated vein-quarz clasts were sampled at the base of 10-15 m high former gravel pits.

Additionally, a gravel pit in Beringen (SH) representative for the Klettgau valley filling (Hochterrasse HT) was chosen to cross-calibrate with recently established luminescence chronologies (Lowick et al., 2015) which question a previously established age estimates based on the interpretation of sedimentary facies and lithostratigraphy (Graf, 2009).Thus, an independent age estimate is desirable. Here, sands and pebbles at the base of the active, 40 m deep gravel pit were collected assuming that shielding was nearly complete and postburial production is negligible.

With the strategy of sampling diverse lithologies and grain sizes, it is attempted to have samples with different pre-burial histories but the same burial and post-burial histories. Different pre-burial histories should enable us to calculate an isochron burial age for the sampled bed.

Low cosmogenic nuclide concentrations require a low total Al background in the samples. Modelling experiments yielded specifically different Al-limits for the assumed age of 2 Myr for HDS, 1 Myr for TDS and 0.3 Myr for HT.
We will present some initial field and preliminary analytical data from these studies.

REFERENCES
Akçar, N., Ivy-Ochs, S., Alfimov, V., Schlunegger, F., Claude, A., Reber, R., Christl, M., Vockenhuber, C., Dehnert, A., Rahn, M., and Schlüchter, C., in press, Isochron-burial dating of glaciofluvial deposits: first results from the Swiss Alps: *Earth Surface Processes and Landforms*, p. n/a-n/a.
Balco, G., and Rovey, C. W., 2008, An Isochron Method for Cosmogenic-Nuclide Dating of Buried Soils and Sediments: *American Journal of Science*, v. 308, no. 10, p. 1083-1114.
Graf, H. R., 2009, Stratigraphie von Mittel- und Spätpleistozän in der Nordschweiz, Bern : Landesgeologie, Beiträge zur geologischen Karte der Schweiz. Neue Folge, 198 S. p.:
Lowick, S. E., Buechi, M. W., Gaar, D., Graf, H. R., and Preusser, F., 2015, Luminescence dating of Middle Pleistocene proglacial deposits from northern Switzerland: methodological aspects and stratigraphical conclusions: *Boreas*, v. 44, no. 3, p. 459-482.
Nagra (2014): Sicherheitstechnischer Bericht zu SGT-Etappe 2: Sicherheitstechnischer Vergleich und Vorschlag der in Etappe 3 weiter zu untersuchenden geologischen Standortgebiete. Nagra Technischer Bericht NTB 14-01.

P 8.8

How politics shape agricultural landscapes: The plant wax record of Lake Lavijärvi, Russia Karelia

Mischa Haas[1,2], Natalya Belkina[3], Dimitry Subetto[3] Nathalie Dubois[1,2]

[1] *Department of Earth Sciences, ETH Zürich, Sonneggstrasse 5, CH-8006 Zürich (mischa.haas@eawag.ch)*
[2] *Department of Surface Waters Research and Management, Eawag, Überlandstrasse 133, CH-8600 Dübendorf*
[3] *Northern Water Problems Institute, Russian Academy of Sciences, A. Nevskogo Str. 50, 185003 Petrozavodsk*

Agriculturally induced soil erosion has a strong influence on the global carbon cycle, however, the historical evolution of its extent and rate is poorly known. This study seeks to address this issue by investigating lacustrine sediments from Lake Lavijärvi (Russia Karelia) to reconstruct past soil loss and soil degradation in the catchment, with a focus on soil carbon dynamics.

The region of Sortavala in the Russian Republic of Karelia has witnessed severe changes in land-use in the last century. During World War II, intensive field cultivation with regular plowing occurred in the catchment of Lake Lavijärvi, initiating soil erosion and consequently lake eutrophication. In the post-war period, the arable fields were mostly converted to pastures as the land was ceded to the Soviet Union by Finland. Shifts in pollen and diatom assemblages revealed that the lake became eutrophic in the 1920s-30s, with the mechanization of agriculture, and oligotrophic again following the relaxation of human pressure in the post-war-period.

In this study we test whether rapid changes in intensities of human land-use, such as the transition from ploughing to grazing, can be detected on a molecular level by analyzing the distribution of leaf wax biomarkers, such as *n*-alkanes and *n*-carboxylic acids, in lacustrine sediments. Investigations of the soil derived plant waxes in the sediments allow us to evaluate the influence of different agricultural practices on soil degradation. In this regard, compound-specific radiocarbon dating of the fossil molecules, will be key to trace changes in the organic carbon pool.

We will present preliminary results of the *n*-alkane and *n*-carboxylic acid homologue patterns in comparison with the grainsize distribution, magnetic susceptibility, concentration of detrital elements (i.e. Ti, Fe, Mn) as well as the $CaCO_3$, biogenic Silica, total organic carbon (TOC), and total nitrogen (TN) content.

P 8.9

Spatial variability of 10Be-derived erosion rates in Ghezel-Ozan Basin, NW Iran

Amaneh Kaveh Firouz[1], Jean-Pierre Burg[1], Negar Haghipour[1], Sanjay Kumar Mandal[2], Ramin Elyaszadeh[3], Marcus Christl[4]

[1] *Geological Institute, ETH Zurich, Sonneggstrasse 5, CH -8092 Zurich, Switzerland (amaneh.kaveh@erdw.ethz.ch)*
[2] *Geochemistry of the Earth's surface, Helmholtz Centre Potsdam, 14473 Potsdam, Germany*
[3] Geological Survey of Iran (GSI), Northwestern Regional Office, PO Box 5167733551, Tabriz, Iran
[4] *Laboratory of Ion Beam Physics, ETH Zurich, Schafmattstrasse 20, CH-8093 Zurich, Switzerland*

Active convergence between the Arabian and Eurasian Plates formed mountainous regions in NW-Iran. The role of active tectonics, climate and lithology in modulating this landscape had not been explored. We measured ^{10}Be concentration in river sands of the Ghezel-Ozan catchment to determine catchment-averaged erosion rates and to test the hypothesis that active tectonics and exhumation of crystalline basement rocks led to transience in the landscape. The Ghezel-Ozan basin is one of the largest catchment of NW-Iran. It receives annually ~400 mm precipitation. The upper, middle and lower parts of the basin drain three tectonostratigraphic zones: the Sanandaj-Sirjan Zone with crystalline rocks and low relief in the upstream, Central Iran with mostly sedimentary rocks and moderate relief in the middle stream and West Alborz with mixed sedimentary and crystaline rocks and high relief in the lower stream. Historical and instrumental seismicity indicates fault activity in both Central Iran and West Alborz zones.

We analyzed the hillslope and channel metrics using digital elevation models and explored their relationship with the millennial-scale erosion rates. The upper catchment (Sanandaj-Sirjan zone) with a smooth topography and gentle slope yields a low erosion rate (0.27 mm/yr) whereas the middle (Central Iran) and lower (West Alborz) parts of the catchment with moderate to high topography, steeper slope and active fault systems show high erosion rates (ca. 0.54 mm/yr). This difference indicates that active tectonics in Central Iran and West Alborz affect erosion rates under semi arid climatic conditions.

P 8.10

Multiproxy approach in assessing the downcore variations of Lake Pupuke, North Island, New Zealand during the last 1700 cal yr BP

Ronald B Lloren[1,2], Paul Augustinus[3], Nathalie Dubois[1,2]

* Department of Earth Sciences, ETH Zürich, Sonneggstrasse 5, CH-8006 Zürich (ronald.lloren@eawag.ch)
** Department of Surface Waters Research and Management, Eawag, Überlandstrasse 133, CH-8600 Dübendorf
[3] School of Environment, University of Auckland, Private Bag 92019, Auckland 1142, New Zealand

Changes in sediment input are caused by several factors which include geologic hazards (landslides caused by earthquakes and volcanic eruptions), climate (changes in rainfall patterns) and anthropogenic activities. Often, sediment input variations are dificult to tease out when climate changes and human activities are both simultaneously involved.

In New Zealand, the arrival of Polynesians around 800 years ago brought tremendous alterations in the landscape, including clearing of forests by burning and cultivations. These environmental changes have been well documented in the Southern Island, whereas only few studies exist for the Nothern Island. A key remaining question is, in which islands did the Polynesians first setlle?

Here we present initial results of the downcore variations of plant wax biomarkers (n-alkanes), coupled with elemental counts of Ti, Al and Zr in Lake Pupuke to study sediment input before and after the arrival of Polynesians in the North Island of New Zealand. The final results will help us to further define the timing of the arrival of Polynesians in New Zealand as well as possible implications of concurrent climatic changes.

P 8.11

Long-term productivity and meromixis dynamics on the Swiss Plateau (Lake Moossee, Switzerland) inferred from Hyperspectral Imaging

Stamatina Makri[1], Martin Grosjean[1], Fabian Rey[2], Erika Gobet[2]

[1] *Institute of Geography & Oeschger Centre for Climate Change Research, University of Bern, Erlachstrasse 9a, CH-3012 Bern, Switzerland*
[1] [1]*Institute of Plant Sciences & Oeschger Centre for Climate Change Research, University of Bern, Altenbergrain 21, CH-3013 Bern, Switzerland*

The Anthropocene has seen unprecedented environmental change and fundamental ecosystem services are increasingly at stake. Anthropogenically altered biogeochemical cycles, combined with climate change have resulted in adverse ecosystem impacts, increased productivity and anoxia in freshwater systems (Chapman, 1998; Hecky, 2010). However, little is known about lake eutrophication and episodes of hypoxia and meromixis in the past, because this is difficult to measure analytically. With this project, we intend to extend applications of the recently developed lake sediments HSI-VNIR methodology by our group. The aim is to investigate the folowing research questions: How did meromixis/hypoxia develop in small eutrophic lakes over Holocene/Late Glacial time scales? Which were the forcing factors (climate, land use, vegetation cover) and what was the influence of human impact?

A sound scientific assessment of such changes must rely on on a long-term perspective and high-resolution data. Hyperspectral Imaging (HSI) is a novel method to detect diagnostic sedimentary pigments at ultra-high resolution. These provide quantitative information about paleoproductivity, past mixing regimes and anoxia in lakes over long (i. e. Holocene) time scales (Butz et al, 2015, 2017). Hyperspectral imaging refers to measurement of reflected light at very high spectral (3 nm) and spatial (40 μm pixel size) resolution. The reflectance spectrum depends on the absorption properties of organic and inorganic species under the sensor field, and can be used to characterize the sediment composition (e.g. sedimentary pigments). Hence, Hyperspectral Imaging spectroscopy has a great potential for ultra-high resolution biogeochemical analysis of lake sediments (sedimentary pigments).

We are currently focusing on small eutrophic lakes on the Swiss Plateau, Lakes Moossee and Burgäschisee with biogenic varves. Further work is planned in biochemically varved lakes in the Mesurian Lakeland, NE Poland (Lakes Żabińskie, Łazduny and Jaczno). We use hyperpectral imaging proxies, quantitative Chl a and chlorins for aquatic productivity and quantitative Bphe a for meromixis (Butz et al, 2016). Bphe a is a diagenetic product of Bacteriochlorophyll a (Bchl a), produced by anoxygenic phototrophic bacteria. Pigment compositions are inferred from sets of spectral indices, such as the Relative Absorption Band Depths (RABD). Indices are calibrated with absolute pigment concentrations of selected samples, as measured by HPLC.

Lake Moossee contains a complete record of paleoproductivity and meromixis at annual resolution (varve years) for the Holocene and Late-Glacial times (past 15,500 years). Preliminary results of hyperspectral data diagnostic for Bphe a provide evidence for repeated meromixis events in the mid-Holocene. Pollen data of paleoecological studies on the same site suggest that changes in meromixis were related to Neolithic and Early Bronze Age land use (deforestation and reforestation after land abondonment).

REFERENCES
Butz C, Grosjean M, Fischer D, Wudnerle S, Tylmann W, Rein B (2015), Hyperspectral imaging spectroscopy: a promising method for the biogeochemical analysis of lake sediments. J Appl Remote Sens 9:096031
Butz C, Grosjean M, Poraj-Górska A, Enters D, Tylmann W. (2016), Sedimentary Bacteriopheophytin a as an indicator of meromixis in varved lake sediments of Lake Jaczno, north-east Poland, AD 1891–2010, Glob. Planet. Change 144: 109–118.
Chapman, L. J., C. a. Chapman, T. L. Crisman, and F. G. Nordlie (1998), Dissolved oxygen and thermal regimes of a Ugandan crater lake, Hydrobiologia, 385, 201–211.
Hecky, R. E., R. Mugidde, P. S. Ramlal, M. R. Talbot, and G. W. Kling (2010), Multiple stressors cause rapid ecosystem change in Lake Victoria, Freshw. Biol., 55, 19–42, doi:10.1111/j.1365-2427.2009.02374.x.

P 8.12

Reconstruction of deglaciation chronology and relative sea level change in northern Norway using cosmogenic nuclides

Katja Mettler[1], Ola Fredin[2,3], Anders Romundset[2], Marcus Christl[4], Christof Vockenhuber[4], Naki Akçar[1]

[1]Institute of Geological Sciences, University of Bern, Baltzerstrasse 1-3, 3012 Bern, (katja.mettler@geo.unibe.ch)
[2]Geological Survey of Norway (NGU), Leiv Eirikssons vei 39, 7491 Trondheim, Norway
[3]Norwegian University of Science and Technology (NTNU), 7491 Trondheim, Norway
[4]Laboratory of Ion Beam Physics (LIP), ETH Zurich, Otto-Stern-Weg 5, 8093 Zurich

Fennoscandia has repeatedly been covered by ice sheets during the Quaternary. The last Scandinavian ice sheet (SIS) reached its maximum volume and extent during the global Last Glacial Maximum (LGM) at around 21 ka and coalesced with the Svalbard–Barents–Kara (SBKIS) and the British-Irish (BIIS) ice sheets (Hughes et al., 2016). The load of the several km thick SIS depressed the Earth's crust beneath the ice into the mantle, which slowly convected away from the glacial loading. After the LGM, warming climate and raising eustatic sea level led to collapse of the marine sectors of the SIS and deglaciation of terrestrial sectors. As a consequence of reduced glacial loading, the crust and mantle immediately responded through mantle convection and isostatic uplift of the crust. The amount of isostatic depression and subsequent uplift is directly proportional to glacial loading and hence ice thickness. Prime landforms and deposits related to the isostatic uplift and fluctuations of the SIS during the Lateglacial can be observed in Finnmark, northern Norway.

Finnmark (~48,000 km^2) represents an important sector of SIS, situated in the northernmost terrestrial part of Fennoscandia, right at the border to Barents sea. The area is poorly mapped and only few studies exist. The most important work was accomplished by Sollid et al. in the early 1970's where they, based on mapping of ice marginal features (moraines, raised deltas etc.) and raised shorelines (e.g., perched deltas, beaches and wavecut platforms), established a framework for the last deglaciation and relative sea level change (Sollid et al.,1973). They defined seven principle deglaciation stages roughly spanning when the ice margin first migrated from Barents sea onto Finnmark about 15 ka BP to the Younger Dryas (YD). It should be stressed that this chronology is poorly constrained, based on only a few radiocarbon dates and correlations to shorelines together with better dated stages in other parts of Norway. In addition, they mapped shorelines, reflecting the maximal sea level stand at the time of local deglaciation at elevations of between 20 m to 70 m above the current sea level. This maximum relative sea level stand is called the marine limit and increases from North towards South corresponding to greater ice load towards central areas of Fennoscandia. Recently, Romundset et al. (2011) used the "isolation basin method" to improve shoreline displacement reconstructions in key areas of Finnmark. One intriguing find from this study is that the region exhibits significantly higher marine limit and lower gradient shorelines compared to equivalent areas along the Norwegian coast. This can only be explained with the Finnmark coast being influenced not only by the SIS but also by the glacial load of the SBKIS. A concept that is very little tested and difficult to verify. It is thus clear that many outstanding questions on the last deglaciation and post-glacial sea level change remain.

In this study we aim at improving the deglaciation chronology and relative sea level change reconstructions across large swaths of Finnmark. First, we establish a local deglaciation chronology since/because the highest sea level stand at any given location (marine limit) is directly linked to local deglaciation. Second, we date raised shorelines at different elevations to reconstruct relative sea level change. To reconstruct the chronology, we apply cosmogenic ^{10}Be surface exposure and depth-profile dating techniques. In addition, Quaternary landforms and deposits will be mapped in detail using the latest remote sensing data (digital aerial photographs and LiDAR). During the first field campaign, in summer 2017, we sampled 25 erratic boulders on the crest line of moraines and raised shorelines. In addition, we took three depth profiles for cosmogenic ^{10}Be analysis: one from a raised ice marginal delta and two from raised beach ridges. We also collected five clasts from the topmost surface of a raised beach ridge. The first results will be shown.

REFERENCES

Hughes, A. L., Gyllencreutz, R., Lohne, Ø. S., Mangerud, J., Svendsen, J. I. 2016. The last Eurasian ice sheets – a chronological database and time-slicecreconstruction, DATED-1. Boreas, 40, 1-45.

Romundset, A., Bondevik, S., Bennike, O. 2011. Postglacial uplift and relative sea level changes in Finnmark, northern Norway. Quaternary Science Reviews, 30, 2398-2421.

Sollid, J. L., Andersen, S., Hamre, N., Kjeldsen, O., Salvigsen, O., Sturød, S., Tveitå, T., Wilhelmsen, A. 1973. Deglaciation of Finnmark, North Norway. Norsk geogr. Tidsskr., 27, 233-325.

P 8.13

A novel 4D-view on sediments: insights to sedimentation processes and post-sedimentary mineral formation

Marina A. Morlock[1], Hendrik Vogel[1], Jebril Hadi[2], Anneleen Foubert[3], Daniel Ariztegui[4], Martin Melles[5], James M. Russell[6], Satria Bijaksana[7] & the TDP science team

[1] *Institute of Geological Sciences and Oeschger Centre for Climate Change Research, University of Bern, 3012 Bern, Switzerland, marina.morlock@geo.unibe.ch*
[2] *Institute of Geological Sciences, University of Bern, 3012 Bern, Switzerland*
[3] *Department of Geosciences, University of Fribourg, 1700 Fribourg, Switzerland*
[4] *Department of Earth Sciences, University of Geneva, 1205 Geneva, Switzerland*
[5] *Institute of Geology and Mineralogy, University of Cologne, 50674 Cologne, Germany*
[6] *Department of Geological Sciences, Brown University, Providence, RI 02912*
[7] *Faculty of Mining and Petroleum Engineering, Institut Teknologi Bandung, Bandung 40132, Indonesia*

Lake sediment archives are well studied around the globe and contribute greatly to our understanding of past environments and climates. Yet, traditional sedimentological analyses are either limited to a 2D study of the sediment core surface, or volumetric analysis, for which the sedimentological structure needs to be destroyed. To overcome these limitations, we combined high-resolution 3D-microCT-scanning (µm-scale) of fresh lake sediment with XRF-scanning, micro-XRF mapping, and traditional thin section analysis. MicroCT-scanning facilitates the observation of sedimentary structures at the mm-scale in 3D prior to analysis, while high-resolution mapping in 2D aids characterisation of the observed structures once the fragile sample is conserved in resin.

We present a study of sediments from Lake Towuti (2.75°S, 121.5°E), one of the oldest and deepest lakes in Indonesia. Cores of the entire sediment infill have been recovered in the ICDP Towuti Drilling Project in 2015, including lacustrine sediments covering several glacial-interglacial cycles. Located in the ultramafic East Sulawesi Ophiolite, the lake is highly ferruginous but poor in sulphur and among the least productive tropical lakes on Earth (ultra-oligotrophic). In the cores, high density contrasts between the clay-rich sediment matrix and postdepositional alteration products such as siderite ($FeCO_3$) and Millerite (NiS) provide an ideal setting for microCT analysis on characteristic sediment core sections. Geochemical information from the embedded sections is provided by high-resolution XRF-scanning (200 µm spacing) and micro-XRF mapping (50 µm spacing) of the samples.

MicroCT scans reveal µm-thick vertical voids filled with high density mineral precipitates related to post-depositional fluid circulation, as well as coatings of high-density material (mainly siderite), around low-density centres. We also observe beds of high-density minerals, which appear continuous in 2D, but prove to be separated structures in 3D space. The combination of high-resolution imaging with XRF element scans allows a novel, very detailed 4D-view of sedimentary structures that identifies processes involved in authigenic mineral formation and their relation to paleoenvironmental changes in the lake and its catchment.

P 8.14

Optically stimulated luminescence dating of the Western Makran marine terraces (Iran)

Raphaël Normand[1], Guy Simpson[1], Rabiul Haque Biswas[2], Frederic Herman[2] & Abbas Bahroudi[3]

[1] *Department of Earth Sciences, University of Geneva, Rue des Maraichers 13, CH-1205 Genève. (Raphael.Normand@unige.ch)*
[2] *Institute of Earth Surface Dynamics, Faculty of Geosciences and Environment, University of Lausanne, CH-1012 Lausanne*
[3] *Exploration department, School of Mining Engineering, University of Tehran, Northern Kargar avn, P.O. Box 11365-4563, Tehran.*

The western part of the Makran subduction zone (Iran) has not experienced a great megathrust earthquake in recent human history. Yet, the presence of uplifted marine terraces along the coast indicates that the margin is still tectonically active during at least the Quaternary. To better assess the seismic hazard of the region, it is important to understand the uplift rate variations in the overriding plate. This will enable estimation of the seismotectonic segmentation of the plate and therefore highlight regions of potentially higher seismic risk.

Several attempts have been made to date the Makran marine terraces using 14C or Th/U, however most of the terraces are older than the upper limit of 14C and the scarcity of coral constructions limits the use of Th/U. Since, layers of beach to foreshore sediments are deposited on top of the wave-cut surfaces, optically stimulated luminescence (OSL) dating seems a more appropriate method. We mapped the marine terraces along the 400km long Iranian Makran coast and prepared fourteen samples for OSL dating. This contribution will present the preliminary results of this dating.

P 8.15

Uranium accumulation and leaching in Swiss plateau wetlands

Anja Pregler[1] and Simon Werthmüller[2]

[1] *Paul Scherrer Institut, CH - 5232 Villigen and Department of Chemistry and Biochemistry, University of Berne, Freiestr. 3, CH - 3012 Bern (anja.pregler@psi.ch)*
[2] *Geologische Beratungen SCHENKER KORNER RICHTER AG, Büttenenhalde 42, CH - 6006 Luzern*

Under anoxic conditions, uranium (U) is insoluble and can be accumulated in wetland sediments. Input of U into these sediments may occur through leaching of external rocks or soils and subsequent transport by creeks or springs. Even if U concentrations in the input water are only in the range of ppb, an accumulation over thousands of years can lead to considerable concentrations in the receptive sediments. Such an accumulation of more than 200 ppm U has been detected in a peat horizon of the ancient Lyssbach wetland northwest of Berne (Surbeck et al. 2015, Werthmüller et al. 2016). During drainage of the wetland in the 19th century and puncturation of the impermeable layer below the peat, groundwater level was significantly lowered, leading to a change in redox conditions from anoxic to oxidizing. As a result, oxidation of accumulated insoluble U(IV) to its soluble form U(VI) was initiated. The peat horizon is now leached by infiltration of oxygen-rich rainwater, resulting in high U concentrations in the drainage water of up to some 100 µg/l (Schmidt 2013).

As the origin of the U source remains unclear, two different scenarios have been proposed: i) leaching of U-rich quaternary sediments derived from Permo-Carboniferous rocks in the Lower Valais, ii) leaching of U-rich fossils from the interface between Lower Freshwater Molasse (USM) and Upper Marine Molasse (OMM). Despite the occurrence of several Permo-Carboniferous erratic blocks with clearly enhanced gamma dose rates in the Lyssbach region, soil samples from above and below the peat horizon do not show increased U concentrations. We therefore consider it very unlikely that quaternary sediments have been the source for U accumulation in the peat. According to the geological map (Lyss, Nr. 76), there is no outcrop of the USM/OMM interface close to the Lyssbach site. However, the interface is present farther north, near the Limpach Valley, where increased U concentrations in a creek have been reported (Riedo 2016). Furthermore, enhanced U concentrations were detected in a coal sample at a Molasse outcrop (probably late USM) southwest of the Lyssbach site.

This is in line with a clearly increased frequency of enhanced U concentrations in drinking water close to the USM/OMM interface in Western Switzerland. However, the transition zone between USM and OSM is not always precisely differentiated and U accumulation is rather found in the youngest USM marls than in the oldest OMM sandstones.

A situation well comparable to the Lyssbach site can be found at Mt. Vully, a hill between Lake Murten and Lake Neuchâtel, where high U concentrations of some springs deriving from the USM/OMM interface with U-rich fossils are known (Schott and Wiegand, 2003). The wetlands north of Mt. Vully are fed by these springs (fig. 1). Since gamma dose rates above ground and U concentrations in drainage waters are clearly enhanced, the wetland seems to have accumulated significant amounts of U under anoxic conditions, identically to the Lyssbach site.

We thus favour an USM/OMM interface with U-rich fossils as the source for enhanced U concentrations in Swiss plateau wetlands.

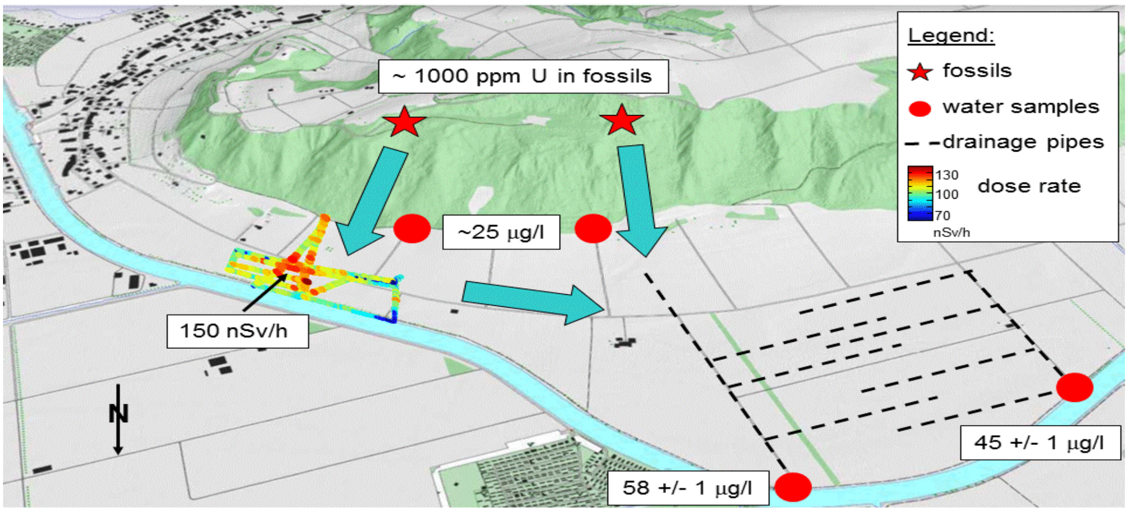

Figure 1. The Mt. Vully site with U concentrations in fossils, springs, creeks and drainage waters and gamma dose rates from ground survey with a 2”x2” NaI-detector.

REFERENCES

Riedo, J. 2016: Uran in bernischen Gewässer. Obligatorische Berufspraxis im Master Umweltnaturwissenschaften. Technischer Bericht, ETH-Zürich.

Schmidt, F. 2013: Schwermetalle im Lyssbach – Herkunft und Bedeutung. BSc thesis, Department of Earth Sciences, ETH-Zurich.

Schott, B. & J. Wiegand 2003: Process of radionuclide enrichment in sediments and groundwater of Mont Vully (Canton Fribourg, Switzerland). Eclogae Geologicae Helvetiae 96, 99-107.

Surbeck, H., Wertmüller, S., Perret, R. 2015: Aeroradiometrie mit einer Drohne zur Suche nach Urananreicherungen, Proceedings Geoforum Umhausen, 111-116.

Werthmüller, S., Surbeck, H., Ryser, R. 2016: Airborne exploration of anomalous high uranium contents in water and soil in the region of the “Lyssbach” – Canton of Bern. Proceedings Swiss Geoscience Meeting, 385.

P 8.16

Mangrove Forest Sedimentary Environments along Iranian Coasts of The Persian Gulf (Bushehr to Naybad Bay)

Alireza Salehipour Milani,

Department of Physical Geography, Faculty of Earth Science, Shahid Beheshti University, Tehran, Iran (Ar_Salehipour@sbu.ac.ir)

Mangrove ecosystems are coastal estuarine systems confined to the tropical and subtropical regions. In the Persian Gulf mangroves have been principally affected by the large oil spill from the Persian Gulf War (1991) and even though they have mostly recovered from this event, oil pollution still represents one of the main threats. Camel grazing has been reported as another relevant threat, while shrimp aquaculture represents one of the emerging threats to this ecosystem. Then investigation of mangrove forest is from view of pollution effects is necessary and sedimentological studies helps us to detect this problem in mangrove forest. The mangrove forest of Iranian that located in Coasts of The Persian Gulf (Boushehr to Naybad Bay), has suffered constant disturbances during the past 20 years, due to industrial wastewater release. However, there are no published data for heavy metals present in its sediments and the relationship with anthropogenic disturbance. The accumulation of Six heavy (Cu, Pb, Ni, Cr, Zn, Mn and Fe) metals in fine-grained sediments from the mangrove fringed coast study area is evaluated. 18 sampling sites were chosen for collection of sediments. The heavy metal concentrations were normalized to reference elements to facilitate comparison between mangrove sitesIn conclusion, the overall average concentrations of above metals exceed the primary standard criteria but meet the standard criteria. Besides mangrove forest area changes were investigate during 1973 to 2017. Results shows heavy metal concentrations in sediment at most heavy metal elements in study area (except Nayband Bay) are lower than standard and pollution had no effect on mangrove trees. mangrove forest area increased during 40 years and this proved our results for heavy metal concentration in sediments of this regions.

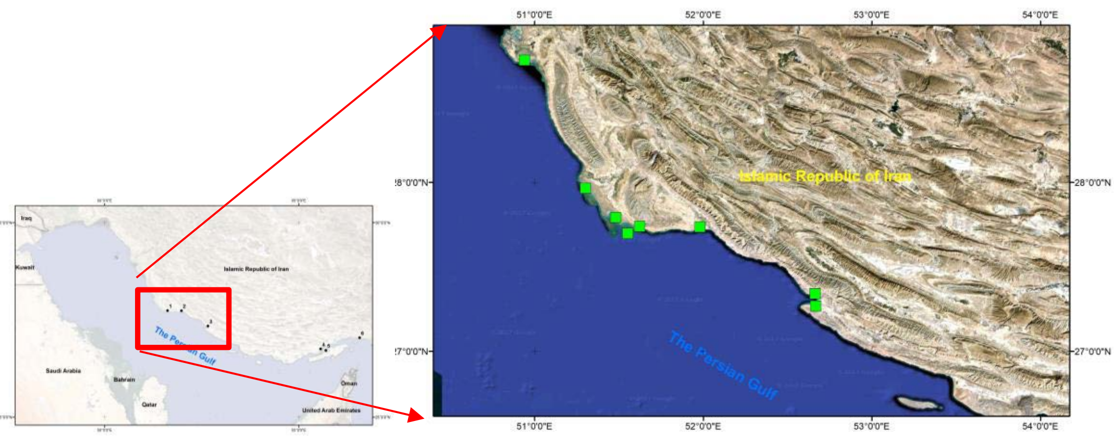

Location of study area and Sediment Samples in The Persian Gulf

REFERENCES

Khosravi, M., 1992: Ecological studies plan of Iranian mangrove forests. Report of mangrove forests identification phase, Department of the Environment, Tehran, Iran

Zahed A,. Rouhani M,. Mohajeri S,. and Bateni F., 2010: An overview of Iranian mangrove ecosystems, northern part of the Persian Gulf and Oman Sea. Acta Ecologica Sinica. Vol. 30, 240–244.

Danehkar, A., 1996: Iranian mangroves forests. The Environment Scientific Quarterly Journal 8–22.

Alloway, B.J., 2013: Heavy Metals in Soils—Trace Metals and Metalloids in Soils and Their Bioavailability; Springer: Dordrecht, The Netherlands.

Liu, J,. Ma, K,. Qu, L., 2015**:** Ecological risk assessments and context-dependence analysis of heavy metal contamination in the sediments of mangrove swamp in Leizhou Peninsula, China. Mar. Pollut. Bull., 100, 224–230.

P 8.17

Sediment input fluctations to Lake Geneva – climate and human impact

Tiago A. Silva[1,2], Anna Costa[3], Stéphanie Girardclos[2,4], Laura Stutenbecker[5], Maarten Bakker[6], Fritz Schlunegger[5], Stuart N. Lane[6], Peter Molnar[3] & Jean-Luc Loizeau[1,2]

[1] *Departement F.-A. Forel for Environmental and Aquatic Sciences, Uni. of Geneva, Geneva, 1205, Switzerland (Tiago.Adriao@unige.ch);*
[2] *Institute for Environmental Sciences, Uni. of Geneva, Geneva, 1205, Switzerland;*
[3] *Institute of Environmental Engineering, ETH Zürich, Zurich, 8093, Switzerland;*
[4] *Departement of Earth Sciences, Uni. of Geneva, Geneva, 1205, Switzerland.*
[5] *Institute of Geological Sciences, Uni. of Bern, Bern, 3012, Switzerland*
[6] *Institute of Earth Surface Dynamics, Univ. of Lausanne, Lausanne, 1015, Switzerland.*

At the Holocene time-scale, climate changes coupled with long-term exhumation processes, short-term seismic activity, glacial inheritance and bed rock lithology drive the sediment production and transfer processes in Alpine environments. However, in the context of the Anthropocene, the sediment delivery from Alpine watersheds to sedimentary sinks, often perialpine lakes, is additionally controlled through direct and indirect human impacts. We can observe the results of all these factors in the Lake Geneva basin, sediment sink of the Rhone and Dranse catchments.

In the past ca.150 years, the Rhone River sediment input to Lake Geneva fluctuated following the influence of both climatic variability and anthropogenic activities. Previous work indicate that suspended sediment loads (SSLs) in the Rhone River and sedimentation rates in Lake Geneva decreased by a factor of 2 to 4 after 1964 (Loizeau and Dominik, 2000; Loizeau, 2012). This decrease was interpreted as the result of the flow abstraction and/or regulation linked to dam construction on the upper Rhone River watershed during the 1950's and 1960's. Costa et al. (2017) identified a simultaneous step-like increase in basin-averaged temperature and suspended sediment concentration (SSC) at the outlet of the catchment in 1987 and show that SSC fluctuations are closely linked to mean temperature changes. They also suggest that colder temperature during 1960´s could have contributed to the SSL reduction observed after 1964.

In this study, 19 short-sediment cores were collected in 2014 in eastern Lake Geneva. Based on sediment radiodating (^{137}Cs and ^{210}Pb) performed in seven short-sediment cores, we could calculate the mass accumulation rates (MAR) in this area. Results (Table 1) show that values are high for the period 1953 to 1964 and then decreases from 1964 to 1986. From 1986 to 2014, preliminary results show that MAR's increase again but reamain lower than the values from the 1953-64 period. The correlation of all sediment cores using lithology and magnetic susceptibility data completes our analysis on the core subset and shows that these MAR trends are present over the whole eastern Lake Geneva, and independent of the various and contrasted in-situ sedimentological processes.

Following our results and earlier studies, we interpret the observed decrease in MAR during the 1964-87 period as due to anthropogenic impacts and climatic effects (colder temperatures) on the watershed, and the MAR increase since 1987 as linked to the mean temperature increase. Knowing that mean air temperature for 1953-64 was lower than the mean air temperature for 1986-2014, and assuming that the impact of anthropogenic activites on the Rhone river sediment transfer remained stable since 1964, we can estimate the relative human impact via hydropower system management on the reduction of sediment delivery to Lake Geneva. These preliminary results suggest that the decrease in MAR's since 1964, linked to anthropogenic activities, vary between 20 and 50% depending on core location, with greater differences in areas that are heavily influenced by the Rhone river input and smaller values away from the Rhone lobe-canyon-fan system (Silva et al., submitted).

	Mass accumulation rates (g cm^{-2} yr^{-1})						
Period\Core	KK-1	TS-4	TS-9	TS-2	TS-12	TS-8	TS-14
1986-2014	0.19 ± 0.02	0.32 ± 0.03	0.53 ± 0.04	0.63 ± 0.04	0.81 ± 0.06	0.60 ± 0.04	1.20 ± 0.06
1964-1986	0.09 ± 0.03	0.11 ± 0.04	0.19 ± 0.05	0.35 ± 0.06	0.43 ± 0.08	0.32 ± 0.06	0.51 ± 0.09
1953-1964	0.24 ± 0.06	0.79 ± 0.11	0.66 ± 0.13	0.73 ± 0.09	0.98 ± 0.16	0.89 ± 0.14	---
^{210}Pb	0.21 ± 0.04	0.28 ± 0.08	---	0.47 ± 0.08	---	0.45 ± 0.09	---

Increase distance from the Rhone River inflow to Lake Geneva

Table 1. Mass accumulation rates (g cm^{-2} yr^{-1}) in seven sediment cores of eastern Lake Geneva. MAR's decrease away from the Rhone lobe-canyon-fan system in Lake Geneva (Silva et al., submitted). Preliminary results show that the 1953-64 period consistently has higher

MAR's than the 1986-2014 period.

REFERENCES

Costa, A., Molnar, P., Stutenbecker, L., Bakker, M., Silva, T. A., Schlunegger, F., Lane, S. N., Loizeau, J.-L., and Girardclos, S. 2017. Temperature signal in suspended sediment export from an Alpine catchment, Hydrol. Earth Syst. Sci. Discuss., https://doi.org/10.5194/hess-2017-2.

Loizeau, J.-L., Dominik, J. 2000. Evolution of the Upper Rhone River discharge and suspended sediment load during the last 80 years and some implications for Lake Geneva. Aquat. Sci. 62, 54. doi:10.1007/s000270050075.

Loizeau, J.-L., Girardclos, S., Dominik, J. 2012. Taux d'accumulation de sédiments récents et bilan de la matiére particulaire dans le Léman (Suisse - France). Arch. des Sci. 65, 81–92.

Silva, T.A., Girardclos, S., Stutenbecker, L., Bakker., Costa, A., Schlunneger, F., Lane., S.N., Molnar, P. and Loizeau, J.-L. 2017 The sediment budget and dynamics of a delta-canyon-lobe system over the Anthropocene timescale: the Rhone River Delta, Lake Geneva (Switzerland/France), Sedimentology, submitted.

P 8.18

Würmeiszeit und die Rückzugsstadien im Alpenrheintal

Peter Zwahlen

BTG Büro für Technische Geologie AG, Grossfeldstrasse 74, Postfach 78, CH-7320 Sargans

Korrelation von ^{14}C-Datierungen aus Bohrprofilen mit Glazialstadien und -schwankungen, Klimaphasen, archäologischen Kulturen und Biozonen.

Die Korrelationstabelle bildet den Kern der vorliegenden Daten und Folgerungen. Anlass dazu gaben viele unpublizierte Projektberichte von Sondierbohrungen und Tunnelaufnahmen im Archiv des BTG, die ^{14}C-Altersdaten von fossilen Holzfunden enthalten und stratigraphisch korrelierbar sind. BTG-Projektgeologen haben die Holzproben gesichert, zur Datierung vorbereitet und archiviert (Finanzierung weitgehend BTG-intern).

Die ersten Holzfunde wurden in den 1970er Jahren am Radiocarbonlabor des Physikalischen Instituts der Universität Bern und bis 2015 (Bohrung 2/15, Posterprofil) zusätzlich am Labor für «Ion Beam Physics» an der ETH Zurich datiert. Sämtliche gemessenen ^{14}C-Altersdaten, auch die Literaturzitate, wurden auf Jahre BP (1950) standardisiert (braune Balken in den Tabellenspalten b—d mit Fehlerbereich 2σ) und in der Spalte a den kalibrierten Altern cal. Jahre BP gegenübergestellt (Kalibrationskurven nach Stuiver 1998 bzw. INTCAL04). Geographisch umfassen die datierten Fundpunkte die Projektgebiete des BTG mit Schwerpunkten im Alpenrheintal, Sarganserbecken, Seeztal-Walenseebecken und Linthtal, sowie in den Bündner Tälern. Für die vorliegende Korrelationstabelle wurden v.a. BTG-Daten und ergänzend dazu zitierte Alter (siehe Literaturverzeichnis) aus den erwähnten Tälern der Nordalpen inkl. Zürichseebecken berücksichtigt. Die Zuordnung der Glazialstadien auf der Karte basiert auf eigenen Arbeiten und René Hantkes Lebenswerk „Eiszeitalter“ 1978 - 1983 und fokussiert auf den **Sarganser-Stand** (Tabelle 1, Spalte d).

Resultate:
Die ausseralpinen Rückzugsstadien (Spalte b) und das alpeninterne Stadium **Koblach-Feldkirch-Weesen** (Spalte c) beschränken den **Sarganser-Stand** auf Älteste Dryas oder jünger. Die **interneren Stadien** (Prättigau) bedingen ein Minimalalter Bølling/Allerød.
Der **Sarganser-Stand** belegt einen Rückzugshalt (gestaffelte randglaziale Schotterterrassen ohne Vorstossmoränen) an der Wende Älteste Dryas/Bölling. Entsprechende Schotter sind bis weit in die Surselva und das Prättigau hinauf verfolgbar.
Das **Stadium Koblach-Feldkirch** (mehrere Moorprofile mit basalen Pollenspektren der Ältesten Dryas) stellt einen Glazialvorstoss mit ausgeprägten Moränenwällen innerhalb der Ältesten Dryas (? Heinrich1-Event) dar. Der Rückzug vom Feldkirch-Stadium zum Sarganser-Stand ist altersäquivalent zum klassischen Gschnitz-Stadium (Tirol, Ivy-Ochs 2006).
Gleichzeitig breitete sich im Mittelland die jungpaläolithische Kultur des Jung-Magdalénien (Leesch/Leuzinger 2012/2016) aus, allerdings ohne dem Gletscherrückzug in die Alpentäler unmittelbar zu folgen. Dies taten auch die eiszeitlichen Grosssäuger nicht.

Tabelle 1: Korrelation von Altersklassen, Probenalter, Talbildungsprozessen, Klimadaten, Glazialstadien und Quartärstufen

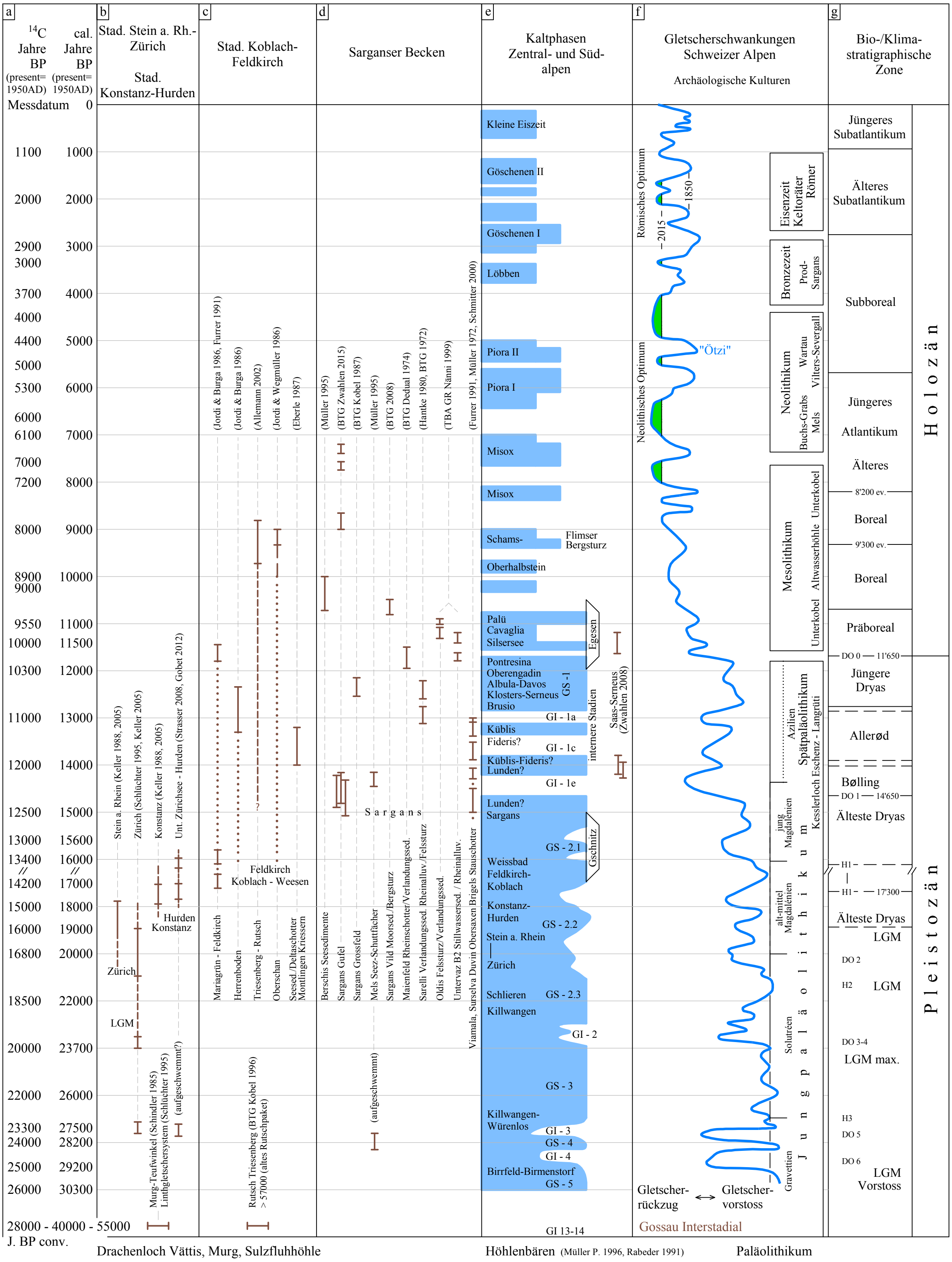

Legende:

	14C - Datierungen ± 2σ, Unsicherheitsbereich	GI	1 bis 4 Grönland Interstadial	8'200 ev.	Event
	Älteste Dryas pollenanalytisch bestimmt	GS	2 bis 5 Grönland Stadial	DO 0 bis 6	Dansgaard-Öschger-Event.
	Warmzeiten			H 1 bis 3	Heinrich-Event

9. Cryospheric Sciences

Margit Schwikowski, Martin Heggli, Matthias Huss, Jeannette Nötzli, Daniel Tobler, Andreas Vieli

Swiss Snow, Ice and Permafrost Society

TALKS:

9.1 **Barbieux K.**, Charitsi A., Merminod B.
Observation of the Ice Coverage of Great Lakes with Landsat 8 Multispectral Imagery

9.2 **Bernhard P.**, Zwieback S., Leinss S. , Hajnsek I.
Large-scale monitoring of rapid permafrost thaw with satellite radar interferometry

9.3 **Capelli A.**, Reiweger I., Schweizer J.
A fiber bundle model with healing mechanisms for snow failure modelling

9.4 **Cohen D.**, Jouvet G., Gillet-Chaulet F., Haeberli W., Machguth H., Seguinot J., Imhof M., Fischer U.H.
Numerical Reconstructions of the Flow and Basal Conditions of the Rhine Glacier at the Last Glacial Maximum

9.5 **Gugerli R.**, Huss M., Salzmann N.
Using a cosmic ray sensor and weather radar composites to estimate the snow water equivalent on a Swiss glacier

9.6 **Heck M.**, Hobiger M., van Herwijnen A., Fäh D.
Localization of avalanches using seismic monitoring

9.7 **Kenner R.**, Phillips M., Hauck C., Hilbich C., Mulsow C., Bühler Y., Stoffel A., Buchroithner M.
Genesis and conservation of permafrost excess ice in the Flüelapass talus slope

9.8 **Leysinger Vieli G.**
Basal-ice accretion – pushing boundaries within ice sheets

9.9 **Mercenier R.**, Luethi M.P., Vieli A.
Using Continuum Damage Mechanics to Simulate Iceberg Calving from Tidewater Outlet Glaciers

9.10 **Prohaska Y.M**., Werder M.A., Farinotti D.
The roughness of englacial R-channels determined by physical experiments

9.11 **Rohrer M.**, Steinegger U., Nötzli C., Lorenzi D., Schwarb M. (solicited)
75 years snow water equivalent measurements in the Wägital catchment

9.12 **Sommer C.G**., Fierz C., Lehning M.
Wind tunnel experiments: influence of erosion and deposition on wind-packing of fresh snow

9.13 **Steiner J.F**., Kraaijenbrink P.D.A., Jiduc S.G., Immerzeel W.W.
A rapid glacier surge in the Karakoram – employing new high-resolution satellite products for coupled research and hazard assessment

9.14 **Haeberli W.** *(see 9.14 Nötzli et al.)*
Hoelzle M. *(see 9.14 Nötzli et al.)*
Vieli A., Cicoira A. *(see 9.14 Nötzli et al.)*

9.14 **Nötzli J.**, Cicoira A., Haeberli W., Hoelzle M., Vieli A., Vonder Mühll D.
Special Session: 30 years Borehole Murtèl-Corvatsch

POSTERS:

P 9.1 **Barandun M.**, Huss M., Usubaliev R., Azisov E., Berthier E., Kääb A., Bolch T., Hoelzle M.
Long-term mass changes on three Kyrgyz glaciers

P 9.2 **Bobillier G.**, Capelli A., Schweizer J.
Effect of load-sharing rules in modeling snow failure with a fiber bundle model

P 9.3 **Buri P**, Steiner J.F, Miles E.S., Ragettli S., Pellicciotti F.
How much do supraglacial ice cliffs contribute to the mass-balance of glaciers? A modelling approach for the Langtang catchment, Nepalese Himalaya

P 9.4 **Crivelli P.**, Paterna E., Lehning M.
Mass-flux dynamics in a drifting snow wind-tunnel

P 9.5 **Dal Farra A.**, Kaspari S., Beach J.J., Bucheli T.D., Schaepman M., Schwikowski M.
Spectral signatures of submicron scale light absorbing impurities in snow and ice using hyperspectral microscopy

P 9.6 **Delaney I.**, Werder M.A., Farinotti D.
A model for subglacial sediment discharge and comparison with available measurments

P 9.7 **Förster S.**, Huss M., Gudmundsson H.
Applying the ice flow model Úa to the Alpine region: first simulations of Rhonegletscher

P 9.8 **Gerber F.**, Besic N., Sharma V., Mott R., Gabella M., Germann U., Bühler Y., Marty M., Berne A., Lehning M.
From the clouds to the ground – snow precipitation vs. snow accumulation patterns

P 9.9 **Gerling B.**, Löwe H., van Herwijnen A.
Measuring the elastic modulus of snow

P 9.10 **Gräff D.**, Walter F.
Analysis of Borehole Measurements and Determination of the Basal Sliding Velocity of Rhonegletscher

P 9.11 **Groos A.R**., Mayer C., Smiraglia C., Diolaiuti G., Lambrecht A.
A first attempt to model region-wide glacier surface mass balances in the Karakoram: findings and future challenges

P 9.12 **Haberkorn A.**, Fierz C., Marty C., Macelloni G., Morin S., Schöner W.
The European Snow Booklet

P 9.13 **Heil K.**, Kaitna R., Fischer J.T., Reiweger I.
Properties of flowing snow – measurements in a rotating drum

P 9.14 **Imhof M.**, Jouvet G., Seguinot J., Cohen D., Funk M.
Modelled and reconstructed ice thickness of the Rhine Glacier during the Last Glacial Maximum

P 9.15 **Irarrazaval I.**, Mariethoz G., Herman F.
Stochastic subglacial hydrology model for water pressure and mass transport data assimilation.

P 9.16 **Jouvet G.**, Stastny T., Oettershagen P., Hugentobler M., Mantel T., Melzer A., Weidmann Y., Funk M., Siegwart R.
Sun2Ice: Monitoring calving glaciers from solar-powered UAVs

P 9.17 **Kronenberg M.**, Machguth H., Stainbank W., Hoelzle M.
Investigating firn changes of Abramov glacier, Pamir Alay

P 9.18 **Landmann J.**, Huss M., Farinotti D.
Cryospheric Monitoring and Prediction Online (”CRAMPON”) – a first version

P 9.19 **Le Bris R.**, Paul F.
Glaciers of Patagonia in 2016: A new inventory from Landsat 8 and the TanDEM-X DEM

P 9.20 **Lindner F.**, Laske G., Walter F.
Seismic azimuthal anisotropy in crevasse fields

P 9.21 **Lüthi M.P**., Mercenier R., Vieli A.
A new parametrization and minimal model for glacier calving

P 9.22 **Magrani F.**, Ayres-Neto A., Vieira R., Rosa K., Ferreira F.
Glaciomarine Sedimentation and Submarine Landforms in Admiralty Bay, South Shetland Islands

P 9.23 **Nötzli J.**, Phillips M.
Borehole measurements in Alpine permafrost – acquired experience and best practices for long-term monitoring

P 9.24 **Preiswerk L.E**., Michel C., Walter F., Fäh D.
Analysis of surface waves from ambient vibrations on Alpine glaciers in Switzerland

P 9.25 **Pruessner L.**, Phillips M., Lehning M., Hoelzle M., Farinotti D.
Near-surface energy balance on an Alpine rock glacier

P 9.26 **Rastner P.**, Notarnicola C., Nicholson L., Prinz R., Sailer R., Paul F.
Processing of multi-temporal Landsat images to detect fractional snow cover and the snow line altitude for large glacier samples

P 9.27 **Roth F.**, Schneebeli M.
Sensitivity of snow specific surface area measurements to different μCT settings

P 9.28 **Richter B.**, Schweizer J., Rotach M.W., Herwijnen V.A.
Using snow cover models driven with meteorological data to predict snow instability for avalanche forecasting

P 9.29 **Scherler M.**, Hoelzle M., Huss M., Hauck C.
Present and future runoff regimes at Murtèl-Corvatsch rockglacier

P 9.30 **Schlögl S.**, Mott R., Lehning M.
How do patchy snow covers affect turbulent sensible heat fluxes?

P 9.31 **Seguinot J.**, Ivy-Ochs S.
Modelled transfluences and crosswise divides in the Last Glacial Maximum Alpine ice flow

P 9.32 **Steiner L.**, Geiger A.
GPS for the Point-wise Quantification of Snow Water Equivalent in alpine Terrain

P 9.33 **Trachsel J.**, Avak S., Edebeli J., Schneebeli M., Eichler A., Bartels-Rausch T.
Microscale Distribution of Impurities in Snow

P 9.34 **Walter A.**, Lüthi M.P., Vieli A., Funk M.
Using terrestrial radar interferometry for understanding calving processes

P 9.35 **Weber S.**, Faillettaz J., Meyer M., Beutel J., Vieli A.
Characteristics of acoustic and micro-seismic signals in steep bedrock permafrost on Matterhorn (CH)

P 9.36 **Wicky J.**, Hauck, Ch.
Influence of slope angle on the convective heat transfer in porous permafrost substrate

9.1
Observation of the Ice Coverage of Great Lakes with Landsat 8 Multispectral Imagery

Kévin Barbieux[1], Antigoni Charitsi[1], Bertrand Merminod[1]

[1]Geodetic Engineering Laboratoy, Ecole Polytechnique Fédérale de Lausanne

The ice coverage of great lakes is a very impactful phenomenon for their local ecosystems. The ice formation and melt influence heavily the organic life of the lakes, like the carbon cycle [1] or the phytoplankton dynamics [2], but also acts as an indicator of climate change [3]. Consequently, it is of interest to study the evolution of the ice coverage of great lakes, in terms of spatial distribution, ice characteristics (structure, temperature, radiative properties, optical properties) and temporal evolution.

The availability of the Landsat 8 data allows to monitor the ice coverage of great lakes. We have designed a simple procedure to segment the lake body and the ice in the Landsat multispectral images. This procedure combines radiometric indexes, mathematical morphology and information about the object texture for the segmentation. The ice-water discrimination performed has been proven consistent with concurrent classification from Sentinel-2 SAR imagery, with a Kappa coefficient of 0.92 between the two classification of lake Ladoga (Russia).

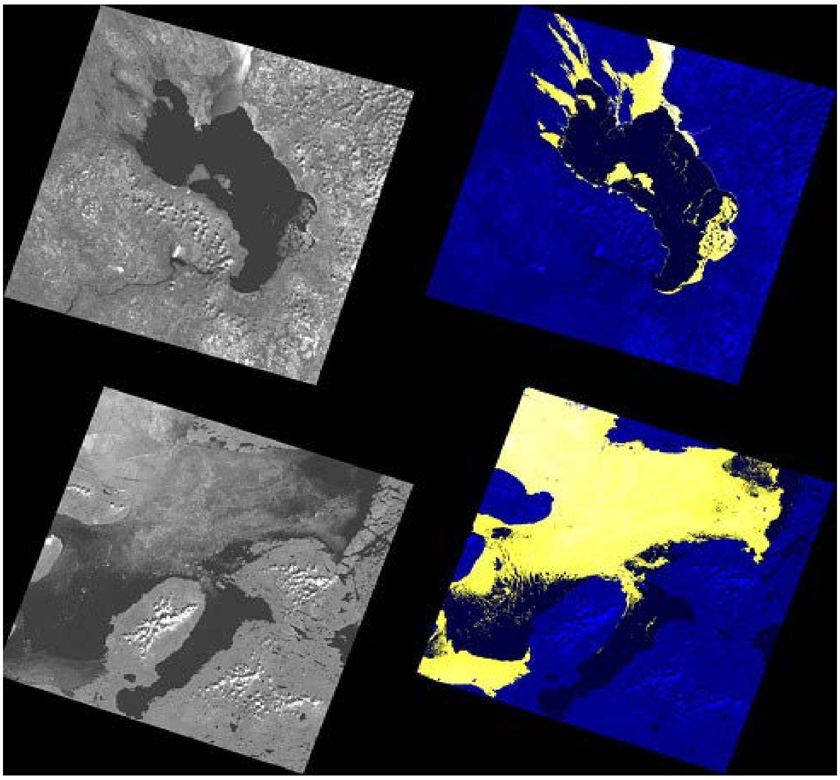

Figure 1. Examples of classifications performed on lake Onega, Russia (top) and the Great Bear Lake, Canada (bottom). The original images are on the left and the processed image on the right, with ice in yellow overlaid on the original image in blue.

Additionally, for the date of April 11th, 2015, merging the Landsat and the Sentinel-2 SAR information allows us to quantify the variations of the ice coverage on the shore of lake Ladoga. The Landsat image and the SAR image were taken respectively at 9:03 and 15:31 (UTC). Our processing shows that in the meantime, the ice cover maximum reach decreased by almost 2 kilometers.

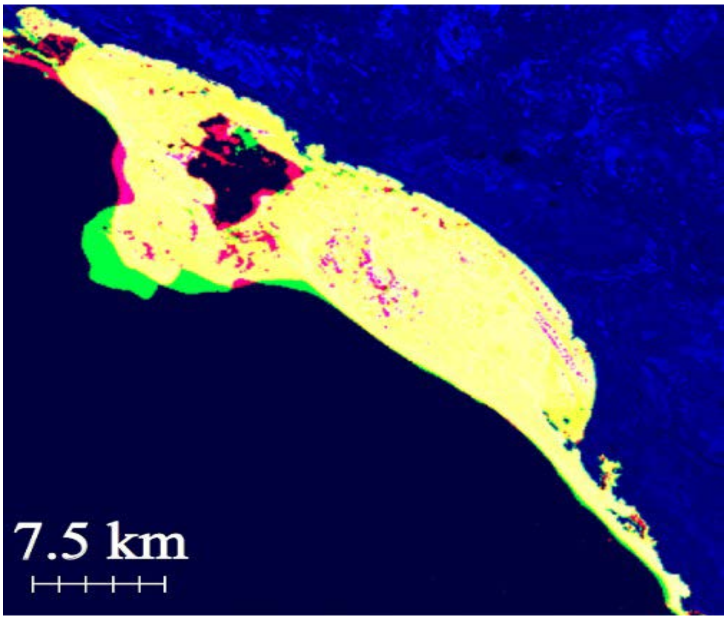

Figure 2. North shore of lake Ladoga. The blue background is the original image; the green and the red colors represent respectively the classifications of ice from the SAR and Landsat 8 images; the yellow colors is where both classifications agree.

REFERENCES

[1] Claude Belzile, John AE Gibson, and Warwick F Vincent. Colored dissolved organic matter and dissolved organic carbon exclusion from lake ice: Implications for irradiance transmission and carbon cycling. Limnology and Oceanography, 47(5):1283–1293, 2002.
[2] Christian H Fritsen and John C Priscu. Seasonal change in the optical properties of the permanent ice cover on lake bonney, antarctica: consequences for lake productivity and phytoplankton dynamics. Limnology and Oceanography, 44(2):447–454, 1999.
[3] Glenn A Hodgkins, Ivan C James, and Thomas G Huntington. Historical changes in lake ice-out dates as indicators of climate change in New England, 1850–2000. International Journal of Climatology, 22(15):1819–1827, 2002.

9.2

Large-scale monitoring of rapid permafrost thaw with satellite radar interferometry

Philipp Bernhard[1], Simon Zwieback[2], Silvan Leinss[1] and Irena Hajnsek[1]

[1] *Institute for Environmental Engineering, ETH Zürich,Stefano-Franscini-Platz 3, 8093 Zürich (bernhard@ifu.baug.ethz.ch)*
[2] *Intitute of Geography, University of Guelph, 50 Stone Road East Guelph, ON, Canada*

Vast areas of the Arctic host ice-rich permafrost, which is becoming increasingly vulnerable to rapid thaw in a warming climate. Rapid permafrost degradation has major impacts on the local hydrology and ecosystems, and it can also reinforce climate change by mobilizing organic carbon leading to the emission of large amounts of the greenhouse gases CO_2 and CH_4 (Schuur et al. 2015). However, on the pan-Arctic scale the prevalence and rates of rapid thaw remain poorly constrained, and so is their contribution to climate change. Here we outline an observational strategy to quantify hillslope thermokarst and its contribution to the carbon-climate feedback on the pan-Arctic scale. At its core are radar interferometric data acquired by the german TanDEM-X satellite, from which accurate measurements of elevation changes can be derived.

The data we will be using are obtained during the TanDEM-X operational phase between 2011 to 2016. This provides us with at least three observations over this timespan to generate digital elevation models (DEMs). Due to the spatial resolution of about 12m and the height sensitivity of 0.5-1m we will focus on forms of abrupt permafrost thaw that are noticeable at these scales, namely active layer detachment slides (ALDS) and retrogressive thaw slumps (RTS). RTS and ALDS evolve by retreat of the headwall which lead to the mobilization of soil resulting in detectable height changes in the landscape (Fig 1). Annual rates of headwall retreat can reach rates of several tens of meters per summer (Jorgenson et. al. 2008, Swanson 2012).

For processing and generating DEMs of the TanDEM-X data we will use the Gamma Remote Sensing Software (Werner et al. 2004). This process should be optimized and automated as much as possible to be able to cover large areas of the northern hemisphere. This includes detecting common problems with the data and apply appropriate algorithms to obtain DEMs with high accuracy. Additionally we will implement methods to deal with problematic features like old firn patches, vegetation and water bodies. It is not clear yet if it will be feasible and necessary to generate DEMs for the whole pan-Arctic land masses or if it will suffice to limit our study on specific regions and upscale the results. After generating the DEMs we will identify and classify different thermokarst features and investigate if a simple rule-based classifier suffices and if not consider other possibilities like classifiers based on machine learning. After the correct classification we will be able to investigate our dataset with regard to spatial variability as well es volumetric changes which is a first estimate for the amount of carbon that is mobilized.

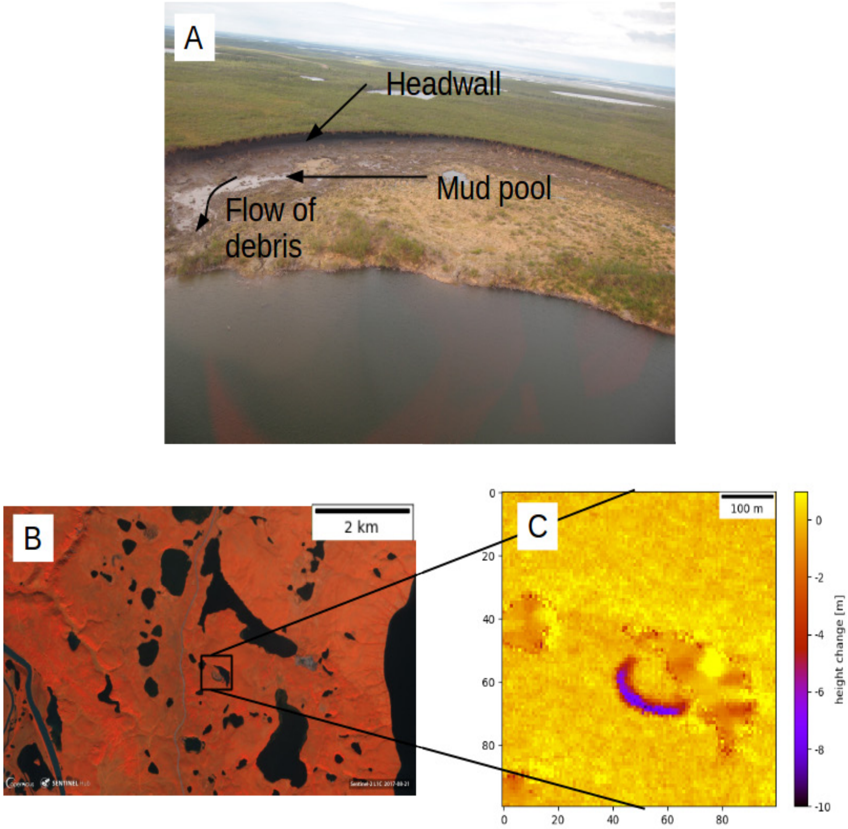

Figure 1. Observations of a thaw slump in the Mackenzie River Delta, Canada. A: Aerial photo of a thaw slump (picture by Simon Zwieback) B: Sentinel-2 L1C image of part of the area in the Mackenzie River Delta (Date: 21.08.2017), C: Result after DEM generation process for single-pass TanDEM-X observation in the Science Phase (01.06.2015). The heigt change shows the difference to a previous TanDEM-X DEM from 2013. The strong height change of up to -8m indicate that the thaw slump shown in A was increasing in size between the two observations.

REFERENCES

Jorgenson M.T., Grosse G., 2016: Remote Sensing of Landscape Change in Permafrost Regions: Permafrost and Periglacial Processes 27: 324-338

Schuur E.A.G. , McGuire A. , Schädel C., Grosse G., Harden J.W. , Hayes D.J., Hugelius G. , Koven C.D., Kuhry P. , Lawrence D.M., Natali S.M., Olefeldt D., Romanovsky V.E., Schaefer K., Turetsky M.R., Treat C.C., Vonk J.E., 2015: Climate change and the permafrost carbon feedback: Nature, v. 520.

Swanson MK. 2012: Monitoring of retrogressive thaw slumps in the Arctic Network: Three-dimensional modeling of landform change. Natural Resources Report NPS/ARCN/NRDC-2012/247

Werner C., Wegmüller U., Strozzi T., Wiesmann A. 2001: Gamma SAR and Interferometric Processing Software, Proc. ERS-ENVISAT Sym., European Space Agency, Gothenburg, Sweden, 16-20 Oct

9.3
A fiber bundle model with healing mechanisms for snow failure modelling

Achille Capelli[1], Ingrid Reiweger[2], Jürg Schweizer[1]

[1] *WSL Institute for Snow and Avalanche Research SLF, Flüelastrasse 11, 7260 Davos Dorf, (achille.capelli@slf.ch)*
[2] *BOKU University of Natural Resources and Life Sciences, Department of Civil Engineering and Natural Hazards, Institute of Mountain Risk Engineering, Peter-Jordan-Strasse 82, 1190 Wien, Austria*

Snow is a heterogeneous material with strain/load rate dependent strength. In particular, a transition from brittle to ductile failure at low loading rates is observed. The rate dependent behavior can partly be explained with the existence of a unique healing mechanism in snow. As soon as broken elements in the ice matrix get in contact, they start sintering and the structure may re-gain strength – or at least the damage process slows down. The failure process of heterogeneous materials is often studied with fiber bundle models (FBM) that consist of a set of linear elastic fibers with heterogeneous strength subjected to an external load. The fibers fail as the load exceeds the strength. The load of failed fibers is then redistributed to the intact fibers possibly causing a cascade of failures. A non-linear failure process emerges from the interaction of the single fibers. We present a new version of a FBM with two concurrent time dependent healing mechanisms: sintering of broken fibers and relaxation of load inhomogeneity. The speed of the two processes can be controlled by two characteristic times. We performed a sensitivity analysis for the speed of the two healing mechanisms.

Both healing mechanisms cause an increase of bundle strength, sintering by distributing the load among more fibers and load relaxation by distributing the load to the fibers carrying less load. The two healing mechanisms have opposite effects on the fiber failure dynamics. The sintering cause larger bursts of failing fibers resulting in a lower b-value, whereas the b-value is higher for faster relaxation. (The b-value describes the distribution of burst sizes, which is assumed to be power-law distributed with the b-value as exponent.) Without healing mechanisms the rate of failing fibers increases towards failure following a power law. The sintering mechanism increases the exponent of the power law. On the other hand, the relaxation inhibits the divergence of the rate of failing fibers, which grows exponentially. Comparing the model with snow failure experiments and in particular the resulting acoustic emissions, we aim to better understand the snow failure process in view of avalanche formation.

9.4

Numerical Reconstructions of the Flow and Basal Conditions of the Rhine Glacier at the Last Glacial Maximum

Denis Cohen[1], Guillaume Jouvet[2], Fabien Gillet-Chaulet[3], Wilfried Haeberli[4], Horst Machguth[4,5] Julien Seguinot[2], Michael Imhof[2], and Urs H. Fischer[6]

[1] *Department of Earth and Environmental Science, New Mexico Tech, Socorro, NM, 87801, USA (denis.cohen@gmail.com)*
[2] *VAW, ETH Zürich, 8093 Zürich, Switzerland*
[3] *Univ. Grenoble Alpes, CNRS, IRD, Grenoble INP, IGE, 38000 Grenoble, France*
[4] *Department of Geography, University of Zürich, 8006 Zürich, Switzerland*
[5] *Department of Geography, University of Fribourg, 1700 Fribourg, Switzerland*
[6] *Nagra, 5430 Wettingen, Switzerland*

At the Last Glacial Maximum (LGM), the Rhine glacier in the Swiss Alps covered an area of about 16,000 km^2. We modeled the Rhine glacier using (1) a fully-coupled, three-dimensional, thermo-mechanical Stokes flow model (Elmer/Ice) down to a horizontal resolution of about 500 m and (2) a shallow-shelf/shallow ice flow model (PISM) with a resolution of 1 km. Both models ran transient simulations: Elmer/Ice was used for short-term constant-climate forcing simulations around the LGM; PISM simulated full glacial cycles.

Using Elmer/Ice, the accumulation and ablation gradients that roughly reproduced the geomorphic reconstruction of glacial extent and ice thickness suggested extremely cold and dry climatic conditions (T_{July} close to 0 °C at the glacier terminus; about 10 to 20% of today's precipitation). The geomorphically reconstructed ice thickness could not be obtained with PISM. Forcing either models with warmer and wetter conditions that better matched LGM climate proxy records yielded a glacier on average 500 to 700 m thicker than geomorphic reconstructions (Fig. 1). In both models, mass balance gradients controlled ice velocities, fluxes, and sliding speeds. These gradients, however, had only a small effect on basal conditions. Although the two models use different model representation of the basal boundary condition, all simulations indicated that basal ice reached the pressure melting point over much of the Rhine and Linth piedmont lobes, and in the glacial valleys that fed these lobes. Only the outer margin of the lobes, some bedrock highs beneath the lobes, and Alpine valleys at high elevations in the accumulation zone remained cold-based. The Rhine glacier was thus polythermal. In all simulations, relatively cold and dry climatic conditions yielded a LGM Rhine glacier that moved rather slowly with maximum ice surface speeds of 150 to 530 m a^{-1} in the Rhine valley and 25 to 80 m a^{-1} in the piedmont lobe. Sliding speed ranged from 20 to 100 m a^{-1} in the lobes to 50 to 250 m a^{-1} in Alpine valleys depending on climate parameters. Velocity ratios (sliding to surface speeds) were > 80% (lobes) and about 60% (valleys). Results with Elmer/Ice indicate that basal shear stresses were very low in the lobes (0.03 to 0.1 MPa), much higher in Alpine valleys (> 0.2 MPa). In these valleys, viscous strain heating was a dominant source of heat, particularly when shear rates in the ice increased due to flow constrictions, confluences, or flow past large bedrock obstacles, contributing locally up to several W m^{-2} but on average of the order of 0.1 W m^{-2}. For comparison, the geothermal heat flux varies between 0.06 and 0.12 W m^{-2}. In the lobes, despite low surface slopes and low basal shear stresses, sliding dictated main fluxes of ice which closely followed bedrock topography: ice was channeled in between bedrock highs along troughs, some of which coincide with glacially eroded overdeepenings. These sliding conditions may have favored glacial erosion by abrasion and quarrying. In contrast, several bedrock highs remained frozen. Some of these coincide with Deckenschotter deposits that have suffered little erosion in the last 1 to 2 million years. Our results confirmed general earlier findings but provide more insights into the detailed flow and basal conditions of the Rhine glacier at the LGM. Ongoing work includes the effect of permafrost on the basal temperature and a systematic parametric study of sliding and ice rheology to see if models can match the geomorphic reconstruction of glacier thickness. Our model results thus far suggest that the trimline could have been buried by a significant thickness of cold ice. These findings have significant implications for interpreting trimlines in the Alps and for our understanding of ice-climate interactions.

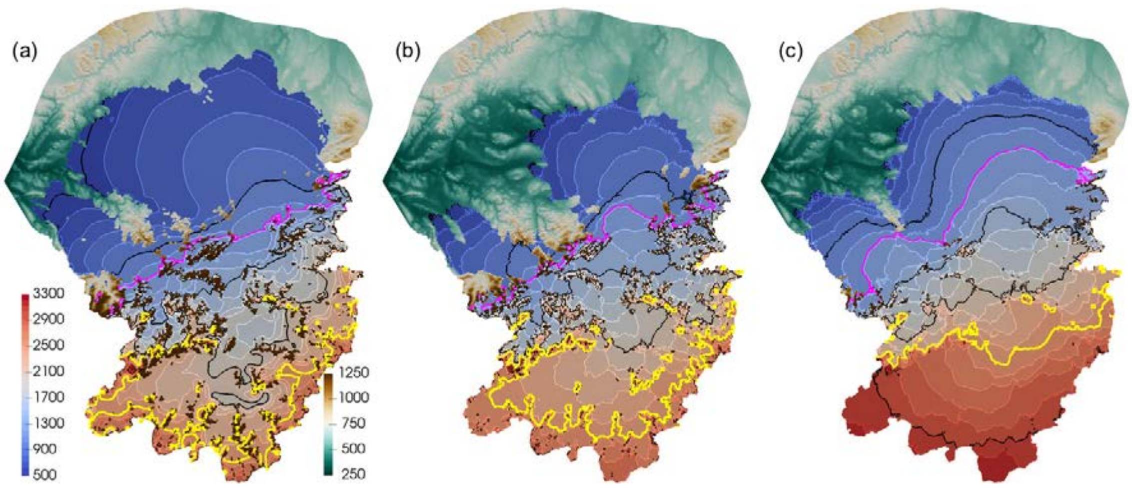

Figure 1. Ice thickness reconstruction. (a) Geomorphic reconstruction of Benz-Meier (2003). (b,c) Numerical reconstructions using Elmer/Ice. Simulation (b) uses an extremely cold and dry climate. Simulation (c) uses a warmer and wetter climate that better matches LGM climate proxy records. Black contours are every 500 m. The 2500 m contour is shown in yellow. The equilibrium line in purple is at 1200 m. Present-day topography is shown in ice-free areas with a different color scheme.

REFERENCES

Benz-Meier, C. 2003: Der würmeiszeitliche Rheingletscher – Maximalstand. Digitale Rekonstruction, Modellierung und Analyse mit einem Geographischen Informationssytem, Ph.D. thesis, Universität Zürich.

9.5

Using a cosmic ray sensor and weather radar composites to estimate the snow water equivalent on a Swiss glacier

Rebecca Gugerli[1], Matthias Huss[1/2], Nadine Salzmann[1]

[1] *Department of Geosciences, University of Fribourg, Chemin de Musée 4, 1700 Fribourg, Switzerland (rebecca.gugerli@unifr.ch)*
[2] *Laboratory of Hydraulics, Hydrology and Glaciology (VAW), Swiss Federal Institute of Zurich, Hönggerbergring 26, 8093 Zürich, Switzerland*

Precipitation estimates in high-mountain regions are essential for environmental studies in many research fields (glaciology, meteorology, hydrology, climate risk and adaptation). Although precipitation data exist for the Swiss Alps, accuracy is limited by data sparsity and measurement challenges in high-mountain regions (e.g., Goodison et al., 1998, Martinaitis et al., 2015). We propose a novel approach to estimate the snow water equivalent (SWE) on glaciers and to spatially integrate these measurements by combining continuous measurements of SWE, conventional glaciological measurements and operational measurements of solid precipitation.

Reliable and continuous measurements of SWE are indispensable for inferring temporal snow-accumulation dynamics. Therefore, we investigate the application of a cosmic ray sensor to measure SWE continuously on the Glacier de la Plaine Morte in Switzerland. The sensor is located on the glacier surface below the snowpack and counts low-energy neutrons at an hourly interval. The neutron count is negatively correlated to SWE. Comparing the cosmic ray sensor with manual measurements of SWE in snow pits, we find a mean overestimation of 1.03+/-0.16 in SWE measured by the cosmic ray sensor. After adjusting with snow height measurements, the overestimation is reduced to a mean factor of 1.01+/-0.10.

In a further step, we compare operational weather radar composites compiled by MeteoSwiss (Germann et al., 2006, Sideris et al., 2014) to continuous SWE measurements on the Glacier de la Plaine Morte. These weather radar composites show precipitation estimates over Switzerland at a horizontal grid resolution of one kilometer and a temporal grid resolution of one hour. This grid resolution is sufficient to directly compare these solid precipitation estimates to hourly SWE measurements from the field site. A further advantage of the weather radar composite is that several grid cells in the weather radar composites cover the glacier area, and, therefore, allow an analysis of the spatial variability in precipitation. First results from the winter season 2016/17 show an underestimation of accumulated solid precipitation by the radar composites (696mm) compared to the SWE measured by the cosmic ray sensor (1330mm) on the Glacier de la Plaine Morte. Precipitation events often agree in time, but the weather radar generally underestimates the amount of solid precipitation.

In future work, we aim to verify the applicability of weather radar composites for solid precipitation information in high mountain regions by comparing accumulated solid precipitation to conventional glaciological field measurements on several monitored glaciers in Switzerland (Glaciological Reports, 1881-2017).

REFERENCES

Germann, U., Galli, G., Boscacci, M., and Bolliger, M. (2006). Radar precipitation measurement in a mountainous region. Quarterly Journal of the Royal Meteorological Society, 132(618):1669–1692.

Glaciological Reports.(1881-2017). The Swiss Glaciers, 1880-2014/2015, Yearbooks of the Cryospheric Commission of the Swiss Academy of Sciences (SCNAT), 1-136. Published since 1964 by VAW-ETH. Zürich.

Goodison, B. E., Louie, P., and Yang, D. (1998). WMO solid precipitation measurement intercomparison. Technical Report 67, World Meteorological Organization.

Martinaitis, S. M., Cocks, S. B., Qi, Y., Kaney, B. T., Zhang, J., and Howard, K. (2015). Understanding winter precipitation impacts on automated gauge observations within a real-time system. Journal of Hydrometeorology, 16(6):2345–2363.

Sideris, I. V., Gabella, M., Erdin, R., and Germann, U. (2014). Real-time radar-rain-gauge merging using spatio-temporal co-kriging with external drift in the alpine terrain of Switzerland. Quarterly Journal of the Royal Meteorological Society, 140(680):1097–1111.

9.6

Localisation of avalanches using seismic monitoring

Matthias Heck[1], Manuel Hobiger[2], Alec van Herwijnen[1], Donat Fäh[2]

[1] *WSL Institute for Snow and Avalanche Research SLF, Flüelastr. 11, CH-7260 Davos (heck@slf.ch)*
[2] *Swiss Seismological Service, ETH Zurich, Sonneggstr. 5, CH-8092 Zurich*

Seismic monitoring systems are well suited for the remote detection of mass movements, such as landslides, rockfalls and debris flows. For snow avalanches, this has been known since the 1970s and seismic monitoring could potentially provide valuable information for avalanche forecasting.

Avalanche warning services try to estimate the avalanche danger level based on information about the snow pack, weather conditions and current avalanche activity.

Using a geophone array, we are able to detect seismic wavefields produced by avalanches and to estimate the avalanche activity in a remote area.

Apart from the avalanche activity we are also interested in the release area and path of the avalanches. To obtain these information, we use array processing techniques such as multiple signal classification (MUSIC) and beam-forming.
The MUSIC method seperates the signal subspace from the noise space and multiple sources can be determined. The beam-forming method shifts the time traces and searches for the maximal enegry stack.

By determing the sources for the MUSIC method or the maximal energy stack for the beam-forming method, the back-azimuth, i.e. the direction of the signals is also calculated.

Applying the methods to small sliding windows, changes in the back-azimuth for avalanche signals can be observed. Analysing theses back-azimuths, we are able to backtrack the moving front of an avalanche.

By combing the back-azimuth results with a map of the local area, we are able to estimate the path of the avalanche.
For a high avalanche activity period in March 2017 we identified around 20 avalanche events and tried to locate them. 14 events could be located using the MUSIC method and confirmed with visual observations.

Seismic arrays are able to detect avalanches and using array processing techniques events can also be located.
These information will help avalanche warning services to improve the estimation of the current danger level.

9.7

Genesis and conservation of permafrost excess ice in the Flüelapass talus slope

Robert Kenner[1], Marcia Phillips[1], Christian Hauck[2], Christin Hilbich[2], Christian Mulsow[3],Yves Bühler[1], Andreas Stoffel[1], Manfred Buchroithner[4]

[1] *WSL Institute for Snow and Avalanche Research SLF, Davos, Switzerland*
[2] *Department of Geosciences University of Fribourg, Switzerland*
[2] *Institute of Photogrammetry and Remote Sensing, Dresden University of Technology, Germany*
[2] *Institute of Cartography, Dresden University of Technology, Germany*

The genesis of ice-rich permafrost at relatively low elevations such as talus slope foot positions or in low elevation rock glaciers is a phenomenon which is not entirely understood. In several cases, one dimensional modelling of ground temperatures at low elevation permafrost sites shows that permafrost would not be possible here without high ground ice contents (Hipp et al., 2012). How can large amounts of ground ice develop at sites which are unfavourable for permafrost as long as they are free of ice? Some of these permafrost sites could be attributed to intra-talus air ventilation, which causes a cooling of the ground (Delaloye and Lambiel, 2005). But can ventilation allow the development of excess ice, without causing a sealing of the ventilation channels with ice? And what causes the permafrost at sites without ventilation? Finally, the process of excess ice development in a rough talus slope including massive ice lenses could not be documented in experimental studies so far.

Kenner et al. (2017) investigating these questions at the oldest permafrost study site in Switzerland, the talus slope at Flüelapass in the eastern Swiss Alps, which is located above the lakeshore of Schottensee. Based on a photogrammetric DEM of the lake bottom and geomorphological observations, an interesting reconstruction of the geomorphologic history of the site could be established. It revealed the presence of a rock glacier within the lake, which was flooded by the latter as a rock fall dammed the current lake basin.

A 14 year temperature-time series measured in two boreholes in the talus slope, one at the base in permafrost ground and one further upslope in permafrost free terrain allowed the analysis of thermal processes within the ground. Additionally, the influence of avalanche snow at the talus slope base could be quantified, which was focused on as possible factor contributing to the presence of permafrost in the talus slope base by Haeberli (1975) (Figure 1). Geophysical investigations provided an insight in the distribution and thickness of the ground ice body and terrestrial laserscanning was used to analyse the snow distribution during winter.

Our investigations suggest that permafrost did not cause the development of ground ice in this talus slope, but that mass movement deposits (avalanches and rock fall) caused the onset of permafrost here. The ground ice distribution corresponds to the main deposition zones of snow avalanches, which were perennial here in the past. The formation of the approximately 30 m thick talus slope during the Holocene most probably covered similar snow deposits with rock fall material and led to the insulation of the snow and to the formation of ground ice. A slight intra-talus ventilation and the insulation effect of long lasting avalanche snow fields against radiation and atmospheric warming turned out to have a measureable but limited effect on the ground temperatures.

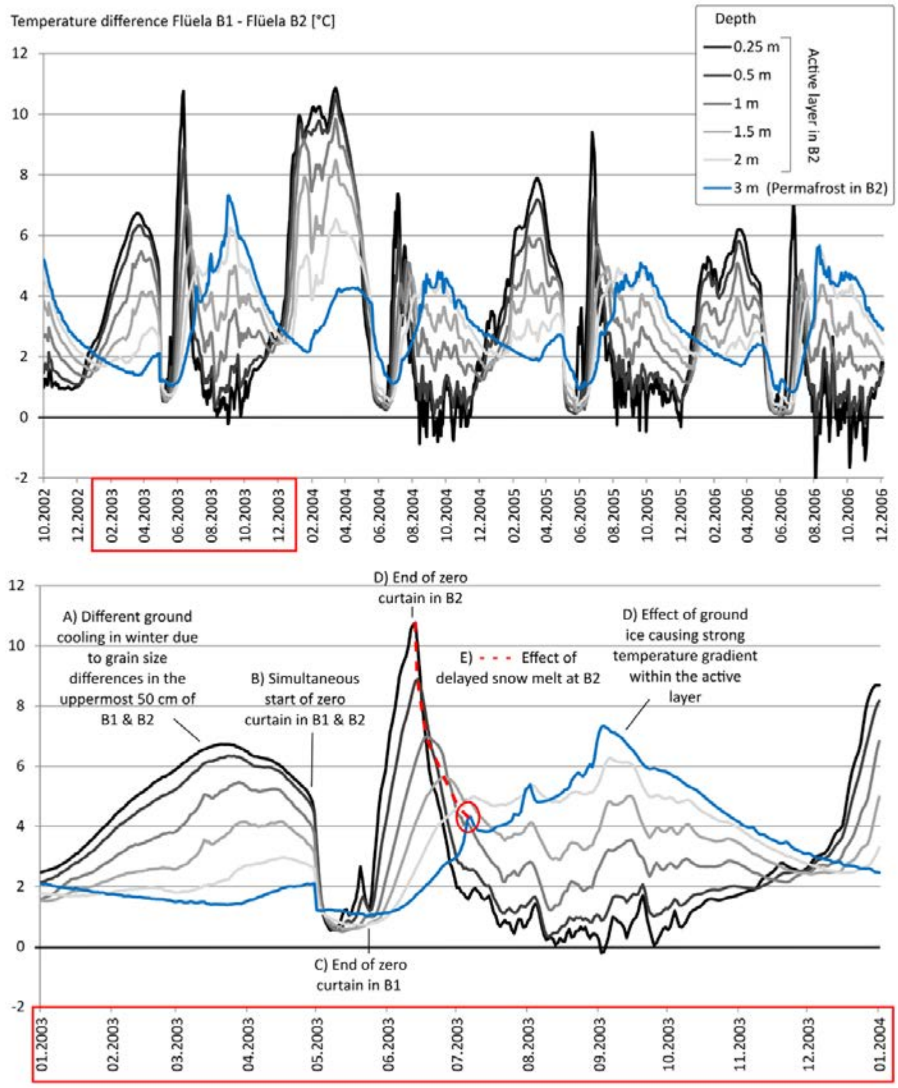

Figure 1. Temperature differences between both boreholes in the Flüela talus slopes at different depths. Whereas temperatures differ strongest close to the surface in winter, the largest differences in summer occur at 3 m, close to the permafrost table in B2. The effect of different snow melt out dates is limited.

REFERENCES

Delaloye R & Lambiel C. 2005: Evidences of winter ascending air circulation throughout talus slopes and rock glaciers situated in the lower belt of alpine discontinuous permafrost (Swiss Alps). Norsk geogr. Tidsskr. 59: 194-201

Haeberli W, 1975: Untersuchungen zur Verbreitung von Permafrost zwischen Flüelapass und Piz Grialetsch (Graubünden). Mitteilungen der Versuchsanstalt für Wasserbau, Hydrologie und Glaziologie der ETH Zürich, 17, Zurich, 221 pp

Hipp T, Etzelmüller B, Farbrot H, Schuler TV, Westermann S. 2012: Modelling borehole temperatures in Southern Norway – insights into permafrost dynamics during the 20th and 21st century. The Cryosphere 6(3): 553-571. doi: 10.5194/tc-6-553-2012

Kenner R, Phillips M, Hauck C, Hilbich C, Mulsow C, Bühler Y, Stoffel A, Buchroithner M. 2017. New insights on permafrost genesis and conservation in talus slopes based on observations at Flüelapass, Eastern Switzerland. Geomorphology 290: 101-113. doi: https://doi.org/10.1016/j.geomorph.2017.04.011

9.8
Basal-ice accretion – pushing boundaries within ice sheets

Gwendolyn Leysinger Vieli[1]

[1] *Department of Geography, University of Zurich, Winterthurerstrasse 190, CH-8057 Zürich (gwendolyn.leysinger@geo.uzh.ch)*

Large, englacial, plume-like structures, rising from the ice-sheet base up to half of the ice thickness, have been observed in modern radio echo sounding data from the Greenland and Antarctic ice-sheet (e.g. Fig. 1). The mechanism behind the formation is not fully understood. However, freeze-on at the ice-sheet base is amongst one of the possible processes.

Here I explain the theory behind the freeze-on process and show by means of numerical modelling how such accreted ice-structures evolve within the ice sheet and cause deformation of the surrounding meteoric ice. Further, by means of spatial analysis using data sets from the Greenland ice-sheet, I show that potential constraints and relationships between the observed complex, near-basal layer structures and the prevailing spatial conditions are consistent with the hypothesis of basal freeze-on.

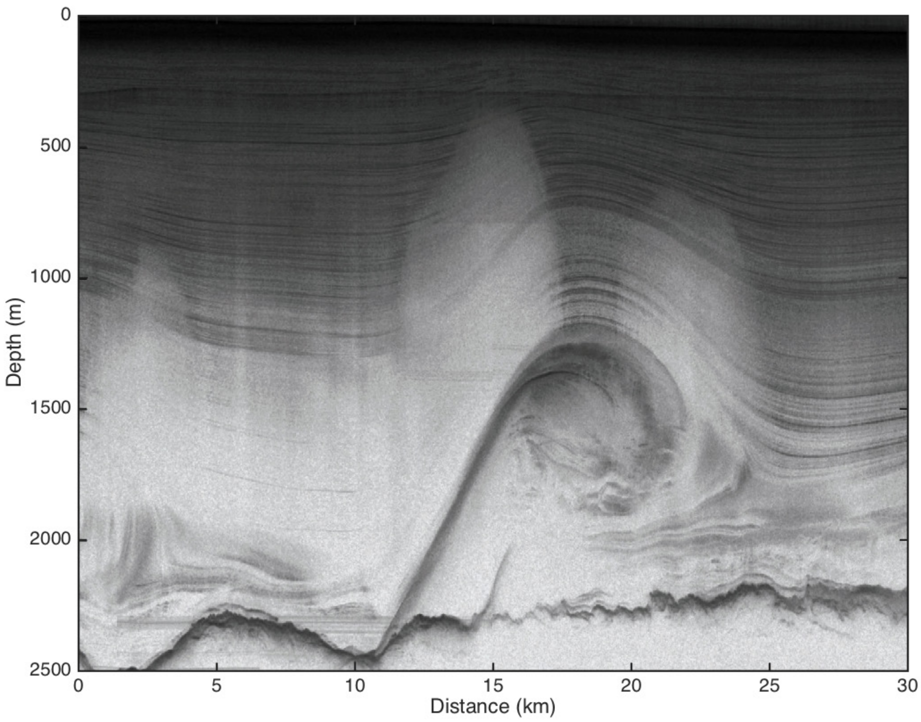

Figure 1. Radio echo sounding profile 20120507_07_001&002 in NorthEast Greenland from NASA's Operation IceBridge (Leuschen et al., 2014).

REFERENCES

Leuschen, C., Gogineni, P., Hale, R., Paden, J., Rodriguez, F., Panzer, B. & Gomez, D. 2014: IceBridge MCoRDS L1B geolocated radar echo strength profiles, version 2. Boulder Colorado USA: National Snow and Ice Data Center. http://dx.doi.org/10.5067/90S1XZ%BAX5N.

9.9

Using Continuum Damage Mechanics to Simulate Iceberg Calving from Tidewater Outlet Glaciers

Rémy Mercenier, Martin P. Lüthi, Andreas Vieli

Department of Geography, University of Zurich, Zurich, Switzerland (remy.mercenier@geo.uzh.ch)

Many ocean terminating glaciers in the Arctic are currently undergoing rapid retreat, thinning and strong accelerations in flow. The process of iceberg calving plays a crucial role for the related dynamical mass losses and occurs when the stresses at the calving front exceed the fracture strength of ice, driving the propagation of cracks and eventually leading to the detachment of ice blocks from the glacier front. However, the understanding of the processes involved in iceberg calving as well as the capability of flow models to represent the calving mechanism remain limited.

Here, we use a time-dependent two-dimensional finite-element flow model coupled to a damage model to simulate the break-off of ice at the front of idealized tidewater outlet glaciers. The flow model computes flow velocities and the resulting stresses, which are in turn used to calculate the evolution of the glacier geometry and damage. Damage is defined as a change of rheological properties, e.g. viscosity, due to increasing material degradation. Elements of ice are removed when the damage variable reaches a critical threshold. The effects of material properties and of geometrical parameters such as water depth, ice thickness and submarine frontal melting on the simulated calving rates are explored through systematic sensitivity analyses.

The coupled ice flow/damage model allows for successful reproduction of calving front geometries typically observed for different water depths. We further use detailed observations from real glacier geometries to better constrain the model parameters. The proposed model approach should be applicable to simulate iceberg calving on arbitrary glaciers, and thus be used to analyse the evolution of tidewater glacier variations from the past to the future.

9.10

The roughness of englacial R-channels determined by physical experiments

Yuri M. Prohaska[1], Mauro A. Werder[1] & Daniel Farinotti[1,2]

[1] *Laboratory for Hydraulics, Hydrology and Glaciology (VAW), ETH-Zürich, Hönggerbergring 26, Zürich, CH 8093*
[2] *WSL, Züricherstrasse 111, Birmensdorf, CH, 8903*

In 1972, Röthlisberger presented a theoretical study describing the evolution of pressurised en- and subglacial channels. The existence of these so-called R-channels has later been confirmed through field observations. To our knowledge, however, no physical experiment has ever been conducted to actually measure the properties of such channel flow in the laboratory. Here, we present a setup for such a laboratory experiment and results showing that the Darcy-Weisbach roughness of such channels is very high.

The aim of our experiment is to measure the Darcy-Weisbach friction factor. For our experiment, we produce transparent ice blocks of 1.6m length and a cross section of up to 25x25cm. A small metal tube is frozen into the ice block and removed before the experiment to create an initial R-channel. Pipes attached to flanges frozen into the ice block allow us to let water flow under pressurised conditions. Water pressure is measured at the inlet and outlet of the ice block as well as within. The evolution of the channel diameter is captured by photographic imaging. A magnetic flow meter measures the discharge. During a typical experiment, the diameter of the R-channel evolves from 1 to 9cm with flow speeds of up to 2m/s, the Reynolds number is around 5×10^4, and the friction factor increases from about 0.024 to 0.12.

9.11
75 years snow water equivalent measurements in the Wägital catchment

Mario Rohrer, Urs Steinegger, Christian Nötzli, Daniela Lorenzi, Manfred Schwarb

Meteodat GmbH, Technoparkstr. 1, 8005 Zürich, Switzerland

The Wägital snowcover measurements have started in the early 1940ies as a basis of inflow forecasts for the dammed lake of Wägital. The Wägital hydro-electric power plant was - after completion - the largest pumping power plant of the world. But in the 1980ies, the forecasts where not any longer of interests for the power company - as in meantime Wägital was one of the tiniest pumping power plants of Switzerland. Thereafter, the snow measurements have been continued by the Geographical Institute of the ETH, and - after 1998 - by Meteodat. As Meteodat could not finance the full costs of the measurement campaign; the WSL Institute for Snow and Avalanche Research SLF, the Geographical Institute of the ETH and of the University of Zurich co-financed these measurements. Since 2010, the Wägital snow cover measurements are co-financed by the Federal Office of Meteorology and Climatology MeteoSwiss in the framework of GCOS (Global Climate Observing System) Switzerland. In our knowledge, the snow-cover water equivalent series of the Wägital are the longest of its kind of the world. A lot of students and senior scientist have helped us from Meteodat to perform the measurements and - on the other hand - these data have been a basis for publications and master thesis (e.g. Nötzli & Rohrer, 2014 or Tilg, 2013). The Wägital data series are open access under Creative Commons Attribution 4.0 Licence (Steinegger et al., 2017). Let's hope that GCOS and all of you will help us also in future to continue this long snow cover data series. Particularly in times of climate change, such time series can serve as a valuable basis for the assessment of the state and fate of the snow cover in pre-alpine Switzerland.

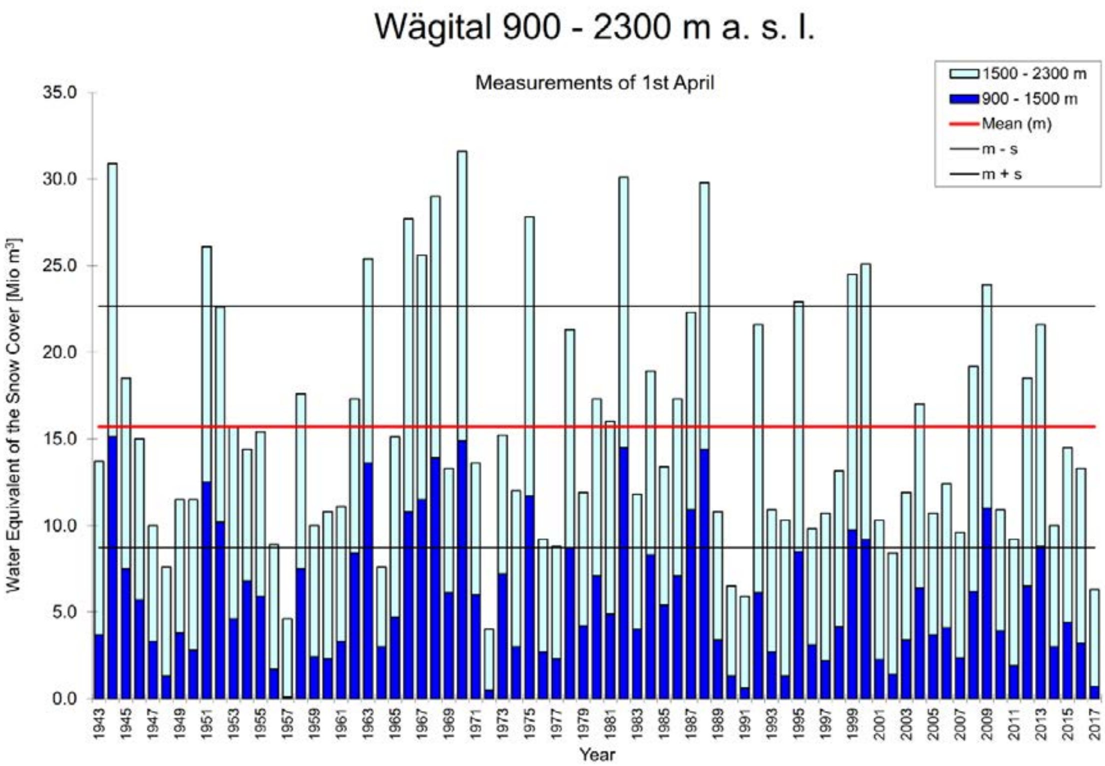

Figure 1.: Data series of the water equivalent of the snow cover (SWE) in the Wägital catchment. In dark blue the values of the altitude zone between 900 and 1500 m asl. and in light blue the SWE-values for the altitude zone between 1500 and 2300 m asl.

REFERENCES

Noetzli Christian & Rohrer, Mario 2014. Schneemessungen in alpinen Einzugsgebieten im Zeichen des Klimawandels, Wasser Energie Luft - 106. Jahrgang, 2014, Heft 4, CH-5401 Baden, p. 280-284.

Steinegger, Urs; Rohrer, Mario; Schwarb, Manfred; Lorenzi, Daniela; Nötzli, Christian; Schauwecker, Simone & Siegenthaler, Hans, 2017: Snow water equivalent for reference date April 1 for Wägital catchment, 1943-2017, https://doi.org/10.5281/zenodo.583656.

Tilg, Anna-Maria 2013. Parametrization and Trend Analysis of Snow Water Equivalent in the Alpine region. Master thesis at the University of Innsbruck, 213p., www.acinn.uibk.ac.at/file/396/download?token=uca6R_Ct.

9.12

Wind tunnel experiments: influence of erosion and deposition on wind-packing of fresh snow

Christian Gabriel Sommer[1,2], Charles Fierz[1], Michael Lehning[1,2]

[1] *WSL Institute for Snow and Avalanche Research SLF, Davos, Switzerland (sommer@slf.ch)*
[2] *CRYOS, School of Architecture, Civil and Environmental Engineering, EPFL, Lausanne, Switzerland*

We observed the formation of wind crusts in an obround wind tunnel. A SnowMicroPen was used to measure the snow hardness and a Microsoft Kinect provided spatially resolved snow depth data. Earlier experiments showed that no crust forms without drifting snow and that the dynamics of erosion and deposition may be an important factor to explain wind-packing. The Kinect data could be used to quantify spatial erosion and deposition patterns and the combination with the SnowMicroPen data allowed to study the effect of erosion and deposition on wind-hardening. We found that erosion had no hardening effect on fresh snow and that deposition is a necessary but not sufficient condition for wind crust formation. In fact, deposited snow was only hardened in wind-exposed areas as revealed by the wind-exposure parameter Sx, which was derived from the Kinect data. We observed no significant hardening for Sx>0.25.

9.13

A rapid glacier surge in the Karakoram – employing new high-resolution satellite products for coupled research and hazard assessment

J.F.Steiner[1], P.D.A. Kraaijenbrink[1], Sergiu G. Jiduc[2], W.W. Immerzeel[1]

[1] *Utrecht University, Department Physical Geography, Utrecht, The Netherlands*
[2] *Imperial College London, Centre for Environmental Policy, Faculty of Natural Sciences, SW7 1NA, London, United Kingdom*

Numerous glaciological studies have addressed glacier surges in the Karakoram in the past and some examples have been identified that result in hazards for downstream communities. Using recent ASTER and TanDEM-X DEMs as well as Landsat imagery in combination with high-resolution Planet imagery we quantify surface elevation changes and flow velocities to document a glacier surge of the Khurdopin glacier in the first half of 2017.

Results reveal an accumulation of ice mass leading to a rapid surge peaking with velocities above 5000 m a^{-1} or 0.5 m h^{-1} during a few days. Velocities increase during a four-year build-up phase prior to the actual surge, while the remaining 15 years of the recurring cycle the glacier is quiescent. We believe that the surge is mainly initiated as a result of increased pressure melting caused by ice accumulation, i.e. the thermal switch hypothesis. However, surface observations show increased crevassing and disappearance of supra glacial ponds, which could have led to increased lubrication of the glacier bed. As a consequence of the surging tongue blocking the main valley a lake has formed and grown continuously in size over two months, culminating in a rapid release of water over a few days, resulting in downstream infrastructure damage.

Using satellite imagery with a frequent overpass rate we are able to identify peak surging better and describe the development of the actual surge in great detail. It also enabled us to monitor the formation and drainage of the lake with a delay of sometimes less than a day. We use this data for a better scientific understanding of surges and with a close connection to local stakeholders as a means of hazard assessment for a remote region of the Karakoram.

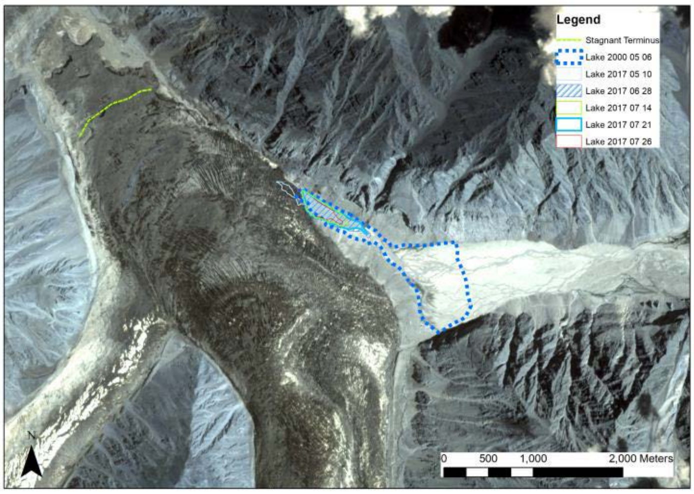

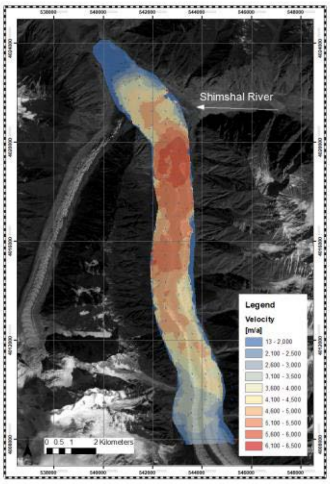

Figure 1. The Glacier terminus with the lake extents (left) as well as the peak velocities derived from Planet imagery (right).

REFERENCES

Quincey, D. J. and Luckman, A.: Brief communication: On the magnitude and frequency of Khurdopin glacier surge events, The Cryosphere, 8(2), 571–574, doi:10.5194/tc-8-571-2014, 2014.

Quincey, D. J., Braun, M., Glasser, N. F., Bishop, M. P., Hewitt, K. and Luckman, A.: Karakoram glacier surge dynamics, Geophysical Research Letters, 38(18), 1–6, doi:10.1029/2011GL049004, 2011.

Round, V., Leinss, S., Huss, M., Haemmig, C. and Hajnsek, I.: Surge dynamics and lake outbursts of Kyagar Glacier, Karakoram, The Cryosphere, 11, 723–739, doi:10.5194/tc-11-723-2017, 2017.

9.14
Special Session: 30 years Borehole Murtèl-Corvatsch

Jeannette Nötzli[1], Alessandro Cicoira[2], Wilfried Haeberli[2], Martin Hoelzle[3], Andreas Vieli[2], Daniel Vonder Mühll[4]

[1] *WSL Institute for Snow and Avalache Research, Flüelastrasse 11, 7260 Davos Dorf (jeannette.noetzli@slf.ch)*
[2] *Department of Geography, University of Zurich, Winterthurerstrasse 190, 8057 Zürich*
[3] *Department of Geosciences, University of Fribourg, Chemin du Musée 4, 1700 Fribourg*
[4] SystemsX.ch, ETHZ, Zürich, Clausiusstr. 45, 8092 Zürich

The longest detailed and continuous permafrost temperature time series in mountain permafrost is measured in the borehole on the Murtèl rock glacier on Corvatsch, Upper Engadine, Switzerland. As the first series in mountain permafrost it reaches the significant length of 30 years this year, i.e. one normal climate period. Since the first drilling campaign in 1987, a large number of additional permafrost research studies were performed at and in the region of the Murtèl-Corvatsch rock glacier, making it the likely best-investigated mountain permafrost site with global relevance (e.g. the 4th EU Framework Project «Permafrost and Climate in Europe – PACE» from 1997–2001 also originates from this site). Due to its unique length, the Murtèl series is of high importance for long-term monitoring activities, both at national and international level in the framework of the Swiss Permafrost Monitoring Network PERMOS, respectively the Global Terrestrial Network for Permafrost (GTN-P).Today it can be considered a role model for education, research as well as longterm monitoring.

Due to considerable internal shearing of the rock glacier at 28 m depth as well as the limited lifetime of the instruments the risk of loosing parts or even all of the permafrost temperature time series continuously increased in the past years. A replacement borehole was drilled only 5 m apart in summer 2015 to validate, secure and continue the measurements. The overlapping period of the old and new measuring systems enables to assess the quality and accordance of the two records.

For the celebration of the 30 year anniversary of the Murtèl borehole, the Swiss Society for Snow, Ice and Permafrost (SEP-NGP) organized an excursion to the drill site as well as a special session at the Swiss Geosciences Meeting 2017. In this session, we will look back to the drilling and installation of the borehole in 1987, and outline the intense large number of field investigations. The Murtèl rock glacier was a key site for method testing or model development concerning mainly the following topics: borehole temperatures and deformation, core-analysis (physico-chemical properties), photogrammetry, geophysical soundings, energy balance measurements, and approaches for modeling the mountain permafrost distribution. The concept and drilling campaign for the new borehole 2015 will be outlined and the first ca. 1.5 years of comparing data as well as an outlook on future activities will be presented.

Figure 1. View on the rock glacier Murtèl on Corvatsch from the cable car to the summit station. Photo: J. Nötzli, August 2010.

P 9.1

Long-term mass changes on three Kyrgyz glaciers

Martina Barandun[1], Matthias Huss[1,2], Ryskul Usubaliev[3], Erlan Azisov[3], Etienne Berthier[4], Andreas Kääb[5], Tobias Bolch[6] & Martin Hoelzle[1]

[1] Department of Geosciences, University of Fribourg, Fribourg, Switzerland
[2] Laboratory of Hydraulics, Hydrology and Glaciology (VAW), ETH Zurich, Zurich, Switzerland
[3] Central Asian Institute of Applied Geosciences (CAIAG), Bishkek, Kyrgyzstan
[4] CNRS, LEGOS, University of Toulouse, Toulouse, France
[5] Department of Geoscience, University of Oslo, Norway
[6] Department of Geography, University of Zurich, Switzerland

Glacier mass balance observations in the Tien Shan and Pamir mountains are sparse and often discontinuous. However, glaciers are one of the most important components of the high-mountain cryosphere and crucially influence water availability of the arid, continental and intensely populated downstream areas (Duethmann et al., 2014; Chen et al., 2016).

With this study, we aim at improving the temporal and spatial representation of long-term glacier mass balance series to create accurate and continuous baseline data for three selected glaciers located in the Tien Shan and Pamir mountains (Fig. 1). We used a combination of three independent methods to reconstruct robust mass balance series for the three benchmark glaciers Abramov, Golubin and No. 354, for the past two decades. Through the consideration of the different approaches, we bridge the limitations and shortcomings of each individual method. Here, we propose the use of transient snowline observations throughout the melting season obtained from satellite imagery and terrestrial automatic cameras. By combining remotely acquired information on summer snow depletion with mass balance modelling, glacier mass changes can be inferred even for unmeasured years at high temporal and spatial resolution. Multi-annual mass changes based on high-accuracy digital elevation models and in-situ glaciological surveys are used to validate the results for every investigated glacier.

Continued mass loss was confirmed for the three studied glaciers by all three methods. Figure 2 compares the geodetic mass balance to the snowline derived mass balance for all three glaciers. Abramov exhibited a mean annual mass balance of -0.30±0.04 m w.e. a^{-1} from 2004 to 2016 derived from our snowline-approach. For Golubin Glacier and Glacier No. 354 a slightly more negative annual mean balance of -0.41±0.09 m w.e. a^{-1} and -0.36±0.09 m w.e. a^{-1}, respectively, was calculated for the same time period using the same method. Model experiments revealed relatively small sensitivity to the input parameters and the meteorological data used, indicating a considerable advantage in comparison to conventional mass balance modelling not including direct observations. Our results show that integration of snowline observations into the conventional mass balance modelling significantly narrows the uncertainty ranges of mass balance estimates for the here studied glaciers and, hence, highlights the potential of the methodology for application to inaccessible glaciers at larger scales for which no direct glaciological measurements are available.

Today mass balance observations in the Pamir and Tien Shan mountains are sparse but essentially needed to improve understanding of the glacier behaviour in the region and its effect on future water availability (Hoelzle et al., in review). For remote and inaccessible regions and countries, lacking financial power and infrastructure to support such monitoring, our proposed approach delivers a tool to investigate and reconstruct the mass balance of inaccessible and remote glaciers with minimal effort.

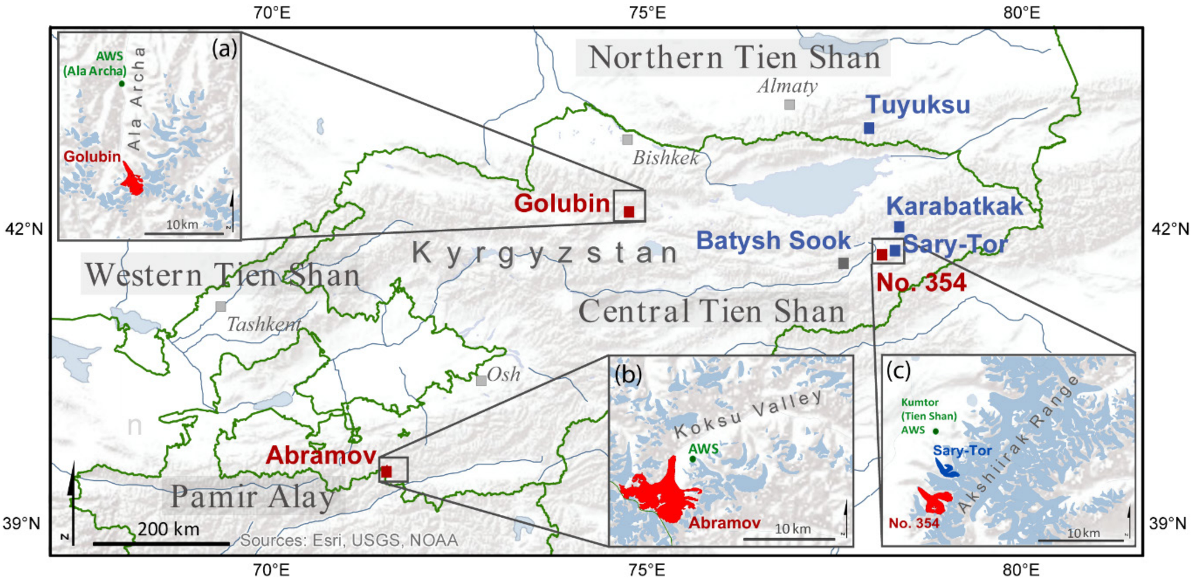

Figure 1: Overview map of Central Asia and the location of glaciers (blue) with available mass balance long-term measurements. Glaciers investigated for this study are marked in red. The insets show the position of the automatic weather station for (a) Golubin Glacier, (b) Abramov Glacier and (c) Glacier No. 354.

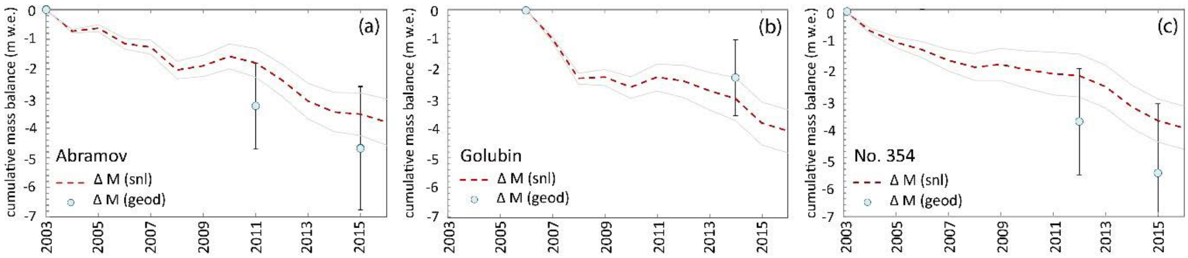

Figure 2: Cumulative snowline-derived mass change (red) in comparison to the geodetic mass change (circles) for (a) Abramov, (b) Golubin and (c) Glacier No. 354. The grey lines indicate the uncertainty range of the snowline-derived mass change.

REFERENCES

Chen, Y., Li, W., Deng, H., Fang, G., & Li, Z. 2016: Changes in Central Asia's Water Tower: Past, Present and Future. Scientific reports, 6, 35458.

Duethmann, D., Peters, J., Blume, T., Vorogushyn, S., & Güntner, A. 2014: The value of satellite-derived snow cover images for calibrating a hydrological model in snow-dominated catchments in Central Asia. Water Resources Research, 50(3), 2002-2021.

Hoelzle, M. et al. in review: Re-establishing glacier monitoring in Kyrgyzstan and Uzbekistan, Central Asia, Geosciencitific Instrumentation, Methods and Data Systems.

P 9.2

Effect of load-sharing rules in modeling snow failure with a fiber bundle model

Gregoire Bobillier[1], Achille Capelli[1], Jürg Schweizer[1]

[1]*WSL Institute for Snow and Avalanche Research SLF, CH-7260 Davos Dorf (gregoire.bobillier@slf.ch)*

Fiber bundle models (FBM) are widely used to model the failure process of heterogeneous materials and hence considered an appropriate tool to study snow failure in view of snow avalanche formation. The fiber bundle consists of a set of linear elastic fibers with variable strength. As during a snowfall, the load on the fibers is progressively increased. When the load on a fiber exceeds its strength, the fiber fails and the load is redistributed to the intact fibers according to a load-sharing rule.

A sharing rule with a variable range of load redistribution can be used to study the transition between two distinct regimes. Global load sharing where the load is distributed equally to all fibers, and local load sharing where the load is redistributed to the nearest neighbors. If the range of interaction decreases, the stress is distributed to fewer fibers and stress concentrations occur. They enable a failure to grow. Finally, the bundle fails at lower stress than with a large range of interaction. For a large sample, the probability is higher for a weak zone to exist, which then can serve as nucleus for the failure process. Therefore, for local load sharing the strength of the sample decreases with increasing sample size, whereas for global load sharing the strength of the sample is independent of sample size.

Furthermore, we developed a new version of the local load-sharing rule taking into account the spatial distribution of already broken fibers, With the new, more realistic load sharing rule, the load is redistributed locally and recursively to all fibers (also to the failed ones) until the load on the failed fiber is negligible. In this way, the load is redistributed more widely around damaged zones instead to be limited to the nearest neighbors. As a consequence, the strength of the bundle is increased.

Dry-snow slab avalanche formation starts with the formation of an initial, localized failure that progressively grows due to stress concentrations in a weak layer below a cohesive snow slab. The developed fiber bundle models are intended to investigate failure initiation, eventually followed by rapid crack propagation in weak snow layers.

P 9.3

How much do supraglacial ice cliffs contribute to the mass-balance of glaciers? A modelling approach for the Langtang catchment, Nepalese Himalaya

Pascal Buri[1], Jakob F. Steiner[2], Evan S. Miles[3], Silvan Ragettli[4] & Francesca Pellicciotti[5]

[1] *Institute of Environmental Engineering, ETH Zurich, Stefano-Franscini-Platz 3, CH-8093 Zürich (buri@ifu.baug.ethz.ch)*
[2] *Faculty of Geosciences, Utrecht University, Heidelberglaan 2, NL-3584 CS Utrecht*
[3] *School of Geography, University of Leeds, Garstang North, UK- Leeds LS2 9JT*
[4] *hydrosolutions ltd., Lindenbachstrasse 11, CH-8006 Zurich*
[5] *Department of Geography, Northumbria University, Ellison Building, UK-Newcastle upon Tyne NE1 8ST*

Supraglacial ice cliffs are typical surface features of debris-covered glaciers worldwide, affecting surface evolution and mass balance by providing a direct ice-atmosphere interface where melt rates can be very high. Their role as windows of energy transfer suggests they may explain the anomalously high mass losses of debris-covered glaciers observed in High Mountain Asia despite the insulating debris, currently at the centre of a debated controversy.

However, their contribution to glacier mass balance has never been quantified at the glacier scale, and all inference has been obtained from extrapolating results of point-scale models or observations at selected cliffs. Here we use a 3D, physically-based backwasting model to estimate the volume losses associated with the melting and backwasting of supraglacial ice cliffs for the entire debris-covered glacier area of the Langtang catchment. We estimate mass losses for the 2014 melt season and compare them to recent values of glacier mass balance determined from geodetic and numerical modelling.

We derive cliff outlines and -topography from high-resolution stereo SPOT6-imagery from April 2014. Meteorological data to force the model are provided by automatic weather stations on- and off-glacier within the catchment. The model simulates ice cliff backwasting by considering the cliff-atmosphere energy-balance, reburial by debris and the effects of adjacent ponds.

In the melt season of 2014, cliffs' distribution and patterns of mass losses vary considerably from glacier to glacier, and we relate rates of volume loss to both glaciers' and cliffs' characteristics. Only cliffs with a northerly aspect account for substantial losses. Uncertainty in our estimates is due to the quality of the stereo DEM, uncertainties in the cliff delineation and the fact that we use a conservative approach to cliff delineation and discard very small cliffs and those for which uncertainty in topography is high.

Despite these uncertainties, our work presents the first estimate of the importance of supraglacial ice-cliffs to total glacier mass-balance, and shows that the volume lost by backwasting of ice cliffs is a non-negligible term in the total glacier mass balance of debris-covered glaciers, providing a partial explanation of the higher-than-expected mass losses of debris-covered glaciers of High Mountain Asia.

P 9.4

Mass-flux dynamics in a drifting snow wind-tunnel

Philip Crivelli[1], Enrico Paterna[1] & Michael Lehning[1,2]

[1] *WSL Institute for snow and avalanche research SLF, Flüelastrasse 11, CH-7260 Davos Dorf, Switzerland (philip.crivelli@slf.ch)*
[2] *CRYOS, School of Architecture, Civil and Environmental Engineering, Ecole Polytechnique Federal de Lausanne, CH-1015 Lausanne, Switzerland*

For the observation the snow surface changes during events of drifting snow, we introduce a Kinect sensor as a new, low-cost tool enabling relatively high resolutions both in time and space which is unmatched by most other current systems. The goal is to compare changes in the surface mass balance recorded with this new method to flux measurements based on traditional measurements such as particle counters in the saltation layer. And investigate how the dynamics of surface erosion and deposition are related to the snow particles mass-flux in the saltation layer above the snow cover.

The conducted experiments consisted of stepwise increasing wind-speeds from the threshold velocity towards strong saltation.

For the specific setting in our wind tunnel, we found that for low wind speeds, there is a balance between erosion and accumulation on the snow surface, while at higher wind speeds erosion dominates.
Furthermore we found that the mean mass flux calculated from the snow surface change correlates well with the mean mass flux in the saltation layer (r^2 = 0.93). Based on this good initial correlation we investigated different parameterizations to establish a link between the particle mass flux in the saltation layer and the dynamic of the snow surface erosion.

P 9.5

Spectral signatures of submicron scale light absorbing impurities in snow and ice using hyperspectral microscopy

Anna Dal Farra[1,2, 3,] Susan Kaspari[4], James Beach[5], Thomas D. Bucheli[6], Michael Schaepman[7], Margit Schwikowski[1,2, 3]

[1] Laboratory of Environmental Chemistry, Paul Scherrer Institute, 5232 Villigen PSI, Switzerland
[2] Department of Chemistry and Biochemistry, University of Bern, 3012 Bern, Switzerland
[3] Oeschger Centre for Climate Change Research, University of Bern, 3012 Bern, Switzerland
[4] Department of Geological Sciences, Central Washington University, Ellensburg, WA 98926, USA
[5] CytoViva, Inc., 570 Devall Drive, Suite 301, Auburn, Alabama 36832, USA
[6] Environmental Analytics, Agroscope, 8046 Zürich, Switzerland
[7] Remote Sensing Laboratories, Department of Geography, University of Zurich, Winterthurerstrasse. 190, 8057 Zurich, Switzerland

Glaciers are important sources of water in many regions, and are vital components of the Earth’s climate system. Widespread decline in glacier size has occurred in recent decades. Previous studies have suggested that along with rising temperatures, a decrease in surface albedo plays a role in their decline. Albedo is defined as the ratio of the radiant flux reflected from a unit surface area into the whole hemisphere to the incident radiant flux of hemispherical angular extent. For snow and ice light absorbing impurities (LAI) . LAI cause darkening of the snow/ice surface resulting in greater absorption of solar energy, heating of the snow/ice, and accelerated snow and glacier melt. In regions with high LAI deposition, LAI can be a larger driver of snow/ice melt than temperature. LAI include Black Caron (BC), mineral dust and organic Carbon (OC). Previous research investigating the role of LAI in albedo reduction has utilized chemical analysis to determine the relative abundances of LAI. Snow albedo models such as the Snow, Ice, and Aerosol Radiation (SNICAR) model have been widely used to determine albedo based on LAI. A key limitation of this approach is that most users utilize generic optical properties for the dust that are based on global means, and that may not accurately reflect the unique optical properties of LAI inherent to different sampling locations. Poorly constrained optical properties of LAI, particularly dust and organics, can result in differences in observed and modelled snow albedo. Advanced methods are needed to constrain the optical properties of LAI, which will improve our ability to identify the contribution of the different LAI constituents to albedo reductions and snow and ice melt.

The aim of this study is to establish a method to analyse the reflectance of LAI in environmental samples using a Hyperspectral Imaging Microscope Spectrometer (HIMS). This instrument allows the collection of hyperspectral images, in which for each pixel a spectrum is obtained. The use of HIMS is unique in measuring LAI in snow and on glacier surfaces, and has the potential to improve quantifying the contributions of different LAI classes to albedo reduction and therefore to attribute causes of snow and ice melt. We describe modifications made to HIMS to allow particle reflectance to be measured at the submicron scale. We present the results comparing reflectance spectra of various reflectance standards with the HIMS to spectra of the bulk materials obtained with a spectroradiometer (FieldSpec 3, PANalytical Analytical Spectral Devices (ASD)). Lastly, for a sample collected on Glacier de la Plaine Morte, reflectance spectra of various particles belonging to different classes of LAI were measured. These spectra provide information on how much radiation is reflected from each class of LAI and allow, taking into account their relative abundances, quantifying their relative contributions to the decrease of surface albedo on the glacier system.

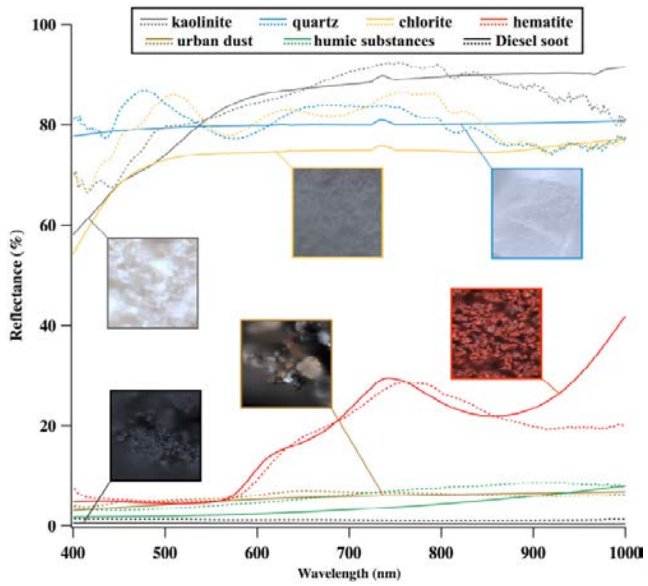

Figure 1.Reflectance spectra of the different standard materials (Diesel soot, minerals and humic substances). Dotted lines: HIMS measurements at the particle scale, solid lines: field spectroradiometer measurement of bulk samples. The images represent examples of the measured standards; the colours of the frames correspond to the spectra (humic substances are not present).

REFERENCES

Warren, S. G., and Zender, C. S.: Bounding the role of black carbon in the climate system: A scientific assessment, Journal of Geophysical Research-Atmospheres, 118, 5380-5552, 2013

Gabbi, J., Huss, M., Bauder, A., Cao, F., and Schwikowski, M.: The impact of Saharan dust and black carbon on albedo and long-term mass balance of a Alpine glacier, Cryosphere, 9, 1385-1400, 2015.

Huss, M., Voinesco, A., and Hoelzle, M.: Implications of climate change on Glacier de la Plaine Morte, Switzerland, Geogr. Helv., 68, 227-237, 2013

Kaspari, S., Painter, T. H., Gysel, M., Skiles, S. M., and Schwikowski, M.: Seasonal and elevational variations of black carbon and dust in snow and ice in the Solu-Khumbu, Nepal and estimated radiative forcings, Atmospheric Chemistry and Physics, 14, 8089-8103, 2014.

P 9.6

A model for subglacial sediment discharge and comparison with available measurments

Ian Delaney[1], Mauro A. Werder[1] & Daniel Farinotti[1,2]

[1] *Laboratory for Hydraulics, Hydrology and Glaciology (VAW), ETH-Zürich, Hönggerbergring 26, Zürich, CH 8093*
[2] *Swiss Federal Institute for Forest, Snow and Landscape Research WSL, Züricherstrasse 111, Birmensdorf, CH 8903*

Glaciers not only release water as they melt, they also erode and transport sediment from their beds. Similar to water, changes to sediment discharge from glacierized catchments has implications for those who use glaciers' resources and are affected by processes such as reservoir sedimentation. This is especially pronounced in Switzerland, where much hydropower infastructure lies close to glaciers. Although some sediment orginates from areas around the glacier that have been exposed by glacier retreat, subglacial sediment contributes greatly to material being expelled from glacierized catchments. This is because glaciers are far more effcient at transporting sediment than their fluvial counter parts. Due to the observed increases in sediment discharge from some Swiss glaciers and its effects on hydropower operations, parameterizing subglacial sediment discharge is of great importance. Implimentation of a model will help understand and predict how forthcoming hydrological shifts and glacier retreat will effect sediment discharge.

Here a 1-dimensional subglacial sediment transport model consisting of three parts is presented. A simple hydraulics model is used to establish the shear stress between the presurized meltwater and the glacier bed. This is then implemented in a sediment transport relationship. Finally, till processes including sediment exhaustion and creation of transportable sediment by processes such as quarrying are parameterized. The model is driven by surface hydrology and calibrated to measured suspended sediment and bedload data from Gornergletscher, Canton Vallis collected over the 2016 and 2017 melt seasons. Comparision with these measured data show, that the model can capture seasonal evolution of sediment transport and approximate proper quantities of sediment. However, the model has difficulties in capturing dramatic extreme events such as high sediment discharge following high precipitiation or lake drainages. Despite these short-comings, the results suggest, that the model is able to successfully parameterize subglacial sediment transport.

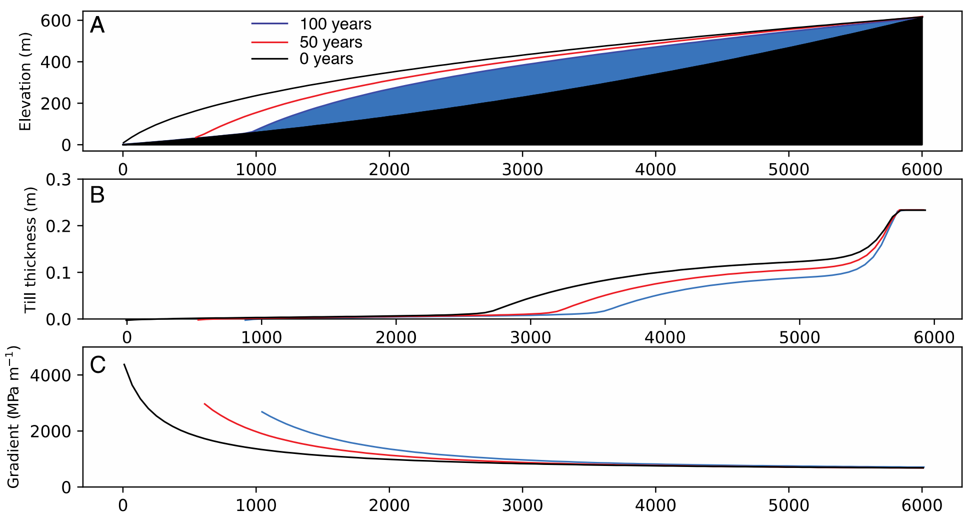

Figure 1. A) Glacier surface under three scenerios. B) Till height after 20 years of water input. C) Change in hydraulic gradient as surface evolves. Note increase erosion rate under conditions of glacier retreat (blue lines).

P 9.7

Applying the ice flow model Úa to the Alpine region: first simulations of Rhonegletscher

Simon Förster[1], Matthias Huss[1], Hilmar Gudmundsson[2]

[1] *Laboratory of Hydraulics, Hydrology and Glaciology (VAW), ETH Zürich, Hönggerbergring 26, CH-8093 Zürich (foerster@vaw.baug.ethz.ch)*
[2] *British Antarctic Survey, High Cross, Madingley Rd., Cambridge, CB3 0ET, UK*

At the end of the Little Ice Age (around 1850), glaciers in the Alps reached their last maximum extent. However, it is still uncertain what caused the preceding advance and the following retreat. Several studies have concluded that temperature alone cannot explain this behaviour. A precipitation increase of about 25% could explain the anomaly, but this is not supported by observations. Further processes have been proposed, including changes in solar radiation (due to either solar activity variations or aerosols in the atmosphere), surface impurities on ice and snow, and dynamical effects in both the atmosphere and the glaciers. We will test some of these processes in a model study and determine their relative importance by coupling the ice flow model Úa to a mass balance model.

In a first step, we are assessing the performance of Úa, which has previously been used primarily for simulations of the Greenland and Antarctic ice sheets, in the Alpine environment. Initial test simulations of Rhonegletscher between 1874 and today, driving the model with mass balance records, showed that Úa is capable of simulating the glacier›s retreat reasonably well. We now extend the simulations to between 1600 and today using a simple mass balance based on different temperature and precipitation reconstructions, e.g. Casty et al. (2005), the PAGES2k database, and Pauling et al. (2006). To validated these simulations, we compare them with observations of glacier length change, flow velocity, and geometry change.

REFERENCES

Casty, C., Wanner, H., Luterbacher, J., Esper, J., & Böhm, R. 2005: Temperature and precipitation variability in the European Alps since 1500. International Journal of Climatology, 25, 1855-1880. doi:10.1002/joc.1216.
PAGES2k Consortium. 2017: A global multiproxy database for temperature reconstructions of the Common Era. Scientific Data, 4, 170088. doi:10.1038/sdata.2017.88.
Pauling, A., Luterbacher, J., Casty, C., & Wanner, H. 2006: Five hundred years of gridded high-resolution precipitation reconstructions over Europe and the connection to large-scale circulation. Climate Dynamics, 26, 387-405. doi:10.1007/s00382-005-0090-8.

P 9.8

From the clouds to the ground – snow precipitation vs. snow accumulation patterns

F. Gerber[1,2], N. Besic[3,4], V.Sharma[1], R. Mott[2], M. Gabella[4], U. Germann[4], Y. Bühler[2], M. Marty[5], A. Berne[3], and M. Lehning[1,2]

[1] Laboratory of Cryospheric Sciences (CRYOS), School of Architecture and Civil Engineering, École Polytechnique Federale de Lausanne, Bâtiment GR, Station 2, CH-1015 Lausanne (gerberf@slf.ch)
[2] WSL Institute for Snow and Avalanche Research SLF, Flüelastrasse 11, CH-7260 Davos Dorf
[3] Environmental Remote Sensing Laboratory (LTE), School of Architecture and Civil Engineering, École Polytechnique Federale de Lausanne, Bâtiment GR, Station 2, CH-1015 Lausanne
[4] Radar, Satellite, Nowcasting Department, MeteoSwiss, Via ai Monti 146, CH-6605 Locarno-Monti
[5] Swiss Federal Institute for Forest, Snow and Landscape Research (WSL), Zürcherstrasse 111, 8903 Birmensdorf

Knowledge about snow distribution and snow accumulation patterns is important and valuable for different applications such as the prediction of seasonal water resources or avalanche forecasting. Furthermore, accumulated snow on the ground is an important ground truth for validating meteorological and climatological model predictions of precipitation in high mountains and polar regions. Snow accumulation patterns are determined by many different processes from ice crystal nucleation in clouds to snow redistribution by wind and avalanches. In between, snow precipitation undergoes different dynamical and microphysical processes, such as ice crystal growth, aggregation and riming, which determine the growth of individual particles and thereby influence the intensity and structure of the snowfall event. In alpine terrain the interaction of different processes and the topography (e.g. lifting condensation and low level cloud formation, which may result in a seeder-feeder effect) may lead to orographic enhancement of precipitation. Furthermore, the redistribution of snow particles in the air by wind results in preferential deposition of precipitation. Even though orographic enhancement is addressed in numerous studies, the relative importance of micro-physical and dynamically induced mechanisms on local snowfall amounts and especially snow accumulation patterns is hardly known.

To better understand the relative importance of different processes on snow precipitation and accumulation we analyze snowfall and snow accumulation between January and March 2016 in Davos (Switzerland). We compare MeteoSwiss operational weather radar measurements on Weissfluhgipfel to precipitation patterns in very high resolution Weather Research and Forecasting (WRF) model simulations. Snow precipitation estimated from the radar and meteorological parameters from our WRF simulations are in reasonable agreement with measurements from automatic weather stations close to the weather radar. Deriving snow accumulation based on radar data is challenging as the close-ground precipitation patters cannot be resolved by the radar due to shielding and ground clutter in highly complex terrain. Nonetheless, radar measurements show distinct patterns of snowfall and accumulation, which may be the result of orographic enhancement. Furthermore, large-scale radar snow accumulation patterns show a snowfall gradient consistent with the prevailing wind direction. The general gradient is partially represented by the large-scale WRF simulations. However, WRF generally overestimates precipitation, but is able to represent larger scale spatial precipitation patterns and an elevation gradient. Additionally, a spatially continuous snow accumulation map derived from airborne digital sensing (ADS) snow height for the area of Dischma valley in the vicinity of the weather radar is available. Overall, snow height ground measurements show a distinct pattern of much smaller scale structures, which are a sign of snow redistribution by wind.

P 9.9

Measuring the elastic modulus of snow

Bastian Gerling[1], Henning Löwe[1] & Alec van Herwijnen[1]

[1]*WSL Institute for Snow and Avalanche Research SLF, Flüelastrasse 11 , 7260 Davos, Switzerland (bastian.gerling@slf.ch)*

The elastic modulus is a fundamental mechanical property of snow and key for the interpretation of seismic measurements, assessment of slope stability or development of constitutive models. However literature values scatter by orders of magnitude due to visco-plastic peculiarities of ice and microstructural variability. Hitherto still no cross-validated measurement exists.

To this end we employ P-wave propagation experiments under controlled laboratory conditions on decimeter-sized snow specimen prepared from artificial snow and subjected to isothermal sintering, to cover a considerable range of densities (170 − 370 kgm^{-3}). The P-wave modulus was estimated from wave propagation speeds in transverse isotropic media and compared to microstructure-based finite element calculations (FEM) facilitated by X-ray tomography imaging of sub-sample microstructures. Heterogeneities and size differences between acoustic and FEM sample volumes were characterized by SnowMicroPen measurements, yielding an elastic modulus as a by-product. The moduli derived from the acoustic and FEM method are in very good agreement (R^2 = 0.99) over the entire range of densities covering values from 10 − 340 Mpa. A remaining bias (24 %) between both methods can be explained by layer heterogeneities which systematically reduce the estimates from the acoustic method.

The consistency of these first-principle methods supports the validity of long-standing, published FEM moduli for various snow types and opens non-destructive routes to time-resolved elasticity measurements during fast sintering.

P 9.10

Analysis of Borehole Measurements and Determination of the Basal Sliding Velocity of Rhonegletscher

Dominik Gräff[1], Fabian Walter[1]

[1] *Laboratory of Hydraulics, Hydrology and Glaciology, ETH Zürich, Switzerland, graeff@vaw.baug.ethz.ch*

Basal sliding of glaciers and the ratio between the sliding velocity at the bed-ice interface and the glacial surface motion is of critical importance for ice flow models. Although the surface velocities of glaciers can be measured easily by satellite, GPS or classic geodetic methods, the sliding velocity at the ice-bedrock interface is difficult to determine experimentally.

During a field campaign on the tounge of Rhonegletscher in August 2017, we drilled three boreholes from the glacier surface to the bed by using a hot water drill. For one borehole, fine-grained sediments that were swirled up by the turbulent outflow of the hot water drill, settled on the bottom of the borehole and thus made it possible to observe the glacier bed visually with a borehole camera. Pictures of the glacier bed taken with the borehole camera show a hard bedrock partially covered by a thin till layer of a few centemeters thickness. Isolated and repeated measurements within a ten-day period allow estimation of basal sliding velocity and sliding direction of the glacier.

Here we present the deduced sliding velocity vector together with data from surface motion measurements at four differential GPS stations in the neighborhood of the borehole. We discuss these results in terms of general glacier dynamics and offer an outlook on future applications of our approach.

P 9.11

A first attempt to model region-wide glacier surface mass balances in the Karakoram: findings and future challenges

Alexander R. Groos[1], Christoph Mayer[2], Claudio Smiraglia[3], Guglielmina Diolaiuti[3] & Astrid Lambrecht[2]

[1] *Institute of Geography, University of Bern, Hallerstrasse 12, CH-3012, Bern (alexander.groos@giub.unibe.ch)*
[2] *Commission for Geodesy and Glaciology, Bavarian Academy of Sciences and Humanities, Alfons-Goppel Straße 11, D-80539, München*
[3] *Dipartimenta di Scienze della Terra, Università degli Studi di Milano, Via Mangiagalli 34, I-20133, Milano*

In contrast to the central and eastern part of High Mountain Asia (HMA), no extensive glacier mass loss has been observed in the Karakoram during previous decades. However, the potential meteorological and glaciological causes of the so-called Karakoram Anomaly are manifold and still under debate. This study introduces and presents a novel glacier Surface Mass Balance Model (glacierSMBM) to test whether the characteristic regional mass balance pattern can be reproduced using recent field, remote-sensing and reanalysis data as input. A major advantage of the model setup is the implementation of the non-linear effect of supra-glacial debris on the sub-surface ice melt. In addition to a first assessment of the annual surface mass balance from 1st August 2010 until 31st July 2011, a sensitivity analysis was performed to investigate the response of Karakoram glaciers to recent climate change and to identify meteorological and glaciological processes that promote stable mass balances. The mean glacier mass balance for the Karakoram during the observation period is -0.92 m w.e. (water equivalent) a-1 and corresponds to an annual melt water contribution of ~12.66 km3. Data inaccuracies and the neglected process of snow redistribution from adjacent slopes in the accumulation area are probably responsible for the negative bias in the model output. Despite the general offset between mass gain and mass loss, the model captures the characteristic features of the anomaly and indicates that positive glacier mass balances are mainly restricted to the central and northeastern part of the mountain range. From the evaluation of the sensitivity analysis it can be concluded that the complex glacier response in the Karakoram is not the result of a single driver, but related to a variety of regional peculiarities such as the favourable meteorological conditions, the extensive supra-glacial debris and the timing of the main precipitation season.

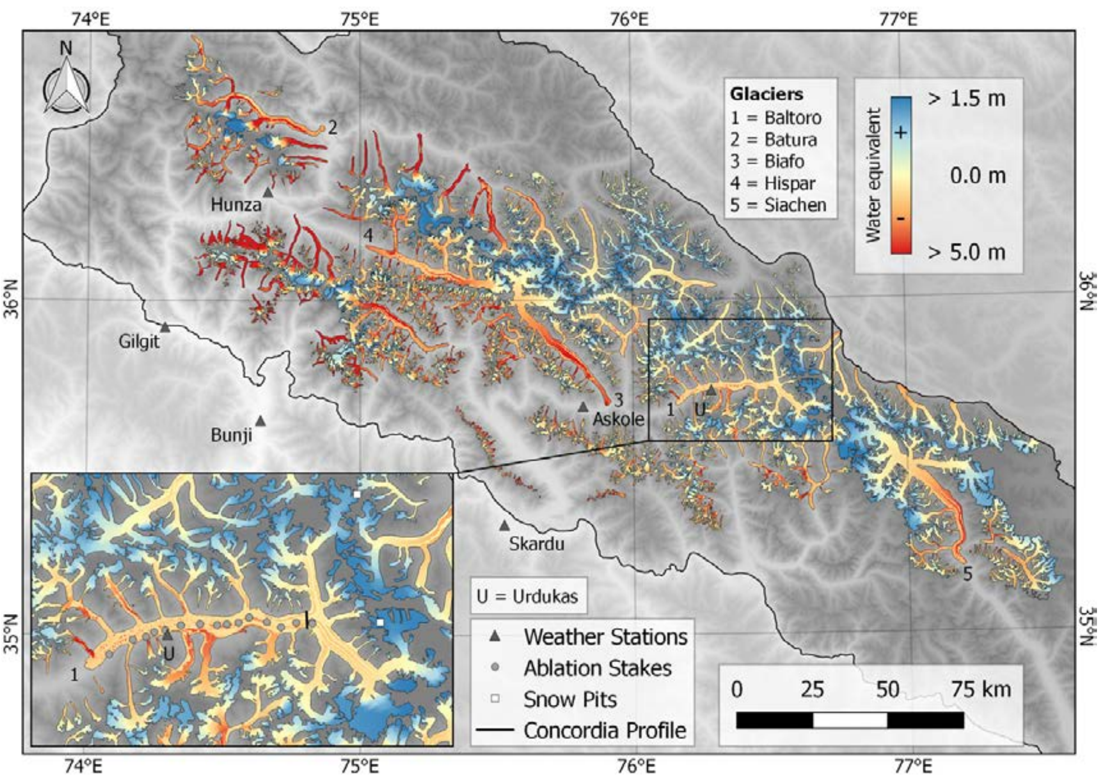

Figure 1. Modelled surface mass balances from 1st August 2010 until 31st July 2011 for all Karakoram glaciers included in our inventory. The spatial mass balance pattern of the debris-covered Baltoro glacier is highlighted in more detail in the lower left box.

P 9.12

The European Snow Booklet

Anna Haberkorn[1], Charles Fierz[1], Christoph Marty[1], Giovanni Macelloni[2], Samuel Morin[3], Wolfgang Schöner[4]

[1] WSL Institute for Snow- and Avalanche Research SLF, Flüelastrasse 11, CH-7260 Davos Dorf (anna.haberkorn@slf.ch)
[2] Institute of Applied Physics, Nello Carrara - IFAC, Via Madonna del Piano 10, IT-50019 Sesto Fiorentino
[3] Meteo France - CEN, 1441 rue de la piscine, FR-38400 St Martin d'Heres
[4] Department of Geography and Regional Science, University of Graz, Heinrichstrasse 36, AT-8010 Graz

Practitioners and researchers worldwide have developed different best practices for snow-related in-situ measurements. However, these practices lack harmonization and thus hamper further developments, for example, of numerical weather prediction models, remote sensing applications and homogenization of long-term records needed for hydrological and climatological applications. Indeed, homogenizing long-term data series of snow depth are scientifically challenging mostly because of the marked spatial variability of this essential climate variable. Another aspect is the determination of snow cover onset and disappearance in order to assess changes in the duration of the snow cover. Beside the need of harmonizing practices across the borders, there is a strong interest from both the operational and the researcher communities to rely on data that can be interpreted globally the same way.

The European Union COST action ES1404 "HarmoSnow" aims at assessing and harmonizing practices and standards applied to snow measurements, building a better connection between snow measurements and models, between snow observers, researchers and forecasters, for the benefit of various stakeholders and the entire society. Since we not even know which European countries operationally measure snow, not to mention which snow variables, "HarmoSnow" produces a "European Snow Booklet". The main objective of this book of reference is an inventory of basic snow measurements realised in each European country, as well as an evaluation of the methods used and on the data availability of these measurements. In addition, best practice recommendations on snow cover monitoring currently developed in close collaboration with WMO's Global Cryosphere Watch will complete the "European Snow Booklet".

P 9.13

Properties of flowing snow – measurements in a rotating drum

Kilian Heil[1], Roland Kaitna[1], Jan-Thomas Fischer[2] & Ingrid Reiweger[1]

[1]University of Natural Resources and Life Sciences (BOKU), Department of Civil Engineering and Natural Hazards, Peter-Jordan-Strasse 82, A-1190 Vienna (ingrid.reiweger@boku.ac.at)
[2]Austrian Research Centre for Forests (BFW), Department of Natural Hazards, Rennweg 1, A-6020 Innsbruck

Snow avalanches represent a severe natural hazard in snow covered, mountainous regions. The flow behaviour and thus destructive potential of snow avalanches depend, among other things, on the physical properties of the flowing snow. However, the snow properties and consequently also flow behaviour change over time as the snow travels downwards along the avalanche path. Recent field investigations aimed to study the effect of physical properties of snow on the flow behaviour and found significant changes at snow temperatures above -2°C. We aim to measure snow properties and their influence on flow behaviour under laboratory-like conditions and present an experimental setup of flowing snow in a rotating drum. With our vertically rotating drum with a diameter 2.5 m and a rectangular cross section of 0.45 m, we created a continuous movement of flowing snow. Our experimental set-up allowed us to measure the temperature of the snow and the ambient air, the flow height, the basal normal stress, and the volumetric liquid water content of the snow. We conducted thirteen continuous flow experiments with air temperature ranging from -5°C to +10°C and rotational speeds ranging from 5.2 rpm to 15.2 rpm. Considerable changes in the flow behaviour of the snow such as the onset of granulation and the formation of free liquid water could be observed. Granulation was particularly pronounced at temperatures above -1°C. Moreover, the experiments showed that the temperature of the snow could significantly exceed the ambient air temperature if the flow moved fast. Concluding, we feel that the rotating drum constitutes an applicable technique for investigating the flow behaviour of snow. Future research could concentrate on a comprehensive consideration of the energy balance of the flow to enhance physical modelling and improve avalanche simulation programs.

P 9.14

Modelled and reconstructed ice thickness of the Rhine Glacier during the Last Glacial Maximum

Michael Imhof[1], Guillaume Jouvet[1], Julien Seguinot[1], Denis Cohen[2], Martin Funk[1]

[1] Laboratory of Hydrauclics, Hydrology and Glaciology, ETH Zürich, Hönggerbergring 26, CH-8093 Zürich (imhof@vaw.baug.ethz.ch)
[2] Department of Earth and Environmental Science, New Mexico Tech, Socorro, NM, 87801, USA

Despite available geological evidence, only a few ice flow modelling studies have been done on the European Alpine ice cap during the Last Glacial Maximum (LGM). These studies show a good agreement with maximum glacier tongue extent reconstructed from moraines. However, the ice flow models systematically overestimate the ice thickness by up to 800 m when compared to reconstructions based on trimlines, unless extremely low precipitation rates are assumed. This discrepancy between model results and geological reconstructions is calling for a more detailed exploration of model sensitivity to uncertain ice physical parameters.

In this study, we investigate the effect of model parameters related to basal motion of the Parallel Ice Sheet Model (PISM) at the Rhine Glacier. We evaluate whether a set of realistic parameters can reproduce the thickness of the Rhine Glacier at the LGM reconstructed from trimlines, without involving extremely low precipitation rates. PISM is a state-of-the-art ice sheet model, that computes the extent and thickness of ice and its thermal and dynamic state, for given initial basal topography and climate forcing. Since PISM is based on simplified ice mechanics (combining shallow ice approximation and shallow shelf approximation), it is computationally inexpensive, making it possible to perform a large number of simulations representing the evolution of the Rhine Glacier during the last 35,000 years of the Würm ice age.

We find that the basal motion is playing a minor role around the highest peaks in the accumulation zone because the ice is mostly cold based there. The piedmont lobes and large Alpine valleys, however, had mostly tempered basal conditions and basal motion plays a key role there. We suggest that trimlines mapped in the Rhine valley may instead depict a transition zone between temperate and cold ice, or characterise a different period than the LGM.

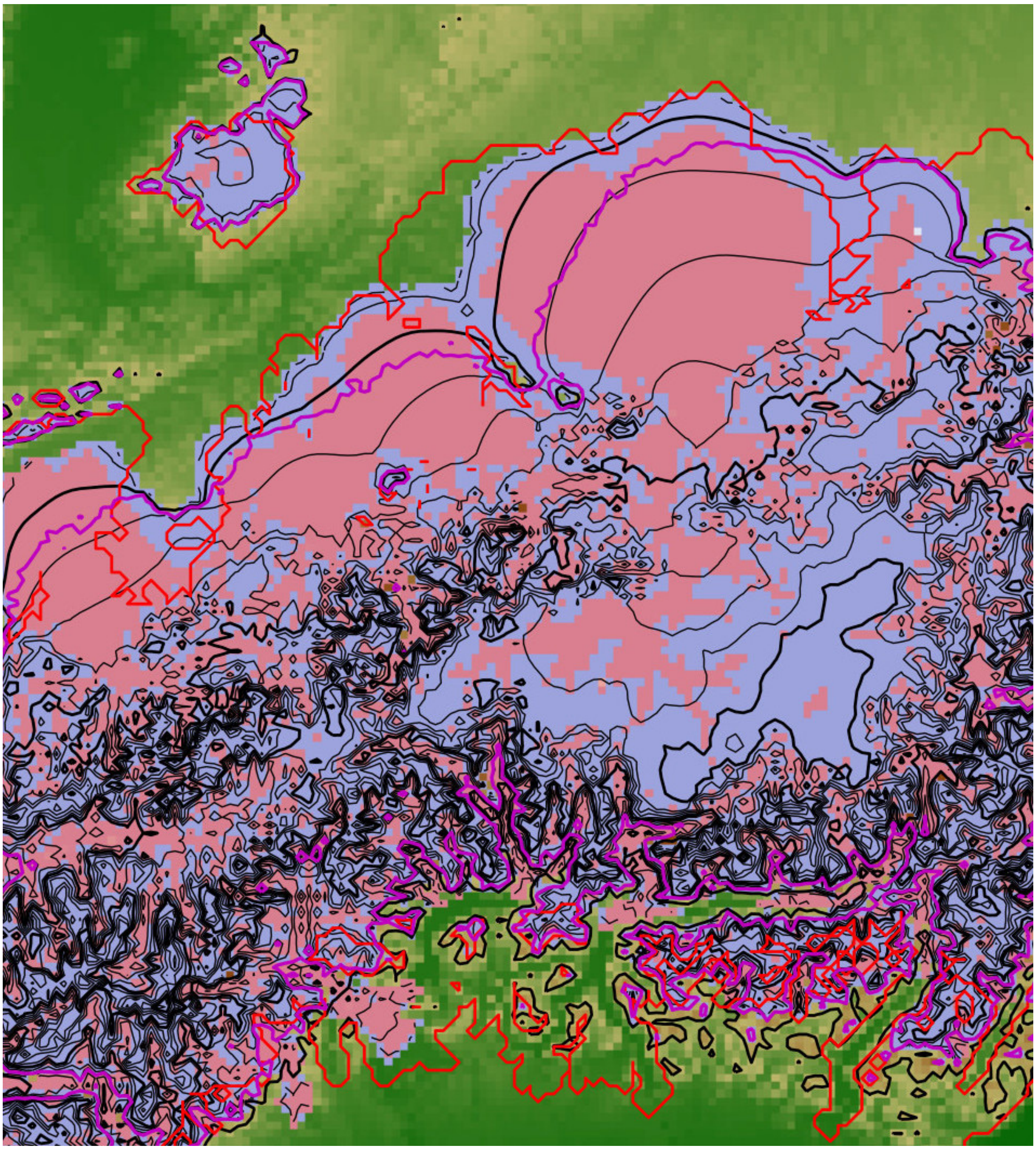

Figure 1: Modelled ice extent in the Rhine basin 24 ka ago. Red indicates warm based ice while blue indicates cold based ice. The red line represents the reconstructed ice margin and purple the equilibrium line. Thick and thin black lines have an elevation spacing of 1000 m and 200 m respectively.

P 9.15

Stochastic subglacial hydrology model for water pressure and mass transport data assimilation.

Inigo Irarrazaval[1], Gregoire Mariethoz[1] & Frederic Herman[1]

[1] *Institute of Earth Surface Dynamics , Faculty of Geosciences and Environment, University of Lausanne. UNIL-Mouline, CH-1015, Lausanne. (inigo.irarrazavalbustos@unil.ch)*

Glacier-bedrock interface plays an important role in understanding glacier dynamic processes such as glacier motion, erosion processes and catchment hydrology, as well as potential hazards such as glacial outburst floods (Benn and Evans, 2010). In general, the subglacial drainage system, made of channelized and distributed hydraulic pathways at the base of the glacier, is not directly accessible and measurable. In addition, the transient processes of melt, freezing and the advance of the glacier make it a very complex system to study. Numerical models that aiming to represent the physics of this system have been built, however, existing models require to know a number of physical parameters that are usually impossible to uniquely determine based on the available data (Flowers 2015).

This work investigates, for the first time, the use of inverse geostatistical modeling for identifying inaccessible subglacial features. The aim is to assimilate observations coming from boreholes (water pressure) and breakthrough curves from tracer experiments in moulines, and retrieve the model parameters values and channel geometries that are able to match the observations.

The inversion framework consists three steps carried out iteratively:

- First, generate subglacial features (discrete channels and a distributed system) using a combination of stochastic and physics-based processes;
- Second, compute the water pressure and mass transport in the system using a finite element groundwater model (Cornaton 2007);
- Third, using a likelihood function, compare the pressure and mass transport outputs with the observations, and update the model parameters for the next iteration.

When convergence is reached the probability distribution of the model parameters is retrieved.

The model is set up for a synthetic ice sheet under different recharge scenarios, and constrained by different number of water pressure observations from boreholes and tracer tests. By comparing the different cases, it is possible to assess the sensitivity of the model parameters and to quantify the uncertainty reduction in the characterization of the subglacial system when adding more observations.

The proposed methodology is able to represent and identify the type of connected patterns that drive subglacial dynamics and allows conditioning to observed data. As such, this work is a step towards a better understanding and a rigorous assessment of parameters uncertainty in subglacial modeling.

REFERENCES

Cornaton, F. 2007: Ground water : A 3-d ground water and surface water flow, mass transport and heat transfer finite element simulator. Internal report, University of Neuchâtel.

Flowers, G. E. 2015: Modelling water flow under glaciers and ice sheets. Proceedings of the Royal Society A: Mathematical, Physical and Engineering Sciences, 471, 20140907-20140907.

Benn, D. I., and Evans, D. J. A., 2010, Glaciers and Glaciation., London, Hodder Education, 802 p.

P 9.16

Sun2Ice: Monitoring calving glaciers from solar-powered UAVs

Guillaume Jouvet[1], Thomas Stastny[2], Philipp Oettershagen[2], Michael Hugentobler[2], Thomas Mantel[2], Amir Melzer[2], Yvo Weidmann[1], Martin Funk[1], Roland Siegwart[1]

[1] *ETH Zürich, VAW, Hönggerbergring 26, 8093 Zürich (jouvet@vaw.baug.ethz.ch)*
[2] *ETH Zürich, ASL, Leonhardstrasse 21, 8092 Zürich*

Here we present the first outcomes of ETHZ‘s Sun2Ice project, which aims to use a state-of-the-art, highly-optimized, solar-powered Unmanned Aerial Vehicle (UAV), AtlantikSolar (Oettershagen, 2017), for long-range, and multi-day monitoring of calving glaciers in the Arctic. The „midnight sun“ in polar summer time offers unique conditions for solar-powered flights, including potentially energetically perpetual flight, consequently enabling frequent, high-resolution and large-scale glacier surveys. In Sun2Ice, this cutting-edge technology is dedicated to the monitoring of iceberg calving (Jouvet, 2017), a still poorly understood process which plays a major role in the observed retreat of many ocean-terminating glaciers. The main achievement of Sun2Ice‘s 2017 fieldwork was the undertaking of the first-ever autonomous, solar-powered flights of a UAV in a polar region, including a flight of more than 12 hours duration, and the survey of the calving front of Bowdoin Glacier, Northwest Greenland, see Fig. 1. This monitoring revealed the opening of a major crack, which led to a major calving event one week later. This presentation will focus on the technical challenges, the glaciological outcomes, and the potential of using such a technology for monitoring the Cryosphere with a spatial and temporal resolution not achievable by satellite remote sensing.

Figure 1. AtlantikSolar on the way to Bowdoin Glacier on the 3rd of July 2017.

REFERENCES

Jouvet, G., Weidmann, Y., Seguinot, J., Funk, M., Abe, T., Sakakibara, D., Seddik, H. & Sugiyama, S. 2017: Initiation of a major calving event on the Bowdoin Glacier captured by UAV photogrammetry, The Cryosphere, 11, 911-921.

Oettershagen, P., Melzer, A., Mantel, T., Rudin, K., Stastny, T., Wawrzacz, B., Hinzmann, T., Leutenegger, S., 2017: Design of small hand-launched solar-powered UAVs: From concept study to a multi-day world endurance record flight. Journal of field robotics.

P 9.17

Investigating firn changes of Abramov glacier, Pamir Alay

Marlene Kronenberg[1], Horst Machguth[1,2], Warren Stainbank[1], Martin Hoelzle[1]

[1] *Department of Geosciences, University of Fribourg, Chemin de Musée 4, CH-1700 Fribourg (marlene.kronenberg@unifr.ch)*
[2] *Department of Geography, University of Zurich, Winterthurerstrasse 190, CH-8057 Zürich*

Despite their effects on glacier mass balance, processes within the firn cover of mountain glaciers such as melt water refreezing are poorly explored. Therefore, understanding and modelling the evolution of glacier firn are regarded as an asset to overcome numerous uncertainties in mass balance studies. Moreover, long-term simulations of firn processes may provide valuable information in the context of climate change.

In our study we investigate firn changes of the Abramov glacier, located in the Pamir Alay mountain range of Central Asia. To simulate and understand the firn evolution of Abramov glacier an existing multi-layer snow model coupled to a surface energy balance model (van Pelt et al. 2012) is iteratively adapted and applied. The model is forced from meteorological measurements from local weather stations. Furthermore, we apply re-analysis data to fill gaps in the measurements and to extend our simulations beyond the duration of direct measurements (2011 to present). Model calibration and validation at various time steps will on one hand rely on (i) ongoing (glaciological) and (ii) planned measurements including the drilling of firn cores to measure firn properties such as stratigraphy, density and temperatures. On the other hand (iii) a unique data set of historical data including accumulation rates from several firn cores drilled in the 1970s will be used. Furthermore, we aim on reproducing expected changes between firn stratigraphies, temperatures and densities measured in the 1970s (Figure 1) and todays firn properties at the same locations.

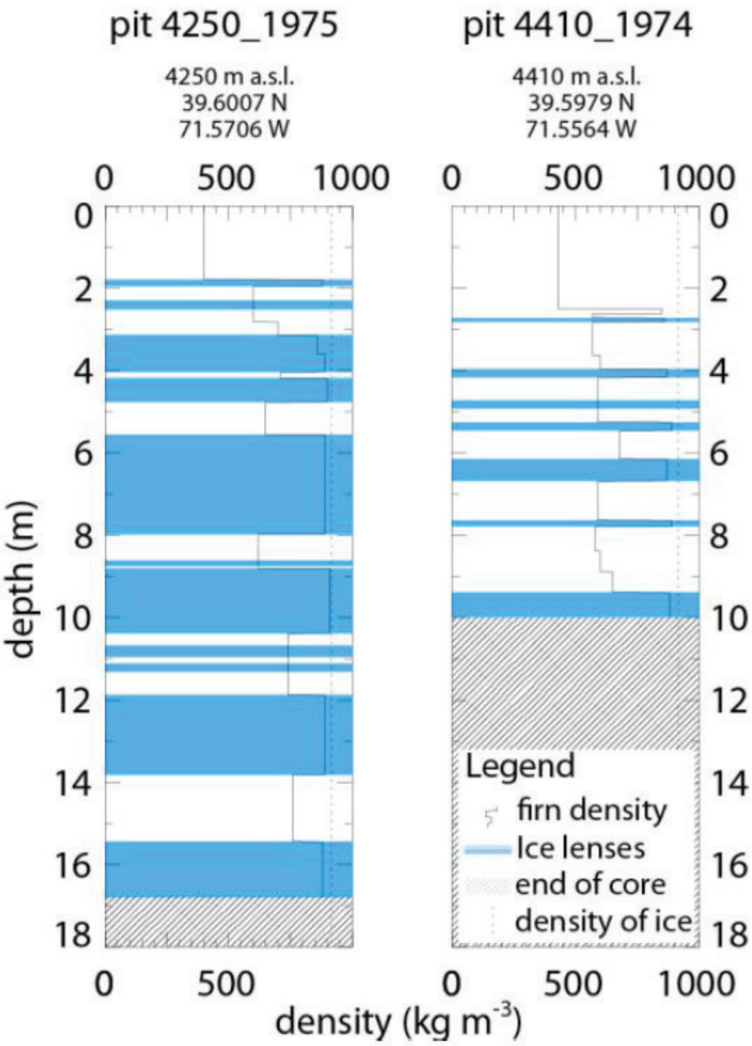

Figure 1. Two examples of firn stratigraphy and density measured in 1974/75 deep snow pits on Abramov glacier (source: Suslov & Krenke 1980, stratigraphy is simplified compared to original source).

REFERENCES

Suslov, V. F. & Krenke, A. N. 1980. Lednik Abramova: Alajskij Khrebet (Abaramov Glacier: Alay Range). Gidrometeoizdat.

van Pelt, W. J. J., Oerlemans, J., Reijmer, C. H., Pohjola, V. A., Pettersson, R. & van Angelen, J. H. 2012. Simulating melt, runoff and refreezing on Nordenskiöldbreen, Svalbard, using a coupled snow and energy balance model. The Cryosphere, 6, 641–659.

P 9.18

Cryospheric Monitoring and Prediction Online (”CRAMPON”) – a first version

Johannes Landmann[1,2], Matthias Huss[1,3], Daniel Farinotti[1,2]

[1] *Versuchsanstalt für Wasserbau, Hydrologie und Glaziologie (VAW), Swiss Federal Institute of Technology (ETH), Hönggerbergring 26, CH-8093 Zürich (landmann@vaw.baug.ethz.ch)*
[2] *Eidgenössische Forschungsanstalt für Wald, Schnee und Landschaft (WSL), Zürcherstrasse 111, CH-8903 Birmensdorf*
[3] *Département des Géosciences, Université de Fribourg, Chemin du Musée 4, CH-1700 Fribourg*

Under the impacts of climate change, the present and future potential of energy production from water resources in mountainous environments is crucial. In Alpine regions, glacial runoff often plays a significant role in the hydrological budget. Knowledge about glacier mass balance and runoff can therefore be critical. In situ mass balance measurements, however, are demanding in terms of both time and manpower, and are thus not always available.

The “Cryospheric Monitoring and Prediction Online” project (CRAMPON) addresses this difficulty and aims at developing a model-based, near real-time glacier monitoring and prediction platform for Swiss glaciers. At the moment, the operational modeling workflow relies on meteorological analyses, whilst field-based data from the Glacier Monitoring Switzerland (GLAMOS) program, elevation changes from Fischer et al. (2015) and multitemporal Digital Elevation Models (DEMs) from the Swiss Forest Inventory (Ginzler & Hobi 2015) are used for calibration and validation. In a next step, we additionally plan to assimilate satellite data as in situ constraints into the workflow.

The basis for the modeling infrastructure and parts of the preprocessing is the Open Global Glacier Model (OGGM; Maussion et al. 2017). We extend OGGM with a workflow to digest operational high-resolution, daily meteorological grids and refine the model in order to address regional/local modeling needs.

Workflow uncertainty is addressed through variation of model parameters within given thresholds (e.g. Huss & Fischer 2016, Farinotti et al. 2012) as well as through considering uncertainty of the input DEMs, elevation changes and meteorological data. In this manner we are able to provide ensemble-like results for translating meteorological forcing into mass change. The ensemble of realizations is used to estimate a probability distribution of the model results at any time step. The median serves as the most likely predictor.

Our glacier mass balance calculations will be made publicly available on a web portal which will include (a) a “mass balance status map” displaying the current state of every glacier with respect to the long-term average and (b) the temporal evolution of the current mass balance year with respect to long-term conditions (Figure 1).

The work results in an operational data assimilation workflow capable of providing near-real time information on glacier mass balance. We expect this will enable a better management of water resources and hydropower operations.

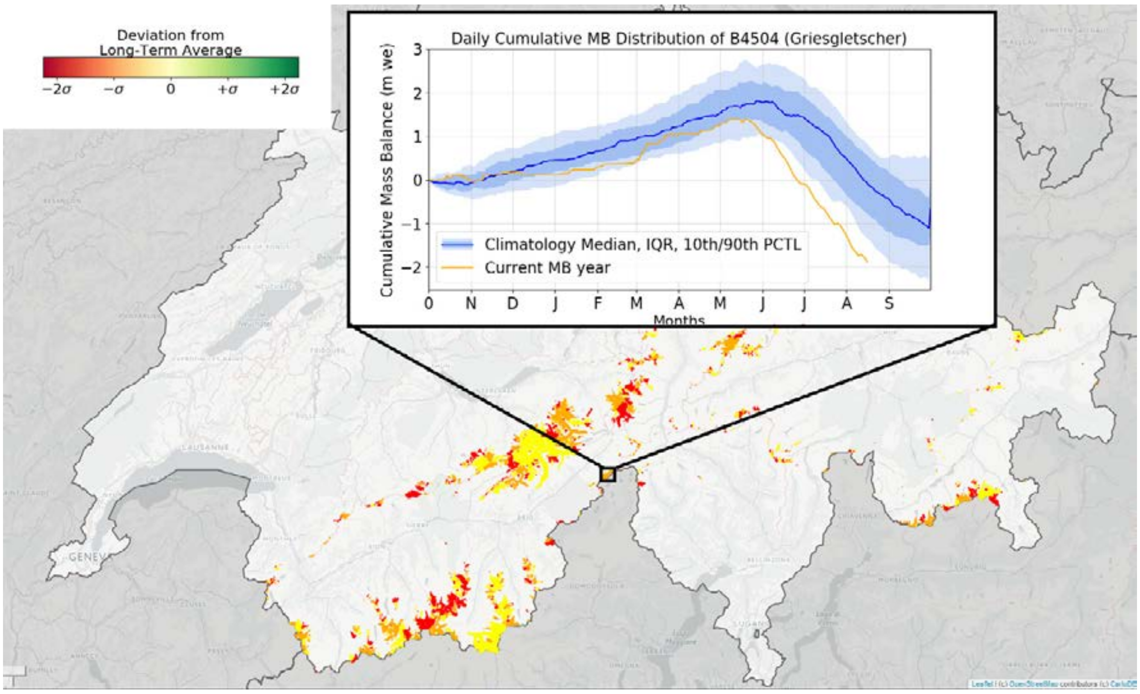

Figure 1. Preview of the anticipated web portal. The illustration shows a preview of a status map for Switzerland as well as a current mass balance figure for Griesgletscher as of August 15th in the mass balance year 2016/2017.

REFERENCES

Farinotti, D., Usselmann, S., Huss, M., Bauder, A. & Funk, M. 2012: Runoff evolution in the Swiss Alps: projections for selected high-alpine catchments based on ENSEMBLES scenarios, Hydrological Processes, 26, 1909-1924.

Fischer, M., Huss, M. & Hoelzle, M. 2015: Surface elevation and mass changes of all Swiss glaciers 1980–2010, The Cryosphere, 9, 525-540.

Ginzler, C. & Hobi, M. 2015: Countrywide Stereo-Image Matching for Updating Digital Surface Models in the Framework of the Swiss National Forest Inventory, Remote Sensing, 2015, 7, 4343-4370.

Huss, M. & Fischer, M. 2016: Sensitivity of Very Small Glaciers in the Swiss Alps to Future Climate Change, Frontiers in Earth Science, 4, 1-17.

Maussion, F., Rothenpieler, T., Marzeion, B., Landmann, J., Oesterle, F., Jarosch, A., Recinos, B., & Vlug, A. 2017: Oggm/oggm: v0.1.1. doi: 10.5281/zenodo.292630

P 9.19

Glaciers of Patagonia in 2016: A new inventory from Landsat 8 and the TanDEM-X DEM

Raymond Le Bris, Frank Paul[1]

[1] *Department of Geography, University of Zurich, Switzerland, (raymond.lebris@geo.uzh.ch)*

A recent study revealed that glaciers in Northern Patagonia, including the larger ones, have shown a dramatic shrinkage over the past three decades. Consequently, the landscape is changing rapidly, glacier fore-fields grow and new and / or growing lakes can often be found where glacier ice had been a decade ago. These rapid changes require repeating glacier inventories more frequently than elsewhere. Unfortunately, adverse weather conditions with clouds and seasonal snow remaining at high elevations typically allow only regional inventory updates. In March 2016, however, near cloud free Landsat 8 scenes were acquired under near-optimal snow conditions covering the entire region from Mt. Tronador to the Gran Campo Nevado (GCN) ice cap.

This study presents the results of a new glacier inventory for entire study region, largely based on Landsat 8 OLI scenes acquired in March 2016. The region encompasses more than 7000 glaciers larger than 0.05 km^2 and covering about 20650 km^2 of ice. The study also extends on currently used methods for glacier classification. In particular, the outlines for 2016 are derived from the 15 m resolution panchromatic band of Landsat 8 and two different thresholds are applied to the band ratio for improved mapping of ice in shadow. The new TanDEM-X DEM is used to derive drainage divides as well as topographic parameters, and lakes and other water surfaces are classified automatically considering DEM information. We also utilize Sentinel-2 images acquired in February 2017 for intercomparsion and correction of remaining seasonal snow in the northern and southern part of the study region. Comparison with glacier extents being currently available in the RGI 6.0 (from around 2000) reveal both a massive shrinkage of glaciers and a huge overestimation of glacier area in the RGI due to inclusion of seasonal snow, in particular for small glaciers being located at high elevations.

P 9.20

Seismic azimuthal anisotropy in crevasse fields

Fabian Lindner[1] , Gabi Laske[2] , and Fabian Walter[1]

[1] *Laboratory of Hydraulics, Hydrology and Glaciology, ETH Zürich*
[2] *Institute of Geophysics and Planetary Physics, Scripps Institution of Oceanography, UC San Diego, USA*

Crevasses and englacial fracture networks route meltwater from a glacier's surface to the subglacial drainage system and thus strongly influence glacial hydraulics. However, rapid frac- ture growth may also lead to sudden (and potentially hazardous) structural failure of unstable glaciers and ice dams, rifting of ice shelves, or iceberg calving.

Here, we use passive seismic recordings from Glacier de la Plaine Morte, Switzerland, to investigate the englacial fracture network. Located in the Bernese alps and bordering the canton of Valais, Glacier de la Plaine Morte is the largest plateau glacier in the European Alps. The annual drainage of an ice-marginal lake gives rise to numerous icequakes, thereby demonstrating the interplay between hydraulics and fracturing. The majority of these naturally occurring events exhibits dispersed, high-frequency Rayleigh waves at about 10 Hz and higher. A wide distribution of events allows us to study azimuthal anisotropy of englacial seismic velocities in regions of preferentially oriented fractures.

Results from beamforming applied to a 100m-aperture array show strong (up to ≈ 9%) azimuthal anisotropy of Rayleigh wave velocities. We find that the fast direction coincides with the observed surface strike of the fractures and that anisotropy is strongest for high-frequency (around 30 Hz) Rayleigh waves that are sensitive only to the uppermost (few tens of meters) part of the glacier. Whereas ice bodies are often assumed to resemble homogeneous media, our results demonstrate that even comparatively narrow crevasses (few tens of decimeters wide at the surface) considerably impact seismic wave propagation.

P 9.21

A new parametrization and minimal model for glacier calving

Martin P. Lüthi, Rémy Mercenier, Andreas Vieli[1]

[1]*Geographical Institutet, University of Zurich, Winterthurerstr. 190, CH-8057 Zurich (martin.luethi@geo.uzh.ch)*

The iceberg calving process influences the geometry of a tidewater glacier, and is in turn controlled by the terminus geometry through the stress field which controls damage and fracture of the ice. A simple parametrization of the stress field at the glacier terminus is obtained from the results of a Finite Element model with varying water depths. Using this stress field in an isotropic damage evolution equation yields calving rates in dependence of calving front thickness and water depth. These parametrized calving rates compare favorably with observations, and extend well established parametrizations. The proposed calving parametrization is easy to implement in numerical ice sheet models. Using these parametrized calving rates in a minimal calving model allows us to analyze the intricate feedbacks of the calving process, reproduce observed tidewater glacier dynamics, and to analyze the stability of glacier termini.

P 9.22

Glaciomarine Sedimentation and Submarine Landforms in Admiralty Bay, South Shetland Islands

Fabio Magrani[1,2], Arthur Ayres-Neto[2], Rosemary Vieira[2], Katia Rosa[3] & Fabricio Ferreira[2]

[1] *Institute of Geological Sciences and Oeschger Center for Climate Research, University of Bern, 3012 Bern, Switzerland. (fabiomagrani@gmail.com)*
[2] *Sedimentary and Environmental Processes Laboratory (LAPSA-UFF). Institute of Geosciences. Universidade Federal Fluminense (UFF). Niteroi-RJ, 24210-346. Brazil.*
[3] *Department of Geography. Centro Polar e Climático (CPC-UFRGS). Universidade Federal do Rio Grande do Sul. Bento Gonçalves-RS, 91540-000. Brazil.*

The objective of this work is to analyze and understand the evolution of Admiralty's Bay deglaciation since the Last Glacial Maximum (LGM). The area has atypical characteristics compared to other Antarctic regions that allow a modern analogue during its past interglacials. The main question we ought to answer is: which glaciomarine records and submarine landforms present in Admiralty Bay can broaden our understanding of the evolution and dynamics of its deglaciation during advances and retreats of the glaciers that once dominated the fjord?

Admiralty Bay, at King George Island, is a fjord with an U-shaped valley, approximately 16 km long and 4 km wide. Its mild climate, with higher temperatures and precipitation, compared to the Antarctic Peninsula and other Antarctic regions, makes the South Shetland Islands an exception of the typical Antarctic glaciomarine environments (Anderson, 1999). Providing high sedimentation rates and, therefore, high-resolution climate data. The integration and interpretation of seismic profiles, echo-characters, geological samples and multibeam bathymetry can significantly improve paleoenvironmental studies and the interpretation of its dynamics through time.

Geological samples were acquired with piston and gravity corers and analyzed on laser granulometers and Multi-Sensor Core Loggers (MSCL), for density, magnetic susceptibilities, resistivity and P-waves velocity. Multibeam data were processed using CARIS®, were spikes and incoherent data have been removed, providing a detailed map of the bay's seafloor. Seismic profiles were acquired with Konsberg's SBP 300 (2.5 – 6.5 kHz) and SIMRAD 3002 (300 kHz). Interpretation was made on SMT KINGDOM®, where four different echo-characters were identified and correlated to glaciomarine processes (Figure 1).

Echoes I and II show good resolution and are characterized by continuous and sharp echoes with sub-parallel reflections and presence of glaciomarine muds. Echo III, a very prolonged echo with absence of sub-parallel reflectors, is associated with the shallower portions of the bay, providing little sediment cover, sandier samples and presence of ice rafted debris. Echo IV is associated with morainical banks and grounding zones.

Submarine landforms show that the region experienced major glacial advance, with subsequent rapid retreat of the glaciers in the deeper parts of the fjord, followed by slower retreat, with the presence of several recessional moraines in the shallower portions (Figure 2).

Submarine channels up to 1.5 km long and 50-80m wide identified in the records indicate the large contribution of meltwater sedimentation in the fjord. The presence of morainical banks and sills show a possible grounding of glaciers at these positions and a maximum extent at the shelf break during the LGM.

ECHO	DESCRIPTION	INTERPRETATION	
I	Continuous sharp bottom echo with weak sub-parallel reflections	Combination of meltwater plumes, ice rafted debris and hemipelagic sediments	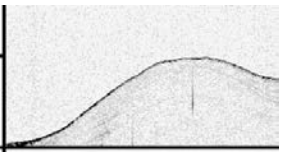
II	Continuous sharp bottom echo with strong sub-parallel reflexions	Combination of meltwater plumes and hemipelagic sediments	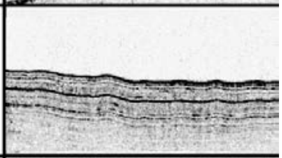
III	Very prolonged bottom echo and no sub-bottom reflectors	Combination of ice rafted debris/ dropstones, meltwater plumes and diamictons	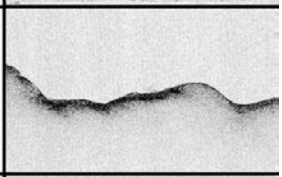
IV	Very prolonged and diffuse bottom echo with no sub-bottom reflectors and irregular morphology	Diamictons in paleo-grounding zones. Associated to iceberg scours on the sill and recessional moraines	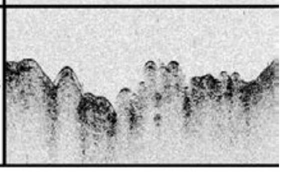

Figure 1. The four different echo-characters found with its description and associated processes interpretation.

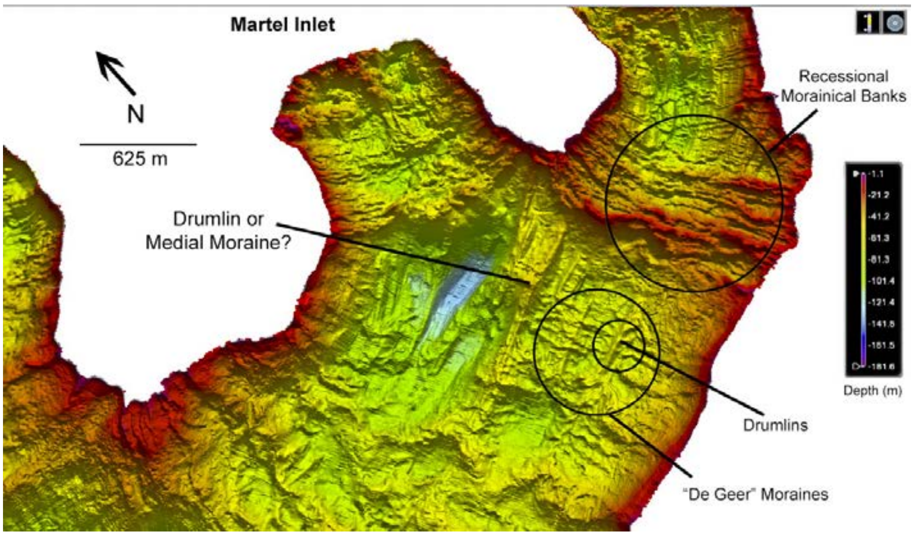

Figure 2. Submarine morphology of Martel Inlet showing the presence of several recessional moraines and a variety of interpreted submarine landforms.

REFERENCES

Anderson, J.B. 1999: Antarctic Marine Geology. Cambridge University Press. 289p.

P 9.23

Borehole measurements in Alpine permafrost – acquired experience and best practices for long-term monitoring

Jeannette Nötzli[1] and Marcia Phillips[1]

[1]WSL Institute for Snow and Avalache Research SLF, Flüelastrasse 11, 7260 Davos Dorf (jeannette.noetzli@slf.ch)

Temperature time series measured in boreholes are the cornerstones of long-term monitoring in permafrost because they are the only direct and continous observation of the thermal subsurface phenomenon. Around 30 boreholes are operated in the scope of the Swiss Permafrost Monitoring Network (PERMOS). It is the core task of the network – but at the same time a considerable challenge – to deliver reliable, robust and comparable measurements from key sites over decades. The main difficulties relate to a) the selection of a limited number of sites in a highly variable environment, b) drilling in ice rich underground in terrain that is difficult to access, c) robust instrumentation for harsh and cold conditions, and d) considerable shearing in the underground at many of the high alpine sites, which can cause thermistor chains to be blocked in the borehole or shear off completely (preventing recalibration or replacement). Additional requirements that a sound long-term climate-related monitoring service has to meet are a robust data management as well as the standardization and quality control of the measured data and their timely publication in a useful way.

PERMOS started in 2000 as a loose network of research-based sites with differing installations and measurement procedures. Many of the borehole installations are now 15 years old or more and will require renovation or complete re-drilling in the coming years in order to validate and secure the time series. A first and successful replacement drilling was performed in 2015 for the 30-year temperature series measured in rock glacier Murtèl-Corvatsch.

The (stepwise) standardization and professionalization of the field installations, measurement protocols and documentation, as well as the data flow are essential to further evolve towards a sustainable operational network. Corresponding guidelines are lacking, both at the national and the international level. Based on the 17 years of experience within PERMOS and in the scope of the ongoing overall evaluation of the network, we are compiling guidelines and standard procedures for the installation and operation of boreholes in mountain permafrost. They include the entire process from site selection, drilling and instrumenttation, maintenance and documentation to data flow and processing. Our experience will address a number of mountain specific aspects but may also be useful for long-term global permafrost monitoring.

Figure 1. Drilling a new 60 m borehole on rock glacier Murtèl-Corvatsch (eastern Swiss Alps) in September 2015 about 5 m apart from the old borehole. Photo: J. Nötzli.

P 9.24

Analysis of surface waves from ambient vibrations on Alpine glaciers in Switzerland

Lukas E. Preiswerk[1], Clotaire Michel[2], Fabian Walter[1] & Donat Fäh[2]

[1] Laboratory of Hydraulics, Hydrology and Glaciology, ETH Zürich, Switzerland, preiswerk@vaw.baug.ethz.ch
[2] Swiss Seismological Service, ETH Zürich, Switzerland

With an increasing data volume from seismic installations in environmentally challenging settings, a growing number of more established techniques from traditional seismology are applied to the frontiers of geoscience. In the general contexts of environmental seismology, scientists seek solid and portable methods to monitor environmental parameters using passive seismology. For glaciologists, ice thickness and englacial or subglacial characteristics such as water flow, fracture state or bed properties are of interest.

Here, we study the surface waves mainly composing the ambient wavefield on a glacier using methods established in seismic site characterization such as H/V (horizontal-to-vertical) spectral ratios, array processing (beamforming) and wavefield polarization analysis. These techniques allow the characterization of the subsurface structure (such as the thickness of the glacier) and the analysis of 3D effects caused by the englacial structure.

We explore the feasibility of monitoring, i.e. the detection of variations over time from seismological observations (resonance frequencies, dispersion curves, wavefield polarization), which can be attributed to changes of glaciologically relevant parameters. We analyze data from several temporary seismic arrays of Alpine glaciers in Switzerland. These networks include an array on Aletschgletscher, with 9 seismometers (corner frequencies: 1 Hz, array aperture: ~1200m, installed for 10 days) as well as one on Bisgletscher, with 5 seismometers (corner frequencies: 1 Hz, array aperture: ~500m, installed for 2 months). We find that the combination of H/V and array processing allow to determine the depth of the bedrock, whereas wavefield polarization seems to allow the monitoring of the glacial properties.

P 9.25

Near-surface energy balance on an Alpine rock glacier

Luisa Pruessner*,**, Marcia Phillips**, Michael Lehning**,[3], Martin Hoelzle[4] & Daniel Farinotti*,**

* Laboratory of Hydraulics, Hydrology and Glaciology (VAW), ETH Zurich, Zurich, Switzerland (pruessner@vaw.baug.ethz.ch);
** WSL, Swiss Federal Institute for Snow and Avalanche Research, SLF, Flüelastrasse 11, CH- 7260 Davos Dorf, Switzerland;
[3] Laboratory of Cryospheric Sciences CRYOS, School of Architecture, Civil and Environmental Engineering, Ecole Polytechnique Fédérale de Lausanne (EPFL), Lausanne, Switzerland;
[4] Alpine Cryosphere and Geomorphology, Department of Geosciences, University of Fribourg, Chemin du musée 4, CH-1700 Fribourg, Switzerland

Glaciers, rock glaciers and ice-rich permafrost are currently undergoing important changes caused by the continuous increase in atmospheric temperatures. While glaciers are retreating, rock glaciers are expected to be less sensitive to climate change as their composition is quite complex with a very variable mixture of debris and ice, and their active layer on the top consists mainly of debris protecting the ice from excessive melt. As they sometimes contain high amounts of ice, they could become important for water resources in regions which currently rely on glacial runoff, when the runoff from glaciers has diminished. In order to determine whether rock glaciers can provide a viable source of water, it is important to make reliable long-term projections about their thermal regime. The latter, however, can be difficult to model due to the blocky surface layer allowing for modes of heat transport other than conduction and diffusion. The large pore spaces in coarse blocky layers allow for advective forms of heat transport, either in form of the chimney effect in the case of open pore spaces or in the form of Rayleigh-Benard convection in the case of closed ones.

The 1D physics-based model SNOWPACK (Lehning et al. 1999) is employed testing different setups for the study site Murtèl-Corvatsch, for which long-term series of borehole temperature measurements and meteorological data are available (Hoelzle and Gruber 2008). The setups considered are: simple standard SNOWPACK functionality without additional modules, an added ventilation module (Lehning et al. 2002), an added canopy module (Gouttevin et al. 2015) and an added advective heat flux (Luethi et al. 2016). In each case, SNOWPACK's soil module was used to represent the rock glacier. Furthermore, different setup parameters were tested to study the effect of e.g. blocky layer thickness, ice content, porosity and grain size. Adding an advective heat flux is the only way to include any lateral effects, which are otherwise not accounted for by the model. The ventilation module presents a parameterisation of air flow from the atmospheric boundary layer into the open pore spaces of the blocky layer. Finally, the canopy module is considered to test whether it can be used to simulate direct throughfall and interception of precipitation at the blocky layer.

It was found that for the Murtèl site ventilation is needed to reproduce the low measured ground temperatures. While the advective heat flux was able to reproduce the rate of cooling well, a value for it needs to be prescribed for each time step. This makes the procedure unsuitable for long term projections as the temporal evolution of these values is unknown.
The canopy module was found to be unsuitable for modelling the blocky layer on rock glaciers, as it caused modelled and measured temperatures to diverge.

For the initialisation, setting the correct thickness of the blocky layer is important since this affects the depth at which zero-curtains occur in the modelled ground temperatures. Furthermore, the ice content of the icy layer has a significant effect for long term modelling as it limits the maximal amount of ice that can melt. The porosity and field capacity (calculated from the grain size of the soil material) determine the water transport and retention in the considered layer and thus exhibit a major influence on the ground thermal regime due to latent heat involved in phase changes.

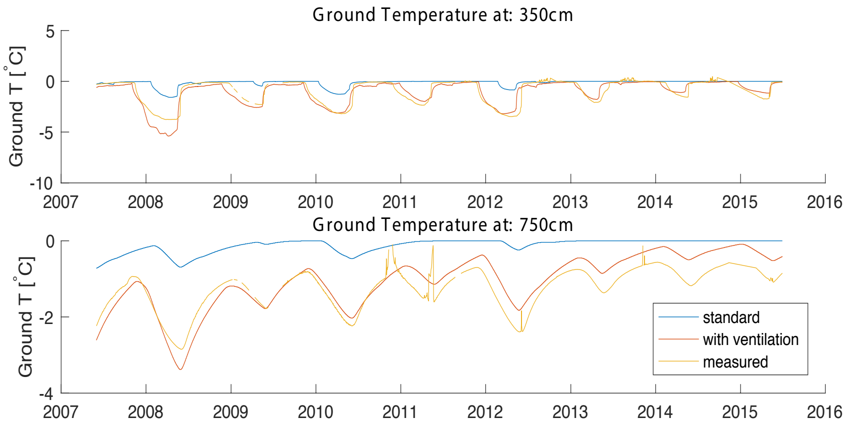

Figure 1. Ground temperatures of the Murtel-Corvatch rock glacier at 3.5 m (top) and 7.5 m depth (bottom). Measured and modelled (standard: blue, ventilation: red) temperatures are shown for the for period June 2007 to June 2016.

REFERENCES

Gouttevin, I., Lehning, M., Jonas, T., Gustafsson, D. & Mölder, M. 2015: A two-layer canopy model with thermal inertia for an improved snowpack energy balance below needleleaf forest (model snowpack, version 3.2.1, revision 741). Geosci. Model Dev. 8, 2379–2398. doi: 10.5194/gmd-8-2379-2015.

Hoelzle, M., Gruber, S. 2008: Borehole and ground surface temperatures and their relationship to meteorological conditions in the Swiss Alps. In: 9th International Conference on Permafrost, Fairbanks, Alaska, 29 June 2008 - 3 July 2008, 723-728. doi: 10.5167/uzh-2825.

Lehning, M., Bartelt, P., Brown, B., Russi, T., Stöckli, U., & Zimmerli, M. 1999: SNOWPACK model calculations for avalanche warning based upon a new network of weather and snow stations. Cold Reg Sci Technol 30, 145–157. doi: 10.1016/S0165-232X(99)00022- 1.

Lehning, M., Bartelt, P., Brown, B., and Fierz, C. 2002: A physical SNOWPACK model for the Swiss avalanche warning Part III: meteorological forcing, thin layer formation and evaluation. Cold Reg Sci Technol 35, 169–184. doi: 10.1016/S0165-232X(02)00072-1.

Luethi, R., Phillips, M., and Lehning, M. 2016: Estimating Non-Conductive Heat Flow Leading to Intra-Permafrost Talik Formation at the Ritigraben Rock Glacier (Western Swiss Alps). Permafrost Periglac 28, 183–194. doi: 10.1002/ppp.1911.

P 9.26

Processing of multi-temporal Landsat images to detect fractional snow cover and the snow line altitude for large glacier samples

P. Rastner[1], C. Notarnicola[2], L. Nicholson[3], R. Prinz[4] , R. Sailer[5], F. Paul[1]

[1]Department of Geography, University of Zurich, Switzerland (philipp.rastner@geo.uzh.ch)
[2]Institute of Applied Remote Sensing (EURAC), Bozen/Bolzano, Italy
[3]Institute of Meteorology and Geophysics, University of Innsbruck, Austria
[4] Integrative Geography Department, University of Graz, Austria
[5]Institute of Geography, University of Innsbruck, Austria

The cryosphere of mountain regions is highly sensitive to climate change. This is particularly evident in region-wide retreat of glaciers and reduced snow cover in mountain areas. Snow cover is not only an important parameter in the water regime of a catchment, but also for glacier mass- and energy balance, as it controls the energy fluxes on the glacier surface and protects the glacier from melt. However, monitoring glaciers and their characteristics in the field is laborious. Satellite remote sensing is a most valuable approach, as parameters like snow cover (SC) or snow line altitude (SLA) can be observed for a large number of individual glaciers. The SLA at the end of the ablation season is of particual interest because it may be considered as a proxy for the equilibrium line altitude (ELA) on Alpine glaciers, which is an indicator of the annual mass balance. In this study we have developed an automated tool, named “multi-temporal glacier parameter tool; MultiGlaPa”, to map firstly the SC and secondly to derive the SLA on single glaciers based on multi-temporal Landsat satellite imagery and an already existing glacier inventory. The method is developed in the Ötztal Alps where reliable in-situ data (ELA) are available for several glaciers for a period longer than 30 years. Two new ways of processing are introduced in this study. First, the approach is able to derive a threshold automatically to separate snow from ice on glacier surfaces (Fig. 1) and, secondly, a robust method to map the SLA based on the consideration of several elevation bins of more than 50% snow cover has been developed. The results indicate a high mapping accuracy of about 90% and a snow line detection capability of more than 80%. For the whole study period (1985-2016) a clear drop in the SC of all glaciers (~ 10%) and a clear rise in the SLA is visible (1.6 m/year; 65 m rise). The approximation of the ELA by using in each case the max. SLA of each year indicates a rather weak correlation, due to the temporal acquisition plan of Landsat (some years with only one image available). If removing such years, the max SLA indicates an average rise of 5 m per year. Overall, MultiGlaPa is a promising tool for future applications like with Sentinel 2 for monitoring the SLA and the SCF through time.

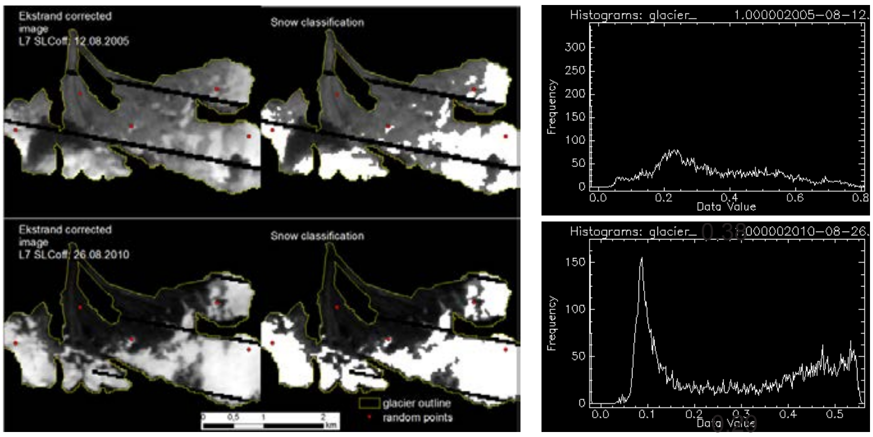

Figure 1: Snow cover mapping performance for Landsat 7 ETM, SLC off scene (left). On the right hand side, the respective histogram of the Ekstrand corrected image is shown with its automatic derived threshold.

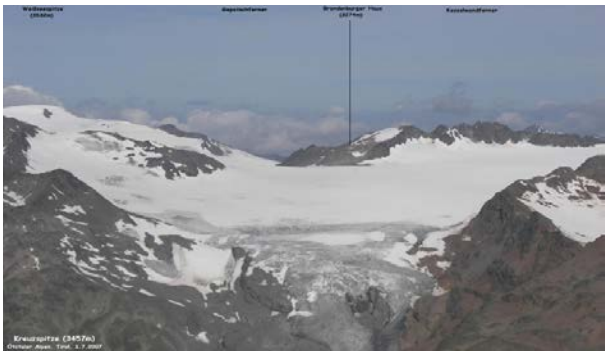

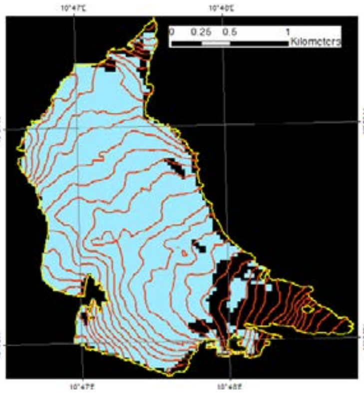

Figure 2: The oblique photo on the left hand shows the patchy distribution of snow cover on Kesselwandferner. The map on the right shows the classified snow cover distribution for a similar day during summer. Using only one elevation bin to map the SLA would result in a wrong snow line altitude.

P 9.27

Sensitivity of snow specific surface area measurements to different µCT settings

Franziska Roth, Martin Schneebeli

WSL Institute for Snow and Avalanche Research SLF, Flüelastrasse 11, 7260 Davos Dorf, Switzerland (franziska.roth@slf.ch, schneebeli@slf.ch)

Snow fascinates human beings since time immemorial. First written evidence of snowflake observations date back to 135 BC (Needham & Gwei-Djen 1961). While snow crystals captivate us due to their hexagonal symmetry, snow on the ground has a not less unique structure. It is a complex, three-dimensional material with various grain shapes and sizes. Different parameters as the density, the snow specific surface area, porosity, curvature or connectivity have been established to describe the snow microstructure (Fierz et al. 2009). The snow specific surface area (SSA), which is defined as the area of the ice-air interface per unit mass or per ice volume, is an important microstructural parameter for understanding the electromagnetic properties and chemical processes in the snow. To determine the SSA, different measurement techniques have been proposed, one being micro computed tomography (µCT) where the SSA is calculated from 3D-images. µCT became a widely used technique in snow research, not only to measure the SSA, but also to investigate processes occurring during the metamorphism of snow (Kämpfer 2007, Löwe 2011). Another measurement technique is the IceCube, a device which derives the SSA from the mid-infrared reflectance of the snow.

Compared to the measurements using a Scanco Medical µCT40, up to 80 % larger SSA were measured with the IceCube (SLF, 2016). While the different algorithms used for the SSA computation from the 3D-images have been already examined by Hagenmuller et al. (2016) as source for variation, the impact of different µCT settings on the measured SSA has not been systematically investigated. So far, the hypothesis has been that the influence of different µCT settings on the SSA measurements is negligible. Hence the goal was to quantify the sensitivity of the image quality and the SSA measurements to different µCT settings. The impact of the nominal resolution, the X-ray tube settings, namely the tube-voltage and tube-current, and the integration time has been investigated. The image quality has been assessed in terms of the signal-to-noise ratio, beam hardening, and the spatial resolution using clear ice and plastic cylinders, which have absorption coefficients similar to snow. Furthermore two different types of snow were scanned with different µCT settings and the SSA was calculated from the reconstructed images.

While the nominal resolution and the X-ray tube settings impacted all image quality characteristics, different integration times only significantly affected the signal-to-noise ratio. The signal-to-noise ratio showed a higher sensitivity to X-ray tube settings than the spatial resolution. Varying the voltage and current settings increased the signal-to-noise ratio by up to 84%, while changes in the spatial resolution were below 10%. Although the increase in the attenuation coefficient due to beam hardening showed a high sensitivity to the µCT settings, the absolute effect of beam hardening on the attenuation coefficient over the entire sample was small.

At a low nominal resolution changes in the X-ray tube settings had no significant effect whereas at higher nominal resolutions changes up to 7% could be observed. The integration time did not impact the measured SSA significantly at any nominal resolution. Generally higher SSA were measured at a higher nominal resolution. The combined effect of changes in the nominal resolution and X-ray tube settings was 19%. It is assumed that higher SSA measurements better represent the real SSA, based on the previous comparison of the µCT and the IceCube measurements. Thus, it is suggested to use a high voltage, low current setting combined with a high nominal resolution for future measurements. The measured SSA was subsequently linked to the image quality characteristics. A correlation between the measured SSA and the spatial resolution was observed. This correlation was however not incontrovertible and needs further investigations.

The above mentioned deviations between the µCT and the IceCube measurements were smaller for lower SSA. For values in the order of magnitude of the SSA measured in this work, differences around 40% to 50% were observed (SLF, 2016). The observed maximum effect of different µCT settings on the measured SSA is distinctively smaller and can thus not etirely explain the difference. To completely understand the deviation further research will be necessary taking the combined effect of all possible sources of uncertainties into account, including the IceCube. Nonetheless, this work contributes to a better understanding of how SSA measurements are influenced by different µCT settings and image quality characteristics.

REFERENCES

Fierz, C. R. L. A., Armstrong, R. L., Durand, Y., Etchevers, P., Greene, E., McClung, D. M., ... & Sokratov, S. A. 2009: The international classification for seasonal snow on the ground (Vol. 25). Paris: UNESCO/IHP.

Hagenmuller, P., Matzl, M., Chambon, G., & Schneebeli, M. 2016: Sensitivity of snow density and specific surface area measured by microtomography to different image processing algorithms. The Cryosphere, 10(3), 1039-1054, doi: 10.5194/tc-10-1039-2016.

Kaempfer, T. U., & Schneebeli, M. 2007:. Observation of isothermal metamorphism of new snow and interpretation as a sintering process. Journal of Geophysical Research: Atmospheres, 112(D24).

Löwe, H., Spiegel, J. K., & Schneebeli, M. 2011: Interfacial and structural relaxations of snow under isothermal conditions. Journal of Glaciology, 57(203), 499-510.

Needham, J., & Gwei-Djen, L. 1961: The earliest snow crystal observations. Weather, 16(10), 319-327.

SLF 2016: Comparison of micro-CT and IceCube SSA measurements at Weissfluhjoch, unpublished results. WSL Institute for Snow and Avalanche Research SLF, Davos.

P 9.28

Using snow cover models driven with meteorological data to predict snow instability for avalanche forecasting

Bettina Richter[1], Jürg Schweizer[1], Mathias W. Rotach[2], Alec van Herwijnen[1]

[1]*WSL Institute for Snow and Avalanche Research SLF, Flüelastrasse 11, CH-7260 Davos (richter@slf.ch)*
[2]*Institute of Atmospheric and Cryospheric Sciences, University of Innsbruck, Innrain 52f, A-6020 Innsbruck*

In mountain regions in winter, snow avalanches are relatively frequent and widespread. Avalanche forecasts are issued in many regions on a daily basis to warn the public. The forecasting process is data-driven, but mainly experience-based. Snow instability is operationally assessed by linking present snow stratigraphy with future weather. Therefore, information on snow stratigraphy plays a key role, but obtaining such data is difficult and time consuming. The ability to forecast avalanches, i.e. predicting snow instability, is limited by the poor resolution in space and time of snow stratigraphy data that can only be overcome with numerical modeling. In this study, we therefore investigated the ability of the snow cover model SNOWPACK driven with meteorological data from automatic weather stations (AWS) to evaluate snow instability. Data on snow instability were collected throughout three winter seasons at two field sites above Davos, Switzerland. Both sites are equipped with an AWS to guarantee the best possible input for snow cover modeling. Stability was assessed by evaluating the critical crack length from modeled snow properties and compared to results of in-situ propagation saw tests. Overall, we observed an increase in stability with time on both field sites, which could be quite well reproduced by the snow cover model. However, the modeled critical crack length was overestimated by up to 40%. The discrepancy was explained by an overestimation of the densification of the critical weak layer in the snow cover simulation. Using density derived from daily in-situ snow micro-penetrometer measurements improved the stability estimates to an error of 15%. Furthermore, avalanche cycles were associated with a decrease in critical crack length in the snow cover model as well as in the field results. This study shows that it is feasible to predict the critical crack length from snow cover simulations solely driven with meteorological data. Operational use of spatially distributed snow instability data derived from a numerical weather prediction model for numerical avalanche forecasting requires to further investigate influences of input uncertainties on modeled snow density and subsequently modeled snow instability.

P 9.29

Present and future runoff regimes at Murtèl-Corvatsch rockglacier

Martin Scherler[1], Martin Hoelzle[1], Matthias Huss[1], Christian Hauck[1]

[1] *Unit of Geography, Department of Geosciences, University of Fribourg, 1700 Fribourg*

As glaciers are expected to continue to retreat during the 21st century due to climate change, an important source of water will be diminishing, especially during the summer months. Regarding this fact, other sources of water, such as meltwater from permafrost and rockglaciers, will become more important to the runoff regime and the total amount of water transported to areas downstream. This study is concerned with modelling the melt of permafrost with regard to runoff. We use and compare two different models to simulate the hydrologic behavior of Murtèl-Corvatsch rockglacier form 1991 to 2100. One model is a physically based 1D heat and mass transfer model (Coup Model), the other a spatially distributed hydrologic model (GERM). We present the simulated runoff regimes of both models for the periods 1991-2020 and 2061-2090. The contributions of snow melt, ice melt and liquid precipitation to runoff are studied and discussed.

P 9.30

How do patchy snow covers affect turbulent sensible heat fluxes?

Sebastian Schlögl[1,2], Rebecca Mott[1] and Michael Lehning[1,2]

[1] *WSL Institute for Snow and Avalanche Research SLF, Davos, Switzerland*
[2] *School of Architecture, Civil and Environmental Engineering, École Polytechnique Fédérale de Lausanne, Lausanne, Switzerland*

The surface energy balance of a snow cover significantly changes once the snow cover gets patchy. The substantial progress in knowledge about the surface energy balance of patchy snow covers is a mandatory requirement to reduce biases in flux parameterizations in larger scale meteorological or climatological models.

The aim of this project was to numerically improve energy balance calculations late in the melting season when the spatial variability of turbulent fluxes is especially high owing to the complex feedback between bare/snow-covered areas and the atmosphere above.

In order to account for the feedback between the atmosphere and the patchy snow-cover we calculated three-dimensional air temperature and wind velocity fields with the non-hydrostatic atmospheric model ARPS for one clear-sky day and for an idealized flat test site initialized with different snow distributions and atmospheric conditions. The physics-based surface process model Alpine3D has been forced with these atmospheric fields close to the snow surface in order to resolve the small-scale spatial variability.

Turbulent sensible heat fluxes over snow increase with increasing number of snow patches and decreasing snow-cover fraction. This is mainly attributed to an increase in the mean near-surface air temperature over snow due to horizontal and vertical exchange processes induced by the heterogeneous land-surface. The increase in daily near-surface air temperatures is larger for high wind velocities than for low wind velocities.

P 9.31

Modelled transfluences and crosswise divides in the Last Glacial Maximum Alpine ice flow

Julien Seguinot[1] & Susan Ivy-Ochs[2]

[1]*Laboratory of Hydraulics, Hydrology and Glaciology, ETH Zürich, Hönggerbergring 26, CH-8093 Zürich, Switzerland (seguinot@vaw.baug.ethz.ch)*
[2]*Laboratory of Ion Beam Physics, ETH Zürich, Otto-Stern-Weg 5, CH-8093 Zürich, Switzerland*

During the Last Glacial Maximum (LGM), Alpine glaciers extending far onto the foreland coalesced to form a continuous ice expanse 750 km across. Ice flow was largely governed by subglacial topography, yet perched glacial deposits and high-altitude erosion marks show that Alpine glaciers occasionally flowed across major topographic features. This explains why the Alpine ice complex has alternatively been referred to as an ice cap (surface topography-controlled flow), an ice field (basal topography-controlled flow) and a network of valley glaciers.

Here, we use the Parallel Ice Sheet Model (PISM) to model the entire last glacial cycle (120–0 ka) in the Alps, and analyse ice flow patterns during the LGM. The modelled fast-flow regions generally occur along the main river valleys, while ice domes and ice divides are predominantly located over major reliefs. Nevertheless, the model results depict ice flow across mountain passes (transfluences) in 55 locations, ice divide above topographic lows (hereafter referred to as crosswise divides) in 27 locations (preliminary numbers), and self-sustained ice domes characteristic of ice caps in two locations over Flüelapass and Ötztal.

In the Eastern Alps, modelled transfluences and crosswise divides are generally incompatible with geological reconstructions, indicating that climate deterioration was overestimated in the model input. In the Western Alps, however, transfluences generally occur where they have been documented by geologic evidence. Interestingly, crosswise divides are often found over valley bottlenecks where glacial erosion has apparently been less efficient. These model results depict the LGM Alpine ice complex as an intermediate between ice fields and ice caps, bearing characteristics of both and perhaps no modern analogue.

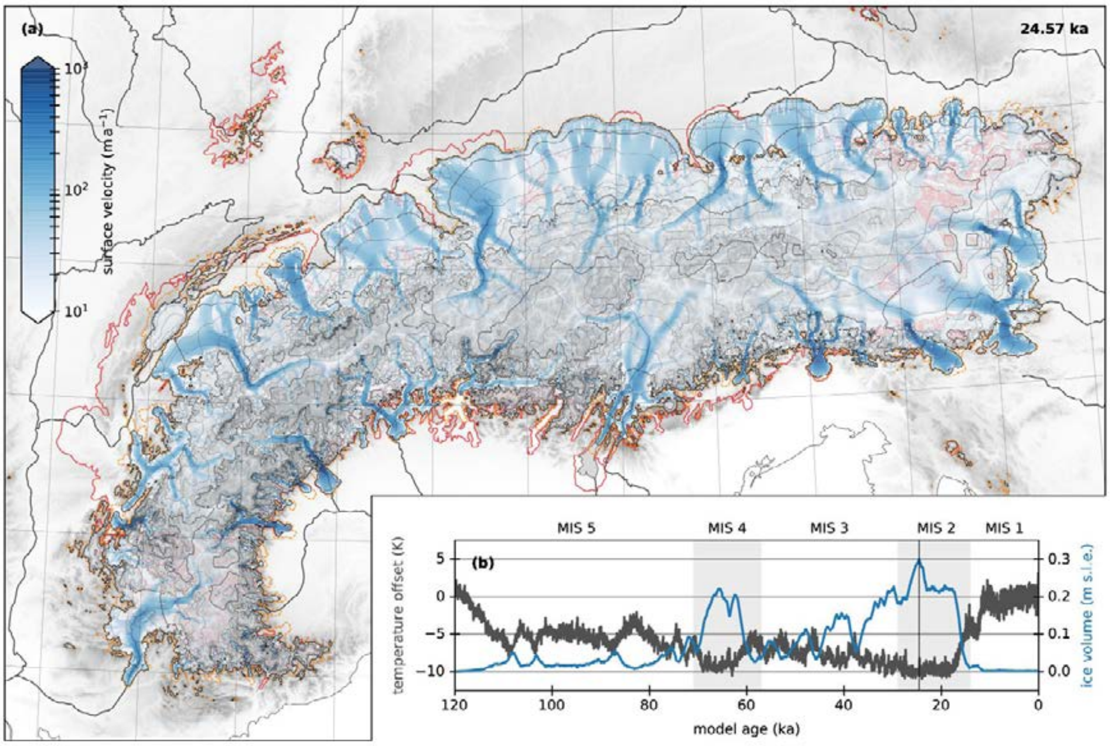

Figure 1. **(a)** Modelled bedrock topography (grey), ice surface topography (200 m contours), and ice surface velocity (blue) in the Alps 24.57 ka before present, corresponding to the maximum modelled ice cover. Modelled Last Glacial Maximum (LGM) ice extent (dashed orange line) and geomorphological reconstruction (solid red line). **(b)** Temperature offset time-series from the EPICA ice core used as palaeo-climate forcing for the ice flow model (black curve), and modelled total ice volume through the last glacial cycle (120–0 ka), expressed in meters of sea level equivalent (m s.l.e., blue curve).

P 9.32

GPS for the Point-wise Quantification of Snow Water Equivalent in alpine Terrain

Ladina Steiner[1] and Alain Geiger[1]

[1]Institute of Geodesy and Photogrammetry, ETH Zurich, Switzerland (ladinasteiner@ethz.ch)

Extensive amount of water stored in snow covers has a high impact on flood development during snow melting periods. Early assessment of the snow water equivalent in mountain environments enhance early-warning and thus prevention of major impacts. Sub-snow GNSS techniques are lately suggested to determine liquid water content, snow water equivalent or considered for avalanche rescue. This technique is affordable, flexible, and provides accurate and continuous observations independent on weather conditions. However, the characteristics of GNSS observations for applications within a snow-pack still need to be further investigataed.

Liquid water exerts the largest influence on GPS signal propagation through a snow-pack. Therefore, we focus on determining the characteristics of GNSS observables under water. An experiment was set-up to investigate the characteristics and limitations of submerged GPS observations using a pool, a level control by communicating pipes, a geodetic GPS antenna, and a water level sensor. The GPS antenna was placed into the water. The water level was increased daily by a step of two millimeters up to thirty millimeters above the antenna. Based on this experiment, the signal penetration depth, satellite availability, the attenuation of signal strength and the quality of solutions are analysed. Our experimental results show an agreement with the theoretically derived attenuation parameter and signal penetration depth. The water level above the antenna could be estimated with submillimeter accuracy compared to the independent water level sensor.

The potential to quantify snow water equivalent above a GPS antenna placed underneath a snowpack is evaluated in a next step. Therefore, a measurement network is set-up at the WSL SLF test site “Weissfluhjoch” consisting of a GPS reference station above the snow pack and a geodetic as well as low-cost GPS antenna mounted on the ground underneath the snowpack. These measurements are analysed for the winter 2016/2017 and compared to the reference sensors provided by the WSL SLF. The preliminary results of this point-wise estimation of snow water equivalent agree with the reference sensors at centimeter level during the first month and diverges around 10 centimeter during the rest of the winter.

P 9.33

Microscale Distribution of Impurities in Snow

Trachsel J., Avak S., Edebeli J., Schneebeli M., Eichler A., Bartels-Rausch T.

Chemical compounds from the atmosphere are deposited on the ground during snowfall. If the snow does not completely melt, like on polar and alpine glaciers, these impurities will be preserved in the snowpack and later incorporated into the glacier ice. To use the impurity records of an ice core as a proxy for past changes of climate, the processes leading to the final embedding of these chemical impurities have to be better understood. Especially the recrystallization of the snowpack during metamorphism processes can cause a redistribution of embedded compounds. We therefore investigated the transport of compounds as major ions, stable water isotopes and black carbon in the dynamic snow. The project is a joint project between the Paul Scherrer Institute (PSI) and the WSL Institute for Snow and Avalanche Research (SLF).

In an elution experiment, originally chemically homogeneous ice droplets were metamorphosed and then rinsed with zero-degree water, to measure the accumulation of ions on the surface of the ice crystals and their inclusion in the ice. Further, from January to May 2017, we monthly sampled the vertical distribution of the compounds in the natural snowpack at a field site above Davos, Switzerland.

First results show a strong separation of the ions during snow metamorphism. The concentration of sulfate and calcium on the outside of the crystals increased of up to 6 times with storage time.

In the next step, the fluxes inside the snow during the experiments have to be quantified and the behavior of stable oxygen isotopes and black carbon at the surface snow has to be investigated.

P 9.34

Using terrestrial radar interferometry for understanding calving processes

Andrea Walter[1], Martin P. Lüthi[1], Andreas Vieli[1], Martin Funk[2]

[1] *Department of Geography, University of Zurich, Winterthurerstr. 190, CH-8057 Zurich (andrea.walter@geo.uzh.ch)*
[2] *ETH Zürich, VAW, Hönggerbergring 26, 8093 Zürich*

Recently, many marine-terminating glaciers of the Greenland ice sheet revealed rapid retreat, thinning and flow acceleration. These glaciers lose mass by calving, a process which can change on short timescales. An increase of the calving rate can increase the contribution of outlet glaciers to global sea level rise significantly. However, major limitations in understanding the dynamics of calving glaciers remain. Terrestrial radar interferometry provides displacement and topographical data with a high spatial and temporal resolution. We observed two Greenland outlet glaciers in one minute interval with a resolution of 5 meters. We use these data to establish detailed calving statistics which can be compared to environmental forcings like tides or weather conditions. Addtionally, we are able to identify source areas and ice volumes of individual calving events at the front. This also allows us to recognize a relationship between the geometry of the calving front and the calving rate. A better understanding of the calving process is crucial to predict the future evolution of marine-terminating outlet glaciers in an appropriate way.

P 9.35

Characteristics of acoustic and micro-seismic signals in steep bedrock permafrost on Matterhorn (CH)

Samuel Weber[1], Jérome Faillettaz[1], Matthias Meyer[2], Jan Beutel[2] & Andreas Vieli[1]

[1] Department of Geography, University of Zurich, Winterthurerstr. 190, CH-8057 Zurich (samuel.weber@geo.uzh.ch)
[2] Computer Engineering and Networks Laboratory, ETH Zurich, Gloriastr. 35, CH-8092 Zurich

Understanding processes and factors affecting rock slope stability are essential for detecting and assessing the stability of potentially hazardous slopes. Despite ever increasing range of possibilities for the instrumentation of steep rock slopes, our ability to detect precursor events remains limited. Analysis based on surface displacement measurements may successfully be complemented by passive monitoring of acoustic emission and micro-seismic activity, providing a potential integrated signal of a rock mass.

However, analyzing such signals raises significant challenges, since it depends on (i) the nature and positioning of sensors as well as (ii) the attenuation of signals in the rock mass under observation. To explore these properties in detail through a set of controlled experiments simulating surface detachment events, we installed an experimental setup in steep, fractured bedrock permafrost on Matterhorn (CH) acquiring acoustic and micro-seismic activity in the range 1-10^5 Hz (Figure 1).

The analysis of artificial forcing using a rebound hammer led to two major findings: First, a strong change in waveform characteristics during propagation was observed, disabling feature detection by cross-correlation. Second, significant signal amplification in the frequency band 33-67 Hz was observed (Figure 2). The origins of this phenomenon remains unclear, especially whether this frequency band of amplification is site or location dependent and is a general characteristic for fractured bedrock conditions. However, this latter effect leads to an enhanced detection in this particular frequency band, an observation that is strongly supported by evidence from artificial rock fall events and natural fracture displacement.

Furthermore our analysis of the two-years time series suggested that filtering raw data in such frequency band might be a first important step towards the constitution of an unbiased catalogue of micro-seismic events. Indeed, the energy rate of the triggered events in this frequency band is not sensitive to positive temperature values. However, anthropogenic noise, e.g. caused by mountaineer activity, is also detected in this frequency band and complicates statistical analysis. Further analysis is required to label and eventually distinguish anthropogenic activity from bedrock-internal activity.

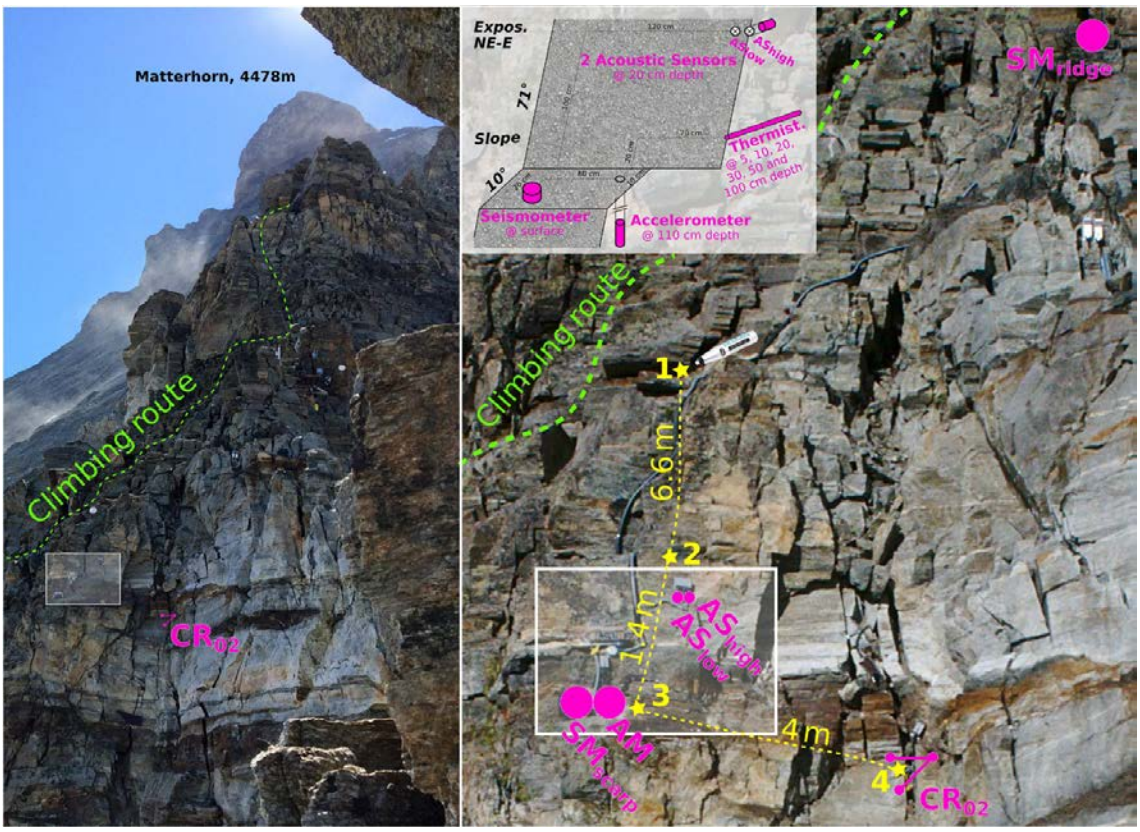

Figure 1. Detailed view on the Hörnligrat field site on the North-East ridge of the Matterhorn in the Swiss Alps with an average slope >60°C. Instrumentation setup for measuring acoustic (AS = acoustic sensor), micro-seismic (SM = seismometer; AM = accelerometer) and fracture kinematics (CR = crackmeter with displacement directions) are indicated in pink. A schematic zoom-in of the AE/MS instrumentation in the scarp is shown in the top white box. The yellow stars show the locations of the artificial events generated by the rebound hammer method.

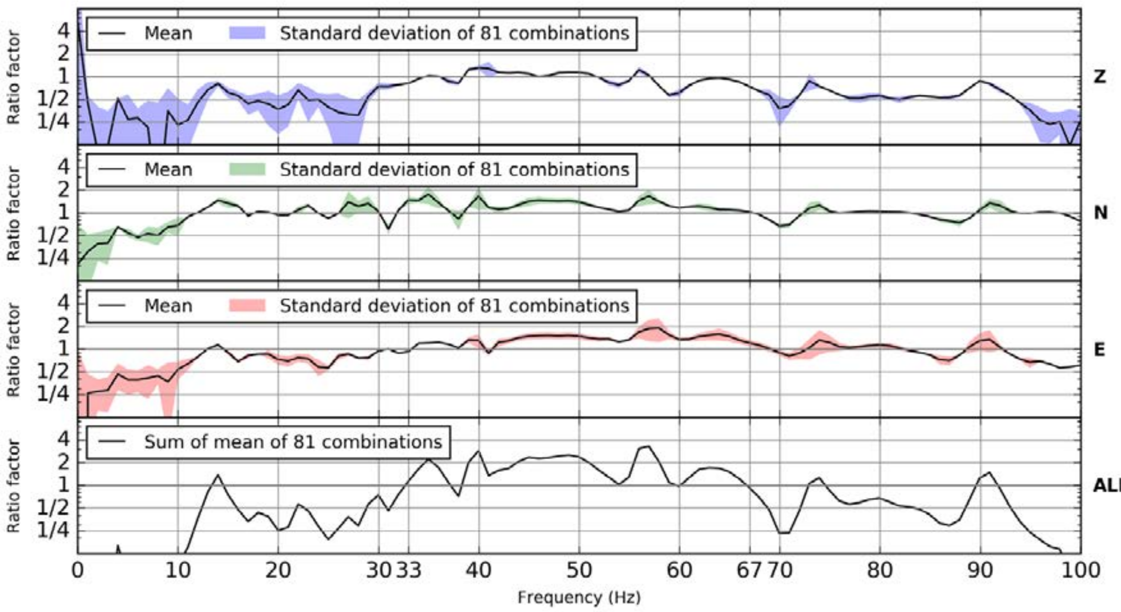

Figure 2. Filter spectrum between Location 3 and Location 4 indicating mean and standard deviation of 81 combinations. Amplification in the middle part of the frequency range (33-67 Hz).

P 9.36

Influence of slope angle on the convective heat transfer in porous permafrost substrate

Jonas Wicky[1], Christian Hauck[1]

[1] Alpine Cryosphere and Geomorphology Group, Department of Geosciences, University of Fribourg, Chemin du Musée 4, 1700 Fribourg. Contact: jonas.wicky@unifr.ch

Permafrost is a widespread phenomenon in the Swiss Alps. Its occurrence is not only influenced by meteorological and topographical parameters of the site, also landform and soil substrate have a significant impact on the ground thermal regime. Many studies showed that especially coarse blocky material with a high porosity influences the ground temperature (Kneisel et al., 2000; Delaloye & Lambiel, 2005; Gudong et al., 2007; Wicky & Hauck, 2017). The high porosity allows air (in addition to water) to circulate within the ground and thus convective heat transfer takes place. Convective heat transfer can lead to a cooling of the ground, which has the largest effect on low elevation permafrost sites, which would otherwise be unfrozen. On steep slopes, the gradient between the temperature of the air in the atmosphere and the ground temperature leads to a seasonally alternating circulation which is generally referred as the “chimney-effect”. On flatter terrain, the lateral extension of the circulation is smaller and vertical convection cells are forming. This is referred to the “Rayleigh-Bénard-Circulation” (Gudong et al., 2007).

In this study, we will present results from numerical experiments on the changing slope angle of an idealised talus slope to show the transition from vertical convection cells to a more lateral dominated convection (advection) and its influence on the ground thermal regime in the context of permafrost. The model setup consists of three domains (bedrock, porous talus and air as a simplified atmosphere; for material properties and other details refer to Wicky & Hauck 2017), where the governing equations for heat transfer, pressure and air flow are solved with the finite element method in GeoStudio2016©.

The results show that the slope angle has a major influence on the air circulation pattern and thus also on the temperature distribution in the ground. Flat terrain and low slope angles (<10°) result in a vertically dominated circulation. This is characterized by (i) the air velocity amplitude being higher in the vertical direction (ii) the air flow direction often close to +-90° and (iii) lower summer temperatures than winter temperatures compared to the mean over all slope angles due to the absence of air circulation in summer. Advection can also be observed on low inclines but has a minor influence. Steeper slopes (>20°) lead to a bi-directional chimney-type circulation characterized by (i) a seasonal reversal of 180° in main air flow direction parallel to the surface and (ii) temperatures being high/low in summer/winter compared to the mean over all slope angles due to the pronounced aspiration of warm/cold air. Slope angles in between show both vertical convection cells and advection over the whole domain depending on the boundary condition. A higher temperature gradient between air and talus temperatures generally leads to a convection dominated by one horizontal cell, whereas lower gradients lead to a vertical convection regime. The transition period in spring and autumn with air temperatures around the freezing point are often characterized by a phase of vertical convection.

The different circulations regimes are also reflected in the temperature distribution. Steeper slopes lead to a more pronounced chimney-type circulation and thus to a higher temperature difference between the lower and the upper part of the talus. This results in a strong cooling at the foot of the slope and can be favourable for azonal permafrost as observed in many field cases (e.g. Kneisel et al., 2000). Still, also at high Alpine sites, these circulations can lead to colder ground temperatures and in some cases explain the inhomogeneous distribution of permafrost in an Alpine setting (Delaloye & Lambiel, 2005).

REFERENCES

Delaloye, R. & Lambiel, C. 2005: Evidence of winter ascending air circulation throughout talus slopes and rock glaciers situated in the lower belt of alpine discontinuous permafrost (Swiss Alps). Norsk Geografisk Tidsskrift-Norwegian Journal of Geography, 59(2), 194-203.

Guodong, C., Yuanming, L., Zhizhong, S., & Fan, J. 2007: The ‘thermal semi-conductor’effect of crushed rocks. Permafrost and Periglacial Processes, 18(2), 151-160.

Kneisel, C., Hauck, C., & Mühll, D. V. 2000: Permafrost below the timberline confirmed and characterized by geoelectrical resistivity measurements, Bever Valley, eastern Swiss Alps. Permafrost and Periglacial Processes, 11(4), 295-304.

Wicky, J. & Hauck, C. 2017: Numerical modelling of convective heat transport by air flow in permafrost talus slopes. The Cryosphere, 11(3), 1311.

10. Hydrology, Limnology and Hydrogeology

Pascal Blanc, Michael Doering, Tobias Jonas, Michael Sinreich, Massimiliano Zappa

Swiss Society for Hydrology and Limnology SGHL,
Swiss Hydrological Commission CHy,
Swiss Hydrogeological Society SGH

TALKS:

10.1 **Addor N.**
Keynote: Two ways to overcome boundaries in hydrology

10.2 **Gaudard A.**, Schmid M., Wüest A.
Using lakes and rivers for the extraction and disposal of heat

10.3 **Hunkeler D.**, Cochand M., Christe P., Ornstein P.
Keynote: Seasonal groundwater storage in alpine catchments and its influence on stream discharge

10.4 **Kiewiet L.**, Meerveld V.I., Seibert J.
Spatio-temporal variability in shallow groundwater chemistry in a small pre-alpine catchment

10.5 **Mastrotheodoros T.**, Pappas C., Molnar P., Burlando P., Hadjidoukas P., Fatichi S.
Alpine ecohydrology across scales: propagating fine-scale heterogeneity to the catchment and beyond

10.6 **Peleg N.**, Fatichi S., Paschalis A., Molnar P. and Burlando P.
Keynote: AWE-GEN-2d: A new gridded stochastic weather generator

10.7 **Pool S.**, Viviroli D., Seibert J.
Prediction of hydrographs and flow-duration curves in almost ungauged catchments: which runoff measurements are most informative for model calibration?

10.8 **Roques C.**, Jachens E., Rupp D., Selker J., Grant G., Lewis S., Walter C., Nolin A.
On the origin of low flows in alpine systems: Insights from a year without snow in the Cascade Mountains of Oregon, USA

10.9 **Round V.**, Huss M., Farinotti D.
The hydropower potential of future ice-free basins worldwide

10.10 **Scheidler S.**, Anders B., Eichenberger U., Calonder G.-P., Aebli H., Huggenberger P.
Integrating geological structures into hydraulic-geothermal models to evaluate the productivity of alpine geological systems; the case study Davos

10.11 **Tischer J.**, Zopfi J., Giglio E., Su G., Cojean A., Lepori F., Lehmann M.F.
Dynamics and isotope effects of denitrification in Lake Lugano

POSTERS:

P 10.1 **Alcolea A.**, Becker J.K.
Automatic interpretation of geophysical well logs

P 10.2 **Bergami G.**, Drummond A., Molnar P., Burlando P.
Flow regulation effects on riparian vegetation: the Maggia River case

P 10.3 **Bolay S.**, Regli C., Eichenberger U., Calonder G.P., Aebli H., Siddiqi G.
Case study: Site investigation and geothermal exploitation of an alpine, fractured, artesian aquifer in Davos, Switzerland

P 10.4 **Botter M.**, Burlando P., Fatichi S.
Water quality in Swiss rivers: analysis of magnitude, trends and concentration-discharge relations

P 10.5 **Ceperley N.**, Michelon A., Beria H., Larsen J., Schaefli B.
Isotopes in water shed light on changing alpine water resources

P 10.6 **Cotte G.**, Vennemann T.
Tracing of the Rhône River within Lake Geneva using the stable isotope composition of water

P 10.7 **De Palézieux L.**, Loew S., Zwahlen P.
Recharge and Transient Pore Pressure Propagation in steep Alpine Mountain Slopes near Poschiavo, Switzerland

P 10.8 **Dembélé M.**, Mariéthoz G., Schaefli B.
Gap filling of streamflow time series using Direct Sampling in data scarce regions

P 10.9 **Ehrenfels B.**, Kalvelage T., Wehrli B.
How biogeochemistry shapes the ecosystem of Lake Tanganyika

P 10.10 **Fluixá-Sanmartín J.**, García-Hernández J., Fluixá-Sanmartín P., Paredes-Arquiola J.
Impacts of climate change on the water resources of an Alpine catchment in the Upper Rhone Basin, Valais, Switzerland

P 10.11 **Guermazi E.**, Milano M., Reynard E., Zairi M.
Impact of climate change and anthropogenic pressure on groundwater resources in Regueb basin, Central Tunisia

P 10.12 **Hyman J.**, Jimenez-Martinez J.
Dispersion and mixing in fractured media: interplay between structural and hydraulic heterogeneity

P 10.13 **Kouame A.A**., Jaboyedoff M., Goola Bi Tie A., Derron M., Kouamé Kan J.
Assessment of potential pollution of an unconfined aquifer in Abidjan by hydrocarbons

P 10.14 **Michelon A.**, Ceperley N., Beria H., Larsen J., Schaefli B.
Role of snowcover on water balance and melt dynamics in the Vallon de Nant, Switzerland

P 10.15 **Pavia D.**, Lebrenz H., Bárdossy A.
Parameter estimation: drivers of extreme discharge in the Northwestern Switzerland

P 10.16 **Remondi F.**, Fatichi S., Kirchner J.W., Burlando P.
Water transit time variability in time and space by fully distributed hydrology-transport modelling

P 10.17 **Schmocker-Fackel P.**, Hüsler F., Zahner S., Hohmann R., Overney O.
Hydro-CH2018: Climate change and its consequences on hydrology in Switzerland

P 10.18 **Sy B.**, Frischknecht C., Dao H., Consuegra D., Giuliani G.
What role for citizen science in flood hazard mapping?

P 10.19 **Vogt M.-L.**, Zwahlen F., Ibrahim H., Brunner P., Hunkeler D.
Modern recharge and flowfield organization of the Nubian Sandstone Aquifer System in Northern Chad

P 10.20 **Voytek E.B**., Jougnot D., Singha K.
Evaluating groundwater flow at multiple temporal scales using passive electrical measurements

P 10.21 **Wienhues G.**, Makri S., Grosjean M., Rey F.
Iron speciation in lake sediments of Moossee (Swiss Plateau) as anoxia proxy by applying a new sequential extraction technique

P 10.22 **Yao F.Z**., Ouattara I., Reynard E., Savané I.
Analysis of trends of hydroclimatic variables in the White Bandama Basin, Northern Côte d’Ivoire

10.1
Two ways to overcome boundaries in hydrology

Nans Addor[1]

[1] *Climatic Research Unit, School of Environmental Sciences, University of East Anglia, Norwich, UK (n.addor@uea.ac.uk)*

In this presentation, I will discuss two kinds of boundaries, boundaries between catchments and boundaries between scientists and decision makers. I will argue that both kinds can be overcome. First, I will discuss some recent progress in large-sample hydrology. Using a new data set of hundreds of catchments, I will illustrate that information at the catchment scale can be generalised to the continental scale. Although the boundaries of catchments are well defined, and streamflow describes what happens within those boundaries, catchment attributes, such as their topography, land cover, soil and geology can be used to explore hydrological similarity and to extrapolate beyond those boundaries. I will show how this is particularly useful for hydrological modelling. Second, I will discuss how, in the context of adapting to climate change impacts, it is key to overcome existing boundaries between researchers and decision makers. I will present the outcomes of a workshop-seminar series I co-organised at the University of Zurich. It is based on the premise that interdisciplinary and iterative dialogue can help to improve the understanding of and adaptation to climate change impacts, in particular on hydrological systems. We conducted an opinion survey among the participants before and after the event. We found that the event stimulated new perspectives on research products and communication processes, which suggests that similar events may contribute to the midterm goal of improving support for decision making, by overcoming boundaries between researchers, decision makers, and students.

10.2

Using lakes and rivers for the extraction and disposal of heat

Adrien Gaudard[1], Martin Schmid[1], Alfred Wüest[1,2]

[1] *Department Surface Waters - Research and Management, Eawag, Seestrasse 79, CH6047 Kastanienbaum (adrien.gaudard@eawag.ch)*
[2] *Physics of Aquatic Systems Laboratory – Margaretha Kamprad Chair, EPFL, CH1015 Lausanne*

The extraction and disposal of heat from lakes and rivers is a large yet scarcely exploited source of thermal energy. In Switzerland, this renewable source of heating and cooling would be readily available, as many urban centers are located near lakes and rivers. Its use would help to reduce consumption of fossil fuels and emissions of CO_2.

Using waterbodies as heat sources and sinks implies the discharge of thermally-altered water into aquatic systems (**thermal discharge**). We review the possible physical, chemical and ecological impacts of thermal discharge in lakes and rivers. In most cases, it appears that the main impacts remain local (e.g., certain species avoid the discharge area). However, intense thermal discharge could potentially cause large-scale impacts such as disruption of mixing (in lakes) or of fish migration (in rivers). Warming in summer is particularly critical, as many ecosystems are already under stress due to climate warming.

Based on simple assumptions, we estimate the potential for heating and cooling of the main lakes and rivers in Switzerland. We observe that this potential is remarkably large, often well above the regional demand. This thermal energy is particularly adapted at the scale of a neighborhood, a large company or industrial parks. The sustainable use of this resource requires a well-thought-out energy strategy and good coordination between the different actors.

Given judicious management and supportive policies, lakes and rivers could become a significant source of thermal energy in Switzerland in the near future. The main challenge of using this renewable, local and reliable energy will be to prevent negative impacts on aquatic systems.

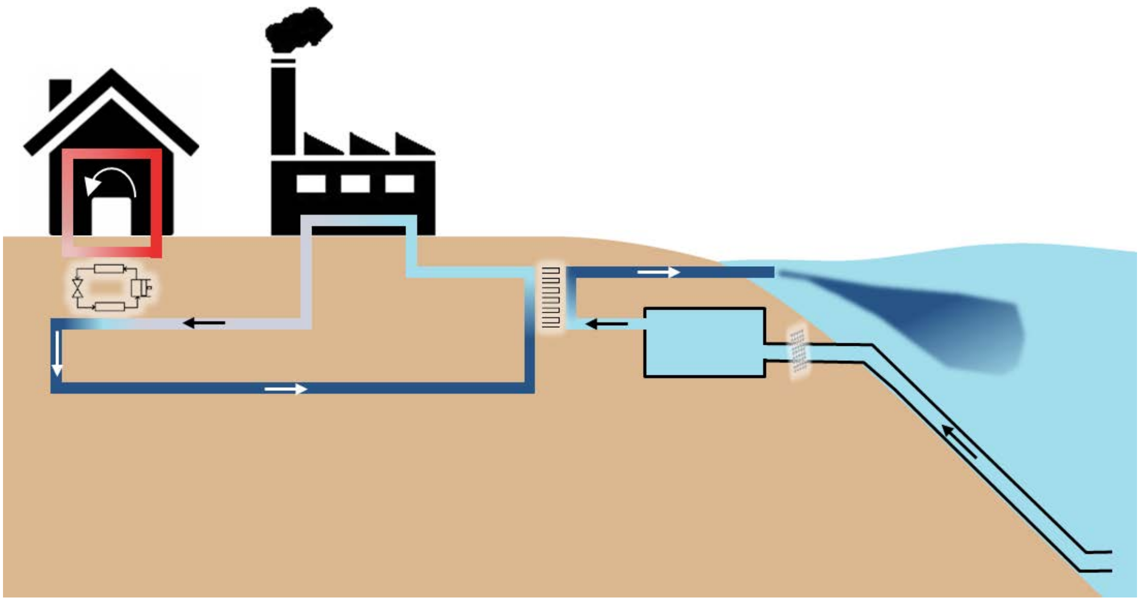

Figure 1. Example system where lakewater, through a heat exchanger, provides cooling for an industry and heating for a building, before being discharged back to the lake.

REFERENCES

Fink, G., Schmid, M. & Wüest, A. 2014: Large lakes as sources and sinks of anthropogenic heat: Capacities and limits. Water Resources Research, 50(9), 7285-7301.
Gaudard, A., Schmid, M. & Wüest, A. 2017: Wärme- und Kältenutzung von Oberflächengewässern: mögliche physikalische und ökologische Auswirkungen. Aqua & Gas, 5, 40-45.
Langford, T.E.L. 1990: Ecological effects of thermal discharges. Springer Netherlands, London, 468 pages.

10.3

Seasonal groundwater storage in alpine catchments and its influence on stream discharge

Daniel Hunkeler[1], Marion Cochand[1], Pierre Christe[2] & Pascal Ornstein[3]

[1] Centre for Hydrogeology and Geothermics (CHYN), University of Neuchâtel, Rue Emile Argand 11, CH-2000 Neuchâtel (daniel.hunkeler@unine.ch)
[2] Service de l'Environnement, Canton du Valais, Rue des Creusets 5, CH-1950 Sion
[3] CREALP, Rue des l'Industrie 45, CH-1951 Sion

In mountain areas, water storage in form of snow and ice leads to a seasonal water redistribution, making water available during hot and dry periods in form of melt water. Numerous studies have highlighted that this storage dynamics could be strongly altered by climate warming. The disappearance of glacier together with earlier snow melt might lead to surface water drought in summer and late fall. However, there is considerable uncertainty to what extent groundwater storage of meltwater could dampen this effect by delaying runoff to lowland regions. Compared to lowland areas, there is limited knowledge about the hydrogeological functioning of alpine areas. A key challenge for alpine hydrogeological studies is the stark contrast between the complexity of such sites versus the usually low data density due to the difficult conditions for instrumentation and data acquisition.

In this presentation, methodological approach to evaluate the groundwater dynamics in Alpine areas are discussed. The methods are applied to a research catchment to quantify seasonal groundwater storage and to relate it to water storage in form of snow. Based on hydrochemical methods and groundwater dating, storage locations and time-scales within the catchment are inferred. The study highlights that a substantial amount of water can be stored in alpine headwater catchments in form of groundwater, which will likely influence how such catchments respond to climate change.

10.4

Spatio-temporal variability in shallow groundwater chemistry in a small pre-alpine catchment

Leonie Kiewiet[1], Ilja van Meerveld[1], Jan Seibert[1,2]

[1] *Department of Geography, University of Zurich, Zürich (leonie.kiewiet@geo.uzh.ch)*
[2] *Department of Earth Sciences, Uppsala University, Uppsala, Sweden*

Landscape characteristics influence the storage and release of water and thus groundwater dynamics and groundwater chemistry. Even though it is well known that shallow groundwater is not one well-mixed storage and shallow groundwater chemistry varies spatially, often only one groundwater sample is used in hydrograph separation studies to determine the contribution of groundwater to streamflow. Quantification of catchment scale variability in groundwater chemistry may help to better understand hydrological flow pathways and to interpret variations in streamwater chemistry, in terms of which parts of the catchment contribute to streamflow.

We present the results from eight snapshot campaigns in a 20-ha steep mountainous catchment in the Swiss pre-Alps during baseflow conditions. During each campaign, shallow groundwater was sampled in 34 - 47 wells and analysed for major ion concentrations and stable isotopes ($\delta^{2}H$ and $\delta^{18}O$).
Electrical Conductivity (EC) was low in the early summer (mean: 284 ± 130 µS/cm) and increased throughout the summer (mean: 442 ± 100 µS/cm). The spatial variability in EC was large for all sampling campaigns. The mean standard deviation of the EC was 115 ± 13 µS/cm; the lowest measured EC was 68 µS/cm and the highest measured EC was 825 µS/cm. Temporal variability in $\delta^{2}H$ and $\delta^{18}O$ was used as a proxy for shallow groundwater residence time and to distinguish between sites with a more dynamic and a more constant water influx. The water influx is hypothesized to be related to aquifer connection and the amount of groundwater storage, thereby being critical in the conceptualization of groundwater contributions to streamflow. The spatial variability in the isotopic composition of the groundwater was smallest in early summer and autumn (standard deviation: $\delta^{2}H$ 2.3 ‰ and 3.4 ‰, respectively) and largest during the dry conditions in late August (standard deviation: $\delta^{2}H$ 9.5 ‰). The temporal variability of the isotopic composition was largest at sites in the upper part of the catchment, close to the catchment water divide, and at sites near (local) ridges.

The solute concentrations and isotopic composition of the groundwater were related to landscape characteristics, such as (local) slope and upslope accumulated area, and indices that describe groundwater dynamics, such as the skewness of the groundwater levels and the fraction of time that groundwater levels were close to the soil surface (i.e. persistence of near-surface groundwater levels). The concentrations of redox-associated solutes, such as manganese and iron(II), were highest at sites that had persistent high groundwater levels, especially during very dry conditions. Chloride-concentrations were lowest at locations with predominantly low groundwater levels but with large increases during large events. Potassium-concentrations were highest at predominantly forested sites with deeper groundwater tables and a more flashy response to rainfall events. Potassium and sodium concentrations were least temporally variable at sites with a more normally distributed groundwater levels (skewness between -1 and 1). However, all relations were weak (spearman correlation coefficients <0.55), indicating that it is difficult to determine the spatial variability in shallow groundwater from a few point measurements. The observed large spatial variability in groundwater chemistry highlights the need to sample groundwater at more than one location, even in small catchments.

10.5

Alpine ecohydrology across scales: propagating fine-scale heterogeneity to the catchment and beyond

Theodoros Mastrotheodoros[1], Christoforos Pappas[2], Peter Molnar[1], Paolo Burlando[1], Panagiotis Hadjidoukas[3], and Simone Fatichi[1]

[1] *Institute of Environmental Engineering, ETH Zürich, Stefano-Franscini-Platz 5, CH-8093 Zürich*
[2] *Département de géographie and Centre d'études nordiques, Université de Montréal, 520 chemin de la Côte-Sainte-Catherine, Montréal, Québec H2V 2B8, Canada*
[3] *Computational Science and Engineering Laboratory, ETH Zürich, Clausiusstrasse 33, CH-8092 Zürich*

In mountainous ecosystems, complex topography and landscape heterogeneity govern ecohydrological states and fluxes. Here, we investigate topographic controls on water, energy and carbon fluxes across different climatic regimes and vegetation types representative of the European Alps. We use an ecohydrological model to perform fine-scale numerical experiments on a synthetic domain that comprises a symmetric mountain with eight catchments draining along the cardinal and intercardinal directions. Distributed meteorological model input variables are generated using observations from Switzerland. The model computes the incoming solar radiation based on the local topography. We implement a multivariate statistical framework to disentangle the impact of landscape heterogeneity (i.e., elevation, aspect, flow contributing area, vegetation type) on the simulated water, carbon, and energy dynamics. This allows us to identify the sensitivities of several ecohydrological variables (including leaf area index, evapotranspiration and net primary productivity) to topographic and meteorological inputs at different spatial and temporal scales. We also use an alpine catchment as a real case study to investigate how the natural variability of soil and land cover affects the idealized relationships that arise from the synthetic domain. Our analysis shows that patterns of ecosystem sensitivity to topography-driven heterogeneity differ depending on the hydrological regime (i.e., wet vs. dry conditions). Topography-driven variability in ecohydrological variables (e.g. transpiration) at the fine spatial scale can exceed 50%, but it is substantially reduced (~5%) when integrated at the catchment scale.

10.6
AWE-GEN-2d: A new gridded stochastic weather generator

Nadav Peleg[1], Simone Fatichi[1], Athanasios Paschalis[2], Peter Molnar[1] and Paolo Burlando[1]

[1] *Institute of Environmental Engineering, Hydrology and Water Resources Management, ETH Zurich, Zurich (nadav.peleg@sccer-soe.ethz.ch)*
[2] *Faculty of Engineering and the Environment, University of Southampton, Southampton, UK*

A new stochastic weather generator, Advanced WEather GENerator for a 2-dimensional grid (AWE-GEN-2d) was recently presented by Peleg et al. (2017). The model combines physical and stochastic approaches to simulate key climate variables (e.g. precipitation, cloud cover, near-surface air temperature, solar radiation, vapor pressure, atmospheric pressure and near-surface wind) at high spatial and temporal resolution. The use of a combined stochastic-physically based methods makes possible accounting for the dependence between meteorological variables and simulating them at sub-daily temporal scales, which typically exceed the capabilities of empirical-statistical weather generators because the statistical correlations at sub-daily scales are complex to model. The resolution of the input data to the model conditions the resolution of the simulated fields (e.g. 2 km x 2 km and 5 min for precipitation when using MeteoSwiss weather radar composite, and 100 m x 100 m and 1 h for other climate variables when using hourly data from ground stations).

AWE-GEN-2d is parsimonious in terms of computational demand and therefore is particularly suitable for studies where exploring internal climatic variability at multiple spatial and temporal scales is fundamental. The model is suitable for studying the impacts of stochastic climate variability, spatial heterogeneity and temporal and spatial resolutions of climate forcing, as well as for climate downscaling. In this respect, the model can also be conveniently used in the context of climate change by modifying the model parameters using climate data derived from dynamical climate models (i.e. GCMs and RCMs).

Applications of the model include modelling of environmental systems, where high spatial and temporal resolution of meteorological forcing is crucial for the correct simulation of hydrological, ecological, agricultural and geomorphological processes.

The weather generator was calibrated and validated for the Engelberg region, an area with complex topography in the Swiss Alps. Model test show that the climate variables are generated by AWE-GEN-2d with a level of accuracy that is sufficient for most of practical applications.

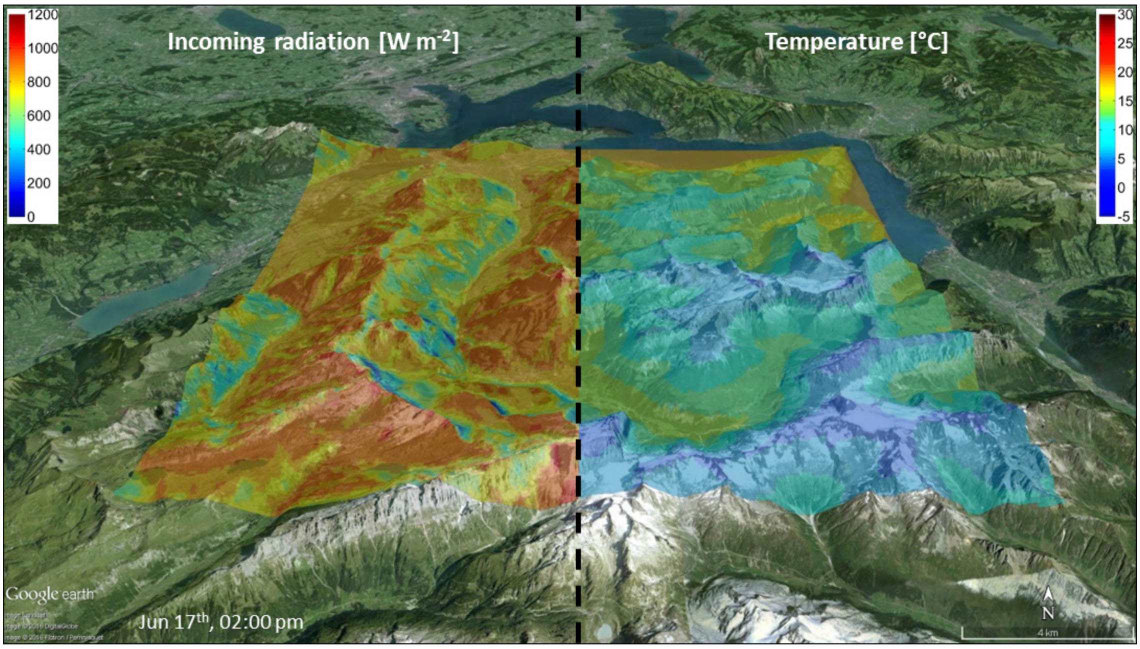

Figure 1. An example of the high-resolution simulation of AWE-GEN-2d. Incoming short-wave radiation (left) and temperature (right) are simulated for spatial resolution of 100 m by 100 m and 1 h in time. The example presented is taken from one member (year) from the ensemble that was simulated for Engelberg area for present climate, representing a realistic climate realization for the region.

REFERENCES

Peleg, N., Fatichi, S., Paschalis, A., Molnar, P., & Burlando 2017: An advanced stochastic weather generator for simulating 2-D high resolution climate variables, Journal of Advances in Modeling Earth Systems, 9(3), 1595-1627.

10.7

Prediction of hydrographs and flow-duration curves in almost ungauged catchments: which runoff measurements are most informative for model calibration?

Sandra Pool[1], Daniel Viviroli[1] & Jan Seibert[1]

[1]*Department of Geography, University of Zurich, Winterthurerstrasse 190, CH-8057 Zürich (sandra.pool@geo.uzh.ch)*

Applications of runoff models often rely on long continuous runoff time series for model calibration. However, many catchments around the world are ungauged and simulating runoff for these catchments is a challenging task. Assuming that it would practically be possible to make a few runoff measurements in such catchments, the question arises which runoff measurements would be most informative for a subsequent model calibration. We therefore tested the hypothesis that a few strategically selected runoff measurements can support runoff simulations in previously ungauged catchments. The study was based on twenty catchments along the eastern US Coast underlying a humid climate with varying importance of snow related runoff processes. The continuous runoff time series of the catchments was used to strategically select twelve runoff measurements within a hydrological year. The strategies ranged from simply selecting monthly flow maxima's to a more process oriented selection of runoff measurements. Each strategy was used to select the 100 best model parameter sets using a Monte Carlo calibration approach. Simulation results from these 'informed' parameter sets were then evaluated in an independent time period in terms of the Nash-Sutcliffe efficiency of the hydrograph and the mean absolute relative error of the flow-duration curve. The hydrographs were generally best simulated for model calibrations based on sampling strategies containing high runoff magnitudes. In contrast, sampling strategies consisting of mean and low flows were most informative for flow-duration curve simulations. The case of sampling the whole range of flow magnitudes with a single strategy provided valuable information for both hydrograph and flow-duration curve estimates. The exact timing of these runoff measurement was not crucial, because differences in model efficiency among strategies sampling the full range of runoff magnitudes were small. Simulation results from calibrations with a few runoff measurements were compared to a lower and an upper benchmark represented by a non-informed Monte Carlo calibration and a well-informed calibration using a continuous fourteen year time series. Taking the effort of making runoff measurements clearly improved model simulations compared to the non-informed case and simulation efficiencies close to a well-informed situation could be achieved. This study therefore confirmed that a small number of strategically selected runoff measurements can be informative for simulating runoff with a bucket-type runoff model in almost ungauged catchments.

10.8

On the origin of low flows in alpine systems: Insights from a year without snow in the Cascade Mountains of Oregon, USA

Clément Roques[1], Elizabeth Jachens[3], David Rupp[3], John Selker[3], Gordon Grant[2], Sarah Lewis[3], Cara Walter[3] and Anne Nolin[3]

[1] *Department of Earth Sciences, ETH Zürich, Zürich, Switzerland 8092 (clement.roques@erdw.ethz.ch)*
[2] *USDA Forest Service, PNW Research Station, Corvallis, OR 97331*
[3] *Oregon State University, Corvallis, OR 97331*

In the Oregon Cascades, the winter snow conditions in 2015 were equivalent to 4 degree Celsius climate warming scenario, representing a unique opportunity to test fundamental hypotheses of streams response to changes in the amount and timing of recharge. The Cascade Mountain range is characterized in two groups: 1) the Western Cascades are old volcanic flows with well-defined drainage basins and high snowmelt runoff, and 2) the High Cascades are younger volcanic flows where precipitation infiltrates into deep aquifer system. We explored the consequences of anomalous recharge processes on streamflow, focusing on how different mountain landscapes in the Cascades would respond. While summer stream tied records, flows did not go as low as predicted by established models for some catchments, revealing some specific hydrological properties. Analysis of stream flow recessions revealed a clear stratification of the hydrological properties for the different alpine zones. Watersheds in old volcanic formations has stream flows an order of magnitude lower than previous years. Catchments within the young High Cascades volcanic systems exhibits sustained flows, similar to previous years despite substantial differences in precipitation and recharge. Deatailled stream flow recession analysis and numerical simulations allow us to discuss morphological and hydrological properties of the landscape which controls the low flow regimes. We demonstrate that a year-to-year variation in recharge is substantially buffered by the deeper compartment which sustains the low flows from regional circulations.

10.9
The hydropower potential of future ice-free basins worldwide

Vanessa Round[1,2] Matthias Huss[2,3] & Daniel Farinotti[1,2]

[1] *Swiss Federal Institute for Forest, Snow and Landscape Research, CH-8903 Birmensdorf (vanessa.round@wsl.ch)*
[2] *Laboratory of Hydraulics, Hydrology and Glaciology, ETH Zurich, CH-8093 Zurich*
[3] *Department of Geosciences, University of Fribourg, CH-1700 Fribourg*

Over the next century, the ongoing retreat of glaciers will continue to cause dramatic changes to the landscape and present new challenges related to water availability. Newly ice-free basins may provide suitable locations for new water storage and hydropower infrastructure, with relatively low conflict in terms of established ecosystems and land use. At the same time, such installations could mitigate impacts arising from changing runoff regimes (Farinotti et al. 2016) or potentially hazardous glacier lakes (Haeberli et al. 2016).

We present an evaluation of the total theoretical hydropower potential of currently glaciated regions worldwide, and assess how this potential will evolve until the end of the century. The theoretical reservoir storage volume and energy production potential of each individual glacier location is determined. In addition, the feasibility in terms of social, economic, technical and ecological parameters is taken into account to present a ranking of potential locations for major glacierized regions around the world.

Potential retention dam volumes are determined by simulating dams in future ice-free terrain, using the subglacial topography of Huss & Farinotti 2012. The theoretical hydropower potential is based on projected runoff from the Global Glacier Evolution Model (GloGEM, Huss & Hock 2015) and site specific hydraulic heads. Additionally, the timing of potential reservoir locations becoming ice-free is revealed by the GloGEM modelled glacier evolution. Installation cost proxies provide an estimate of economic feasibility, and lithology and topographical data give further insight into technical feasibility. Population distribution and a suite of World Development Indices are used to assess the demand for new electricity production. Environmental and cultural risks are identified though the density of vulnerable species and presence of UNESCO sites.

REFERENCES

Farinotti, D., Pistocchi, A. & Huss, M. 2016: From dwindling ice to headwater lakes: could dams replace glaciers in the European Alps? Environmental Research Letters, vol.11, n.054022.

Haeberli, W., Buetler, M., Huggel, C., Lehmann, T., Schaub, Y. and Schleiss, A. 2016: New lakes in deglaciating high-mountain regions - opportunities and risks. Climatic Change, 139, 201-214

Huss, M. & Hock, R. 2015: A new model for global glacier change and sea-level rise. Frontiers in Earth Science, vol.3, n.54.

Huss, M. & Farinotti, D. 2012: Distributed ice thickness and volume of all glaciers around the globe. Journal of Geophysical Research, Earth Surface, vol.117, n.F4.

10.10

Integrating geological structures into hydraulic-geothermal models to evaluate the productivity of alpine geological systems; the case study Davos

Stefan Scheidler[11], Birte Anders[1], Urs Eichenberger[2], Gian-Paul Calonder[3], Hansruedi Aebli[4], Peter Huggenberger[1]

[1] *University of Basel, Department of Environmental Sciences, Applied and Environmental Geology (AUG), Bernoullistrasse 32, 4056 Basel, Switzerland*
[2] *Institut Suisse de Spéléologie et de Karstologie (ISSKA), Case Postale 818, CH-2301 La Chaux-de-Fonds, Switzerland*
[3] *Umweltbeauftragter Gemeinde Davos*
[4] *Amt für Natur und Umwelt Graubünden (ANU), Gürtelstrasse 89, 7001 Chur*
[1] *Corresponding author: Stefan Scheidler, e-mail: stefan.scheidler@unibas.ch, phone: +41 61 207 34 47, fax: +41 61 207 29 98*

Within the framework of the INTERREG VB project GRETA (Near-surface Geothermal Resources in the Territory of the Alpine Space) geothermal resources near the surface in the Alpine region and their sustainable use are to be examined as a contribution to the reduction of CO_2 emissions. Together with the project partners, Office of Nature and Environment Chur, the Federal Office for Spatial Development ARE, the Gemeinde Davos and the Geotest AG Davos, the AUG is working on the pilot study Switzerland located in Davos (Canton Grisons) and its surroundings.

The objective of the pilot study is to work out the use potential and productivity of shallow geothermal energy from an alpine aquifer, the Arosa Dolomite, an aquifer of regional spatial extent, embedded in a sequence of tectonic units in the eastern alpine system. Geologically, the Arosa Dolomite unit includes mainly rocks of the Triassic Hauptdolomit-Formation. It is sandwiched between the austroalpine and penninic tectonic units.

In spite of low data availability regarding the hydraulic conditions of the subsurface the main challenge was to create a regional groundwater model which maps the large-scale circulation systems. The basis for this was the integration of the constructed 3D geological model (GOCAD©) into a numerical groundwater flow model (COMSOL©).

We start from a purely conceptual approach defining hydraulic boundary conditions. A comprehensive measuring program (GNAMA) around the exploration borehole in the spa gardens of Davos (400 m deep) served to examine a sustainable operation of the production well and to monitor potential negative impacts on existing geothermal applications. All the data have been available also for the geological and groundwater flow models. Further hydrogeological data concentrate on the Landwasser valley of the Davos area which are the basis for the setup of the models and the hydraulic calibration.

The 3D geological-hydrogeological model allows evaluating pumping tests and to understand the dynamic character of capture zones of pumping wells as well as to test how different boundary conditions and hydraulic property distribution influence calculated flow regimes. In addition, the model enables us to test the effects of hydraulic regimes changes at different scales. In the year 2016, the focus was laid on the development of the 3D geological model and in 2017 on the hydraulic model for understanding the dynamics of deeper confined and artesian aquifers including the interaction with near surface groundwater resources in the unconsolidated rocks of valley fills.

10.11

Dynamics and isotope effects of denitrification in Lake Lugano

Jana Tischer[1], Jakob Zopfi[1], Elena Giglio[1], Guangyi Su[1], Adeline Cojean[1], Fabio Lepori[2] & Moritz F. Lehmann[1]

[1] *Aquatic and Stable Isotope Biogeochemistry, Department of Environmental Sciences, University of Basel, Bernoullistrasse 30, CH-4056 Basel (jana.tischer@unibas.ch)*

[2] *Institute of Earth Sciences, University of Applied Sciences of Southern Switzerland, Via Trevano, CH-6952 Canobbio*

Lakes are important ecosystems where reactive nitrogen (N) species are removed from inland waters. Particularly, in redox transition zones of permanently stratified lakes, a variety of microbial processes occur in close vicinity, including nitrification, (nitrifier-) denitrification and anammox. Classical organotrophic denitrification and the potentially underestimated sulfur (S) dependent chemolithotrophic denitrification are important nitrate removal processes. The meromictic north basin of Lake Lugano represents an anthropogenically-influenced ecosystem, where a dominance of S-oxidizing denitrifiers over chemotrophic denitrifiers in the water column has been proposed, at least during some periods of the year. Within this context, nitrate isotopes can be used to characterize different denitrification pathways/metabolisms. The $\Delta\delta^{18}O:\Delta\delta^{15}N$ ratios of nitrate during its reduction are diagnostic for specific processes, in particular the use of the nitrate reductases Nar vs. Nap, and overlapping nitrite-oxidation by nitrification or anammox. Using a combination of biogeochemical and microbiological approaches, we aimed at studying (i) the seasonal dynamics of (and controls on) the different modes of denitrification, (ii) isotopic fingerprints of organo- vs. lithotrophic nitrate reduction, and (iii) the identity of the responsible N-transforming microorganisms. Several incubation experiments show varying contributions of chemotrophic vs. S-driven denitrification, depending on water column depth, season, and availability of organic electron donors. The $\Delta\delta^{18}O:\Delta\delta^{15}N$ ratios seem mostly determined by the active denitrifying organisms and the enzymes they use, respectively. Pure culture studies of denitrifying species will further characterize isotope effects of nitrate reduction. The assessment of the microbial diversity via high-throughput sequencing of ^{16}S rRNA genes will help to identify the organisms responsible for S-dependent and organotrophic denitrification.

REFERENCES

Wenk, C.B. et al. 2013: Anaerobic ammonium oxidation (anammox) bacteria and sulfide-dependent denitrifiers coexist in the water column of a meromictic south-alpine lake. Limnol Oceanogr 58, 1-2.

P 10.1

Automatic interpretation of geophysical well logs

Andrés Alcolea[1], Jens Karl Becker[2]

[1] HydroGeoModels, Tösstalstrasse 23, CH-8400 Winterthur (andres.alcolea@hydrogeomodels.ch)
[2] Nagra, Hardstrasse 73, CH-5430 Wettingen

Facies interfaces are often located by interpreting combinations of well logs (e.g., natural and spectral gamma with caliper). Generally, this interpretation is made long after the logs were collected. This often leads to a loss of “first hand” information, as collected on-site. In addition, well log interpretation is usually slow and tedious, what hinders on-site decisions. To make things worse, (1) the standard interpretation is subjective and based on subtle “manipulations” of the raw data that are hardly traceable in the long run, and (2), small lithological changes (e.g., in clay content) or intercalated thin layers presenting different lithologies are often combined in one single (notably thicker) stratigraphic unit. Yet, such thin layers may be clearly visible in geophysical logs and are important (e.g., as preferential flow paths for contaminant migration or as water conducting features). Therefore, an automated, parameter based (and thus traceable) quick look of the lithology after log completion represents a valuable tool to help with on-site decisions (e.g., depth of the different lithological sub-units). To that end, an interpretation workflow and corresponding algorithm has been developed.

The algorithm consists of two main parts, i.e., the identification of facies and corresponding interfaces and the inference of hydrogeological properties (hydraulic conductivity and porosity). First, the algorithm uses a set of Walsh functions which enhances transitions in signal levels and weighs/combines information from all available well logs (e.g. caliper, density, natural and spectral gamma, neutron, etc.) to select a set of interfaces between facies. Identified facies can be as thin as the log accuracy (usually centimetre). In a second step, the algorithm identifies the lithology of the inferred facies using the Schlumberger standard diagram correlating Thorium to Potassium contents, provided that spectral gamma was measured. Third, the distribution of shale volume is inferred from the gamma log. Fourth, an estimate of the distribution of effective porosity along the borehole is obtained if the total porosity is known. Such distribution can also be correlated to that of hydraulic conductivity through empirical laws after some calibration process. The variability of the estimated (per facies) hydraulic properties, allows the deterministic estimation of variograms and other higher order statistics that are the starting point of the necessary posterior geostatistical (either deterministic or stochastic) modelling exercises.

This work presents the methodology and its application to a set of 16 boreholes in Mont Terri and northern Switzerland (Figures 1 and 2).

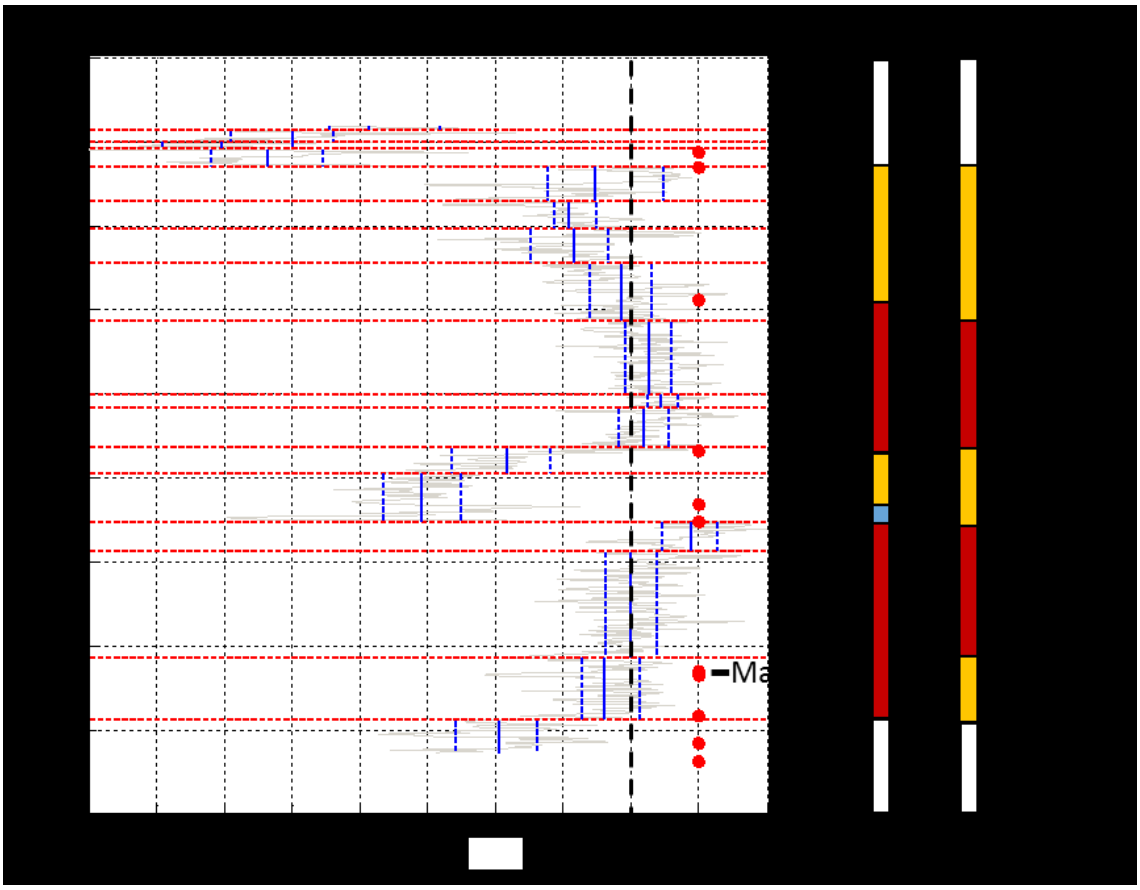

Figure 1. Identified facies mineralogy in borehole BDB-1 (Mont Terri). Orange, brown and blue rectangles on the right depict sandy, shaly and carbonate-rich sandy facies respectively. Red dots depict the facies interfaces from the manually interpreted lithostratigraphic logs, dashed red lines indicate the facies interfaces picked by the algorithm.

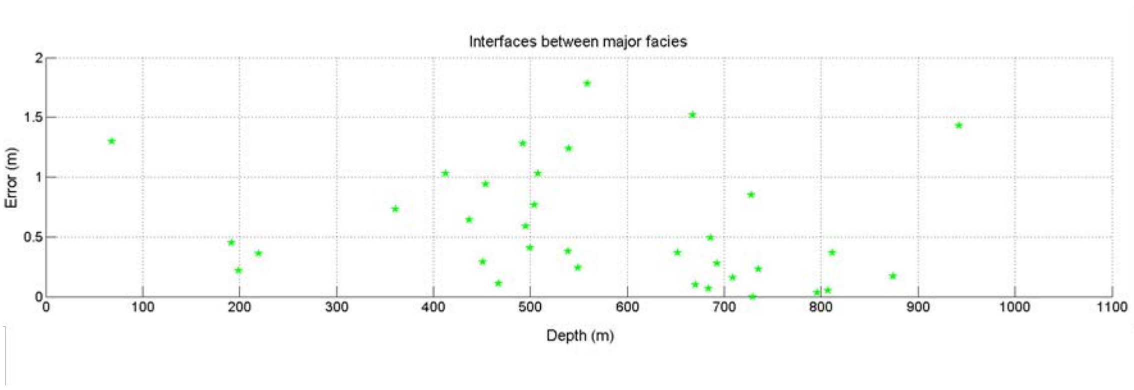

Figure 2. Identification errors of observed interfaces in Benken borehole.

P 10.2

Flow regulation effects on riparian vegetation: the Maggia River case

Gianluca Bergami[1], Alice Drummond[1], Peter Molnar[1] & Paolo Burlando[1]

[1] *Institute of Environmental Engineering, ETH Zürich, Stefano-Franscini-Platz 5, CH-8093 Zürich (bergami@ifu.baug.ethz.ch)*

In a context of increasing energy demand, hydropower is currently the leading renewable source. However, the benefits of hydropower production are counterbalanced by negative effects of human modifications, such as damming and water abstraction, which pose threats to the river hydrology, sedimentology and ecology. In particular, interventions on Alpine rivers in Europe led in many cases to the disruption of river-aquifer flow interactions, a lateral disconnection of floodplains, the disturbance of sediment fluxes and a drop in aquatic habitat quality and extent. The prediction of the impact of such changes on the ecology of rivers requires a combined effort of numerical modelling and field observations, which is to date missing.

We intend to simulate the response of river and groundwater systems to different environmental flow strategies (e.g. constant releases, seasonal releases, etc.) and to quantify the effects of such response on riparian vegetation growth and spatial distribution in Alpine streams. To achieve this goal, we designed numerical models of river-aquifer flow interactions and of their impact on riparian vegetation growth in the Maggia River: a heavily regulated Alpine gravel-bed braided river. The modelling tasks are being supported by field measurements of hydrology (river stage, groundwater levels), plant-scale phenology (dendrometers) and reach-scale vegetation change (terrestrial camera monitoring) (Džubáková et al. 2015). Long-term changes in vegetation cover are gleaned from historical aerial photography (Figure 1).

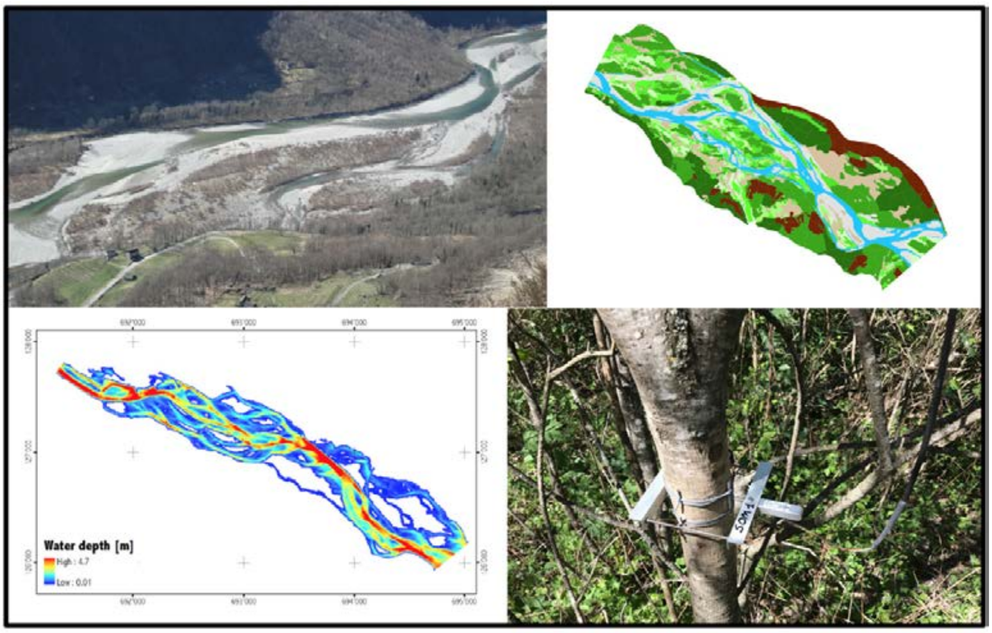

Figure 1. The Maggia floodplain and some numerical and experimental analyses thereof. Photos and illustrations by Gianluca Bergami. The Maggia floodplain is a particularly suitable site for the calibration and validation of such a modelling system, since the flow of the Maggia River is regulated by hydropower dams and riparian vegetation is present on the gravel bars along the floodplain with rather natural dynamics, responding to flood and inter-flood periods as well as low flows (Perona et al. 2009).

Among the expected results of this research, we foresee that: a) an improved surface water – groundwater coupled model will be obtained, able to accurately simulate river-aquifer exchange fluxes in a braided Alpine stream, also accounting for surface processes (evapotranspiration) and dynamics in the hyporheic zone, and capable of long-term simulations at the river corridor scale; b) the coupling of such model with a riparian vegetation model will be accomplished, allowing to estimate the water stress of riparian species in regulated streamflows and their response to environmental flow policies; c) a model-based quantitative assessment of how riparian species respond to different flow conditions, as well as to new minimum flow release strategies, will be achieved.

The final aim of this research is to produce a valuable tool for the fine-tuning of environmental flow releases in the Maggia valley, improving the state of the riparian ecosystem while maintaining sufficient water withdrawals and electricity production at the same time. This research could serve as a methodological prototype for other Alpine streams where river restoration actions aiming to restore or maintain natural dynamics in riparian vegetation downstream of dams are planned.

REFERENCES

Džubáková, K., Molnar, P., Schindler, K. & Trizna, M. 2015. Monitoring of riparian vegetation response to flood disturbances using terrestrial photography. Hydrol. Earth Syst. Sci. 19, 195-208, doi:10.5194/hess-19-195-2015.

Perona, P., Molnar, P., Savina, M. & Burlando, P. 2009. An observation-based stochastic model for sediment and vegetation dynamics in the floodplain of an Alpine braided river, Water Resour. Res., 45, W09418, doi:10.1029/2008WR007550.

P 10.3

Case study: Site investigation and geothermal exploitation of an alpine, fractured, artesian aquifer in Davos, Switzerland

Stephan Bolay[1], Christian Regli[1], Urs Eichenberger[2], Gian Paul Calonder[3], Hansruedi Aebli[4], Gunter Siddiqi[5]

[1] GEOTEST AG, Bahnhofstrasse 8A, 7260 Davos Dorf (corresponding author: stephan.bolay@geotest.ch)
[2] Schweizerisches Institut für Speläologie und Karstforschung, Rue de la Serre 68, 2301 La Chaux-de-Fonds
[3] Gemeinde Davos, Berglistutz 1, 7270 Davos Platz
[4] Amt für Natur und Umwelt Graubünden, Gürtelstrasse 89, 7001 Chur
[5] Bundesamt für Energie, Mühlestrasse 4, 3063 Ittingen

Alpine areas are more sensitive to the expected impacts of climate change and geothermal energy plays an important role in the energy strategy of the alpine space [Gloersen et al (2012)]. This holds also true for the community of Davos which actively promotes the growth of renewable energy sources and is therefore certified with the European energy award Energiestadt (energy city). To explore the geothermal potential of Davos the pilot project GNAMA (Geothermie-Nutzung alpiner mitteltiefer Aquifere, geothermal exploitation of non-shallow alpine aquifers) was launched which is expected to save 400 MWh per year of fossil fuels in the upcoming years [Gemeinde Davos 2016]. The project is part of the Swiss national geothermal research program and is funded by the community of Davos, the cantonal department of nature and environment (ANU) and the Swiss ministry of energy (BFE).

The pilot project included site investigation with seismic measurements carried out in 2010 and drilling of a 400 m deep exploration borehole in the vicinity of the Congress Centre Davos in 2012. The borehole was drilled in the fractured dolomite aquifer (Arosa Dolomite aquifer, Schiahorn nappe) which is located below a quaternary, layered, unconfined aquifer. The Arosa Dolomite aquifer is confined and artesian with groundwater flow mostly along fractures.

Extensive measurements were carried out to characterise the reservoir; the applied methods are borehole geophysics, pumping tests and analysis of water chemistry including stable isotopes. The aquifers main features are natural artesian flow of about 1’200 l/min with a water temperature of 11.3 °C and a pressure of 2.3 bar. The results also showed that the aquifer can be used for heating or cooling applications and that it is of regional importance.

The conducted studies serve as a basis for the evaluation of the preliminary exploitation of the borehole which started in 2014. The ground water from the exploration borehole is used to power a local district heating network, which features cooling and heating with heat pumps. The outcomes of the studies are also used as input parameters for a 3D geological model and a numerical groundwater flow model developed by the University of Basel within the scope of the INTERREG VB project GRETA (near-surface geothermal resources in the territory of the alpine Space) [Scheidler et. al 2017]. The results of both projects GNAMA and GRETA are to be incorporated in developing guidelines for improved exploration of further hydrogeothermal applications in the alpine regions of Switzerland.

REFERENCES

Regli, C., Kleboth, P., Eichenberger, U., Schmassmann, S., Nyfeler, P., & Bolay, S. 2014. First insights in the prospection and characterisation of the aquifer of the Arosa Dolomites, Switzerland. Grundwasser, 19, 29-38.
Gemeinde Davos 2016: Energiestadt-Bericht. Erneuerung Energiestadt-Label Gemeinde Davos.
Gloersen, E., Bausch, T., Hurel, H. Pfefferkorn, W., Del Fiore, F., Ratti, C. & Zovodnik-Lamovsek, A. 2012: Strategy-development for the Alpine Space.
Scheidler, S., Anders, B., Eichenberger, U., Calonder G. P., Aebli, H. & Huggenberger, P. 2017: Integrating geological structures into hydraulic-geothermal models to evaluate the productivity of alpine geological systems; the case study Davos. 15th Swiss Geoscience Meeting 2017 Davos. Abstract.

P 10.4

Water quality in Swiss rivers: analysis of magnitude trends and concentartion-discharge relations

Martina Botter[1], Paolo Burlando[2], Simone Fatichi[2]

[1] Institute of Environmental Engineering, ETH Zurich, Zurich, Switzerland (botter@ifu.baug.ethz.ch)
[2] Institute of Environmental Engineering, ETH Zurich, Zurich, Switzerland

Pollutants, nutrients and solute concentrations in streams represent the hydrological and biogeochemical response to natural processes and increasing anthropogenic pressure on watersheds.

This study analyses the Swiss National River and Survey Programme (NADUF) database, comprising almost 40 years of water quality data sampled every two weeks in eleven Swiss catchments. The solutes are divided into five categories: geogenic solutes (Ca, Mg, Na, silicic acid and K), deposition derived solutes (Cl), nitrogen species (NO_3, total N), phosphorus species (DRP, total P and suspended solids) and organic carbon (DOC, TOC).

Firstly, the magnitude and trends in time of the concentration patterns are explored. Then, the concentration-discharge (C-Q) relationships, expressed as $C = a\ Q^b$, are studied in the different catchments. The behavior of each solute is classified as chemostatic ($b \approx 0$), source limited ($b<0$) or transport limited ($b>0$) depending on the value of b coefficient. The C-Q relations are computed separating low flows (Q < median daily Q) and high flows (Q ≥ median daily Q). As some solute concentrations have changed in time, the trend in time of b is also considered.

Among geogenic solutes, calcium has the highest concentration, while NO_3 is about half of the total nitrogen concentration, similarly DRP is half of the total phosphorus concentration. DOC, instead, is about 2/3 of the TOC concentration. Suspended solids have a two order of magnitude higher concentration than phosphorus species. The concentrations patterns are highly influenced by seasonality and this is particularly clear in Alpine catchments. Some solute concentrations show trends in time. Sodium and Chloride have increased likely due to the salt (NaCl) used for roads during winter. Total nitrogen, DRP and total phosphorus have decreased due to the adoption of phosphate ban measures. DOC concentrations have also decreased in most catchments, but decrease of TOC concentration is more remarkable. C-Q relationships analysis provides a classification of the solute behavior. Geogenic solutes and chloride are source limited (dilution effect), as b coefficient is negative in almost all cases. Only silicic acid does not show a clear evidence of dilution. Nitrogen species mainly show a source limited behavior during low-flow events and a chemostatic behavior during high flows. This behavior is consistent with the nitrogen element characteristics, as it is a mobile solute, which leaches easily. Suspended solutes are clearly transport limited, as higher flows increase erosion and therefore the sediment concentration. DRP does not show a clear behavior, but there is prevalence of chemostatic behavior during high flows. The total phosphorus is influenced by both DRP and suspended sediments. While for low flow events total phosphorus shows all the three possible behaviors, during high flow events the behavior is clearly transport limited (effect of erosion).

DRP concentration has the most evident decreasing trend in time, and the trend is reflected in the b coefficient. Overall, results provide a comprehensive picture of the behavior, seasonality and trends of solutes in Swiss rivers.

P 10.5

Isotopes in water shed light on changing alpine water resources

Natalie Ceperley[1], Anthony Michelon[1], Harsh Beria[1], Joshua Larsen[1,2], Bettina Schaefli[1]

[1] *Institute of Earth Surface Dynamics, Faculty of Geosciences and the Environment, University of Lausanne, Switzerland*
[2] *School of Earth and Environmental Sciences, The University of Queensland, Australia*

In alpine areas, loss of glaciers and changes in snow pack and cover dynamics present direct and indirect consequences to water resources. The hydrologic, biologic, and physical environment can be expected to change, for example opening up new surfaces for vegetation growth and forestation. We are operating an intensive monitoring program of hydrological processes in the Vallon de Nant, Switzerland (area of 14 km², altitude ranging from 1200 to 3051 m). This site is both a karst system and a protected area, making it a particularly interesting site to study eco-hydrologic processes. Monitoring of stable isotopes (δO18 and δD) in water combined with measurements of climate and hydrologic parameters help to quantify flows through different components of the water balance and assess their certainty. Our presentation will highlight the importance of in situ measurements to quantify the spatial and temporal variations in the water balance. Predicting feedbacks between changes in vegetation and climate is challenging due to the complexity of the hydro-ecological processes. In this presentation, we will review the state of current knowledge regarding these interrelated phenomena and discuss how we will answer open questions in our study catchment in the Swiss Vaudois Alps.

P 10.6

Tracing of the Rhône River within Lake Geneva using the stable isotope composition of water

Cotte Gabriel[1], Vennemann Torsten[2]

[1]*IDYST, University of Lausanne, Géopolis 1015 Lausanne (Gabriel.Cotte@unil.ch)*
[2]*IDYST, University of Lausanne, Géopolis 1015 Lausanne (Torsten.Vennemann@unil.ch)*

Determining the hydrodynamics of lake water is essential for a better understanding of nutrient transport but also of the distribution of potential pollutants through the lake. The objective of this study is to understand the mixing of Rhône River water within Lake Geneva. During summer and autumn, when the lake is thermally well stratified, the Rhône River water can potentially flow more or less directly towards and finally out of the “Petit Lac” (small lake basin close to Geneva) more than 60 km from its mouth. During winter, when stratification is weakened, the water from the Rhône River mixes more diffusively with the water of Lake Geneva. The aim of this study is to determine the path of the Rhône River through the lake more precisely and identify the thermal and meteorologic conditions favourable for different types of flows as suggested by physical circulation models of the Rhône River interflows.

Waters are sampled from different North-South transects across the lake. Bathymetric profiles are measured for temperature, pH, conductivity and oxygen concentrations. In addition, the H- and O-isotope compositions of water, the C-isotope composition of dissolved inorganic carbon and the major ions are analysed. Sampling campaigns are carried out every two months to study the hydrodynamics of the lake at varying thermal conditions. The isotopic composition of water was already proven to be a powerful tool to trace the Rhône River interflow within the lake (Halder et al., 2013) but the details of this interflow remain debatable. It is the aim of the present study to use the isotopic tracer method in much more detailed cross-sections as a tool to both test and verify interflow models based on wind patterns and thermal dispersion of the waters.

The chosen cross-sections, to be sampled regularly and “event-based”, that is after extended periods of similar meteorological conditions, should allow for more precise estimates of the path of the Rhône water interflow and the control of different wind conditions on the formation of resultant gyres of circulation within Lake Geneva. For example, an anticlockwise gyre forces Rhône River water to flow at intermediate depths towards the northern shore of the lake and a return interflow close to the southern shore of the lake. Isotopic mixing models coupled to physical hydrodynamic models of the lake will help constrain the flow paths of the Rhône.

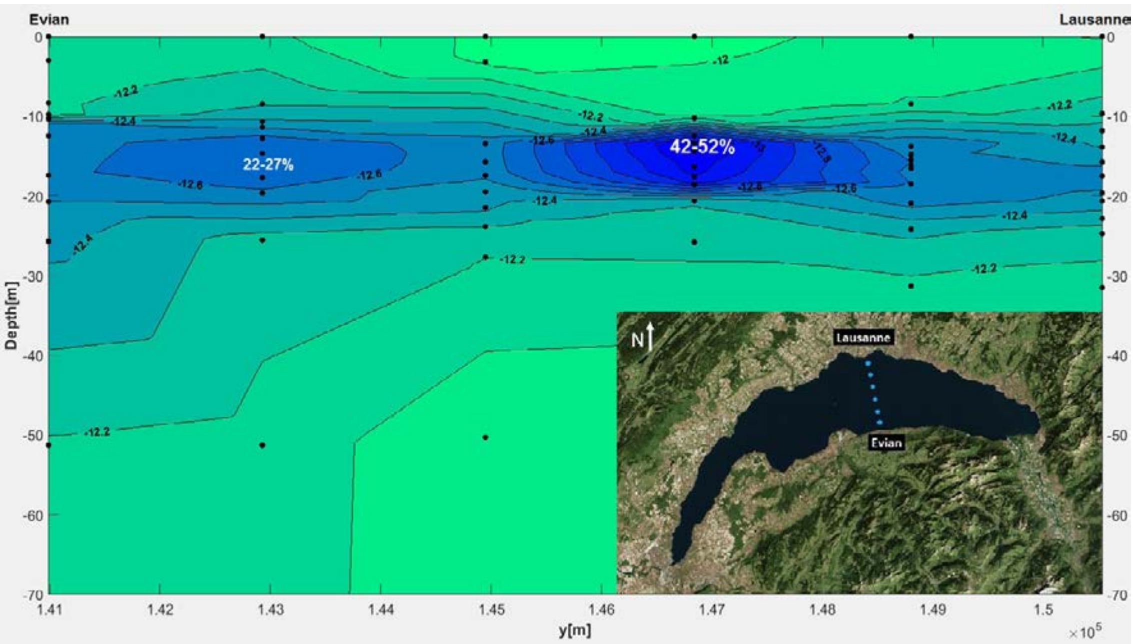

Figure 1. Isotopic composition of oxygen of water $\delta^{18}O_{VSMOW}$ (‰) measured on the Evian-Lausanne cross section in August 2015.

REFERENCES

Halder J., Decrouy L. & Vennemann T. 2013 : Mixing of Rhône River water in Lake Geneva (Switzerland–France) inferred from stable hydrogen and oxygen isotope profiles, Journal of Hydrology 477:152–164

P 10.7

Recharge and Transient Pore Pressure Propagation in steep Alpine Mountain Slopes near Poschiavo, Switzerland

Larissa de Palézieux[1], Simon Loew[1], Peter Zwahlen[2]

* Geological Institute, ETH Zurich, Sonneggstrasse 5, CH-8092 Zurich (larissa.depalezieux@erdw.ethz.ch)
[2] *Büro für Technische Geologie, Grossfeldstrasse 74, CH-7320 Sargans*

Within the scope of planning a hydropower pump storage plant in the Poschiavo valley by Lagobianco SA (Repower AG), numerous cored boreholes with depths of 50 to 300 m were drilled at elevations between 963 and 2538 m a.s.l. (Fig. 1). In several boreholes Lugeon and transient pressure packer tests were executed at various depths and pore water pressure sensors were properly installed in short monitoring intervals, which have been recording since 2011/12/13 until today (Fig. 2). Several of the boreholes intersect large suspended rock slides showing the characteristic zones of highly fragmented rock mass above a kakirite layer of several tens of meters thickness.

This study presents long term transient pressure records from these deep boreholes and relates them to seasonal recharge trends from snow melt and summer rainstorm events. Annual pore pressure amplitudes at depths between 45 and 278 meters, range between 4 and 40 meters. Meteoric pressure signals from snow melt and rain storm events are clearly visible in the pressure records with stronger pressure increase during snow melt than during rainstorms.

First estimations of storage properties of the aquifers intersected by the boreholes are determined by fitting a combined snow melt and precipitation pressure function to the observed (delayed and attenuated) pore pressure records using a convolution of the one-dimensional pressure diffusion equation for a semi-infinite aquifer of constant thickness (De Marsily, 1986). Recharge from snow melt water production is obtained from the Degree-Day Method (Rango and Martinec, 1995) and initial hydraulic conductivity values were taken directly from hydraulic tests executed by Lagobianco SA in similar rock types (Figi et al., 2014). Although simplifying the problem to a single homogeneous layer, this approach yields impressively good fits of the transient pressure records in both damping and temporal delay. Realistic specific storage/yield values for most boreholes are obtained, which vary significantly as a function of sensor depth below the piezometric level.

The obtained values for specific storage and the assumed values for hydraulic conductivity were then verified with a 1D finite element free-surface hydraulic model under steady-state and transient conditions, as a column with two superposed materials of differing permeability, storage properties, and porosity. The simulated values were again fitted to the observed pore water pressure records. The results support the observed values for hydraulic conductivity as obtained from the packer tests with low permeabilities in the intact rock mass and a higher permeability in the rock slide masses. Furthermore, the pore pressure values and amplitudes could be reproduced and the values for specific storage found by convolution could be confirmed.

In the light of changing climatic conditions and the related changes in spatial and temporal precipitation patterns, the understanding of recharge mechanisms and rates of alpine aquifers is crucial. This study contributes to the relatively scarce knowledge in this area, by delimiting realistic ranges of hydraulic conductivity, specific storage, and volumetric water content via the fitting of an analytical solution and numerical modeling results to observed pore water pressures. In the reaction of the pore water pressure to different meteoric events we see a significant sensitivity to the timing, type, and amount of recharge. The increasing annual temperatures and thus decreasing precipitation fallen as snow are likely to affect the general recharge and circulation regime of the aquifers at the scale of the Alps.

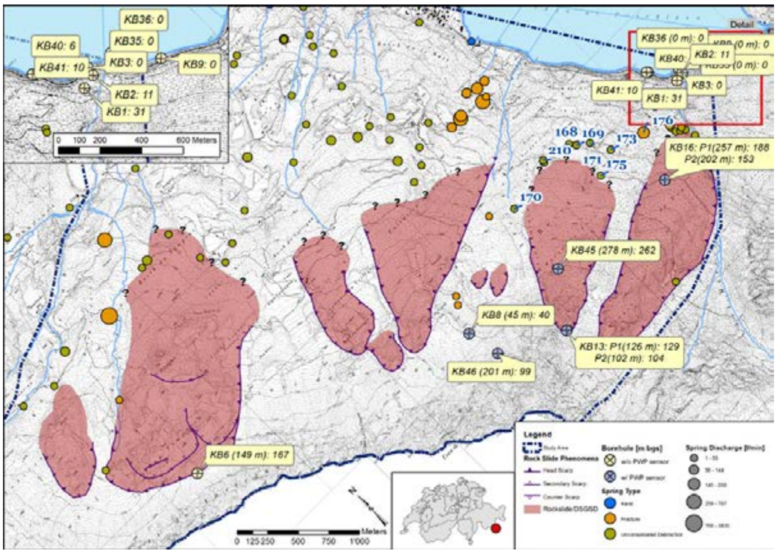

Figure 1. Topographic map of the study area with boreholes (with average water table), springs (type and annual discharge), and rockslide outlines.

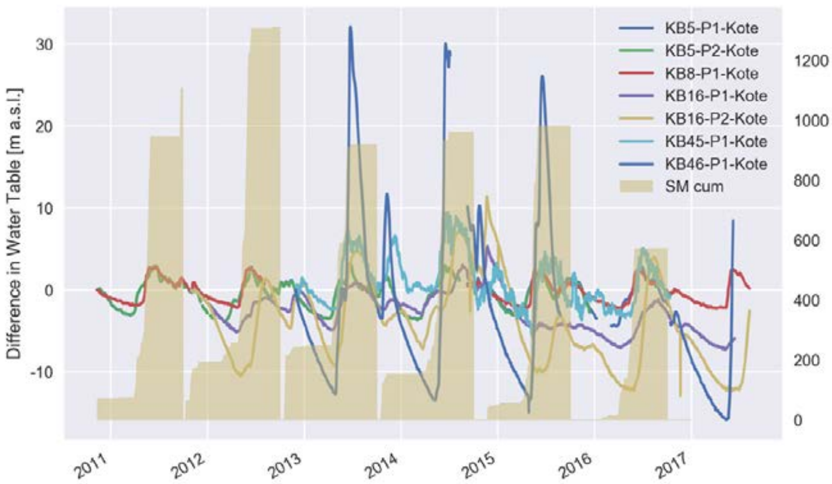

Figure 2. Water table of the boreholes in the study area normalized by the initial water table elevation over the available time-span and cumulative snow melt (per hydrological year) as calculated with Rango and Martinec (1995).

REFERENCES

De Marsily, G. (1986), Quantitative Hydrogeology (pp. 198–199). Masson.

Figi, D., Brunold, F. & Zwahlen, P. (2014), Felskennwerte - Kennwertebericht, Projekt Lagobianco. Büro für Technische Geologie AG, Sargans.

Rango, A., & Martinec, J. (1995), Revisiting the Degree-Day Method for Snowmelt Computations. JAWRA Journal of the American Water Resources Association, 31(4), 657–669.

P 10.8

Gap filling of streamflow time series using Direct Sampling in data scarce regions

Moctar Dembélé[1], Grégoire Mariéthoz[1] & Bettina Schaefli[1]

[1] *University of Lausanne, Faculty of Geosciences and Environment, Institute of Earth Surface Dynamics, Lausanne, Switzerland (moctar.dembele@unil.ch)*

In many regions around the world, observed streamflow time series show too many missing data for a direct use in the context of water resources management, engineering applications or hydrological modelling. Here, we propose the use of the Direct Sampling (DS) method, which was originally designed for the generation of random fields, but sees an increasing number of applications focused on time series. The principle of DS is that it generates new simulated values based on a conditional resampling of a provided training set. In the case of reconstructing gaps in time series, the training set consists of historical data in the same time series during periods not affected by gaps. The method can be extended to multisite time series by considering patterns that span across several neighboring locations. Most importantly, the approach is stochastic and considers short as well as long-range variability of the considered variable. Compared to other methods, one advantage of the DS is that it is almost entirely data-driven, can fit any data structure and simulate the outcome of a complex natural process without assuming a specific statistical model.

This study aims at using the DS technique to fill gaps in daily streamflow data in the Volta river basin (VRB). This is a transboundary river basin (400,000 km^2) that encompasses six countries in West Africa. The area is known to be a data scarce region due to the poor density of gauging stations on the hydrographic network. The average area for stations density is about 3,000 km^2/station while the World Meteorological Organization recommends a maximum of 1,900 km^2/station. The available data are often unreliable because of long gaps in the time series. Many stations show gaps up to an average of 65% of daily records per year, while some of them have complete time series .

Fifteen years of daily streamflow data have been collected for the VRB with some stations and years more complete than the others. In a first step, different scenarios of missing data with continuous and discontinuous, regular and irregular gap size, ranging from days to months, are used to assess the performance of the DS technique in reproducing the data patterns. Results from the DS simulations are compared to results from other methods such as ARMAX, NARMAX and the Thornthwaite-Matter hydrological model. Once validated, the method is used to generate continuous streamflow data across the VRB. Given the simplicity of the DS technique, the method is readily transferable to any other variable and is thus very promising for environmental modeling in general.

P 10.9

How biogeochemistry shapes the ecosystem of Lake Tanganyika

Benedikt Ehrenfels[1 2], Tim Kalvelage[2], Bernhard Wehrli[1]

[1] *Department Surface Waters Research and Management, Eawag, Seestrasse 79, CH-6047 Kastanienbaum (benedikt.ehrenfels@eawag.ch)*
[2] *Institute of Biogeochemistry and Pollutant Dynamics, ETH Zurich, Universitätstrasse 16, CH-8092 Zurich*

Lake Tanganyika is the world's second largest lake by volume and sustains the second largest inland fishery of the African continent. Despite the lake's oligotrophy, upwelling of nutrients from deep waters fuels significant productivity in the euphotic zone. There is evidence that fixation of atmospheric dinitrogen (N2) by cyanobacteria also plays a significant role. Productivity is generally highest in the dry season (period of pronounced upwelling) and in the southern basin of the lake. Fish catches have experienced a long-term declining trend, which has been ascribed to amplified lake stratification in the course of global warming. However, the drivers of spatiotemporal patterns in phytoplankton assemblages and ultimately the fluctuations in pelagic fish catches are not fully understood.

This PhD project will explore how the pelagic food web of Lake Tanganyika responds to spatial and temporal heterogeneity in biogeochemistry. My research objectives are in particular:

1. to assess subsurface nitrogen (N) losses and N regeneration as well as the relative importance of N2 fixation and nutrient upwelling for primary production along a north-south transect during dry and wet season
2. to characterize the functional phytoplankton composition with respect to large-scale spatial and temporal variability in nutrient availability
3. to trace the isotopic signal of dominant phytoplankton functional groups through the pelagic food web

The N sources and sinks will be examined using high resolution biogeochemical profiling, chemical analyses of the dissolved and particulate N species, and 15-15N2 incubations along a north-south transect during different seasons. Primary productivity and phytoplankton community composition will be investigated by wet-chemical analysis and continuous monitoring of photopigment concentrations across Lake Tanganyika. The food web structure will be elucidated by bulk isotopic and amino acid specific isotopic analyses of four trophic levels (phytoplankton, zooplankton, planktivorous and piscivorous fish). The biogeochemical investigations will be complemented by an ecological and genetic study of the relevant pelagic fish species. The new insights gained from this interdisciplinary collaboration will facilitate better predictions about future responses of the lake ecosystem to global warming and direct human impacts and thus, add to a sustainable fishery management strategy.

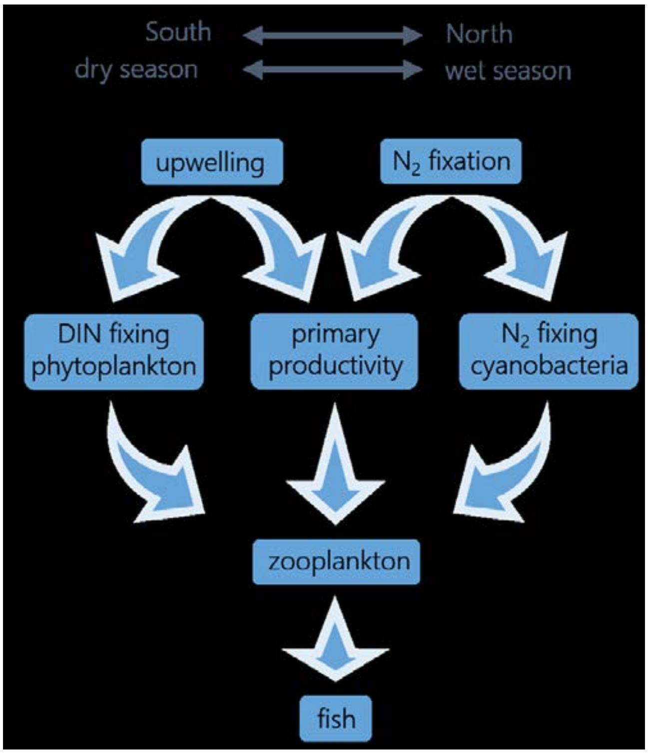

Figure 1. Upwelling and dinitrogen (N2) fixation are the major nutrient cycling mechanisms in Lake Tanganyika. Our underlying hypothesis is that N2 fixation is more important during stratified conditions, whereas upwelling will favor dissolved inorganic nitrogen (DIN) fixers. Upwelling intensities are highest in the South and in the North of the lake. The diffent signals among N2 and DIN fixers in nitrogen isotopy might be traceable through the food web.

REFERENCES

Descy, J. P. et al. 2005: Phytoplankton pigments and community composition in Lake Tanganyika, Freshwater Biology, 50, 668–684.

Edmond, J. M., Stallard, R. F., Craig, H., Craig, V., Weiss, R. F. & Coulter, G. W. 1993: Nutrient chemistry of the water column of Lake Tanganyika, Limnology and Oceanography, 38, 725–738.

O'Reilly, C. M., Alin, S. R., Plisnier, P.-D. D., Cohen, A. S. & McKee, B. 2003: Climate change decreases aquatic ecosystem productivity of Lake Tanganyika, Africa, Nature, 424, 766–768.

P 10.10

Impacts of climate change on the water resources of an Alpine catchment in the Upper Rhone Basin, Valais, Switzerland

Javier Fluixá-Sanmartín[1], Javier García-Hernández[1], Paula Fluixá-Sanmartín[2] & Javier Paredes-Arquiola[2]

[1] Centre de Recherche sur l'Environnement Alpin (CREALP), Rue de l'Industrie 45, CH-1951 Sion (javier.fluixa@crealp.vs.ch)
[2] Department of Hydraulic Engineering and Environment, Universitat Politècnica de València (UPV), camino de Vera s/n, 46022 Valencia, Spain

An adequate management and planning of river basins requires the assessment of the availability of water resources. In Alpine basins, snow covers and glacial zones play an important role in the hydrological cycle. In autumn and winter, a significant part of the precipitation is stored in glacial and non-glacial high mountains areas, creating natural reservoirs. In spring and summer, rivers experience an increase of flow due to the melt of snow and glacier deposits.

Climate change is very likely to have a significant impact on different climatic conditions. Glacier retreat and changes of the meteorological variables are expected, which in turn will affect the water resources availability and discharge conditions. Climate projections for this century show a generalized rise in temperature as well as regional precipitation fluctuations (Figure 1).

Based on these assumptions, the present work aims at analyzing the effects of climate change on the water resources of the Reckingen subbasin, an Alpine catchment located in the Upper Rhone River Basin in Switzerland. A glacio-hydrological model has been created and calibrated using the semi-distributed hydrological software RS MINERVE (García Hernández et al., 2017). This software allows the distinction between glacial and non-glacial regions, to better capture the hydrological processes. Based on previous studies (CH2011, 2011; Funk et al., 2011), 3 emission scenarios (A1B, A2 and RCP3PD) have been analyzed for three 30-year future periods (centered at 2035, 2060 and 2085). For each of them, the meteorological conditions (namely the precipitation and temperature variables) and the glacier coverage have been re-evaluated.

Results show significant fluctuations in the projected discharges of an average year at the outlet of the Reckingen basin (Figure 2). This is specially marked during the spring-summer seasons (May to September). In general, there is a combined tendency to a change of total discharges (mainly due to reduced precipitations coupled with increased temperatures and glacier shrinkage/melt) and a shift toward earlier maximum summer flows (due to an early melting of existing glaciers). This may first entail an increase in the discharges, but a reduction in the water resources availability in the long term.

The analysis of climate change impacts on water resources in alpine catchments helps anticipating climate change effects and adapting management strategies.

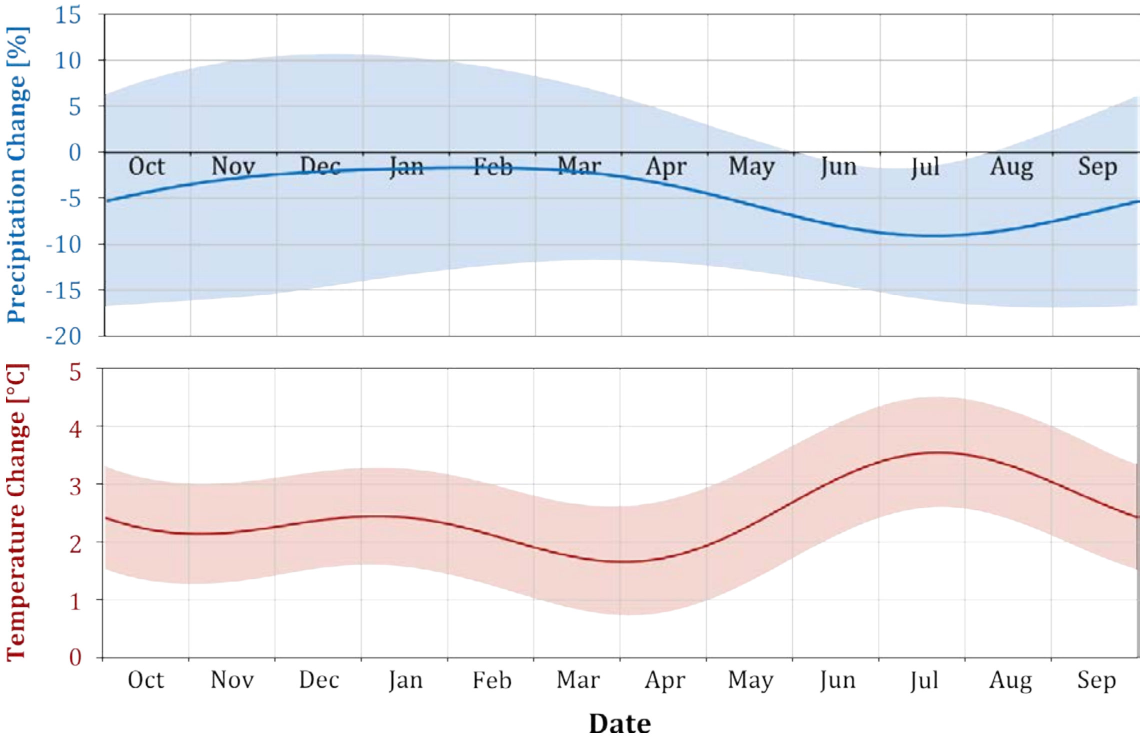

Figure 1. Projected Precipitation (%) and Temperature (°C) changes at the Grimsel-Hospiz station for the 2060-centered period and the A1B emission scenario, including the 95% confidence interval (source: CH2011, 2011).

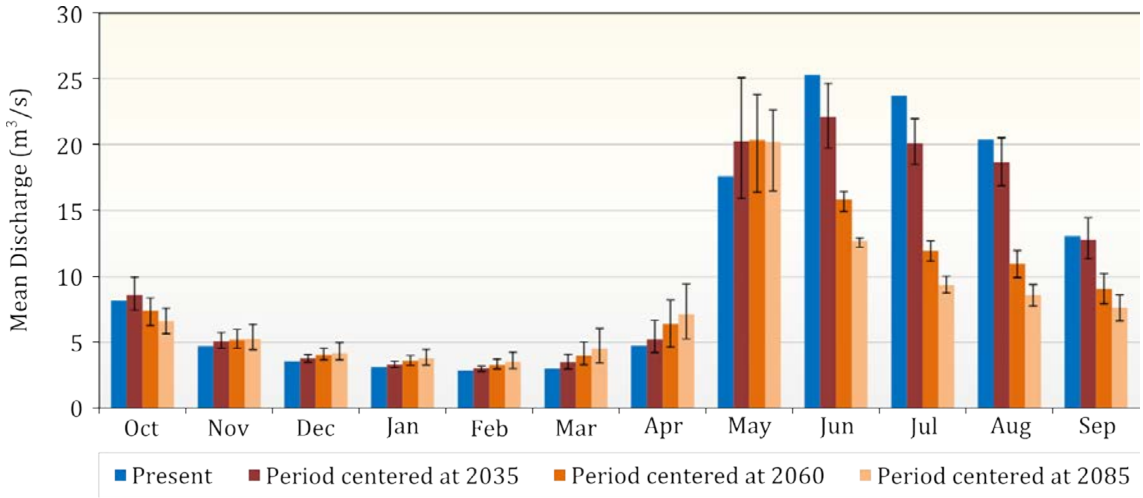

Figure 2. Resulting discharges for an average year at the outlet of the Reckingen basin for 3 periods (centered at 2035, 2060, 2085) and the 95% confidence interval, applying the A1B emission scenario.

REFERENCES

CH2011, 2011: *Swiss Climate Change Scenarios CH2011*, published by C2SM, MeteoSwiss, ETH, NCCR Climate, and OcCC, Zurich, Switzerland, 88 pp.

Funk, M., Bauder, A., Farinotti, D., Usselmann, S., & Jeannette Gabbi, J. 2011: *Gletscher-und Abflussveränderungen im Zeitraum 1900-2100 in sieben Einzugsgebieten der Schweiz*. VAW-Teilprojekt von CCHydro, Schlussbericht. Zurich, Switzerland.

García Hernández, J., Paredes Arquiola, J., Foehn, A. and Roquier, B. (2017). *RS MINERVE – Technical manual*. RS MINERVE Group, Switzerland.

P 10.11

Impact of climate change and anthropogenic pressure on groundwater resources in Regueb basin, Central Tunisia

Emna Guermazi[1,2], Marianne Milano[1], Emmanuel Reynard[1], Moncef Zairi[2]

[1] *University of Lausanne, Institute of Geography and Sustainability, Building Géopolis, CH-1015 Lausanne, Switzerland (guermaziemna@ymail.com)*
[2] *University of Sfax, Department of Geology, National Engineering School of Sfax, PB: 1173-3038, Sfax, Tunisia*

The Intergovernmental Panel on Climate Change (IPCC) expects that renewable surface water and groundwater resources will decrease in most of the dry subtropical regions due to climate change by the 2100 horizon (IPCC, 2014). In addition, population growth, urbanization and economic development apply significant pressures on water resources that lead to the increase of water scarcity, particularly in arid regions. In this context, the present study was conducted in order to analyze the impact of both anthropogenic and climate pressures on groundwater availability in the Regueb basin.

The study area is located in Central-Eastern Tunisia and covers approximately 1'900km^2 (Fig. 1a,b). It is characterized by an average annual rainfall of 193mm and an extended dry season from March to December (Fig. 1c). The land surface elevation in Regueb ranges from 500m in the mountainous region to less than 70m in the main oued (Fig. 1d). The rural aspect of the Regueb basin as well as the good quality of soil and groundwater resources availability have led to the development of the irrigated agriculture sector. Important amounts of water are therefore pumped annually, particularly during the summer season, in order to satisfy the agriculture water needs.

An integrated approach was developed to quantify the water resource balance and to evaluate the current and future pressure applied on groundwater resources.

First, a conceptual model of the unconfined aquifer of Regueb was simulated and calibrated in steady-state and transient-state conditions. Monthly groundwater storage was estimated over a reference (1976-2005) and future period (2036-2065) using the modular finite-difference groundwater flow model (McDonald & Harbaugh 1988). Three climate models were used by the 2050 horizon, based on the outputs of three selected GCMs provided by the Fifth Assessment Report (AR5) of the IPCC (2014): CSIRO-Mk3.6.0, CNRM-CM5 and MPI-ESM-MR. Secondly, monthly irrigation water withdrawals were evaluated based on the decision support system for irrigation CropWat developed by the FAO in 1992. Remote sensing techniques were used to generate the land use map and to identify irrigated areas. Thirdly, urban water use was estimated from population growth and monthly specific water consumption data. The current average specific use is evaluated to be 38.6l/cap/day. It was assumed that this value remained the same all year-round. Three future water use scenarios were considered: (1) a climate scenario (CS) including climate changes only and the projection of land use observation of 2010; (2) a business-as-usual scenario (BAU) considering climate changes and an extension of irrigated surfaces following the recent trends (crops, areas); (3) and an adaptation scenario considering climate changes and an extension of irrigated areas following the recent trends but only with crops requiring few water. Finally, using the data of groundwater resource availability and water use, the impacts of climatic and anthropogenic changes on water resources and management was assessed based on two indicators: the groundwater balance (GB) and the water stress index (WSI).

By 2050, the groundwater balance should decrease by 97%, 30% or 22% compared to the reference period according to climatic projections based on CSIRO-Mk 3.6.0 model, MPI-ESM-MR model and CNRM-CM5 model, respectively. The average annual water use should increase by 3.8% to 16.4% under climate change scenario while it should double under BAU scenario and increase by 50% under the adaptation scenario. The evaluation of WSI shows that water demand should be satisfied by the 2050 horizon under climate change only, while a severe water stress is predicted by 2040 according to the other scenarios.

In conclusion, the applied methodology represents an initiative to raise decision-makers' awareness about the water stress risk on groundwater availability under climate and human pressures.

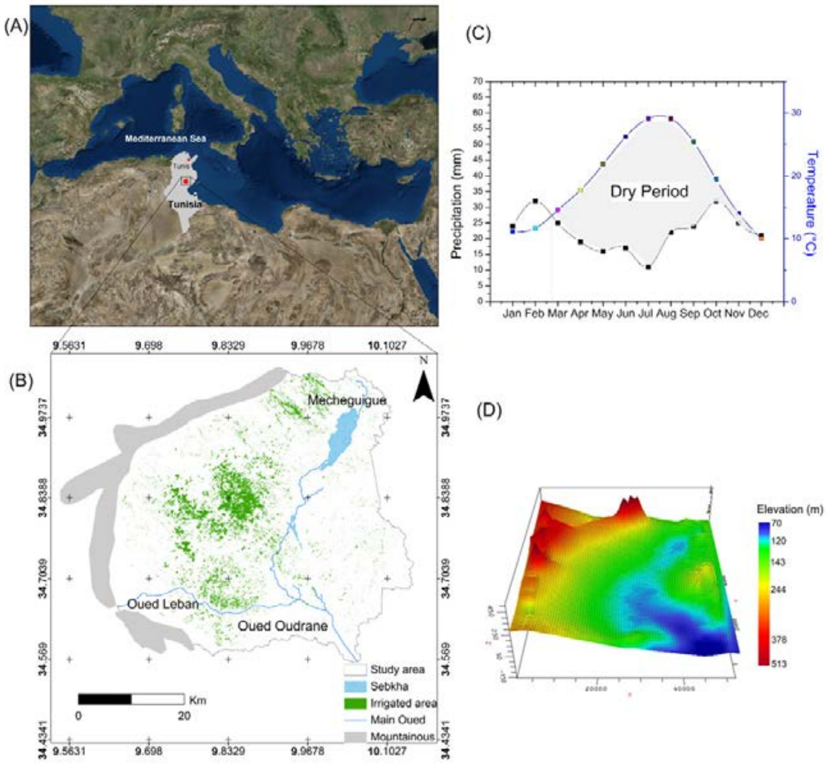

Figure 1. Location of the study area (A). Regueb watershed limit (B). Ombrothermique diagram (C). Land surface elevation (D).

REFERENCES

IPCC, 2014: Climate Change 2014: Synthesis Report. Contribution of Working Groups I, II and III to the Fifth Assessment Report of the Intergovernmental Panel on Climate Change [Core Writing Team, R.K. Pachauri and L.A. Meyer (eds.)]. IPCC, Geneva, Switzerland, 151.

McDonald, MG. & Harbaugh AW. 1988: A modular three-dimensional finite-difference ground-water flow model: Techniques of Water-Resources Investigations of the United States Geological Survey, Book 6, Chapter A1, 586.

P 10.12

Dispersion and mixing in fractured media: interplay between structural and hydraulic heterogeneity

Jeffrey Hyman[1], Joaquin Jimenez-Martinez[1,2,3]

[1] *Earth and Environmental Sciences Division, Los Alamos National Laboratory, Los Alamos, NM 87545, USA (jhyman@lanl.gov)*
[2] *Department Water Resources and Drinking Water, EAWAG, 8600 Dubendorf, Switzerland (joaquin.jimenez@eawag.ch)*
[3] *Department of Civil, Environmental and Geomatic Engineering, ETH Zurich, 8093 Zurich, Switzerland (jjimenez@ethz.ch)*

We study the impact of topological, geometric, and hydraulic heterogeneity on transport processes in fractured media from three-dimensional discrete fracture networks (DFN). We compare transport through analogous structured and disordered fracture networks with varying degrees of hydraulic heterogeneity. Only the two largest scales of heterogeneity, individual fracture and network structure, are considered. For the moderate levels of hydraulic heterogeneity, network structure is the dominant control of transport. Independently of the level of hydraulic heterogeneity, less dispersion in the structured than in the random network is observed, associated to the higher connectivity in the structured network. Increases in dispersion with higher hydraulic heterogeneity are larger in the disordered network than in the structured network, indicating that the interplay between structural and hydraulic heterogeneity is nonlinear. We propose a measure of disorder in fracture networks based on the Shannon entropy definition that integrates structural and hydraulic properties. This can be seen as a first approach to the dispersion potential and mixing capacity of a fracture network.

P 10.13

Assessment of potential pollution of an unconfined aquifer in Abidjan by hydrocarbons

Amenan Agnès Kouame[1], Michel Jaboyedoff[1], Albert Goola Bi Tie[2], Marc-Henri Derron[1] and Kouamé Kan Jean[3]

[1] *Institute of Earth Sciences, University of Lausanne, Geopolis 3129 , CH-1015 Lausanne (amenanagnes.kouamé@unil.ch)*
[2] *UFR of Sciences and Environment management, University of Nangui-Abrogou (Abidjan, Côte d'Ivoire)*
[3] *UFR of Earth Sciences and Mineral Resources, University of Félix Houphouët-Boigny Cocody (Abidjan, Côte d'Ivoire)*

This study of the aquifer of the Continental Terminal is carried out in the Abidjan District located on the coastal sedimentary basin in southern Côte d'Ivoire (West Africa). This unconfined aquifer of the city of Abidjan of Mio-Pliocene age is called "Abidjan groundwater" (Jourda, 1987). The water quality of this aquifer is facing diverse sources of anthropogenic pollution such as scattered deposits of solid and liquid wastes of all kinds. Indeed, the inadequacy of sanitation and drinking water supply systems increases the pollution risk of the Abidjan's groundwater (Kouamé, 2007).
Besides, the proliferation of gas stations, including tank breaking, needs to be considered in the event of an accident, which poses a real threat to groundwater given the complex hydrogeological structure of the region. In order to ensure the effective protection and management of the Abidjan water table, this work proposes to evaluate the risk of contamination of groundwater in the Abidjan aquifer by hydrocarbons such as benzene for the purpose of the implementation of protective measures. This evaluation consist to implement hydrogeological models with FEFLOW 6.2 software.

Various kinds of data have been used to achieve such objectives: in particular, geological maps of Abidjan and Grand-Bassam, the inventory map of the exploitation structures, the reconnaissance structures and the 1: 50,000 piezometric map prepared by SOGREAH, weather data from Abidjan International airport and the piezometric data. These data were also obtained from field surveys carried out for soil sampling. The parameters of models are porosity, hydraulic conductivity, storage coefficient and recharge, Henry constancy, molecular diffusion coefficient, steady-state constant, and Van Genuchten shape parameters.

Using the FEFLOW software, the predictive simulation of underground flow coupled with the transport of dissolved benzene deposited on the soil surface at the N'Dotré and Anador station was implemented. Dissolved benzene initial concentrations are 43,12 and 14,17 mg/l for the two sites respectively for variably saturated zone.The results revealed that between 1 year 10 months and 4 years 3 months the pollutant is detected on the surface of the aquifer at N'Dotré and Anador respectively. In saturated zone, 0.37 mg / l of dissolved benzene was injected at the two stations. This pollutant is detected between 6 and 14 years in certain boreholes in the East Zone and Anonkoua-Koute catchments. In the end, the threat would appear between 38 and 60 years. This overall time of dissolved benzene transport could be 10 time faster if it travels in channels with high hydraulic conductivity. Figure 1 shows the benzene plume at 7305 days (around 20 years) in saturated zone.

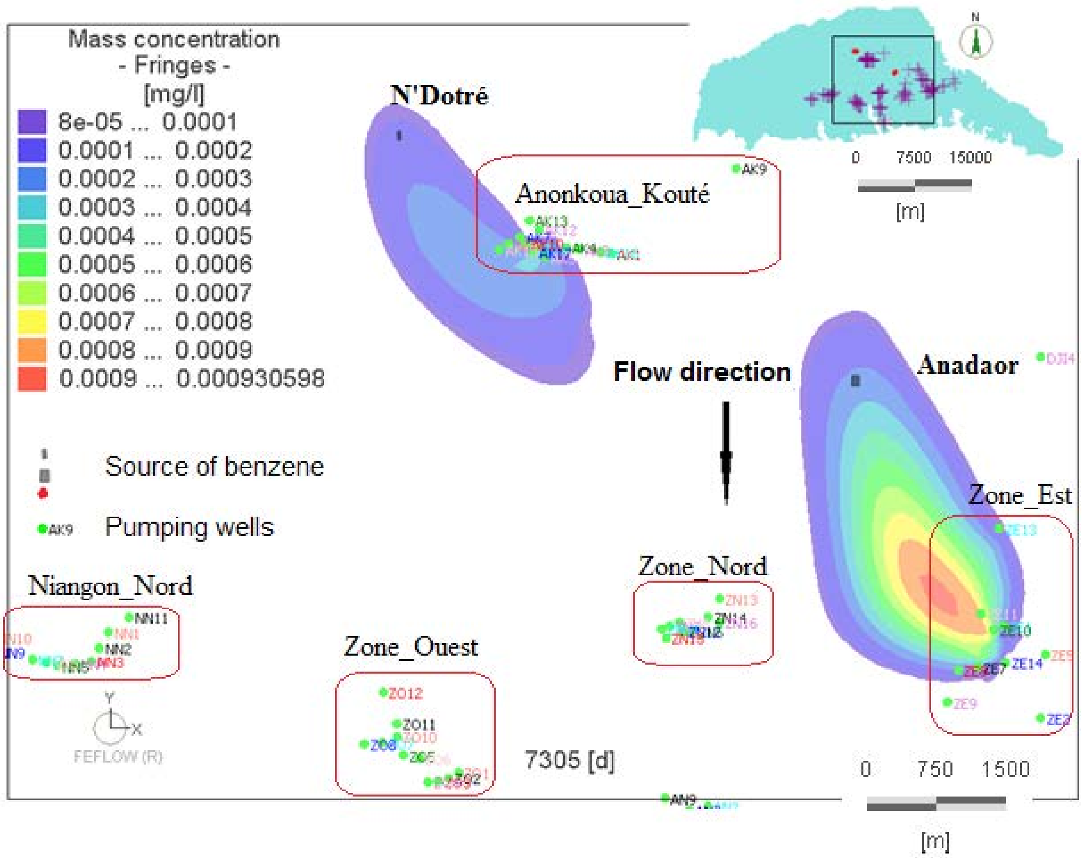

Figure 1. Benzene at 7305 days in saturated zone

REFERENCES

Jourda J. P.1987. Contribution à l'étude géologique et hydrogéologique de la région du Grand Abidjan (Côte d'Ivoire). Thèse de doctorat de 3ème cycle, Université scientifique, technique et médicale de Grenoble, 319p.
Kouamé K. J. 2007. Contribution à la Gestion Intégrée des Ressources en Eaux (GIRE) du District d'Abidjan (Sud de la Côte d'Ivoire) : Outils d'aide à la décision pour la prévention et la protection des eaux souterraines contre la pollution, Thèse de doctorat unique de l'Université de Cocody, 229p.

P 10.14

Role of snowcover on water balance and melt dynamics in the Vallon de Nant, Switzerland

Anthony Michelon[1], Natalie Ceperley[1], Harsh Beria[1], Josh Larsen[1], and Bettina Schaefli[1]

[1]University of Lausanne, IDYST, Geosciences, Lausanne, Switzerland

In Switzerland, water from Alpine catchments provides a large proportion of available water resources. However, large uncertainties regarding changes in glacier volume and snow accumulation can have significant impacts on hydrologic, biologic, physical and economic processes. Accurately quantifying, modeling, and predicting these water resources is therefore an on-going challenge. Given the well-known difficulty observing solid precipitation (snowfall), it can be assumed that most of the uncertainty in water balance estimates for snow-dominated environments is due to: 1) Poor measurement of winter precipitation and 2) A poor estimation of timing and amount of snow melt. It is noteworthy that the timing of melt plays a crucial role even for annual water balance estimates since it might significantly influence melt runoff flow paths and thereby groundwater recharge.

We are monitoringstable water isotopes in an Alpine catchment to shed light on how such observations can constrain water balance estimates. The data set currently spans over more than one year. The selected catchment is the experimental Vallon de Nant catchment in the Vaud Alps of Switzerland, where detailed hydrologic observations have started in 2016 addition to the existing vegetation and soil investigations. The Vallon de Nant (14 km^2, and an altitude ranging from 1200 to 3051 m) is a narrow valley that accumulates large amounts of snow during winter. In spring and summer, the river discharge is mainly supplied by snowmelt, with additional inputs from a small glacier and rainfall. Continuous monitoring of water stable isotopes (δO18 and δD) is combined with measurements of climatic and hydrological parameters to quantify water fluxes. Measurements and sampling in such an environment is challenging and has rarely been done at such a high temporal resolution for a full annual cycle. We will discuss the advantage of our approach for 1) evaluating the dominant hydrological processes and pathways in Alpine environments and 2) for reducing the uncertainties of water resource estimation in Alpine catchments.

P 10.15

Parameter estimation: drivers of extreme discharge in the Northwestern Switzerland

Daniela Pavía[1], Henning Lebrenz[1] & András Bárdossy[2]

[1] *Institute of Civil Engineering, University of Applied Sciences and Arts Northwestern Switzerland FHNW, Gründenstrasse 40, CH-4132 Muttenz (daniela.paviasantolamazza@fhnw.ch)*
[2] *Institute for Modelling Hydraulic and Environmental Systems, University of Stuttgart, Pfaffenwaldring 61,DE- 70569 Stuttgart*

Hydrologists are challenged to estimate extreme discharges from catchment basins with data of relative poor temporal and spatial resolution. In addition, the probability of occurrence of the input driver (i.e. extreme precipitation) is assumed the same as the proabbility of the response (i.e. extreme discharge). However, extreme discharges are complex processes derived from catchment responses from diverse meteorological inputs. A better understanding of driving precipitation inputs, catchment properties and a-priori conditions is required in order to characterize flood procceses and to determine shape, volume and peak of the hydrograph of the extreme discharges.

Therefore, we investigate on the driving spatial and temporal variability of extreme precipitation and the heteoreogenity of the catchments in order to describe different procceses and to identify hydrologically relevant parameters for extreme discharges (Fig. 1.). We use entropy as a descriptor of the precipitation patterns. First results from data of 46 catchments (<200 km^2), located within Northwestern Switzerland, with temporal resolutions of 10-15 minutes are presented.

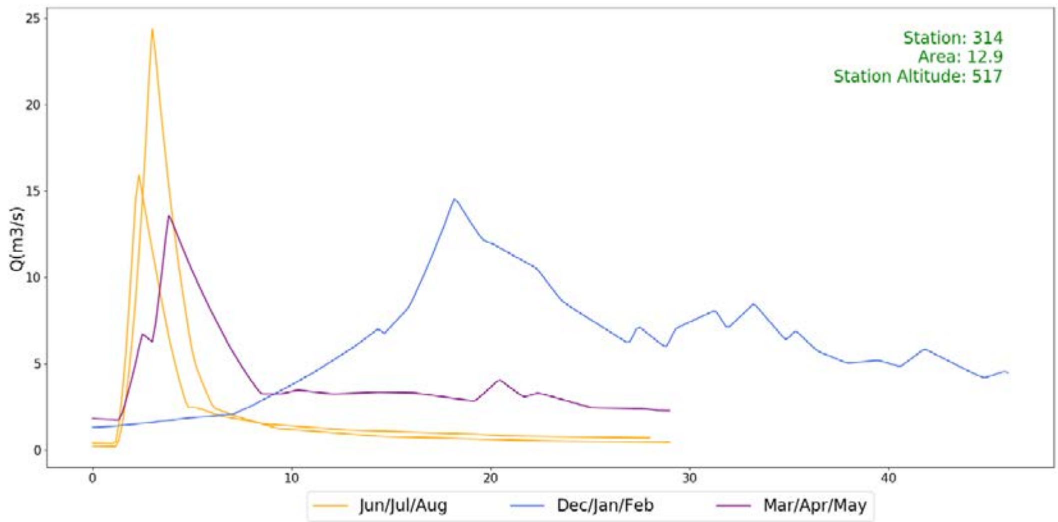

Figure 1. Hydrographs of the 4 highest peaks of a catchment (12.9 km^2) in Northwestern Switzerland, indicating different event dynamics and parameters, leading to different shapes, peaks and volumes.

P 10.16

Water transit time variability in time and space by fully distributed hydrology-transport modelling

Federica Remondi[1], Simone Fatichi[1], James W. Kirchner[2,3] & Paolo Burlando[1]

[1] Institute of Environmental Engineering, ETH Zürich, Stefano-Franscini-Platz 5, CH- 8093 Zürich (*remondi@ifu.baug.ethz.ch*)
[2] Department of Environmental Systems Science, ETH Zürich, Universitätstrasse 16, CH-8092 Zürich
[3] Swiss Federal Research Institute WSL, Zürcherstrasse 111, CH-8903 Birmensdorf

The time water takes to travel in a catchment and the pathways it follows are crucial elements in characterizing hydrologic response. Understanding their variability in time and space sheds light on the link between discharge formation and water quality at the catchment scale. Here, we introduce a novel modeling framework to explore water transport mechanisms using the Hafren basin in Wales (UK) as a case study. We show that a fully distributed process-based hydrological model coupled with a transport component for conservative tracers can successfully reproduce water and conservative tracer fluxes. We present results from using the model as a tracking tool to follow the paths of water parcels that entered the catchment as rainfall over 2 years. The agreement between tracer simulations and observations demonstrate that dynamic transit time distributions both forward and backward in time can be directly estimated from a hydrochemical model with a high spatial and temporal resolution without assuming a priori any transit and solute selection laws. The approach proves useful in quantifying how hydrometeorological conditions and spatial heterogeneity affect water transit time and age distributions in a real catchment.

P 10.17

Hydro-CH2018: Climate change and its consequences on hydrology in Switzerland

Petra Schmocker-Fackel[1], Fabia Hüsler[1], Samuel Zahner[1], Roland Hohmann[1], Olivier Overney[1]

[1] *Federal Office for the Environment FOEN, Papiermühlestrasse 172, CH-3063 Ittigen (petra.schmocker-fackel@bafu.admin.ch)*

In the framework of the recently established National Center for Climate Services (NCCS), the FOEN's Hydrology Division is in charge of the focus area "Climate Change and its consequences on Hydrology in Switzerland Hydro-CH2018". This focus area aims at preparing the hydrological basics required to address climate adaptation measures. In addition to the continued development and maintenance of the long-term hydrological monitoring, this also includes further improving our understanding of the hydrological processes through targeted research projects. The update of hydrological scenarios based on the new CH2018 climate scenarios, potential multi-purpose use of lakes and reservoirs, water quality and ecology, as well as future changes in the hydrological cycle are of particular interest. The expected products are a state-of-the-art summary of the hydrological knowledge and the closing of knowledge gaps in order to meet the measures formulated in the national climate change adaptation strategy. Furthermore, climate services in the field of water will be developed. Such services comprise scientific information and data on the climate of the past, present and future, as well as its consequences and shall serve as the basis for decision-making in the context of climate issues. As such, they are expected to support government, political and business sectors and society to minimise climate-related risks, recognise opportunities and optimise benefits and costs.

P 10.18

What role for citizen science in flood hazard mapping?

Bocar Sy[1], Corine Frischknecht[1], Hy Dao[2], David Consuegra[3] & Gregory Giuliani[4]

[1] *Department of Earth Sciences, University of Geneva, Rue des Maraichers 13, CH-1205 Geneva (Bocar.Sy@unige.ch)*
[2] *Department of Geography and Environment, University of Geneva, Boulevard Carl-Vogt 66, CH-1205 Geneva*
[3] *Institute of Territorial Engineering, School of Management and engineering Vaud, Route de Cheseaux 1, CH-1401 Yverdon-les-Bains*
[4] *Institute for Environmental Sciences, University of Geneva, Boulvard Carl-Vogt 66, CH-1205 Geneva*

Flood events cause substantial losses, on human life or economic income. One of the key elements necessary for developing efficient strategies in hazard and risk mitigation is flood hazard mapping.

Current flood hazard mapping strategies are based on data coming from hydrometeorological stations, remote sensing and hydrological/hydraulic modelling. These classical tools are used for input data acquisition such as topographic information, soil characteristics, rainfall data or land use typology, and for output results such as flood extent, water depth, flow velocity or velocity*depth products (De Moel et al., 2009; Prinos et al., 2009). Despite the numerous advantages of these tools for flood hazard mapping, they also present some limitations. For ground data acquired by instruments, extensive spatial and temporal coverage is a challenge as well as the maintenance and data processing cost (Houghton-Carr, 2014). In the field of remote sensing, depending on the type of sources (e.g. active or passive) and the location on Earth, issues can raise from incomplete or low spatio-temporal coverage, alteration of the quality of the scene or even its cost. As for hydrological modelling, the output is highly dependent on the quantity, accuracy and precision of the input data.

With the rise of web 2.0 technologies (Batita et al., 2012) and participatory research (Cornwall and Jewkes, 1995), we argue that citizen science, i.e. participation of the public in scientific research projects (Wiggins and Crowston, 2011) has the potential to provide valuable spatial data for flood hazard analysis.

This work presents the contribution of citizen science in flood hazard analysis in a pilot study: a suburban area of Dakar, Senegal, where flooding has emerged lately as major threat for poor people and is also an area undergoing rapid changes. This area is characterized by a) lack of a catalogue of past events, b) poor coverage of hydrometeorological stations, c) no regular update of basic data, such as topography, and d) some quality and frequency issues with satellite images.

Using a combination of citizen science techniques, such as participatory mapping, participatory GIS and social media, the citizens of the area were able to provide different thematic spatial data. Figure 1 illustrates the contribution of citizen science on basic data acquisition and output results. Figure 1a shows an example of rainfall data reported by local citizens at different locations, from August to September 2016. Contributors collected daily average rainfall through simple devices implemented in this regard, and posted their data on our Facebook page (https://www.facebook.com/xeex.meude), whereas figure 1b displays water depth reached during past floods, independently of the event, provided by local representatives across participatory mapping and participatory GIS.

Figure 1. The contribution about citizen science for flood hazard mapping a) with rainfall data and b) with water depth

These promising results show how citizen science through participatory mapping and participatory GIS can provide useful information in flood hazard analysis, in particular for areas where no instrumental network is available and financial resources are scarce.

REFERENCES

Batita, W., Roche, S., Bédard, Y. & Caron, C. 2012: WikiSIG et GeoDesign collaboratif: Revue internationale de géomatique–n, 255, p. 285.

Cornwall, A. & Jewkes, R. 1995: What is participatory research?: Social science & medicine, v. 41, no. 12, p. 1667-1676.

De Moel, H., Jongman, B., Kreibich, H., Merz, B., Penning-Rowsell, E. &Ward, P. 2015: Flood risk assessments at different spatial scales: Mitigation and Adaptation Strategies for Global Change, 20, 865-890.

Houghton-Carr, H. 2014, Surface water handbook: water level, stage-discharge and flow. Indian Hydrology Project

Prinos, P., Kortenhaus, A., Swerpel, B., Jiménez, J. A. & Samuels, P. 2009: Review of flood hazard mapping.

Wiggins, A. & Crowston, K. 2011: From conservation to crowdsourcing: A typology of citizen science, *in* Proceedings System Sciences (HICSS), 2011 44th Hawaii international conference on 2011, IEEE, p. 1-10.

P 10.19

Modern recharge and flowfield organization of the Nubian Sandstone Aquifer System in Northern Chad

Marie-Louise Vogt[1], François Zwahlen[1], Hamza Ibrahim[2], Philip Brunner[1] and Daniel Hunkeler[1]

[1] *Centre d'Hydrogéologie et Géothermie, University of Neuchâtel, rue Emile-Argand 11, 2000 Neuchâtel, Switzerland (marie-louise.vogt@unine.ch)*
[2] *Institut de Géologie, Faculté des Sciences Exactes et Appliquées, University of N'Djaména, Chad*

We aim to understand the potential contribution of modern recharge from the mountainous regions of Northern Chad (Ennedi, Tibesti) to the very large fossil Nubian Sandstone Aquifer System (NSAS); the most important aquifer system of Northern Africa. Previous studies concluded that in the current climate, the system does not receive significant recharge, in contrast to the middle Holocene when rainfall was estimated to be around 400 mm/y. Geographical remoteness and political instability have so far prevented a detailed investigation seeking to understand recharge pathways and dynamics.

Combining remote sensing and hydrochemistry provides new insights into recharge mechanisms and dynamics from the mountainous regions at the margins of the NSAS. Previous studies have shown that stable isotopes are an excellent tool to discriminate between modern and paleorecharge. Along wadis and at specific accumulation points, surface and near surface water changes occur on a spatial scale < 100 m and on a temporal scale of a few days. At these locations, surface water can infiltrate and generate recharge. Therefore, we employed LandSat8OLI images (spatial resolution 30 m, temporal resolution 16 days) in combination with rainfall estimates products (FEWS-NET) to understand surface water occurrence and to build a relationship between geographical variability and intensity of precipitation with superficial flow response. Ground-truth observations of surface water occurrences were collected during several field campaigns (2013 - 2016) within the framework of the ResEau project (https://reseau-tchad.org/). Surface and groundwater samples were obtained at 180 locations, covering an area of 88'000 km^2. They were analyzed for their stable isotopes and major ion signatures.

LandSat images show that when high intensity precipitation occurs in the mountains of Northern Chad, surface water is rapidly transferred to the lower lands over distances of 100 km. Frequencies of such events are spatially variable, with the southern slopes receiving more frequent and intense rainfall than the northern slopes. The hydrochemical variability shows the same pattern: stable isotopes have ratios comparable to current rainfall over the mountains of the Ennedi (where rains amount at 100 mm/y) and on the southern slopes of the Tibesti (40 mm/y). The spatial evolution of stable isotopes is also in strong agreement with the hydraulic gradient at a regional scale, meaning that flow velocities and mean residence time could be determined based on conceptual groundwater flow models. Groundwater flows from the mountains towards the lakes of Ounianga where depleted isotopic ratios are comparable to values found in other parts of the NSAS (e.g. Kufra oases in Libya), where groundwater age was identified to be between 9'000 and 36'000 yrs.
The results obtained indicate that a significant amount of modern recharge is happening. We are able to geographically constrain the areas involved which collect and transmit effective precipitation to the NSAS.

P 10.20

Evaluating groundwater flow at multiple temporal scales using passive electrical measurements

Emily B. Voytek[1], Damien Jougnot[2] & Kamini Singha[3]

[1] *Institute of Earth Science, University of Lausanne, Géopolis, CH-1015 Lausanne (emily.voytek@unil.ch)*
[2] *Sorbonne Universités, UPMC Univ Paris 06, CNRS, EPHE, 75005 Paris, France*
[3] *Hydrologic Science and Engineering Program, Colorado School of Mines, Golden, Colorado.*

Accurate quantification of groundwater flow patterns, both in magnitude and direction, is a necessary component of evaluating any hydrologic system. Groundwater flow patterns are often determined using a dense network of wells or piezometers, which can be limited due to logistical or regulatory constraints. The self-potential (SP) method, a passive geophysical technique that relies on currents generated by water movement through porous materials, is another method which can be used in addition to traditional piezometer networks to evaluate flow patterns. Naturally generated currents can be measured as voltage differences at the ground surface using only two electrodes, or using a more complex electrode array installed in the ground. The method can be used to analyze hydrologic processes at various temporal and spatial scales. Here we present the results of SP surveys collected at multiple scales (1 to 10s of meters) and demonstrate how these measurements can be used to evaluate changing patterns of groundwater flow at the daily or seasonal time scale.

P 10.21

Iron speciation in lake sediments of Moossee (Swiss Plateau) as anoxia proxy by applying a new sequential extraction technique

Giulia Wienhues*, Stamatina Makri*, Martin Grosjean*, Fabian Rey**

* Institute of Geography & Oeschger Centre for Climate Change Research, University of Bern, Erlachstrasse 9a, CH-3012 Bern, Switzerland
** Institute of Plant Sciences & Oeschger Centre for Climate Change Research, University of Bern, Altenbergrain 21, CH-3013 Bern, Switzerland

Fluctuations in temperature and nutrient input influence the mixing regime of lakes and also the various biochemical processes in the water and water-sediment interface. Laminated lake sediments are useful archives to reconstruct climatic and environmental changes through time, due to their high temporal resolution.
A current issue is the progressing anoxia in marine and freshwater systems during the last century (Diaz 2001). There are only a few proxies established (e.g. bacterio-pheophytins, µXRF Mn/Fe-ratios, among others…) established to reconstruct the oxidation history and paleoredox conditions of bottom waters in lakes. In many paleolimnological studies, µXRF Mn/Fe-ratios are used as paleo-redox proxies with the reasoning that Fe and Mn have a different redox behavior. However, µXRF does not reveal information about the different Fe and Mng species, which may or may not be related to redox-driven precipitation but rather reflect soil erosion, carbonate precipitation or aquatic productivity. Long-term studies regarding oxygenation and redox state changes of lake bottom water are analytically challenging difficult and rarepoorly done. However, it is necessary to understand anoxia because of its heavy impact on lake ecology. The aim of this study is to assess the sources of Fe and Mn and the processes of their precipitation to the sediments by analysing different Fe and Mn fractions and, thus, to better understand establish a new method to reconstructpast oxygenation and mixing regimes in of the lalake ke system by applying a sequential extraction method to determine Fe and Mn fractions of the lake sediment of Moossee.

We present an adapted sequential extraction technique (from soil sciences) that enables the quantitative (concentration) distinction between mineralogical fractions. We are able to distinguish between seven iron and manganese fractions: (F1) Fe(II)-Phosphates, (F2) adsorbed / exchangeable / carbonates (AEC), (F3) humic material, (F4) amorphous Fe-oxyhydroxides and Mn oxides, (F5) crystalline Fe oxides, (F6) Fe sulphides and organics and (F7) residuals and silicates.

The quantitative composition of these fractions indicates paleo environmental depositional conditions (Poulton and Canfield 2005) such as anoxia. Sequential extraction techniques have never been applied to lake sediments before. Understanding the cycling and deposition behaviour of metals in the lake can provide additional information about paleo environmental and –climatic conditions and how they affect the lake system.
In addition, we measured We compared the resulting Fe and Mn species with the Mn/FeµXRF ratio (redox proxy), loss on ignition LOI, data, C/N/S data, µXRF elemental composition and sedimentary pigments as inferred from scan data and hyperspectral imaging. data, in order to understand their speciation behaviour. Finally, we tested whether the different Fe and Mn fractions can be attributedssigned to specific lake or catchment processes and assessed to prove whichat factors finally drive the total Mn/Fe ratio (as e.g. measured with uXRF).

The lake sediment samples were taken in a wide temporal ime rrange from the Late Glacial to Mmodern Ttimes. The preliminary results show, based on the vertical distribution of Fe and Mn fractions, that it is possible to reconstruct the oxygenation states of the bottom water in Moossee. Periods of reducing and anoxic conditions coincided with enhanced formation of reduced Fe species and are expressed in increased relative amounts of these species in to the total metal fractionconcentration. Furthermore, we find that also long-term (Holocene) ecosystem changes such as the natural eutrophication of the lake system, forest and vegetation dynamics, soil development, deforestation and land use changes as well as the erosion history since the Early Holocene are clearly shown by the Fe speciation pattern.
We conclude that, in Moossee, the Mn/Fe ratio is mainly driven by redox-sensitive behaviour of the two metals but also by detrital inputs from the catchment.

With an appropriate research design the detection of Fe speciation in lake sediments with the here presented sequential extraction method has a great potential for reconstructing biochemical metal cycles in lakes and for providing information about paleo environmental conditions.

REFERENCES

Diaz R.J. 2001: Overview of Hypoxia around the World. Journal of Environmental Quality, 30, 275–281.
Poulton, S.W. & Canfield D.E. 2005: Development of a sequential extraction procedure for iron: implications for iron partitioning in continentally derived particulates. Chem Geology, 214, 209–221.

P 10.22

Analysis of trends of hydroclimatic variables in the White Bandama Basin, Northern Côte d'Ivoire

Franck Zokou Yao[1], Ismailia Ouattara[1], Emmanuel Reynard[2] & Issiaka Savane[1]

[1] *Faculty of Sciences and Environmental Management, University Nangui Abrogoua, 02 BP 801 Abidjan 02, Côte d'Ivoire (f.zokou@yahoo.fr)*
[2] *Institute of Geography and Sustainability, University of Lausanne, Géopolis, CH–1015 Lausanne*

The Sahelian climate is characterized by a rainy season of a few months in summer and an average annual rainfall of less than 700 mm. The surface water dries up very quickly during the long dry season. The Sudano-Sahelian zone of West Africa, which encompasses northern Côte d'Ivoire is no exception. This part of the African continent is therefore a concern for the scientific community, so for its socio-economic development as for the well-being of the populations.

In this poster, trends on hydroclimatic variables in the White Bandama Basin in northern Côte d'Ivoire are studied. The non-parametric CUSUM test and parametric t-Student test are used to detect changes in series of data. The parametric Mann Kendall test, linear regression test and Sen's test show amplitude of changes. All these tests are applied on data from 15 rainfall stations, and 5 hydrometric and temperature stations over the period 1944-2015.

This basin-scale and monthly data analysis shows a decreasing trend in precipitation and runoff from 1971 to 2010, while temperature increases over the same period.

11. Environmental Biogeochemistry of Trace Elements

Andreas Voegelin, Moritz Bigalke, Montserrat Filella, Adrien Mestrot, Lenny Winkel

Swiss Society of Mineralogy and Petrology (SSMP)

TALKS:

11.1 **Bhattacharya S.**
Arsenic contamination in the groundwater and soil and subsequent bioaccumulation in the edible crops in Bengal Delta

11.2 **Cojean A.**, Zopfi J., Robertson E., Thamdrup B., Lehmann M.F.
Fe^{2+}, H_2S and Mn^{2+} Availability modulate the Balance between N-Removal and N-Recycling in Lake Lugano Sediments

11.3 **Feinberg A.**, Stenke A., Suess E., Peter T., Winkel L.H. E.
Tracing the atmospheric transport and fate of selenium using a chemistry-climate model

11.4 **Filella M.**
Beauty, bottlenecks and progress in the study of the environmental behaviour of less-studied technology-critical elements

11.5 **Gfeller L.**, Mestrot A.
Spatial distribution of mercury and methylmercury in an industrially polluted floodplain soil.

11.6 **Imseng M.**, Wiggenhauser M., Frossard E., Müller M., Keller A., Wilcke W., Bigalke M.
Copper and zinc stable isotopes as analytical tool to trace sources and processes in agricultural systems

11.7 **Kretzschmar R.**, Christl I., Kotsev T. (Keynote)
Arsenic pollution of Ogosta River floodplain by legacy mining: Assessing pollution and environmental impacts at different scales

11.8 **Mueller E.**, von Gunten U., Bouchet S., Winkel L.H.E.
New insights into the oxidation of marine organic sulfur compounds by reactive bromine species

11.9 **Müller B.**
Trace elemental analysis of arsenic-contaminated groundwater in the lowlands of Nepal suggest the initial source of arsenic in the High Himalayas

11.10 **Peter Hug D.**, Castella E., Slaveykova V.I.
Metal availability to invertebrate community: integrating field experimentation and modelling

11.11 **Su G.**, Niemann H., Zopfi J., Lehmann M.F.
Limitation of anaerobic oxidation of methane in sulfate-rich lake sediments

11.12 **Wick S.**, Fischer M., Pfenninger N., Voegelin A.
Solubility of thallium in soils: role of Tl uptake by illite

11.13 **Wiggenhauser M.**, Bracher C., Imseng M., Keller A., Rehkämper M., Eikenberg J., Wilcke W., Frossard E., Bigalke M.
The fate of P fertilizer derived Cd in soil-wheat systems

POSTERS:

p 11.1 **Blattmann T.M**., Liu Z., Wen K., Lin S., Li J., Zhao Y., Zhang Y., Wacker L., Haghipour N., Plötze M., Eglinton T.I.
Geochemical tracing of sedimentary organic matter and associated clay minerals in the South China Sea

P 11.2 **Caplette J.**, Mestrot A.
Trapping of volatile antimony (Sb): current work and future developments

P 11.3 **Chonova T.**, Slaveykova V.I.
Inorganic mercury adsorption and internalization kinetics and the role of dissolved organic matter

P 11.4 **Deonarine A**, Gfeller L, Neuhaus P and Mestrot A.
Mercury and methylmercury quantification in floodplain soils, canal sediments, and plants in the Upper Valais

P 11.5 **Groß-Schmölders M.**, Woodard J., Krüger J., Leifeld J., Alewell C.
Depth profile of $\partial^{15}N$ indicates drainage effects on peat

P 11.6 **Guilmot S.**, Slaveykova V.I.
Toxicity and uptake of mercury compounds to the cyanobacterium *Synechocystis* PCC603

P 11.7 **Hoffmann K.**, Christl I., Kaegi R., Kretzschmar R.
Effects of metal-to-sulfide ratio, NOM, and Mn^{2+} on metal sulfide nanoparticle characteristics

P 11.8 **Marafatto F.F**., Ferreira-Sanchez D., Dähn R., Grolimund D., Voegelin A.
Synchrotron X-ray beam-induced chemical transformations: The case study of Tl redox changes as a function of photon flux and temperature

P 11.9 **Rodríguez-Murillo J.C**. , Filella M.
Exploring the application of time series analysis methods to concentration data from Swiss rivers and lakes

P 11.10 **Van Groeningen N.**, Christl I., Kretzschmar R.
Mn(II) and Cd(II) sorption to synthetic montmorillonite

11.1

Arsenic contamination in the groundwater and soil and subsequent bioaccumulation in the edible crops in Bengal Delta

Sayan Bhattacharya[1]

[1]*School of Ecology and Environment Studies, Nalanda University, Rajgir, District: Nalanda, Bihar-803116, India.*

Arsenic (As) is a metalloid of great environmental concern because of its highly toxic nature and colossal abundance. The Bengal basin is considered as one of the most acutely arsenic affected geological provinces in the world. The research work was performed in a part of Bengal Delta [Kalinarayanpur (23°14’ N, 88°59' E), Nadia, West Bengal, India] for exploring the status of arsenic contamination.

Pre monsoonal and post monsoonal water samples were collected from the tube wells and the groundwater parameters were studied in HG-AAS and spectrophotometric methods. Sediment layers were collected up to 160 ft. depth in each 5 ft. interval and the samples were analysed for arsenic (As) in HG-AAS. Oxidizable organic carbon (OOC) and organic matter (OM) of the soil samples were measured. Rice (*Oryza sativa*) and jute (*Corchorus capsularis*) plant samples of different age groups were studied for arsenic bioaccumulation; different plant parts were dried, digested and analyzed in HG-AAS.

The results showed that the groundwater samples were highly contaminated with arsenic. Analysis of the sediments showed that arsenic levels decreased from the surface (2.89 mg/kg of soil) till a depth of about 45 feet (0.3 mg/kg), following which there was a constant concentration of arsenic along the gradient of increasing depth. Both the percentage of oxidizable organic carbon (OOC) and organic matter (OM) in soil showed a gradual decrease with depth till approximately 45-50 feet and constant levels at depths beyond 45-50 feet. A strong correlation was found between the distribution of As and OOC. This was in synchrony with the fact that arsenic was co-deposited with OOC in soil, and the correlation between them was due to arsenic retention and high OOC inputs in the vegetated zones of the Bengal basin.

There was a time-dependent decline of arsenic content in the diverse parts of *Oryza sativa*. The accumulation of arsenic remained significantly high in the initial phase (i.e. 1 month age); particularly in root zones it was 149.4 mg./kg, in stem basal part 22.5 mg./kg., in stem middle part 6.34 mg./kg., in stem apical part 2.78 mg./kg., in leaves 1.53 mg./kg and in the early phase of grains (apical parts in tillering stage) 0.29 mg./kg. In the 3 months old plants, arsenic bioaccumulation in rice roots was 31.4 mg./kg, in stem basal part 7.72 mg./kg., in stem middle part 0.52 mg./kg., in stem apical part 0.43 mg./kg., in leaves 0.12 mg./kg and in the grains 0.07 mg./kg. The possible reason behind it is the existence of oxidized zone around the rice root zone which helps to form oxidized iron plaque (Bhattacharya *et al.*, 2012). Iron plaque can efficiently bind arsenic and can reduce its translocation to the above ground tissues (straw, husk and grain) of the plant (Liu *et al.*, 2004; Norra *et al.,* 2005). Accumulation of arsenic showed a root> basal stem> median stem> apical stem> leaves> grains trend in *Oryza sativa*. *Corchorus capsularis* followed a trend of arsenic bioaccumulation similar to *Oryza sativa*. In the initial phase of growth (i.e. in 1 month), arsenic bioaccumulation in jute roots was 8.701 mg./kg, in stem basal part 6.08 mg./kg., in stem middle part 5.71 mg./kg., in stem apical part 3.92 mg./kg., in leaves 2.07 mg./kg. However, in the 3 month old plants, arsenic accumulation level in all parts of jute plants was within the permissible limit. The overall scenario can reflect that the contamination of arsenic in water, soil as well as in the food chain in Bengal Delta must be addressed properly to understand the importance of arsenic exposure from food sources.

REFERENCES

Bhattacharya, S., Gupta, K., Debnath, S., Ghosh, U.C., Dhrubajyoti Chattopadhyay & Aniruddha Mukhopadhyay. 2012: Arsenic bioaccumulation in rice and edible plants and subsequent transmission through food chain in Bengal basin: a review of the perspectives for environmental health. Toxicolology and Environmental Chemistry 94(3), 429-441.

Liu, W.J., Zhu, Y.G., Smith, S.A. & Smith, S.E. 2004: Do iron plaque and genotypes affect arsenate uptake and translocation by rice seedlings (Oryza sativa L.) grown in solution culture? Journal of Experimental Botany 55, 1707-1713.

Norra, S., Berner, Z.A., Agarwala, P., Wagner, F., Chandrasekharam, D. & Stüben, D. 2005: Impact of irrigation with As rich groundwater on soil and crops: a geochemical case study in West Bengal Delta Plain, India. Applied Geochemistry 20, 1890–906.

11.2

Fe^{2+}, H_2S and Mn^{2+} Availability modulate the Balance between N-Removal and N-Recycling in Lake Lugano Sediments?

Adeline Cojean[1], Jakob Zopfi[1], Elizabeth Robertson[2], Bo Thamdrup[3], Moritz F. Lehmann[1]

[1] *Department of Aquatic and Isotope Biogeochemistry, University of Basel, Bernoullistrasse 30, CH-4056 Basel (adeline.cojean@unibas.ch)*
[2] *Department of Geology, Lund University, Sölvegatan 12, SE-223 62 Lund, Sweden*
[3] *Nordic Centre for Earth Evolution, Institute of Biology, University of Southern Denmark DK-5230 Odense, Denmark*

Intensive human activities have dramatically altered the natural nitrogen (N) cycle in lakes by increasing reactive-N concentrations in surface waters. Anaerobic microbial N_2-producing processes help to counteract excessive fixed-N loading, specifically within lacustrine sediments where bacterial communities are dense. Denitrification, the stepwise NO_3^- reduction to N_2 is considered the most important fixed-N removal process in anoxic lake sediments. Anammox, anaerobic oxidation of ammonium to N_2 using NO_2^- as electron acceptor, is also a prominent benthic N-transformation pathway in certain environments, particularly in organic-poor sediments. In contrast, dissimilatory nitrate reduction to ammonium (DNRA) fuels eutrophication by retaining a bioavailable form of nitrogen (i.e., NH_4^+) within the system. During canonical denitrification and DNRA, microorganisms use mainly organic matter as sole electron donor to reduce NO_3^-. But recent work has revealed the existence of chemolithotrophic denitrification and DNRA using Fe^{2+} and H_2S as terminal electron donor in pure culture experiments, as well as in slurry incubation work using natural sediments. In these studies, substrate concentrations were often very high and non-representative of *in situ* conditions in freshwater sediments. To our knowledge, there is no clear evidence for NO_3^- reduction coupled to Mn^{2+} oxidation in aquatic environments. Quantifying the relative partitioning between denitrification, anammox and DNRA in lacustrine sediments, as well as understanding the biogeochemical controls is essential to better constrain N budgets in lakes. The main goal of this study was to assess the role of Fe^{2+}, H_2S and Mn^{2+} in modulating the balance between denitrification, anammox and DNRA, using experimental substrate concentrations that are pertinent to natural conditions. Eutrophic Lake Lugano (south basin) is an excellent study site for this purpose due to its high, and variable, Fe^{2+} and Mn^{2+} concentrations in the sediments. Laboratory incubation experiments were conducted using benthic microbial biomass from the sediments with additions of ^{15}N-labeled substrates and dissolved Fe^{2+}, H_2S and Mn^{2+} at two sites, Figino (Fe^{2+}/Mn^{2+}-rich) and Melide (Fe^{2+}-poor/Mn^{2+}-rich). Our experiments revealed that denitrification was the main benthic NO_3^--reduction process at both locations, and DNRA contributed about 35% to the total NO_3^- reduction. Anammox was negligible. The ratio of denitrification to DNRA was very similar (~1.8) at the two sites despite different biogeochemical conditions. Fe^{2+} additions at relatively low level (e.g. 170-250 µM Fe^{2+}) stimulated denitrification at the two sites, but did not significantly affect DNRA. In contrast, higher Fe^{2+} concentrations (400-2500 µM) seemed to inhibit denitrification at both sites, while stimulating DNRA in Figino. An analogous response was observed with H_2S additions. So far, we did not observe any evidence for NO_3^- reduction coupled to Mn^{2+} oxidation, but further experiments with addition of various amounts of Mn^{2+} will be performed. Our results indicate that locally, chemolithotrophic denitrification and DNRA play an important role in benthic nitrate turnover of Lake Lugano (south basin). While, it seems that the balance between denitrification and DNRA is modulated by Fe^{2+} and H_2S availability, the exact controls remain ambigous. The differential microbial response to Fe^{2+} and H_2S additions at the two sites, as well as their inhibitory effect on denitrification await further investigation through phylogenetic analyses and additional incubation experiments.

11.3

Tracing the atmospheric transport and fate of selenium using a chemistry-climate model

Aryeh Feinberg[1,2], Andrea Stenke[1], Elke Suess[1,2] Thomas Peter[1], & Lenny H. E. Winkel[1,2]

[1] *Department of Environmental Systems Science, ETH Zürich, Universitätstrasse 16, CH-8092 Zürich (aryeh.feinberg@env.ethz.ch)*
[2] *Eawag, Swiss Federal Institute of Aquatic Science and Technology, Überlandstrasse 133, CH-8600 Dübendorf*

Humans and animals require selenium in their diet for proper physiological functioning. The optimal intake range of selenium is rather narrow, with risks of toxicity occurring for high levels (>900 μg day^{-1}) and deficiency for low levels (<30 μg day^{-1}). Whereas selenium toxicity is mostly a local issue, selenium deficiency affects large-scale regions, impacting an estimated 0.5 - 1 billion people globally. Soils low in selenium can lead to low selenium content in plant-based foods, ultimately causing insufficient dietary intakes. Selenium deposition from the atmosphere, for example through rainfall, can act as a source of selenium to soils. Atmospheric deposition has been suggested to be an important control of soil selenium in several locations. However, the atmospheric selenium cycle has not been extensively studied in the literature. It is unknown which are the dominant atmospheric selenium species, how far selenium travels in the atmosphere after being emitted, and whether selenium is present in significant amounts in the stratosphere. We will investigate these questions by incorporating selenium for the first time into a global chemistry-climate model, SOCOL-AER. Selenium chemistry was implemented analogously to the existing sulfur chemistry in the model, due to the expected chemical similarities between selenium and sulfur. In the model, selenium species (SeO_2, DMSe, H_2Se, OCSe, …) are emitted from the surface based on estimates from previous field campaigns or atmospheric budgets. Low volatility selenium compounds can be taken up by sulfate aerosols, which are explicitly described by an aerosol microphysics module. Since gas phase selenium species are quickly oxidized to become low volatility compounds, far range transport of selenium occurs mainly on aerosols. We will show the importance of atmospheric deep convection in spreading selenium globally. Our model will be used to fill major research gaps on atmospheric selenium cycling, speciation, and transport. Our results can motivate future field studies, by identifying regions where atmospheric selenium speciation and deposition should be further investigated. Furthermore, the deposition maps derived by SOCOL-AER will be a valuable input for soil models that predict soil selenium concentrations.

11.4

Beauty, bottlenecks and progress in the study of the environmental behaviour of less-studied technology-critical elements

Montserrat Filella[1]

[1]*Institute F.-A. Forel, University of Geneva, Boulevard Carl-Vogt 66, CH-1205 Geneva (montserrat.filella@unige.ch)*

Nature has governed biogeochemical cycles for millions of years but now humans are mining and redistributing material at a very fast rate, probably contributing to shape the geology and biology of the Earth. This fast element turnover is accompanied by an increasing diversity of the material used in all types of products. A number of trace elements that until recently were only considered to be laboratory curiosities have now become essential components in a variety of applications ranging from information to 'green energy' related technologies. The current strategic importance of these elements is such that they have now been labelled as 'energy-critical elements' or 'technology-critical elements' (TCEs) and initiatives at national levels are underway to secure their availability in the coming years. The list of elements considered as TCEs is variable, depending on the source but it generally includes: Pt-group elements, lanthanides and Ta, Nb, Ga, In, Ge and Te. These are, for instance, the elements considered in the EU COST action TD1407 (www.costnotice.net). This last group of 'less-studied' elements are the object of this communication.

We are now in a much better position than we were in the past to tackle the environmental challenges that the increasing use of chemical elements might create. Today, we have highly performing analytical techniques and, more importantly, a solid theoretical background. Pitfalls, such as those derived from not taking chemical speciation into account when performing (eco)toxicological experiments, will surely be avoided. However, difficulties encountered in the study of these less-studied TCEs are so far many. Main bottlenecks are, on the one hand, the lack of adequate analytical methods (and the improper use of the existing ones) and, on the other hand, the absence of adequate equilibrium and solubility constants and of a satisfactory description of the interactions of these elements with natural organic matter and potentially binding mineral surfaces. Progress is however fast both in the analytical front and in the improvement of the knowledge of their behaviour in solution. Discussion of current bottlenecks and recent progress is the object of this communication.

11.5

Spatial distribution of mercury and methylmercury in an industrially polluted floodplain soil.

Lorenz Gfeller[1], Adrien Mestrot[1]

[1] *Institute of Geography, University of Bern, Hallerstrasse 12, CH-3012 Bern (lorenz.gfeller@giub.unibe.ch)*

Mercury (Hg) is a ubiquitous global pollutant cycling through all environmental compartments. Microbially formed methylmercury (MeHg) is the most toxic and bioavailable form of Hg (Sakamoto et al. 2012). The bio-methylation of mercury is well studied in the marine environment. However, there is still a lack of knowledge concerning MeHg formation soils. The aim of this study is to characterize parameters potentially driving MeHg formation in agricultural soils and terrestrial ecosystems.

From the 1930s to 1980s, the agricultural floodplain between Visp and Raron (Canton of Valais) was polluted by an acetaldehyde producing plant. The chemical plant released an estimated 50 t of Hg into a discharge canal. During this period, the canal was dredged multiple times. The extracted Hg-rich canal sediments were used to fertilize agricultural fields and private gardens. To estimate the extent of the Hg pollution in the area, a screening was conducted by a geo engineering office. Despite these efforts, little is known about the meter-scale distribution of Hg and the concentration of MeHg in the agricultural soils in Valais.

As a first step, we aim to assess the three-dimensional distribution of Hg species in the area. Based on the previous screening, five sites were selected for this study. Soil was sampled in a rectangular grid system to a depth of 50 cm. MeHg is extracted with a newly developed method including a three-step selective extraction with 35% HCl, dichloromethane and L-cysteine. The Hg species are measured with HPLC-ICP-MS, while total Hg, and a range of selected metals, are measured by ICP-MS. Further, parameters potentially affecting MeHg formation (organic C, N, S, and pH) are measured. Maximum Hg concentrations (59.3 mg kg^{-1}) in the agricultural soils are almost 3 times the federal threshold value of 20 mg kg^{-1}.

In the terrestrial environment, future impacts on Hg cycling due to changes in climate and land-use remain unclear. Changes in soil saturation and redox may potentially promote Hg release and biomethylation. Our future research will include soil incubation experiments to assess the influence of flooding and agricultural practices on the mobilization and biomethylation of Hg in soils.

REFERENCES

Sakamoto, M., Murata, K., Akiyoshi, K., Sasaki, M., 2012: A review of mercury toxicity with special reference th methylmercury, In: Guangliang L., Nelson J. OD. und Yong C., Environmental chemistry and toxicology of mercury. Hoboken, N.J Wiley, 501–516.

11.6

Copper and zinc stable isotopes as analytical tool to trace sources and processes in agricultural systems

Martin Imseng[1], Matthias Wiggenhauser[2], E. Frossard[2], Michael Müller[3], Armin Keller[3], Wolfgang Wilcke[4] and Moritz Bigalke[1]

[1] Geographic Institute, University of Bern, Hallerstrasse 12, CH-3012 Bern
[2] Institute of Agricultural Sciences, ETH Zürich, Eischikon 33, CH-8315 Lindau
[3] Swiss Soil Monitoring Network (NABO), Agroscope, Reckenholzstrasse 191, CH-8046 Zürich
[4] Institute of Geography and Geoecology, Karlsruhe Institute of Technology (KIT), Reinhard-Baumeister-Platz 1, D-76131 Karlsruhe

In agriculture, copper (Cu) and zinc (Zn) are used as feed additives and pharmaceuticals and can accumulate with farmyard manure in agricultural soils. Although being micronutrients, high Cu and Zn concentrations are toxic for microorganisms and invertebrates and endanger in that way the soil fertility. Former studies revealed Cu and Zn accumulations in Swiss agricultural soils in the past decades. However, these studies were not completely based on in-situ measured data. The aim of this study was to fill this gap and measure Cu and Zn fluxes at selected Swiss agricultural sites. Specifically, we aimed to trace the metals in the soil and to differentiate between anthropogenic and geogenic sources. Additionally, we further elucidated metal redistribution in Swiss agricultural systems, based on the measurements of stable metal isotope ratios of system fuxes and soil pools.

For that purpose, metal balances of three three grassland sites were determined by measuring the soil metal concentrations and all inputs (atmospheric bulk deposition, manure & parent material) and outputs (seepage water and grass harvest) during one hydrological year (May 2014 – May 2015). Furthermore, stable metal isotopes of the soil and all inputs will be measured.

Cu and Zn mass balances showed that manure application is by far the most important Cu (146-340 g ha^{-1} yr^{-1}) and Zn (947-1'742 g ha^{-1} yr^{-1}) input. Inputs with bulk deposition and through parent material weathering were by 1-2 orders of magnitude smaller. Beside the Cu and Zn budgets, stable isotope data (not yet analysed) will be presented and discussed to assess the biogeochemical processes and redistribution of (anthropogenic) Cu and Zn in agricultural systems.

REFERENCES

Keller, A., Rosser, N. & Desaules A. 2005:Schwermetallbilanzen der nationalen Bodenbeobachtung: NABO – Nationales Bodenbeobachtungsnetz der Schweiz, Agroscope FAL.
Schultheiß, U., Döhler, H., Roth, U., Eckel, H., Goldbach, H., Kühnen, V., Wilcke, W., Uihlein, A., Früchtenicht, K. & Steffens, G. 2004: VDLUFA-Schriftenreihe, 59, 232-243.
Sheppard, S. C. & Sanipelli, B. 2012: Trace Elements in Feed, Manure, and Manured Soils, Journal of Environmental Quality, 41, 1846-1856.

11.7

Arsenic pollution of Ogosta River floodplain by legacy mining: Assessing pollution and environmental impacts at different scales

Ruben Kretzschmar[1], Iso Christl[1] & Tsvetan Kotsev[2]

[1] Soil Chemistry Group, Institute of Biogeochemistry and Pollutant Dynamics, CHN, ETH Zurich, 8092 Zurich, Switzerland (kretzschmar@env.ethz.ch)
[2] Department of Geography, NIGGG, Bulgarian Academy of Sciences, Sofia, Bulgaria

In many industrialized regions, riverine floodplains have accumulated legacies of toxic trace metals and metalloids. These contaminations often arise from past or present mining and ore processing, releasing dissolved metal(loid)s and their mineral host phases into downstream floodplains by mine waste discharge or tailings dam failures. Since river floodplains cover extensive areas and are commonly used for settlements and agriculture, they can pose greater risks with respect to human exposure than the tailings themselves. Even moderate concentrations of toxic metal(loid)s in soils may threaten soil fertility and ecosystem health if the contaminants are bioavailable to soil organisms and plants. Contaminated floodplains may also represent a persisting source for polluting surface and groundwater even long after mining and metallurgical activities have ended.

One such example is Ogosta River, which is one of the largest tributaries to the river Danube in Bulgaria. Ogosta originates in the Balkan Mountains and joins the Danube approximately 140 km northeast. Soils and sediments in the Ogosta floodplain are heavily contaminated with As resulting from historic mining and a large tailing dam failure in 1964. This presentation will give an overview of past and ongoing research on soil contamination and environmental impact assessment at different spatial scales in the upper Ogosta floodplain.

Soil contamination with As is investigated at various spatial scales (Figure 1). At the floodplain scale, our goal is to identify contamination “hotspots” and to develop improved contamination maps for the entire floodplain based on the analysis of soil samples (to date 1352) in combination with LIDAR-derived mapping of geomorphographic units, flood modeling, and geostatistical methods. For detailed process studies, transects perpendicular to the floodplain were selected and characterized at the (lateral) transect scale to the (vertical) soil profile scale. Within soil profiles, detailed studies were conducted to investigate As speciation at the microscopic to molecular scale using X-ray diffraction, fluorescence, and absorption spectroscopy (Mandaliev et al., 2014). Environmental impact assessment of the As pollution of the Ogosta floodplain includes studies on human bioaccessibility of As in soils studied by *in-vitro* extraction tests (Mikutta et al., 2014), plant uptake of As along a contamination gradient (Simmler et al., 2016), As release during simulated soil flooding by microbial reduction (Simmler et al., 2017), influence of the soil contamination on As in Ogosta river and groundwater, and the effects of soil contamination on microbial communities. Selected results of these studies will be highlighted and discussed.

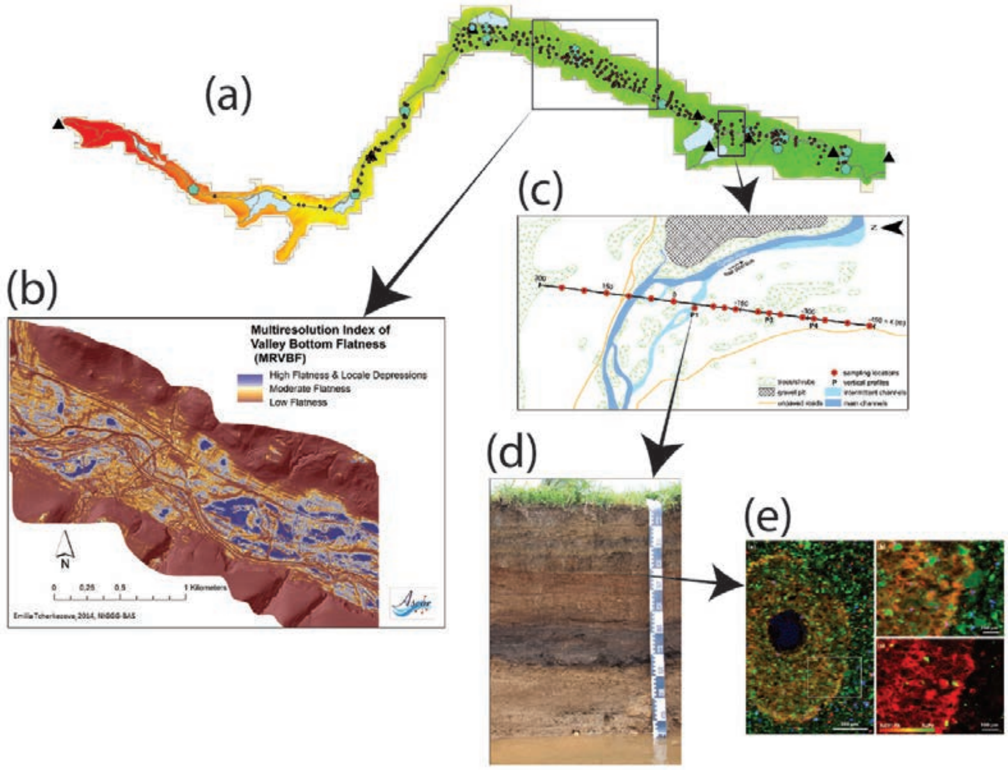

Figure 1. Investigating As contamination on various spatial scales: (a) Upper Ogosta river valley with soil and groundwater sampling locations, (b) LIDAR derived image for a section of Ogosta valley showing flatness and depressions vulnerable to flooding, (c) transect across Ogosta valley used for studies on processes along contamination gradients, (d) soil profile investigated within the transect showing Mn enriched layers, and (e) µ-X-ray fluorescence maps of As (red), Fe (green), and S (blue) around a soil macropore.

REFERENCES

Simmler, M.; J., B.; Frischknecht, S.; Christl, I.; Kotsev, T.; Kretzschmar, R., Reductive solubilization of arsenic in a mining-impacted river floodplain: Influence of soil properties and temperature. *Environ. Poll*. 2017, 231, 722-731.

Simmler, M.; Suess, E.; Christl, I.; Kotsev, T.; Kretzschmar, R., Soil-to-plant transfer of arsenic and phosphorus along a contamination gradient in the mining-impacted Ogosta River floodplain. *Sci. Total Environ*. 2016, 572, 742-754.

Mandaliev, P. N.; Mikutta, C.; Barmettler, K.; Kotsev, T.; Kretzschmar, R., Arsenic species formed from arsenopyrite weathering along a contamination gradient in circumneutral river floodplain soils. *Environ. Sci. Technol*. 2014, 48, 208-217.

Mikutta, C.; Mandaliev, P. N.; Mahler, N.; Kotsev, T.; Kretzschmar, R., Bioaccessibility of arsenic in mining-impacted circumneutral river floodplain soils. *Environ. Sci. Technol*. 2014, 48, 13468-13477.

11.8

New insights into the oxidation of marine organic sulfur compounds by reactive bromine species

Emanuel Müller[1,2], Urs von Gunten[1,2,3], Sylvain Bouchet[1,2], Lenny H.E. Winkel[1,2]

[1] *Eawag, Swiss Federal Institute of Aquatic Science and Technology, Department of Water Resources and Drinking Water (W+T),* **Überlandstrasse** *133, CH-8600 Dübendorf*
[2] *ETH Zürich, Swiss Federal Institute of Technology, Institute of Biogeochemistry and Pollutant Dynamics (IBP), Department of Environment Systems (D-USYS), Rämistrasse 101, 8092 Zürich*
[3] *EPFL, École polytechnique fédérale de Lausanne, Route Cantonale, 1015 Lausanne*

Volatile marine organic sulfur and bromine compounds are important players in climatic processes.[1, 2] A key compound in the production of volatile bromine compounds (e.g., bromoform, dibromomethane) is enzymatically produced bromine (e.g., Br_2, HOBr, OBr^-), via reactions with dissolved organic matter (DOM) in marine waters.[2, 3] Indirectly, these reactions are also important for atmospheric chemistry, as the volatile bromine species can photolyze to Br atoms, which are known to degrade ozone.[4] However, apart from reacting with DOM, in marine waters, bromine potentially also reacts with biogenic marine organic sulfur compounds (e.g., dimethylsulfoniopropionate (DMSP), dimethylsulfide (DMS), dimethylsulfoxide (DMSO)) and could thus play an additional role in controlling concentrations of these species in marine waters. Nevertheless, the reactivity of bromine towards these species is largely unknown.

Therefore, we studied the reactions between HOBr and organic sulfur compounds in marine waters by determining second order rate constants for their reactions, and analyzing reaction products via HPLC/ICP-MS. We observed a high reactivity between HOBr and DMS, with an apparent second order rate constant of $3 \cdot 10^9$ M^{-1} s^{-1} at pH 8. In contrast, reactions of HOBr with other studied organic sulfur compounds are slow (DMSO: 8 M^{-1} s^{-1}; DMSP: < 1 M^{-1} s^{-1}; dimethylsulfone ($DMSO_2$): < 0.1 M^{-1} s^{-1}; methanesulfonicacid (MSA): < 0.1 M^{-1} s^{-1}). Furthermore, we found that DMS is oxidized to DMSO. With an excess of HOBr relative to DMS, DMSO is further slowly oxidized to the stable compound $DMSO_2$. Also low amounts of MSA and sulfate (SO_4^{2-}) were detected after long reaction time.

Further experiments are planned to study reactions between marine bromine and sulfur species as well as DOM, using diffusion reactors in which transport of DMS and HOBr through biological membranes is simulated. These experiments will show to what extent concentrations of marine organic sulfur species may influence the formation of volatile bromo-organic compounds, and thus the concentrations of both volatile organic sulfur and bromine compounds in marine waters and ultimately in the atmosphere.

REFERENCES

[1] Stefels et al. 2007: Environmental constraints on the production and removal of the climatically active gas dimethylsulphide (DMS) and implications for ecosystem modelling. Biogeochemistry 83, 245-275.
[2] Wever, R., & van der Horst M.A. 2013: The role of vanadium haloperoxidases in the formation of volatile brominated compounds and their impact on the environment. Dalton Transactions 42, 11778-11786.
[3] Rehder D. 2014: Vanadate-Dependent Peroxidases in Macroalgae: Function, Applications, and Environmental Impact. Oceanography 2, 121.
[4] Salawitch, R. 2006: Atmospheric chemistry: Biogenic bromine. Nature 439, 275-277.

11.9

Trace elemental analysis of arsenic-contaminated groundwater in the lowlands of Nepal suggest the initial source of arsenic in the High Himalayas

Barbara Müller

Horbenstrasse 4 8356 Ettenhausen (Switzerland)

Arsenic contamination of groundwater used ubiquitously as potable water in South Asia remains a serious health issue to the inhabitants living on alluvial plains of the Himalayan foreland in countries like Bangladesh, India, Nepal, Myanmar, China, Vietnam and Cambodia. Even the geological and geochemical conditions favoring the release of the highly poisonous contaminant from the sediments hosting the groundwater are fairly well understood, there is still am ongoing debate about the origin of arsenic. All the sediments forming a huge proportion of the Terai (lowlands of Nepal) aquifers are derived from two main sources, (i) sediments deposited by large rivers that erode the upper Himalayan crystalline rocks, (ii) weathered meta-sediments carried by smaller rivers originating in the Siwalik forehills adjacent to the Terai. But a sor far underestimated source of As will be presented here: The peraluminous leucogranites found ubiquitously in the Nepal Himalaya. The relationship between the trace elements analyzed in the groundwater in the Terai and trace elements found in this peculiar felsic rocks reflect the origin of the arsenic in the high Himalayas of Nepal. A striking feature besides the high concentration of As is the presence of the lithophile trace elements like Li, B, P, Mn, Br, Sr and U in the groundwater. Preliminary results concerning the mentioned elements point to a felsic initial source like metapelites or leucogranites – all rocks showing a high abundance of especially B, P and As along with Cd and Pb.

11.10

Metal availability to invertebrate community: integrating field experimentation and modelling

Dorothea Hug Peter[1,2], Emmanuel Castella[1,2], Vera I. Slaveykova[1,2]

[1] Department F.-A. Forel for Environmental and Aquatic Sciences, Earth and Environmental Science Section, University of Geneva, Uni Carl Vogt, Boulevard Carl-Vogt 66, CH-1205 Genève
[2] Institute for Environmental Sciences (ISE), University of Geneva, Uni Carl Vogt, Boulevard Carl-Vogt 66, CH-1205 Genève

Bioavailability is a key concept allowing to integrate the environmental metal concentrations and speciation with the effects induced in the biota, e.g. macroinvertebrates. Bioavailability is increasingly included in regulatory frameworks. While such refinements of regulatory dispositions are currently based on laboratory experiments, evidence from the field of such mechanisms would improve their relevance. Among different modelling approaches, biodynamic model combining the uptake from water and food with elimination, provides a mechanistic basis for predicting of the bioaccumulation of trace metals in aquatic organisms (Luoma and Rainbow, 2005). Nonetheless, extrapolation based on the lab-based research with model species to the field as well as the transferability of uptake and loss parameters to phylogenetically close taxa and even for the same species under different ambient conditions is still to explore. What is more such approach do not allow to model whole-body concentrations for an entire community, where the link between exposure conditions to uptake or toxicity is explore by multiple regression models (Esbaugh et al. 2012).

The present study aims to determine the metal availability to invertebrate community and to test the applicability of the existing bioavailability models in field situation, as well as to explore the avanue for their improvement.Twelve floodplain sites from the two extremes of the lateral connectivity gradient (permanent connection upstream and downstream vs. disconnected at base flow) of Rhône River were studied. They were chosen because of their diverse invertebrate community and a variety of physico-chemical conditions. Metal bioavailability to invertebrates was characteized by measurement of the whole- body concentrations of Al, Cr, Mn, Fe, Co, Ni, Cu, Zn, Cd, Pb and U (Hug Peter et al. 2017). In paralel the concentrations of these metals were determined in different environmental compartments including, water, suspended particulate matter (SPM), sediments. For selected metals, bioanalogical diffusive gradients in thin films (DGT) were used to evaluate the bioaccessible metal fractions in water and sediments. Conductivity and pH, dissolved organic carbon, major ion concentrations were also analyzed. All the above mentioned parameters were used to evaluate the concentration in food and water input parameters into the tested models.

Results showed no significant differences of the concentrations in invertebrates between site types. Concentrations in invertebrates differed significantly between macroinvertebrate taxa. For a given taxa, the whole body metal concentrtaions decreased in the order Zn, Al, Cu, Ni, Pb, Cr, Cd, U. Contrasting trends for metal concentrations in water, sediment, SPM and macroinvertebrates were found, suggesting that more than one environmental compartment should be considered in the evaluation whole-body metal concentrations. No direct link with a single environmental compartments, confirming the necessity of an approach integrating the potential contribution of different environmental compartments.

The application of the biodynamic model to the field showed that the choice of input parameters was crucial for the accuracy of the model prediction. Sediment and SPM concentrations as input lead to a strong overestimation of whole-body concentrations. DGT-labile trace metal concentrations in water and sediments, for water and food exposure provided better results. Transferability of uptake and loss rate constants from model to non-model taxa was possible with very good acuracy for gastropoda than for amphipoda.

In a novel approach to model whole-body concentrations for an entire community, functional traits were used as input parameters of a statistical model. The possibility to include the traits is very important since aquatic invertebrates in the natural environment are diverse concerning their biological and ecological traits (e.g. feeding, life history, locomotion) leading to different interactions and exposure pathways towards trace metals in the field. Indeed the inclusion of functional traits of the taxa reduced the bias of the model to predict whole-body metal concentrations in the field sampled invertabrates. For large scale risk assessment, trait based models could be a valuable tool to improve the estimation of potential exposure. As macroinvertebrate traits are increasingly available, the model can be applied in large scale studies, risk assessment and for the determination of water quality guidelines.

REFERENCES

Esbaugh A J, Brix K V, Mager E M, De Schamphelaere K and Grosell M 2012: Multi-linear regression analysis, preliminary biotic ligand modeling, and cross species comparison of the effects of water chemistry on chronic lead toxicity in invertebrates Comp. Biochem. Physiol. Part C Toxicol. Pharmacol. 155 423–31.

Hug Peter, D., Castella, E., et Slaveykova, V., 2017: Lateral and longitudinal patterns of water physico-chemistry and trace metal distribution and partitioning in a large river floodplain: Science of the Total Environment, 587-588, 248-257.
Luoma S N and Rainbow P S 2005: Why Is Metal Bioaccumulation So Variable? Biodynamics as a Unifying Concept Environ. Sci. Technol. 39 1921–31.
Rainbow P S 2002: Trace metal concentrations in aquatic invertebrates: why and so what? Environ. Pollut. 120 497–507

11.11

Limitation of anaerobic oxidation of methane in sulfate-rich lake sediments.

Guangyi Su, Helge Niemann, Jakob Zopfi & Moritz F. Lehmann

Department of Environmental Sciences, University of Basel, Bernoullistrasse 30, CH-4056 Basel (guangyi.su@unibas.ch)

Sulfate reduction coupled to anaerobic oxidation of methane (AOM) has been recognized as an important sink in marine environments. This microbial process is mediated by anaerobic methanotrophic archaea (ANME-1, 2 and 3) probably in syntrophy with sulfate-reducing bacteria (SRB). However, in anoxic lake sediments, AOM is likely to be limited by relatively low sulfate concentrations, and alternative electron acceptors (e.g., Fe and Mn oxides) may be involved.

We assessed methane oxidation rates in the anoxic sediments of a sulfate-rich lake in Switzerland: Lake Cadagno. Our data provide clear geochemical evidence for AOM in the sediments. The highest rate occurred at the zone where sulfate became exhausted, which suggests sulfate-linked AOM. However, different from most diffusive marine settings, a well-defined sulfate-methane transition zone that corresponds to peak AOM rates was not developed and we did not find typical sequences of ANME that couple AOM to sulfate reduction. The involvement of electron acceptors other than sulfate remains uncertain. Yet, geochemical porewater profiles indicate the reduction of iron and manganese at and below the AOM zone, including depths where we detected abundant sequences of *Candidatus* Methanoperedens, which was reported to be closely related to archaea that perform Fe/Mn-dependent methane oxidation. Our observation raised the question as to whether AOM in Lake Cadagno may be partly modulated by the availability of Fe/Mn oxides. We will also present data on lipid biomarkers in the sediments, possibly providing information on methanotrophic organisms responsible for AOM and, hence, on the pathways involved. Ongoing $^{13}CH_4$ incubation experiments with amorphous manganese and iron oxides will provide further constraints on the controls on AOM limitation in Lake Cadagno sediments.

REFERENCES

Ettwig, K. F., Zhu, B., Speth, D., Keltjens, J. T., Jetten, M. S. & and Kartal, B. 2016: Archaea catalyze iron-dependent anaerobic oxidation of methane. Proceedings of the National Academy of Sciences of the United States of America, 113, 12792–12796.

11.12
Solubility of thallium in soils: role of Tl uptake by illite

Silvan Wick[1], Marlene Fischer[1], Numa Pfenninger[1] & Andreas Voegelin[1]

[1] *Eawag, Überlandstrasse 133, CH-8600 Dübendorf, Switzerland (silvan.wick@eawag.ch)*

Thallium (Tl) is a highly toxic trace element. In the environment, Tl commonly occurs as monovalent Tl^{I}. The clay mineral illite has long been assumed to be a key sorbent for Tl in soils and sediments. This hypothesis was based on the similarity of the ionic radius and hydration energy of the cations Tl^{+} and Cs^{+}. For the latter, highly specific adsorption at the frayed edges of illite and fixation in the illite interlayer is the well-documented. In a study on geogenically Tl-rich soils from the Erzmatt in the Swiss Jura mountains, first spectroscopic evidence for the sequestration of Tl by illite was presented (Voegelin et al., 2015). In a recent laboratory study, we confirmed the high affinity of Tl^{+} for adsorption onto illite and showed that K^{+} and NH_4^{+} are important competing cations (Wick et al., in preparation). To further constrain the role of Tl^{+} adsorption and fixation by illite in soils, we examined the solubility of geogenic Tl and freshly spiked Tl^{+} in soils from the Erzmatt.

In four soils with geogenic Tl contents of 10 to 300 mg/kg, adsorption isotherms were recorded for ~3 to 1000 mg/kg spiked Tl. Using our model for Tl adsorption by illite (Wick et al., in preparation), the adsorption isotherms could be reasonably reproduced. Extraction of the spiked soil samples with 10 mM $CaCl_2$ and 1 M NH_4-acetate showed that these extracts were suitable to determine soluble Tl ($CaCl_2$) and the pool of exchangeable Tl (NH_4-acetate), with a recovery of about 80% of the adsorbed Tl by 1 M NH_4-acetate. The extraction of 36 Erzmatt topsoil samples with ~3 to 1000 mg/kg geogenic Tl revealed nearly the same relationship between soluble Tl ($CaCl_2$) and the exchangeable Tl pool (NH_4-acetate) as observed for the Tl-spiked soils. On average, however, only 3.5±1.8% of the geogenic Tl was NH_4-exchangeable, whereas Tl L_{III}-edge X-ray absorption spectra of 12 soils suggested that most geogenic Tl was associated with illite. These findings suggest that most geogenic Tl had become fixed in the interlayers of illite (and maybe other phyllosilicate minerals like muscovite) over the time-scales of soil formation.

In combination, our results gained on soils with spiked and geogenic Tl confirmed that illite affected Tl solubility in two important ways: (i) as an adsorbent of exchangeable Tl and (ii) as a host for structural Tl fixation.

REFERENCES

Voegelin, A., Pfenninger, N., Petrikis, J., Majzlan, J., Plötze, M., Senn, A.C., Mangold, S., Steininger, R. and Gottlicher, J. (2015): Thallium speciation and extractability in a thallium- and arsenic-rich soil developed from mineralized carbonate rock, Environmental Science and Technology, 49, 5390-5398.

Wick, S., Baeyens, B., Marques Fernandes, M. and Voegelin, A. (in preparation) Thallium adsorption onto illite.

11.13

The fate of P fertilizer derived Cd in soil-wheat systems

Matthias Wiggenhauser[1] & Christoph Bracher[2], Martin Imseng[2], Armin Keller[3], Mark Rehkämper[4], Jost Eikenberg[5], Wolfgang Wilcke[6], Emmanuel Frossard[1], Moritz Bigalke[2]

[1] Institute of Agricultural Sciences, ETH Zurich, Eschikon 33, CH-8315 Lindau, matthias.wiggenhauser@usys.ethz.ch
[2] Institute of Geography, University of Bern, Hallerstrasse 12, CH-3012 Bern
[3] Swiss Soil Monitoring Network (NABO), Agroscope, Reckenholzstrasse 191, CH-8046 Zürich
[4] Department of Earth Science & Engineering, Imperial College, London SW7 2AZ, UK
[5] Paul Scherrer Institute (PSI), Radioanalytics Laboratory, PSI Aarebrücke, CH- 5232 Villigen
[6] Institute of Geography and Geoecology, Karlsruhe Institute of Technology (KIT), P.O. Box 6980, D-76049 Karlsruhe

Applications of phosphorus (P) mineral fertilizer can lead to Cd accumulation in soils and potentially increase Cd concentrations in edible crop parts. A Cd source-tracing experiment was conducted in three soil-fertilizer-wheat systems by using a ^{109}Cd radioisotope labeled P mineral fertilizer in order to determine the fate of freshly applied Cd. Additionally, it was tested whether Cd can be traced by using stable Cd isotopes ratios at natural abundance ($\delta^{114/110}$Cd). The ^{109}Cd radiotracer results revealed that 5 to 11 % of the Cd in the shoot derived from the fertilizer. With regard to the total amount of ^{109}Cd introduced, a maximum of 2 % reached the shoots while 98% stayed in the roots and soils. Source-tracing using stable isotope at natural abundance led to inadequate results since the differences in isotope ratios in the Cd sources were too small (max. = $\delta^{114/110}$Cd 0.02 to 0.62 ‰). The low recoveries of Cd applied with fertilizer suggest that continuous P mineral fertilizer application in the past decades might have led to a build-up of a residual Cd pool in arable soils.

In a follow up study we investigate the hypothesized residual Cd pool from past P fertilization in more detail by applying a stable ^{111}Cd tracer. A P mineral fertilizer is isotopically labeled with an enriched ^{111}Cd spike and applied to soils from long-term field trials. Soils with distinct P fertilizer application histories were selected and wheat is grown on them in a pot trial. By using an isotope mass balance approach based on altered $^{111/110}$Cd ratios due to the presence of the tracer, the share and recovery of fertilizer derived Cd in 3 plant parts of wheat (roots, straw, grains) and 3 operationally defined soil fractions (using a 3-step sequential extraction procedure) can be calculated. The use of soils with a distinct fertilization history should allow us to assess the contributions of a hypothesized residual Cd pool and freshly introduced Cd to the total Cd concentration in plant parts and soil fractions. We will present the first results on the fate of freshly applied fertilizer and the influence of past P fertilizer applications on Cd fluxes in soil-fertilizer-wheat systems.

P 11.1

Geochemical tracing of sedimentary organic matter and associated clay minerals in the South China Sea

Thomas Blattmann[1], Zhifei Liu[2], Ke Wen[2] Shun Lin[2], Jianru Li[2], Yulong Zhao[2], Yanwei Zhang[2], Lukas Wacker[2], Negar Haghipour[2], Michael Plötze[2], Timothy Eglinton[2]

[1] *ETH Zurich, Zurich, Switzerland (correspondence: thomas.blattmann@erdw.ethz.ch)*
[2] *State Key Laboratory of Marine Geology, Tongji University, Shanghai, China*

Sediment traps deployed in the South China Sea (SCS) were used to collect a one-year time series of sinking particles in order to study sediment provenance and organic matter (OM)-mineral interactions from source-to-sink. The traps were deployed at water depths ranging from 500 to nearly 4000m across three mooring sites with a sediment trap time collection window of 18 days yielding intraseasonal resolution. The SCS, one of the largest marginal seas bordering the Pacific Ocean, is influenced by widespread sediment dispersal processes (Zhang et al., 2014). It is also characterized by strong spatial gradients in phyllosilicate mineralogy that lends itself to constraining sediment provenance based on smectite, kaolinite, chlorite, and illite abundances (Liu et al., 2010).

The stable and radiocarbon isotopic compositions of bulk OM from the time series samples has been measured to gain insight into the provenance and type of OM discharged from land and carried into the deep ocean. Measurements of mineral-specific surface area, cation exchange capacity, and quantitative mineralogial composition yield exciting new insights into the stabilization effect of different phyllsilicates on OM in the ocean. The radiocarbon isotopic composition exhibits significant variability over the time series, reflecting changes in the source material. During time windows with elevated sediment flux, radiocarbon concentrations of bulk OM are lower, indicating the export of aged terrestrial OM. This aged material reflects contributions of bedrock-derived OM emanating from Taiwan (Hilton et al., 2011). The SCS sediments reveal trends in OM-mineral associations as a function of phyllosilicate mineralogy with smectite and illite/chlorite enriched fractions showing strongly contrasting behavior.

REFERENCES

Hilton, R.G., Galy, A., Hovius, N., Horng, M.-J. and Chen, H. 2011: Efficient transport of fossil organic carbon to the ocean by steep mountain rivers: An orogenic carbon sequestration mechanism. Geology 39, 71-74.

Liu, Z., Li, X., Colin, C. and Ge, H. 2010: A high-resolution clay mineralogical record in the northern South China Sea since the Last Glacial Maximum, and its time series provenance analysis. Chinese Science Bulletin 55, 4058-4068.

Zhang, Y., Liu, Z., Zhao, Y., Wang, W., Li, J. and Xu, J. 2014: Mesoscale eddies transport deep-sea sediments. Scientific Reports 4, 5937.

P 11.2

Trapping of volatile antimony (Sb): current work and future developments

Jaime Caplette[1] and Adrien Mestrot[1]

[1] *Trace Element Speciation Group, Geographisches Institut, Universitat Bern, Hallerstrasse 12, CH-3012 Bern (jaime.caplette@giub.unibe.ch)*

Antimony (Sb) in the environment is ubiquitous, ranging from 0.3 – 8.4 mg kg^{-1} in the soil environment (Filella et al. 2002) biological and geochemical samples. Antimony and its compounds are considered to be priority pollutants interest by the USEPA and the EU. In this first review paper on antimony occurrence in natural waters, 420 papers on freshwaters, marine waters, estuaries, soils, and sediments have been reviewed. All data are quoted from the original sources. Typical concentrations of total dissolved antimony are usually less than 1.0 \u03bcg/l in non-polluted waters. When redox speciation determinations are performed, most studies report the dominance of Sb(V. Antimony concentrations can be elevated due to anthropogenic actitivies such as: mining and smelting, industrial, and shooting range activities. The United States Environmental Protection Agency and European Union consider Sb a priority pollutant of interest (Filella et al. 2002; Wilson et al. 2010)biological and geochemical samples. Antimony and its compounds are considered to be priority pollutants interest by the USEPA and the EU. In this first review paper on antimony occurrence in natural waters, 420 papers on freshwaters, marine waters, estuaries, soils, and sediments have been reviewed. All data are quoted from the original sources.

Typical concentrations of total dissolved antimony are usually less than 1.0 \u03bcg/l in non-polluted waters. When redox speciation determinations are performed, most studies report the dominance of Sb(V. Volatile Sb, stibine (SbH_3), monomethylstibine (MeSb), dimethylstibine (Me_2Sb), and trimethylstibine (Me_3Sb), can be produced at low temperatures from inorganic substrates under aerobic and anaerobic conditions and represent an understudied portion of the biogeochemical cycle of Sb. Volatile antimony has been detected as a product of sewage sludge fermentation and hydrothermal vents, landfills, produced in headspace gases from fungi (*S. brevicaulis)* and methanogenic Archaea bacteria (Feldmann et al. 1994; Filella et al. 2007; Jenkins et al. 1998; Smith et al. 2002; Wehmeier and Feldmann. 2005) bismuth, mercury, arsenic, antimony and tellurium could be found by boiling point calibration, respectively. Some technical and methodical concepts towards quantification of the results are indicated. “Direct analysis of the volatile antimony compounds stibine (SbH3. Volatile species also have different residence times in the environment, ranging from 1 hour to 42 days in the light and dark, respectively, indicating potential long term dispersal in the environment (Feldmann et al. 1994).

Common techniques used for trapping volatile compounds include cryotrapping and liquid trapping in HNO_3 (Feldmann et al. 1994; Pecheyran et al. 1998; Vriens et al. 2014). Though these methods are successful, they are not convenient for field measurements. This work focuses on the development of a method for trapping volatile antimony applying a successful method for arsine (Mestrot and Uroic. 2009). Hydride generation is used to produce volatile trimethylstibine and stibine from trimethylantimony and antimony (III) standards, respectively. The gaseous products are collected in inert Teldar bags and chemo-trapped using $AgNO_3$ impregnated silica gel tubes and subsequently digested for total Sb concentration on the traps. Results indicate ≥ 99.1% efficiency of hydride generation and yields of approximately 30% SbH_3, and 50% Me_3Sb trapped on the gel tubes. Future developments and potential uses of the method will be discussed.

REFERENCES

Feldmann, J., Grümping, R., & Hirner, A. V., 1994: Determination of volatile metal and metalloid compounds in gases from domestic waste deposits with GC/ICP-MS, Fresenius. J. Anal. Chem, 350, 228–234.

Filella, M., Belzile, N., & Chen, Y.W., 2002: Antimony in the environment: a review focused on natural waters I, Earth-Science Rev, 57, 125–176.

Filella, M., Belzile, N., & Lett, M.C., 2007: Antimony in the environment: A review focused on natural waters. III. Microbiota relevant interactions, Earth-Science Rev, 80, 195–217.

Jenkins, R.O., Craig, P.J., Miller, D.P., Stoop, L., Ostah, N., & Morris, T.A., 1998: Antimony biomethylation by mixed cultures of micro-organisms under anaerobic conditions, Appl. Organomet. Chem,12, 449-445.

Mestrot, A., & Uroic, M.K., 2009: Quantitative and Qualitative Trapping of Arsines Deployed to Assess Loss of Volatile Arsenic from Paddy Soil, Environ. Sci. Technol, 43, 8270–8275.

Pecheyran, C., Quetel, C.R., Martin Lecuyer, F.M., & Donard, O.F.X., 1998: Simultaneous Determination of Volatile Metal (Pb, Hg, Sn, In, Ga) and Nonmetal Species (Se, P, As) in Different Atmospheres by Cryofocusing and Detection by ICPMS, Anal. Chem, 70, 2639–2645.

Smith, L.M., Maher, W.A., Craig, P.J., & Jenkins, R.O., 2002: Speciation of volatile antimony compounds in culture headspace gases of Cryptococcus humicolus using solid phase microextraction and gas chromatography-mass

spectrometry, Appl. Organomet. Chem, 16, 287–293.
Vriens, B., Ammann, A.A., Hagendorfer, H., Lenz, M., Berg, M., & Winkel, L.H.E., 2014: Quantification of Methylated Selenium, Sulfur, and Arsenic in the Environment, PLoS One, 9, 1–9.
Wehmeier, S., & Feldmann, J., 2005: Investigation into antimony mobility in sewage sludge fermentation, J. Environ. Monit, 7, 1194–1199.
Wilson, S.C., Lockwood, P. V., Ashley, P.M., & Tighe, M., 2010: The chemistry and behaviour of antimony in the soil environment with comparisons to arsenic: A critical review, Environ. Pollut, 158, 1169–1181.

P 11.3

Inorganic mercury adsorption and internalization kinetics and the role of dissolved organic matter

Teofana Chonova[1], Vera I. Slaveykova[1]

[1] *Environmental Biogeochemistry and Ecotoxicology, Department F.-A. Forel, Faculty of Sciences, University of Geneva, 66, boulevard Carl-Vogt, 1211, Geneva, Switzerland.*

Mercury (Hg) is a priority contaminant of global concern, because of its toxicity and biomagnification in aquatic food webs. However, mercury interactions with phytoplankton, central for its incorporation in the food web, as well as the role of environmental modifying factors are still not well elucidated and quantified (Le Faucheur et al., 2014).

The present work aims to characterize Hg uptake dynamics and explore the influence of the dissolved organic matter (DOM) ubiquitous for surface waters, as a modifying factor. DOM is key environmental parameter that is expected to reduce toxic metal bioavailability (e.g. Ravichandran et al., 2004); however, in the case of Hg there are rather few controversial studies.

The uptake dynamics were characterized in terms of adsorbed and intercellular contents, and as uptake and efflux rate constants. Adsorbed and intercellular Hg in *Chlamydomonas reinhardtii* was followed over period of 2h at three different, environmentally relevant concentrations (10^{-8} M, 10^{-9} M and 10^{-10} M). To that aim, cells grown in 4 × diluted Tris-Acetate-Phosphate medium were resuspended in simplified medium (Beauvais-Flueck et al., 2017) and exposed to the respective Hg concentration. Subsequently, one part was washed with Hg free exposure medium in order to obtain the total (adsorbed and intercellular) Hg content, and the second part was washed with 10^{-3} M cysteine (Sigma-Aldrich, Buchs, Switzerland) to determine the intracellular Hg concentration. To get insights into the role of DOM in Hg uptake dynamics, *Chlamydomonas reinhardtii* was exposed to Hg in natural waters rich in dissolved organic matter from Onego Lake, Russia.

Results showed, that at Hg exposure at 10^{-10} M, adsorbed and intracellular concentrations were similar. With increasing Hg exposure concentration, the ratio between intracellular and adsorbed mercury increased. A plateau of adsorbed mercury over time was reached faster with increasing Hg exposure concentrations. Inversely, plateau of intracellular concentration over time was attended faster when Hg exposure concentrations decreased. The latter may result from protection mechanisms of *Chlamydomonas* which were activated faster when concentrations were increasing. Indeed, calculated uptake and efflux constants evidence decelerating of influx, and acceleration of efflux rates with increasing Hg exposure concentrations.

The uptake of Hg decreased by approximately 50% when exposure experiments were performed in organic matter rich waters (6.4 - 16.6 mg.L^{-1}). This may result from the strong binding ability of Hg to DOM that affects speciation, solubility, mobility and toxicity of Hg in aquatic environments (Ravichandran et al., 2004). However, the variation of DOC between sites did not result in significantly different Hg bioaccumulation, except for the site with highest DOC concentration (16.6 mg.L^{-1}), where total Hg was lower compared to other sites. Nonetheless, the importance of other environmental factors (e.g. trace metals) has to be taken into account and evaluated as well. Laboratory experiments under controlled conditions are necessary in order to comprehend better the effect of DOM on Hg bioaccumulation excluding the potential influence of competitors or other environmental factors.

REFERENCES

Beauvais-Flueck, R., Slaveykova, V., Cosio, C. 2017: Cellular toxicity pathways of inorganic and methyl mercury in the green microalga Chlamydomonas reinhardtii. Scientific Reports, vol. 7, no. 1, p. 8034.

Le Faucheur, S., Campbell, P. G. C., Fortin, C., Slaveykova, V. I. 2014: Interactions between mercury and phytoplankton: Speciation, bioavailability, and internal handling. Environ Toxicol Chem 33(6), 1211–1224.

Ravichandran, M., 2004. Interactions between mercury and dissolved organic matter—a review. Chemosphere, 55(3), 319-31.

P 11.4

Mercury and methylmercury quantification in floodplain soils, canal sediments, and plants in the Upper Valais

Amrika Deonarine[1], Lorenz Gfeller[1], Patrick Neuhaus[1], Adrien Mestrot[1]

[1]*Institute for Geography, University of Bern, Hallerstrasse 12, CH-3012 Bern (amrika.deonarine@giub.unibe.ch)*

From 1930 to 1976, Hg was utilized as a catalyst for acetaldehyde production by an industrial plant in Visp. The Hg-containing wastewater was discharged into a canal which flows along an agricultural floodplain and then converges with the Rhone River. The canal sediments were later dredged and re-distributed as soil conditioner for agricultural fields and private gardens, resulting in widespread Hg contamination within the floodplain. To better understand the distribution and fate of this Hg, soils and sediments from agricultural fields, tree groves within the floodplain, and the impacted canal were collected and analyzed for total Hg, methylmercury (MeHg), total carbon (C)-nitrogen (N)-sulfur (S), organic-CNS, loss on ignition, and major and minor elements (e.g., iron (Fe), manganese (Mn)). Plant material (roots and leaves/shoots) from agricultural fields were also collected for total Hg quantification.

Our data indicated that there was low Total Hg and MeHg in the canal sediments and agricultural field soils. In the canal, Total Hg concentrations (0.2-1.5 mg/kg) were lower than the guideline of 2 mg/kg for areas that are considered contaminated. MeHg concentrations were generally ≤ 1 μg/kg, with %MeHg ≤ 0.8%. In the agricultural fields, Total Hg (≤ 1.34 mg/kg) and MeHg concentrations (≤ 1 μg/kg) were also low, with two exceptions: 3.7 and 5.7 μg/kg MeHg (%MeHg = 0.3 and 2.4%, respectively) were observed at two field sites downstream of the plant. Total Hg was positively correlated with organic-C ($R_s = 0.54$, $p < 0.05$) and organic-N content ($R_s = 0.78$, $p < 0.01$). Lg(Total Hg/C) was negatively correlated with C/N ratio ($R_s = -0.58$, $p < 0.05$), suggesting that Hg methylation was associated with increased humification of organic-C. In soils collected from tree groves, low Total Hg (≤ 0.4 mg/kg) and elevated MeHg concentrations (≤ 29.6 μg/kg; %MeHg = 17.7%) were observed. In these soils, MeHg was negatively correlated with Fe ($R_s = -0.94$, $p < 0.01$) and Mn ($R_s = -0.83$, $p < 0.05$), suggesting that lower occurrence of Fe and Mn oxides in these areas may increase Hg availability for methylation. In plants, Total Hg concentrations in roots and leaves/shoots were ≤ 0.13 mg/kg, and roots:leaves/shoots concentration factors were ≤ 1.33.

Future work involves performing sequential extractions and quantification of acid volatile sulfide to further investigate the biogeochemical parameters which control Hg methylation in the tree grove soils.

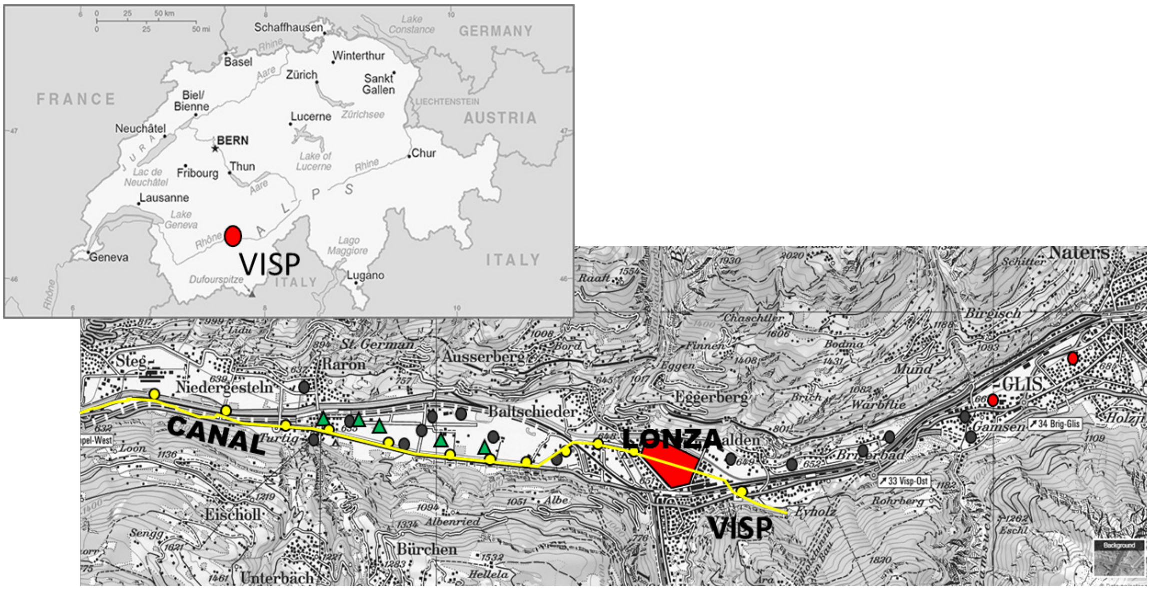

P 11.5

Depth profile of ∂^{15}N indicates drainage effects on peat

Miriam Groß-Schmölders,[1] Jennifer Woodard[2], Jan-Paul Krüger, Jens Leifeld[2] & Christine Alewell[1]

[1] *Institut für Umweltgeowissenschaften, University of Basel, Bernoullistrasse 32, CH-4056 Basel (miriam.gross-schmoelders@unibas.ch)*
[2] *Agroscope, Reckenholzstraße 191, CH-8046 Zürich*

Peatlands are powerful sinks for carbon dioxide (CO_2) and large stores of organic carbon. During the last centuries a substantial fraction of peatlands degraded for different reasons, reducing their sink function and turning them in long-term sources of CO_2. In view of climate change and the need to reduce emission of greenhouse gases, it becomes increasingly important to restore the natural state of degraded peatlands in order to reduce CO_2 emissions and to re-establish CO_2 sink activity.

Evaluation of the state of peatlands and the success of restoration projects calls for cost-efficient and reliable methods that indicate the current state of a peatland. Changes in the natural abundance of stable isotopes (^{15}N, ^{13}C) during degradation and restoration provide a promising opportunity (Krüger et al. 2015; Krüger et al. 2017). This project extends the former work of our group with a focus on ∂^{15}N depth trends and their value in interpreting the current state and recent history of peatlands. We investigated five peatlands in Southern Germany, central Sweden and Southern Finland. At all locations cores were taken from drained and natural sites in parallel to identify trends that could indicate changes due to drainage. Changes in ∂^{15}N with depth were compared to those in ∂^{13}C, bulk density (BD) and the carbon to nitrogen ratio (C:N).

In general we found that there are specific changes in all investigated parameters connected with drainage. In addition there are strong correlations between the different parameters. A negative correlation between ∂^{15}N and C:N (r: -0.89) was found at all locations (similar to Conen et al. 2008). There were distinct positive correlations between BD and the value of ∂^{15}N (r: 0.70). A consistent trend in ∂^{15}N with depth was detectable at all drained sites, similar to what Hobbie & Ouimette (2009) and Krull & Skjemstad (2003) found in other soils. At our locations the ∂^{15}N value first increased from the surface to a shallow depth, similar to other locations (e.g. Nadelhoffer et al., 1996; Högberg, 1995). However, at mid-depth in the drained profile there was a distinct peak in ∂^{15}N values at all our locations, before the ∂^{15}N values sharply decreased again close to the greatest depth to which the drainage had been effective. In deeper, always water saturated layers, there was a monotone depth trend similar to that in natural (undisturbed) peatlands. The feature of a peak in ∂^{15}N at mid-depth in the drained profile contrasts with a more frequently observed steady increase in ∂^{15}N with depth (Fig. 1). We hypothesise the peak in ∂^{15}N could be caused (1) by microbial activity and a depth-depending ratio of mineralization and leaching of N to N immobilization (e.g. Dijkstra et al. 2008), or by (2) by a shift from bacterial to fungal communities dominating activity (e.g. Hobbie 2012).

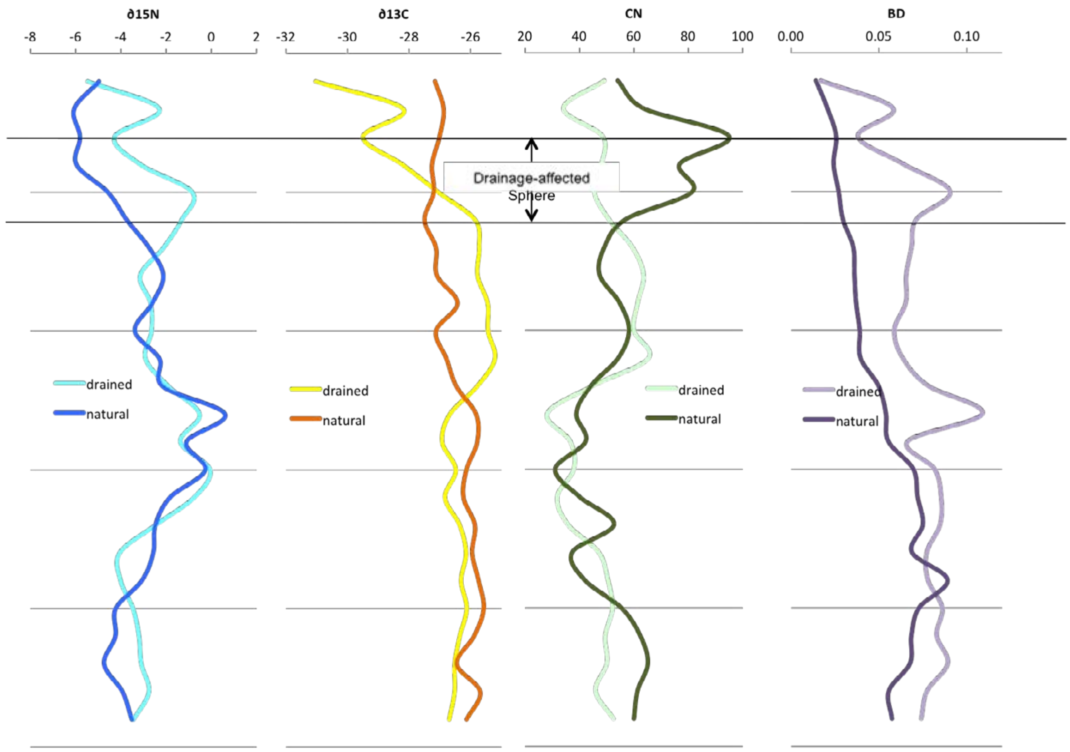

Figure 1. Depth trends in drained and natural locations of (a) $\partial^{15}N$, (b) $\partial^{13}C$, (c) CN and (d) BD in Lakkasuo

REFERENCES

Conen, F., M. Zimmermann, J. Leifeld, B. Seth & C. Alewell 2008: Relative stability of soil carbon revealed by shifts in $\partial^{15}N$ and C:N ratio. Biogeoscience, 5, 123 – 128.

Dijkstra P., C. LaViolette, J. Coyle, R. Doucett, E. Schwartz, S. Hart & B. Hungate 2008: ^{15}N enrichment as an integrator of the effects of C and N on microbial metabolism and ecosystem function. Ecology Letters, 11, 389 – 397.

Hobbie E., & A. Ouimette 2009: Controls of nitrogen isotope patterns in soil profiles. Biogeochemestry, 95, 355 – 371.

Hobbie E. & P. Högberg 2012: Nitrogen isotopes link mycorrhizal fungi and plants to nitrogen dynamics. The New Phytologist, 196, 367 – 382.

Högberg, P. 1995: ^{15}N Natural Abundance in Soil-Plant Systems. The New Phytologist, 137, 179 – 203.

Krüger, J.-P., L. Leifeld, S. Glatzel, S. Szidat & C. Alewell 2015: Biogeochemical indicators of peatland degradation – a case study of a temeprate bog in nothern Germany. Biogeoscience, 12, 2861 – 2871.¨

Krüger, J. P., F. Conen, J. Leifeld & C. Alewell 2017: Palsa Uplift Identified by Stable Isotope Depth Profiles and Relations of $\partial^{15}N$ to C/N Ratio. Permafrost and Periglacial Processes, 28, 485 – 492.

Krull, E. & J. Skjemstad 2003: $\partial^{13}C$ and $\partial^{15}N$ profiles in ^{14}C-dated Oxisol and Vertisols as a function of soil chemestry and mineralogy. Gerderma, 112, 1 – 29.

Nadelhoffer, K., G. Shaver, B. Frey & A. Giblin 1996: ^{15}N natural abundance and N use by tundra plants. Oecologia, 107, 386 – 394.

P 11.6

Toxicity and uptake of mercury compounds to the cyanobacterium *Synechocystis* pcc6803

Sébastien Guilmot[1], Vera Slaveykova[1]

[1] *Département F.-A. Forel des sciences de l'environnement et de l'eau, Université de Genève, Uni Carl Vogt - 2ème étage, 66, boulevard Carl-Vogt CH-1211 Genève 4*

Mercury is one of the most potent toxic trace metal of global concern. In surface waters it will undergo transformations, those transformations are a key factor of mercury toxicity, especially its methylation, enabling its biomagnification through the food chain (Dranguet et al. 2014).
Various forms of mercury possess different rates of absorption, metabolism, excretion and consequently toxicity. Interaction of Hg compounds and phytoplankton are important because it consists in the entrance point of the trophic chain (Gre and Poulain 2014).

The cyanobacterium *Synechocystis* pcc6803 has been chosen as it is a widely used model for phototrophs and photosynthesis understandings. Cyanobacteria are early ubiquitous phototrophic organisms reponsible for more than half of the global oxygen production, on the other hand they can bloom and alter their environment characteristics dramatically.

This work focuses on the Hg bioauptake to a cyanobacterium *Synechocystis* pcc6803, an entrance point of aquatic food chains in order to get a better understanding of the mechanistic insight of the phytoplankton's role in the mercury cycle. The aim of the present study is to determine and compare the kinetics of uptake of inorganic and methylmercury as well as their toxicity.

Uptake experiments were conducted as followed : anexic cultures of the cyanobacterium were exposed to increasing concentrations of mercury and methylmercury from 10^{-7} to 10^{-10} M.
An aliquot of the exposed culture was sampled after 10, 20, 30, 45, 60 and 120 min. Intracelluar and adsorbed mercury quantities were measured after a cysteine wash with a direct mercury analyzer (DMA)

In parallel, the toxicity of both Hg species on *Synechocystis* pcc6803 was assessed under the same mercury concentrations during 5 days.
Effective concentrations (EC) 50, 20 and 10 values were calculating using the absorbance and fluorescence relative to the chlorophyll a and the phycocianin.

Toxicity results show EC 50 values for MeHg at 10-8 M, whereas it is 10-7 M for inorganic Hg. MeHg being 10 times more toxic than inorganic Hg for *Synechocystis pcc6803.* It shows also an increase of EC 50 values over time for both compounds.

Preliminary uptake results show a faster uptake for MeHg than for inorganic Hg. A plateau is usually reached between 1 and 2 hours depending on the concentration of exposition.

REFERENCES

Dranguet, Perrine et al. 2014. "Towards Mechanistic Understanding of Mercury Availability and Toxicity to Aquatic Primary Producers." 68(11): 799–805.
Gre, Daniel S, and A J Poulain. 2014. "A Little Bit of Light Goes a Long Way : The Role of Phototrophs on Mercury Cycling." : 396–407.

P 11.7

Effects of metal-to-sulfide ratio, NOM, and Mn^{2+} on metal sulfide nanoparticle characteristics

Kevin Hoffmann[1], Iso Christl[1], Ralf Kaegi[2] & Ruben Kretzschmar[1]

[1] Institute of Biogeochemistry and Pollutant Dynamics, CHN, ETH Zurich, Zurich, Switzerland
[2] Eawag, Swiss Federal Institute of Aquatic Science and Technology, Dübendorf, Switzerland

Trace metals can be enriched in natural environments either naturally or anthropogenically. In redox-dynamic environments (e.g., river floodplains, wetlands) that are subject to periods of prolonged waterlogging, anoxic conditions can establish within a few days as a consequence of microbial respiration. The absence of O_2 favors the use of alternative electron acceptors (e.g., Fe^{III}, $Mn^{III/IV}$, and S^{VI}) in biotic and abiotic reactions. With the onset of sulfate reduction, readily generated bisulfides form sparingly soluble nanoscale precipitates with chalcophile trace metals (e.g., Cu_xS, CdS). Depending on soil pore water composition, these natural metal sulfide nanoparticles (MS NPs) may have a crucial impact on trace metal mobility in natural environments. In highly contaminated soils, pore water concentration of trace metals can be in excess with respect to sulfide, or in deficit in sulfur-rich environments. In this regard, reaction stoichiometry has been shown to influence particle size and surface site composition of CdS NPs formed in the presence of cysteine (Mullaugh and Luther III, 2010). However, effects of various reaction stoichiometries on formation of Cu_xS and CdS in the presence of natural organic matter (NOM) are still unknown. The relevance of NOM as key modulator for particle growth and stability has been shown for other metal sulfides, e.g., HgS (Deonarine and Hsu-Kim, 2009).

Up to now, respective knowledge of NOM effects on Cu_xS and CdS NPs is lacking. As in waterlogged soils, microbial respiration leads to the reductive dissolution of $Mn^{III/IV}$-oxides and the resulting elevated Mn^{2+} concentrations in the pore water may influence particle formation of metal sulfides. Though several divalent cations are known to induce aggregation, to our knowledge the impact of Mn^{2+} ions on formation and aggregation of MS NPs has not been addressed, yet. Given the lack of information on MS NP formation processes relevant in redox-variable environments, our objective was to investigate the effects of initial metal-to-sulfide ratio, NOM type and concentration, and Mn^{2+} concentration on particle size, particle morphology and colloidal stability.

We performed experiments on Cu_xS and CdS nanoparticle formation from anoxic solutions with low metal and sulfide concentrations (50-100 µM) at different metal-to-sulfide ratios (1:2, 1:1, 2:1), absence and presence of different NOM types and concentrations (humic and fulvic acid, 0–50 mg C/L), and varying Mn^{2+} concentrations (0.1–1 mM). All experiments were conducted at pH 7.5 (1 mM MOPS) in a 10 mM NaCl electrolyte. Dynamic light scattering (DLS), electrophorectic mobility measurements, and transmission electron microscopy (TEM) were used to investigate the properties of the Cu_xS and CdS nanoparticles after 24h equilibration time.

The influence of the metal-to-sulfide ratio on particle size and surface charge of CdS NPs in the absence and presence of fulvic acid is shown in Figure 1A. The excess of the metal over sulfide favored aggregation when fulvic acid was absent. With increasing Cd concentration, the hydrodynamic diameter of the precipitates increased and the zeta potential became less negative (~-15 mV). The presence of fulvic acid counteracted this effect and substantially reduced the tendency of CdS NPs to aggregate as indicated by the smaller hydrodynamic diameters. Moreover, in the presence of 5 mg C/L fulvic acid, Cu_xS NPs occurred as well-dispersed, single particles ($d_{median} \approx 10$nm) whereas CdS NPs ($d_{median} \approx 43$nm) were mostly present as small aggregates (Figure 1B and C).

Our results suggest that the metal-to-sulfide ratio of the solution is critical for the stability of the precipitating MS NPs when NOM is absent. Even rather low NOM concentrations can stabilize MS NPs against aggregation by adding negative charges to the particles. We further demonstrated that the extent of stabilization was dependent on the MS species (Cu_xS vs. CdS). As a consequence, the mobility of some MS NP species may be enhanced in NOM-rich natural waters.

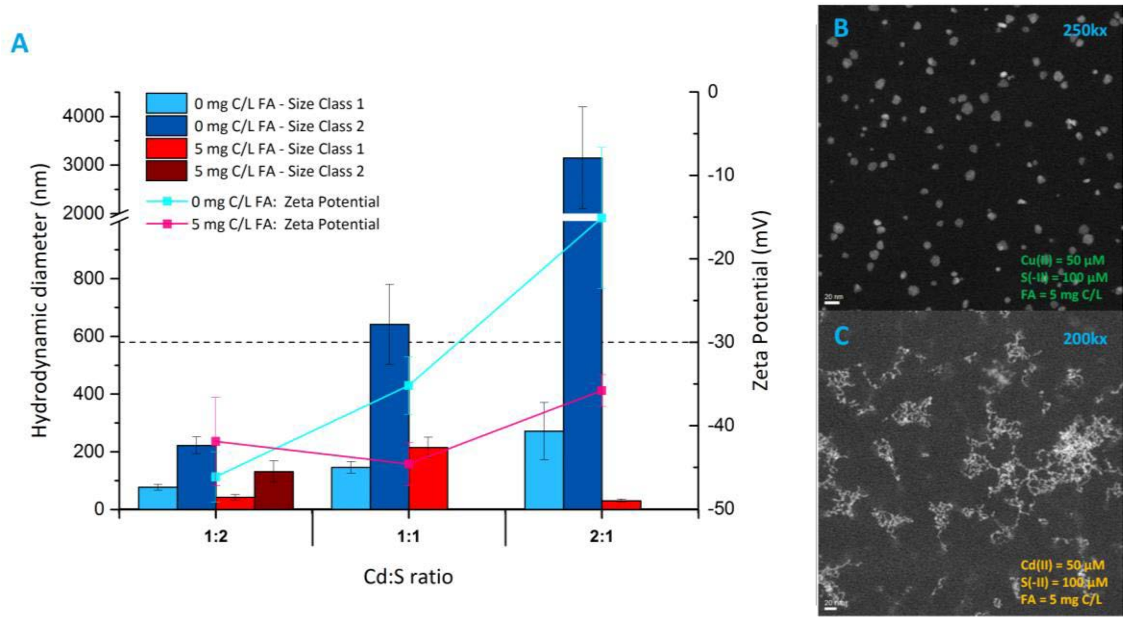

Figure 1. (A) Influence of cadmium-to-sulfide ratio on median hydrodynamic diameters (d_h) and zeta potentials of CdS NPs at pH 7.5 and 10 mM NaCl electrolyte after 24h equilibration time in the absence and presence of fulvic acid (FA). Due to bimodal size distributions of the NPs, two size classes were considered for size evaluation using the multi narrow mode algorithm in the DLS software. Electrophoretic mobility measurements were converted into zeta potential values using the Smolouchowski assumption. All values were compiled from at least two sample replicates (n = 2–5) and multiple measurement replicates. The dashed line at -30 mV indicates the colloidal stability threshold. (B, C) TEM images of selected samples at different magnifications for direct comparison of Cu_xS and CdS morphology and aggregation state. Note the different magnifications when comparing the particle sizes.

REFERENCES

Deonarine, A. and Hsu-Kim, H. 2009: Precipitation of mercuric sulfide nanoparticles in NOM-containing water: Implications for the natural environment. Environ. Sci. Technol. 43, 2368-2373.

Mullaugh, K.M. and Luther III, G.W. 2010: Spectroscopic determination of the size of cadmium sulfide nanoparticles formed under environmentally relevant conditions. J. Environ. Monitor. 12, 890-897.

P 11.8

Synchrotron X-ray beam-induced chemical transformations: The case study of Tl redox changes as a function of photon flux and temperature

Francesco Femi Marafatto[1], Dario Ferreira-Sanchez[1], Rainer Dähn[1], Daniel Grolimund[1], Andreas Voegelin[2]

[1] *Paul Scherrer Institute, CH-5232 Villigen PSI*
[2] *Eawag, Überlandstrasse 133, CH-8600 Dübendorf*

The mobility and toxicity of trace elements in environmental systems largely depends on their speciation, including their redox state. Therefore, information on the (redox) speciation of trace elements is crucial for an improved process-based understanding of the environmental fate and impact of micronutrients and contaminants. Synchrotron based X-ray absorption spectroscopy (XAS) provides information on the redox state and speciation of trace elements, with a spatial resolution down to the micro-meter scale when using a micro-focused X-ray beam.

However, the high brilliance and photon flux density of third-generation synchrotron facilities such as the Swiss Light Source (SLS) have raised concerns about beam-induced transformations in some systems. In particular, a micro-focused X-ray beam may damage the sample either by ablating the atoms on the surface (physical radiation damage) (Teng and Moffat, 2000) or by promoting chemical changes due to the breaking of chemical bonds and/or promoting the formation of radical species (chemical radiation damage) (Weik et al., 2000)). A number of studies have shown that the rate of radiation damage induced by high photon flux densities in certain systems can be slowed down at low (cryogenic) temperatures. Ideally, effective sample cooling thus offers a means to obtain spatially-resolved speciation information on dilute samples with minimal instrumental artifacts.

The current study was undertaken in the framework of a project aimed at setting up a stage at the micro-XAS beamline at the SLS that enables spatially resolved speciation studies on radiation-sensitive (environmental) samples with at the micrometer scale. As a scientific test-case, we aim to examine the nature of Tl-rich minerals formed in geogenically Tl-rich soils (Voegelin et al., 2015). Apart from the importance of Tl as highly toxic but poorly studied trace element, this test case is ideally suited for our purposes as Tl occurs as Tl(I) and Tl(III) in environmental samples and is often associated with radiation-sensitive solids such as Mn-oxides.

In this study, as a baseline for the future evaluation of system performance, we systematically evaluated changes in Tl redox state in two Tl reference materials ($TlNO_3$ in BN matrix and Tl_2O_3 in cellulose or BN matrix) as a function of sample temperature, photon flux density, and exposure time using an $N_{2(g)}$ cryo-blower for temperature control. Experiments were run at the microXAS beamline at the SLS by irradiating the sample with 3 different photon flux densities (different beam sizes) at three different temperatures.

Our results confirm that X-ray irradiation of the pellets results in changes in the Tl redox state by promoting Tl(III) reduction in cellulose pellets or Tl(I) oxidation (from Tl(I)-nitrate), with greater effects at higher photon flux density and exposure time. Importantly, the changes were dependent on the matrix, as evidenced by experiments showing a greater reduction of Tl(III) in a cellulose matrix than in a BN matrix. We also observed that lower temperature reduced the rate of chemical changes induced by the X-ray photons (Figure 1).

These results have strong implications on the design of experiments where information on both the spatial distribution and the speciation of elements in natural samples is desired. Furthermore, the upgrade to diffraction limited storage rings in many synchrotron facilities with multi-bend achromat lattice magnets (Einfeld, 2014) will result in an even greater photon flux density (reduction in beam size). Solutions to avoid beam damage will need to be developed either through technical upgrades (i.e. cryostats) or methodological strategies (i.e. chemical maps at selected energies around the absorption edge). The future part of this project aims to test both these solutions on a pilot study to evaluate the speciation (and therefore potential mobility) of Tl in a Tl-rich soil from the Erzmatt site in the Swiss Jura mountains, in particular through chemical imaging at low temperature (Voegelin et al., 2015).

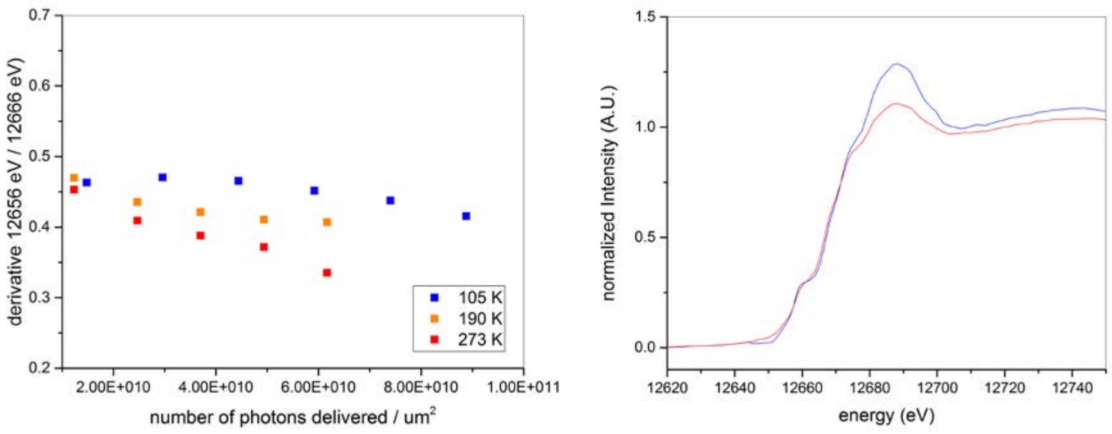

Figure 1.A – left) Temperature-dependent reduction of Tl(III) in Tl_2O_3 with a 70 µm² spot size as a function of number of photons delivered per square micron. The decrease in the ratio between the normalized absorbance at 12656 eV and that at 12666 eV indicates a reduction of Tl; B – right) Tl L_3-edge XANES for the first scan at 105K (blue) and the last scan at 273K (red) of which the derivative ratio is shown in A.

REFERENCES

Einfeld, D. 2014 Multi-bend Achromat Lattices for Storage Ring Light Sources. Synchrotron Radiation News 27, 4-7.

Teng, T.-y., et al. 2000 Primary radiation damage of protein crystals by an intense synchrotron X-ray beam. J Synchrotron Radiat 7, 313-317.

Voegelin, A., et al. 2015 Thallium Speciation and Extractability in a Thallium- and Arsenic-Rich Soil Developed from Mineralized Carbonate Rock. Environ Sci Technol 49, 5390-5398.

Weik, M., et al. 2000 Specific chemical and structural damage to proteins produced by synchrotron radiation. Proc Natl Acad Sci U S A 97, 623-628.

P 11.9

Exploring the application of time series analysis methods to concentration data from Swiss rivers and lakes

Juan Carlos Rodríguez-Murillo[1] and Montserrat Filella[2]

[1] *Museo Nacional de Ciencias Naturales-CSIC, C/ Serrano 115 dpdo. E-28006 Madrid, Spain (jcmurillo@mncn.csic.es)*
[2] *Institute F.-A. Forel, University of Geneva, Boulevard Carl-Vogt 66, CH-1205 Geneva, Switzerland (montserrat.filella@unige.ch)*

Concentration data series in natural waters have mostly been used to determine whether the corresponding element or compound was accumulating or being depleted in a given system. However, time data series analysis can provide much more information. A time series can be expressed as a sum of a deterministic trend and a stochastic component. In concentration data series, the deterministic component is the cause of the above mentioned accumulation or depletion and the stochastic part is the final result of the physical and chemical processes that affect solute concentrations and have an apparently random output. The study of this non-deterministic component can give information on those processes.

The application of time series analysis pervades many areas of knowledge from financial predictions to signal processing but has been much less applied to concentration data. It includes a wide variety of approaches, ranging from probabilistic methods based in time series autocorrelation functions (ACF) (e.g., moving average (MA), autoregressive (AR) and ARMA models) to spectrum calculations (e.g., periodograms). Unfortunately, most of these methods require data to be stationary but as clearly stated by Thomson 1994: “Experience with real-world data soon convinces one that both stationarity and Gaussianity are fairy tales invented for the amusement of undergraduates”. This adds a further difficulty to the analysis~~.~~ Exploration of the advantages and weaknesses of the existing methods will be discussed in this communication through their application to Swiss freshwater data. Preliminary results show that there are clear differences between time series stochastic properties of different solutes and also between the solutes at the surface and bottom of Lake Geneva and between the lake and River Rhône data.

REFERENCES

Thomson, D.J. 1994: Jackknifing multiple-windows spectra. *In:* Proceedings of the IEEE International Conference on Acoustics, Speech and Signal Processing*, VI, 73-76*.

P 11.10

Mn(II) and Cd(II) sorption to synthetic montmorillonite

Natacha Van Groeningen[1], Iso Christl[1] & Ruben Kretzschmar[1]

[1] *Soil Chemistry Group, Institute of Biogeochemistry and Pollutant Dynamics, Department of Environmental Systems Science, CHN, ETH Zurich, Universitätstrasse 16, CH-8092 Zurich, Switzerland*

Redox variable environments such as riparian floodplain soils, wetlands, and rice paddies are of great importance in the mobilization of trace elements from terrestrial environments into aquatic systems. Elevated dissolved concentrations of trace elements in terrestrial and aquatic systems are of concern since they can cause detrimental effects on the biosphere due to toxic responses in plants (e.g. Mn, Zn, Cu) as well as in animals and humans (e.g. Cd, Pb). Both natural sources (e.g., presence of trace metal-enriched minerals) and anthropogenic sources (e.g., agriculture, industrial and mining activities) can lead to local enrichments of trace elements in the environment. During periods of water-saturation, high concentrations of dissolved Mn^{2+} are observed in redox variable environments as a result of the reductive dissolution of Mn(IV,III)-(oxyhydr)oxides. Consequently, the high concentrations of Mn^{2+} are expected to compete with trace elements cations (e.g. Ca^{2+}, Zn^{2+}, Cd^{2+}) for adsorption to mineral surfaces and therefore influence their fate in the environment. Herein, the mobility and the bioavailability of trace elements in soils is mainly controlled by surface adsorption to soil solids including clay minerals, oxides of iron, manganese and aluminium, as well as natural organic matter. Clay minerals are widespread in soils and are among the most important sorbents for trace elements due to their large specific surface area, negative surface charge and reactive surface hydroxyl groups.

To date, it is not well known how and to which extent the sorption of Mn^{2+} to clay minerals surfaces influences the retention of other trace elements under reducing conditions. To investigate this, we first performed single metal sorption experiments under anoxic conditions (O_2 < 0.1 ppm) using a synthetic iron-free montmorillonite (Syn-1) to elucidate the sorption of Mn^{2+} and Cd^{2+} at the clay mineral-water interface as function of pH (4-10), total metal concentration (0.001-1 mM) and $CaCl_2$ background electrolyte concentration (0.1-30 mM).

The sorption of Mn^{2+} and Cd^{2+} to Syn-1 as function of the dissolved metal concentration (sorption isotherm) and pH (sorption edge) are shown in Figure 1. An increase of Mn^{2+} and Cd^{2+} sorption was observed with increasing metal concentration in solution (1a, c) and pH (1b, d) due to proton-metal cation competition for binding sites. In the sorption isotherm data (1a, c), a sorption maximum was not observed for either cation indicating that the sorption sites had not been saturated with respect to Mn^{2+} and Cd^{2+}, respectively. This also applies to the data on pH-dependent sorption (1b, d) considering the chosen total metal concentrations. However, noted that the amount Mn^{2+} and Cd^{2+} sorbed at pH 7.8 and 7.4 respectively, clearly exceed the CEC of Syn-1 (~0.07 mol/kg), indicating an additional sorption mechanism through surface complexation. The pronounced effect of Ca on Mn and Cd sorption at pH ≤ 5.5 and the virtual absence of a pH-dependence at pH below 5 and [Ca] ≥ 1 mM indicate the binding to permanently negatively charged surfaces sites dominated the sorption of Mn and Cd under these conditions (Fig 1b, d). The clear influence of Ca on the pH-dependent sorption of Mn and Cd at pH 6–9 (Fig 1b, d) further suggests that outer-sphere surface complexation to negatively charged edge surfaces sites of Syn-1 significantly contributed to Mn and Cd sorption at circumneutral to alkaline conditions. The absence of Ca-independence in Mn and Cd sorption data at trace levels of dissolved Mn and Cd implies that inner-sphere surface complexation to edge surface sites is marginal even at low concentrations. The quantitative similarity of Mn and Cd sorption at 0.1 mM Ca in both sorption isotherm data (Fig 1a, c) and pH-dependent data (Fig 1b, d) indicates that elevated levels of dissolved Mn, as observed in water-saturated terrestrial environments, may very effectively compete with Cd bound to clay minerals. As a consequence, increased Mn concentrations may trigger Cd release from clay surfaces and increase Cd mobility and bioavailability.

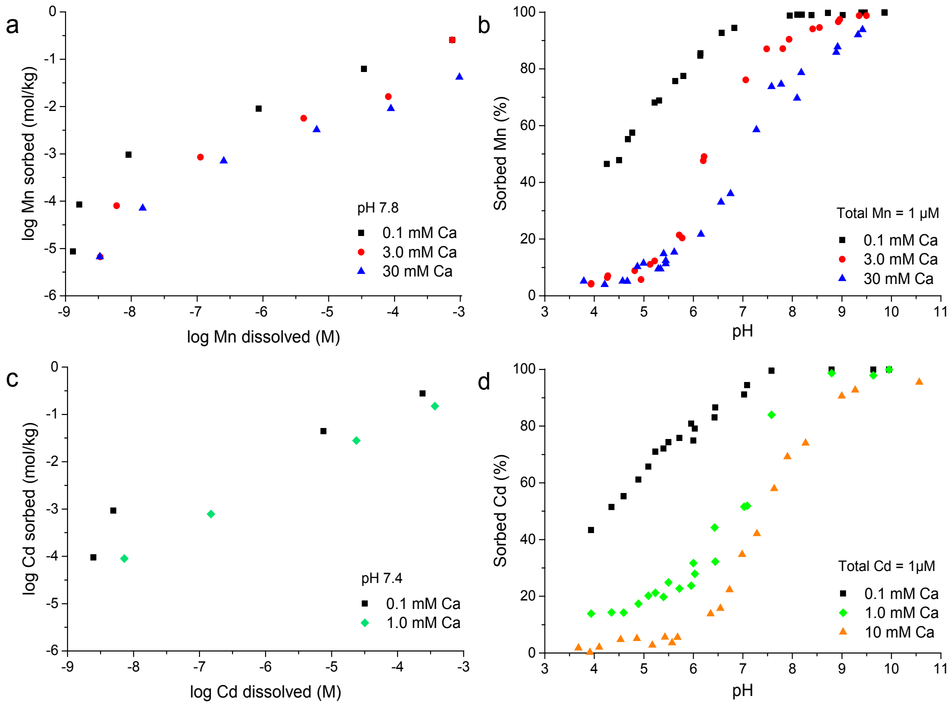

Figure 1. Sorption of Mn^{2+} (a, b) and Cd^{2+} (c, d) on Syn-1 smectite (~1 g/L) as function of dissolved metal concentration (10^{-3} to 10^{-8} M) (a, c) and pH (b, d), at different $CaCl_2$ concentrations. Sorption isotherms were recorded at fixed pH 7.8±0.1 for (Mn^{2+}) and for pH 7.4±0.1 for Cd^{2+}. Total metal concentrations of 1 μM were used to investigate pH-dependence of sorption (b, d). All samples were equilibrated for 1 day.

12. Atmospheric Processes and Interactions with the Biosphere + 13. Aerosols and clouds in a changing world

Convenors 12: Christof Ammann, Stefan Brönnimann, Susanne Burri, Martin Steinbacher
Convenors 13: Christopher Hoyle, Ulrich Krieger

ACP – Commission on Atmospheric Chemistry and Physics

TALKS:

12.1 **Bartels-Rausch T**.
Fundamentals of multiphase chemistry at the surface of environmental snow with relevance to the Atmosphere

12.2 **Berhanu T.A**., Szidat S., Brunner D., Satar E., Schanda R., Nyfeler P., Battaglia M., Steinbacher M., Hammer S., Leuenberger M.
Estimation of the fossil-fuel component in atmospheric CO_2 based on radiocarbon measurements at the Beromünster tall tower, Switzerland

12.3 **Buchmann N.**, Brinkmann N., Kahmen A., Eugster W.
Changes in water uptake of temperate tree species in response to low soil moisture

12.4 **Carozzi M.**, Loubet B.
Estimating NH_3 volatilisation from multi-plot agronomic trials measured with low-cost samplers

12.5 **Emmel C.**, Winkler A., Hörtnagl L., Revill A., Buchmann N., Eugster W.
Long-term C budget of a cropland site on the Swiss plateau

12.6 **Etzold S.**, Burri S., Haeni M., Zweifel R.
Tree growth patterns and water relations of beech, spruce, pine, fir and oak trees across Switzerland

12.7 **Gharun M.**, Vervoort W., Turnbull T., Adams M.
Testing the influence of vegetation coupling to the atmosphere on catchment-scale hydrological processes in Australia

12.8 **Gilgen A.**, Huang K., Ickes L., Neubauer D., Lohmann U.
Future changes in Arctic aerosol emissions and their impact on clouds and radiation

12.9 **Jeannet P.**
Comparison of tropospheric temperature trends based on radiosondes and satellite instruments

12.10 **Krieger U.K**., Luo B.P., Corral-Arroyo P., Alpert P., Ammann M., Peter T.
Feedbacks between microphysics and photochemical aging in viscous aerosols

12.11 **Malle J.**, Mazzotti G., Jonas T.
Influence of sub-canopy energy fluxes on snowpack dynamics in forest

12.12 **Müller M.**, Berchet A., Graf P., Meyer J., Brunner D., Hüglin C., Emmenegger L.
Low-cost sensors for CO_2 monitoring: sensor calibration and first data from the Carbosense network

12.13 **Voglmeier K.**, Ammann C., Jocher M., Menzi H.
Nitrous oxide emissions of a Swiss rotational grazing system: how important are small scale emissions

12.14 **Volk M.**, Bassin S., Enderle J., Fuhrer J.
Atmospheric N deposition causes carbon balance gains in a seven year field experiment in subalpine grassland

POSTERS:

P 12.1 Winther M., **Blunier T.**, Balslev-Harder D., Christensen S., Priemé A., Elberling B.
Continuous measurements of nitrous oxide isotopomers during incubation experiments

P 12.2 **Imhof S.**, Steinbacher M., Conen F.
Large-scale CO_2 flux estimated from CO_2 and ^{222}Rn measurements on Jungfraujoch

P 12.3 **Hörtnagl L.**, Baur T., Burri S., Eugster W., Etzold S., Haesler R., Käslin F., Meier P., Merbold L., Pluess P., Zielis S., Buchmann N.
Two decades of ecosystem CO_2 and H_2O gas exchange above a sub-alpine coniferous forest in Switzerland

P 12.4 **Meier P.**, Burri S., Merbold L., Eugster W., Hörtnagl L., Buchmann N.
Beyond CO_2 – Tackling the full greenhouse gas budget of a sub-alpine forest ecosystem

P 12.5 **Satar E.**, Berhanu T., Brunner D., Henne S., Herrmann L., Leuenberger M.
Four years of continuous CO_2/CH_4/CO measurements (2012-2016) at the Beromünster tall tower station in Switzerland

P 12.6 **Steinbacher M.**, Wyss S.A., Emmenegger L.
Harmonization of atmospheric greenhouse gas observations in Europe

12.1

Fundamentals of multiphase chemistry at the surface of environmental snow with relevance to the Atmosphere

Thorsten Bartels-Rausch

[1]*Paul Scherrer Institut, Laboratory of Environmental Chemistry, 5232 Villigen PSI*

Earth's surface snow plays an active part in atmospheric chemistry. Research over the past decades has provided an impressive observational basis of the resulting large scale effects, such as substantial modification of the composition and of the chemical reactivity of the lowermost atmosphere in polar regions.

Here, I present details on the chemical mechanisms operating in environmental snow and ice derived from well controlled laboratory based experiments.
The research is taking full advantage of the Near Ambient Pressure Photoelectron spectroscopy (NAPP) end station at PSI/SLS reveals the ability of atmospheric trace gases to modify the structure of ice at the upper few nanometers at the air-ice interface upon adsorption. Particular focus is placed on the interfacial dissociation mechanism of acids.

Even with a focus of this presentation on adsorption of acidic trace gases (HCl, HNO_3, formic acid, acetic acid) to ice, on the molecular structure of the hydrogen bonding network at the air-ice interface, and on the kinetics of halogen reactions in sea-salt, the details on chemistry at extreme concentration and temperature conditions at interfaces might be of high relevance not only in environmental science but also in general chemistry, material science, catalysis, cryobiology, and astrophysics.

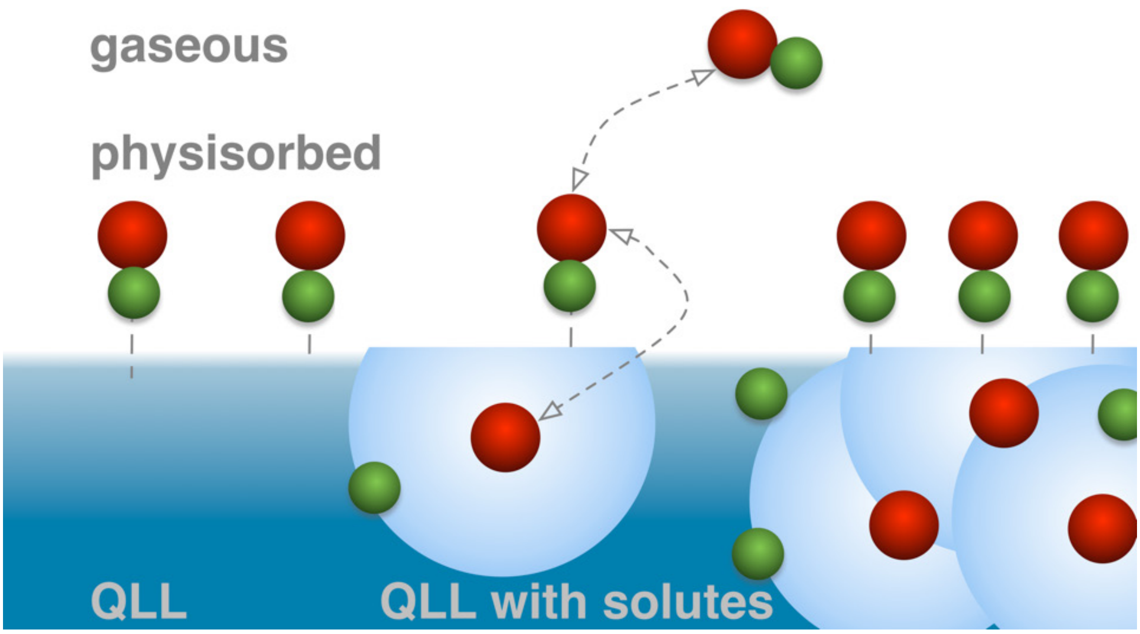

12.2

Estimation of the fossil-fuel component in atmospheric CO_2 based on radiocarbon measurements at the Beromünster tall tower, Switzerland

Berhanu T.A[1]., Szidat S., Brunner D., Satar E., Schanda R., Nyfeler P., Battaglia M., Steinbacher M., Hammer S., Leuenberger M.

[1]Climate and Environmental Physics, Physics Institute, University of Bern, Sidlerstrasse 5, 3012 Bern

Fossil fuel CO_2 (CO_{2ff}) is the major contributor of anthropogenic CO_2 in the atmosphere, and accurate quantification is essential to better understand the carbon cycle. Since October 2012, we have been continuously measuring the mixing ratios of CO, CO_2, CH_4 and H_2O at five different heights at the Beromünster tall tower, Switzerland. Air samples for radiocarbon ($\Delta^{14}CO_2$) analysis have also been collected from the highest sampling inlet (212.5 m) of the tower on a bi-weekly basis. A correction was applied for $^{14}CO_2$ emissions from nearby nuclear power plants (NPPs), which have been simulated with the Lagrangian transport model FLEXPART-COSMO. The $^{14}CO_2$ emissions from NPPs offset the depletion in ^{14}C by fossil-fuel emissions resulting in an underestimation of the fossil-fuel component in atmospheric CO_2 by about 16 %. An average observed ratio (R_{CO}) of 13.4 ± 1.3 mmol/mol was calculated from the enhancements in CO mixing ratios relative to the clean air reference site Jungfraujoch (ΔCO) and the radiocarbon-based fossil-fuel CO_2 mole fractions. The winter time R_{CO} estimate of 12.5 ± 3.3 is about 30 % higher than the winter time ratio between in-situ measured CO and CO_2 enhancements at Beromünster over the Jungfraujoch background (8.7 mmol/mol) corrected for non-fossil contributions due to strong biospheric contribution despite the strong correlation between ΔCO and ΔCO_2 in winter. By combining the ratio derived using the radiocarbon measurements and the in-situ measured CO mixing ratios, a high-resolution time series of CO_{2ff} was calculated exhibiting a clear seasonality driven by seasonal variability in emissions and vertical mixing. By subtracting the fossil-fuel component and the large-scale background, we have determined the regional biospheric CO_2 component that is characterized by seasonal variations ranging between -15 to +30 ppm. A pronounced diurnal variation was observed during summer modulated by biospheric exchange and vertical mixing while no consistent pattern was found during winter.

12.3

Changes in water uptake of temperate tree species in response to low soil moisture

Nina Buchmann[1], Nadine Brinkmann[1,2], Ansgar Kahmen[2] & Werner Eugster[1]

[1] *ETH Zürich, Universitätstr. 2, CH-8092 Zürich (nina.buchmann@usys.ethz.ch)*
** University of Basel, Schönbeinstrasse 6, CH-4056 Basel

Forests play an important role in biospheric-atmospheric gas exchange, affect and are affected by climate change, while providing many valuable ecosystem services. How forests react to changes in climate and to extreme weather events is thus of high interest.

Within the Swiss FluxNet (http://www.swissfluxnet.ch/), CO_2 and H_2O vapor fluxes of two forests have been intensively studied: at the Lägeren (mixed deciduous forest at 682 m asl; dominated by beech) and at Davos (subalpine evergreen forest at 1639 m asl, dominated by spruce). These ecosystem flux measurements are running at Lägeren since 2004 and at Davos since 1997, making the latter one of the oldest ecosystem flux sites globally. In addition, these sites serve as platforms for additional studies, e.g. on tree water relations or on tree responses to extreme events like dry spells and droughts.

Although both forests have been carbon sinks since ever since measurements started, they acclimate fast to changing environmental conditions such as a spring drought. Increasing the ratio of gross primary production to evapotranspiration, sometimes also called ecosystem water use efficiency, clearly shows that tree responses to reduced soil water availability are highly plastic. However, how tree species differ in their water uptake patterns and how plastic species-specific responses to a changing environment really are is still unclear.

We used stable oxygen and hydrogen isotopes to follow the fate of precipitation within the Lägeren forest and studied the spatial and temporal variations of root water uptake of the four dominant tree species (*Fagus sylvatica*, *Acer pseudoplatanus*, *Fraxinus excelsior*, and *Picea abies*) over four years. All species took up water from the top soil, when soil water was not limiting. Under low soil moisture conditions in the top soil, the deciduous trees shifted their uptake depth to deeper soil layers, while spruce trees did stay shallow. In addition, we modeled the residence time of water in different soil depths and quantified the age of the water taken up for beech and spruce trees. Both species rely on water which precipitated during the growing season (about 50%), but also on water originating from the previous winter (about 40%).

Thus, while the deciduous tree species are highly plastic in their responses to low soil moisture conditions, spruce was not, making the evergreen species highly vulnerable to future droughts. In addition, deciduous species benefit from their reliance on summer AND winter precipitation, with the latter acting as a buffer against water deficits during summer.

12.4

Estimating NH_3 volatilisation from multi-plot agronomic trials measured with low-cost samplers

Marco Carozzi[1] & Benjamin Loubet[2]

[1] *Agroscope Research Station, Climate and Air Pollution, CH-8046 Zurich, Switzerland*
[2] *INRA, UMR ECOSYS, INRA, AgroParisTech, Université Paris-Saclay, FR-78850, Thiverval-Grignon, France*

Ammonia (NH_3) plays a central role in the global biogeochemical cycle of reactive nitrogen as well as in soil acidification, ecosystem eutrophication, aerosol formation and climate. Ammonia is a highly reactive gas that is mostly produced by agricultural activity (93.3% in EU-28, and 92.9% in Switzerland; Eurostat, 2016). It is mainly emitted through management of livestock excreta and their subsequent application in the field as fertiliser, and to a lesser extent through the application of mineral fertilisers.

While in recent decades many studies have been addressed to assess NH_3 emission from fertiliser application at plot or field scales (Hafner et al., 2015), most of them were restricted to explore a single combination of management (as a fertiliser type, a distribution method, a soil cover) in a climatic conditions. The main reason of this simple experimental designs derives from the interferences that replicated multiple sources can play towards the others, due to local advection phenomena. To overcome this lack and statistically assess the effect of agronomic management in the same pedo-climatic conditions, a repeated experimental design is needed.

Among existing methods for measuring NH_3 emissions, micrometeorological methods are the most reliable. However they require large surfaces to be applied and are expensive. Consequently they are not adapted for multiple sources assessments. Inverse modelling approaches (Flesch et al., 1995; Loubet et al., 2001), conversely, have been demonstrated to be suitable for estimating NH_3 volatilisation from intensive NH_3 sources based on concentration mesurements.

A novel method to quantify NH_3 emission from multiple treatment based on the combination of low-cost concentration-based passive sensors (Sutton et al., 2001) and a short-range inverse dispersion model, is proposed.

This method was tested in silica with over a block scheme composed by three treatments with three repeated sources mimicinc real emissions. Different patterns (constant, linear decreasing, exponential decreasing, and gaussian emission potentials) and strengths (ratios between sources up to 100) were simulated over a range of semi-oceanic meteorological conditions.

In order to assess the method, the surface of the plot, the height and the integration time of the samplers (from few hours to a week), as well as sources strengths and background concentrations have been taken into account. This method revealed suitable for estimating NH_3 emissions from replicated agronomic plots, and in line with the uncertainty fo other measurement methods (Loubet et al., 2010). Preliminary results shown an overall underestimations of the method compared to generated data, lower than -25±15% for a multi-plots scheme with NH_3 sources differing by at most a factor of 10, and an underestimation of -12±7% for an isolated plot. The method was not sensitive to the emission pattern.

REFERENCES

Eurostat. 2016. Agriculture - ammonia emission statistics. http://ec.europa.eu/eurostat/statisticsexplained/index.php/Agriculture_-_ammonia_emission_statistics.

Flesch, T.K., Wilson, J.D. & Yee, E., 1995. Backward-time Lagrangian stochatic dispertion models and their application to estimate gaseous emissions. Journal of Applied Meteorology, 34: 1320-1332.

Hafner S., Vilms Pedersen S. & Sommer S.G., 2016. The ALFAM2 project: Predicting ammonia loss from field-applied manure. In Körner I, editor, RAMIRAN 2015: Proceeding of the 16th International Conference Rural-Urban Symbiosis. TuTech Verlag. 289-292.

Loubet, B., Milford, C., Sutton, M.A. & Cellier, P., 2001. Investigation of the interaction between sources and sinks of atmospheric ammonia in an upland landscape using a simplified dispersion-exchange model. Journal of Geophysical Research-Atmospheres, 106(D20): 24183-24195.

Loubet, B., Génermont, S., Ferrara, R., Bedos, C., Decuq, C., Personne, E., Fanucci, O., Durand, B., Rana, G. & Cellier, P., 2010. An inverse model to estimate ammonia emissions from fields. European Journal of Soil Science, 61: 793–805.

Sutton, M.A., Miners B., Tang Y.S., Milford C., Wyers G.P., Duyzer J.H., Fowler D., 2001. Comparison of low cost measurement techniques for long-term monitoring of atmospheric ammonia. J Environ Monit, 3(5): 446-53.

12.5

Long-term C budget of a cropland site on the Swiss plateau

Carmen Emmel[1], Annina Winkler[1], Lukas Hörtnagl[1], Andrew Revill[1], Nina Buchmann[1], Werner Eugster[1]

[1]*Institute of Agricultural Sciences, ETH Zürich, Universitätstr. 2, CH-8092 Zürich (carmen.emmel@usys.ethz.ch)*

The FLUXNET field site CH-OE2 in Oensingen (canton Solothurn) is the only long-term monitoring cropland site in Switzerland and has been running since the end of 2003. The site is managed under the regulations of the Swiss proof of ecological performance (ÖLN) featuring a crop rotation focusing on winter wheat, but also including winter barley, rapeseed, peas, potatoe and an intermediate cover crop (*Phacelia)*. Field management information is regularly provided by the farmer. Eddy covariance, meteorological and soil observations as well as carbon (C) imports and exports from sowing, organic fertilization and harvesting are used in this study to 1) analyze the C budget of the crop field over thirteen years, (2) determine the effect of the different crop types on the C budget, and (3) assess the interannual variability of the C exchange.

In this study we used the following equation to calculate the C budget (*CB*) of the field based on net ecosystem exchange (*NEE*) measured with the eddy covariance system, harvest exports ($E_{harvest}$), organic fertilization imports ($I_{fertilizer}$) and sowing imports (I_{sowing}):

$$CB = E_{harvest} + NEE + I_{fertilizer} + I_{sowing} CB = E_{harvest} + NEE + I_{fertilizer} + I_{sowing}$$
(1)

The different crop types resulted during their cropping seasons in an average C loss of between 55 (rapeseed) and 85 g m^{-2} (barley), except for peas, which lost on average 310 g m-2 partly due to extreme weather conditions. However, the crop-type specific interannual variability was relatively large (standard error typically between 30 and 60 g m^{-2}), mainly caused by meteorological variations and extreme events.

Seven out of thirteen years were close to C neutral (within ±50 g m^{-2}), while in all other years, the field was a net C source of 67 to 617 g m^{-2}. In total, the field lost approximately 1550 g C m^{-2} between 2004 and 2016 corresponding to an average annual loss of 120 g m^{-2} and $E_{harvest}$ was the largest term of the C budget equation (on average 290 g m^{-2} $year^{-1}$) followed by NEE (on average –120 g m^{-2} $year^{-1}$). At the same time, $I_{fertilizer}$ played only a minor role (on average –45 g m^{-2} $year^{-1}$) while I_{sowing} was rather negligible (–5 g m^{-2} $year^{-1}$). Soil C measurements to a depth of 12 cm showed that C stocks decreased by 790 g m^{-2} between 2004 (4270 g m^{-2}) and 2017 (3480 g m^{-2}), corresponding to a decrease of 18.6%. Assuming that the decrease was comparable all the way to the typical ploughing depth of 30 cm and roughly estimating a soil C loss of 1975 g m^{-2}, the soil C measurements confirm the findings of the C budget determined with equation (1).

12.6

Tree growth patterns and water relations of beech, spruce, pine, fir and oak trees across Switzerland

Etzold S.[1], Burri S.[2], Haeni, M.[1], Zweifel R.[1]

[1] *Swiss Federal Institute for Forest, Snow and Landscape Research WSL, Switzerland*
[2] *Department of Environmental Systems Science, ETH Zürich, Switzerland*

Changes in climatic conditions highlight the need for a better understanding of climatic forcing of tree growth in Central European forests. Within TreeNet, the biological drought and growth indicator network, stem radius changes of 140 tree individuals at 25 study sites across Switzerland were analyzed at an hourly resolution since 2011. We analyzed tree growth and water relations derived from stem radius variations of beech, spruce, pine, fir and oak trees in relation to meteorological conditions. The main objectives of the study were (i) to identify the main driving forces of tree growth at a high temporal resolution (hourly), (ii) to compare the optimum conditions for tree growth with the actually occurring conditions, and (iii) to interpret the discrepancies between the two ranges of conditions in order to better understand the physiological limits of the different tree species.

We found the main fraction of annual growth of beech, spruce and pine trees occurring during a relatively short time span of one to two months. Moving correlation analysis of daily growth values and meteorological conditions indicated precipitation and relative humidity as most important predictors for daily growth rates, independent of species and site conditions. Further, growth was closely negatively related to the tree's water deficit (TWD) with highest correlations at the beginning of the growing season, followed by a decreasing trend. During peak growth, other driving factors became important. This highlights the importance of tree water status especially for growth initiation, and thus, the timing of drought events as a decisive factor to judge about drought impacts on tree growth.

Frequency distributions of percentage annual growth binned by meteorological conditions, e.g., temperature, VPD, compared to the frequency distribution of maximum hourly growth rates binned by meteorological conditions were only partly congruent. This was interpreted as follows: the larger the difference between the two distributions frequencies were, the more the tree species grew away from its optimal conditions. Between 2012 and 2015, beech trees grew within the climate conditions of their maximum growth rates, and might be able to benefit from increasing temperatures in the future, if water availability is sufficient (Fig. 1). Further, spruce trees grew already near their upper temperature limit for maximum growth rates, whereas pine, fir and oak trees grew already 2-3°C above their optimal range, indicating a possible negative impact on growth rates of these tree species with potentially further increasing temperature in the future.

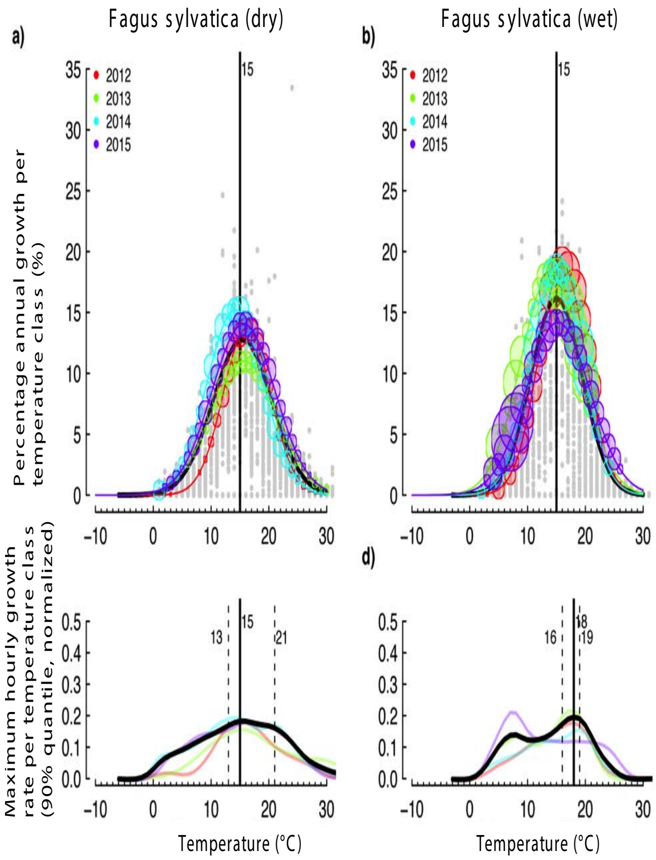

Figure 1: Frequency distribution of growth rates of beech trees (*Fagus sylvatica*) binned in temperature classes. Trees are grouped in **a)** dry and **b)** wet locations concerning their soil water balance (<400mm). Upper panel: Percentage annual growth rate per temperature class with the black line indicating the mean 90% quantile. Size of the circles indicate the maximum hourly growth rate per temperature class (90% quantile), as also shown in the lower panels c) and d) as black line. Beech trees grew most at 15°C (vertical black line in a) and b)). Maximum hourly growth rates were obtained at 15°C at dry sites (c) and at 18°C at wet sites. The dashed vertical lines in c) and d) indicate the temperature range in which 25% of growth occurred.

12.7

Testing the influence of vegetation coupling to the atmosphere on catchment-scale hydrological processes in Australia

Mana Gharun[1], Willem Vervoort[1], Tarryn Turnbull[1] , Mark Adams[1]

[1] *School of Life and Environmental Sciences, Faculty of Science, University of Sydney, NSW 2015 (mana.gharun@sydney.edu.au)*

Evapotranspiration (ET) is a major component of the water balance in Australia and is often simulated as supply-limited, i.e. depending on the soil moisture availability. In reality, vegetation canopy transpiration is also strongly controlled by atmospheric demand, particularly during demand-limited periods. In this study we investigate the atmospheric control over catchment-scale hydrological processes through atmospheric influence on Evapotranspiration. For this purpose we used a simple conceptual rainfall- runoff model (HBV) to test the hypothesis that atmospheric constraints to canopy transpiration, especially during conditions when soil moisture is not limiting, determine the variations in catchment water yield in mountainous eucalypt forests in Australia.

In the second part we test the hypothesis that spatial aggregation of climatic variables can improve lumped model simulations. Spatial surfaces of the climatic inputs (air temperature, rainfall, vapour pressure deficit and potential ET) were generated, taking into account the topographic influence of the forcing meteorological variables.

Inclusion of atmospheric-induced limitations to transpiration into the ET sub model improved streamflow simulation, especially during demand-limited periods. This is because the canopies of eucalypt forests are well-coupled to the atmosphere – changes in atmospheric demand have a large influence on transpiration. In addition, high resolution (30 m) surfaces of potential ET, temperature, and vapour pressure deficit, developed by including the influence of topography on forcing variables, improved model performance compared to point-based inputs.

12.8

Future changes in Arctic aerosol emissions and their impact on clouds and radiation

Anina Gilgen[1], Katty Huang[1], Luisa Ickes[1,2], David Neubauer[1], Ulrike Lohmann[1]

[1]Institute for Atmospheric and Climate Science, ETH Zürich, CH-8092 Zürich (anina.gilgen@env.ethz.ch)
[2]Now at Department of Meteorology, Stockholm University, 106 91 Stockholm

The Arctic climate is expected to change dramatically within the next decades as a consequence of climate change. Models predict that the Arctic temperature increase will be approximately twice as large as the global mean, among others due to the ice-albedo feedback. Higher temperatures reduce sea ice extent and thickness, especially in summer and autumn. The removal of sea ice can lead to increases in both natural and anthropogenic aerosol emissions: since sea ice acts like a barrier, less sea ice enables the emission of more aerosol particles from oceanic sources (such as sea salt) to the atmosphere. Furthermore, ship traffic through the Arctic Ocean is expected to increase; ships emit aerosol particles like black carbon or precursor gases such as sulphur dioxide.
Clouds can be affected by this increase in aerosol particles, which are crucial for both cloud droplet and ice crystal formation. In addition, clouds are impacted by the increase in temperature and the consequential increase in specific humidity. A simplified sketch (Fig. 1) illustrates these links and feedbacks.

In this work, we analyse how aerosol particles and clouds in the Arctic might change in late summer (July/August) and early autumn (September/October). We also assess how aerosol particles and clouds interact with radiation and therefore feedback on temperature. With the global aerosol-climate model ECHAM6-HAM2, we simulate and compare the years 2050 and 2004; for each year we chose an ensemble size of 10 to account for the high variability in Arctic climate. A new aspect of this study is the inclusion of future ship emissions, which are associated with traffic shipping and oil and gas extraction in the Arctic region based on the inventory by Peters et al. 2011.

We find that natural aerosol emissions increase until 2050, thereby leading to larger cloud droplet number concentrations. However, the impact of aerosol particles and clouds on radiation mainly changes because of the reduction in sea ice: since both aerosol particles and clouds have a lower albedo than ice but a higher albedo than water, the melting of sea ice reverses the effect of aerosols and clouds on temperature from a cooling to a warming over ice.
Future ship emissions over the Arctic Ocean do not have a large impact on climate. Only if the ship emissions are increased by a factor of ten, significant changes in aerosol burdens and cloud properties occur. Impacts on radiation are dominated by the Twomey effect (higher albedo of the polluted clouds), which is significant for changes in low cloud optical thickness.

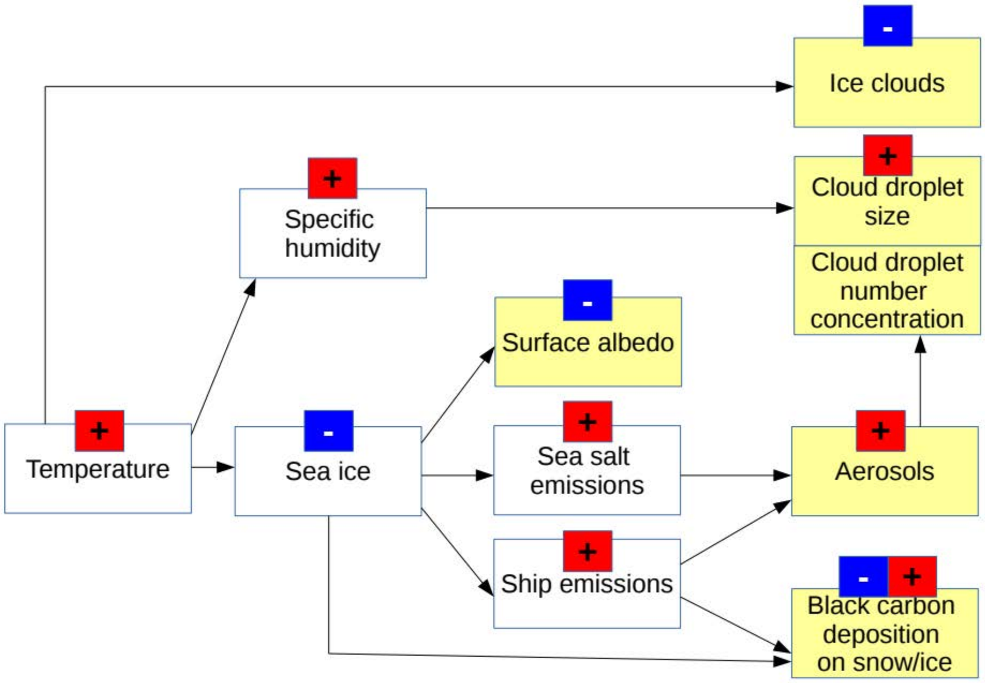

Figure 1. Simplified sketch showing how different variables will or might change in a warming Arctic. Yellow boxes indicate variables which affect radiation and therefore again temperature.

REFERENCES

Peters, G. P., Nilssen, T. B., Lindholt, L., Eide, M. S., Glomsrød, S., Eide, L. I., & Fuglestvedt, J. S. 2011: Future emissions from shipping and petroleum activities in the Arctic, Atmospheric Chemistry and Physics, 11, 5305-5320.

12.9

Comparison of tropospheric temperature trends based on radiosondes and satellite instruments

Pierre Jeannet

retired from MeteoSwiss Payerne, now 2068 Hauterive (famille.jeannet@bluewin.ch)

Long-term temperature changes are not only observed at the Earth surface, but also in the troposphere and the stratosphere. The world radiosonde network has been put in operation more than 60 years ago, followed by different satellite technologies. Microwave instruments onboard satellites started to monitor the global Earth troposphere and stratopshere since 1979 (MSU). Global Positioning System (GPS) radio occultation (RO) temperature series have been recently reprocessed back to 2006 (COSMIC 2013).
This presentation first focuses on tropospheric temperature trend comparisons between Swiss mountain surface stations, Payerne radiosonde and MSU series. Then it extends such comparisons to other parts of the world using gridded results from the Radiosonde Observation Correction Using Reanalyses (RAOBCORE). Finally, it shows comparisons between the Payerne radiosonde and the COSMIC temperature profiles.

Figure 1 is an extended version of Fig. 8.6 that we published in chapter 8 of Willemse & Furger (2016), in which three new MSU time series are included. The first two ones are provided by the University of Alabama in Huntsville (UAH v6.0), and the third one by the NOAA (STAR v4). Contrary to surface stations and radiosondes, the MSU only distinguishes two or three levels in the troposphere, mainly the low (TLT) and middle (TMT) troposphere. Here the MSU pixel used covers the longitude and latitude rectangle 5 – 7.5 / 47.5 – 50, slightly NE of Payerne. Temperature trend values (^{o}C/decade) given in the bottom of the Figure are calculated with a simple linear model over the full period with satellite data (1979-2016). The Swiss series based on in situ thermometric measurements show quite close results and only a weak vertical trend structure. All MSU annual values follow rather well the interannual variability depicted in the Swiss observations. However, both UAH MSU series (TLT and TMT) underestimate the tropospheric temperature trends given by the two independent surface and radiosonde Swiss observations by roughly a factor a two. The NOAA MSU TMT trend lies over the UAH one, but is still well under the Swiss results. These features are extreme over Switzerland, where the tropospheric warming is twice the global one.

Comparisons between radiosonde and MSU temperature trends averaged over different large regions of the world show various features, e.g. radiosondes mostly deliver similar trends between 850 and 300 hPa whereas UAH TMT trends are really smaller than the UAH TLT trends and the smallest ones in our analysis. On a near global scale, NOAA TMT trends remain slightly under the radiosonde trends. The numerous studies on the differences in the multi-decadal tropospheric trends provided by the major observation and adjustment techniques did not bring so far full conclusive answers and the political debate is intense in the USA (Santer & al. 2017).
COSMIC data are now used for the detection of temperature bias of widely used radiosonde types (Ho & al. 2017). Possibility and limits of this technique for the Swiss radiosonde will be presented.

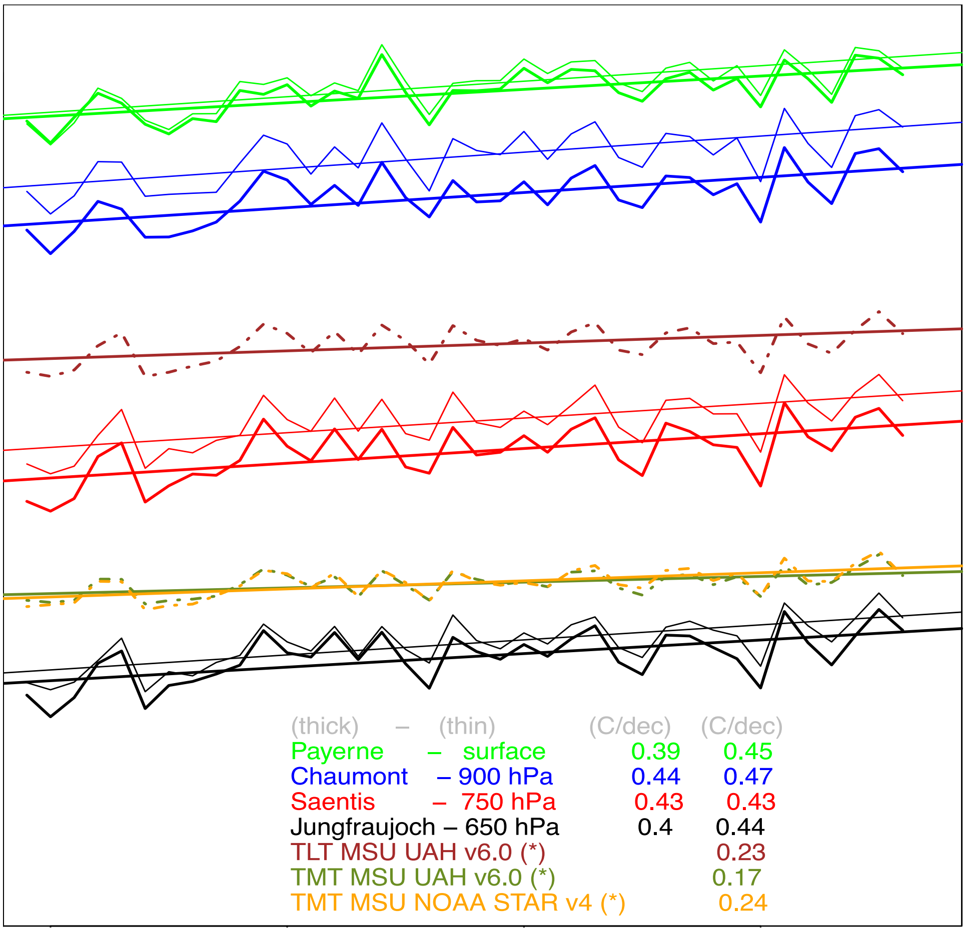

Figure 1. Comparison of temperature series and trends 1979-2016 of Swiss mountain surface stations (heavy lines: homogenised series), of Payerne radiosonde at nearby pressure levels (thin lines: reevaluated series), as well and of the newest MSU series in the low (TLT) and middle (TMT) troposphere (dashed lines) on the pixel close to Payerne (MSU (*): vertically shifted series).

REFERENCES

Ho, S.-P., Peng L. & Vömel H. 2017: Characterization of the long-term radiosonde temperature biases in the upper troposphere and lower stratosphere using COSMIC and Metop-A/GRAS data from 2006 to 2014, Atmos. Chem. Phys., 17, 4493-4511, doi:10.5194/acp-17-4493-2017.

Santer, B., & al. 2017: Tropospheric Warming Over The Past Two Decades, Scientific Reports 7, 2336, doi:10.1038/s41598-017-02520-7.

Willemse, S., & Furger M. (eds.) 2016: From weather observations to atmospheric and climate sciences in Switzerland, vdf Hochschulverlag, doi:10.3218/3746-3.

12.10

Feedbacks between microphysics and photochemical aging in viscous aerosols

Ulrich. K. Krieger[1], Luo Beiping[1], Pablo Corral Arroyo[2], Peter Alpert[2], Markus Ammann[2], Thomas Peter[1]

[1] Institute for Atmospheric and Climate Science, ETH Zürich, Zürich, Switzerland (ulrich.krieger@env.ethz.ch)
[2] Laboratory of Environmental Chemistry, Paul Scherrer Institute, 5232 Villigen PSI, Switzerland

Fe(III)-citrate complex photochemistry, which plays an important role in aerosol aging, especially in the lower troposphere, has been widely recognized in both solution and solid states. The complex can get excited by light below about 500 nm, inducing the oxidation of carboxylate ligands and the production of peroxides (e.g., OH•, HO2•), which will lead to more decarboxylation and oxygenated volatile organic compounds (OVOC) production, having a significant impact on the gas-particle partitioning. Recently, there is literature reporting that aqueous aerosol particles may attain highly viscous, semi-solid or even glassy physical states under a wide range of atmospheric conditions. However, systematic studies on the effect of high viscosity on photochemical processes are scarce.

In this research, mass and size changes of a single, aqueous Fe(III)-citrate/citric acid particle levitated in an electrodynamic balance (EDB) are tracked during photochemical processing. Low temperature and/or low relative humidity can result in reduced molecular mobility and low water content, which affects chemical reaction rates in the liquid phase, but also slows down the diffusion of components in the liquid phase. With the assistance of a numerical model, which includes the equilibria of each component, main chemical reactions, and the transport of volatile and semi-volatile products, we found the evaporative loss through photochemical processing and fragmentation in aqueous Fe(III)-citrate/citric acid particles being quite sensitive to relative humidity with temperature unchanged. This is mainly due to water acting as a plasticizer changing viscosity drastically. We will compare the high and low viscosity experiments with model predictions and discuss these comparisons.

12.11

Influences of sub-canopy energy fluxes on snowpack dynamics in forest

Johanna Malle[1], Giulia Mazzotti[1], Tobias Jonas[1]

[1]*WSL Institute for Snow and Avalanche Research SLF, Flüelastrasse 11, CH-7260 Davos Dorf (johanna.malle@slf.ch)*

Seasonal snow is an important component of the hydrological cycle since it acts as a natural reservoir for water storage during the winter and is a fundamental water resource during spring and summer for many regions worldwide. To facilitate water resources management and climate change impact assessments, it is therefore important to have models that allow accurately quantifying snow water resources. However, while current snow models are capable of representing snow dynamics in open areas rather accurately, modelling snow in forested areas remains a challenge. The micrometeorological conditions are strongly influenced through the presence of trees which also drives the large spatial and temporal variation of the forest snow cover.

In an attempt to improve the representation of both turbulent and radiative fluxes in forest snow models, we analyzed sub-canopy air temperature, short and longwave radiation, and wind speed measurements from within the forest stand. Corresponding field work was conducted in the canton of Grisons, Switzerland during the winter season 2016/17 at 24 field sites with variable canopy coverage using mobile measuring infrastructure. With the collected data we were able to relate the radiative temperature of the canopy to above-canopy air temperatures while also accounting for site-specific canopy parameters. At the same time, air temperatures inside forests were shown to be similar to the above-canopy air temperatures with remaining differences not being correlated to the canopy parameters considered in this study. Finally, a simple wind-model was developed to relate above canopy wind measurements to sub-canopy wind conditions.

To test the sensitivity of forest snow models to the representation of these micrometeorological conditions we implemented parameterizations corresponding to the above findings into the physically based snow model FSM (Factorial Snow Model). Validation with measured meteorological data demonstrated both parameterizations for radiative canopy temperature and wind to be much improved over standard assumptions build into FSM. The model results showed further a considerable effect on SWE and snow depth as well as on the snow disappearance date. This study emphasizes the importance of accurately representing longwave radiation and turbulent fluxes in forested areas when aiming to model sub-canopy snowpack dynamics.

12.12

Low-cost sensors for CO_2 monitoring: sensor calibration and first data from the Carbosense network

Michael Müller[1], Antoine Berchet[1], Peter Graf[1], Jonas Meyer[2], Dominik Brunner[1], Christoph Hüglin[1], Lukas Emmenegger[1]

[1] *Empa, Swiss Federal Laboratories for Materials Science and Technology, Dübendorf, Switzerland (michael.mueller@empa.ch)*
[2] *Decentlab, CH-8600 Dübendorf, Switzerland*

Monitoring the success of CO_2 reduction measures requires detailed understanding and accurate quantification of CO_2 fluxes. While there are reliable estimates for annual total CO_2 emissions in Switzerland, our current knowledge of their temporal variability and attribution to individual sources such as individual cities is limited. Furthermore, we are lacking detailed information on fluxes between the atmosphere and the biosphere which considerably vary in space and time. New measuring and modelling techniques have the potential to enhance our understanding of anthropogenic CO_2 emissions, atmospheric transport and biospheric uptake in Switzerland.

A unique dense CO_2 low power sensor network is being deployed and operated within the Swiss project Carbosense. The network consists of 300 sensor nodes across Switzerland plus additional 40 nodes in the city of Zurich. The data of this network shall be combined with atmospheric transport models and CO_2 inventories at different scales to better constrain the anthropogenic emissions as well as the fluxes of the biosphere.

The network relies on three levels of CO_2 measurements: (i) 300 nodes of battery-powered CO_2 low-cost diffusive NDIR sensors (SenseAir LP8), (ii) 30 temperature stabilized, mains-powered NDIR low-cost instruments with active sampling and zero-air connection (SenseAir HPP (Hummelgard 2015)), and (iii) high-precision laser spectrometers (Picarro G1301/ G2401, CRDS) as reference instruments. The sensors are distributed mainly at Swisscom radio transmitter locations and at MeteoSwiss meteorological stations. All LP8 and HPP data is transmitted as 10 minute averages through Swisscom's new Low Power Network (LPN).

Over 300 LP8 CO_2 sensors have been integrated with relative humidity and temperature measurements and with LoRaWAN communication (www.lora-alliance.org). All sensors were characterized in climate and pressure chambers with respect to carbon dioxide (350 – 1000 ppm), temperature (-5 to 50 °C) and pressure (770 – 1010 hPa). A calibration model was developed based on Beer-Lambert law, and relating the raw signal of the IR detector to the true CO_2 mixing ratio, determined by CRDS, and referenced to the WMO scale.
The impact of temperature and pressure variations on the IR detector signal is modelled by including polynomial correction terms in the Beer-Lambert equation. Largest IR signal changes are related to temperature variations. Pressure effects are slightly higher than expected for an ideal gas due to factors such as spectral line broadening and sensor design (Gaynullin 2017). Relative humidity becomes a critical issue above ca. 95%, likely because of local condensation within the non-heated sensor unit.
Before network deployment and in addition to the chamber measurements, all 300 sensors were placed next to a Picarro instrument for several weeks. To account for a wide range of operating conditions, these deployments took place at the rural site Dübendorf (432 masl) and the mountain site Rigi (1031 masl).

Two of the more expensive and precise HPP instruments were also characterized with respect to pressure (770 to 1010 hPa) and CO_2 (450 to 900 ppm) and operated in the field next to a reference instrument for several months. Pressure correction was based on measurements of integrated sensors, and zero drift was measured in the field by supplying CO_2 free air to the instrument for 36 minutes every 37 hours.

This paper presents findings obtained from the extensive CO_2 sensor characterization tests. These include the accuracy of the LP8 and HPP sensors, variability in performance between sensors, long-term sensor behaviour, power consumption and reliability of the data transmission. Furthermore, we present our first experiences from their deployment within the network and discuss operational aspects such as the assessment and assurance of the long-term data quality.

REFERENCES

Hummelgard, C. et al. 2015: Low-cost NDIR based sensor platform for sub-ppm gas detection. Urban Climate, 14, pp. 342-350.

Gaynullin, B. et al. 2017: A practical solution for accurate studies of NDIR gas sensor pressure dependence. Lab test bench, software and calculation algorithm. Proceedings of IEEE Sensors, art. no. 7808828.

12.13

Nitrous oxide emissions of a Swiss rotational grazing system: how important are small scale emissions

Karl Voglmeier[1,2], Christof Ammann[1], Markus Jocher[1] & Harald Menzi[3]

[1] *Climate and Air Pollution Group, Agroscope Research Station, Reckenholzstrasse 191, CH-8046 Zürich (karl.voglmeier@agroscope.admin.ch)*
[2] *Institute of Agricultural Sciences, ETH Zurich, Tannenstrasse 1, CH-8092 Zürich*
[3] *Ruminant nutrition, Agroscope Research Station, Tioleyre 4, CH-1725 Posieux*

Grazed pastures are considered as strong sources of the greenhouse gas nitrous oxide (N_2O) with local hot-spots resulting from the uneven spatial distribution of the excretion of the grazing animals. Especially urine patches can result in a high local nitrogen surplus, which can only partly be taken up by nearby plants (Moir et al. 2011). The strong spatial and temporal variability of the gaseous emissions represents an inherent problem for the quantification of gaseous emissions from pastures. For this reason, micrometeorological methods that integrate emissions over a larger domain like the eddy covariance (EC) method are well suited to quantify the total N_2O emissions of grazed fields. In contrast, chamber methods are better suited to study the underlying processes and to measure the spatial and temporal variability of individual emission sources (urine and dung patches). We present first results of the Posieux pasture experiment with dairy cows in 2016 where N_2O fluxes were measured during the entire grazing season. Field-scale emission were obtained with the EC technique using fast response Quantum cascade lasers (QCL) for N_2O quantification. Small scale emissions of N_2O from dung and urine patches as well as from “background” surface areas were quantified using an optimized chamber technique (Hensen et al. 2006). These so called ‘fast box’ measurements also made use of a QCL and allowed to measure a flux value within 60-90 s. We carried out these measurements at selected intensive observation areas within the pasture on naturally and artificially applied urine and dung patches. High temporal and spatial dynamics of the N_2O emissions were observed and related to driving parameters. We discuss the feasibility and limitations of our measurement methods and highlight the advantages of a combined chamber-EC approach to understand the dynamics of pasture N_2O emissions. Additionally we present a first approach to up-scale the chamber measurements to the field-scale and compare the results with the results of the EC method. Using excretion estimates derived from animal C and N budgets, net emission factors for the individual emission sources (urine, dung) and for the pasture field are presented.

REFERENCES

Hensen, A., Groot, T.T., van der Bulk, W.C.M., Vermeulen, A.T., Olesen, J. & Schelde, E.K. 2006: Dairy farm CH_4 and N_2O emissions, from one square metre to the full farm scale, Agriculture Ecosystems and Environment, 112 (2/3), 146–152.

Moir, J.L., Cameron, K.C., Di, H.J. & Fertsak, U. 2011: The spatial coverage of dairy cattle urine patches in an intensively grazed pasture system, Journal of Agricultural Science, 149, 473-485.

12.14

Atmospheric N deposition causes carbon balance gains in a seven year field experiment in subalpine grassland

Matthias Volk[1], Seraina Bassin[1], Jan Enderle[1] & Jürg Fuhrer[1]

[1] *Agroscope Zürich, Air Pollution/Climate Group, Reckenholzstrasse 191, 8046 Zurich, Switzerland (matthias.volk@agroscope.admin.ch)*

Air pollution agents interact when affecting biological sinks for atmospheric CO_2, e.g. the soil organic carbon (SOC) content of grassland ecosystems. Factors favoring plant productivity, like atmospheric N deposition, are usually considered to favor SOC storage. In a seven year experiment in subalpine grassland under N-deposition treatment, we examined C-fluxes and -pools. Total N deposition was 4, 9, 14, 29 and 54 kg N ha^{-1} yr^{-1} (N4, N9, etc.). We hypothesized that SOC of this mature ecosystem would not change in control treatments, but that effects of the air pollutant on plant yield, net ecosystem productivity (NEP) and SOC content would develop in parallel, leading to SOC content to increase with N deposition. In the control treatment SOC increased significantly by 9% in seven years. Cumulative plant yield showed a highly significant N effect (+38% in N54). Cumulative NEP did show a strong, yet statistically insignificant, hump shaped response pattern to N deposition with a +62% increase in N14, and only +39% increase in N54. SOC had a similar response to N, with highest gains at intermediate N deposition rates (9 and 14 kg N ha^{-1} yr^{-1}), suggesting a unimodal response, too. We assume the strong, pollutant-independent soil C sink developed as a consequence of the management change from grazing to cutting. The non-parallel response of SOC and NEP compared to plant yield under N deposition is likely the result of increased respiratory SOC losses, following mitigated microbial N-limitation or priming effects, and a shift in plant C allocation leading to smaller C input from roots.

P 12.1

Continuous measurements of nitrous oxide isotopomers during incubation experiments

Malte Winther[1], Thomas Blunier[1], David Balslev-Harder[1,2], Søren Christensen[3], Anders Priemé[4,5] & Bo Elberling[5]

[1]Centre for Ice and Climate, Niels Bohr Institute, University of Copenhagen, Juliane Maries Vej 30, DK-2100 Copenhagen (blunier@nbi.ku.dk)
[2]Danish National Metrology Institute, Matematiktorvet 307, DK-2800 Kgs. Lyngby
[3]Section for Terrestrial Ecology, Department of Biology, University of Copenhagen, *Universitetsparken 15, DK-2100 Copenhagen*
[4]Section for Microbiology, Department of Biology, University of Copenhagen, *Universitetsparken 15, DK-2100 Copenhagen*
[5]Center for Permafrost, Department of Geosciences and Natural Resource Management, University of Copenhagen, Øster Voldgade 10, DK 1350 Copenhagen

Nitrous oxide (N_2O) is an important and strong greenhouse gas in the atmosphere. It is produced by microbes during nitrification and denitrification in terrestrial and aquatic ecosystems. The main sinks for N_2O are turnover by denitrification and photolysis and photo-oxidation in the stratosphere. In the linear N=N=O molecule ^{15}N substitution is possible in two distinct positions, central and terminal. The respective molecules, $^{14}N^{15}N^{16}O$ and $^{15}N^{14}N^{16}O$, are called isotopomers. It has been demonstrated that N_2O produced by nitrifying or denitrifying microbes exhibits a different relative abundance of the isotopomers. Therefore, measurements of the site preference (SP, the difference in the abundance of the two isotopomers) in N_2O can be used to determine the source of N_2O i.e. nitrification or denitrification. Recent instrument development allows for continuous position dependent d^{15}N measurements at N_2O concentrations relevant for studies of atmospheric chemistry. We present results from continuous incubation experiments with denitrifying bacteria, *Pseudomonas fluorescens* (producing and reducing N_2O) and *Pseudomonas chlororaphis* (only producing N_2O) with a prototype of the Picarro G5101-i analyzer.

The continuous analysis of N_2O isotopomers reveals the transient isotope exchange between KNO_3, N_2O, and N_2. We find bulk isotopic fractionation of about -5‰ for *P. chlororaphis*, in line with previous results for production from denitrification. For *P. fluorescens*, the bulk isotopic fractionation during production and reduction differ largely we found 52‰ and 9‰, respectively. The SP isotopic fractionation for *P. chlororaphis* is 3.5‰. For *P. fluorescens*, we obtain positive fractionation in SP for both production and reduction conflicting with previous findings.

In summary, we implemented continuous measurements of N_2O isotopomers during incubation of denitrifying bacteria and believe that similar experiments will lead to a better understanding of denitrifying bacteria and N_2O turnover in soils and sediments and ultimately hands-on knowledge on the biotic mechanisms behind greenhouse gas exchange of the globe.

REFERENCES

Winther, M., et al. 2016: Continuous measurements of nitrous oxide isotopomers during incubation experiments, Biogeosciences Discuss., doi 10.5194/bg-2016-258.

P 12.2

Large-scale CO_2 flux estimated from CO_2 and ^{222}Rn measurements on Jungfraujoch

Simon Imhof[1], Martin Steinbacher[2] & Franz Conen[1]

[1] *Department of Environmental Sciences, University of Basel, Bernoullistrasse 30, CH-4056 Basel (s.imhof@unibas.ch)*
[2] *Laboratory for Air Pollution/Environmental Technology, Swiss Federal Laboratories for Materials Science and Technology (Empa), Überlandstrasse 129, CH-Dübendorf*

The High Altitude Research Station Jungfraujoch (3580 m a.s.l.) contributes high precision data to the Integrated Carbon Observation System (ICOS), a pan-European research infrastructure for monitoring the carbon cycle and its perturbations. Here, we explore the potential of carbon dioxide (CO_2) and radon (^{222}Rn) data from Jungfraujoch to provide estimates of monthly CO_2 flux in central Europe. Radon is emitted relatively homogenously in space and time from land surfaces, which, together with its half-life of 3.8 days, makes it a useful tracer of gas exchange between boundary layer and free troposphere. We analysed hourly data of the year 2016 by using ^{222}Rn concentrations below the 10th percentile of a month as guidance for free tropospheric (baseline) conditions, and three different percentiles as guidance for enhanced boundary layer influence.

Results show that episodes of enhanced ^{222}Rn concentrations at Jungfraujoch were usually accompanied by elevated CO_2 for most of the year 2016, except during the period from May to August when the surrounding surface acted as a net CO_2 sink. Although the temporal pattern of monthly net CO_2 flux was plausibly reproduced, the annual CO_2 budget was underestimated by a factor of about 10 compared to the national CO_2 inventory. One reason for the low estimate could be that boundary layer influence on Jungfraujoch is during summer particularly frequent in the afternoon or early evening. This leads, during the main growing season, to a bias in observations towards the time of day when photosynthetic activity has most strongly reduced CO_2 concentration in the boundary layer. Another reason for the underestimate could be a that the uptake of CO_2 by vegetation has been greater in 2016 than in other years. In Switzerland, 2016 started warmer than usual, the first half was particularly wet and there was little snow in the mountains towards the end of the year. Whether this led to larger than usual CO_2 uptake by vegetation could be verified by looking at annual CO_2 budgets over the past years obtained through eddy-covariance measurements above forests.

P 12.3

Two decades of ecosystem CO_2 and H_2O gas exchange above a sub-alpine coniferous forest in Switzerland

Lukas Hörtnagl[1], Thomas Baur[1], Susanne Burri[1], Werner Eugster[1], Sophia Etzold[1,2], Rudolf Haesler[2], Florian Käslin[1], Philip Meier[1], Lutz Merbold[1,3], Peter Pluess[1], Sebastian Zielis[1], and Nina Buchmann[1]

[1] *ETH Zürich, Institute of Agricultural Sciences, Department of Environmental Systems Science, Zürich, Switzerland (lukas.hoertnagl@usys.ethz.ch)*
[2] *Swiss Federal Institute for Forest, Snow and Landscape Research WSL, Switzerland*
[3] *Mazingira Centre, International Livestock Research Institute (ILRI), Kenya*

The ICOS Class 1 Ecosystem Station candidate site in Davos, located in a sub-alpine coniferous forest in Switzerland, is one of the longest running eddy covariance (EC) flux stations in the world. Carbon and water exchange above the canopy, i.e. fluxes of carbon dioxide (CO_2) and water vapor (H_2O_v), were first recorded in 1995, continuous measurements are available since 1997. The availability of these long-term measurements allows detailed analyses of intra- as well as inter-annual variability of forest carbon and water dynamics and thus facilitates the identification of potential trends in ecosystem functioning over a time period of two decades. An additional EC system for CO_2 and H_2O_v fluxes, compliant with ICOS guidelines, was installed in 2014.

Here we present CO_2 and H_2O_v flux results from the last 20 years and give insights into the complex functioning of the forest ecosystem in response to biotic and abiotic drivers. Flux calculations for all years were standardized, with each year following the same processing steps and corrections. To ensure only data of highest quality go into subsequent analyses, all fluxes were subjected to rigorous quality tests, consistent among all years.

In addition, we compare new fluxes from the ICOS eddy covariance system with fluxes from the previously installed EC system between 2014 and 2016. This comparison aims to investigate the impact of switching to the ICOS EC setup on observed ecosystem fluxes in order to identify potential offsets between the two EC systems.

P 12.4

Beyond CO_2 - Tackling the full greenhouse gas budget of a sub-alpine forest ecosystem

Philip Meier[1], Susanne Burri[1], Lutz Merbold[1,2], Werner Eugster[1], Lukas Hörtnagl[1], Nina Buchmann[1]

[1] Department of Environmental Systems Science, ETH Zurich, Switzerland (philip.meier@usys.ethz.ch)
[2] Mazingira Centre, International Livestock Research Institute (ILRI), Kenya

In order to tackle the full greenhouse gas (GHG) budgets of forest ecosystems, it is desirable but challenging to quantify the three major GHGs, i.e. CO_2, CH_4 and N_2O simultaneously in-situ. At the long-term forest research site Davos (Candidate Class I Ecosystem Station within the Integrated Carbon Observation System - ICOS), we have recently installed a state-of-the-art measuring system to simultaneously observe the three GHGs on a high temporal resolution and both within and above the forest canopy. Thereby, we combine above-canopy eddy covariance flux measurements and forest floor chamber flux measurements (using five custom-made fully automated chambers). Both systems are connected to a quantum cascade laser absorption spectrometer (QCL, Aerodyne) and measurements are switched between three hours of above-canopy and one hour of forest floor GHG flux measurements. Using this approach, we will be able to study the full GHG budget as well as the dynamics of the individual fluxes on two vertical levels within the forest using a single instrument. The first results presented here will highlight the suitability of this promising tool for quantifying the full GHG budget of forest ecosystems.

P 12.5

Four years of continuous CO_2/CH_4/CO measurements (2012-2016) at the Beromünster tall tower station in Switzerland

Ece Satar[1], Tesfaye Berhanu[1], Dominik Brunner[2], Stephan Henne[2], Lars Herrmann[1] & Markus Leuenberger[1]

[1] *Climate and Environmental Physics, Physics Institute and Oeschger Centre for Climate Change Research, University of Bern, Bern, Switzerland (satar@climate.unibe.ch)*
[2] *Empa, Laboratory for Air Pollution/Environmental Technology, Dübendorf, Switzerland*

Tall tower measurements of greenhouse gases can provide important information about diurnal and synoptic variability as well as seasonal and multi-annual trends. Due to their large footprint, tall-tower measurements are representative for a comparatively large region such that a network of such sites can be used to constrain greenhouse gas budgets from regional to continental scales.

In Switzerland, the CarboCount CH project (2012-2015), established a network of greenhouse gas measurement sites in order to estimate greenhouse gas fluxes on the country scale. An important component of this network is the Beromünster tower (47° 11′ 23″ N, 8° 10’ 32″ E, 217 m tall, base at 797 m a.s.l.) that is located on the Swiss plateau between the Alps in the south and the Jura mountains in the northwest. Since November 2012 the mixing ratios of CO_2, CH_4 and CO have been measured with a cavity ring down spectroscopy (CRDS) analyzer (Picarro G2401) from five sampling lines with inlets at 12.5, 44.6, 71.5, 131.6 and 212.5 m above ground level. Moreover, since April 2016 a LICOR 7000 instrument has measured the CO_2 mixing ratios at the highest sampling line with high frequency alongside with a 3D turbulence measurements in order to establish the turbulent CO_2 flux at the top of the tower and further constrain the local carbon budget.

Here we extend the discussion of the previously published dataset, and present four years (December 2012-December 2016) of continuous measurements of CO_2, CH_4 and CO. We investigate the seasonal and diurnal variations, the development of the vertical gradients, their resulting flux estimates, and draw inferences about the correlations between different species. This multi-species, multi-level observation based study aims at discussing typical variability patterns of the different species at the Beromünster site in order to investigate influences of sinks and sources of local and regional origin.

P 12.6

Harmonization of atmospheric greenhouse gas observations in Europe

Martin Steinbacher[1], Simon A. Wyss[1], Lukas Emmenegger[1]

[1] *Laboratory for Air Pollution/Environmental Technology, Swiss Federal Laboratories for Materials Science and Technology (Empa), Überlandstrasse 129, CH-8600 Dübendorf*

The Integrated Carbon Observation System Research Infrastructure (ICOS RI) is a European effort to quantify and understand greenhouse gas (GHG) fluxes.
Its concept is a high precision long-term network of stations measuring GHG concentrations in the atmosphere and GHG fluxes from ecosystems and the oceans, designed around a set of central facilities.

The quantification of the sources and sinks is a prerequisite for developing and implementing appropriate reduction measures. This requires international coordination and homogenization of the observations. Measurements must be of high quality and comparable across countries to allow detecting small regional differences and trends, and to draw reliable conclusions.

Therefore, three dedicated Thematic Centres for the atmospheric, ecosystem and oceanic domains, two Central Analytical Laboratories and a Carbon Portal were established in ICOS RI to ensure that highly standardised and coordinated data is recorded and disseminated.

Based on the atmospheric observations at Jungfraujoch, this paper will give a comprehensive overview of the benefits of the central facilities and commonly developped standardized operation procedures in order to achieve maximum homegeneitiy within the infrastructure. Moreover, it will be shown how synergies can be exploited when applying centralized data processing, quality control and provision of reference gases to a multinational monitoring network.

14. Remote Sensing of the Spheres + 15. High alpine remote sensing

Convenors 14: Stefan Wunderle, Mathias Kneubühler, Dominik Brunner, Alain Geiger +
Convenors 15: Yves Bühler, Christian Ginzler

Swiss Commission for Remote Sensing
Swiss Geodetic Commission

TALKS:

14.1 **Caduff R.**, Strozzi T., Wiesmann A., Wegmüller U.
Monitoring glacial, periglacial and landslide surface motion with Sentinel-1 over the Swiss Alps every 6 days.

14.2 **Dizerens C.**, Huesler F., Wunderle S.
Webcam-based snow cover monitoring in the Swiss Alps: methods and evaluation

14.3 **Kuhlmann G.**, Clément V., Fuhrer O., Marshall J., Meijer Y., Löscher A., Brunner D.
Atmospheric CO_2 simulations to study the capability of future imaging CO_2 satellites to observe emissions from cities and power plants

14.4 **Li C.**, Wulf H., Schaepman M.
The impacts of human activities and environmental variables on grassland canopy traits on the Qinghai-Tibetan Plateau

14.5 **Manconi A.**, Galletti M., Loew S.
Remote sensing of rock fall events in high alpine environments

14.6 **Mazzotti G.**, Bühler Y., Webster C., Schirmer M., Stoffel A., Jonas T.
Mapping snow depth distribution in forested terrain using Unmanned Aerial Vehicles and Structure-from-Motion

14.7 **Meier L.**, Jäger D., Steinacher R., Funk M.
Remote Monitoring of Glaciers and Landslides Using Interferometric Radar and High-Resolution Cameras

14.8 **Meyer U.**, Arnold D., Bentel K., Jean Y., Jäggi A.
GRACE satellite gravimetry to assess global hydrology and ice melt

14.9 **Paul F.**, Rastner P.
Recent glacier changes in western Greenland and glacier mapping challenges in mountain topography

14.10 **Payne D.**, Adler C., Krauer J., Sayre R.
The GEO-GNOME Mountain Explorer – visualizing and comparing commonly applied mountain definitions

14.11 **Schmidt S.**, Alewell C., Borrelli P., Meusburger K.
Seasonal dynamics and spatial patterns of the cover management factor for Swiss grassland

14.12 **Strozzi T.**, Caduff R., Barboux C., Delaloye R., Kääb A., Lambiel C.
Inventory and state of activity of rockglaciers and periglacial slope instabilities from satellite SAR interferometry (InSAR)

14.13 **Vivero S.**, Meyrat R., Delaloye R., Lambiel C.
UAV-photogrammetry for rock glacier monitoring: Examples from the Swiss Alps

14.14 **Wilgan K.**, Geiger A.
High-resolution troposphere models based on numerical weather prediction and Global Navigation Satellite Systems data

14.15 **Xie J.**, Kneubühler M., Garonna I., de Jong R., Schaepman M.E.
Influence of meteorological factors on the autumn land surface phenology in alpine grasslands

POSTERS:

P 14.1 **Vallat R.**, Mariéthoz G.
UAV-based thermal remote sensing to highlight groundwater inputs in rivers

P 14.2 **Bühler Y.**, Schneebeli M., Schwank M., Fierz C., Jonas T., Lehning M., Löwe H., Caduff R., Ginzler C.
High alpine remote sensing test site Davos: validating remote sensing technology in complex terrain

14.1

Monitoring glacial, periglacial and landslide surface motion with Sentinel-1 over the Swiss Alps every 6 days.

Rafael Caduff[1], Tazio Strozzi[1], Andreas Wiesmann[1] & Urs Wegmüller[1]

[1]Gamma Remote Sensing AG, Worbstrasse 225, CH-3073 Gümligen (caduff@gamma-rs.ch)

A large number of slopes in the Swiss Alps is in a state with active continuous movement. Different process types such as flow, glide, creep or slide can be identified. Using satellite based radar interferometry data, up to now more than 2000 active zones with movement rates ranging from several mm up to few meters per year could be identified. Most of the observed slope movements with velocities higher than 2-4 m/year are rock glaciers. A second common type is the process of slow moving continuous landslides. For both process types, there are strong needs to determine the current state by means of extension and surface velocity. Slope movement processes are seen as hazardous processes that can pose significant risk to life or result in damage to infrastructures. In addition, changes in rockglacier motion are believed to be the most indicative short- to medium-term response of rockglaciers to environmental changes and thus an indicator of mountain permafrost conditions in general. Different actively sensing SAR satellites are currently observing the earth surface and offer the possibility to quantify slope deformation by means of SAR interferometry (InSAR). The European Sentinel-1 mission became operational by the end of 2014 with the launch of the C-band satellite Sentinel-1A. In the meantime, the mission was extended with Sentinel-1B. Over the Swiss Alps Sentinel-1A/B acquisitions have been operationally acquired every 6 days since the beginning of 2017. Since interferometric radar observations are highly sensitive to changes in the state of the surface (e.g. decorrelation of the signal caused by vegetation and snow cover) and the absolute line-of-sight deformation in between two acquisitions, Sentinel-1A/B offers an unprecedented monitoring capability by means of a combination of spatial coverage, temporal resolution, data quality, timeliness of the data-availability and the open data philosophy. The short revisit time of 6 days dramatically reduces phase noise effects and decorrelation caused by slope movements drastically exceeding the wavelength of the system. An example of decorrelation of a fast rock-glacier after 12 days is given in Figure 1. The 6-day repeat cycle on the other hand still permits determining the LOS-velocity of the rock-glacier.

With the Sentinel-1 swath width of 250 km, the entire Swiss territory can be covered with two and three acquisitions in either ascending orbits (ENE-looking) or descending orbits (WNW-looking). In each of these 5 geometries the interferometric repeat cycle is 6 days. Data is available for download usually in less than 24 hours after acquisition, offering the possibility for relatively quick data availability after the satellite pass.

We are currently processing data at national level on supervised automated basis in near-real time. Since data handling with large datasets is difficult and time consuming, there is a strong need of down-scaling the processing to the local scale (e.g. watershed or mountainside) or even object scale (e.g. single landslide). With the use of an inventory of pre-existing slope movement objects, that was created by the interpretation of InSAR data, the automated data processing can be continued and refined for local area of interests. The inventory contains the spatial extent of the instability and a nearby coherent stable reference point for automated data-processing, including treatment of atmospheric disturbances to increase the quality of the observations.

We present numerous examples of current active slope instabilities over the Swiss Alps, including glacier and rock-glacier flow and continuous land- and rockslides. We will show to what level the 6-day acquisition cycle enhances the applicability of the technique even at times with frozen snow cover in the area of interest. Finally, we present the architecture and prerequisites necessary for an object based automated processing workflow.

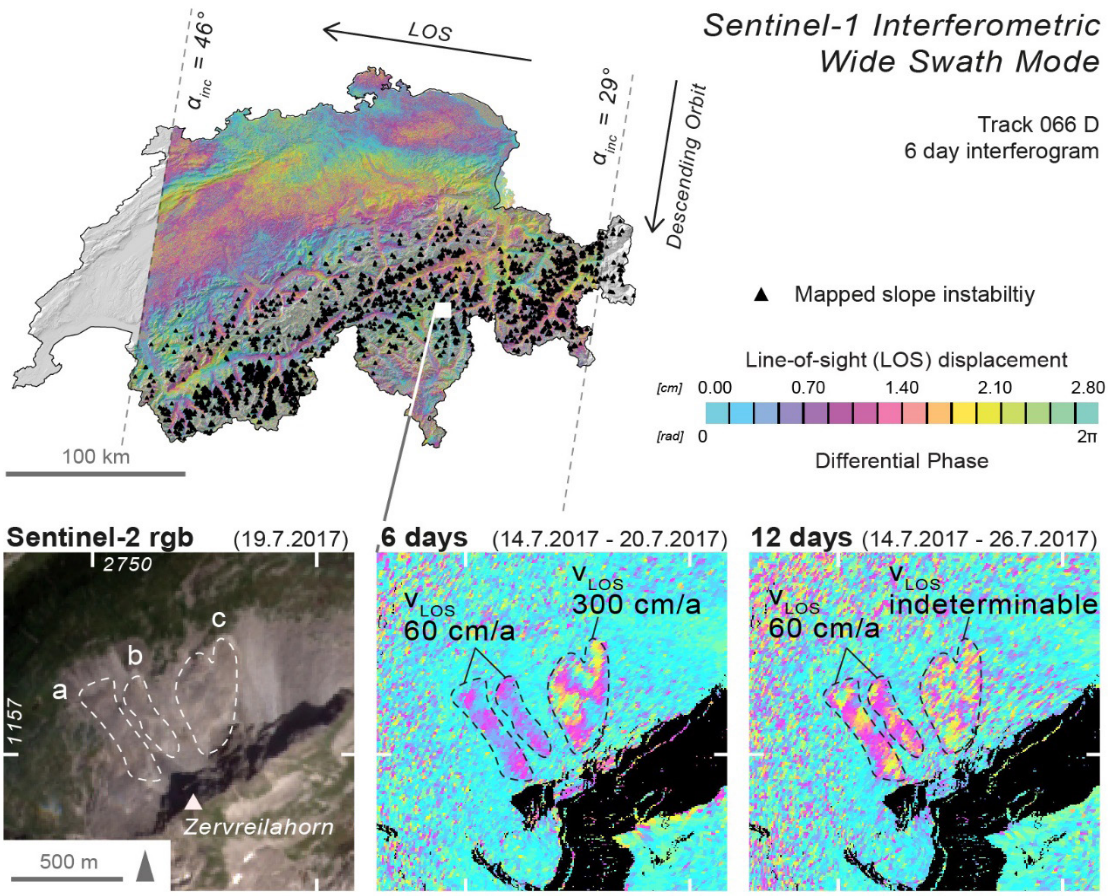

Figure 1. Full Sentinel-1 swath over Switzerland. The details of rockglaciers on the toe of the Zervreilahorn/GR demonstrate the value of 6 day repeat cycles: While in 6 days, the LOS-velocity (v_{LOS}) of area c) can be estimated as ~3 m/year, the same rate cannot be determined due to decorrelation after 12 days. Areas a) and b) are still coherent and v_{LOS} can be determined as ~60 cm/year. (S1 and S2 data source: Copernicus Sentinel data 2017)

14.2

Webcam-based snow cover monitoring in the Swiss Alps: methods and evaluation

Céline Dizerens[1], Fabia Hüsler[1,2] & Stefan Wunderle[1]

[1]Institute of Geography and Oeschger Centre for Climate Change Research, University of Bern, Hallerstrasse 12, CH-3012 Bern (celine.dizerens@giub.unibe.ch)
[2]Hydrology Division, Federal Office for the Environment FOEN, Papiermühlestrasse 172, CH-3063 Ittigen

Hundreds of publicly available outdoor webcams are located in the Swiss Alps. Most of these webcams are provided by mountain railway operators, restaurants, hotels, and private citizens and are located at elevations ranging from 800m to 3600m a.s.l.. Its images offer the possibility to observe snow cover variability on a high spatio-temporal resolution. Derived snow cover maps could not only serve as a reference for improved validation of satellite-based approaches but also offer unique potential for complementing satellite-derived snow retrieval in steep alpine terrain and under cloudy conditions. Our procedure allows to almost automatically derive snow cover maps from webcam images by using an estimate of the webcams position and a high-resolution digital elevation model (DEM). Mountain silhouettes are used to register the webcam images with the DEM and therewith to automatically resolve webcam parameters such as camera orientation, principal point, and field of view. Combined with automatic snow classification and image alignment using SIFT features, our procedure can be applied to arbitrary webcam images to generate snow cover maps with a minimum of effort. We discuss the assets and drawbacks of our procedure and evaluate the mapping accuracy using ground control points. Furthermore, we compare our webcam-based snow cover maps to the Sentinel-2 snow cover product provided by the Theia land data services centre and show some possible applications of a webcam-based snow cover dataset.

14.3

Atmospheric CO_2 simulations to study the capability of future imaging CO_2 satellites to observe emissions from cities and power plants

Gerrit Kuhlmann[1], Valentin Clément[2,3], Oliver Fuhrer[3], Julia Marshall[4], Yasjka Meijer[5], Armin Löscher[5], and Dominik Brunner[1]

[1]*Empa, Swiss Federal Laboratories for Materials Science and Technology, Dübendorf, Switzerland (gerrit.kuhlmann@empa.ch)*
[2]*Center for Climate Systems Modelling (C2SM), ETH Zürich, Zürich, Switzerland*
[3]*Federal Office of Meteorology and Climatology, MeteoSwiss, Zürich, Switzerland*
[4]*Max Planck Institute for Biogeochemistry, Jena, Germany*
[5]*ESA ESTEC, Noordwijk, the Netherlands*

Under the Paris climate agreement, the signatory countries have set ambitious goals to reduce CO_2 emissions and limit global warming to below 2°C. The ability to implement long-term policies and manage them effectively will require consistent, reliable, and timely information on CO_2 emissions [1]. The majority of these emissions are concentrated on a tiny fraction of the globe, notably on cities and power plants. Cities, for example, have been estimated to contribute roughly two thirds of global anthropogenic CO_2 emissions [2]. A growing number of cities therefore acknowledges both the responsibility for, and the vulnerability to, climate change as indicated by several international initiatives of city governments [3,4]. Cities often take more aggressive mitigation measures to reduce CO_2 emissions compared to the country average, but are lacking reliable means to monitor the success of their policies. The European Space Agency (ESA) and the European Commission are therefore proposing a constellation of CO_2 satellites to support the quantification of anthropogenic and natural CO_2 fluxes and to assist greenhouse gas mitigation policies at the national, city and facility level. The satellites are envisioned as an essential component of a CO_2 observation system to be established under Europe's Earth observation programme Copernicus.

Previous studies have demonstrated that an imaging CO_2 satellite with sufficient precision will have the potential to quantify emissions from strong point sources such as cities and power plants during single overpasses [5].
Here, we present the results of a high-resolution model simulation study conducted on behalf of ESA, which aims to investigate the capabilities of such a CO_2 satellite mission, to analyze the benefit of auxiliary measurements of anthropogenic tracers such as NO_2 and CO, and to specify the requirements in terms of observation strategy and measurement accuracy. For this purpose, we have set up a highly optimized version of the COSMO numerical weather prediction model [6] extended for the simulation of CO_2, CO and NO_x for a domain centered over the city of Berlin and covering a large number of power plants in Germany and neighbouring countries. The simulations were conducted at a horizontal resolution of 1 km x 1 km and sampled along the tracks of a future satellite mission expected to have a pixel size of up to 2 km x 2 km and a swath width of approximately 250 km. Different levels of unstructured and structured noise were applied to the simulated satellite observations in order to investigate the capability of observing the CO_2 plumes of Berlin and individual large power plants. In addition, several different scenarios for auxiliary measurements of NO_2 and CO on either the same or a different satellite platform (with different overpass time) were tested for their ability to support the detection of the plumes and the quantification of the CO_2 emissions.

The results emphasize the need for both high measurement precision and high observation frequency, because the detectability of the plumes is highly dependent on the meteorological situation and clouds frequently obscure the view.

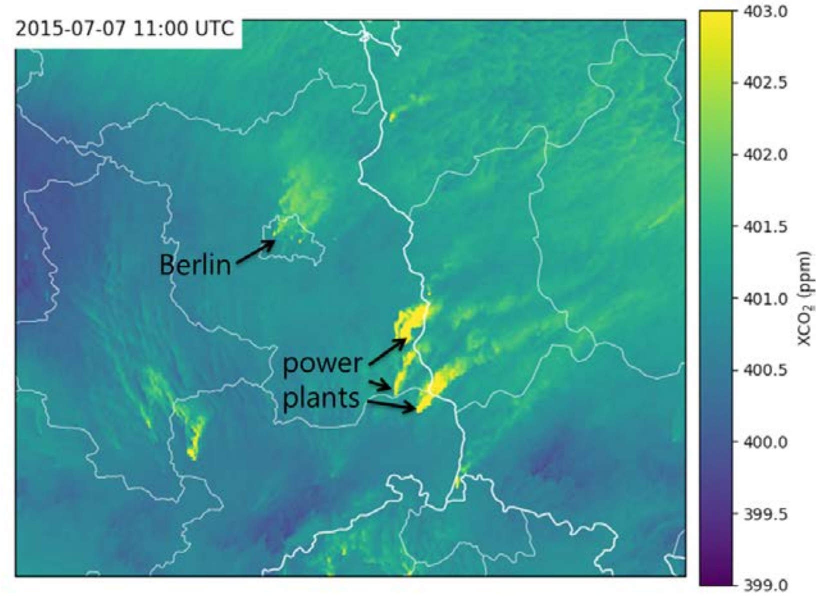

Figure 1: Column averaged dry air mixing ratios of CO_2 simulated for 7 July 2015, 11 UTC highlighting the plumes of the city of Berlin and several power plants.

REFERENCES

[1] Ciais, P., Crisp, D., Gon, H. v. d., Engelen, R., Heimann, M., Janssens-Maenhout, G., Rayner, P., and Scholze, M.: Towards a European Operational Observing System to Monitor Fossil CO2 emissions - Final Report from the expert group. European Commission, Copernicus Climate Change Service, 2015.

[2] UN-HABITAT, Cities and Climate Change: Global Report on Human Settlements, 2011. Global Report on Human Settlements. 2011: Earthscan. 300.

[3] http://www.c40.org

[4] http://www.covenantofmayors.eu

[5] Bovensmann, H., et al., A remote sensing technique for global monitoring of power plant CO2 emissions from space and related applications. Atmos. Meas. Tech., 2010. 3(4): p. 781-811.

[6] Fuhrer, O., Osuna, C., Lapillonne, X., Gysi, T., Cumming, B., Bianco, M., Arteaga, A., & Schulthess, T.: Towards a performance portable, architecture agnostic implementation strategy for weather and climate models. Supercomputing frontiers and innovations, 1(1), 5-62, doi:10.14529/jsfi140103, 2014.

14.4

The impacts of human activities and environmental variables on grassland canopy traits on the Qinghai-Tibetan Plateau

Chengxiu Li[1], Hendrik Wulf[1], Michael Schaepman[1]

[1] *Remote Sensing Laboratories, University of Zurich, Winterthurerstrasse 190, CH-8057 Zurich, Switzerland (chengxiu.li@geo.uzh.ch)*

In order to understand an ecosystem's response to global change, the relationships between plant traits, environmental variables and human factors need to be identified. This understanding is of particular importance for the Qinghai-Tibetan Plateau, where the ecosystem is highly sensitive to global changes. In this study, we analyze the impacts human activities (grazing intensity, roads and residential areas) and environmental variables (climatic variables, elevation and soil properties) on the spatial distribution of three selected canopy traits: (1) chlorophyll content, (2) specific leaf area and (3) leaf dry matter content on the Qinghai-Tibetan Plateau. We derive canopy traits based on empirical models that combine satellite data and field measurements. We perform a Multiple Linear Regression of the predicted canopy traits against the selected explanatory variables based on their relative importance. Our preliminary results indicate that precipitation, soil PH, altitude and soil nitrogen availability could explain 67% of the spatial variation in canopy traits. Canopy chlorophyll content and specific leaf area decrease towards roads and residential areas within 2 kilometers distance, indicating that human activities impact those canopy traits within certain surroundings. Such findings are important to better understand the impact of human activities and climate change on ecosystem degradation in the Qinghai-Tibetan Plateau.

14.5

Remote sensing of rock fall events in high alpine environments

Andrea Manconi[1], Maud Galletti & Simon Loew

[1]Swiss Federal Institute of Technology, Department of Earth Sciences, Zurich, Switzerland (andrea.manconi@erdw.ethz.ch)

Remote sensing is referred to as the capability of retrieving information of an object without physical contact. This definition is generally used to describe methodologies leveraging active and/or passive electromagnetic radiations, and relying on space borne, airborne, and/or terrestrial sensors (optical, multispectral, LiDAR, radar, etc.). However, seismic sensors may fall also into the broader definition of remote sensing, as they are capable of detecting and accurately measure the ground shacking caused by events located hundreds of kilometers away, such as earthquakes and other mass wasting phenomena (rockslides, rock falls, debris flows, avalanches).

Several authors have recently shown how the analysis of seismic signals generated from rock falls can be very useful to investigate their physical properties (Manconi et al., 2016 and reference therein). The goal of this study is to test how low-cost seismic sensors can be used to identify and monitor rock fall activity in alpine environments, when the use of classical remote sensing methods might be hindered because of logistic problems and/or severe weather conditions. Our area of study is a large instability adjacent to the Great Aletsch glacier in the Swiss Alps, i.e. the Moosfluh slope, which is undergoing an acceleration phase since the late summer 2016. During the acceleration phases, rock fall activity also increases. Due to the limited access to the site, rock falls are identified and investigated by analyzing the data acquired with a local seismic network composed of 3 Raspberry Shake (RS) seismometers (see figure 1). RS are a low-cost, all-in-one plug-and-go solution developed by OSOP S.A., which integrate vertical velocity sensor (4.5 Hz Racotech RGI-20DX), digitizer, and micro-computer in a single box (100x120x50 mm, 0.35 kg). Installation of the RS was achieved by beginning of July 2017, when we expected to start recording a further increase of rock fall activity. Seismic data are currently collected and analyzed to identify and locate rock fall phenomena. Moreover, a webcam was installed on the opposite side of the Moosfluh slope, acquiring images every 10 minutes to map the surface deformation and to validate the occurrence of slope failure events.

Our preliminary results show that the data acquired from RS sensors allow to well discriminate between local events (i.e., rockfall phenomena) and distant events (mainly regional earthquakes and teleseisms). In particular, we show a number of examples where seismic data can be the only viable approach to retrieve information on rock fall activity in an alpine environement .

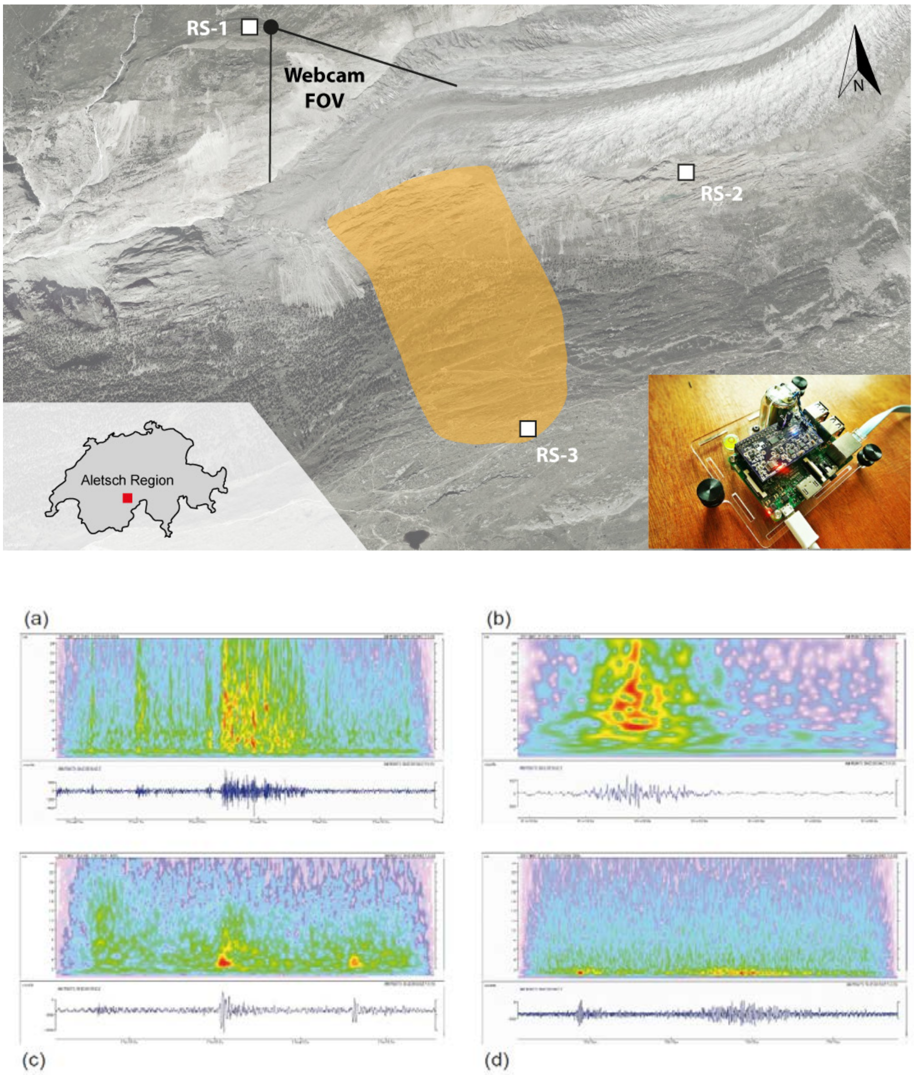

Figure 1. (top panel) Overview of the area of investigation, the Moosfluh rock slope instability, in the Aletsch region (Swiss Alps). White squares indicate the position of the Raspberry Shake sensors (RS 1-3, see picture in the inset on the bottom right, www.raspberryshake.org). (bottom panel) Examples of seismic signals measured by the RS sensors. (a) seismic signal recorded by the raspberry shake, but not visible changes are recognized in the optical imagery; (b) rockfall activity confirmed by the optical imagery; (c) Seismic signal associated to a Magnitude ML= 2 earthquake occurred in Montreaux, Switzerland, (about 80 km distance) on 29/05/2017; (d) Seismic signal associated to a Magnitude Mw= 4.5 earthquake occurred in Poland (about 800 km distance) on 31/05/2017.

REFERENCES

Manconi, A., Picozzi, M., Coviello, V., De Santis, F., Elia, L., 2016: Real-time detection, location, and characterization of rockslides using broadband regional seismic networks. Geophys. Res. Lett. 43, 2016GL069572. doi:10.1002/2016GL069572.

14.6

Mapping snow depth distribution in forested terrain using Unmanned Aerial Vehicles and Structure-from-Motion

Giulia Mazzotti[1 2], Yves Bühler[1], Clare Webster[1], Michael Schirmer[1], Andreas Stoffel[1], Tobias Jonas[1]

[1] *WSL Institute for Snow and Avalanche Research SLF, Davos Dorf, Switzerland*
[2] *Swiss Federal Institute of Technology ETHZ, Zurich, Switzerland*

In forested areas, snow distribution is strongly affected by the spatial layout of canopy elements and thus exhibits strong spatial heterogeneity compared to adjacent open sites. Given the wide extent of forested areas that feature seasonal snow cover, forest snow dynamics strongly impact on the hydrological cycle from the local to the global scale. Measurement of snow depths in forests is currently limited to in-situ measurements, which are time-intensive and have limited spatial coverage, or airborne LiDAR acquisition, which is expensive and may deteriorate in denser forests. Limited knowledge of the snow distribution has hampered our abilities to accurately quantify forest snow water resources.

We present the application of unmanned aerial vehicles in combination with structure-from-motion (SfM) methods to map snow depth distribution in forests.
Two separate flights were carried out 10 days apart across a heterogeneous forested area of 900x500m. Corresponding snow depth maps were computed by subtracting DTM data from the surface elevation model derived by SfM. Manual measurements collected following each flight were used to validate the snow maps. In semi-closed forest, small-scale spatial variability of snow depth typical to forested areas was well visible. Differential snow depth maps revealed distinct spatial patterns in local ablation rates particularly around exposed trees. While these findings are promising, resolving snow depths below trees or in very narrow gaps remains challenging.

This new application of SfM demonstrates an efficient method which could be extended to more frequent observations of the forest snow cover, surveys with wider areal coverage, or in unaccessible terrain. It constitutes an encouraging tool to explore snow patterns in forests and enhance our understanding of spatial variability of snow accumulation and depletion rates; And it could contribute to improving estimates of hydrological resources stored in the forest snow pack if coupled to in-situ measurements of snow water equivalent.

14.7

Remote Monitoring of Glaciers and Landslides Using Interferometric Radar and High-Resolution Cameras

Lorenz Meier[1], Dominik Jäger[1], Richard Steinacher[1], Martin Funk[2]

[1] *GEOPRAEVENT AG, Technoparkstrasse 1, CH-8005 Zürich (lorenz.meier@geopraevent.ch)*
[2] *ETH Zurich, Laboratory of Hydraulics, Hydrology and Glaciology VAW, CH-8093 Zurich*

Monitoring surface deformations is a common challenge when assessing natural hazards in the high alpine environment like glacier- or rock-instabilities or landslides. Different technologies are available and the selection depends on multiple requirements, among them:

- Which measurement precision is necessary?
- Are absolute deformation values necessary or is the relative deformation sufficient?
- Is a monitoring based on single points sufficient, or should it be area-wide?
- Are one, two or three-dimensional measurements required?
- Are measurements needed during times of bad weather or at night (data availibility)?

A large part of the glacierized northwest face of Weissmies in the Saas Valley (Switzerland) recently became unstable. The likely causes of this instability are climate-induced glacier thinning of the supporting Triftgletscher and a progressive warming from freezing to melting temperatures at the ice-bed interface.

Starting in October 2014, a ground-based interferometric radar system was installed on the roof of the cable-car station Hohsaas at 3’142 m.a.s.l. Until April 2017, the radar permanently scanned the face and surface velocities with high precision and availability could be obtained. Several small size ice falls (< 20’000 m3) could be predicted in advance with a few days warning time. In February 2017, we additionally installed a high-resolution camera with 42 megapixels to monitor this area. Every day, an image processing algorithm automatically determined the surface deformations based on a correlation analysis. The goal was to provide a more cost-effective monitoring solution. Both instruments were operated simultaneously during three months.

We compared the deformations obtained with both systems. While the radar data allows a prediction of small ice falls even during no visibility conditions (bad weather), the camera only provides data during the day and good visibility conditions. The image processing technique is sensitive to deformations of a few centimeters between two acquisitions. It relies on the existence of persistent optical surface features that vary with for example snow fall events. For the Weissmies monitoring during the summer months, the camera performance turned out to be a sufficient and cost-effective monitoring solution.

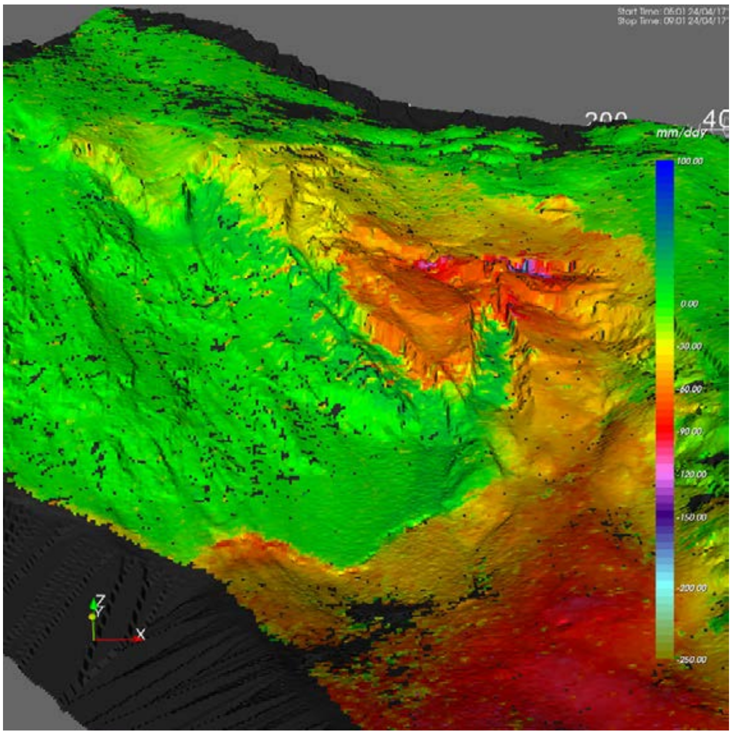

Figure 1. Surface deformations measured by the interferometric radar (line-of-sight). Units are mm per day.

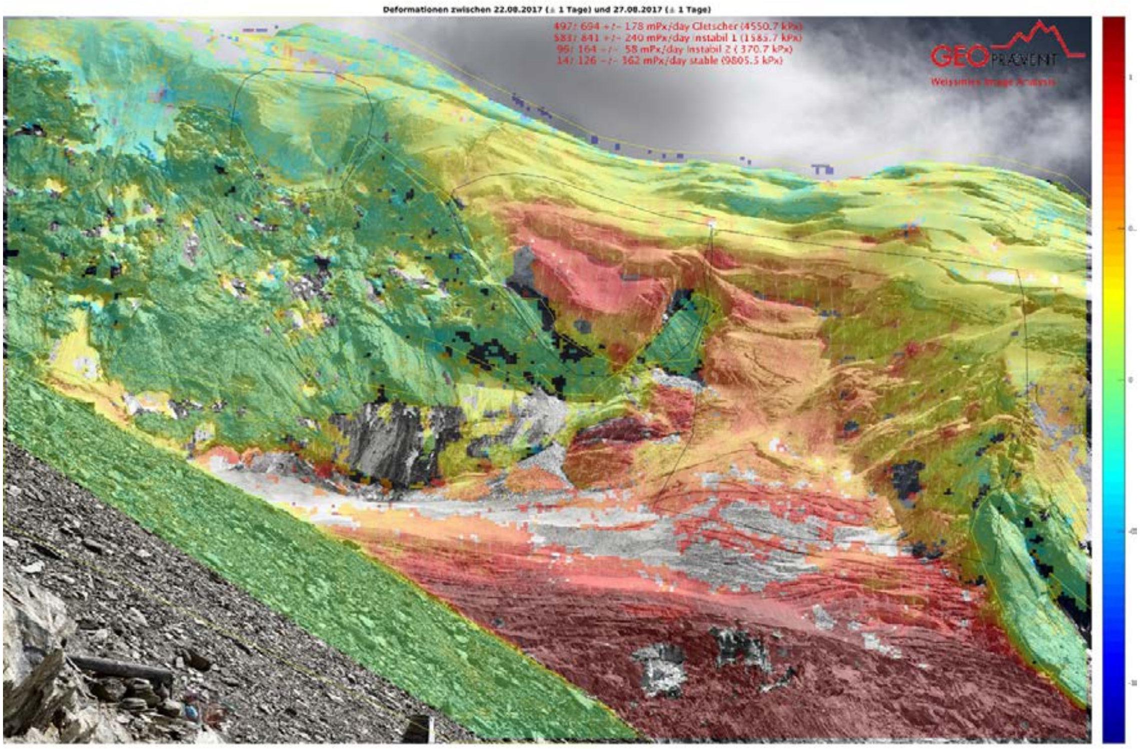

Figure 2. Surface deformations measured by the high-resolution camera (cross line-of-sight). Units are pixels per day.

REFERENCES

Lorenz Meier, Mylène Jacquemart, Bernhard Blattmann, Sam Wyssen, Bernhard Arnold, Martin Funk 2016: Radar-based Warning and Alarm Systems for Alpine Mass Movements. Conference Proceedings INTERPRAEVENT 2016

14.8
GRACE satellite gravimetry to assess global hydrology and ice melt

Ulrich Meyer[1], Daniel Arnold[1], Katrin Bentel[1], Yoomin Jean[1] & Adrian Jäggi[1]

[1]*Astonomisches Institut, University of Bern, Sidlerstrasse 5, CH-3012 Bern (ulrich.meyer@unibe.ch)*

The satellites of the GRACE and the upcoming GRACE Follow-On missions are dedicated to observing the Earth's gravity field and its temporal variations. These variations are related to global mass transport caused by the water cycle, polar and mountain ice mass loss, changes in ocean surface currents and sea level rise.

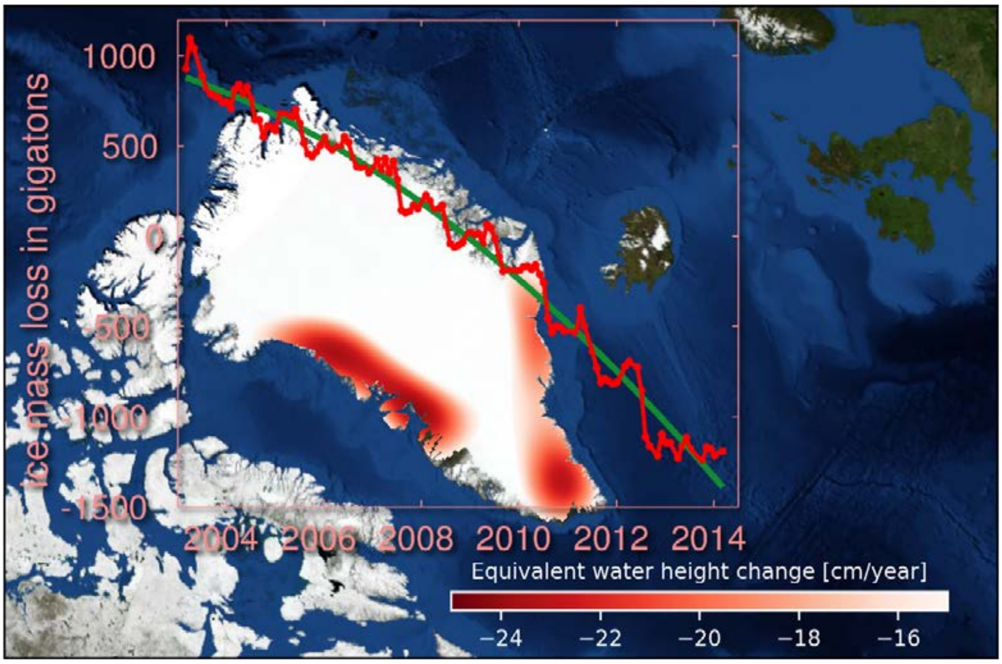

Figure 1. Mass loss (red) at the coasts of Greenland indicates ice melt associated with climate change. It amounts to 200 billion tons per year.

AIUB is leading the Horizon 2020 EGSIEM project, a European initiative to provide the best satellite derived gravity field models with a short latency for applications in Earth and environmental sciences to demonstrate their value for flood and drought monitoring services. In the frame of EGSIEM three services are beeing installed: 1) a scientific combination service, 2) a near real-time / regional service and 3) a hydrological / early warning service.

We here focus on the scientific combination service, where monthly gravity field models of different analysis centers (AC) are combined. All ACs perform independent analyses but apply consistent standards. A combination thus enhances the quality, robustness, and reliability of the monthly gravity models. The products are combined on normal equation level to correctly take into account all correlations between model parameters and the orbit parameters of the GRACE satellites. The resulting combined monthly gravity models are provided in spherical harmonic representation as well as user-friendly global grids of equivalent water hight, pre-filtered and tailored to the needs of hydrological or oceanographic applications.

The EGSIEM scientific combination service is in transition to become COST-G, a combination center under the umbrella of the International Gravity Field Service (IGFS) of the International Association of Geodesy (IAG). It is envisaged to provide a consistently reprocessed and combined time series of monthly gravity fields spanning the entire GRACE mission and, in the future, also its successor, GRACE Follow-On.

REFERENCES

Meyer, U., Jäggi, A. & Beutler, G. 2012: Monthly gravity field solutions based on GRACE observations generated with the Celestial Mechanics Approach, Earth and Planetary Science Letters, 345, 72-80.

Meyer, U., Jäggi, A., Jean, Y. & Beutler, G. 2016: AIUB-RL02: an improved time-series of monthly gravity fields from GRACE data, Geophysical Journal International, 205, 218-233.

Jean, Y., Meyer, U. & Jäggi, A. 2017: Combination of GRACE monthly gravity field solutions from different processing strategies, submitted to Journal of Geodesy.

14.9

Recent glacier changes in western Greenland and glacier mapping challenges in mountain topography

Frank Paul[1], Philipp Rastner[1]

[1] Department of Geography, University of Zurich, Winterthurerstr. 190, CH-8057 Zurich (frank.paul@geo.uzh.ch)

The region to the NW of Jacobshavn Isbrae (e.g. Disko Island, Nuussuaq and Svartenhuk Peninsula) in western central Greenland is hosting >1000 glaciers and ice caps that receive comparably little attention. A previous study presented a glacier inventory for 2001 derived from Landsat ETM+ scenes and area changes since their assumed LIA maximum extent as mapped from trim-lines (Citterio et al. 2009). The region is well known for its high number of surge-type glaciers of which the largest one (Kuannersuit) had a massive surge in 1995/96 with a frontal advance of more than 10 km (Yde and Knudsen 2005). This has to be considered when interpreting length, area or volume changes in climatic terms. With the now available image data from 1985 (Landsat TM and the new orthomap) and 2015/16 (Landsat 8 OLI and Sentinel 2 MSI) it is possible to study recent glacier fluctuations in detail. Additionally, high-quality DEMs from 1985 (aerodem) and around 2012 (ArcticDEM, TanDEM-X) that are now available allow calculation of volume changes over a multi-decadal time period.

In this study we present the new glacier inventory for 2016 derived from three Landsat OLI scenes, a comparsion of the available DEMs (incl. GDEM and GIMP) and elevation changes since 1985, and how spatial resolution and time of image acquisition impacts on the visibility of glacier extents in steep mountain topography casting deep shadows in early autumn. Glaciers were automatically mapped with the band ratio method from three Landsat OLI scenes with a subsequent manual correction for misclassified debris cover, rock glaciers, water, shadow, seasonal snow, sea ice and icebergs. Hill-shades and subtraction of the DEMs (after co-registartion) revealed data voids, interpolation artefacts and outliers that restricted the analysis of elevation changes to selected glaciers. We used the new TanDEM-X DEM to derive new drainage divides and topographic attributes for all glaciers.

A first analysis reveals a general glacier retreat and down-wasting with several local exceptions. In particular on Disko Island glaciers have advanced or surged after 1985, requiring to remove them from the statistical analysis. A strong area decrease is observed for ice caps at higher elevations whereas volume loss (or gain) is strongest for glaciers that have surged. A general trend of increasingly higher snow lines at the end of the ablation period can be observed from 1985 to 2016. Despite recent conditions of mass loss, some small glaciers (<5 km^2) on Disko Island have started advancing or even surging after 2012.

REFERENCES

Citterio, M., Paul, F., Ahlstrøm, A.P., Jepsen, H.F. & Weidick, A. 2009: Remote sensing of glacier change in West Greenland: accounting for the occurrence of surge-type glaciers. Annals of Glaciology, 50 (53), 70-80.

Yde, J.C. & Knudsen, N.T. 2005: Glaciological features in the initial quiescent phase of Kuannersuit Glacier, Greenland. Geografiska Annaler, 87A, 473-485.

14.10

The GEO-GNOME Mountain Explorer - visualizing and comparing commonly applied mountain definitions

Davnah Payne[1], Carolina Adler[2], Jürg Krauer[3] & Roger Sayre[4]

[1] *Global Mountain Biodiversity Assessment, University of Bern, Institute of Plant Sciences, Altenbergrain 21, CH-3013 Bern (davnah.payne@unibe.ch)*
[2] *Mountain Research Initiative, University of Bern, Insitute of Geography, Hallerstrasse 12, CH-3012 Bern*
[3] *Center for Development and Environment, University of Bern, Hallerstrasse 10, CH-3012 Bern*
[4] *United States Geological Survey, 12201 Sunrise Valley Drive, Reston, VA 20192, United States of America*

Mountain ecosystems are globally distributed environments that provide significant societal benefits, yet their ability to provide goods and services to both highland and lowland residents is threatened by changes in climate and land use, environmental pollution, large-scale political and socio-economic transformations, unsustainable management of natural resources and serious gaps in the understanding of mountain systems.

Improving our understanding of mountain regions and sharpenening our future ability to identify context-specific opportunities for sustainable development requires an accurate definition of the world's mountains. How to define mountains has been a topic of controversy for many years, and various definitions using different benchmarks have been proposed for different contexts of use (e.g., biogeographical research versus hydrology or climatology). To date, the three most commonly applied mountain definitions are those of Kapos et al. (2000), Körner et al. (2011), and Karagulle et al. (2017). The definition by Kapos constrains mountains to parameters that combine elevation and ruggedness. The definition by Körner and colleagues, used for the first inventory of the world's mountains for biogeographic applications (Körner et al. 2017), constrains mountains by ruggedness only, irrespective of elevation. This appears to be the most meaninfgul approach from the biodiversity and biogeography perspective. In the work by Karagulle et al. (2017), mountains are one of the many different ecological land units (ELUs) identified while developing a high-resolution and data-derived global ecosystem map. These diverse means for the characterisation and representation of mountains result in fundamental differences in statistics for attributes such as land area size and population, most notably. For example, the approach of Kapos et al. arrives at twice the global mountain area and much higher human population numbers than the one by Körner et al. (Körner et al. 2017). These differences profoundly impact research results and the conclusions drawn on the state and prospects of mountain socio-ecological systems, ultimately affecting decisions on policy and investment.

To support the mountain research and policy community with the layers of information required for a pertinent choice of mountain definition, the Group on Earth Observations Initiative – Global Network for Observations and Information in Mountain Environments (GEO-GNOME) has initiated the creation of a web-based application for the visualization and comparision of existing mountain definitions. The Global Mountain Explorer (GME), developed by the U.S. Geological Survey (USGS), in partnership with Esri, the Center for Development and Environment of the University of Bern (CDE), the Global Mountain Biodiversity Assessment (GMBA), and the Mountain Research Initiative (MRI) allows for visualization and query of all definitions either separately or in pairwise comparisons. The resources are accessible as either mountains only, or as mountain classes (Kapos et al., Karagulle et al.) and bioclimatic belts (Körner et al.). Pan, zoom, and query functionality are included, and a query anywhere on the map returns the binary values for all three definitions in a pop-up query results box.

The GME is the first of a series of initiatives led by GEO-GNOME to address the paucity of observations of- and information on mountains, improve our understanding of mountain regions and sharpen our future ability to provide policy and investment relevant advice, and to create a capacity to combine data and information to meet emerging, often as-yet unarticulated policy needs.

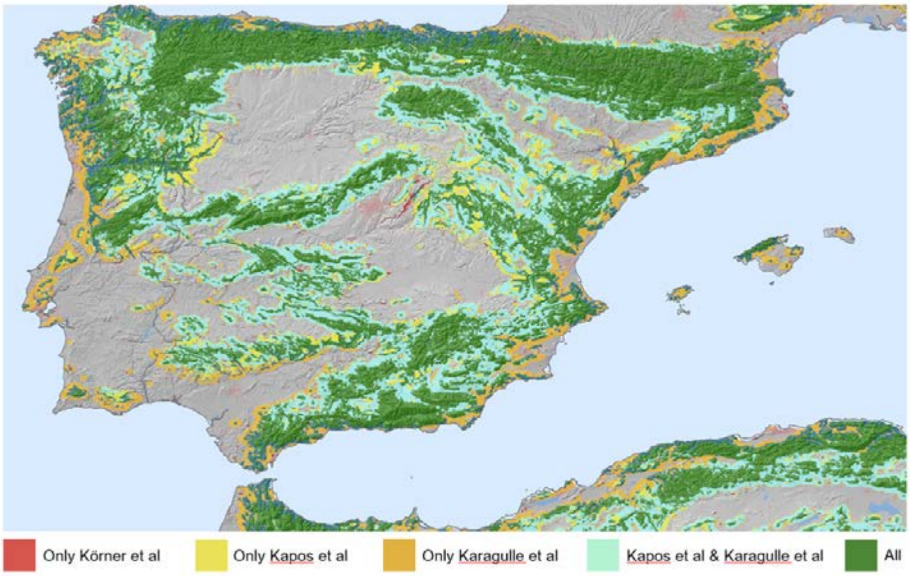

Figure 1. Overlaps and divergences between the three mountain definitions

REFERENCES

Kapos, V., Rhind, J., Edwards, M., Price, M.F. & Ravilious, C. 2000: Developing a map of the world's mountain forests. In: Price MF, Butt N (eds) Forests in sustainable mountain development: a report for 2000. CAB International, Wallingford, pp 4–9.

Körner, C., Paulsen, J. & Spehn, E.M. 2011: A definition of mountains and their bioclimatic belts for global comparisons of biodiversity data. Alpine Botany 121, 73-78.

Körner, C., Jetz, W., Paulsen, J., Payne, D., Rudmann-Maurer, K. & Sephn, E.M. 2017: A global inventory of the worlds mountains for bio-geographic applications. Alpine Botany, 127, 1-15.

Karagulle, D., Frye, C., Sayre, R., Breyer, S., Aniello, P., Vaughan, R. & Wright, D. 2017. Modeling global Hammond landform regions from 250-m elevation data. Transactions in GIS.

14.11

Seasonal dynamics and spatial patterns of the cover management factor for Swiss grassland

Simon Schmidt, Christine Alewell, Pasquale Borrelli & Katrin Meusburger

Environmental Geosciences, University of Basel, Bernoullistrasse 30, 4056 Basel, Switzerland (si.schmidt@unibas.ch)

According to the revised soil erosion equation (RUSLE), soil erosion is controlled by the factors rainfall erosivity R, soil erodibility K, cover management C, slope length and steepness LS, and support practices P. The C-factor represents the effect of cropping and management practices on erosion rates by water (Renard et al. 1997) and is the factor most easily to alter by a change of management and therefore a parameter of high relevance for soil erosion control. Furthermore, it has the highest amplitude of variation among all the RUSLE factors (Zhang et al. 2011). The C-factor of grassland is rather controlled by surface cover then by grassland type and crop rotation like it is common for agricultural land. To derive a Swiss national C-factor map of grassland, we used remote sensing techniques to map fractional vegetation cover (FCV) which enabled both, an assessment of the spatial and temporal variability.

The orthophoto Swissimage FCIR with a high spatial resolution of 0.25 m and the satellite derived product FCover300m with a high temporal resolution (10-day) were used for fractional vegetation cover mapping.
Swissimage FCIR was undergone a linear spectral unmixing (LSU) to estimate the fractional abundance of green vegetation and bedrock/soils with a very high spatial resolution. The FCover300m datasets were averaged over three years to a time-series of 36 mean long-term fractions of green vegetation. The resulting temporal FVC is used for normalizing the spatial results to the day of the year 181 (30th of June) since tiles of Swissimage FCIR were recorded at different periods of the year. The normalized abundances of vegetation are transformed to C-factors according to USDA (1977).

The spatio-temporal maps of the C-factor of Swiss grassland (Fig. 1) show distinct dynamics with very high C-factors in alpine areas in the winter and decreasing values from spring according to increasing vegetation coverage to a maximum soil cover in July/August. Spatially, the alpine grassland indicates a temporal delay in decreasing C-factors in summer with a shorter period of low C-factors (high vegetation cover) in elevated alpine grasslands. In combination with the spatio-temporal dynamics of the Swiss R-factor (Schmidt et al. 2016), the months June and September are the most erosion prone regions with high rainfall erosivity and low vegetation cover (high C-factor) in the alpine grasslands. Lowland grasslands have a higher FCV earlier in the summer season which better protects soils at times of high rainfall erosivity.

A combination of the monthly factors R and C enables a dynamic soil erosion risk assessment which simultaneously allows the identification of susceptible seasons and regions. Based on the results, agronomists can introduce selective erosion control measures for erosion prone regions and seasons and thereby reduce the direct costs of erosion and mitigation measures.

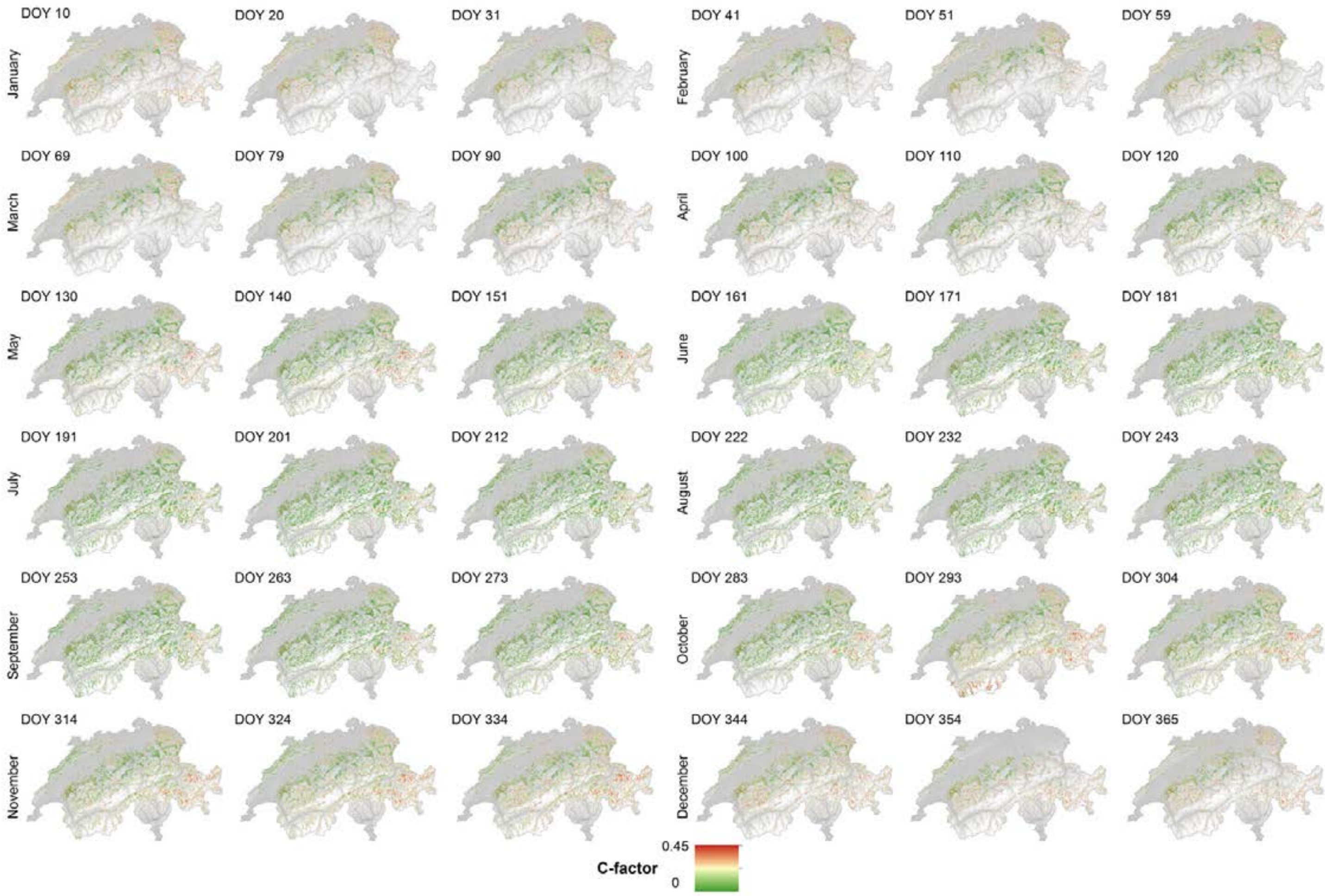

Figure 1. Spatio-temporal dynamics of the C-factor on Swiss grasslands (DOY day of the year; spatial resolution 100 m)

REFERENCES

Renard, K. G.; Foster, G.; Weesies, G.; McCool, D. K.; Yoder, D. C. 1997: Prediction Soil Erosion by Water: A Guide to Conservation Planning with the Revised Universal Soil Loss Equation (RUSLE). Agriculture Handbook (703).

Schmidt, S.; Alewell, C.; Panagos, P.; Meusburger, K. 2016: Regionalization of monthly rainfall erosivity patterns in Switzerland. Hydrol. Earth Syst. Sci. 20 (10), 4359–4373.

USDA US Department of Agriculture S.C.S. 1977: Procedure for computing sheet and rill erosion on project areas. Technical Release (51).

Zhang, W.; Zhang, Z.; Liu, F.; Qiao, Z.; Hu, S. 2011: Estimation of the USLE cover and management factor C using satellite remote sensing. A review. 19th International Conference on Geoinformatics. Shanghai, China, 24.06.-26.06.2011, 1–5.

14.12
Inventory and state of activity of rockglaciers and periglacial slope instabilities from satellite SAR interferometry (InSAR)

Tazio Strozzi[1], Rafael Caduff[1], Chloé Barboux[2], Reynald Delaloye[2], Andreas Kääb[3] & Christophe Lambiel[4]

[1] *Gamma Remote Sensing, Gümligen (BE), Switzerland (strozzi@gamma-rs.ch)*
[2] *Department of Geosciences - Geography, University of Fribourg, Switzerland*
[3] *Department of Geosciences, University of Oslo, Norway*
[4] *Institute of Earth Surface Dynamics, University of Lausanne, Switzerland*

Past investigations conducted in the Swiss Alps demonstrated that the visual analysis of satellite differential Synthetic Aperture Radar (SAR) interferograms can be employed for the estimation of the surface deformation rates of rockglaciers and other periglacial slope instabilities (Strozzi et al., 2004; Barboux et al., 2014; Barboux et al., 2015). Within the GlobPermafrost project funded by the European Space Agency (ESA) we are building up a worldwide long-term monitoring network of active rockglacier motion investigated using remote sensing techniques. Five sites in the European Alps, the Brooks Range of Alaska, the Andes in South America and the Tien Shan and Karakoram regions in the Himalaya Range are analysed through a uniform set of data and methods. Our analysis is divided in two major steps. InSAR data are first considered as a base for an inventory of periglacial slope instabilities, including rock glaciers. Deformation rates are expressed using different classes (e.g. 0-2 cm/a, 2-10 cm/a, 10-50 cm/a, 50-100 cm/a, > 100 cm/a). Classification of the process types and validation of the spatial extent is done using optical imagery. In a second step, matching of repeat optical data and SAR interferometry are considered to quantify the rate of surface movement and the relative changes over time of a few significant active rockglaciers. Changes in rockglacier motion are indeed believed to be the most indicative short- to medium-term response of rockglaciers to environmental changes and thus an indicator of mountain permafrost conditions in general.

In this contribution, we focus on the potential of recent high spatial and temporal resolution SAR data for the analysis of periglacial processes in mountain environments with special attention to the Arolla Valley (Valais), an area which we are actively studying since many years using SAR interferometry along with other in-situ and remote sensing methods. Our area of interest encompasses active rockglaciers with deformation rates ranging typically between 0.1 and 2.0 m/yr, a recently destabilized (or “surging”) rockglacier with rate of motion above 5.0 m/yr, and many other much more slowly moving landforms in which permafrost is likely to occur. We first applied InSAR with the high-resolution satellite radar data (spatial resolution on the order of 20 m) of the ERS-1/2 SAR and JERS-1 sensors during the 1990’s with acquisition time intervals from 1 day to several years to compile a first inventory of slope movements. Results from this inventory were then considered in the set-up of in-situ monitoring sites, showing increased velocity of rock glaciers in recent years. In recent years, new SAR sensors, advanced processing techniques, and very-high resolution Digital Elevation Models (DEM) to more accurately compensate for the topography related phase have become available recently. Very-high resolution SAR data with spatial resolution on the order of 3 m from the TerraSAR-X and Cosmo-SkyMed missions were for instance considered to better spatially characterize the rate of movement of the inventoried landforms. In addition, nowadays the Sentinel-1 mission represents the newest approach to SAR mission design with acquisitions regularly available over nearly all mountainous areas worldwide every 6 to 24 days allowing to better characterize changes of surface motion over time (Caduff et al., 2017). Apart from SAR interferograms, more sophisticated processing approaches, like Persistent Scatterer Interferometry (PSI), Short Baseline Interferometry (SBAS) or Offset-Tracking (OT) (Strozzi et al., 2002; Barboux et al., 2015), are used to quantitatively detect points moving with velocities below a few cm/yr, below several dm/yr and more than 1 m/yr, respectively, with different levels of accuracy and resolution. Finally, besides satellite sensors, a terrestrial radar instrument was used to complement satellite SAR data in time and space (Werner et al., 2012), allowing the measurement of additional displacement vectors and velocity classes. Recent InSAR data processed with up-to-date technologies are considered to update the inventory of slope movements and to quantify over time the rate of motion of the most active rockglaciers.

REFERENCES
Barboux C., Delaloye R. & Lambiel, C., Inventorying Slope Movements in an Alpine Environment Using Dinsar, Earth Surface Processes and Landforms, 39(15): 2087-2099, 2014.

Barboux C., Strozzi T. Delaloye R., Wegmüller U. & Collet C., Mapping slope movements in Alpine environments using TerraSAR-X interferometric methods, Journal of Photogrammetry and Remote Sensing, 109: 178-192, 2015.

Caduff R., Strozzi T., Wiesmann A. & Wegmüller U., Monitoring glacial, periglacial and landslide surface motion with Sentinel-1 for the entire Swiss Alps every 6 days. 15th Swiss Geoscience Meeting, Davos, 2017.

Strozzi T., Luckman A., Murray T., Wegmüller U. & Werner C., Glacier motion estimation using SAR offset-tracking procedures, IEEE Transactions on Geoscience and Remote Sensing, 40(11): 2384-2391, 2002.

Strozzi T., Kääb A. & Frauenfelder R., Detecting and quantifying mountain permafrost creep from in situ inventory, space-borne radar interferometry and airborne digital photogrammetry, Int. J. Remote Sensing, 25(15): 2919-2931, 2004.

Werner C., Wiesmann A., Strozzi T., Kos A. & Wegmüller U., The GPRI Multi-mode Differential Interferometric Radar for Ground-based Observations, Proceedings of EUSAR 2012, Nuremberg, Germany, 24-26 April 2012.

14.13

UAV-photogrammetry for rock glacier monitoring: Examples from the Swiss Alps

Sebastián Vivero[1], Régis Meyrat[1], Reynald Delaloye[2] & Christophe Lambiel[1]

[1] *Institute of Earth Surface Dynamics (IDYST), University of Lausanne, Bâtiment Géopolis UNIL Mouline, CH-1015 Lausanne*
[2] *Department of Geosciences, Geography, University of Fribourg, Chemin du Musée 4, 1700 Fribourg, Switzerland*

The use of Unmanned Aerial Vehicles (UAV) and digital optical cameras for aerial surveying has become a standard practice in the fields of geoscience. Images acquired by UAV platforms are usually employed for generating high-density point clouds, Digital Elevation Models (DEMs) and high-resolution orthorectified images of different landforms. This study focuses on the applications of UAV surveys and Structure-for-Motion (SfM) photogrammetric methods for rock glaciers research. Rock glaciers constitute a significant component of the cryosphere in many mountain regions, where favourable geomorphological and climatic factors allow their development. Rock glacier movement represents the manifestation of creeping mountain permafrost, which has received considerable attention about their current velocity changes in the European Alps. Given the rapid change and hazardous terrain of our study areas, the potential to carry out detailed field observations is demanding and troublesome. To overcome this, we have been employing different UAV configurations to monitor permafrost creep and their environs. We provide the first results after 2-years of UAV surveys from “fast” and “slow” rock glaciers in the Valais Alps. High-resolution images in combination with image classification algorithmic permitted to derive superficial boulder sizes; surface displacement vectors and to improve morphological parameters such as slope and aspect.

14.14

High-resolution troposphere models based on numerical weather prediction and Global Navigation Satellite Systems data

Karina Wilgan[1,2], Alain Geiger[1]

[1] *Institute of Geodesy and Photogrammetry, ETH Zürich, Robert-Gnehm-Weg 15, CH-8093 Zürich, Switzerland (kwilgan@ethz.ch)*
[2] *Institute of Geodesy and Geoinformatics, Wroclaw University of Environmental and Life Sciences, Grunwaldzka 53, 50-357 Wroclaw, Poland*

The microwave signal propagating through the atmosphere is delayed due to the free electron content in the ionosphere and due to the air molecules and the water vapor in the troposphere. The tropospheric delay can be expressed in terms of zenith tropospheric delay (ZTD) or total refractivity depending on the meteorological parameters: air pressure, temperature and humidity (water vapor).

The application of external high-resolution troposphere models in Global Navigation Satellite Systems (GNSS) processing, especially in the Precise Point Positioning (PPP) technique has been proven to enhance the coordinates' accuracy and to shorten the convergence time of the position solution (e.g. Wilgan et al., 2017). The tropospheric models can also be applied to other techniques, where the microwave signal is delayed in the atmosphere, such as space-borne Synthetic Aperture Radar interferometry (InSAR). One of the limitations of InSAR technique are atmospheric effects, especially due to the different values of water vapor during two acquisitions.

In this study, we have reconstructed the total refractivity profiles and ZTD values for Switzerland with main focus on the Valais region. The tropospheric parameters are obtained by the least-squares collocation method using the in-house developed software package COMEDIE (Collocation of Meteorological Data for Interpretation and Estimation of Tropospheric Pathdelays). The troposphere models are based on different combinations of data sources, including GNSS data and numerical weather prediction model COSMO-1 with high spatial resolution of 1.1 km x 1.1 km.

The GNSS-based ZTD model shows the highest agreement with the reference data, with an average bias close to zero and standard deviations of 4 mm. The ZTD models based on COSMO-1 exhibit worse, but still acceptable accuracies, with average biases also close to zero and standard deviations of about 9 mm. Figure 1 shows the average biases and standard deviations for the particular stations in the Valais region. In case of the total refractivity, the profiles reconstructed from COSMO-1 model show the best agreement with the reference radiosonde data in Payerne, with the average bias of 1 ppm and mean standard deviations of 2.6 ppm averaged from the whole profile.

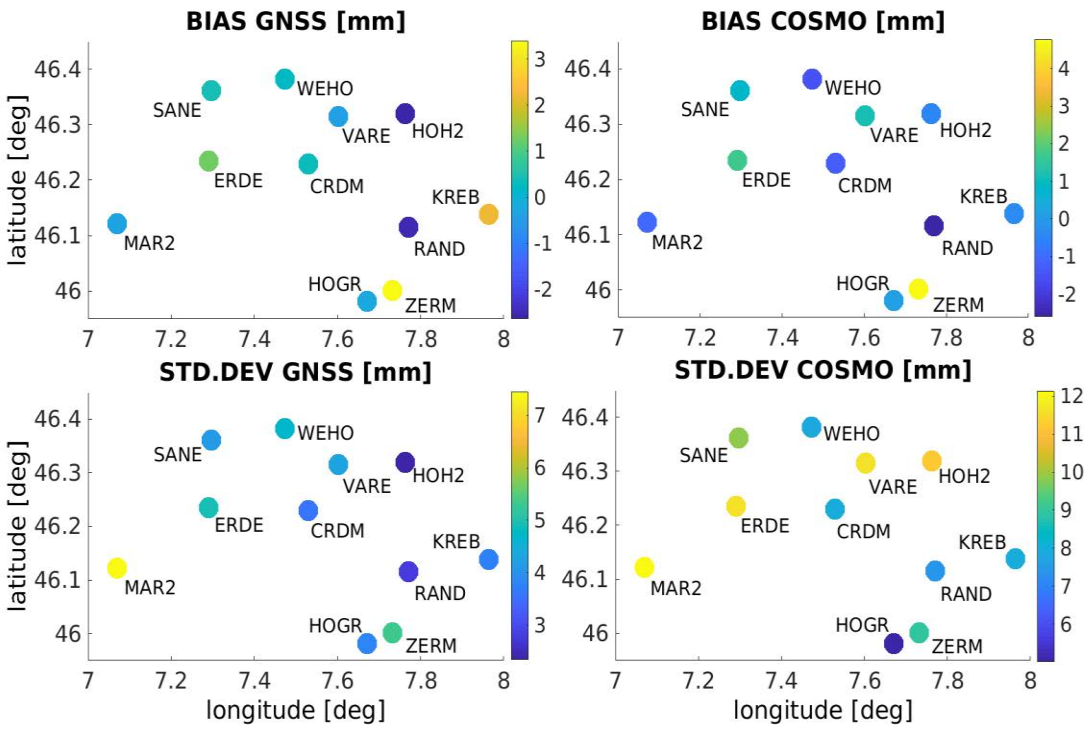

Figure 1. Average biases and standard deviations of residuals ZTD_{ref}-ZTD_{model}, where 'model' is either based on GNSS or COSMO data, 'ref' is a reference GNSS solution for particular station for which the model is calculated; this station is always excluded from building the model. Data is averaged over a period 1.08.-30.09.2016.

REFERENCES

Wilgan, K., Hadas, T., Hordyniec, P., & Bosy, J. 2017: Real-time precise point positioning augmented with high-resolution numerical weather prediction model, GPS Solutions, 21(3), 1341–1353

14.15

Influence of meteorological factors on the autumn land surface phenology in alpine grasslands

Jing Xie, Mathias Kneubühler, Irene Garonna, Rogier de Jong, Michael E. Schaepman

Remote Sensing Laboratories, Department of Geography, University of Zurich, Winterthurerstr. 190, 8057 Zurich, Switzerland (jing.xie@geo.uzh.ch)

Meteorological conditions impact the autumn phenology of alpine grasslands in various ways. However, in comparison to spring phenology our knowledge about the characteristic and magnitude of these effects is still limited and needs further investigation.

We examined the relationships between a number of meteorological factors and phenology in the alpine grasslands of the Swiss Alps using satellite-derived and gridded metrics for the period of 2003–2014. We tested the correlation of interannual differences (Δ) in the timing of the end of season (EOS) with meteorological factors (monthly maximum, mean and minimum temperatures, monthly mean relative sunshine duration and mean precipitation) across elevations (from 1000 up to 3000 meters above sea level (m a.s.l.)) and for four climatic subregions of the Alps.

We found a significant ($p < 0.05$) positive correlation between ΔEOS and interannual differences in autumn temperature (with mean R>0.69) for 31.9% of all pixels. ΔEOS showed the strongest correlation with interannual differences of minimum autumn temperature, except for the eastern Swiss Alps where precipitation showed the strongest relationship with ΔEOS. The areas sensitive to the investigated meteorological metrics were more pronounced in northern and eastern regions and at elevations below 2000 m a.s.l. across the Swiss Alps.

We conclude that a positive linear relationship exists between autumn temperature and autumn phenology of grasslands at elevations below 2000 m a.s.l. in our study area. Besides, autumn precipitation has a slightly higher impact than autumn relative sunshine duration on autumn phenology. Warmer autumn temperatures delay the end of the growing season, thus may indicate easing of growth constraints in alpine grasslands. This may suggest that alpine grassland ecosystems are therefore particularly sensitive to future climate warming scenarios.

P 14.1

UAV-based thermal remote sensing to highlight groundwater inputs in rivers

Raphael Vallat[1], Grégoire Mariéthoz[1]

[1]*Faculté des geosciences de l'environnement, University of Lausanne, 1015 Lausanne.*

Measuring lateral temperature fluctuations can give precious indications on river-groundwater exchanges. However, riverstream temperatures in-situ measurements are challenging to carry out and hardly representative due to the typical heterogeinity in rivers temperatures. Remote sensing methods can provide spatially continuous measurements of the surface of a river and show some of the complexity of its thermal rate. Using UAVs (drones) allows for frequent and inexpensive acquisitions covering a relatively large zone in a limited time (Handcock et al, 2012)

When interpreting such thermal data, it is critical to account for environmental conditions. For example, remotely sensed data are only representative of the stream surface, thus only the water contrasts reaching the surface are visible. Also, in high energy, turbulent rivers, temperatures are uniformized and can be supposed similar at any depth of the water column. Aerial points of views and time of day, such as before sunrise, and at nadir, allow minimizing the influence of day surface warming, reflexions and shadows (Dugdale, 2016). To determine optimal conditions, different data acquisitions settings have been tested, and some influences of hydrological and atmospheric conditions for remote sensed temperatures by UAV have been determined. The use of existing instruments and sofwares has allowed to concentrate the analysis on data acquisition conditions, comparisons to in-situ measurements, image interpretations and the identification of artefacts.

The drone used is a fixed wing Sensefly eBee equiped with ThermoMap and Multispec4 sensors. Two study sites have been monitored: the Avançon de Nant river in Vallon de Nant (VD), with acquisitions of about 1.3 km^2 and the Emme river in Aeschau (BE), with 0.5 km^2 acquisitions. The first site is a natural catchement, with multiple arms and clear groundwater inputs mainly detectable during low melt-water discharge. On the second site, multiple local hot spots have been detected in winter (fig. 1), which partially match cold spots identified in summer, indicating exfiltration zones. Along-stream temperature gradients could indicate zones of more intense groundwater inputs, giving clues of diffuse discharge.

In addition to the thermal band, multispectral datasets (R, G, NIR, R-edge) have been acquired to discriminate water bodies from other surfaces. These additional bands also allow assessing the artefacts in the TIR band and their potential origins (trees, angle, image correlation problems). Flight planning has showed that a unique water stream 2.5 km long and ~20 m wide can be mapped in under 1h at a 0.2 m resolution in the TIR band. Flight planning requires to cover enough non water surfaces (>65%) and high overlap between images (80-90%), however trees and high objects have a negative impact on the mosaicking results. Raw images can be useful to assess individual zones, that allows limiting artifacts resulting from the difficulty of performing image correlation on thermal images.

It was found that the optimal environnemental conditions for thermal UAV-based river monitoring are:

- low water discharge which maximize thermal gradients,
- no rainfall, during and and the day(s) before the flights,
- a stable discharge level and minimal TIR radiation variations during acquisition.

Two main scales of gradients have been analysed: (1) local hotspots reprensenting concentrated inputs of GW and (2) temperature variation along the stream, potentially indicating zones of infiltration and exfiltration. In conclusion, it can be said that thermal maps can contribute to a better understanding of the surface/subsurface water exchanges, and that recent advances in UAVs allow studying a large number of sites with high regularity.

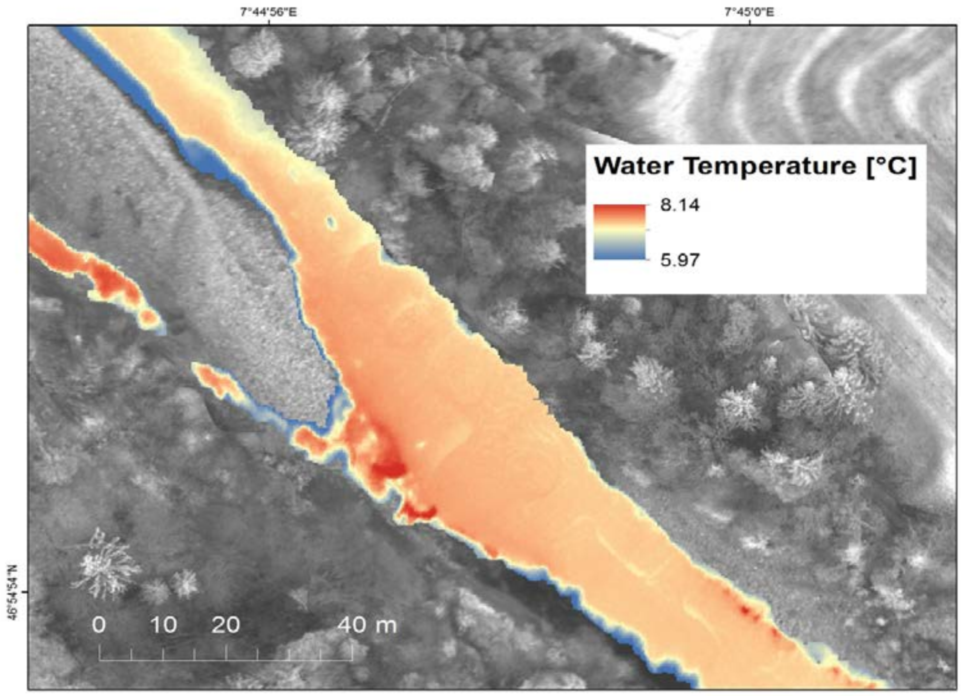

Figure 1 Water temperature on the 15.11.2016 on the Emme river, near Aeschau. Background: red-edge band.

REFERENCES

Dugdale, S. 2016. A practitioner's guide to thermal infrared remote sensing of rivers and streams: Recent advances, precautions and considerations. WIREs Water. 3, 251–268.

Handcock, R., Torgersen, C., Cherkauer, K., Gillespie, A., Tockner, K.,Faux, R., Tan, J. 2012. Thermal Infrared Remote Sensing of Water Temperature in Riverine Landscapes. In: Carbonneau PE, Piégay H, eds. Fluvial Remote Sensing for Science and Management. Chichester: Wiley-Blackwell; 2012, 85–113.

P 14.2

High alpine remote sensing test site Davos: validating remote sensing technology in complex terrain

Yves Bühler[1], Martin Schneebeli[1], Mike Schwank[2], Charles Fierz[1], Tobias Jonas[1], Michael Lehning[1], Henning Löwe[1], Rafael Caduff[2] & Christian Ginzler[3]

[1] *WSL Institute for Snow and Avalanche Research SLF, Flüelastrasse 11, 7260 Davos Dorf, Switzerland (buehler@slf.ch).*
[2] *GAMMA Remote Sensing AG, Worbstrasse 225, 3073 Gümligen, Switzerland (gamma@gamma-rs.ch).*
[3] *Swiss Federal Institute for Forest, Snow and Landscape Research WSL, Zürcherstrasse 111, 8903 Birmenstorf, Switzerland (christian.ginzler@wsl.ch).*

Satellite and airborne remote sensing has proven its value for a wide range of scientifically and socially relevant applications over many years now. However most sensors and data processing algorithms are developed and tested in relatively flat and wide regions. About 20% of the earth surface consists of rugged terrain such as mountains and hills, of which a big part is covered by seasonal or permanent snow and ice. These components of the cryosphere form temporary water storage and – during the summer – provide a crucial source of water for the human population. There is a lack of research on the performance of remote sensing technology over mountainous terrain, as it is particularly difficult to get sound reference datasets.

To close this gap, we are currently developing a well-documented alpine test site in Davos, Graubünden, Switzerland. It is part of the Global Cryosphere Watch (GCW) Cryonet site Weissfluhjoch-Davos and further encompasses the Dischma Valley catchment that is part of the International Network for Alpine Research Catchment Hydrology (INARCH). This high alpine region (elevation range 1400 – 3200 m a.s.l.) is home to the WSL Institute for Snow and Avalanche Research SLF and houses many different long-term observations. SLF operates 10 active automated weather stations measuring snow and weather data, as well as several manned stations for snow observations on the ground, one of them having continuous records for more than 80 years (Marty and Meister, 2012). Measurements include specific observational fields at Weissfluhjoch (2650 m a.s.l.) and Laret (1500 m a.s.l.), where a large variety of snow parameters are recorded. The focus of the intensive observation area (IOA) Laret is on ground-based microwave measurements accompanied by the acquisition of in-situ data relevant to foster the understanding of interactions between microwaves and snow-covered grounds.

Research at this site is conducted in close collaboration with the European Space Agency (ESA) and industry partners (GAMMA) and aims at the development of novel retrieval schemes and their validation. Ground based measurements are complemented by measurement campaigns with airborne remote sensing instruments (UAS and airplanes) to regularly map the distribution of alpine snow depth at high spatial resolution over entire catchments (Bühler et al. 2015, Grünewald et al. 2014) and at selected sites (Bühler et al. 2016). These measurements are already changing paradigms of hydrological modeling in Alpine catchments and lead to improved understanding of snow precipitation (Vögeli et al., 2016). Furthermore, many different ground based measurements performed for different projects at SLF are available. This collection of alpine datasets as well as the good accessibility of the alpine terrain and the availability of skilled field personnel through SLF provides unique opportunities to develop and validate remote sensing technology specifically for high alpine terrain. We aim at consolidating this test site by starting optical, microwave and LiDAR remote sensing validation projects financed by different national and international funding sources.

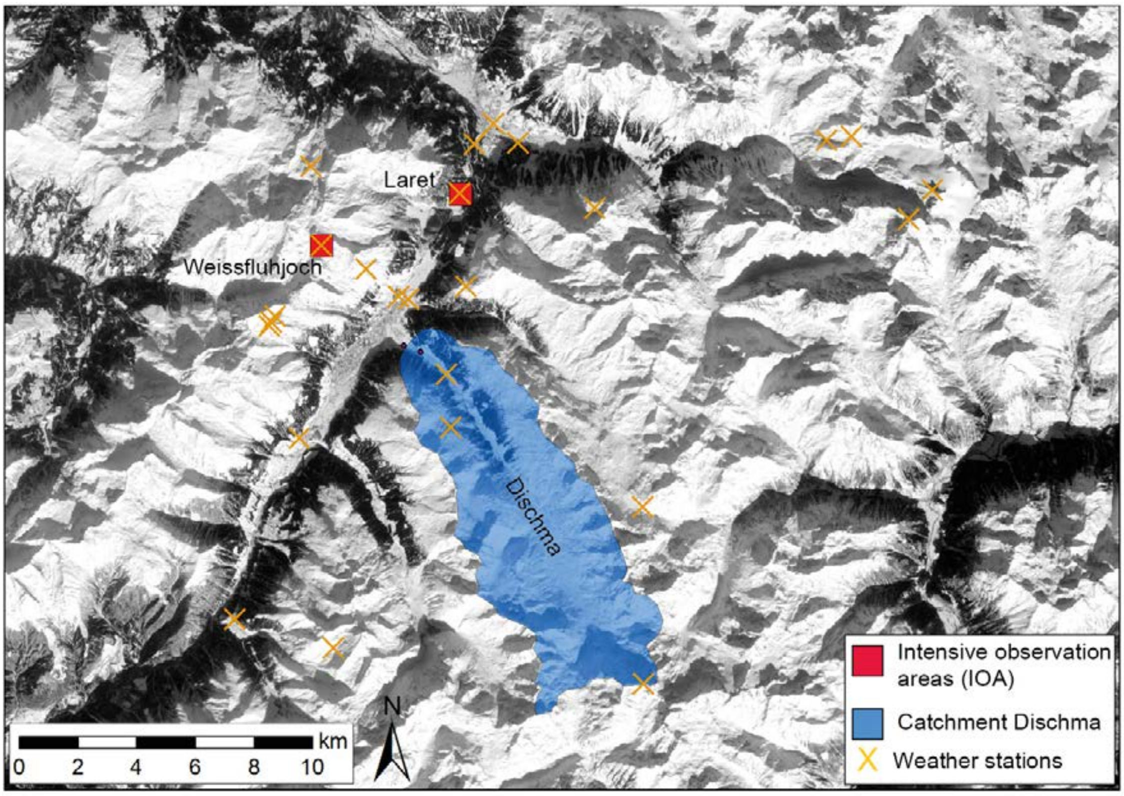

Figure 1. Sentinel-2 satellite image of the high alpine test site Davos acquired on January 27 2017 showing the already available infrastructure and intensive observation areas (IOA).

REFERENCES:

Bühler, Y., M. Marty, L. Egli, J. Veitinger, T. Jonas, P. Thee, and C. Ginzler 2015: Snow depth mapping in high-alpine catchments using digital photogrammetry, The Cryosphere, 9(1), 229-243, doi:10.5194/tc-9-229-2015.

Bühler, Y., M. S. Adams, R. Bösch, and A. Stoffel 2016: Mapping snow depth in alpine terrain with unmanned aerial systems (UASs): potential and limitations, *The Cryosphere*, *10*(3), 1075-1088, doi:10.5194/tc-10-1075-2016.

Grünewald, T., Y. Bühler, and M. Lehning 2014: Elevation dependency of mountain snow depth, *The Cryosphere*, *8*(6), 2381-2394, doi:10.5194/tc-8-2381-2014.

Marty, C. and R. Meister. 2012: Long-term snow and weather observations at Weissfluhjoch and its relation to other high-altitude observatories in the Alps, Theoretical and Applied Climatology, 110(4), 573–583, doi:10.1007/s00704-012-0584-3.

Vögeli, C., Lehning, M., Wever, N., Bavay M., 2016: Scaling Precipitation Input to Spatially Distributed Hydrological Models by Measured Snow Distribution. Front. Earth Sci. 4: 108. doi: 10.3389/feart.2016.00108.

16. Geoscience and Geoinformation – From data acquisition to modelling and visualisation

Nils Oesterling, Adrian Wiget, Massimiliano Cannata, Michael Sinreich

Swiss Geodetic Commission
Swiss Geotechnical Commission
Swiss Geophysical Commission
Swiss Hydrogeological Society)

TALKS:

16.1 **Boulicault L.**, Manzini M., Faubert M., Minnig C., Glaus L., Oesterling N., Baumberger R.
GeoTherm: Public Data Infrastructure for Deep Geothermal Energy in Switzerland

16.2 **Brodhag S.H**., Oesterling N., Baumberger R.
Geological Data Management – An Example for Borehole Data

16.3 **Cannata M.**, Strigaro D., Cardoso M., Hoffman M., Antonovic M.
4 times open weather station: first results of non-conventional cost-effective monitoring system

16.4 **Cledat E.**, Cucci D., Skaloud J.
Planning of UAV mission for precise terrain reconstruction in steep terrain without ground control points

16.5 **Dawes N.**, Suter C.
FeldApp – Fieldwork to final report in the most efficient fashion

16.6 **Galvan B.**
Efficient implementation of complex elasto-plastic models in high performance computing systems

16.7 **Jaeggi D.**, Herfort M., Tabani P.
Long-term performance of fiber optical sensors subjected to HLW repository conditions

16.8 **Nurtaev B.**
Application of solar numeral system in geosciences

16.9 **Plattner G.-K**., Espona Pernas L., Iosifescu Enescu I., Lehning M., Steffen K.
Moving research boundaries by enhancing access to Swiss environmental data

16.10 **Produit T.**, Ingensand J.
Visualisation and analysis of landscape change using crowdsourced historical photographs

16.11 **Wiget A.**, Wicht A.
Moving national boundaries – reasons, documentation and backtracking

POSTERS:

P 16.1 **Dahrabou A.**, Valley B., Ladner F., Guinot F., Meier P.
Optimisation of borehole trajectory in order to minimize borehole failure

P 16.2 **Guignard F.**, Leuenberger M., Kanevski M.
Uncertainty quantification in environmental data driven modelling using machine learning

P 16.3 **Hunziker J.**, Laloy E., Linde N.
Towards probabilistic full-waveform inversion

P 16.4 **Laib M.**, Telesca L., Kanevski M.
Multifractal Detrended Fluctuation Analysis of Wind Speed Connectivity Density Time Series

P 16.5 **Leith K.**, Perras M., Loew S.
Integration of open-source hardware in a low-power, low-cost system to monitor thermally-driven rock fracturing

P 16.6 **Long X.**, Ballmer D.
Intraplate volcanism in northeast China due to upwellings rising from the stagnant slab

P 16.7 **Tonini M.**, Amato F., Kanevski M., Murgante B.
A prospective scenario for Rural Urban Interface based on spatio-temporal LULCC

P 16.8 **Wehrens P.**, Volken S., Preisig G., Gaehwiler M., Möri A.
GeoQuat project: Benefits of standardization and automation for analyzing and modelling data from Quaternary deposits

16.1

GeoTherm: Public Data Infrastructure for Deep Geothermal Energy in Switzerland

L. Boulicault[1], M. Manzini, M. Faubert[1], C. Minnig[1], L. Glaus[2], N. Oesterling[1], R. Baumberger[1]

[1] *Federal Office of Topography swisstopo, Swiss Geological Survey, Seftigenstrasse 264, CH-3084 Wabern (lise.boulicault@swisstopo.ch)*
** SCCER-SoE, ETH Zürich, Sonnegstrasse 5, CH - 8092 Zürich

In the context of the Energy Strategy 2050, Switzerland commits to the development of renewable energy including deep geothermal energy. Lack of coordination or even complete lack of data management and data policies are one of the barriers for the development of deep geothermal projects. For this reason, the Swiss Federal Office for Energy (SFOE) and Swiss Federal Offices of Topography (swisstopo) launched the GeoTherm project (2015 – 2019). GeoTherm is the public federal information system for data related to deep geothermal energy. It aims to establish an infrastructure for the storage and publication of geothermal data on the federal geoportal (map.geo.admin.ch). This paper gives an updated view of the work in progress after 20 months of project duration.

Data collection
Raw and interpreted data relevant for the development of deep geothermal energy are key to the GeoTherm project. Therefore, a first inventory of borehole data from the internal swisstopo archives has been raised since the beginning of the work. In order to complete this inventory as well as to collect additional information (e.g. geothermal potential studies, geothermal projects reports, seismic surveys, chemical and petrophysical databases, etc.), external data providers such as universities, cantons and private companies will be contacted.

Quality control and perennial storage
Every new dataset is quality controlled and harmonized based on swisstopo's data management standards (data models). Where needed, the standards are extended to fit particular needs of geothermal data. Then, the data is integrated into a central borehole database, i.e. existing data is updated. This guarantees a long-termin sustainability of the data.

Data Web – publication
GeoTherm strives to show where data exist and make it accessible. Therefore, metadata of the wells, potential studies, etc., which contains no sensitive information, will be fully published on the federal geoportal. As for the data itself, it might be protected by certain rights. The publication of such data is either based on existing laws [1, 2] or on contracts between the rights owners and swisstopo. At the end, only non-confidential data will be published.

First results and outlooks
Since March 2017 a layer showing geothermal projects deeper than 400 m has been online on the federal geoportal (https://map.geo.admin.ch) (Fig. 1). Two additional layers will be published in 2017: one provides information on boreholes deeper than 500 m and the other one shows available geothermal potential studies.

Further layers are planned to be published in 2018 such as an updated "Heat Flux Map" (in coll. with the Swiss Geophysical Commission SGPK), temperature maps per depth and top horizons, seismic surveys and earthquakes monitoring (in coll. with the Swiss Seismological Service SED). In order to keep these layers up to as well as to provide more information for planners of geothermal energy projects in Switzerland, the SFOE and swisstopo need a close collaboration with the involved stakeholders.

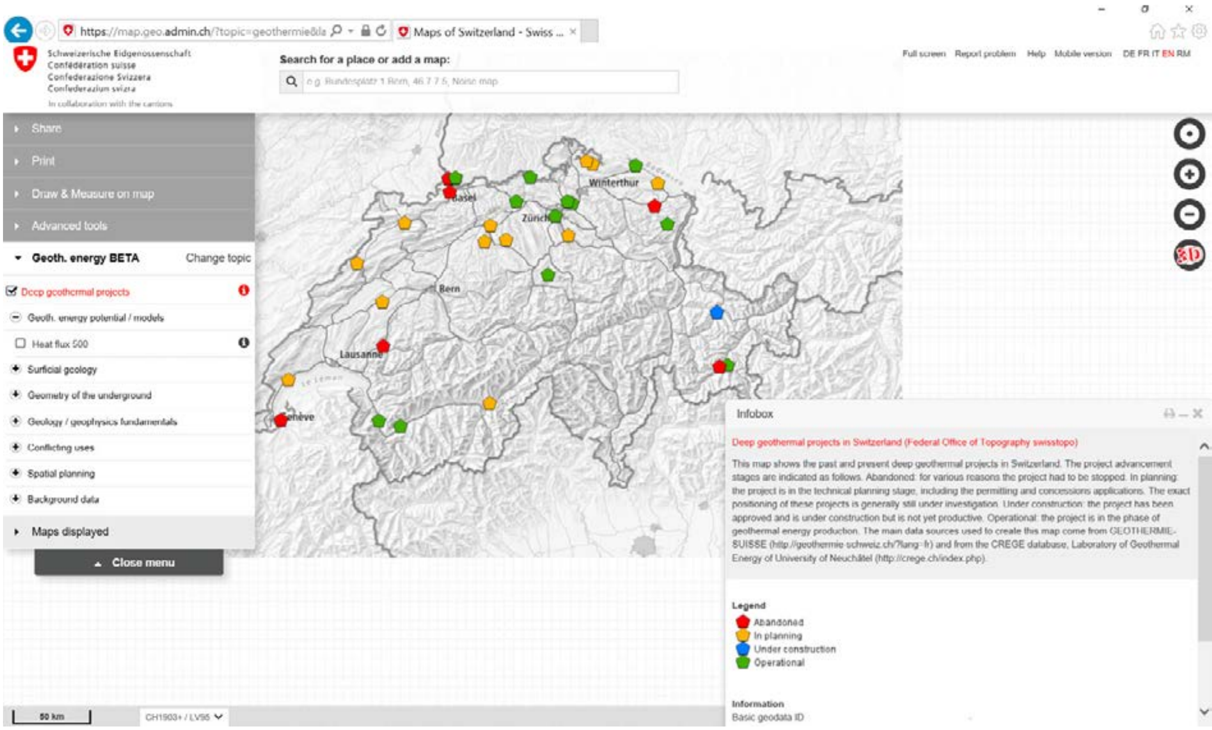

Figure 1: View of the first layer showing the geothermal projects deeper than 400 m on map.geo.admin.ch. The additional layers of the wells deeper than 500 m and the geothermal potential studies will soon also be available on this website

REFERENCES

[1] Energy Act (EnA), SR 730.0
[2] Federal Act on the Reduction of CO_2 Emissions (Co2 Act), SR 641.71

16.2

Geological Data Management - An Example for Borehole Data

[1]Sabine H. Brodhag, [1]Nils Oesterling, [1]Roland Baumberger

[1] *Federal Office of Topography swisstopo, Swiss Geological Survey, Seftigenstrasse 264, CH-3084 Wabern (sabine.brodhag@swisstopo.ch)*

In Switzerland, the use of the subsurface increases year by year. Besides the classical production fields of mineral resources industry, civil engineering, underground construction and the use of groundwater, the exploitation of geothermal energy became a well-established source of energy meanwhile. In the course of this intensive subsurface use, the amount of newly generated borehole data, which has to be managed, is increasing vastly.

The Swiss Geological Survey (SGS) is the national authority for the subsurface (Federal Office of Topography swisstopo, 2017) and the federal competence centre for geological data. To handle the topics mentioned above in the light of legislative regulation and to provide nationwide geological base data and information, data management of the SGS had to be reorganized fundamentally. Fast and effective exchange of data between partners is only possible with a well-structured and harmonized data management. Addtionally, administrative efforts are reduced to a minimum as well. Therefore, several systems for capture, storage and visualisation of geological data are under development or already established. One of those systems is the management system for borehole data, which was acquired in 2015 and refined by the SGS until now to adapt it to the SGS's requirements.

In order to realize a well-structured and harmonized data management geology-related data had to be identified, structured and harmonized in a first step, before data management workflows themselves could be adapted and software solutions found. The structuring of data was done by means of data models, which describe data and their relationship to each other in a standardized descriptive model language. For the federal government, they are obligatory for all basic federal geodata and are stored in the Model Repository for official geodata under federal legislation. Up to now, the SGS published three data models: (i) the Data Model Geology (2012, in revision), (ii) the Data Model Geology – Pixel Maps (2011) and (iii) the Data Model Borehole Data (2014, in revision). Further, non-published data models for internal use do exist.

The Data Models Geology and Borehole Data were developed with the collaboration of representatives of several federal offices, universities, cantonal administration and the private sector to increase the acceptance of the respective model and to guarantee meeting its proper target. Pre-existing geology-related national and international standards like SN, SIA or ISO were integrated into the models as well as the new harmonized tectonic, lithologic chrono- and lithostratigraphic SGS charts for Switzerland (published in Data Model Geology, 2011, and on strati.ch). Both models are available in German and French further languages are planned.

For SGS's new borehole-database management-system, the Data Model Borehole is a crucial basis and was implemented completely into it as well as the stratigraphic SGS charts mentioned above. By means of implementing the data models into the management system, standards, harmonized charts and multilingualism are integrated as well. In the course of the development of the database management system for borehole data, the complete SGS filing system had to be reorganized as well as data capturing for linked databases (e.g. swisstopo address database). Workflow structures for borehole data management were adapted to comply with the new borehole-database management-system and the surrounding infrastructure.

Implementing consolidated data models into one's data management systems results in structured and harmonized data and adds value to the data in the sense of a defined data quality. Sharing these data models with the community simplifies data exchanges and makes exchanges independent of technical systems or formats (Wehrens et al. 2017). Finally, structuring and harmonizing data has a feed backing effect on data management workflows and initial data acquisition.

REFERENCES

Data Model Geology, Version 2.1, 2012. Federal Office of Topography swisstopo, 151 p. https://www.geologieportal.ch/en/knowledge/lookup/data-models/geology-data-model.html

Data Model Geology, Pixel Maps, Version 1.0, 2011. Federal Office of Topography swisstopo, 71 p. https://www.geologieportal.ch/en/knowledge/lookup/data-models/geology-data-model.html

Data Model Borehole Data (German), Version 2.0, 2014. Federal Office of Topography swisstopo, 48 p. https://www.geologieportal.ch/en/knowledge/lookup/data-models/borehole-data-model.html

Lithostratigraphic Lexicon of Switzerland. Federal Office of Topography swisstopo. http://www.strati.ch/

Model Repository for official geodata under federal legislation:
http://models.geo.admin.ch/

Swiss Geological Survey 2017. The Swiss Geological Survey – the authority for subsurface. Swiss Confederation, 20 p.
https://www.swisstopo.admin.ch/en/home/meta/pub-caroussel/brochure-geology.html

Wehrens, P., Volken, S., Preisig, G., Gaehwiler, M., Möri, A., 2017. GeoQuat project: Benefits of standardization and automation for analyzing and modelling data from Quaternary deposits, 15th Swiss Geoscience Meeting, 17-18 November 2017, Davos.

16.3
4 times open weather station: first results of non-conventional cost-effective monitoring system

Massimiliano Cannata[1], Daniele Strigaro[1], Mirko Cardoso[1], Marcus Hoffman[1], Miln Antonovic[1]

[1]*Scuola Universitaria Professionale della Svizzera Italiana (SUPSI), Campus Trevano, CH-6952*

The access to weather information in developing countries is often limited due to non existing or in decline monitoring networks. The main issues that contribute to this lack of data is the inaccessibility to expensive technologies installed with international projects and not adequately supported by replacement parts, local knowledge of the systems and high costs (Snow, 2013). The indaquate availability of information mines the capacity of the community to cope with hydrogeological hazards and to sustainably manage natural resources.

For these reason, the 4ONSE project is studing the effectiveness and sustainability of non-conventional automatic weather monitoring system fully based on open technologies (hardware, software, standard and data). The project of the duration of three year is just entered the second year, and after the design and prototyping of the enginereed solution is going to deploy around 30 station in the Deduru Oya basin in Sri Lanka, which currently monitored with three manual rain gauge. The designed system combines Arduino microcontroller, GPRS communication, Observation and Modelling standard data format, istSOS Sensor Observation Service software and CKan open data portal. The system will enable the acquisition, management and distribution of observations of temperature, humidty, rainfall and pressure with a temporal resolution of 10 minutes.

Preliminary results on the data quality analyses and system replication tests showed enoraging outcomes. These support the idea that such a kind of system may help in filling the gap of missing critical data for effective policy making individuated by the United Nation (2015).

4ONSE is a project funded within the Swiss Programme for Research on Global Issues for Development (r4d programme) financed by the Swiss Agency for Development and Cooperation (SDC) and the Swiss National Science Foundation (SNSF).

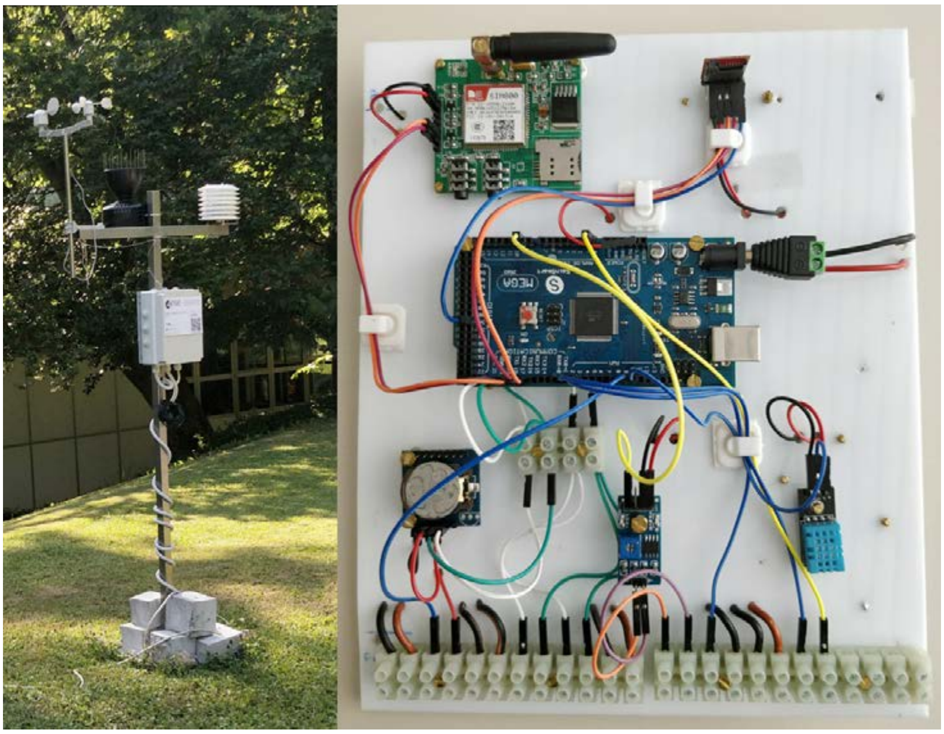

Figure 1. Prototype of the non-conventional weather monitoring station based on open technology designed by the 4ONSE project.

REFERENCES

Snow, J.T. 2013: Non-traditional Approaches to Weather Observations in Developing Countries. International Finance Corporation. Available online at: https://goo.gl/sAZS6u.

United Nations. Department of Economic, & United Nations. Department of Public Information. 2015. The millennium development goals report 2015. United Nations Publications.

16.4

Planning of UAV mission for precise terrain reconstruction in steep terrain without ground control points

Skaloud, J., Cucci, D., Cledat, E.

EPFL-TOPO, Station 18, 1015 Lausanne

The operation efficiency of micro aerial vehicles (MAV) makes them an ideal tool for acquiring imagery for the purpose of mapping/observing small zones of natural interest (e.g. hazards) in the Alpine environment. Such operations are further simplified if the UAV has the ability to geo-tag the acquired photographs with cm-level accuracy. This allows dropping the need for signalization and surveying of ground control points that is otherwise necessary for the purpose of image geo-referencing.

Precise “geo-tagging” or aerial position control is possible with surveying-grade receivers of Global Navigation Satellite Systems (GNSS) if the instantaneous satellite constellation is of sufficient quality. This depends generally on the number of visible satellites and their geometry. The satellite “visibility” requires direct line-of-sight (LOS), which is a function of drone position with respect to its environment. Such function is complex for drone operating close to steep mountainous terrain and in extremity may deny GNSS-position determination of the drone, fact of which hampers its self-guiding capacity and thus the mission execution.

We present the advantage of implementing a software functionality that depicts the expected quality of GNSS positioning for each part of the planned trajectory considering its surroundings during a specific time window. The user can provide a custom high-resolution digital elevation model (DEM) to be employed in substitution of the global models, for better accuracy or to introduce extra features (tree-surface model) or man-made features. The waypoints for which the GNSS constellation is evaluated are represented in color (green to red), giving an intuitive notion of the constellation quality at that point with respect to chosen flight, start time. An aggregated statistics are plotted in a separate plot over a time span of several hours to guide user for choosing optimal mission time.

An impact of the developed feature on the mapping accuracy is empirically evaluated in a natural environment, where the average visibility of satellites is critical. A zone of natural hazard in canton Valais, located northwest from Martigny was chosen for the study. It is a narrow valley that is surrounded by high ridges in all directions but east. During winter 2015-2016 an exceptionally large avalanche fell down from the South-ridge and destroyed part of the forest, the road and some habitations. A flight plan was created to map again a portion of the avalanche run-off zone with fixed-wing senseFly’s drone: ebeeRTK. Benefiting from the developed feature predicting the GNSS constellation quality along the trajectory, the flight was executed in both “sub-optimal” and “close to optimal” conditions of satellite visibility and geometry, which fluctuate considerably during the day. The impact of the image geo-localization quality on the mapping accuracy is evaluated as differences (residuals) of coordinates of the signalized targets determined “from the air” with respect to their values known before hand (ground-truth). The improvement of the mapping accuracy thanks to better geo-localization of the images varies by the factor of 3-10 in vertical and horizontal coordinates, respectively. The root-mean-square error of the positioning residuals on the ground targets during flight executed during planned “optimal flying conditions” is 0.013 m horizontally and 0.018 m vertically.

This research was supported by the Swiss Commission for Technology and Innovation (CTI) via the contract 18442.1 PFWI-IW.

16.5

FeldApp - Fieldwork to final report in the most efficient fashion

Nicholas Dawes[1], Christoph Suter[1]

[1]GEOTEST AG, Bernstrasse 165, CH-3052 Zollikofen (nicholas.dawes@geotest.ch)

Field time is precious to most outdoor professionals. The digitisation of field notes and conversion of these notes into a written product reduces the productive time of skilled personnel. Yet many of these products are repetetive assessments, and their production can largely be automated from digital field notes.

At GEOTEST, we have developed a mobile and web-GIS combination which allows us to optimise the time our experts may spend in the field. The system consists of an iOS application, based around a map interface (in either Swiss or international coordinate systems), which allows us to take georeferenced field notes; paired with a personalized web-GIS application, through which our experts may edit their notes and produce a report based on a pre-defined template.

Notes can be taken in the mobile app using application specific forms. These forms allow us to maintain a structure in the field notes, though unrelated notes and photos are also allowed. Each form type is associated with a report template in the web-GIS, enabling the user to produce a complete report, pre-populated with the field notes, in one click.

Not all objects can be geolocated to a sufficient accuracy in the map interface, so we have added the ability to locate objects on a plan, which is in turn geolocated in the map. These plans could be small-scale plans of a field site, with objects located only a few cm apart; annotated photographs of rock walls; or manual sketches of a hidden object such as a tunnel system. All of the above solutions can be created within the app whilst in the field, and are immediately available for detailed location of e.g. notes and photographs.

The mobile app is designed to be used offline in the field. Maps can be saved for the area of interest. When a data connection is available, the field notes can be synchronised to the web-GIS, securing the data in case of loss. This synchronisation also allows multiple team members to work on the same project simultaneously, or a single user to work on a combination of iPhone and iPad.

It is possible to add new forms and associated report-templates, based on a specific application. One such application is monitoring infrastructure such as natural hazards protection structures. For this use-case, we have several forms implemented for the assessment of protection measures. Based on specific parameters in the form, the map/plan-based object can be coloured to indicate its status, e.g. Red: Requires urgent repairs / Yellow: requires monitoring / Green: no problems assessed. Typically, protection measures are re-assessed at regular intervals. This interval can be entered into the system, and the objects are coloured accordingly, indicating which protection measures must be reassessed. This facilitates fieldwork planning and logistics. Both from within the field and from the office, a complete history of repairs and repair assessments is available for all protection measures, and should a hazard overcome the protection measures, a report on their prior status is available in an instant.

Our solution has been developed over several years for use within our own company, and is used for a broad spectrum of applications. From this summer, it is also being provided as a solution for external customers.

Figure 1. The mobile app map interface

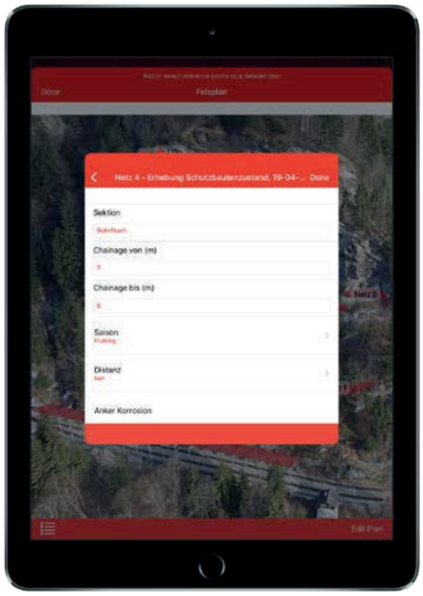

Figure 2. The form data entry interface with a objects located on a plan in the background

Figure 3. The web-GIS interface showing the plan (top-left) with objects coloured according to their status, as well as images and reports related to the objects.

16.6

Efficient implementation of complex elasto-plastic models in high performance computing systems

Boris Galvan[1]

[1] Centre for Hydrogeology and Geothermics of University of Neuchâtel (CHYN)
e-mail: boris.galvan@unine.ch,

New energy production technologies like fracking and enhanced geothermal systems, requires simulation of rock fracturing and fractures evolution. These simulations are computationally challenging, primarily due to different space and time scales of the processes involved and complex geometries of the physical domains under study. In particular, the dynamic solution of the equations related to rock deformation requires very short time steps and introduces different competing deformation modes that translate into program branching. This is the most computing intensive part in field scales thermo-hydro-mechanical (THM) modeling. It represent around 90% of the total computational time.

This computational cost problem could be tackle using next generation computing clusters that have heterogeneous architecture nodes, in which very dense computations are off-loaded to one or more co-processors. These co-processor are single instruction, multiple data (SIMD) highly parallel computing devices like Graphical Processor Units (GPU) or Intel Many Integrated Core (MIC) architecture.

Our work focuses in efficient 2D simulation of THM models in multi-GPU clusters, particularly the mechanical part using explicit finite differences approximation. This involve the implementation of brittle-elasto-plastic models that must be solved efficiently, accounting for the different deformation modes and consequent programming branching.

Normally, program branching imposes a high efficiency penalty when SIMD devices are used. We present different optimization techniques to handle it and to enhance the performance in High Performance Computing systems (HPC). These strategies could be applied to different mechanical models for a variety of problems.

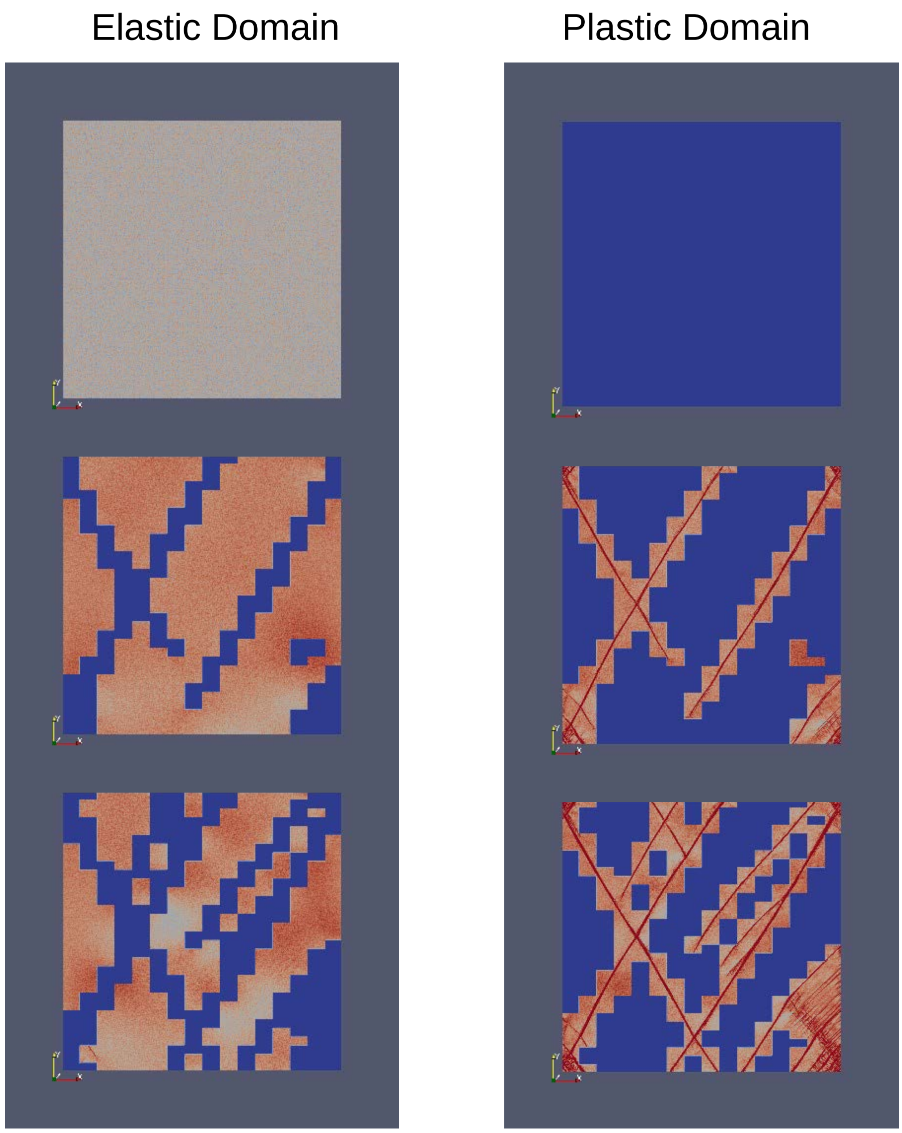

Figure 1. From top to bottom: initial, intermediate and final state of the yield function of an brittle-elasto-plastic material subjected to biaxial compression. Red color means yield function closer to or equal to zero and blue color represent GPU block inactive for depicted failure mode. Domain size is 512x512 divided among 4 GPU's. Decomposition between elastic and plastic failure modes is performed on the fly on each GPU and each failure mode is computed in parallel within GPU's using concurrent GPU streams. The figures show spontaneous fracture generation and evolution within the domain.

REFERENCES

Galvan, B. & Miller, S. 2013. A full GPU simulation of evolving fracture networks in a heterogeneous poro-elasto-plastic medium with effective-stress-dependent permeability, in: D. Yuen, L. Wang, X. Chi, L. J. W. Ge, Y. Shi(Eds.), GPU solutions to multi-scale problems in science and engineering,Lecture Notes in Earth System Sciences, Springer, p. 305-319.

Nvidia Corporation, 2007.NVIDIA CUDA Compute Unified Device Architecture Programming Guide.

16.7

Long-term performance of fiber optical sensors subjected to HLW repository conditions

David Jaeggi[1], Martin Herfort[2], Philippe Tabani[3]

[1] Swisstopo, Seftigenstrasse 264, 3084 Wabern (david.jaeggi@swisstopo.ch)
[2] Ensi, Industriestrasse 19, 5200 Brugg
[3] Andra – Centre de Meuse/Haute-Marne, RD960, 55290 Bure

Long-term monitoring of high-level radioactive waste (HLW) repository performance during closure and early post-closure phases is an integral part of the Swiss concept. Extensive monitoring will be performed in a pilot repository, containing a small, but well-defined quantity of HLW. In view of this, we present experiments using fiber optical sensing systems. The MO (Preparation of technology for long-term monitoring) experiment was established for testing fiber Bragg gratings (FBG) and Brillouin optical time domain analysis (BOTDA) sensors from different suppliers under realistic conditions in order to provide a mature technology for monitoring in a future pilot repository. Fiber optical sensors do not need electric energy downhole and can be used for accurate continuous measurements along a borehole or an installation. Since March 2012, FBG and BOTDA sensors from different suppliers are specifically tested on ageing and long-term signal performance in a heated borehole, backfilled with a mixture of sand/bentonite and saturated with artificial pore water. Maximum temperature reached 85 °C at the borehole bottom of 6 m depth. Four strings of FBG sensors are installed at 5 different depth levels and 3 BOTDA cables from different suppliers are wrapped in a spiral manner onto a carbon basket.

All sensors are protected with strain-free coatings or encapsulated in short steel or heat-shrink tubes. Temperatures of FBG sensors are measured every 30 minutes with 3 repeated measurements within 2 seconds in order to check the repeatability of the measurement. BOTDA cables are measured with a portable interrogator unit 4 times a year. In November 2017 the experiment will be dismantled and the sensor coatings will be tested microscopically, chemically, and mechanically on three different cable sets: i) an initial cable set, where the analysis was carried out in 2012, ii) a retained set stored under warehouse conditions and iii) the set buried in the borehole and subjected to the harsh downhole pressure, temperature and chemical conditions.

Two types of FBG sensors failed shortly after installation or exhibited non-systematic behavior or deviation from the conventional PT1000 signals. For these sensors after every temperature increase on the heater, bandwidth of acquisition needed to be increased. The other two sensors perform well, however strain free installation is not evident. For all 4 types of FBG sensors a recalibration was carried out after 2.5 years of operation. Calibration was performed by using data from a 1D-thermal modeling with Comsol™ and the temperature data of conventional PT1000 sensors as true-value calibration points. The BOTDA sensors needed a recalibration as well. Their long-term behavior is strongly dependent on the sensor type (Figure 1). The smooth shape of the temperature plot of the ST (steel armoring)-sensor shows its long-term stability and reliability. However, the LP (lightly protected)-sensor shows very irregular and undulated shape of the temperature plot after every of the 5 deployed temperature steps. Even in the depth interval between 2.5 and 6.0˙m, where the temperature signal should a priori be more or less smooth, the temperature signals are very irregular. Obviously, the LP-sensor is insufficiently protected and strain free packaging is not at all achieved.

For monitoring a future pilot repository, redundant systems or simple means to check sensor performance and to re-calibrate the sensors at any time are required. Experience with different types of fiber optic sensors for measuring temperature has shown that cross-checking with conventional sensors is indispensable. However, future instrumentation will rely mainly on fiber optical sensors, which allow to increase the spatial density of measurement remarkably. Recent developments with hybrid systems measuring Brillouin and Rayleigh scattering at the same time make a deconvolution of strain and temperature signal, and consequently a continuous auto-calibration, possible. For the MO experiment all 5 conventional sensors installed downhole were lost after 4 years of monitoring. Consequently, and due to the official end of a successful five-year monitoring period, the experiment will be stopped and dismantled by the end of 2017.

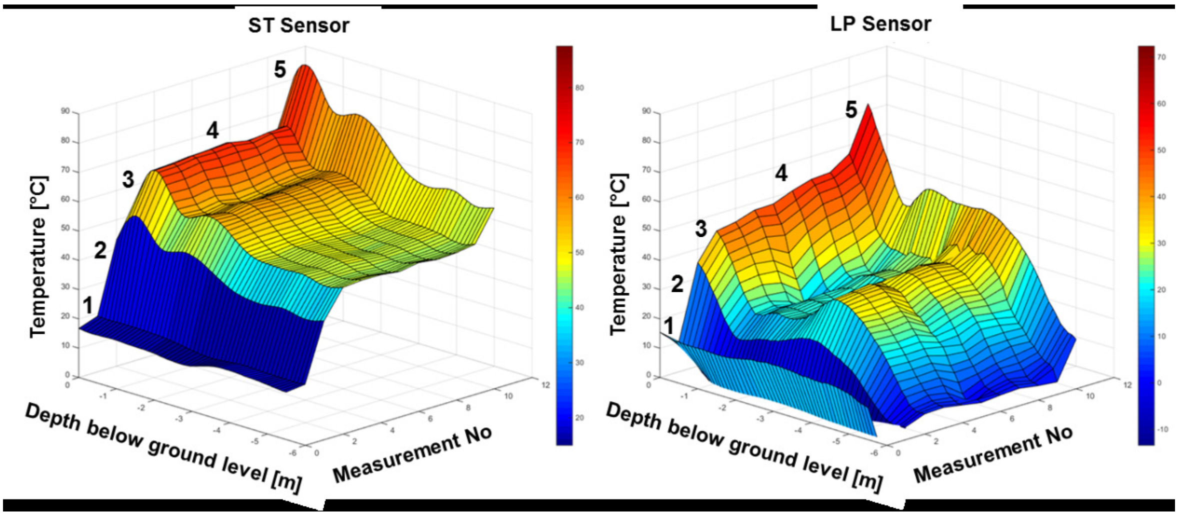

Figure 1. Representation of temperature evolution for ST (left) and LP (right) BOTDA sensors. Sensor performance of the ST sensor is exactly displaying the deployed temperature towards depth and with time. Steps indicate initial equilibration at T=15°C (1), increase to T_{app}=60°C (2), T_{app}=80°C (3), constant temperature at T_{app}=80°C (4) and increase to T_{real}=85°C (5).

16.8

Application of solar numeral system in geosciences.

Bakhram Nurtaev

Institute of Helioclimatology, Kapfenberger Str.17, 50226 Frechen (nurtaev@gmx.net)

The sunspot number time series is the longest record made in science. Almost 400 years of sunspots observation provides a useful tool for studying hydrogeology, engineering geology, geomorphology and climate change. The sun plays a major role in the geological and atmospheric processes. Over many thousands of years, energy from the Sun moves the wind and water at the Earth's surface with enough force to break rocks apart into sand and other types of sediment. Actually all sedimentary rocks came through solar activity: physical and chemical weathering, temperature change diurnal, seasonal, 11 years cycles.

A rise and fall in sunspot counts varies in a cyclical way; the length of the cycle is around eleven years on average, the exact length of the cycle can vary from 8 to 14 years. We have a big accumulated database: about 150 thousand diurnal observations over 400 years for sunspots.

We compared averaged for one solar cycle different solar indices with averaged for the same cycle terrestrial data, such as air temperature, precipitation and river discharge for many weather stations and have found close relationships. This inverse statistical model can explain contribution of solar radiation in many terrestrial processes trends with correlation coefficient more than 0.8.

At present time almost 24 solar cycles have been observed. These 24 cycles measured values of solar indices can be conceived as 24 empirical numeral values for study of terrestrial environmental changes both as in centennial as well as in inter cycle scale.

This study proposes a method of Big Data processing simplification for development of solar terrestrial numeral system in geosciences.

We analyzed the long-term records climate trends in Alpine Region and solar activity and detected close interrelation between these indices.

Results show that above 80% level of statistically significant correlations exist between sunspots and air temperature. Empirical relationships between temperatures in the studied area in dependence on solar activity in weather stations presented below:

Karlsruhe,	T=0,03W +	8,4,	r=0,87
Lugano,	T=0,02W +	10,7,	r=0,81
München,	T=0,02W +	6,6,	r=0,81
Salzburg,	T=0,02W +	6,8,	r=0,77
Stuttgart,	T=0,03W +	7,7,	r=0,81
Zürich	T=0,02W +	7,1,	r=0,87
Bratislava	T=0,02W +	7,7,	r=0,89
Budapest	T=0,02W +	8,9,	r=0,89

where- T is temperature of air in °C, W is the number of sunspots, r- is the coefficient of correlation.The studied period over 1855-1996.

Precipitation trends in the same stations in dependence from solar activity are not so homogeneous, Fig.1

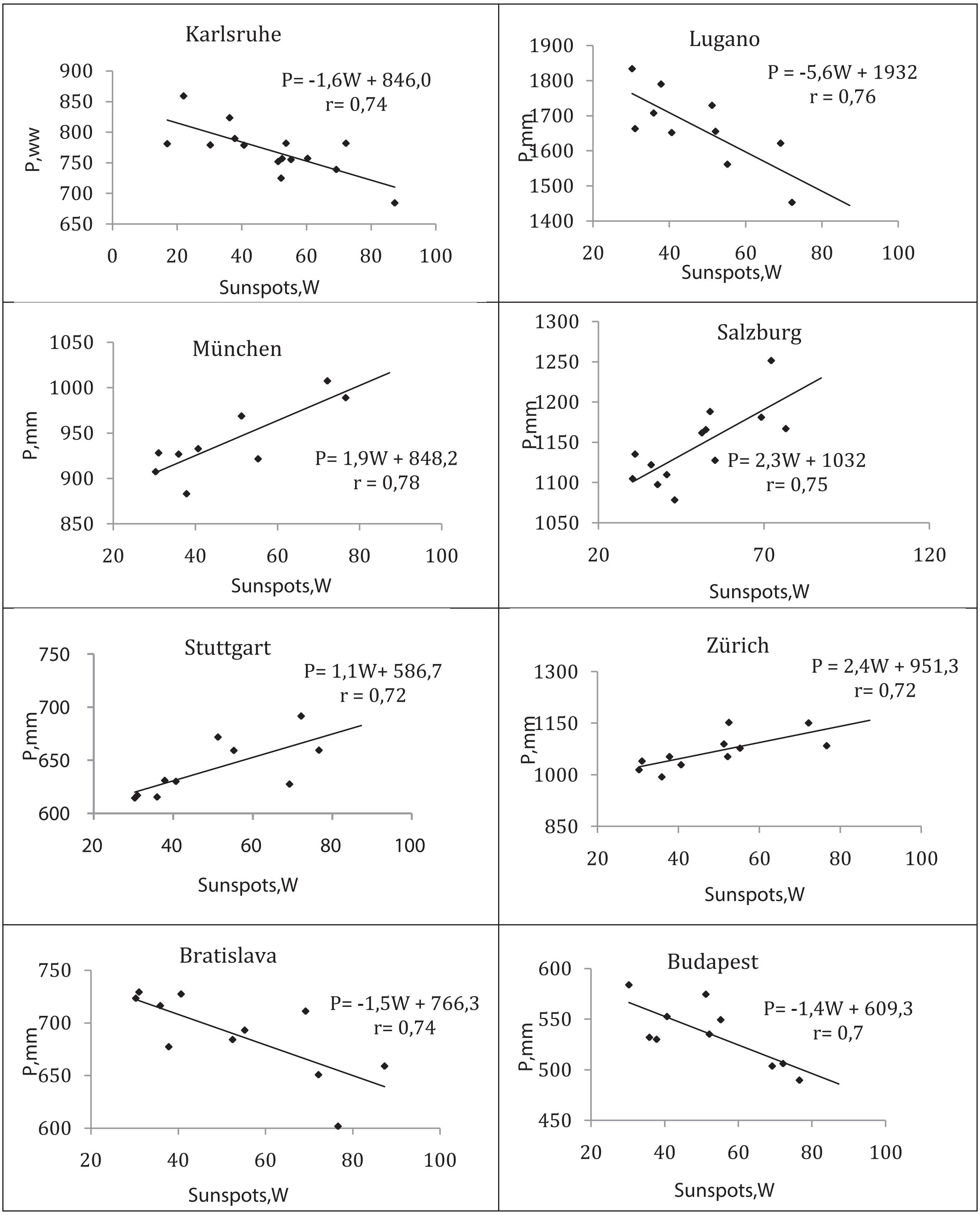

Fig.1. Empirical relationships between precipitation and solar activity over 1878-1996,where P-precipitation in mm, W-number of the sunspots, r-coefficient of correlation.

In accordance with NASA forecasting, the solar cycles 24 and 25 will be very weak, and that will lead to following: the global temperatures will be trending lower over the next 20 years. Precipitation will be change in dependence from geographical location. Source of data -HISTALP.

16.9

Moving research boundaries by enhancing access to Swiss environmental data

Gian-Kasper Plattner[1], Lucia Espona Pernas[1], Ionut Iosifescu Enescu[1], Michael Lehning[2,4] & Konrad Steffen[1,3,4]

[1] *Swiss Federal Research Institute WSL, Zürcherstrasse 111, CH-8093, Birmensdorf*
[2] *WSL Institute for Snow and Avalanche Research SLF*
[3] *ETH Zurich*
[4] *EPF Lausanne*

The amount and quality of environmental data is rapidly increasing. At the same time, challenges related to data sharing and international access to environmental monitoring and research data are rapidly growing. A unified portal allowing simple and efficient access to all kinds of environmental data sets and their metadata does not currently exist. In Switzerland, centralized access to environmental data sets is missing despite plans to move towards open data in the mid- to long-term. Moreover, even a catalogue of existing environmental databases or research data sets is not readily available to interested researchers. Similarly, across Europe, only a few large institutions provide their data in its entirety to the international research community. Institutions have therefore the opportunity to contribute substantially to improving data access across disciplines and thereby moving boundaries and fostering research (Adams, 2013).

The Swiss Federal Research Institute WSL has a long tradition in the collection and curation of environmental research and monitoring data (e.g., Dawes et al., 2008), in particular in the areas of forest and forest ecosystem research but also extending into other fields such as, e.g., snow and natural hazards research (WSL, 2017). Data sets collected by WSL researchers include time series and spatial samplings spanning over one hundred years. WSL operates a comprehensive network for environmental research that includes more than six thousand observation sites for studying the terrestrial environment and its changes in a changing climate.

WSL also succesfully operates environmental web- and data portals and has recently strengthened these activities by developing an overarching Environmental Data Portal (EnviDat). EnviDat facilitates managing, searching, and accessing heretogeneous environmental research data. It is designed to publish, connect and search existing data, rather than a center for the long-term storage of large amounts of research data. The sharing of research data is centrally managed and facilitated; the creation, quality control, and responsibility for curation of the research data, however, remains with the experts and data providers.

EnviDat is based on the conceptual framework illustrated in Figure 1. Its main user requirements include i) to support easy data discovery through full text and map search, ii) to allow publishing of datasets including Digital Object Identifiers (DOI) minting, and iii) to provide a repository for diverse data types. Furthermore, the importance of the future interoperability with the wider data management community influence additional functional requirements such as i) metadata harvesting and provisioning, ii) leveraging existing community software, where possible, and, iii) adoption of national and international standards and best practices in data sharing. A notable example to this end is the decision of building EnviDat based on a reliable software stack that includes CKAN, Apache Solr and PostgreSQL, in a similar manner as pioneered in Switzerland by openresearchdata.ch. Finally, important non-functional requirements such as reliability, security and maintainability are taken into account through a multi-server deployment planned to be finalized in the first half of 2018.

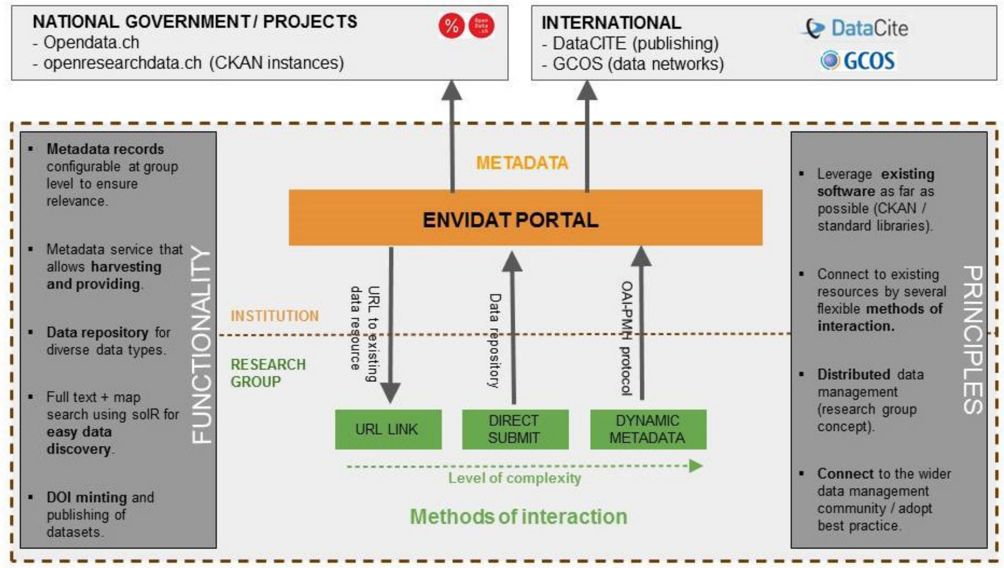

Figure 1. Conceptual framework of the WSL Environmental Data Portal EnviDat. EnviDat serves as an overarching, centralized structure that facilitates publication, searching and accessing of environmental research data. EnviDat offers DOI minting for publication-ready data sets. Data providers decide what, how and with whom to share their research data. The metadata can be searched efficiently through a number of data discovery options. Data providers have the possibility to link data sets, photos and other resources.

As the boundaries in science are moving towards cooperation among research communities, WSL aims to advance environmental science through EnviDat. The availability of rich environmental data in an accessible and effective system such as EnviDat opens unprecedented opportunities for advancing environmental science. The resulting distribution and sharing of data is expected to bring together scientists from different disciplines and to foster new national and international collaborations.

REFERENCES

Adams, J. 2013. Collaborations: The fourth age of research. Nature, 497(7451), 557–60. doi:10.1038/497557a

WSL 2017. http://www.wsl.ch/forschung/index_EN

Dawes, N., Kumar, A.K., Michel, S., Aberer, K., Lehning M., 2008. Sensor metadata management and its application in collaborative environmental research, 4th IEEE E-Science Conference, DOI:10.1109/eScience.2008.27.

16.10

Visualisation and analysis of landscape change using crowdsourced historical photographs

Produit Timothée[1], Ingensand Jens[1]

[1] *Territorial Engineering Institute, University of Applied Sciences and Arts Western Switzerland, CH-1401 Yverdon-les-Bains (timothee.produit@heig-vd.ch)*

Mountain areas have been subject to the effects of human activities that are either direct (e.g. construction of infrastructures) or indirect (e.g. global warming). In order to understand these effects, it is important to offer tools to monitor and analyze the variations during a period of time. These variations are very slow at the time scale of a human being. Hence, there is also the need of showing and communicating these changes to the public and to exhibit the impact of for instance climate change and land planning policies.

Currently, mainly two types of remote sensing data are used to monitor landscape change in mountainous environments: 1) satellite images but the first images were shot in 1972 and had a very rough spatial resolution. 2) Photogrammetric survey started in 1915 in Switzerland, they are used to generate 3D models or orthophotos. On the other hand, photographs of mountain areas exist since the middle of the 19th century and are precise snapshots of the landscape. Unlike most of the photogrammetric images which are top views, photographs are shot with an oblique point of view which is closer to our natural viewpoint. Generally, photographs can not be processed with state of the art photogrammetric software. In Switzerland, Bozzini and Produit have developped a system to compute the location of a single photograph and extract geographic information from it. However collections of photographs remain an underused medium since they are a) often not available in a digitized form b) often stored in disseminated archives that are not easily accessible to researchers c) lack a georeference.

Scientists are mostly interested in metrics of landscape change such as measuring the extent of a natural disaster or the evolution of an area. However, to communicate the landscape variation to the general public the visualization of the variation is sufficient. *swisstopo* provides a web map which shows the evolution through topographic maps. *Google earth engine* uses satellite images to show time-lapses, but it is limited by the quality of past satellite images. Many authors prefer photographs to show changes, because they are closer to our real view. An common method is called rephotography which is a repeated photograph of a historical photograph. Both images can be overlaid and easily compared. This method is widely used in books and web sites. It has the advantage of showing the variation with a natural viewpoint.

The goal of our web platform smapshot is to 1) group disseminated collections in a single platform 2) compute the exact location and orientation of photographs 3) provide a virtual globe to show the landscape variation in mountainous areas through photographs.

Federate collections: smapshot gathers private and public collections of landscape photographs and stores these photos in an efficient geographic search engine. Hence, we ease the access to landscape photographs for both the general public and professionals.

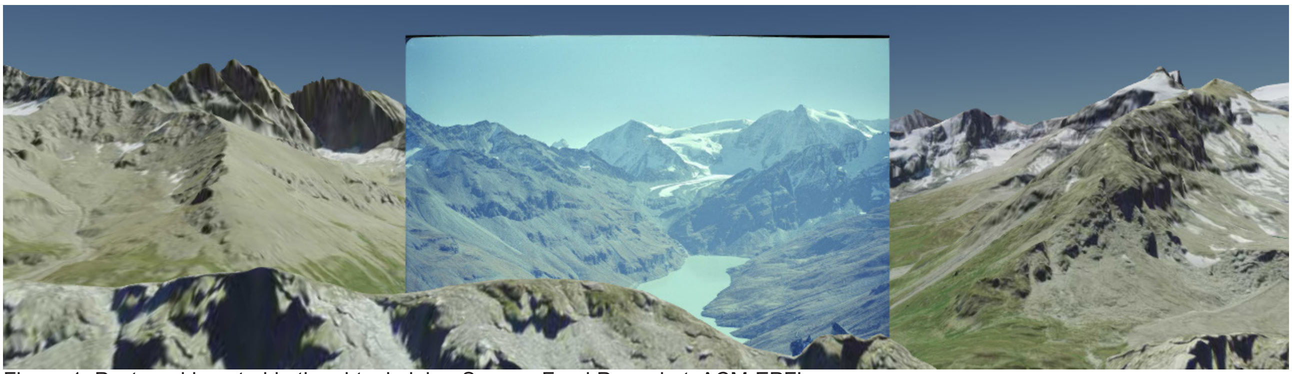

Figure 1. Post card inserted in the virtual globe. Source: Fond Perrochet, ACM-EPFL

Georeferencing: smapshot uses crowdsourcing to find the exact location and orientation of the photographs. To accomplish this goal, we developed a web-based 3D georeferencer. This module computes the photograph location and orientation based on corresponding points where a volunteer clicks in the photograph and in a virtual globe.
The exact location and orientation enables us to compute the points of interest which are visible in the photographs. This information is delivered to the archivists who use it to enrich their collections.

Virtual globe: Finally, the photographs are placed in a virtual globe (Figure 1). The general public can navigate through the virtual space to compare the current virtual landscape with the photographs.

The prototype is currently tested with collections of swiss landscape photographs. Indeed, the mountains of Switzerland have two advantages. First, the jagged horizon line eases georeferencing. Second, mountain areas show drastic changes such as the enlargement of mountain resorts and the retreat of glaciers. Our community of volunteers provides an accurate georeferencing of most of the 1500 photographs stored in the platform. Hence, we can notice that in famous areas, such as the Matterhorn region, photographs provide a continuous remote sensing of the landscape with a high spatial accuracy. This is very promising both from a geospatial scientific point of view to study the landscape evolution and from a web-design point of view to develop time-lapse modules.

In the future, we would like to develop tools dedicated to scientists and other professionals such as land planners and geographers. These tools could be used to improve the geolocation provided by the volunteers and extract accurate 2D and 3D geographic information from the photographs. Moreover machine learning algorithms can be developed and used to automatically detect and classify changes.

REFERENCES

Produit, T., Tuia, D. 2012,An open tool to register landscape oblique images and generate their synthetic model, Open Source Geospatial Research and Education Symposium (OGRS)

Bozzini, C., Conedera, M., Krebs, P., 2012, A new monoplotting tool to extract georeferenced vector data and orthorectified raster data from oblique non-metric photographs, International Journal of Heritage in the Digital Era

16.11

Moving national boundaries – reasons, documentation and backtracking

Adrian Wiget, Alain Wicht

Federal Office of Topography swisstopo, Seftigenstrasse 264, 3084 Wabern

The final definition of the current Swiss national boundary was decided at the Vienna Convention in 1815, along with other European boundaries. Is this definition unchangeable? Generally speaking, yes, especially where it is artificially defined and marked by the more than 7000 boundary monuments – mostly artfully carved stones and interconnected by straight lines. But there
are areas where the two neighbouring countries have agreed on «natural boundaries».

Natural boundaries are formed by lakes, flowing waters and mountains. In lakes and flowing waters the boundary usually runs through the middle of these bodies of water. Alternatively, it may follow the deepest channel in the riverbed, the so called «Talweg» – basically the middle of the river at lowest water level. An example of this is the Rhine River along the Cantons of Aargau and Basel-Land on the border to Germany. It may also follow the river bank, e.g. on the Swiss side along the Doubs River in the Canton of Jura. In the mountains a crest, the so-called «water divide», is commonly defined as a natural boundary.

The course of natural boundaries may vary with time because of natural changes. Examples are meandering rivers or crest changes caused by rockfalls. Especially noticable are changes in the water divide on glaciers when they retreat or advance (the second is less likely to happen these days). Theses variations can reach several meters per year and therefore cause relatively large surface-changes.

Figure 1. Glaciers in the Monte Rosa area, Canton Valais (VS)

This paper presents reasons and examples of moving national boundaries. Furthermore, we show how the representation and documentation of the national boundary has changed from old historic maps to modern GIS techniques and how changes in the boundary line can be backtracked.

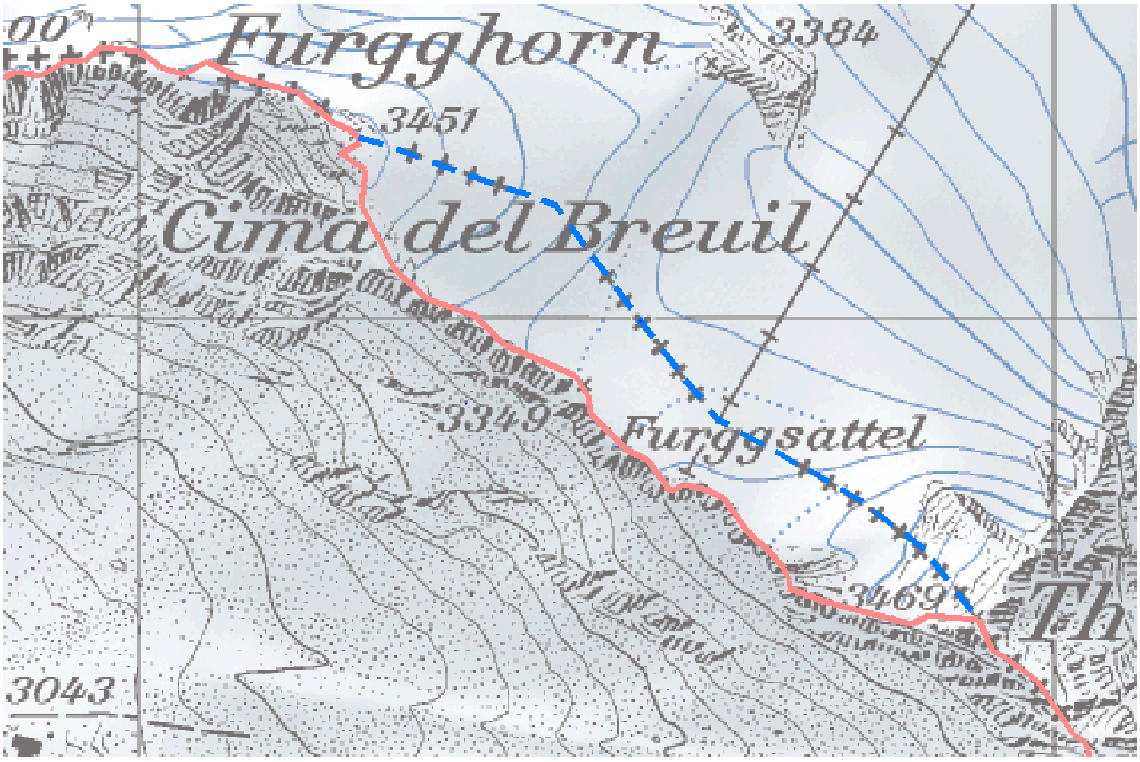

Figure 2. National boundary at Furggsattel (VS) with old (2008, in blue) and new boundary lines (in red) indicated on the topographic map.

Figure 3. Retreat of the Theodul-Glacier viewed from the Furggsattel towards the Matterhorn.

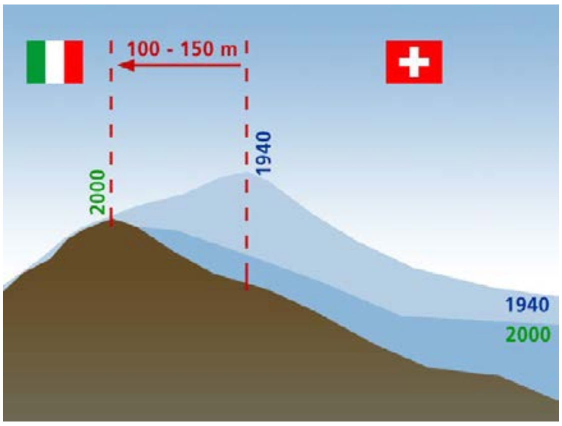

Figure 4. Schema showing boundary on top of the water divide moving as a result of a retreating glacier.

REFERENCES

https://www.swisstopo.admin.ch/en/knowledge-facts/sovereign-border/national-boundary/moving-boundaries.html

P 16.1

Optimisation of borehole trajectory in order to minimize borehole failure

Asmae Dahrabou[1], Benoît Valley[1], Florentin Ladner[2], Frédéric Guinot[2], Peter Meier[2]

[1] *Centre for Hydrogeology and Geothermics (CHYN), University of Neuchâtel, Emile-Argand 11, CH-2000 Neuchâtel (asmae.dahrabou@unine.ch, benoit.valley@unine.ch)*
[2] *Geo-Energie Suisse AG, Reitergasse 11, 8004 Zürich. (f.ladner@geo-energie.ch, f.guinot@geo-energie.ch, p.meier@geo-energie.ch)*

In the frame of a CTI-project the CHYN and Geo-Energie Suisse AG are developing a workflow and associated software tools that allow a fast decision-making process for selecting an optimal well trajectory while drilling deep inclined wells for EGS-projects. The goal is to minimize borehole instabilities and maximize the intersection with natural fractures. Minimizing borehole instability enhances drilling performance and is required when the open hole is completed with swellable packers. Maximizing the intersection with natural fractures increases overall productivity or injectivity of the well. The specificity of the workflow is that it applies to crystalline rocks and includes an uncertainty and risk assessment framework.

Fundamentally the understanding of borehole failure in deep crystalline well is lacunar because the strength and stress parameters are largely unknown independently. Moreover, there is no agreement on the appropriate failure model required to capture all characteristics of borehole failure. A sensitivity study performed on data from the well BS-1 (DHM project Basel) showed that the most influential parameters on borehole stability are the magnitude of the maximum horizontal stress, the uniaxial compressive strength and the internal borehole pressure.

Three geometry descriptors that are potentially more relevant to packer sealing integrity were investigated: breakout width, breakout depth, borehole cross sectional area and the overall final shape of the borehole. Analytical models assuming an elastic-brittle behavior without stress redistribution were calibrated to these observations using various failure criteria. The commonly used Mohr-Coulomb failure criterion was unable to find calibrated parameters satisfying all failure indicators. Thus, alternative failure criteria were tested eventually showing that a purely cohesive failure criterion with no friction ($\phi = 0°$) allows a more consistent calibration across the failure indicators (Fig.1). This result is consistent with the literature that indicates that breakout formation is a cohesion weakening process (Diederichs, M.S. 2007, Damage and spalling prediction criteria for deep tunnelling). In further analyses, the frictionless failure criterion was used. Another difficulty is that the calibrated models on the vertical borehole section lead to non-unique and inconsistent predictions for deviated wells (Fig.2) because of the very simple model used that cannot entirely capture the failure processes.

Moreover, a pragmatic calibration approach was chosen: firstly, realistic ranges for both SHmax and UCS were computed based on admissible stress limits and secondly, independent data (sonic and density data) were used as a proxy to approximate the strength. Eventually, a complete workflow was developed to provide a systematic approach in selecting the optimum drilling direction. In order to select representative scenarios representing different behaviors substantially affecting the decision, cluster analysis will be performed. In fact, It is a multivariate method which aims to classify the different computed scenarios on the basis of different variables (breakout width, breakout depth, fracture frequency), into a number of different groups such that similar scenarios are placed in the same cluster. These analysis will help to select only distinct scenarios having different behaviors in terms of borehole failure and fracture frequency. These results will form the basis of an integrated workflow optimizing geothermal (EGS) well trajectory.

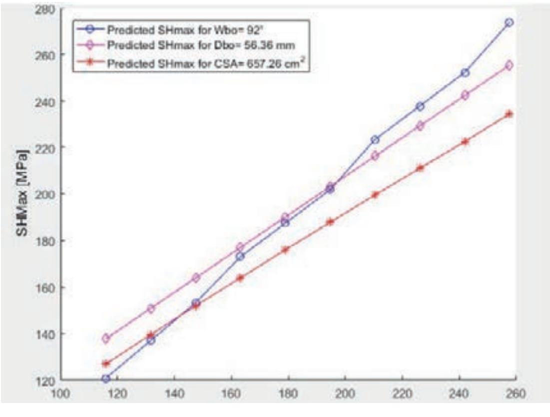

Figure 1. The calibrated couples (SHmax, UCS) for a vertical hole (borehole dip direction = 0°, borehole deviation =0°) for z=3509m with Mohr-Coulomb failure criteria for breakout width calculations and the purely cohesive criteria for both breakout depth and cross sectional area calculations.

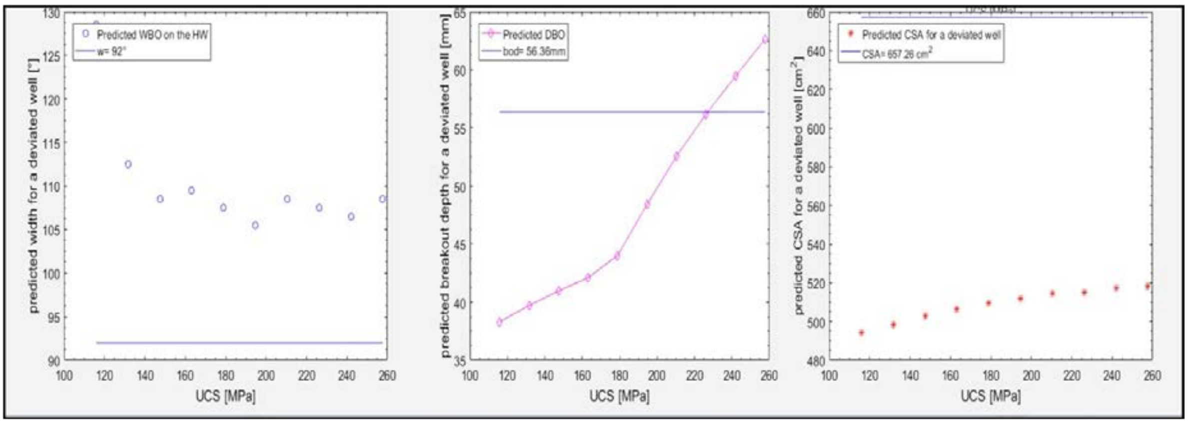

Figure 2. a) The predicted breakout width, b) breakout depth and c) cross sectional area for a horizontal well (deviaton = 90°, dip direction= 0°) using the calibrated couples (SHmax,UCS), obtained in Fig.1. Horizontal lines correspond to the observed values.

REFERENCES

Diederichs, M.S. 2007. The 2003 CGS Geocolloquium Address: Damage and spalling prediction criteria for deep tunnelling. Can. Geotech. J., Vol. 44: 9, pp. 1082-1116(35)

P 16.2

Uncertainty quantification in environmental data driven modelling using machine learning

Fabian Guignard[1], Michael Leuenberger[1] & Mikhail Kanevski[1]

[1]Institute of Earth Surface Dynamics (IDYST), University of Lausanne, CH-1000 Lausanne (fabian.guignard@unil.ch)

Nowadays, the amount of geo- and environmental data has considerably increased due to the development of new and efficient monitoring systems and remote sensing technologies. It requires development of contemporary tools to analyze, model and visualize the data and the results. Machine learning algorithms in this new emerging discipline – environmental data science – play a key role.

The present research deals with an adaptation of recently introduced algorithm, called Extreme Learning Machine (ELM), to the environmental data modelling and spatio-temporal predictions. An important contribution of the work deals with the quantification of prediction uncertainties which is decomposed into the following parts:

1) the uncetainty produced by the modeling error and
2) the uncertainty produced by measurement errors, in other words the data noise.

ELM was introduced by Huang et al. in 2006. It is a very fast one hidden layer feedforward neural network with randomly generated weights between inputs and hidden layer. Due to its speed and stochastic nature, it is common to repeat computations several times to reduce the variability produced by the random weights and thus ensure prediction quality. These repetitions allow us to estimate separately the variability induced by the model and the variability induced by the data noise.

Both uncertainty components can be visualized as maps, providing geographical places where data problems appears, e.g. existing measurements need to be controlled, or additional measurements are necessary. In particular, the model uncertainty map provides places where the model can be improved (active learning) and the measurement uncertainty map provides places where the noise can be reduced by more precise additional measurement.

This new method is tested on both simulated and real environmental datasets.

REFERENCES

Huang, G.-B., Zhu Q.-Y. & Siew C.-K.. 2006: Extreme learning machine: theory and applications. Neurocomputing, 70, 489-501.

P 16.3

Towards probabilistic full-waveform inversion

Jürg Hunziker[1], Eric Laloy[2] & Niklas Linde[3]

[1] *University of Lausanne, Applied and Environmental Geophysics Group, Institute of Earth Sciences, Lausanne, Switzerland (jurg.hunziker@unil.ch)*
[2] *Belgian Nuclear Research Center, Mol, Belgium (eric.laloy@sckcen.be)*
[3] *University of Lausanne, Applied and Environmental Geophysics Group, Institute of Earth Sciences, Lausanne, Switzerland (niklas.linde@unil.ch)*

Full-waveform inversion is a highly non-linear process, which requires the starting model for deterministic inversions to be relatively close to the correct solution (Virieux and Operto, 2009). Otherwise, the algorithm will be trapped in a local minimum. To circumvent this problem, we propose a probabilistic approach for full-waveform inversion. Our approach also has the advantage that prior information can be included in the form of a prior-probability distribution. Furthermore, as we do not only retrieve one solution as it is the case for deterministic algorithms, but a set of solutions sampled from the posterior distribution, an uncertainty quantification is straightforward. The main disadvantage of our approach is the long runtime. A probabilistic inversion approach requires that the forward problem is evaluated several 100'000 times, while a deterministic approach only needs several dozens of forward evaluations. Another disadvantage is that probabilistic algorithms can only solve for a limited amount of unknowns within a useful runtime.

In this study, we show preliminary results of our probabilistic inversion approach to a crosshole full-waveform inversion problem using Ground Penetrating Radar (GPR). Our probabilistic inversion approach uses an efficient implementation of the Markov chain Monte Carlo (MCMC) algorithm (Laloy and Vrugt, 2012; ter Braak and Vrugt, 2008). To reduce the amount of unknowns, we assume that the subsurface can be represented as a multi-Gaussian field and reduce the dimensionality of the problem using circulant embedding (Dietrich and Newsam, 1997). We invert simultaneously for 250 dimension reduction variables describing the subsurface structure, 6 parameters describing the geostatistical model and the standard deviation of the data error, resulting in a total of 257 unknowns. More details about the algorithm can be found in Hunziker et al. (2017).

We created synthetic data based on the subsurface model shown in Figure 1(d). The inversion of these data was run three times. The last model of these three inversion runs is shown in Figure 1(a)-1(c). From each inversion run, we selected from the second half of the Markov chains at regular intervals 128 models. From these 384 models, a mean model (Figure 1(e)) and the standard deviation (Figure 1(f)) were computed. Please note, that as the chains just started sampling the posterior distribution, these last two plots do not properly represent the posterior distribution. However, they demonstrate that the algorithm works properly as it was able to find subsurface models that are close to the true model. The standard deviation is large in between the source positions in the left borehole, indicating that more source locations are necessary to illuminate the subsurface well enough.

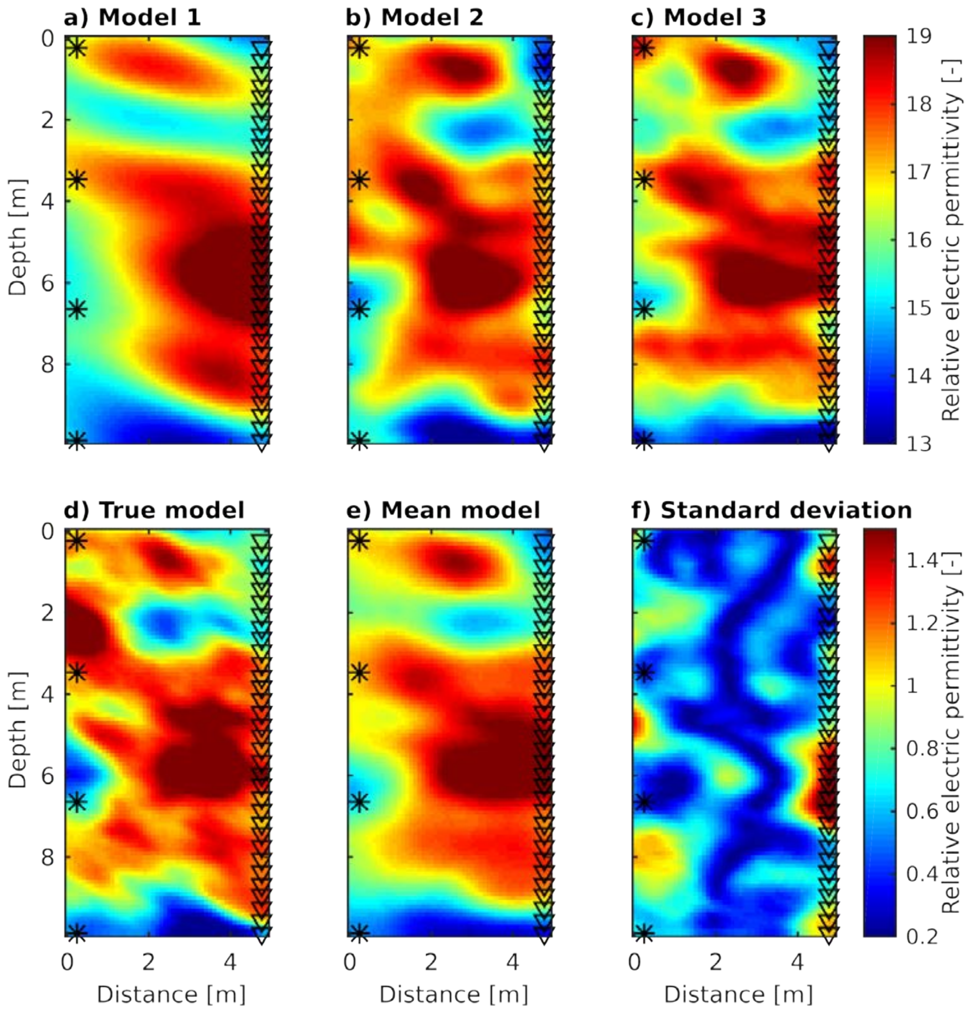

Figure 1. Results of our crosshole probabilistic full-waveform inversion with indicated sources (asterisks) and receivers (triangles). (a) - (c): The last model of three different inversion runs, (d): the true model, (e): the mean model based on 384 models (128 from each run), (f): standard deviation of these 384 models. The colorbar of plot (c) is valid for plots (a) to (e).

REFERENCES

Dietrich, C.R. & Newsam, G.N. 1997: Fast and exact simulation of stationary Gaussian processes through circulant embedding of the covariance matrix, SIAM Journal of Scientific Computation, 18, 1088 – 1107.

Hunziker, J., Laloy, E., & Linde, N. 2017: Addressing the non-linearity of full-waveform inversion with a probabilistic approach, EAGE Near Surface Geoscience 2017, conference proceedings.

Laloy, E. & Vrugt, J.A. 2012: High-dimensional posterior exploration of hydrologic models using multiple-try DREAM (ZS) and high-performance computing, Water Resources Research, 48, WO1526.

ter Braak, C.J.F. & Vrugt, J.A. 2008: Differential Evolution Markov Chain with snooker updater and fewer chains, Statistics and Computing, 18(4), 435– 446.

Virieux, J. & Operto, S. 2009: An overview of full-waveform inversion in exploration geophysics, Geophysics, 74(6), WCC1–WCC26.

P 16.4

Multifractal Detrended Fluctuation Analysis of Wind Speed Connectivity Density Time Series

Mohamed Laib[1], Luciano Telesca[2], Mikhail Kanevski[1]

[1] *IDYST, Faculty of Geosciences and Environment, University of Lausanne, Switzerland.*
[2] *CNR, Istituto di Metodologie per l'Analisi Ambientale, Tito (PZ), Italy.*

Meteorological services have been developing sensors to record environmental parameters with higher and higher frequency; that is crucial to analyse complex, multivariate, and non-linear meteo-climatic phenomena. However, to extract information and understand the underlying dynamical mechanisms of these phenomena, we need robust and advanced statistical methods.

Among the environmental variables, wind speed is very important for the implications in terms of sustainable energy issues. Several studies have been carried out on wind speed, by using machine learning algorithms, time series forcasting, fractal analysis, multifractal analysis, visibility graph, and complex network.

In the present work, we use correlation network and multifractal analysis to investigate the inner structure of the wind speed. Even more, we study the wind phenomena by combining three diffferent aspects: spatial (due to the spatial distribution of the meteorological sensors), temporal (due to the analysis of the network topology on a daily basis), and correlative (due to the selection of the correlation threshold, by which the topology of network is defined).

The study is focused on the daily correlation network (between wind measuring stations) at several thresholds (see Fig. 1). These networks are characterised by the connectivity density, which measure the proportion of wind sensors that are correlated among them. A daily time series of connectivity density is obtained for the period time between 2012 and 2016.

Finally, we apply the multifractal detrended fluctuation analysis (MFDFA) to detect the presence of long-range propreties in the connectivity density time series and quantify possible intermittency. As an example, Fig. 2 shows the results of the MFDFA applied on the connectivity density time series for threshold 0.5.

The present study would contribute to better understand the wind processes in complex areas, like Switzerland. Furthermore, it would help a better planning and design of the characteristics of a wind monitoring system.

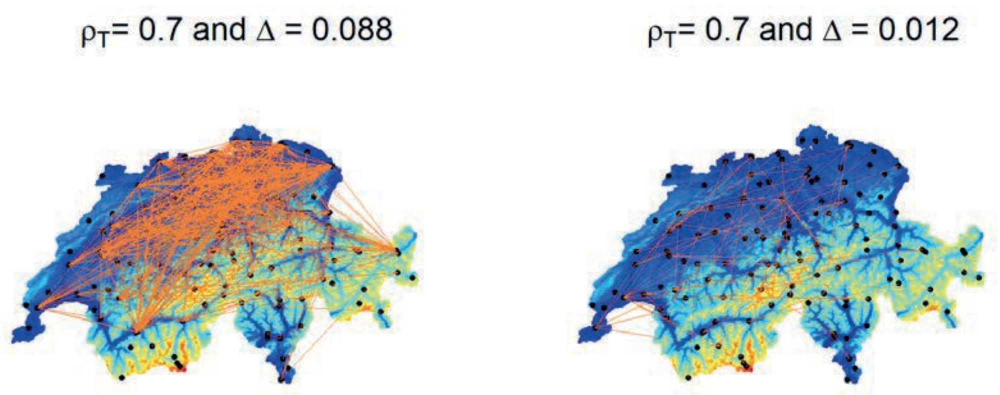

Figure 1: Correlation networks for two different days considering a threshold of 0.7 (April 9, 2012 and September 4, 2016).

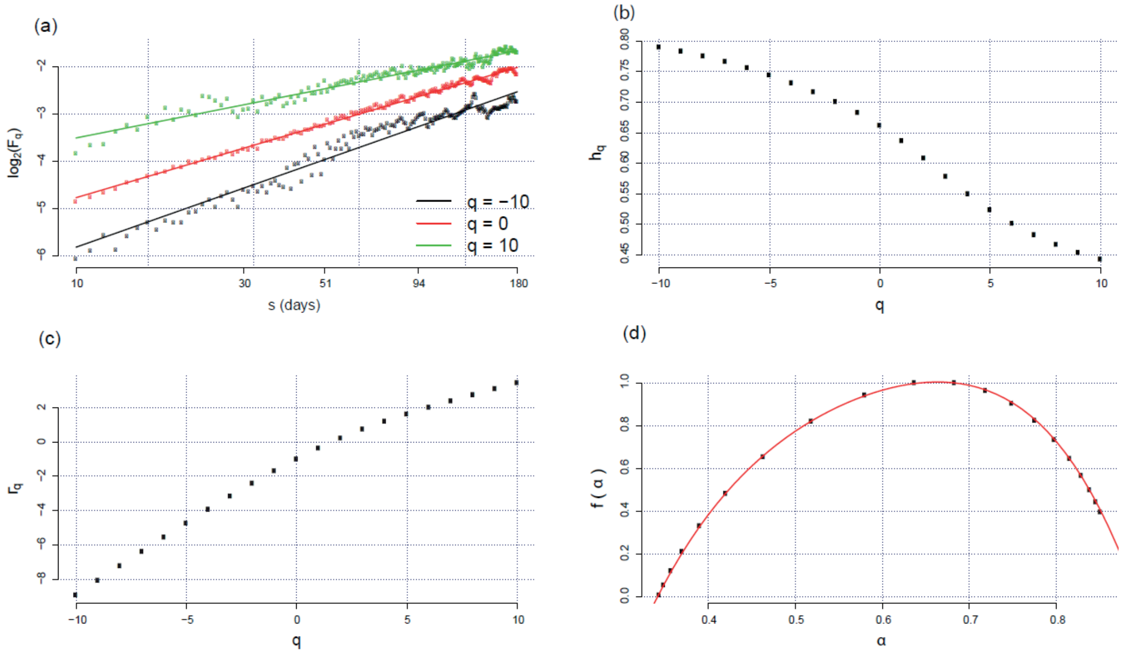

Figure 2: MFDFA results for; (a) fluctuation functions; (b) generalized Hurst exponents; (c) -; (d) multifractal spectrum.

REFERENCES

J. W. Kantelhardt, S. A. Zschiegner, E. Koscielny-Bunde, S. Havlin, A. Bunde, H. Stanley, Multifractal detrended fluctuation analysis of nonstationary time series, Physica A: Statistical Mechanics and its Applications 316 (1) (2002) 87 – 114.

Mohamed Laib, Luciano Telesca, Mikhail Kanevski, Long-range fluctuations and multifractality in connectivity density time series of a wind speed monitoring network, 2017, arXiv:1708.04216.

P 16.5

Integration of open-source hardware in a low-power, low-cost system to monitor thermally-driven rock fracturing

Kerry Leith[1], Matthew Perras[2], Simon Loew[1]

[1]*Geological Institute, ETH Zurich, Sonneggstrasse 5, CH-8092 Zurich (kerry.leith@erdw.ethz.ch)*
[2]*Department of Civil Engineering, York University, 4700 Keele St, Toronto ON. M3J 1P3 Canada*

The global increase in atmospheric temperatures may be accelerating rockfall and landsliding as result of the physical breakdown of bedrock landscapes. Effects may include thermomechanical fracturing of intact bedrock, stress corrosion as a result of water infiltration into normally dry fracture systems (e.g. in arid or permafrost regions), debuttressing as a result of glacier retreat, and rockfalls resulting from a reduction of permafrost in high alpine rock walls. The last few years have seen changes in temperature and/or climate implicated in events occurring at sea level in the Finnish Archipelago (Leith et al., 2017), 1000 m a.s.l. in the Sierra Nevada (Collins et al., 2017), 2000 m a.s.l. in the central Swiss Alps (Kos et al., 2016), and at over 3000 m a.s.l. in the Mont blanc massif (Ravanel et al., 2017). The broad spatial range, incipient nature of associated fracturing, and lack of insight into mechanisms driving rock breakdown (which ultimately facilitates these events), calls for a new low-cost, versatile, and distributed approach to data collection.

Leveraging the increasing popularity of open-source electronics platforms (specifically the Arduino hardware), community-based software development projects, and low-power mini-PC's, we present details of an installation incorporating off-the-shelf sensors with a simple data acquisition platform and tried-and-tested microacoustic monitoring monitoring system to determine the mechanisms responsible for the thermomechanical fracturing of a bedrock island in the Finnish Archipelago (Figure 1). Notably, we incorporate a full weather station, 1 m long bedrock temperature strings, a crack aperture gauge, and continuous acoustic emission monitoring to observe the bedrock response to environmental conditions. Independent remote data access and power management systems allow us to remotely manage the observation system. The data gathered has allowed us to model thermoelastic efects in the subsurface, and characterize the bedrock response to strong thermal cycles during the summer of 2016.

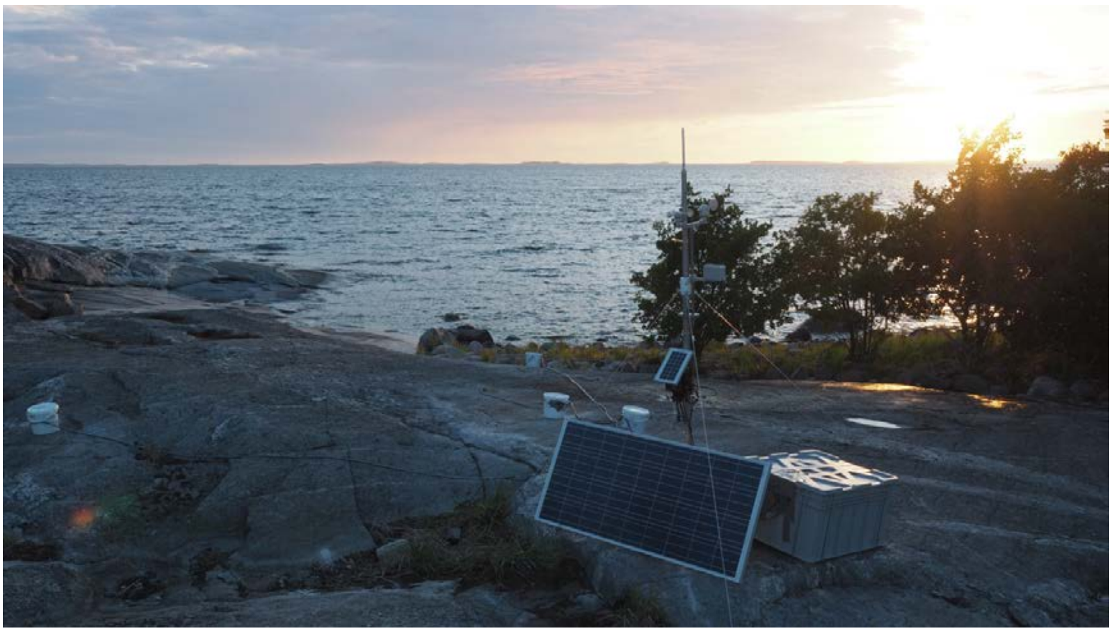

Figure 1. The installed monitoring system on Långören Island, Finland.

REFERENCES

Collins, B.D., Stock, G.M., Eppes, M.C., 2017. Progressive thermally induced fracture of an exfoliation dome: Twain Harte, California, USA, in: Leith, K., Ziegler, M., Perras, M., Loew, S. (Eds.), Progressive rock failure conference 2017. ETH Zurich, Zurich, Switzerland, Ascona, Switzerland, pp. 15 - 16.

Kos, A., Amann, F., Strozzi, T., Delaloye, R., von Ruette, J., Springman, S., 2016. Contemporary glacier retreat triggers a rapid landslide response, Great Aletsch Glacier, Switzerland. Geophysical Research Letters 43, 12,466-412,474.

Leith, K., Perras, M., Siren, T., Rantanen, T., Wolter, A., Heinonen, S., Loew, S., 2017. Development of a new thermally-induced fracture in a 12,000 year old bedrock surface, in: Leith, K., Ziegler, M., Perras, M., Loew, S. (Eds.), Progressive rock failure conference 2017. ETH Zurich, Zurich, Switzerland, Ascona, Switzerland, pp. 17 - 19.

Ravanel, L., Magnin, F., Deline, P., 2017. Impacts of the 2003 and 2015 summer heatwaves on permafrost-affected rock-walls in the Mont Blanc massif. Science of The Total Environment 609, 132-143.

P 16.6

Intraplate volcanism in northeast China due to upwellings rising from the stagnant slab

Xiaogang LONG[1,2], Maxim D. Ballmer[1]

[1] *Institut für Geophysik, Departement für Erdwissenschaften, ETH Zürich, 8092 Zürich, Switzerland*
[2] *School of Ocean and Earth Science, Tongji University, Siping Road 1239, 200092, China*

Major intraplate hotspot volcano chains are well explained by plume theory. However, the mechanisms for non-hotspot continental intraplate volcanism remains controversial. Intraplate continental volcanism commonly occurs in regions located above stagnant subducted slabs, such as in northeast China. Here, we explore the role of the stagnant slab and of mineral water stored in the transition zone for the formation and evolution of intraplate volcanoes in northeast China. We explore two-dimensional regional models of convection in the upper and mid mantle. The effect of water on melting behavior and density are considered. We find that the stagnant slab is unstable and will extend laterally in the transition zone. Upwellings rise from the edges of the slab, out of the warm and buoyant harzburgite underbelly of the slab, as well as from the hydrous layer atop the slab within a couple of Myrs. They rise to ~400 km depth and are then entrained by sub-lithospheric small-scale convection cells to reach the base of the lithosphere after a couple of tens of Myrs. The volumes, patterns and composition of related decompression melting depend on model parameters, such as e.g. the water content in the hydrous layer above the slab. We also explore the effects of lateral heterogeneity within the slab and find that even small heterogeneity is sufficient to significantly advance convective instability, and thus the timing and volumes of related mantle melting. The study of intraplate continental volcanism can indeed improve our understanding of upper-mantle and transition-zone dynamics.

P 16.7

A prospective scenario for Rural Urban Interface based on spatio-temporal LULCC

Marj Tonini[1], Federico Amato[2], Mikhail Kanevski[1], Beniamino Murgante[2]

[1] *Institute of Earth Surface Dynamics, Faculty of Geosciences and Environment, University of Lausanne, CH-1015 Lausanne, Switzerland (marj.tonini@unil.ch)*
[2] *University of Basilicata, Viale dell'Ateneo Lucano 10, 85100 Potenza, Italy*

The Rural Urban Interface (RUI) define the area where humans and their development intermix with wildland fuels, including forest and rural areas. Here human-caused wildfires are more likely to occur and represent a main hazard for people, houses and infrastructures. Compounded by climate changes, urban growth and the fragmentation of rural areas, RUI represents at present the central focus of wildland fire policy and has been identified by recent studies as the most fire prone surface.

Current approaches proposed by the scientific community to map the RUI are prevalently GIS based, marked by the use of a buffer at a pre-defined distance around buildings which define an area overlapping the wild vegetation and forest covers (Conedera et al., 2015). Such maps represent a useful support tool for fire managers but, from a scientific perspective, this procedure does not account for uncertainty (Uusitalo et al., 2015). Moreover, the extension of the RUI changes both spatially and temporally as a result of environmental and anthropogenic variables. A typical example is the urbanisation, following the abandonment of remote rural areas, which increases the likelihood of wildfires to affect houses and infrastructures, prompting the RUI's expansion. Therefore, the delimitation of the RUI is closely relate to the land use/land cover changes (LULCC). In European countries the recent trend in LULCC is characterised by the abandonment of rural areas under the pressure of urbanization and the expansion of costal touristic centers (Antrop, 2004). Therefore, low-intensity agriculture, grazing practices and other rural activities are more and more abandoned, causing the intensification of forest covers and scrubland vegetation, especially in poor accessible areas.

In the preset study authors propose an innovative approach to define the Rural Urban Interface, which escape from the definition of fixed boundaries and their dependence from predefined parameters (Kanevski M., 2008). As an alternative, we introduce an new procedure based on Multilayer Perceptron (MLP) and Fuzzy Set Theory (FST). MLP was first applied to model the probability of having changes in land cover (Eastman et al., 2005), and then FST was used to derive maps expressing the possibility of an area of being included in the RUI. This methodology allowed to elaborate future RUI scenario (for the year 2030) based on the transition between the past (year 1990) and the current land cover (year 2012), including driving variables for urban and rural development (e.g. census data, distance from roads, DEM and derivatives). The case study is Portugal, a country in the Mediterranean basin particularly affected by fires (Tonini et al., 2017), but the model is applicable worldwide. As rusult we obtained continuous and non-categorical 'fuzzy' maps expressing the degree of possibility of being RUI in the near future (Figure 1).

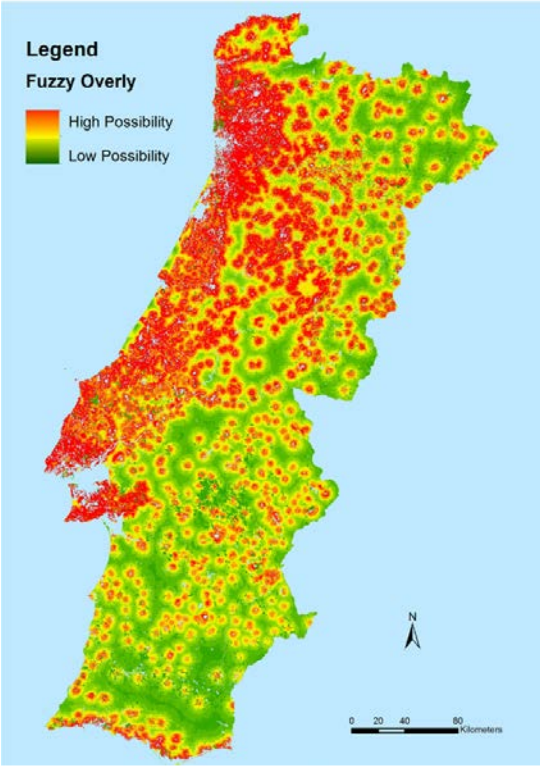

Figure 1. Possibility RUI map for the year 2030 in Portugal. This map was obtained applying Multilayer Perceptron to model the probability of having changes in land cover, followed by fuzzy overlay to combine the predicted changes.

REFERENCES

Antrop, M., 2004. Landscape change and the urbanization process in Europe. Landscape and Urban Planning, 67(1–4), pp.9–26.

Conedera, M., Tonini, M., Oleggini L., Vega Orozco, C., Leuenberger, M., Pezzatti, G. B., 2015. Geospatial approach for defining the Wildland-Urban Interface in the Alpine environment. Computers, Environment and Urban Systems, 52, pp.10–20.

Eastman, J., Van Fossen, M.E. & Solarzano, L.A., 2005. Transition potential modeling for land cover change. GIS, spatial analysis and modeling, ESRI Press, California, pp.357–386

Kanevski, M., 2008. Advanced mapping of environmental data: Geostatistics, Machine Learning and Bayesian Maximum Entropy. Kanveski M. (eds.)., 5072 328, ISTE Ltd and Wiley Press.

Tonini, M., Pereira, M.G., et al., 2017. Evolution of forest fires in Portugal: from spatio-temporal point events to smoothed density maps. Natural Hazards, 85(3), pp.1489–1510.

Uusitalo, L., Lehikoinen A., Helle I., Myrberg, K., 2015. An overview of methods to evaluate uncertainty of deterministic models in decision support. Environmental Modelling & Software, 63, pp.24–31.

P 16.8

GeoQuat project: Benefits of standardization and automation for analyzing and modelling data from Quaternary deposits.

Philip Wehrens[1], Stefan Volken[1], Giona Preisig[2], Michael Gaehwiler[3], Andreas Möri[1]

[1] Federal Office of Topography swisstopo, Swiss Geological Survey (SGS), Seftigenstrasse 264, CH-3084 Wabern bei Bern
[2] Center for Hydrogeology and Geothermics, Rue Emile-Argand 11, CH-2000 Neuchâtel
[3] Service de géologie, sols et déchets (GESDEC), Quai du Rhône 12, CH-1205 Genève

In Switzerland, approximately 90% of subsurface uses take place in unconsolidated rock masses (i.e., Quaternary deposits). These Quaternary deposits accommodate more than half of Switzerland's drinking water resources and contain a substantial volume of raw materials (gravels and sands). Due to the increased demand on these deposits, use conflicts in the shallow subsurface are unavoidable. Knowledge about composition and spatial distribution of these sediments is essential for managing the subsurface.
The GeoQuat project has therefore been launched by the Federal Office of Topography swisstopo in cooperation with the Federal Office for the Environment FOEN and the Federal Office of Energy SFOE in order to:

i). Develop a system for structured storage of unconsolidated rock data (QLG data model and database). Refer to Volken et al. (2016) for more details.
ii) Build workflows and tools for the realization of 3D geological and parametric models (voxel models) of Quaternary deposits (Preisig et al., 2016).
iii) Make the developed tools, models and derived products accessible to users working in the different fields of applied geology.

Here, emphasis is laid on the added-value of data harmonization and workflow automation for analyzing, modelling and processing data from Quaternary deposits.
A homogeneous and structured storage of unconsolidated rock data in Switzerland is vital, as it permits data comparison and exchangeability, as well as it is the basis for 3D geological and parametric models. Therefore, a well-structured Quaternary deposit data model (QLG) has been implemented in the central Swiss Geological Survey (SGS) database (Brodhag et al. 2017). Moreover, data standardization in the QLG harmonized database, in itself allows for the creation of automated tools and workflows, where users can directly apply such tools favoring the exchangeability of standardized data.
Boreholes, geological cross-sections and geophysical data are harmonized, as they are the main components of the QLG database. Automated tools and workflows were built with the Feature Manipulation Engine, i.e. FME (Safe Software, 2017), to i) pre-process data and to ii) generate derived products from the 3D models. i) The raw harmonized data may represent various elements (e.g., geological formations, unified soil classification, etc.) and can exist in many formats (e.g., points along boreholes, polygons on maps or cross-sections). In pre-processing, the automated workflow gathers all those data and converts them to points with specified dimensions as needed for 3D voxel modeling. ii) The 3D voxel models serve as the foundation from which various post-products can be extracted (e.g., map of foundation soil classes, volume and quality map of resources, etc.). These entire derived products are based on the 3D voxel models and they can visualize exhaustive analysis results in a comprehensible manner. Also here, FME is used to automate the generation of these post-products and allows for fast testing of different scenarios or updating the model with the implementation of new input data. Furthermore, FME visually represent transformations on the data, in essence documenting the workflow. Overall, this semi-automated framework greatly enhances the use of (harmonized) observational data (e.g. borehole data) for producing flexible and reproducible 3D voxel models, as well as the realization of comprehensible post-products. Additionally, standardized data in combination with a multitude of tools for derived products are accessible and exchangeable for users in the fields of geology, hydrogeology, geotechnical engineering, contaminated sites, natural hazards, non-energetic mineral resources and geothermics.

REFERENCES

Brodhag, S., Oesterling, N., Baumberger, R.: Geological Data Management - An Example for Borehole Data, 15th Swiss Geoscience Meeting, 17-18 November 2017, Davos
Preisig G., Volken S., Gaehwiler M., Möri A. & Sinreich M. 2016. GeoQuat project: realization of groundwater volumes and vulnerability maps based on 3D parametric modelling. 14th Swiss Geoscience Meeting, 18-19 November 2016, Geneva, Switzerland.
Volken S., Preisig G. & Gaehwiler M. 2016. GeoQuat: Developing a system for the sustainable management, 3D modelling and application of Quaternary deposit data. Swiss Bull Angew Geol, 21(1), 3-16.
Safe Software 2017. FME Software– Feature Manipulation Engine. https://www.safe.com